

**I) BINOL-CATALYZED ASYMMETRIC SYNTHESIS OF CHIRAL
HETEROCYCLES**

**II) EXPERIMENTAL MECHANISTIC STUDY OF BINOL-CATALYZED
CONJUGATE ADDITION OF VINYLBORONIC ACIDS TO ENONES**

**III) ENANTIOSELECTIVE SYNTHESIS OF DIARYLALKANE COMPOUNDS
VIA BINOL-CATALYZED CONJUGATE ADDITION**

A Dissertation Presented to
the Faculty of the Department of Chemistry
University of Houston

In Partial Fulfillment
of the Requirements for the Degree
Doctor of Philosophy

By
Thien Si Nguyen
May 2015

**I) BINOL-CATALYZED ASYMMETRIC SYNTHESIS OF CHIRAL
HETEROCYCLES**

**II) EXPERIMENTAL MECHANISTIC STUDY OF BINOL-CATALYZED
CONJUGATE ADDITION OF VINYLBORONIC ACIDS TO ENONES**

**III) ENANTIOSELECTIVE SYNTHESIS OF DIARYLALKANE COMPOUNDS
VIA BINOL-CATALYZED CONJUGATE ADDITION**

Thien Nguyen

APPROVED:

Dr. Jeremy A. May, Chairman

Dr. Olafs Daugulis

Dr. Don Coltart

Dr. P. Shiv Halasyamani

Dr. John S. McMurray

Dean, College of Natural Sciences and
Mathematics

Dedicated to my family

my parents, my brother, my wife, and kids

for their great love and support

ACKNOWLEDGEMENTS

I would like to express my special appreciation and thanks to my advisor, Professor Dr. Jeremy May. He has been a tremendous mentor for me. His passion for chemistry is the real inspiration to me as well as to other members of our group. It is valuable of him as a supervisor that he has never put us under any pressure. Instead of pushing us to work hard, he has his own way to stimulate the endeavor inside each of us to go to the lab to set up reactions. An example is that we have been narrated with his great enthusiasm the interesting research from many other groups after each of his journey to conferences and meetings. When my research got stuck and it happened frequently, he was very patient and always came up with suggestions and solutions to help me overcome the problems. It is sure that under his guidance I have grown greatly as a research scientist. I would like to wish him a successful career and a happy life with his wonderful family.

A special thanks to my family. Words cannot express how grateful I am to my parents for all of the sacrifices that they have made on my behalf. Their eternal love and prayer for me were what empowered me so far. I would also like to thank my younger brother for all of the playful memories we had together during my childhood. He is always a little brother that I am also very proud of. The greatest support has come from my beloved wife whose devotion to me and our family is truly priceless. Without her by my side, I would have never sustained all the hard time and pressure I had to endure during my graduate study. I also thank her for having with me a wonderful boy who is the real source of joy and happiness for every single day. Our happiness will double soon as the second boy is on his way. We cannot wait to meet him.

Lastly, I would like to thank all of the group members I have worked with during the years, Brian, Santa, Miguel, DK, Ravi, Phong, Edward, Emma, Alan, Krit, Lily, and Truong. I appreciate all the jokes and laughs we had together that really helped us get through the burdensome graduate study more delightfully. I also thank them for all of the useful discussions and suggestions to help me tackle a lot of problems I had in my research. All of them will be remembered to the rest of my life.

**I) BINOL-CATALYZED ASYMMETRIC SYNTHESIS OF CHIRAL
HETEROCYCLES**

**II) EXPERIMENTAL MECHANISTIC STUDY OF BINOL-CATALYZED
CONJUGATE ADDITION OF VINYLBORONIC ACIDS TO ENONES**

**III) ENANTIOSELECTIVE SYNTHESIS OF DIARYLALKANE COMPOUNDS
VIA BINOL-CATALYZED CONJUGATE ADDITION**

An Abstract of a Dissertation Presented to
the Faculty of the Department of Chemistry
University of Houston

In Partial Fulfillment
of the Requirements for the Degree
Doctor of Philosophy

By
Thien Si Nguyen
May 2015

ABSTRACT

A BINOL-catalyzed conjugate addition was shown in our laboratory to be compatible with unprotected indole substrates. This was considered to be an advantage over typical organometallic strategies since it allowed the use of mild boron-based nucleophiles. With this well established method, we investigated the synthesis of a variety of chiral heterocyclic compounds. A new method was developed showing great compatibility with different heteroaryl structures. Along with that, a new BINOL catalyst was introduced that exhibited superior catalytic activity to previously used catalysts.

As proposed for previous studies, the rate determining step of the transformation was the carbon-carbon bond formation. In another project, we carried out a Hammett plot study to investigate the electronic effects of the aryl groups on the reaction rate. The results provided solid support for the proposal mentioned above.

Work in our laboratory showed that heteroaryltrifluoroborates exhibited superior reactivity to boronic acids in the synthesis of chiral bis-heterocycles. Therefore, in the latest project, we made use of aryltrifluoroborates in BINOL catalysis to construct different chiral bis-aryl compounds, whose structures were present in a number of important molecules. As a result, a new strategy was successfully established allowing access to a variety of enantioenriched diarylalkanes.

TABLE OF CONTENTS

Chapter One An introduction to the synthesis of chiral heterocycles via conjugate addition

1.1. Introduction.....	1
1.2. Flinderole C as the inspiration for chiral heterocycles	1
1.3. Metal mediated transformations	3
1.3.1. Chiral Lewis acid	3
1.3.2. Transition metal catalyzed 1,4-addition.....	9
1.4. Organocatalytic transformations.....	10
1.5. Other organocatalytic methods using mild boronate nucleophiles	17
1.5.1. Bifunctional thioureas	17
1.5.2. Tartaric acid catalyzed conjugate addition	18
1.5.3. BINOL-catalyzed conjugate addition	19
1.5.3.1. Chong's work.....	19
1.5.3.2. May's work	20
1.6. References.....	22

Chapter Two BINOL-catalyzed asymmetric synthesis of chiral heterocycles

2.1. Introduction.....	26
2.2. Reaction optimization	26
2.2.1. Initial screening: multi-parameter.....	26
2.2.2. Catalyst screening	27

2.3. Reaction scope	28
2.4. Conclusion	34
2.5. Experimental section.....	34
2.5.1. General consideration	34
2.5.2. HPLC columns for separation of enantiomers.....	35
2.5.3. Materials	36
2.5.4. General procedures for starting material synthesis.....	36
2.5.5. Procedures for catalyst synthesis	45
2.5.6. Procedures for boronic acid/ester synthesis.....	52
2.5.7. General procedure for conjugate addition.....	53
2.5.8. General procedure for cuprate conjugate addition.....	75
2.6. References.....	76
APPENDIX ONE: Spectra relevant to Chapter Two	78

Chapter Three Experimental mechanistic study of BINOL-catalyzed conjugate addition of vinylboronic acids to enones

3.1. Background	192
3.1.1. H. C. Brown's work.....	192
3.1.2. Suzuki's work	194
3.1.3. Chong's work and the proposed mechanism	197
3.1.4. Theoretical study.....	199
3.2. Approach.....	202
3.2.1. Postulated mechanistic scheme.....	202

3.2.2. Hammet plot.....	203
3.3. Results and discussion	205
3.3.1. Electronic effect from β -aryl groups	205
3.3.2. Electronic effect from keto-aryl groups.....	207
3.3.3. Electronic effect from boronic acids.....	209
3.4. Conclusion	211
3.5. Experimental section.....	211
3.5.1. General consideration	211
3.5.2. General procedure for the synthesis of (<i>E</i>)-4-phenylbut-3-en-2-ones	212
3.5.3. General procedure for the synthesis of (<i>E</i>)-chalcones	214
3.5.4. General procedures for the Hammet plot study	218
3.5.4.1. Reactions of β -aryl substrates	218
3.5.4.2. Reactions of keto-aryl substrates	229
3.5.4.3. Reactions of boronic acids	242
3.6. References.....	253

Chapter Four Enantioselective synthesis of diarylalkane compounds via BINOL-catalyzed conjugate addition

4.1. Background.....	256
4.1.1. Introduction.....	256
4.1.2. Method towards chiral diarylalkanes	257
4.1.2.1. Organometallic transformations.....	257
4.1.2.2. Organocatalytic methods	268

4.2. Approach.....	270
4.3. Reaction optimization	272
4.4. Reaction scope	275
4.4.1. Aryltrifluoroborate scope.....	275
4.4.2. Aryl enone scope.....	277
4.5. Conclusion	278
4.6. Experimental section.....	278
4.6.1. General consideration	278
4.6.2. General procedure for the synthesis of starting material	279
4.6.3. General procedure for potassium aryltrifluoroborate synthesis.....	284
4.6.4. Procedures for catalyst synthesis	289
4.6.5. General procedure for the BINOL-catalyzed conjugate addition of potassium aryltrifluoroborate to (<i>E</i>)-4-aryl-3-buten-2-one.....	291
4.7. References.....	312
APPENDIX TWO: Spectra relevant to Chapter Four	316

ABBREVIATIONS AND ACRONYMS

AcO	acetate
app.	apparent
aq.	aqueous
BArF ₂₄	tetrakis[3,5-bis(trifluoromethyl)phenyl]borate
9-BBN	9-borabicyclo (3.3.1)nonane
Bn	benzyl
Bu	butyl
°C	degree Celcius
cod	cyclooctadiene
d	day
DCE	1,2-dichloroethane
DCM	dichloromethane
DME	1,2-dimethoxyethane
DMF	<i>N,N</i> -dimethylformamide
DMSO	dimethylsulfoxide
ee	enantiomeric excess

equiv	equivalent
er	enantiomeric ratio
ESI	electrospray ionization
Et	ethyl
Et ₃ N	
Et ₂ O	diethyl ether
EtOAc	ethyl acetate
EtOH	ethanol
EWG	electron withdrawing group
GC	gas chromatography
h	hour
HMPA	hexamethylphosphoramide
HPLC	high performance liquid chromatography
HRMS	high resolution mass spectrometry
Hz	hertz
IC ₅₀	50% inhibitory concentration
<i>i</i> -Pr	isopropyl

IR	infrared
<i>J</i>	coupling constant
KHMDS	potassium bi(trimethylsilyl)amide
LAH	Lithium aluminum hydride
m	multiplet or mili
Me	methyl
MeCN	acetonitrile
MeOH	methanol
min	minute
mol	mole
MOM	methoxymethyl
MS	molecular sieves
NMR	nuclear magnetic resonance
<i>o</i>	ortho
OTf	triflate
Ph	phenyl
PhH	benzene

PhMe	toluene
pin	pinacol
ppm	part per million
q	quartet
R _F	retention factor
R.T.	room temperature
s	singlet
t	triplet
<i>t</i> -Bu	<i>tert</i> -butyl
TFA	trifluoroacetic acid
THF	tetrahydrofuran
TLC	thin layer chromatography
TMS	trimethylsilyl
Ts	tosyl
UV	ultraviolet

Chapter One

An introduction to the synthesis of chiral heterocyclic molecules via conjugate addition

1.1. Introduction

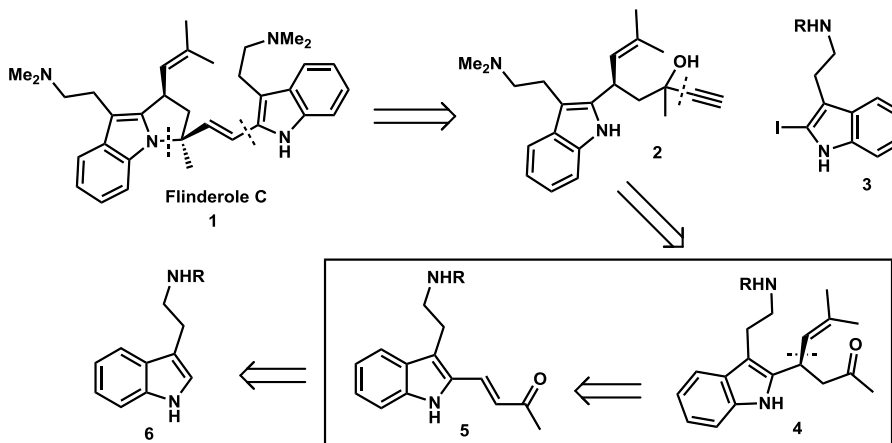
It is undoubted that heterocycles are an important class of organic compounds. They are present in a number of natural products that possess significant bioactivities. They also play important roles as useful synthetic moieties such as chiral auxiliaries¹ and directing groups in regioselective transformations.²

These vital roles of heterocyclic compounds have stimulated synthetic chemists to devote their efforts in developing strategies for their synthesis as well as the functionalization of heterocycles.³ However, stereoselective transformations in the presence of heterocyclic structures, especially with the lack of protecting groups, have received less attention. It is presumably due to the propensity of coordinating atoms on the heterocycles to interact with activating species, therefore preventing the reactions from achieving the desired reactivity and selectivity. In the following sections, we will discuss on different methods for access to α -chiral heterocycles with a focus on 1,4-addition.

1.2. Flinderole C as the inspiration for chiral heterocycles

Flinderole C, a natural product isolated from *Flindersia amboinensis*, exhibits antimalarial activity against the chloroquine-resistant *Plasmodium falciparum* with a low IC₅₀ of 0.34 μ M. This interesting activity makes flinderole C a potential candidate for the treatment of chloroquine-resistant malaria and consequently a target of several synthetic

efforts with the hope of accessing a large quantity of the substance. However, there has been no report of an enantioselective synthesis of flinderole C so far. Being interested in addressing this problem, we joined the field and were able to come up with a synthetic route (Scheme 1.1.2) for an efficient selective preparation of flinderole C.



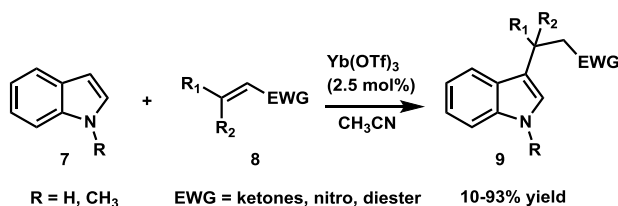
Scheme 1.1.2. Retrosynthesis of flinderole C.

As demonstrated in the retrosynthetic analysis, the most important disconnection requires the introduction of a vinyl group to an indole-appended enone in a highly stereoselective manner (**4** to **5**). The newly formed stereocenter α to the indole moiety will control the formation of the other centers so that the synthesis can be achieved without employing any more chiral reagents. A wide literature search was made to seek an appropriate strategy for that purpose, and to our surprise there are few examples of such transformation. Therefore, the development of an asymmetric conjugate addition that is compatible with indoles and a wider range of heterocycle structures is of great importance.

1.3. Metal mediated transformations

1.3.1. Chiral Lewis acid

The use of a Lewis acid to facilitate the Friedel-Crafts conjugate addition of indole to an α,β -unsaturated enone was first reported by Michael Kerr in 1996.⁴ In this work, 2.5 mol% of $\text{Yb}(\text{OTf})_3$ was used to promote the addition of indole to different enones at room temperature (Scheme 1.3.1.1).

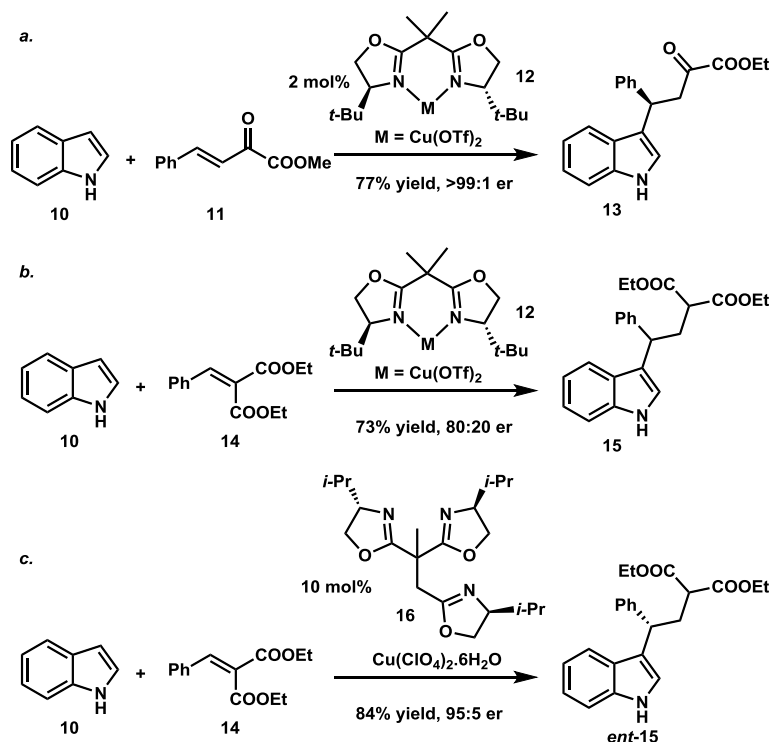


Scheme 1.3.1.1. Racemic Lewis acid catalyzed Friedel-Crafts alkylation of indoles

This pioneering work has triggered a movement in the field of developing an asymmetric version of the addition of indoles to electron deficient olefins. A well-known method is the incorporation of a chiral ligand, which is typically a nitrogen or phosphorus containing compound, with a Lewis acidic metal center. The most widely used are the chiral bisoxazoline (BOX) and bisphosphorus ligands. To apply this catalytic system for the reactions, the substrates have to possess functional groups which can coordinate to the catalyst in a bidentate fashion.

In 2003, Jorgensen *et al.* revealed the enantioselective addition of indoles to different β,γ -unsaturated α -ketoesters with the use of $\text{Cu}(\text{OTf})_2$ in combination with (*S*)-*t*-Bu-BOX (Scheme 1.3.1.2a).⁵ Later in the same year, they extended their strategy to different alkylidene malonates using the same catalyst combination to achieve addition reactions in high yields, although with significantly lower selectivity (Scheme 1.3.1.2b).⁶ This

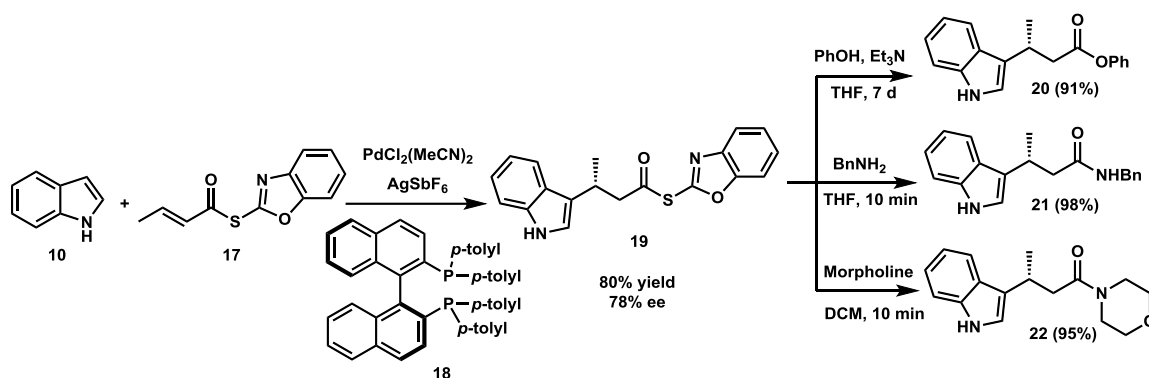
problem was later tackled by Tang *et al.* the year after. They developed the Michael addition of alkylidene malonates with indoles in high enantioselectivity by taking advantage of the combination of $\text{Cu}(\text{ClO}_4)_2$ and a C_3 -trisoxazoline ligand (Scheme 1.3.1.2c).⁷



Scheme 1.3.1.2. Asymmetric addition of indoles to (a) unsaturated ketoesters and (b), (c) diesters

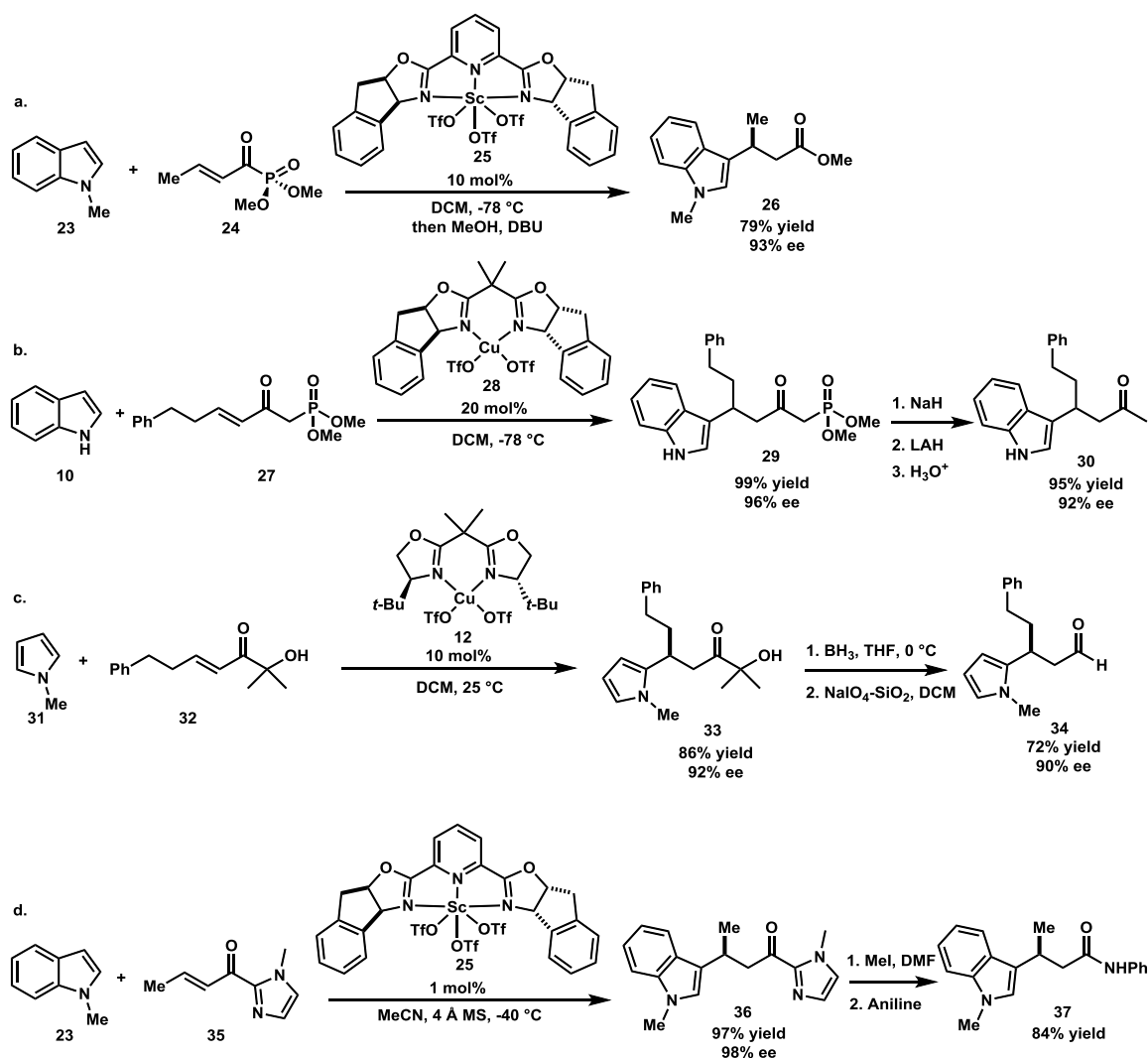
The major problem of the use of bidentate substrates is the difficulty in transforming these functional groups to other useful functionalities. In 2003, Umani-Ronchi *et al.* introduced the α,β -unsaturated thioesters as a new class of substrates with a removable 2-sulfanylbenzoxazole auxiliary for the asymmetric Michael addition reaction with

indoles.⁸ The subsequent treatments of the products with appropriate nucleophiles lead to the formation of different molecules of practical importance (Scheme 1.3.1.2).



Scheme 1.3.1.2. Asymmetric Friedel–Crafts reaction of indoles and unsaturated thioesters

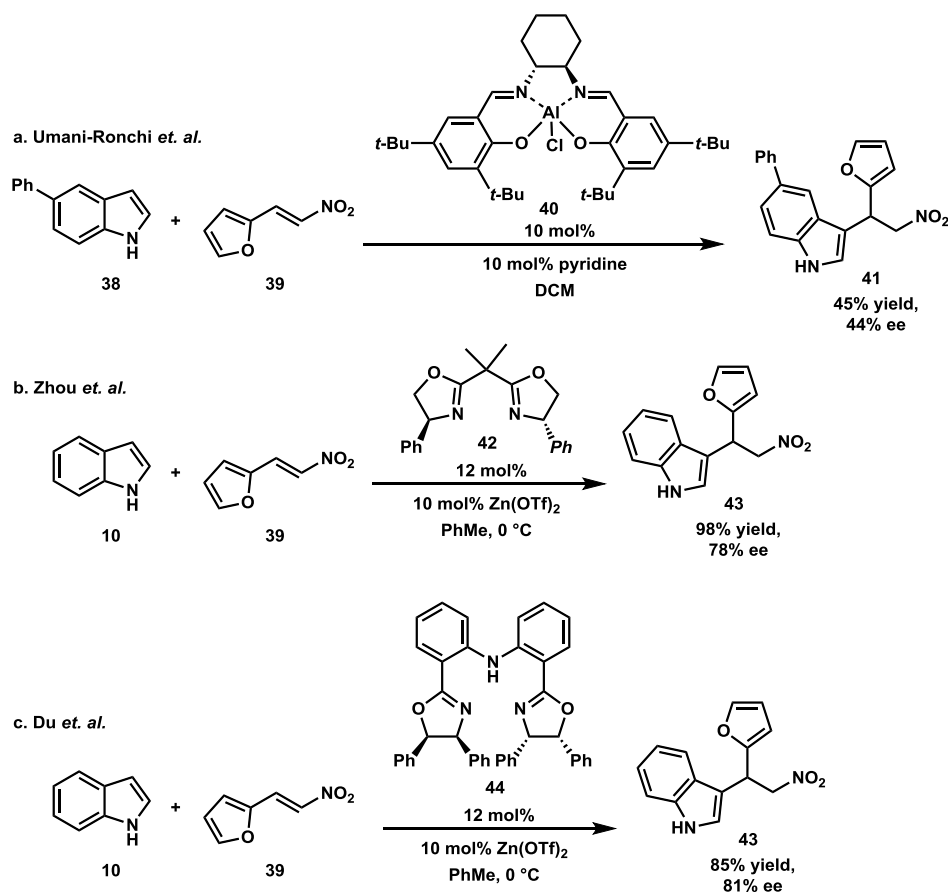
Later, acylphosphonate,⁹ β -ketophosphonate,¹⁰ α^{\prime} -hydroxyketone,¹¹ and acylimidazole¹² substrates were also demonstrated to be effective counterparts for interaction with a chiral metallic center to yield excellent selectivity in the reaction with indoles and pyrroles (Scheme 1.3.1.4). These groups were later transformed to different functionalities, confirming the great utility of the strategy in organic synthesis.



Scheme 1.3.1.4. Enantioselective Friedel-Crafts reactions using (a) acyphosphonates; (b) β -ketophosphonates; (c) α' -hydroxyketones; (d) acylimidazole

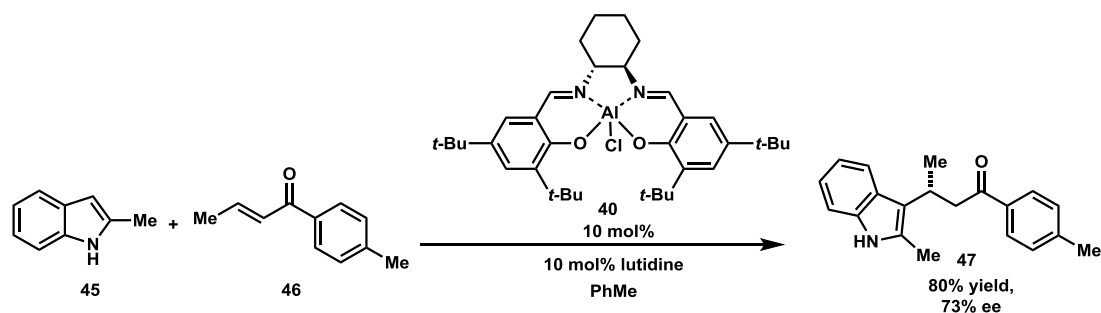
Nitroalkenes were first examined as Michael acceptors for indoles by Umani-Rochi in 2005 using a [SalenAlCl] complex as the catalyst. However, the reactions proceeded in moderate yields and low enantiomeric excesses (Scheme 1.3.1.5a).¹³ Later in 2006, Zhou *et al.*¹⁴ and Du *et al.*¹⁵ independently developed similar zinc-based catalysts to enhance the reactivity and selectivity of the transformation (Scheme 1.3.1.5b-c). The nitro group

was proposed to provide a bidentate coordination to the metal giving an unusual four-membered ring interaction.



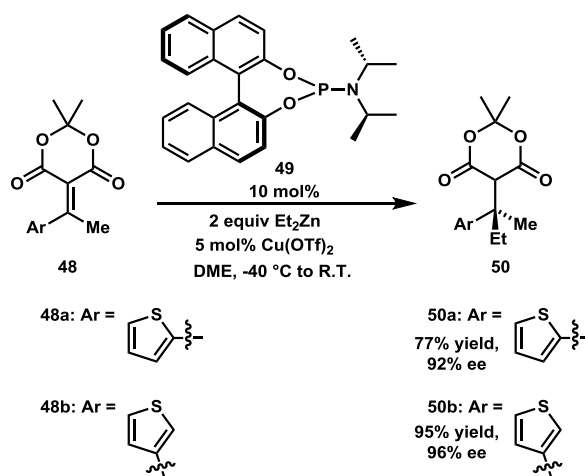
Scheme 1.3.1.5. Asymmetric Friedel-Crafts reactions of indoles and nitroalkenes

In their attempts to make the simple enones viable for the Michael addition with indoles, the Umani-Rochi group employed one more time the chiral aluminum based catalyst [SalenAlCl], which could provide reactions with acceptable yields and moderate enantioselectivities (Scheme 1.3.1.6).¹⁶



Scheme 1.3.1.6. Enantioselective Michael addition of indoles to simple enones.

As shown so far, the Friedel-Crafts reactions of indole have been exploited for the asymmetric Michael addition to various types of substrates. Despite the considerable importance of these transformations in the establishment of a stereocenter adjacent to indole structures, the tendency of indoles to only give functionalization at the C3 position has largely limited the scope of the methods. A potential alternative approach is employing an α,β -unsaturated carbonyl functionalized with indolyl or heteroaryl groups at the desired contact point on the ring. This will eliminate the Friedel-Crafts regioselectivity controlled by the electronic nature of the heteroarenes. The work of Fillion and coworkers in 2009 took advantage of this tactic in synthesizing an array of all carbon quaternary centers neighboring a number of prefunctionalized heterocycles and aromatic structures.¹⁷ As illustrated in Scheme 1.3.1.7, Fillion was successful in introducing alkyl groups to different heterocyclic alkylidene Meldrum's acids by using a dialkylzinc reagent and a chiral copper catalyst. In light of the synthesis of flinderole C, we find this strategy promising for the 2-indole-appended enone that is required to access the key intermediate **4**, which cannot be achieved by reacting indole with an enone substrate.

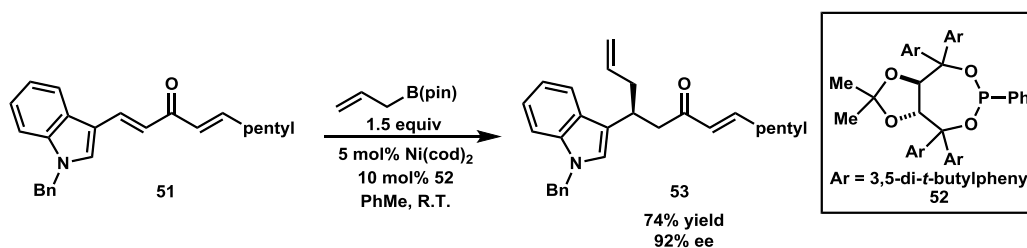


Scheme 1.3.1.7. Asymmetric conjugate addition of diethylzinc to β -arylalkylidene

Meldrum's acids

1.3.2. Transition metal catalyzed 1,4-addition

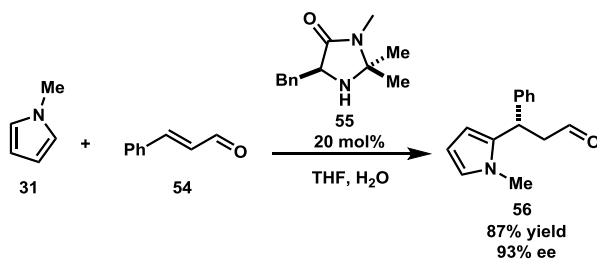
Although the synthesis of chiral α -branched heterocycles via organometallic processes have received comparable attention,¹⁸ 1,4-addition reactions compatible with indoles catalyzed by transition metal have rarely been reported. The only example we were able to find was the work of Morken *et al.* in 2008. They utilized a nickel complex as the catalyst in the presence of a chiral phosphoramidite ligand to bring about the enantioselective conjugate addition of allylpinacolboranes to dialkylidene ketones. The reactions proceeded with good yields and great selectivities (Scheme 1.3.2).¹⁹



Scheme 1.3.2. Nickel catalyzed conjugate allylation of activated enones

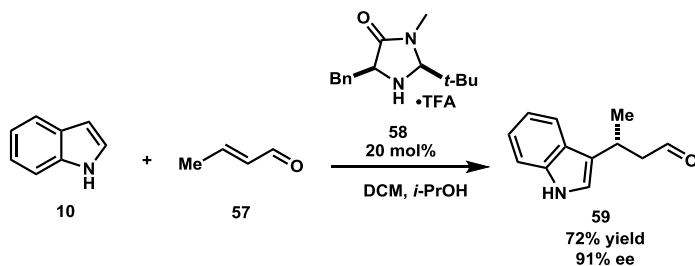
1.4. Organocatalytic transformations

In 2001, MacMillan *et. al.* introduced the first asymmetric organocatalytic conjugate addition of pyrroles to enal substrates using a chiral secondary amine catalyst (Scheme 1.4.1).²⁰ This work takes advantage of the ability of iminium catalysis to facilitate the 1,4-addition to enals, which is known to be prone to 1,2-addition under acidic conditions, due to the inherent steric hindrance of the catalyst.



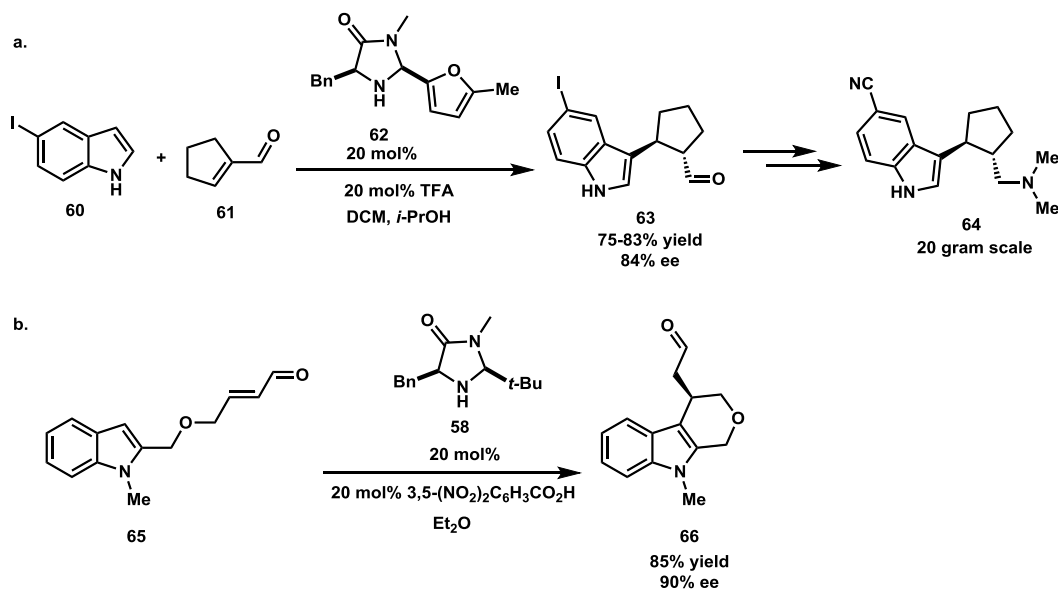
Scheme 1.4.1. Asymmetric Friedel-Crafts alkylation of pyrroles using a chiral secondary amine catalyst

The following year, 2002, they extended it to indole substrates with as much success as they had achieved with pyrroles (Scheme 1.4.2).²¹



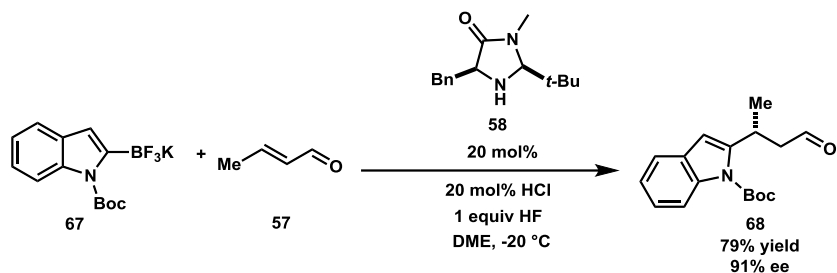
Scheme 1.4.2. Asymmetric Friedel-Crafts alkylation of indoles using a chiral secondary amine catalyst

This strategy was later applied to cyclic enals and proved to be efficient in synthesizing in gram scale compound **64** as a highly potent selective serotonin reuptake inhibitor (Scheme 1.4.3a).²² Later in 2007, an intramolecular version of the transformation was performed by Xiao *et al.* (Scheme 1.4.3b).²³



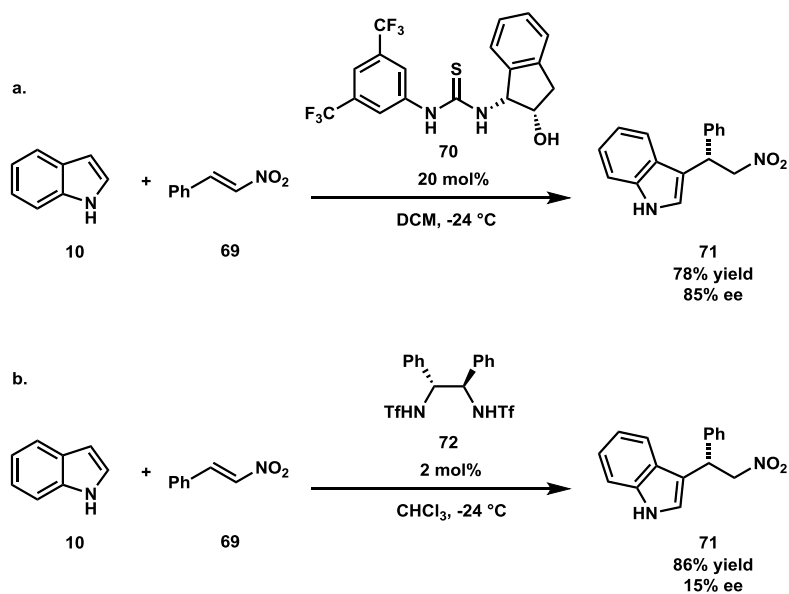
Scheme 1.4.3. Imidazolidinone catalysis in (a) addition of indoles to cyclic enals; (b) intramolecular addition of indoles to enals.

In 2007, the MacMillan group demonstrated the elegant use of nucleophilic 2-indolyl and 2-benzofuranyl trifluoroborate salts to overcome the restriction of Friedel-Crafts regioselectivity of plain nucleophiles (Scheme 1.4.4).²⁴



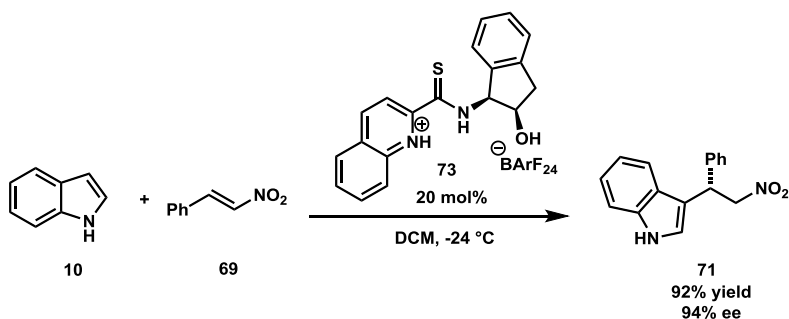
Scheme 1.4.4. Asymmetric conjugate addition of aryltrifluoroborate salts to enals catalyzed by imidazolidinone catalyst

As also mentioned in section 1.3.1, a nitro group could coordinate in a bidentate fashion to a metallic center in the activation of nitroalkenes for the Michael addition of indole reagents. A similar chelating mode can be achieved by the use of a double hydrogen-bonding chiral thiourea²⁵ or chiral diamine catalyst²⁶ (Scheme 1.4.5). The reactions proceeded in good yields with moderate ee's in the former and low ee's in the latter. Subsequent attempts in designing more efficient thiourea catalysts were made Connon²⁷ without significant improvement, although the work introduced a library of interesting novel thiourea structures.



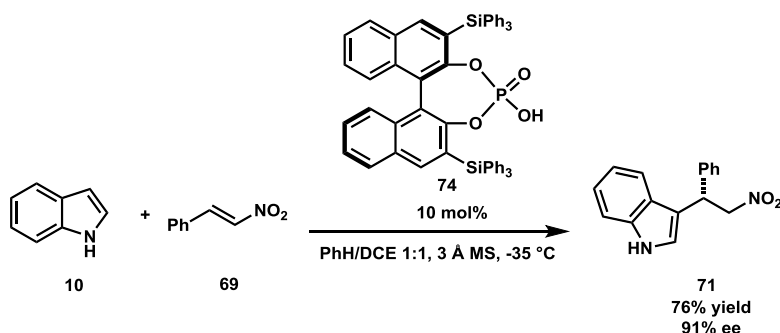
Scheme 1.4.5. Asymmetric conjugate addition of indoles to nitroalkenes catalyzed by
 (a) a chiral thiourea catalyst; (b) a chiral diamine catalyst

Such low selectivity could be overcome by the utilization of more acidic catalyst. Seidel and coworkers designed a novel thioamide containing a protonated quinoline moiety which dramatically enhanced the selectivity (Scheme 1.4.6).²⁸



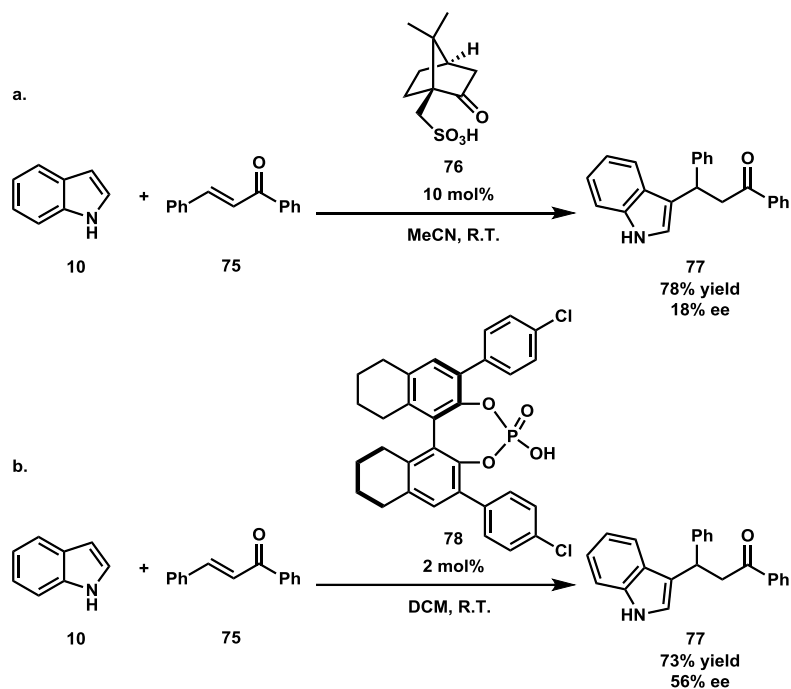
Scheme 1.4.6. Asymmetric conjugate addition of indoles to nitroalkenes catalyzed by
 a cationic thioamide catalyst

Chiral phosphoric acids were introduced by Akiyama and coworkers as efficient catalysts for the Friedel-Crafts addition of indoles to nitroalkenes (Scheme 1.4.7).²⁹ In this transformation, the phosphoric acid was proposed to activate the nitro group and interact with the indole nitrogen both through hydrogen bonding. This proposal was made by the observation of the deterioration of both yield and selectivity when N-methyl indole was in use.



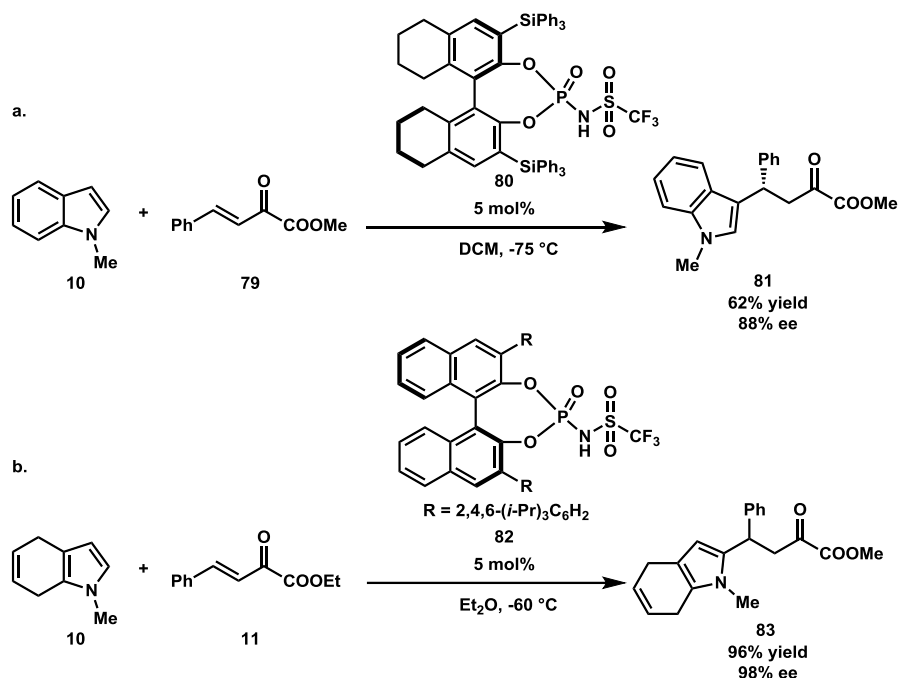
Scheme 1.4.7. Asymmetric conjugate addition of indoles to nitroalkenes catalyzed by chiral phosphoric acid

The above mentioned type of interaction enabled the use of simple α,β -unsaturated carbonyl compounds that can only provide monodentate coordination to an acid. In fact, two years before Akiyama's work was published, Xia *et al.* had discovered that commercial *D*-camphor sulfonic acid could trigger an enantioselective Michael addition of indoles to a variety of aromatic enones albeit in impractical selectivities (Scheme 1.4.8a).³⁰ Two years later, in 2008, Zhou *et al.* utilized a chiral phosphoric acid to facilitate a similar transformation, however without a significant improvement (Scheme 1.4.8).³¹ It is worth mentioning that the viability of simple enones in the reaction with indoles was confirmed by Umani-Ronchi as described in previous section.



Scheme 1.4.8. Asymmetric conjugate addition of indoles to enones catalyzed by (a) *D*-camphor sulfonic acid; (b) chiral phosphoric acid

In 2008, Rueping *et al.* reported their pioneering work in using chiral *N*-triflyl phosphoramidate to catalyze the 1,4-addition of indoles to β,γ -unsaturated α -keto esters (Scheme 1.4.9a).³² The reactions proceeded with high yields and selectivities. Later in the same year, this catalyst system was used with slight modification for the reaction of 4,7-dihydroxyindoles by You *et al.* (Scheme 1.4.9b).³³



Scheme 1.4.9. N-triflylphosphoramidate catalyzed conjugate addition of (a) Indoles and (b) dihydroindoles to unsaturated esters

So far, we have depicted a comprehensive picture of the establishment of a stereocenter alpha to heterocyclic structures through Michael addition reactions. In general, methods have been predominantly built around Friedel-Crafts reactions, which are not appropriate for the synthesis of flinderole C due to the restrictions in regioselectivity. A suitable solution is then to employ either heteroaryl enones (Fillion and Morken) or heteroarylboron reagents (MacMillan), which can suppress the Friedel-Crafts selectivity rendered by the nucleophiles. Among these strategies, MacMillan's work seems to serve as the most suitable system for our study towards flinderole C synthesis. However, this method only works for enals since secondary amine catalysts exhibit poor reactivity towards enones in the formation of iminium species. We also find

that typical organometallic conjugate additions are rarely compatible with heterocycles, and strong nucleophiles such as Grignard reagents are definitely detrimental to unprotected nitrogen atoms on the ring. Therefore, we wish to seek for an organocatalyst system which can enable the employment of mild nucleophiles for compatibility with heterocyclic compounds. In the next section, we will discuss several potential candidates and the one of our choice.

1.5. Other organocatalytic methods using mild boronate nucleophiles

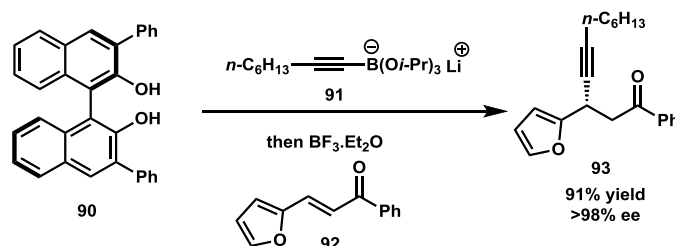
1.5.1. Bifunctional thioureas

Thioureas are known for a doubly hydrogen bonded interaction with electronegative atoms. In all examples described in the previous section, the substrates that contained dicarbonyl or nitro groups could coordinate in a bidentate mode. Consequently, that leads to a high energy four-membered or nine-membered ring binding interaction resulting in low selectivity for the reactions. In 2010, Takemoto *et al.* designed a novel iminophenol thiourea catalyst to catalyze the 1,4-addition of vinylboronic acids to enones containing an γ -hydroxy group (Scheme 1.5.1).³⁴ The proposed transition state invokes a six-membered ring chelation through hydrogen bonds between the N-H's and the carbonyl oxygen as well as dual coordination of the substrate and the catalyst to the boronic acid to trigger the bond formation. Although the conversion and selectivity on the reactions are comparatively high, the requirement for a hydroxyl group from the substrates significantly limits the method.

1.5.3. BINOL catalyzed conjugate addition

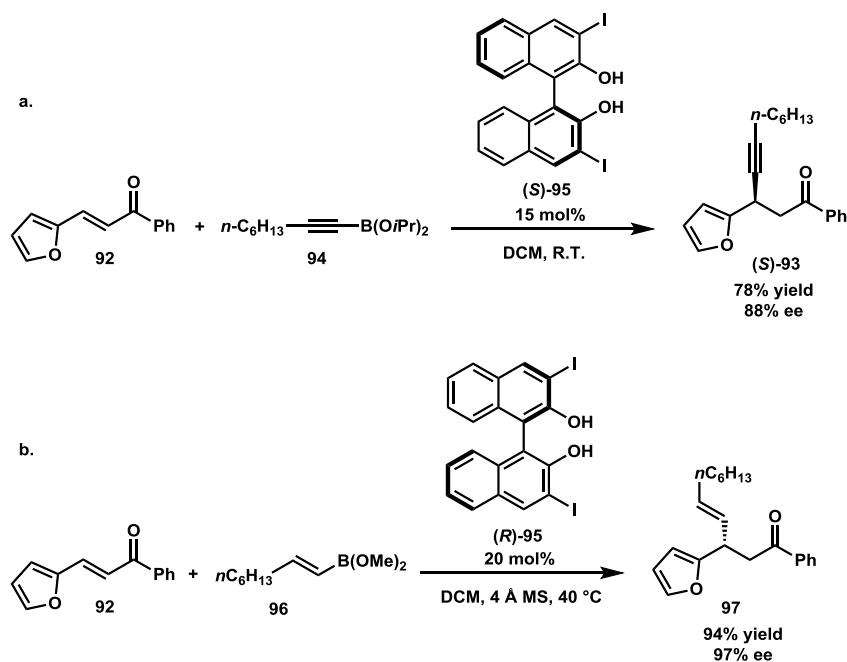
1.5.3.1. Chong's work

In 2000, Chong and coworkers reported the use of a BINOL derivative in the conjugate addition reaction of alkynylborate salts to aromatic enones for the first time (Scheme 1.5.3.1.1).³⁶ Although the reactions advanced with high yields and great selectivities, the requirement for stoichiometric amounts of BINOL was a limitation of the transformation.



Scheme 1.5.3.1.1. Enantioselective conjugate addition of alkynylborate salts to enones facilitated by stoichiometric BINOL

In 2005, they were successful in developing a catalytic version of the strategy in which the loading of BINOL **95** could be dropped to 15 mol% (Scheme 1.5.3.1.2a).³⁷ In this work, the reaction of a furan-appended enone was carried out, showing a potential application to a wider range of heterocyclic substrates. Two years later, in 2007, they disclosed the expansion to different vinylboronates with the same level of success (Scheme 1.5.3.1.2b).³⁸



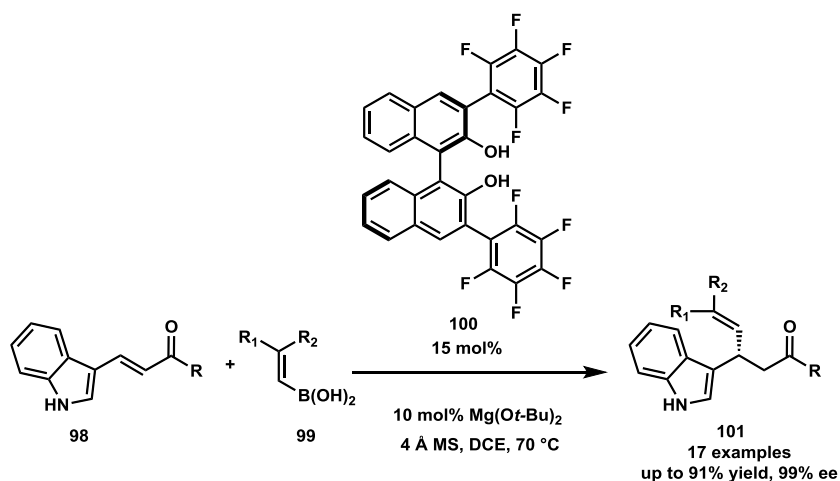
Scheme 1.5.3.1.2. BINOL catalyzed conjugate addition of (a) alkynylboronic esters and (b) vinylboronic esters to enones

At this point, we found this method advantageous for our study since it allows the use of a mild boron nucleophile and simple enone substrates. In addition, it also enables the introduction of not only vinyl groups, but also alkynyl groups. The latter could not be added by typical organometallic processes. Furthermore, the great reactivity and selectivity of the reaction make it a trustable and interesting base for approaching the synthesis of flinderole C. The background of this chemistry will be discussed deeper in chapter 3 where we will present our experimental mechanistic study.

1.5.3.2. May's work

As mentioned in the previous section, we decided to test the viability of an unprotected indole substrate, especially 2-indole enone, in a BINOL-catalyzed conjugate addition. However, due to the scant availability of indoles prefunctionalized at the 2-

position, we made our first investigation on 3-indole-appended enones as model substrates for our study. This work was performed by a former member of our group, Dr. Brian Lundy.³⁹ Although the conditions reported by the Chong group operated smoothly with chalcone substrates, they were ineffective with indole substrates. An extensive examination of reaction conditions led to a great deviation from the original. Specifically, boronic acids were used in place of boronic esters owing to the readiness and ease of handling of the acids. Furthermore, a highly fluorinated BINOL structure was employed to obtain sufficient reactivity and selectivity for the reactions. Finally, a catalytic amount of $\text{Mg}(\text{O}i\text{-Bu})_2$ as an additive was shown to be vital. With those newly established conditions, Lundy was able to build a library of chiral 4-(3-indolyl)-butan-2-ones possessing β -vinyl or alkynyl groups (Scheme 1.5.3.2). The conditions were later applied to the 2-indole enone without great success. Efforts to elevate the efficiency of the reaction to the same degree as with 3-indole enones were not successful, with 55% as the best yield at higher temperature in toluene and with Cs_2CO_3 as the additive.



Scheme 1.5.3.2. BINOL-catalyzed conjugate addition of vinylboronic acids to indole-appended enones

Despite the unexpected low reactivity towards the target 2-indole substrates, the method provided a potentially powerful tool for the construction of different other chiral heterocycles. The following chapter will discuss the main body of our research on the expansion of the scope of the chemistry to a variety of heterocyclic structures that may have great importance in medicinal chemistry.

1.6. References

1. Corey, E. J.; Helal, C. J. *Angew. Chem., Int. Ed.* **1998**, *37*, 1986—2012.
2. (a) Tran, L. D.; Popov, I.; Daugulis, O. *J. Am. Chem. Soc.* **2012**, *134*, 18237—18240;
(b) Yang, W.; Ye, S.; Fanning, D.; Coon, T.; Schmidt, Y.; Krenitsky, P.; Stamos, D.; Yu, J.-Q. *Angew. Chem., Int. Ed.* **2015**, *54*, 2501—2504.
3. (a) Humphrey, G. R.; Kuethe, J. T.; *Chem. Rev.* **2006**, *106*, 2875—2911; (b) Eftekhari-Sis, B.; Zirak, M. *Chem. Rev.* **2015**, *115*, 151—264.
4. Harrington, P. E.; Kerr, M. A. *Synlett.* **1996**, 1047—1048.
5. Jensen, K. B.; Thorhauge, J.; Hazell, R. G.; Jorgensen, K. A. *Angew. Chem., Int. Ed.* **2001**, *40*, 160—163.
6. Zhuang, W.; Hansen, T.; Jorgensen, K. A. *Chem. Commun.* **2001**, 347—348.
7. Zhou, J.; Tang, Y.; *J. Am. Chem. Soc.* **2002**, *124*, 9030—9031.
8. Bandini, M.; Melloni, A.; Tommasi, S.; Umani-Ronchi, A. *Helv. Chim. Acta* **2003**, *86*, 3753—3763.
9. Evans, D. A.; Schiedt, K. A.; Fandrick, K. R.; Lam, H. W.; Wu, J. *J. Am. Chem. Soc.* **2003**, *125*, 10780—10781.
10. Yang, H.; Hong, Y.-T; Kim, S. *Org. Lett.* **2007**, *9*, 2281—2284.

11. Palomo, C.; Oiarbride, M.; Kardak, B. G.; Garcia, J.; Liden, A. *J. Am. Chem. Soc.* **2005**, *127*, 4154—4155.
12. Evans, D. A.; Fandrick, K. R.; Song, H.-J. *J. Am. Chem. Soc.* **2005**, *127*, 8942—8943.
13. Bandini, M.; Garelli, A.; Rovinetti, M.; Tommasi, S.; Umani-Rochi, A. *Chirality* **2005**, *17*, 522—529.
14. Jia, Y.-X.; Zhu, S.-F.; Yang, Y.; Zhou, Q.-L. *J. Org. Chem.* **2006**, *71*, 75—80.
15. Lu, S.-F.; Du, D.-M.; Xu, J. *Org. Lett.* **2006**, *8*, 2115—2118.
16. Bandini, M.; Fagioli, M.; Melchiorre, P.; Melloni, A.; Umani-Ronchi, A. *Tetrahedron Lett.* **2003**, *44*, 5843—5846.
17. Wilsily, A.; Fillion, E. *J. Org. Chem.* **2009**, *74*, 8583—8694.
18. (a) Matsuzawa, H.; Miyake, Y.; Nishibayashi, Y. *Angew. Chem., Int. Ed.* **2007**, *46*, 6488—6491; (b) Pathak, T. P.; Gligorich, K. M.; Welm, B. E.; Sigman, M. S. *J. Am. Chem. Soc.* **2010**, *132*, 7870—7871; (c) Rauniyar, V.; Wang, Z. J.; Burks, H. E.; Toste, F. D. *J. Am. Chem. Soc.* **2011**, *133*, 8486—8489; DeAngelis, A.; Shurtleff, V. W.; Dmitrenko, O.; Fox, J. M. *J. Am. Chem. Soc.* **2011**, *133*, 1650—1653; (e) Matsuzawa, H.; Kanao, K.; Miyake, Y.; Nishibayashi, Y. *Org. Lett.* **2007**, *9*, 5561—5564.
19. Sieber, J. D.; Morken, J. P. *J. Am. Chem. Soc.* **2008**, *130*, 4978—4983.
20. Paras, N. A.; MacMillan, D. W. C. *J. Am. Chem. Soc.* **2001**, *123*, 4370—4371.
21. Austin, J. F.; MacMillan, D. W. C. *J. Am. Chem. Soc.* **2002**, *124*, 1172—1173.
22. King, H. D.; Meng, Z.; Denhart, D.; Mattson, R.; Kimura, R.; Wu, D.; Gao, Q.; Macor, J. E. *Org. Lett.* **2005**, *7*, 3437—3440.

23. Li, C.-F.; Liu, H.; Liao, J.; Cao, Y.-J.; Liu, X.-P.; Xiao, W.-J. *Org. Lett.* **2007**, *9*, 1847—1850.
24. Lee, S.; MacMillan, D. W. C. *J. Am. Chem. Soc.* **2007**, *129*, 15438—15439.
25. Herrera, R. P.; Sgarzani, V.; Bernadi, L.; Ricci, A. *Angew. Chem., Int. Ed.* **2005**, *44*, 6576—6579.
26. Zhuang, W.; Hazell, R. G.; Jorgensen, K. A. *Org. Biomol. Chem.* **2005**, *3*, 2566—2571.
27. Fleming, E. M.; McCabe, T.; Connon, S. J. *Tetrahedron Lett.* **2006**, *47*, 7037—7042.
28. Manesh, M.; Seidel, D. *J. Am. Chem. Soc.* **2008**, *130*, 16464—16465.
29. Itoh, J.; Fuchibe, K.; Akiyama, T. *Angew. Chem., Int. Ed.* **2008**, *47*, 4016—4018.
30. Zhou, W.; Xu, L.-W.; Li, L.; Yang, L.; Xia, C.-G. *Eur. J. Org. Chem.* **2006**, 5225—5227.
31. Tang H.-Y.; Lu, A.-D.; Zhou, Z.-H.; Zhao, G.-F.; He, L.-N.; Tang, C.-C. *Eur. J. Org. Chem.* **2008**, 1406—1410.
32. Rueping, M.; Nachtsheim, B. J.; Moreth, S. A.; Bolte, M. *Angew. Chem., Int. Ed.* **2008**, *47*, 593—596.
33. Zeng, Mi.; Kang, Q.; He, Q.-L.; You, S.-L. *Adv. Synth. Catal.* **2008**, *350*, 2169—2173.
34. Inokuma, T.; Takasu, K.; Sakaeda, T.; Takemoto, Y. *Org. Lett.* **2009**, *11*, 2425—2428.
35. Sugiura, M.; Tokudomi, M.; Nakajima, M. *Chem. Commun.* **2010**, *46*, 7799—7800.
36. Chong, J. M.; Shen, L.; Taylor, N. J. *J. Am. Chem. Soc.* **2000**, *122*, 1822—1823.
37. Wu, T. R.; Chong, J. M. *J. Am. Chem. Soc.* **2005**, *127*, 3244—3245.

38. Wu, T. R.; Chong, J. M. *J. Am. Chem. Soc.* **2007**, *129*, 4908—4909.
39. Lundy, B. J.; Jansone-Popova, S.; May, J. A. *Org. Lett.* **2011**, *13*, 4958—4961.

Chapter Two

BINOL-catalyzed asymmetric synthesis of chiral heterocycles¹

2.1. Introduction

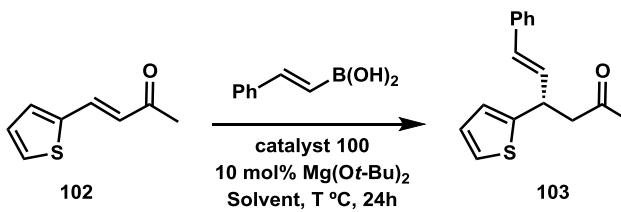
As mentioned in Chapter 1, our laboratory was successful in developing a highly enantioselective conjugate addition of mild vinylboronic acids to indole-appended enones using BINOL as the catalyst. In this chapter, we will report our work on the application of the strategy to access different chiral heterocyclic compounds.

2.2. Reaction optimization

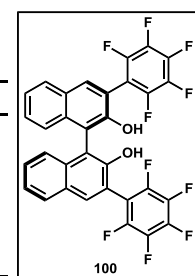
2.2.1. Initial screening: multi-parameter

Starting out with the conditions developed in our previous work, we used a 2-thiophenyl enone as a substrate for reaction optimization (entry 1, Table 2.2.1). However, only an 11% yield of product was obtained. Switching to refluxing toluene gave a better yield (entry 2). Increasing the equivalents of boronic acid significantly improved the conversion (entry 3 and 4). Finally, by increasing the catalyst loading to 20 mol%, we were able to obtain the product in 96% yield and 95:5 ee.

Table 2.2.1. Optimization table

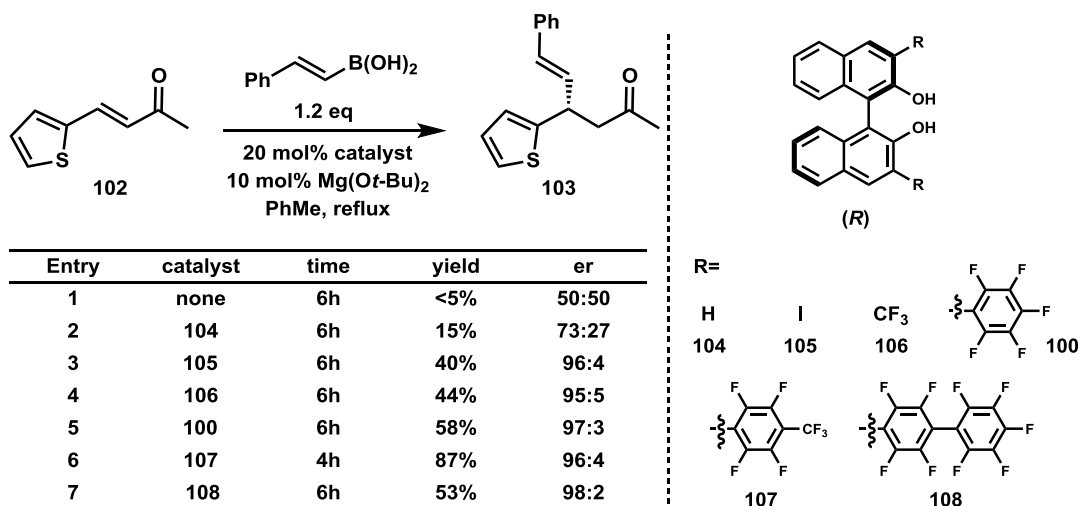


Entry	Solvent	Acid (eq)	catalyst	T °C	yield	er
1	DCE	1.2	15 mol%	70	11%	NA
2	PhMe	1.2	15 mol%	Reflux	26%	96:4
3	PhMe	2	15 mol%	Reflux	41%	95:5
4	PhMe	3	15 mol%	Reflux	57%	94:6
5	PhMe	3	20 mol%	Reflux	96%	95:5



2.2.2. Catalyst screening

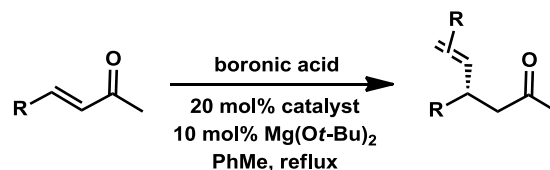
Although catalyst **100** appeared to work well under the optimized conditions, a better catalyst may shorten the reaction time as well as give higher enantioselectivities while still maintaining good reaction yields. A variety of BINOL catalysts that have different electron-withdrawing substituents at the 3,3' positions were then synthesized, and a direct comparison of these catalysts was made with the thiophene substrate **102** (Table 2.2.2). Without the presence of the BINOL catalyst, a small amount of product **5** was observed from a background reaction (entry 1). BINOL (**104**) slightly improved the reaction rate and exhibited a certain degree of stereinduction (entry 2). Better yields and enantioselectivities were obtained using **105**, **106**, and **100** (entries 3,4 and 5). The most effective catalyst, however, was **107**, which gave 87% yield and 92% ee in even shorter time (entry 6). These results showed a correlation between the degree of fluorination and the reaction outcome. Nevertheless, catalyst **108**, which has the highest incorporation of fluorine, only gave 53% yield (entry 7).

Table 2.2.2. Reactivity of different BINOL

2.3. Reaction scope

The reactions of a variety of heterocycle-appended enones were then investigated by employing the first generation catalyst **100** and the novel BINOL **107**. Thiophene and furan enones worked well under the reaction conditions (Table 2.3.1). In some cases, catalyst **107** gave comparable yields and ee's in much shorter time compared to catalyst **100** (entries 1,2 and 9,10). Vinyl and alkynyl substituents were introduced by using various vinylboronic acids and an alkynylboronic ester (entry 6), respectively. As expected, no 1,6- or 1,2- addition product was observed when using a 3-furan dienone substrate (entries 7,8).

Table 2.3.1. Furan and thiophene substrates



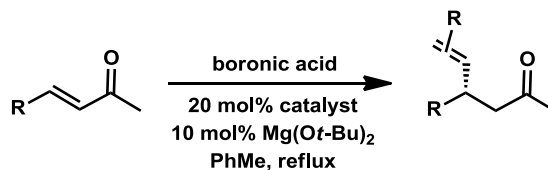
Entry	Product	catalyst	time	yield	er	Entry	Product	catalyst	time	yield	er	
		R= Ph, 109										
1		100	24h	93%	96:4	7		100	72h	74%	98:2	
2		107	4h	99%	95:5	8		107	36h	75%	97:3	
		R= <i>p</i> -F-C ₆ H ₄ , 110					9		100	17h	72%	90:10
3		100	24h	86%	99:1	10		107	2h	99%	96:4	
4		100	24h	95%	99:1			R= H, 116				
	111					11		100	24h	96%	94:6	
5		100 ^a	36h	89%	94:6	12		107	22h	98%	97:3	
	112							R= OMe, 117				
6		100 ^b	36h	99%	95:5	13		100 ^c	16h	64%	92:8	
	113					14		107 ^d	24h	90%	97:3	
								R= F, 118				
						15		100	24h	80%	94:6	
						16		107	22h	92%	98:2	

^a PhCl as solvent at 80 °C. ^b Boronic ester used. ^c Reaction run at 90 °C. ^d Reaction run at 70 °C

Lower enantiomeric excesses were observed for thiazole and benzothiazole products (Table 2.3.2). Presumably, this result can be accounted for by the epimerization of the products under the reaction conditions. A control experiment was conducted in which the thiazole product **119** was resubjected to the reaction conditions. The recovered product had a diminished enantiomeric excess. Therefore, a faster reaction time could help improve the optical purity of the products. In fact, catalyst **107**, to some extent, proved to

be efficient for such purpose. In most cases (entries 4-13), better yields and ee's were achieved when using **107** relative to **100** due to much shorter reaction times.

Table 2.3.2. Thiazole and benzothiazoles substrates



Entry	Product	catalyst	time	yield	er
1		100	24h	89%	88:12
2		107	15h	87%	84:16
3		107^a	4h	82%	84:16
4		100	20h	64%	82:18
5		107	2h	92%	84:16
		R= H, 121			
6		100	60h	53%	76:24
7		107	36h	69%	80:20
		R= OMe, 122			
8		100	42h	77%	89:11
9		107	7h	85%	92:8
		R= F, 123			
10		100	60h	47%	74:26
11		107	24h	84%	87:13
12		100	16h	88%	80:20
13		107	4h	91%	86:14

^a PhCl as solvent, reflux

High conversion was still observed in pyridine, quinoline, and pyrazine products (Table 2.3.3). Epimerization appeared to occur in 2- and 4-pyridyl products (entries 1 and

5). However, this did not occur with the 3-pyridyl adduct. These results reflect that the benzylic protons in 2- and 4-pyridyl products are more acidic than that in the 3-pyridyl product. The same trend was also present in the quinoline product (entry 7) but not in the pyrazine adduct (entry 9). Catalyst **107** again showed its value in improving the reaction outcome. Better optical purities and comparable yields of products were gained when using **107** (entries 2,3,6,8 and 10).

Table 2.3.3. Pyridine, Quinoline and Pyrazine substrates

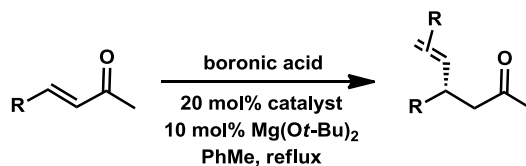


Entry	Product	catalyst	time	yield	er
1		100	3h	71%	86:14
2		107 ^a	16h	95%	94:6
3		107	75 min	92%	93:7
4		100	15h	87%	98:2
5		100	21h	92%	91:9
6		107	22h	91%	95:5
7		100	1h	85%	88:12
8		107 ^a	5h	94%	96:4
9		100	4h	95%	92:8
10		107 ^a	8h	99%	95:5

^a Reaction run at 70 °C

Unprotected pyrrole and imidazolyl enones were also tolerated under the reaction conditions (Table 2.3.4). In the case of pyrrole, the reaction of unprotected substrates (entries 1 and 2) afforded the product in only moderate yields due to the formation of a side product. This side product was not able to be characterized because of the difficulty in isolating it from the mixture with catalyst, which had a similar R_F . The by-product formation increased as the reaction temperature was elevated. Performing the reaction at 70 °C can both give a moderate yield of product and minimize the formation of the by-product. The *N*-methylpyrrole substrate, on the other hand, worked well without side product formation (entries 3 and 4). Unlike pyrrole, unprotected imidazole substrates afforded products in high yields (entries 5,6,7 and 8), though the *N*-methyl enone (entry 9) gave an even better yield. Again, in most cases, catalyst **107** afforded higher conversion, much faster reaction time, and even greater enantioselectivity (entries 2, 6, and 9).

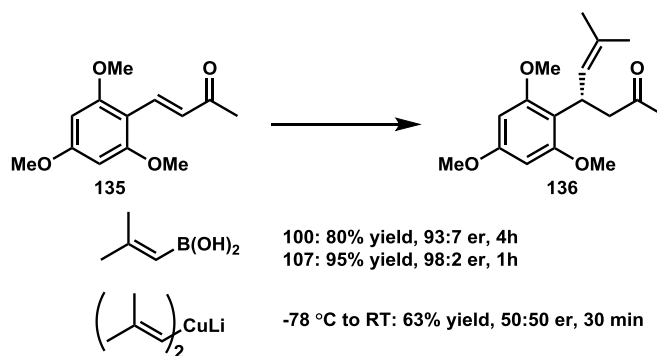
Table 2.3.4. Pyrrole and imidazole substrates



Entry	Product	catalyst	time	yield	er
R= H, 130					
1		100 ^a	48h	23%	92:8
2		107 ^a	24h	39%	96:4
R= Me, 131					
3		100	24h	63%	97:3
4		107	2h	90%	96:4
R= H, 133					
5		100	72h	83%	81:19
6		107	36h	88%	87:13
R= Me, 134					
7		100	32h	76%	83:17
8		107	15h	83%	91:9
9		100	12h	92%	96:4

^a Reaction run at 70 °C

Finally, a very electron rich substrate was tried (Scheme 2.3.1). This enone is predicted to have low reactivity toward nucleophilic attack due to its low electrophilicity and steric hindrance. However, it turned out to be the most reactive substrate under these organocatalytic conditions. Both catalyst **100** and **107** gave excellent yields and enantiomeric excesses in only 4 hours and 1 hour, respectively. This same substrate afforded the product in only 63% yield under cuprate conjugate addition conditions. This cuprate addition was also performed with unprotected pyrrole and imidazole substrates, and no product was obtained.



Scheme 2.3.1. Reactivity of electron rich substrate

2.4. Conclusion

The enantioselective conjugate addition of vinylboronic acids and alkenyl boronic esters to β -heteroaryl α,β -unsaturated carbonyl compounds has been investigated. The method allows for the formation of stereocenters adjacent to a variety of common heterocycles in moderate to good yields and high selectivity. A novel BINOL catalyst (**107**) was created to enhance the reaction rate as well as selectivity. Electron-rich substrates were shown to be very reactive under these reaction conditions. Further investigation in the reaction mechanism as well as development of more efficient catalysts is underway to achieve higher conversion and greater selectivity.

2.5. Experimental section

2.5.1. General consideration

All reactions were carried out in flame- or oven-dried glassware. THF, toluene and CH_2Cl_2 were purged with argon and dried over activated alumina columns. Flash chromatography was performed on 60Å silica gel (EMD Chemicals Inc). Preparative plate chromatography was performed on EMD silica gel plates, 60Å, with UV-254

indicator. Chemical names were generated using Cambridge soft ChemBioDraw Ultra 12.0. Analysis by HPLC was performed on a Shimadzu Prominence LC (LC-20AB) equipped with a SPD-20A UV-Vis detector and a Chiralpak or Chiralcel (250 mm x 4.6 mm) column (see below for column details). Analytical thin layer chromatography was performed on EMD silica gel/TLC plates with fluorescent detector 254 nm. The ^1H , ^{13}C and ^{19}F NMR spectra were recorded on a JEOL ECA- 500 or ECX-400P spectrometer using residual solvent peak as an internal standard (CDCl_3 : 7.25 ppm for ^1H NMR and 77.16 ppm for ^{13}C NMR). Hexafluorobenzene ($\delta = -164.9$ ppm) was employed as an external standard in ^{19}F NMR spectra. NMR yields were determined by addition of 0.5 equivalent of methyl (4-nitrophenyl) carboxylate as an internal standard to the crude reaction mixture. IR spectra were obtained using a ThermoNicolet Avatar 370 FT-IR instrument. HRMS analyses were performed under contract by UT Austin's mass spectrometric facility via ESI method and a US10252005 instrument.

2.5.2. HPLC columns for separation of enantiomers

Chiralpak AY-3: Amylose tris-(5-chloro-2-methylphenylcarbamate) coated on 3 μm silica gel.

Chiralpak AD-H: Amylose tris-(3,5-dimethylphenylcarbamate) coated on 5 μm silica gel.

Chiralpak ID: Amylose tris-(3-chlorophenylcarbamate) immobilized on 5 μm silica gel.

Chiralcel OJ-H: Cellulose tris-(4-methylbenzoate) coated on 5 μm silica gel.

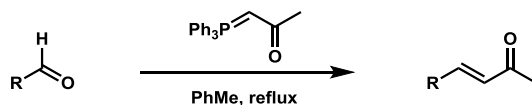
Chiralcel OD-H: Cellulose tris-(3,5-dimethylphenylcarbamate) coated on 5 μm silica gel.

Chiralpak AS-H: Amylose tris-[(S)- α -methylbenzylcarbamate) coated on 5 μ m silica gel.

2.5.3. Materials

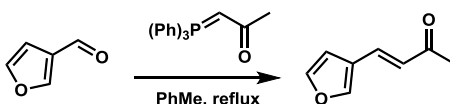
Commercially available compounds were purchased from Aldrich, Acros, and Alfa Aesar and were used without further purification.

2.5.4. General procedures for starting material synthesis



To a flask equipped with a stir bar and a condenser was added carboxaldehyde (4 mmol, 1.0 equiv), 1-(triphenylphosphoranylidene)-2-propanone (5 mmol, 1.25 equiv), and toluene (8 mL). The reaction mixture was refluxed overnight. After completion, the reaction mixture was concentrated via rotary evaporation. The crude mixture was purified via flash column chromatography with an appropriate eluent on silica gel.

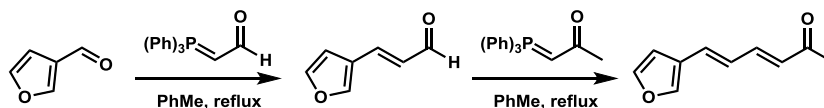
2.5.4.1. Synthesis of (*E*)-4-(furan-2-yl)-6-phenylhex-5-en-2-one, precursor to 111, 112, 113



See the general procedure for enone formation above. The crude reaction mixture was purified via flash column chromatography with a 10–20% gradient of ethyl acetate in hexanes as eluent on silica gel to afford a white solid (539.2 mg, 3.96 mmol, 99% yield). ¹H NMR (400 MHz, CDCl₃): δ 7.66 (s, 1H), 7.41 (s, 1H), 7.39 (d, *J* = 16.5 Hz, 1H), 6.57 (d, *J* = 1.8 Hz, 1H), 6.41 (d, *J* = 16.0 Hz, 1H), 2.30 (s, 3H). ¹³C NMR (125.77 MHz, CDCl₃): δ 198.3, 145.0, 144.6, 133.5, 127.3, 122.8, 107.5, 27.4 LR-MS-EI *m/z*: [M⁺],

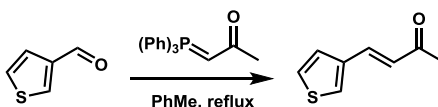
calculated for C₈H₈O₂ 136.1479, found 136. IR (neat): 3115, 2924, 2861, 1666, 1629, 1268, 1158, 974, 869 cm⁻¹.

2.5.4.2. Synthesis of (3*E*,5*E*)-6-(furan-3-yl)hexa-3,5-dien-2-one, precursor to 114



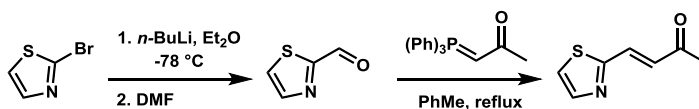
To a flask equipped with a stir bar and a condenser was added furan-3-carbaldehyde (4 mmol, 1.0 equiv), (triphenylphosphoranylidene)acetaldehyde (5 mmol, 1.25 equiv), and toluene (8 mL). The reaction mixture was refluxed overnight. After completion, 1-(triphenylphosphoranylidene)-2-propanone (5 mmol, 1.25 equiv) was added to reaction mixture which was refluxed for another 12 hours. The reaction mixture was then concentrated via rotary evaporation. The crude mixture was purified via flash column chromatography with 5-10% ethyl acetate in hexane on silica gel to obtain a yellowish solid (486.6 mg, 3 mmol, 75% yield). ¹H NMR (400 MHz, CDCl₃): δ 7.56 (s, 1H), 7.41 (s, 1H), 7.23 (dd, J= 16.0, 11.4 Hz, 1H), 6.83 (d, J= 15.6 Hz, 1H), 6.89 (m, 2H), 6.19 (d, J= 15.6 Hz, 1H), 2.29 (s, 3H). ¹³C NMR (100 MHz, CDCl₃): δ 198.6, 144.3, 143.5, 142.9, 131.1, 129.7, 126.6, 124.1, 107.4, 27.5. HR-MS-ESI m/z: [M+Na], calculated for C₁₀H₁₀NaO₂ 185.0573, found 185.0570 IR (neat): 3122, 1625, 1254, 1163, 1086, 990, 868, 788, 638 cm⁻¹.

2.5.4.3. Synthesis of (*E*)-4-(thiophen-2-yl)-but-3-en-2-one (102), precursor to 115, 116, 117, 118



See the general procedure for enone formation above. 897.2 mg of 2-thiophenecarboxaldehyde was used. The crude reaction mixture was purified via flash column chromatography with a 5- 10% gradient of ethyl acetate in hexanes as eluent on silica gel to afford a yellow oil (1.205 g, 7.92 mmol, 99% yield). ^1H NMR (500 MHz, CDCl_3): δ 7.6 (d, $J=15.7$ Hz, 1H), 7.37 (d, $J=4.5$ Hz, 1H), 7.2 (d, $J=3.4$ Hz, 1H), 7.03 (dd, $J= 4.5, 3.4$ Hz, 1H), 6.49 (d, $J = 15.7$ Hz, 1H), 2.30 (s, 3H). ^{13}C NMR (125.77 MHz, CDCl_3): δ 197.8, 139.8, 135.8, 131.6, 129.0, 128.3, 125.8, 27.8. IR (neat): 1663, 1613, 1594, 1254, 966, 710 cm^{-1} .

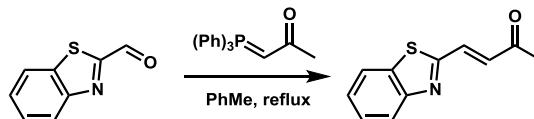
2.5.4.4. Synthesis of (*E*)-4-(thiazol-2-yl)-but-3-en-2-one, precursor to 119, 120



The compound was prepared following the procedure previously reported.² To a solution of 2-bromothiazole (545 mg, 3.3 mmol) in diethyl ether (4ml) at -78°C was added dropwise 1.6 ml of *n*-butyl lithium (2.5M solution in hexanes). The reaction mixture was stirred at -78°C for 45 minutes. Dimethylformamide was then added and the reaction mixture was allowed to stir in 30 minutes at -78°C . Saturated NaCl and pentane were added and aqueous layer was brought to pH 8 by adding 2M HCl. Product was extracted by ether. Combined organic layers was concentrated via rotary evaporation and purified via column chromatography using 10% diethyl ether in pentane as eluent. Thiazole-2-carboxaldehyde was obtained as a yellow liquid. The Wittig reaction was carried out on the aldehyde following the above general procedure with a 10-20% gradient of ethyl acetate in hexanes as eluent on silica gel yielding a light brown solid (187.5 mg, 1.22 mmol, 37% overall yield). ^1H NMR (400 MHz, CDCl_3): δ 7.91 (d, $J= 3.2$ Hz, 1H), 7.61

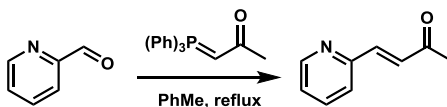
(d, $J=16.4$ Hz, 1H), 7.44 (d, $J= 3.2$ Hz, 1H), 6.91 (d, $J= 16.49$ Hz, 1H), 2.38 (s, 3H). ^{13}C NMR (100.52 MHz, CDCl_3): δ 197.7, 164.0, 144.9, 134.5, 130.8, 121.7, 27.9 IR (neat): 1663, 1256, 1224, 969, 752 cm^{-1} .

2.5.4.5. Synthesis of (*E*)-4-(benzo[d]thiazol-2-yl)-but-3-en-2-one, precursor to 121, 122, 123, 124



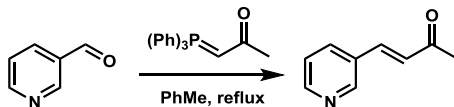
See the general procedure for enone formation above. 726 mg of 2-benzothiazolecarboxaldehyde was used. The crude reaction mixture was purified via flash column chromatography with a 10-20% gradient of ethyl acetate in hexanes as eluent on silica gel to afford a light brown solid (852.1 mg, 4.19 mmol, 94% yield). ^1H NMR (400 MHz, CDCl_3): δ 8.06 (d, $J= 8.2$ Hz, 1H), 7.89 (d, $J= 7.79$ Hz, 1H), 7.70 (dd, $J=16.0, 1.1$ Hz, 1H), 7.52 (m, 1H), 7.45 (m, 1H), 6.98 (dd, $J= 16.0, 1.1$ Hz), 2.43 (s, 3H). ^{13}C NMR (100.52 MHz, CDCl_3): δ 197.5, 164, 153.9, 135.4, 135.3, 133.6, 126.9, 126.7, 124.0, 121.9, 27.8. IR (neat): 1666, 1254, 958, 762, 731 cm^{-1} .

2.5.4.6. Synthesis of (*E*)-4-(pyridin-2-yl)but-3-en-2-one, precursor to 125



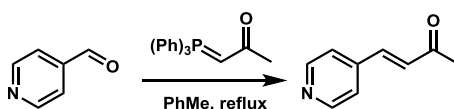
See the general procedure for enone formation above. The crude reaction mixture was purified via flash column chromatography with a 20-40% gradient of ethyl acetate in hexanes as eluent on silica gel to afford light yellow oil (582.8 mg, 3.96 mmol, 99% yield). The spectroscopic data for the compound was identical to that reported in the chemical literature.³

2.5.4.7. Synthesis of (*E*)-4-(pyridin-3-yl)but-3-en-2-one, precursor to 126



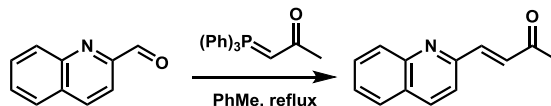
See the general procedure for enone formation above. The crude reaction mixture was purified via flash column chromatography with a 10-20% gradient of ethyl acetate in dichloromethane as eluent on silica gel to afford light yellow oil (541.6 mg, 3.68 mmol, 92% yield). The spectroscopic data for the compound was identical to that reported in the chemical literature.³

2.5.4.8. Synthesis of (*E*)-4-(pyridin-4-yl)but-3-en-2-one, precursor to 127



See the general procedure for enone formation above. The crude reaction mixture was purified via flash column chromatography with a 10–20% gradient of ethyl acetate in chloroform as eluent on silica gel to afford a red brown solid (559.2 mg, 3.8 mmol, 95% yield). The spectroscopic data for the compounds was identical to that reported in the chemical literature.³

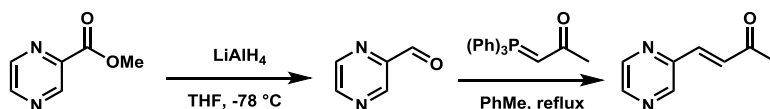
2.5.4.9. Synthesis of (*E*)-4-(quinolin-2-yl)but-3-en-2-one, precursor to 128



See the general procedure for enone formation above. The crude reaction mixture was purified via flash column chromatography with a 10-20% gradient of ethyl acetate in hexanes as eluent on silica gel to afford a brown solid (631.2 mg, 3.2 mmol, 80% yield). ¹H NMR (500 MHz, CDCl₃): δ 8.20 (d, J= 8.6 Hz, 1H), 8.11 (d, J=8.6 Hz, 1H), 7.83 (d,

$J = 8.0$ Hz, 1H), 7.75 (m, 2H), 7.68 (d, $J = 8.6$ Hz, 1H), 7.59 (t, $J = 6.9$ Hz, 1H), 7.15 (d, $J = 16.6$ Hz, 1H), 2.43 (s, 3H). ^{13}C NMR (125.77 MHz, CDCl_3): δ 198.9, 148.2, 143.1, 137.0, 132.0, 130.3, 129.8, 128.2, 127.7, 127.6, 120.1, 27.7. LR-MS-EI m/z : $[\text{M}^+]$, calculated for $\text{C}_{13}\text{H}_{11}\text{NO}_2$ 197.2325, found 197. IR (neat): 1658, 1362, 1348, 1271, 1252, 985, 819, 760, 656 cm^{-1} .

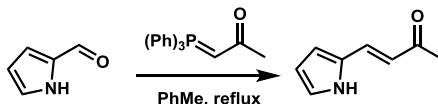
2.5.4.10. Synthesis of (*E*)-4-(pyrazin-2-yl)but-3-en-2-one, precursor to 129



To a flame-dried 100 ml round bottom flask was added methyl pyrazine-2-carboxylate (1.38 g, 10 mmol) and 20 ml THF. The mixture was then cooled to $-78\text{ }^\circ\text{C}$ followed by adding lithium aluminium hydride (189.8 mg, 5 mmol) in THF (5 ml). The reaction was stirred for another 20 minutes and quenched with acetic acid glacial (2 ml) at $-78\text{ }^\circ\text{C}$. When the reaction was warmed up to room temperature, HCl 3N (3 ml) was added and organic layer was separated. The aqueous layer was then extracted with dichloromethane (3 times). The organic layers was combined and concentrated via rotary evaporation. The resulting mixture was purified via flash column chromatography with a 20-30% gradient of ethyl acetate in hexanes as eluent on silica gel to afford crude light yellow oil (235.0 mg, 22% yield). The carboxaldehyde was confirmed by 2,4-dinitrophenylhydrazine stain and was carried into the next reaction. The Wittig reaction was carried out following the general enone formation procedure above and was purified via flash column chromatography with a 10-40% gradient of ethyl acetate in hexanes as eluent on silica gel to afford a light yellow solid (222.2 mg, 1.5 mmol, 15% overall yield after 2 steps). ^1H NMR (500 MHz, CDCl_3) δ 8.70 (s, 1H), 8.60 (s, 1H), 8.54 (s, 1H), 7.52

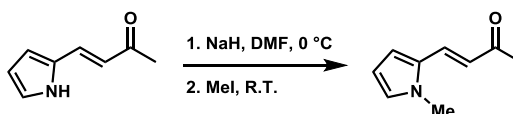
(d, $J=16.0$ Hz, 1H), 7.25 (d, $J=16.0$ Hz, 1H), 2.41 (s, 3H). ^{13}C NMR (125.77 MHz, CDCl_3) δ 197.9, 148.9, 145.4, 145.3, 145.0, 137.8, 132.0, 28.5 LR-MS-EI m/z : $[\text{M}^+]$, calculated for $\text{C}_8\text{H}_8\text{N}_2\text{O}$ 148.1619, found 148. IR (neat): 1670, 1475, 1262, 1015, 984, 883, 640 cm^{-1} .

2.5.4.11. Synthesis of (*E*)-4-(1*H*-pyrrol-2-yl)-but-3-en-2-one, precursor to 130



See the general procedure for enone formation above. 1g of 2-pyrrolecarboxaldehyde was used. The crude reaction mixture was purified via flash column chromatography with a 10-40% gradient of ethyl acetate in hexanes as eluent on silica gel to afford a light yellow solid (1.3092 g, 7.69 mmol, 73% yield). ^1H NMR (400 MHz, CDCl_3): δ 9.27(bs, 1H), 7.42 (d, $J=16.0$ Hz, 1H), 7.00 (m, 1H), 6.60 (m, 1H), 6.39 (d, $J=16.0$ Hz, 1H), 6.30 (m, 1H), 2.33 (s, 3H). ^{13}C NMR (100 MHz, CDCl_3) δ 198.7, 133.8, 128.4, 123.6, 120.8, 115.8, 111.3, 26.9 IR (neat): 3300, 1629, 1617, 1265, 1008, 961, 737 cm^{-1} .

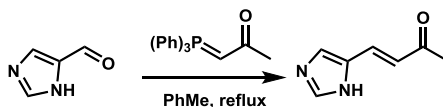
2.5.4.12. Synthesis of (*E*)-4-(1*H*-pyrrol-2-yl)-but-3-en-2-one, precursor to 131



To a flame-dried 25ml round bottom flask was added (*E*)-4-(1*H*-pyrrol-2-yl)-but-3-en-2-one (500mg, 3.7 mmol), NaH (177.6 mg, 4.4 mmol) and 7ml anhydrous DMF. The mixture was then cooled to $0\text{ }^\circ\text{C}$ and stirred in 20 minutes. After 20 minutes, methyl iodide was added and the reaction was allowed to warm up to room temperature. After completion, reaction was quenched with water and extracted with dichloromethane (3 times). Organic layers were combined and washed with water and brine and dried over

magnesium sulfate. The crude mixture was concentrated via rotary evaporation and purified via flash column chromatography using 10-20% gradient of ethyl acetate in hexanes as eluent. The product was obtained as a yellow liquid (353mg, 2.37 mmol, 64% yield). ¹H NMR (400 MHz, CDCl₃): δ 7.45 (d, J=15.57 Hz, 1H), 6.78 (m, 1H), 6.70 (m, 1H), 6.49 (d, J=15.57 Hz, 1H), 6.18 (m, 1H), 3.71 (s, 3H), 2.3 (s, 3H). ¹³C NMR (100.52 MHz, CDCl₃): δ 197.8, 130.7, 129.3, 127.8, 121.6, 112.6, 109.7, 34.5, 28.3. IR (neat): 1613, 1589, 1480, 1415, 1271, 1251, 1059, 967, 730 cm⁻¹.

2.5.4.13. Synthesis of (*E*)-4-(1*H*-imidazol-5-yl)but-3-en-2-one, precursor to 132



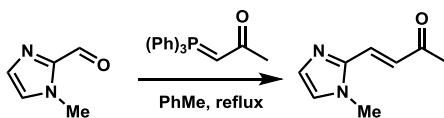
See the general procedure for enone formation above. The crude reaction mixture was purified via flash column chromatography with a 2-5% gradient of methanol in dichloromethane as eluent on silica gel to afford a yellowish solid (381.2 mg, 2.8 mmol, 70% yield). ¹H NMR (500 MHz, CDCl₃): δ 7.72 (s, 1H), 7.47 (d, J= 16.0 Hz, 1H), 7.33 (s, 1H), 2.33 (s, 3H). ¹³C NMR (125.77 MHz, CDCl₃): δ 199.0, 137.4, 134.6 (broad peak), 124.8, 119.1 (broad peak), 27.8. LR-MS-EI m/z: [M⁺], calculated for C₇H₈N₂O 136.1512, found 136. IR (neat): 3140, 1609, 1362, 1270, 1159, 1099, 977, 621 cm⁻¹

2.5.4.14. Synthesis of (*E*)-4-(1*H*-imidazol-2-yl)but-3-en-2-one, precursor to 133

(*E*)-4-(1*H*-imidazol-2-yl)but-3-en-2-one was synthesized following the literature procedure.⁴

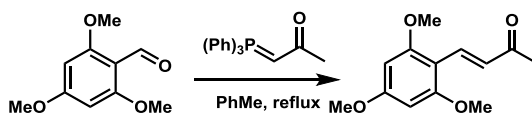
2.5.4.15. Synthesis of (*E*)-4-(1-methyl-1*H*-imidazol-5-yl)but-3-en-2-one, precursor to

134



See the general procedure for enone formation above. The crude reaction mixture was purified via flash column chromatography with a 40-100% gradient of ethyl acetate in hexanes as eluent on silica gel to get a yellowish solid (533.7 mg, 3.98 mmol, 98% yield). ¹H NMR (500 MHz, CDCl₃) δ 7.37 (d, J= 15.5 Hz, 1H), 7.16 (s, 1H), 7.15 (d, J= 15.5 Hz, 1H), 6.99 (s, 1H), 3.75 (s, 3H), 2.34 (s, 3H). ¹³C NMR (125.77 MHz, CDCl₃): δ 197.7, 143.3, 130.6, 127.5, 126.1, 124.1, 33.2, 29.6 LR-MS-EI m/z: [M⁺], calculated for C₈H₁₀N₂O 150.1778, found 150. IR (neat): 3137, 1650, 1632, 1481, 1429, 1263, 980, 789 cm⁻¹.

2.5.4.16. Synthesis of (*E*)-4-(2,4,6-trimethoxyphenyl)-but-3-en-2-one (135), precursor to 136

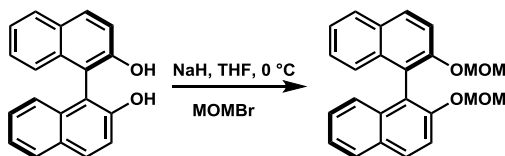


See the general procedure for reaction above. 588.6 mg of 2,4,6-trimethoxybenzaldehyde was used. The crude reaction mixture was purified via flash column chromatography with a 10-40% gradient of ethyl acetate in hexanes as eluent on silica gel to afford a white solid (599 mg, 2.54 mmol, 84% yield). ¹H NMR (400 MHz, CDCl₃): δ 7.93 (d, J= 16.7, 1H), 7.05 (d, J= 16.7 Hz, 1H), 6.10 (s, 2H), 3.86 (s, 6H), 3.86 (s, 3H), 2.33 (s, 3H). ¹³C NMR (100.52 MHz, CDCl₃): δ 200.7, 163.1, 161.4, 135.1,

127.7, 105.7, 90.5, 55.8, 55.4, 27.0 IR (neat): 1595, 1565, 1334, 1264, 1249, 1231, 1154, 1111, 830 cm^{-1} .

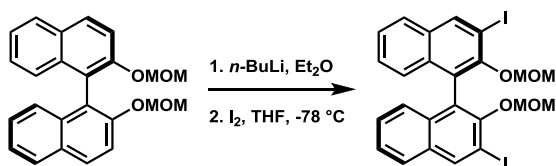
2.5.5. Procedures for catalyst synthesis

2.5.5.1. Synthesis of (*R*)-2,2'-bis(methoxymethoxy)-1,1'-binaphthyl



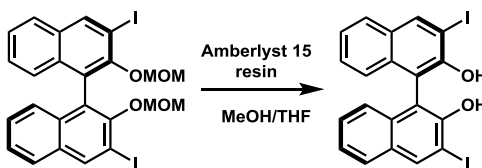
The title compound was prepared via modification of the literature procedure.⁵ To a flame-dried flask fitted with a stir-bar and addition funnel was added NaH (60% dispersion in mineral oil, 840 mg, 21 mmol, 3 equiv) and THF (30 mL). The reaction was cooled to 0 °C. R-(+)-BINOL (2.00 g, 7 mmol, 1.0 equiv) was then added as one portion. The reaction mixture was stirred at 0 °C for 1 h. MOM-Br (1.3 mL, 15.4 mmol, 2.2 equiv) was then added dropwise. The reaction was allowed to stir at 0 °C for 10 min. After completion, the reaction mixture was quenched with saturated aq. NH_4Cl , extracted with Et_2O , and washed with brine. The organic layer was dried with MgSO_4 and the solvent was removed via rotary evaporation. The crude product mixture was purified via column chromatography with a 10–20% gradient of ethyl acetate in hexanes as eluent on silica gel. (2.5162 g, 6.72 mmol, 96% yield).

2.5.5.2. Synthesis of (*R*)-3,3'-diiodo-2,2'-bis(methoxymethoxy)-1,1'-binaphthyl



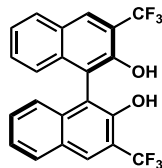
The title compound was prepared as previously described in the literature.⁵ To a flame-dried flask equipped with a stir bar was added (*R*)-2,2'-bis(methoxymethoxy)-1,1'-binaphthyl obtained above (700 mg, 1.87 mmol 1.0 equiv), and then Et₂O (35 mL). 2.5 M *n*-BuLi (2.3 mL, 5.61 mmol, 3.0 equiv) was added to the reaction. The reaction mixture was allowed to stir for 4 hours at room temperature. The reaction mixture was then cooled to -78 °C and I₂ (1.424 g, 5.61 mmol, 3.0 equiv) was added as one portion. The reaction was allowed to slowly warm to R.T. and stir overnight. After completion, the reaction mixture was quenched with saturated aq. NH₄Cl, extracted with Et₂O, and washed with 10% aq. Na₂S₂O₃ followed by brine solution. The organic layer was dried with MgSO₄ and the solvent was removed via rotary evaporation. The crude product mixture was then purified via column chromatography with 5% ethyl acetate in hexanes as eluent on silica gel. (909.5 mg, 1.45 mmol, 78% yield).

2.5.5.3. Synthesis of (*R*)-3,3'-diiodo-1,1'-binaphthyl-2,2'-diol (**105**)



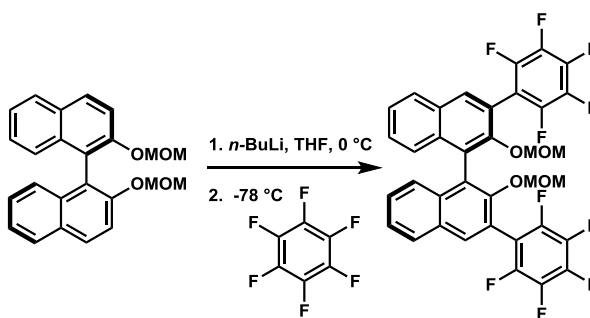
Compound **105** was prepared as previously described in the literature.⁵ To (*R*)-3,3'-diiodo-2,2'-bis(methoxymethoxy)-1,1'-binaphthyl (300 mg, 0.479 mmol) was added MeOH (2 mL) and THF (2 mL). Amberlyst 15 resin (600 mg) was then added, and reaction was allowed to reflux at 65 °C overnight. After completion, the resin was filtered off and the organic layer concentrated to reduce solvent amount. The organic layer was then passed through a silica plug with 5% ethyl acetate in hexanes as eluent to afford the hydrolyzed product. (214.8 mg, 0.399 mmol, 83% yield).

2.5.5.4. (*R*)-3,3'-bis(trifluoromethyl)-[1,1'-binaphthalene]-2,2'-diol (106)



106 was prepared as previously reported.⁶

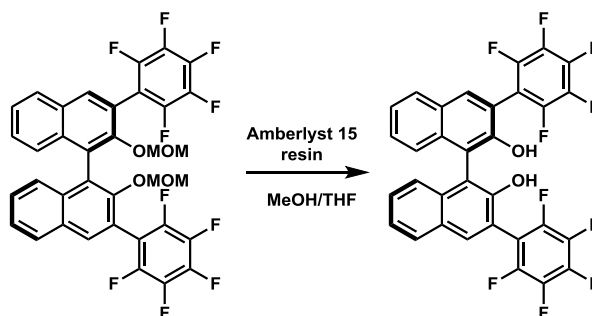
2.5.5.5. Synthesis of (*R*)-2,2'-bis(methoxymethoxy)-3,3'-bis(perfluorophenyl)-1,1'-binaphthyl



The title compound was prepared following the procedure previously described in the literature.⁶ To a flame-dried flask equipped with a magnetic stirbar was added (*R*)-2,2'-bis(methoxymethoxy)-1,1'-binaphthyl (1g, 2.67 mmol, 1 equiv) and 16ml THF. The reaction mixture was then cooled down to 0 °C followed by the addition of 2.5M *n*-BuLi (3.2 ml, 8 mmol, 3 equiv) and allowed to stir in 30 minutes. The reaction temperature was decreased to -78 °C and hexafluorobenzene (2.2 ml, 18.7 mmol, 7 equiv) was added dropwise via syringe. The reaction mixture was then warmed up to R.T. and stirred at this temperature for 12h. After completion, the reaction was quenched with saturated aq. NH₄Cl, extracted with Et₂O, and wash with brine. After the removal of solvents via rotary evaporation, the reaction mixture was purified by column chromatography on silica gel using 5% ethyl acetate in hexanes as eluent. The product was obtained as a

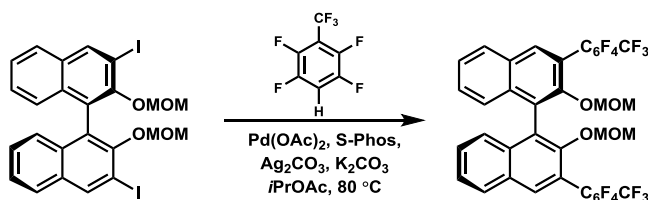
white solid (1.341 g, 1.9 mmol, 71% yield) and the spectral data agreed with the reported data.⁶

2.5.5.6. Synthesis of (*R*)-3,3'-bis(perfluorophenyl)-1,1'-binaphthyl-2,2'-diol (**100**)



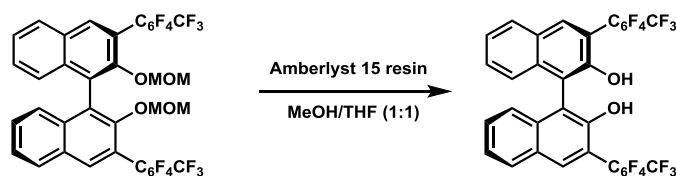
Compound **100** was prepared following the procedure described for the preparation of compound **105** above. 649.5 mg of SI-26 was used. The product was obtained as a white solid (553.4 mg, 0.77 mmol, 96% yield) after column chromatography using 5% ethyl acetate in hexanes as eluent. ¹H NMR (400 MHz, CDCl₃): δ 8.07 (s, 2H), 7.97 (d, J= 7.3 Hz, 2H), 7.48 (m, 4H), 7.26 (d, J= 8.2 Hz, 2H), 5.29 (s, 2H). ¹³C NMR (100 MHz, CDCl₃): δ 150.0, 134.0, 133.8, 129.4, 129.1, 128.9, 125.4, 124.0, 115.5, 111.4. ¹⁹F NMR (470.6 MHz, CDCl₃) δ -58.48 (t, J= 21.8 Hz, 6F), -140.0 (dd, J= 23.1, 12.2 Hz, 2F), -140.3 (dd, J= 21.8, 12.2 Hz, 2F), -143.06- -143.33 (m, 4F). HR-MS-ESI m/z: [M+Na], calculated for C₃₄H₁₂F₁₄NaO₂ 741.0506, found 741.0506.

2.5.5.7. Synthesis of (*R*)-2,2'-bis(methoxymethoxy)-3,3'-bis(2,3,5,6-tetrafluoro-4-(trifluoromethyl)phenyl)-1,1'-binaphthyl



The title compound was prepared following the procedure previously described in the literature.⁷ To a flame-dried sealable flask equipped with a magnetic stirbar was added K₂CO₃ (737.7 mg, 5.33 mmol, 4.0 equiv), Ag₂CO₃ (367.7 mg, 1.33 mmol, 1.0 equiv), S-Phos (109.5 mg, 0.27 mmol, 0.2 equiv), and Pd(OAc)₂ (30 mg, 0.13 mmol, 0.1 equiv). To this mixture 2,3,5,6-tetrafluorobenzotrifluoride (0.73 mL, 5.33 mmol, 4.0 equiv) and *i*-PrOAc (1.5 mL) were added. The reaction mixture was allowed to stir for 2 min at R.T. before the addition of 3,3'-diiodo-2,2'-bis(methoxymethoxy)-1,1'-binaphthyl (835.6 mg, 1.33 mmol, 1.0 equiv). The reaction temperature was increased to 80 °C and stirred at this temperature for 12h. The reaction mixture was then cooled to R.T. and passed through a plug of Celite washing with EtOAc. After the removal of solvents via rotary evaporation, the reaction mixture was purified by column chromatography on silica gel using 5% ethyl acetate in hexanes as eluent. The product was obtained as a white solid (649.5 mg, 0.805 mmol, 60% yield). ¹H NMR (400 MHz, CDCl₃): δ 7.98 (s, 2H), 7.94 (d, J= 7.8 Hz, 2H), 7.52 (dt, J= 6.8, 1.3 Hz, 2H), 7.42 (dt, J= 6.8, 1.3 Hz, 2H), 7.32 (d, J= 8.7, 2H), 4.48 (d, J= 5.9 Hz, 2H), 4.42 (d, J= 6.4 Hz, 2H), 2.62 (s, 6H). ¹³C NMR (100 MHz, CDCl₃): δ 151.7, 134.7, 132.3, 130.3, 128.5, 128.3, 126.2, 125.8, 120.6, 99.5, 56.2.

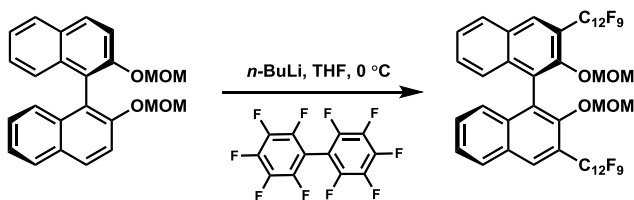
2.5.5.8. Synthesis of (*R*)-3,3'-bis(2,3,5,6-tetrafluoro-4-(trifluoromethyl)phenyl)-1,1'-binaphthyl-2,2'-diol (107**)**



Compound **107** was prepared following the procedure described for the preparation of compound **105** above. 649.5 mg of (*R*)-2,2'-bis(methoxymethoxy)-3,3'-bis(2,3,5,6-

tetrafluoro-4-(trifluoromethyl)phenyl)-1,1'-binaphthyl was used. The product was obtained as a white solid (553.4 mg, 0.77 mmol, 96% yield) after column chromatography using 5% ethyl acetate in hexanes as eluent. ^1H NMR (400 MHz, CDCl_3) δ 8.07 (s, 2H), 7.97 (d, J = 7.3 Hz, 2H), 7.48 (m, 4H), 7.26 (d, J = 8.2 Hz, 2H), 5.29 (s, 2H). ^{13}C NMR (100 MHz, CDCl_3) δ 150.0, 134.0, 133.8, 129.4, 129.1, 128.9, 125.4, 124.0, 115.5, 111.4. ^{19}F NMR (470.6 MHz, CDCl_3): δ -58.48 (t, J = 21.8 Hz, 6F), -140.0 (dd, J = 23.1, 12.2 Hz, 2F), -140.3 (dd, J = 21.8, 12.2 Hz, 2F), -143.06- -143.33 (m, 4F). HR-MS-ESI m/z : $[\text{M}+\text{Na}]$, calculated for $\text{C}_{34}\text{H}_{12}\text{F}_{14}\text{NaO}_2$ 741.0506, found 741.0506.

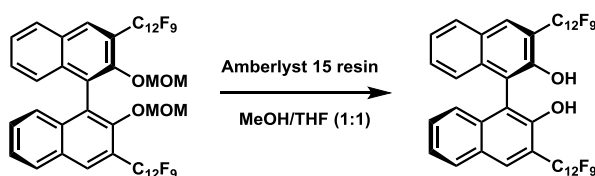
2.5.5.9. Synthesis of (*R*)-bis(methoxymethoxy)-3,3'-bis(perfluorobiphenyl-4-yl)-1,1'-binaphthyl



To a flame-dried flask equipped with a magnetic stirbar was added (*R*)-2,2'-bis(methoxymethoxy)-1,1'-binaphthyl (500 mg, 1.33 mmol, 1 equiv) and 8 ml THF. The reaction mixture was then cooled down to 0 °C followed by the addition of 2.5M *n*-BuLi (2.7 ml, 6.7 mmol, 5 equiv) and allowed to stir in 30 minutes. The reaction temperature was decreased to -78 °C and decafluorobiphenyl (3.122 g, 9.34 mmol, 7 equiv) was added. The reaction mixture was then warmed up to R.T. and stirred at this temperature for 12h. After completion, the reaction was quenched with saturated aq. NH_4Cl , extracted with Et_2O , and washed with brine. After the removal of solvents via rotary evaporation, the reaction mixture was purified by column chromatography on silica gel using 5% ethyl acetate in hexanes as eluent. The product was obtained as a white solid (868 mg, 0.86

mmol, 65% yield). ^1H NMR (400 MHz, CDCl_3): δ 8.07 (s, 2H), 7.96 (d, J = 8.2 Hz, 2H), 7.52 (app.t., J = 7.5 Hz, 2H), 7.42 (app.t., J = 7.5 Hz, 2H), 7.35 (d, J = 8.7, 2H), 4.56 (d, J = 5.04 Hz, 2H), 4.48 (d, J = 5.95 Hz, 2H), 2.68 (s, 6H). ^{13}C NMR (100 MHz, CDCl_3): δ 152.1, 145.8, 143.4, 134.6, 132.4, 130.4, 128.4, 128.1, 126.2, 126.1, 125.9, 121.4, 99.7, 56.1.

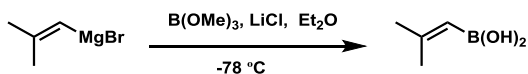
2.5.5.10. Synthesis of (*R*)-3,3'-bis(perfluoro-[1,1'-biphenyl]-4-yl)-1,1'-binaphthalene-2,2'-diol (**108**)



Compound **108** was prepared following the procedure described for the preparation of compound **105** above. 868 mg of (*R*)-bis(methoxymethoxy)-3,3'-bis(perfluorobiphenyl-4-yl)-1,1'-binaphthyl was used. The product was obtained as a white solid (361.7 mg, 0.395 mmol, 46% yield) after column chromatography using 5% ethyl acetate in hexanes as eluent. ^1H NMR (500 MHz, CDCl_3): δ 8.13 (s, 2H), 7.98 (app.d., J = 7.4 Hz, 2H), 7.48 (m, 4H), 7.30 (app.d., J = 7.4 Hz, 2H), 5.33 (s, 2H). ^{13}C NMR (100 MHz, CDCl_3) δ 150.3, 134.1, 133.8, 129.2, 129.1, 129.0, 125.2, 124.1, 116.2, 111.4. F NMR (376 MHz, CDCl_3) δ -139.2 (d, J = 21.6 Hz, 2F), -139.6 (d, J = 22.5 Hz, 2F), -141.0- -141.4 (m, 8F), -152.6 (t, J = 20.8 Hz, 2F), -162.7- -162.9 (m, 4F). HR-MS-ESI m/z : $[\text{M}+\text{Na}]$, calculated for $\text{C}_{44}\text{H}_{12}\text{F}_{18}\text{NaO}_2$ 937.0442, found 937.0426.

2.5.6. Procedures for boronic acid/ester synthesis

2.5.6.1. Synthesis of 2-methylprop-1-enylboronic acid



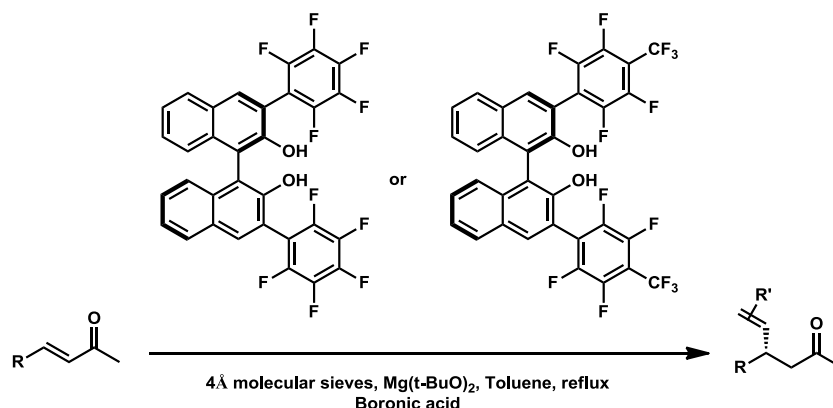
To a 250 ml-flask was added LiCl (1.008 g, 24 mmol, 1.2 equiv) and the flask was flamed-dried under high vacuum. The flask was then back-filled with Argon. 0.5 M 2-Methyl-1-propenyl magnesium bromide in THF (40 mL, 20 mmol, 1.0 equiv) and Et₂O (50ml) were added. The solution was cooled to -78 °C. Trimethyl borate (2.5 mL, 22 mmol, 1.1 equiv) was added dropwise and the reaction was allowed to slowly warm to room temperature and stir overnight. The next day it was quenched with 1 M HCl (30 ml) until the reaction mixture became clear and then stirred for 1 hour. It was then extracted with Et₂O (3 times), and washed with sat. aqueous NaHCO₃ and Brine solution. The organic layer was dried with Na₂SO₄ and then concentrated via rotary evaporation. The crude solid was purified via column chromatography with a 20-30% gradient of ethyl acetate in hexanes as eluent on silica gel to afford a white solid (1.105 g, 11.06 mmol, 55% yield). All spectral properties were identical to those reported in the literature.⁸

2.5.6.2. Diisopropyl hex-1-ynylboronate



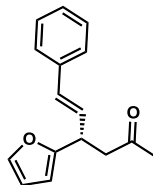
The title compound was prepared as previously reported.⁹

2.5.7. General procedure for conjugate addition



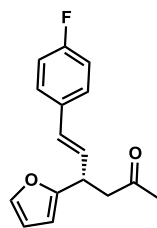
To a flask equipped with a stir bar and a condenser was added 4Å powdered molecular sieves (100mg) and the flask was flamed-dried under high vacuum. The flask was then back-filled with Argon. The heterocycle-appended enone (0.2 mmol, 1.0 equiv), $\text{Mg}(t\text{-BuO})_2$ (3.4 mg, 0.02 mmol, 0.1 equiv), boronic acid (1.2 to 3 equiv), and BINOL catalyst (0.04 mmol, 0.2 equiv) were then added. Freshly dried toluene (4 mL) was added and the reaction was heated to reflux in a 111⁰C oil bath and allowed to stir at this temperature (see each product for specific reaction times). After completion, methanol was added and the reaction mixture was concentrated via rotary evaporation. The crude reaction mixture was then dry-loaded onto silica gel and purified via flash column chromatography on silica gel with appropriate eluents. (See each product for specific eluent)

2.5.7.1. Synthesis of (*E*)-4-(furan-2-yl)-6-phenylhex-5-en-2-one (109)



See the general procedure for 1,4-conjugate addition reaction above. The crude reaction mixture was purified via flash column chromatography with a 30–60% gradient of dichloromethane in hexanes as eluent on silica gel. HPLC Chiralcel OD-H (hexane/*i*-PrOH = 90:10 – 70:30, 0.75 mL/min, UV-254 detector). Trial 1: 47 mg, 0.195 mmol, 97% yield; 97:3 er (with catalyst **100**, 1.3 eq of boronic acid). Trial 2: 44.2 mg, 0.184 mmol, 92% yield; 95:5 er (with catalyst **100**, 1.3 eq of boronic acid). Trial 3: 47.6 mg, 0.198 mmol, 99% yield; 95:5 er (with catalyst **107**, 1.3 eq of boronic acid). Trial 4: 47.5 mg, 0.197 mmol, 98.8% yield, 96:4 (with catalyst **107**, 1.3 eq of boronic acid). ¹H NMR (400 MHz, CDCl₃) δ 7.33-7.36 (m, 3H), 7.26-7.31 (m, 2H), 7.21 (tt, *J* = 7.3, 1.4 Hz, 1H), 6.45 (d, *J* = 15.6 Hz, 1H), 6.31 (app.dd, *J* = 1.8, 3.2 Hz, 1H), 6.25 (dd, *J* = 16.0, 7.8 Hz, 1H), 6.05 (d, *J* = 3.2 Hz, 1H), 4.17 (dd, *J* = 7.8, 14.6 Hz, 1H), 3.02 (dd, *J* = 6.4, 16.5 Hz, 1H), 2.85 (dd, *J* = 16.5, 7.3 Hz, 1H), 2.15 (s, 1H). ¹³C NMR (100 MHz, CDCl₃) δ 206.4, 155.8, 141.6, 136.9, 131.4, 129.2, 128.6, 127.6, 126.4, 110.3, 105.5, 47.3, 37.8, 30.6. HR-MS-ESI *m/z*: [M+Na], calculated for C₁₆H₁₆NaO₂ 263.1042, found 263.1041. IR (neat): 3031, 2930, 1712, 1360, 967, 749, 696 cm⁻¹

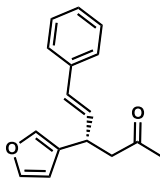
2.5.7.2. Synthesis of (*E*)-6-(4-fluorophenyl)-4-(furan-2-yl)hex-5-en-2-one (**110**)



See the general procedure for 1,4-conjugate addition reaction above. The crude reaction mixture was purified via flash column chromatography with a 30–60% gradient of dichloromethane in hexanes as eluent on silica gel. HPLC Chiralcel OD-H (hexane/*i*-

PrOH = 90:10 – 70:30, 0.75 mL/min, UV-254 detector). Trial 1: 44.9 mg, 0.174 mmol, 87% yield; 99.3:0.7 er (with cat. **100**, 1.3 eq of boronic acid). Trial 2: 43.1 mg, 0.167 mmol, 84% yield; 99.9:0.1 er (with cat. **100**, 1.3 eq of boronic acid). ¹H NMR (400 MHz, CDCl₃) δ 7.26-7.34 (m, 3H), 6.94-6.99 (dapp.t, J = 8.7 Hz, 2H), 6.39 (d, J = 16.0 Hz, 1H), 6.3 (dd, J = 3.2, 2.3 Hz, 1H), 6.14 (dd, J = 15.6, 7.8 Hz, 1H), 6.06 (d, J = 3.2 Hz, 1H), 4.15 (dd, J = 7.3, 14.2 Hz, 1H), 3.00 (dd, J = 16.5, 6.9 Hz, 1H), 2.84 (dd, J = 16.9, 7.3, 1H), 2.14 (s, 3H). ¹³C NMR (100 MHz, CDCl₃) δ 206.3, 163.2, 161.0, 155.7, 144.6, 133.4, 130.2, 129.0, 127.9, 115.5, 110.3, 105.5, 47.2, 37.7, 30.6. HR-MS-ESI m/z: [M+Na], calculated for C₁₆H₁₅FNaO₂ 281.0948, found 281.0948. IR (neat): 2930, 1712, 1600, 1509, 1226, 970, 832, 603 cm⁻¹

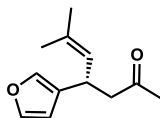
2.5.7.3. Synthesis of (*E*)-4-(furan-3-yl)-6-phenylhex-5-en-2-one (**111**)



See the general procedure for 1,4-conjugate addition reaction above. The crude reaction mixture was purified via flash column chromatography with a 30–60% gradient of dichloromethane in hexanes as eluent on silica gel. HPLC Chiralcel OD-H (hexane/*i*-PrOH = 90:10 – 70:30, 0.75 mL/min, UV-254 detector). Trial 1: 44.2 mg, 0.184 mmol, 92% yield; 99:1 er (with cat. **100**, 1.3 eq of boronic acid). Trial 2: 90.1 mg, 0.375 mmol, 94% yield; 98:2 er (with cat. **100**, 0.4 mmol enone, 1.3 eq of boronic acid). Trial 3: 47.7 mg, 0.198 mmol, 98% yield; 98:2 er (with cat. **100**, 1.3 eq of boronic acid). ¹H NMR (400 MHz, CDCl₃) δ 7.30 (m, 7H), 6.41 (d, J=16.0Hz, 1H), 6.31 (s, 1H), 6.25 (dd, J = 16.0, 7.8, 1H), 4.05 (q, J = 14.2, 7.3, 1H), 2.84 (d, J=7.3, 2H), 2.14 (s, 3H). ¹³C NMR

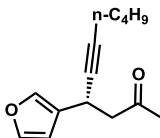
(100 MHz, CDCl₃) δ 206.9, 143.3, 138.9, 137.0, 131.5, 130.4, 128.6, 127.5, 126.3, 110.0, 49.1, 34.9, 30.8. HR-MS-ESI m/z: [M+Na], calculated for C₁₆H₁₆NaO₂ 263.1042, found 263.1041. IR (neat): 3034, 2937, 1712, 1362, 1161, 969, 753, 697 cm⁻¹.

2.5.7.4. Synthesis of 4-(furan-3-yl)-6-methylhept-5-en-2-one (112)



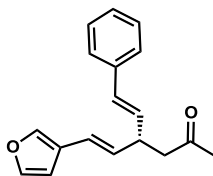
See the general procedure for 1,4-conjugate addition reaction above, chlorobenzene was used as solvent at 80°C. The crude reaction mixture was purified via flash column chromatography with a 30–60% gradient of dichloromethane in hexanes as eluent on silica gel. HPLC Chiralcel OD-H (hexane/*i*-PrOH = 90:10 – 70:30, 0.75 mL/min, UV-230 detector). Trial 1: 34.3 mg, 0.179 mmol, 89% yield; 93.9:6.1er (with cat. **107**, 1.3 eq of boronic acid). Trial 2: 34.4 mg, 0.179 mmol, 89% yield; 94:6 er (with cat. **107**, 1.3 eq of boronic acid). ¹H NMR (500 MHz, CDCl₃) δ 7.32 (t, *J* = 1.6 Hz, 1H), 7.17 (s, 1H), 6.24 (s, 1H), 5.11 (td, *J* = 9.7, 1.2 Hz, 1H), 3.98 (q, *J* = 16.6, 6.9, 1H), 2.71 (dd, *J* = 16.0, 6.9 Hz, 1H), 2.61 (dd, *J* = 16.0, 8.0 Hz, 1H), 2.10 (s, 3H), 1.69 (s, 3H), 1.55 (s, 3H). ¹³C NMR (125.77 MHz, CDCl₃) δ 207.5, 143.1, 138.4, 133.5, 133.0, 126.3, 109.7, 50.1, 30.9, 25.8, 18.1. HR-MS-ESI m/z: [M+Na], calculated for C₁₂H₁₆NaO₂ 215.1042, found 215.1039. IR (neat): 2985, 2937, 1713, 1154, 1154, 1020, 971, 792 cm⁻¹

2.5.7.5. Synthesis of 4-(furan-3-yl)dec-5-yn-2-one (113)



See the general procedure for 1,4-conjugate addition reaction above. 3 equivalents of boronic ester were used. The crude reaction mixture was purified via flash column chromatography with a 30–60% gradient of dichloromethane in hexanes as eluent on silica gel. HPLC Chiralcel OD-H (hexane/*i*-PrOH = 90:10 – 70:30, 0.75 mL/min, UV-190 detector). Trial 1: 43.4 mg, 0.199 mmol, 99% yield; 95:5 er (with cat. **107**, 3 equivalent of boronic ester). Trial 2: 43.3 mg, 0.198 mmol, 99% yield; 95:5 er (with cat. **107**, 3 equivalent of boronic ester). ¹H NMR (400 MHz, CDCl₃) δ 7.32 (ss, 2H), 6.32 (s, 1H), 4.04 (tt, *J* = 9.0, 2.5 Hz, 1H), 2.86 (dd, *J* = 16.5, 7.8 Hz, 1H), 2.15 (s, 3H), 1.40 (m, 6H), 0.89 (t, *J* = 7.3 Hz, 3H). ¹³C NMR (100 MHz, CDCl₃) δ 206.3, 143.1, 139.5, 125.9, 109.7, 82.2, 80.1, 50.8, 31.0, 30.7, 23.8, 22.0, 18.4, 13.7. HR-MS-ESI *m/z*: [M+Na], calculated for C₁₄H₁₈NaO₂ 241.1199, found 241.1198. IR (neat): 2939, 2879, 2348, 1715, 1359, 1163, 1033, 655 cm⁻¹.

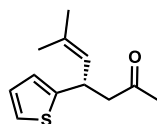
2.5.7.6. Synthesis of (E)-6-(furan-3-yl)-4-((E)-styryl)hex-5-en-2-one (**114**)



See the general procedure for 1,4-conjugate addition reaction above. The crude reaction mixture was purified via flash column chromatography with a 30–60% gradient of dichloromethane in hexanes as eluent on silica gel. HPLC Chiralcel OD-H (hexane/*i*-PrOH = 90:10 – 70:30, 0.75 mL/min, UV-254 detector). Trial 1: 39.3 mg, 0.147 mmol, 74% yield; 98:2 er (with cat. **100**, 1.3 eq of boronic acid). Trial 2: 39.4 mg, 0.147 mmol, 74% yield; 98:2 er (with cat. **100**, 1.3 eq of boronic acid). Trial 3: 39.9 mg, 0.15 mmol, 75% yield; 97:3 er (with cat. **107**, 1.3 eq of boronic acid). Trial 4: 40 mg, 0.15 mmol,

75% yield; 98:2 er (with cat. **107**, 1.3 eq of boronic acid). ^1H NMR (400 MHz, CDCl_3) δ 7.22-7.40 (m, 7H), 6.50 (s, 1H), 6.42 (d, $J=16.0$ Hz, 1H), 6.30 (d, $J=16.0, 7.3$ Hz, 1H), 6.16 (dd, $J=16.0, 7.3$ Hz, 1H), 5.91 (dd, $J=16.0, 6.9$ Hz, 1H), 3.59 (m, 1H), 2.67 (d, $J=6.9$, 2H), 2.16 (s, 3H). ^{13}C NMR (100 MHz, CDCl_3) δ 207.0, 143.5, 140.2, 137.1, 131.1, 130.7, 130.5, 128.6, 127.4, 120.3, 107.5, 48.7, 41.3, 30.8. HR-MS-ESI m/z : $[\text{M}+\text{Na}]$, calculated for $\text{C}_{18}\text{H}_{18}\text{NaO}_2$ 289.1199, found 289.1199. IR (neat): 2976, 1710, 1361, 1260, 1161, 1032, 752, 699 cm^{-1}

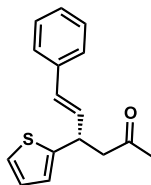
2.5.7.7. Synthesis of 6-methyl-4-(thiophen-2-yl)hept-5-en-2-one (115)



See the general procedure for 1,4-conjugate addition reaction above. The crude reaction mixture was purified via column chromatography with a 30–50% gradient of dichloromethane in hexanes as eluent on silica gel. Trial 1: 30.7 mg, 0.147 mmol, 75% yield; 94:6 er (with 15 mol% catalyst **100**, 4 equiv of boronic acid, 17h, 29.7 mg of starting material). Trial 2: 26 mg, 0.125 mmol, 70% yield; 87:13 er (with 15 mol% catalyst **100**, 4 equiv of boronic acid, 17h, 27.2 mg of starting material). Trial 3: 44.7 mg, 0.214 mmol, 99% yield; 96:4 er (with catalyst **107**, 2 equiv of boronic acid, 2h, 33 mg of starting material). Trial 4: 41.6 mg, 0.199 mmol, 99% yield; 96:4 er (with catalyst **107**, 2 equiv of boronic acid, 2h, 29.6 mg of starting material). ^1H NMR (400 MHz, CDCl_3) δ 7.11 (dd, $J=5.0, 1.3$ Hz, 1H), 6.89 (dd, $J=5.0, 3.6$ Hz, 1H), 6.78 (dd, $J=3.6, 1.3$ Hz, 1H), 5.19 (td, $J=9.6, 1.3$ Hz, 1H), 4.36 (ddd, $J=9.6, 7.5, 6.6$ Hz, 1H), 2.87 (dd, $J=16.0, 6.6$ Hz, 1H), 2.74 (dd, $J=16.0, 7.5$ Hz, 1H), 2.10 (s, 3H), 1.71 (d, $J=1.3$ Hz, 3H), 1.70 (d, $J=1.3$ Hz, 3H). ^{13}C NMR (100 MHz, CDCl_3) δ 207.0, 148.7, 133.5, 126.7, 126.6, 123.2,

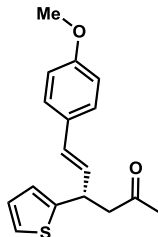
123.0, 51.3, 35.3, 30.8, 25.8, 18.1. HR-MS-ESI m/z: [M+Na], calculated for C₁₂H₁₆NaOS 231.08141, found 231.08126. IR (neat): 1716, 1357, 847, 696 cm⁻¹

2.5.7.8. Synthesis of (*E*)-6-phenyl-4-(thiophen-2-yl)hex-5-en-2-one (117)



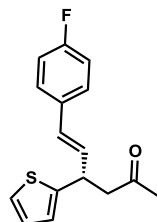
See the general procedure for 1,4-conjugate addition reaction above. 3 equivalent of boronic acid was used. The crude reaction mixture was purified via column chromatography with a 30–50% gradient of dichloromethane in hexanes as eluent on silica gel. Trial 1: 50.3 mg, 0.196 mmol, 98% yield; 96:4 er (with catalyst **100**, 3 equiv of boronic acid, 24h). Trial 2: 47.5 mg, 0.185 mmol, 93% yield; 93:7 er (with catalyst **100**, 3 equiv of boronic acid, 24h). Trial 3: 52 mg, 0.203 mmol, 98% yield; 97:3 er (with catalyst **107**, 3 equiv of boronic acid, 22h). Trial 4: 56 mg, 0.218 mmol, 99% yield, 97:3 er (with catalyst **107**, 3 equiv of boronic acid, 22h). ¹H NMR (400 MHz, CDCl₃) δ 7.26 (m, 6H), 6.94 (d, J= 5.5 Hz, 1H), 6.88 (d, J= 3.2 Hz, 1H), 6.46 (d, J= 16 Hz, 1H), 6.29 (dd, J= 16, 7.3 Hz, 1H), 4.38 (q, J= 7.3 Hz, 1H), 2.98 (m, 2H), 2.15 (s, 3H). ¹³C NMR (100.52 MHz, CDCl₃) δ 206.3, 146.8, 136.9, 131.6, 130.6, 128.6, 127.6, 126.9, 126.4, 124.1, 123.8, 50.3, 39.3, 30.8. HR-MS-ESI m/z: [M+Na], calculated for C₁₆H₁₆NaOS 279.08141, found 279.08139. IR (neat): 1715, 1357, 1163, 965 cm⁻¹

2.5.7.9. Synthesis of (*E*)- 6-(4-methoxyphenyl)-4-(thiophen-2-yl)hex-5-en-2-one (117)



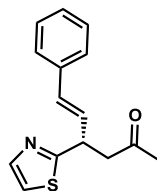
See the general procedure for 1,4-conjugate addition reaction above. 3 equivalent of boronic acid was used. The reactions were done in 24h at 70°C. The crude reaction mixture was purified via column chromatography with a 30–50% gradient of dichloromethane in hexanes as eluent on silica gel. Trial 1: 33.6 mg, 0.117 mmol, 66% yield; 92:8 er (with catalyst **100**, 27 mg of starting material). Trial 2: 34.4 mg, 0.120 mmol, 62% yield; 92:8 er (with catalyst **100**, 29.4 mg of starting material). Trial 3: 50.3 mg, 0.175 mmol, 95% yield; 96:4 er (with catalyst **107**, 28.2 mg of starting material). Trial 4: 48 mg, 0.168 mmol, 86% yield; 98:2 er (with catalyst **107**, 29.7 mg of starting material). ¹H NMR (400 MHz, CDCl₃) δ 7.27 (d, J= 8.9 Hz, 2H), 7.16 (dd, J= 5.0, 0.9 Hz, 1H), 6.93 (dd, J= 5.0, 3.6 Hz, 1H), 6.86 (bd, J= 3.6 Hz, 1H), 6.82 (d, J= 8.9 Hz, 2H), 6.39 (d, J= 15.5 Hz, 1H), 6.14 (dd, J= 15.5, 7.8 Hz, 1H), 4.34 (q, J= 7.3 Hz, 1H), 3.78 (s, 3H), 2.96 (m, 2H), 2.14 (s, 3H). ¹³C NMR (100 MHz, CDCl₃) δ 206.5, 159.2, 147.1, 130.0, 129.6, 129.4, 127.5, 126.9, 123.9, 123.8, 114.0, 55.3, 50.4, 39.3, 30.8. HR-MS-ESI m/z: [M+Na], calculated for C₁₇H₁₈NaO₂S 309.09197, found 309.09221. IR (neat): 1714, 1607, 1511, 1248, 1175, 1033, 967, 824, 702 cm⁻¹

2.5.7.10. Synthesis of (*E*)-6-(4-fluorophenyl)-4-(thiophen-2-yl)hex-5-en-2-one (118)



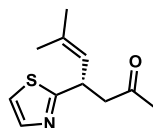
See the general procedure for 1,4-conjugate addition reaction above. 2 equivalent of boronic acid was used. The crude reaction mixture was purified via column chromatography with a 30–50% gradient of dichloromethane in hexanes as eluent on silica gel. Trial 1: 44.2 mg, 0.161 mmol, 87% yield; 95:5 er (with catalyst **100**, 2 equiv of boronic acid, 24h). Trial 2: 36.2 mg, 0.132 mmol, 73% yield; 94:6 er (with catalyst **100**, 2 equiv of boronic acid, 24h). Trial 3: 56.6 mg, 0.206 mmol, 98% yield; 98:2 er (with catalyst **107**, 2 equiv of boronic acid, 22h). Trial 4: 41.5 mg, 0.151 mmol, 87% yield; 97:3 er (with catalyst **107**, 2 equiv of boronic acid, 22h). ¹H NMR (500 MHz, CDCl₃) δ 7.3 (m, 2H), 7.17 (dd, J= 5.15, 1.15 Hz, 1H), 6.96 (m, 3H), 6.86 (d, J= 3.4 Hz, 1H), 6.41 (d, J= 16.04 Hz, 1H), 6.20 (dd, J=16.04, 8.02 Hz, 1H), 4.36 (q, J=7.4 Hz), 2.97 (m, 2H), 2.14 (s, 3H). ¹³C NMR (100 MHz, CDCl₃) δ 206.2, 163.5, 161.1, 146.7, 133.0, 131.4, 129.5, 127.98, 127.90, 127, 124, 123.9, 115.3, 50.2, 39.2, 30.8. HR-MS-ESI m/z: [M+Na], calculated for C₁₆H₁₅FNaOS 297.07199, found 297.07202. IR (neat): 1715, 1508, 1227, 1158, 967, 825, 700 cm⁻¹

2.5.7.11. Synthesis of (*E*)-6-phenyl-4-(thiazol-2-yl)hex-5-en-2-one (119)



See the general procedure for 1,4-conjugate addition reaction above. 3 equivalent of boronic acid was used. The crude reaction mixture was purified via column chromatography with a 1% tetrahydrofuran in dichloromethane as eluent on silica gel. Trial 1: 44.7 mg, 0.174 mmol, 88% yield; 87:13 er (with catalyst **100**, 19h, 30.4 mg of starting material). Trial 2: 46.5 mg, 0.181 mmol, 90% yield; 89:11 er (with catalyst **100**, 20h, 30.6 mg of starting material). Trial 3: 42.1 mg, 0.164 mmol, 82% yield; 84:16 er (with catalyst **107**, 15h, 30.6 mg of starting material). Trial 4: 47.4 mg, 0.184 mmol, 92% yield; 85:15 er (with catalyst **107**, 16h, 30.5 mg of starting material). Trial 5: 43.4 mg, 0.169 mmol, 83% yield; 87:13 er (with catalyst **107**, 4h, 31 mg of starting material). Trial 6: 40.7 mg, 0.158 mmol, 80% yield; 80:20 (with catalyst **107**, 4h, 30.4 mg of starting material). ¹H NMR (400 MHz, CDCl₃) δ 7.68 (d, J= 3.6 Hz, 1H), 7.36 (app.d, J= 7.3 Hz, 2H), 7.29 (app.t, J= 7.5 Hz, 2H), 7.25-7.20 (m, 2H), 6.57 (d, J= 15.5 Hz, 1H), 6.31 (dd, J= 15.5, 8.7 Hz, 1H), 4.47 (q, J= 6.8 Hz, 1H), 3.38 (dd, J= 17.1, 7.3 Hz, 1H), 2.98 (dd, J= 17.1, 6.8 Hz, 1H), 2.19 (s, 3H). ¹³C NMR (100 MHz, CDCl₃) δ 206.1, 172.4, 142.4, 136.5, 132.5, 129.4, 128.6, 127.9, 126.5, 119.0, 48.0, 42.2, 30.6. HR-MS-ESI m/z: [M+H], calculated for C₁₅H₁₅NNaOS 280.07666, found 280.07657. IR (neat): 1715, 1496, 1361, 1161, 967, 750, 694 cm⁻¹.

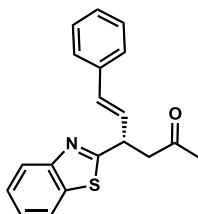
2.5.7.12. Synthesis of 6-Methyl-4-(thiazol-2-yl)hept-5-en-2-one (**120**)



See the general procedure for 1,4-conjugate addition reaction above. 3 equivalent of boronic acid was used. The crude reaction mixture was purified via column chromatography with a 10% of ethyl acetate in hexanes as eluent on silica gel. Trial

1: 27.8 mg, 0.133 mmol, 66% yield; 83:17 er (with catalyst **100**, 20h, 30.8 mg of starting material). Trial 2: 23.8 mg, 0.114 mmol, 62% yield; 82:18 er (with catalyst **100**, 20h, 28 mg of starting material). Trial 3: 37.5 mg, 0.179 mmol, 88% yield; 84:16 er (with catalyst **107**, 2h, 31.1 mg of starting material). Trial 4: 40.2 mg, 0.192 mmol, 95% yield; 84:16 er (with catalyst **107**, 2h, 31.1 mg of starting material). ¹H NMR (400 MHz, CDCl₃) δ 7.63 (d, J= 3.4 Hz, 1H), 7.16 (d, J= 3.4 Hz, 1H), 5.24 (app.dt, J= 9.6, 1.3 Hz, 1H), 4.50-4.44 (m, 1H), 3.24 (dd, J= 16.9, 6.8 Hz, 1H), 2.77 (dd, J= 16.9, 6.8 Hz, 1H), 2.16 (s, 3H), 1.76 (d, J= 1.3 Hz, 3H), 1.73 (d, J= 1.37 Hz, 3H). ¹³C NMR (100 MHz, CDCl₃) δ 206.6, 174.1, 142.2, 135.6, 124.9, 118.5, 48.6, 37.9, 30.6, 25.8, 18.3. HR-MS-ESI m/z: [M+H], calculated for C₁₇H₁₅NNaOS 232.07666, found 232.07643. IR (neat): 1717, 1498, 1360, 1159, 1036, 850, 727 cm⁻¹

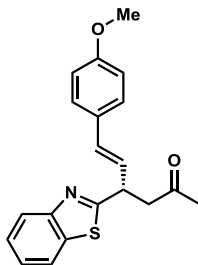
2.5.7.13. Synthesis of (*E*)-4-(benzo[d]thiazol-2-yl)-6-phenylhex-5-en-2-one (**121**)



See the general procedure for 1,4-conjugate addition reaction above. 3 equivalent of boronic acid was used. The reaction was done at 90°C. The crude reaction mixture was purified via column chromatography with a 50–100% gradient of dichloromethane in hexanes as eluent on silica gel. Trial 1: 35.6 mg, 0.116 mmol, 58% yield; 80:20 er (with catalyst **100**, 60h, 40.4 mg of starting material). Trial 2: 29.1 mg, 0.095 mmol, 48% yield; 71:29 er (with catalyst **100**, 60h, 40.4 mg of starting material). Trial 3: 41.5 mg, 0.135 mmol, 69% yield; 74:26 er (with catalyst **107**, 36h, 39.8 mg of

starting material). Trial 4: 42.6 mg, 0.138 mmol, 69% yield; 86:14 er (with catalyst **107**, 36h, 40.9 mg of starting material). ^1H NMR (400 MHz, CDCl_3) δ 7.96 (d, $J=7.8$ Hz, 1H), 7.82 (d, $J=8.7$ Hz, 1H), 7.45 (m, 1H), 7.36 (m, 3H), 7.29 (m, 2H), 7.23 (m, 1H), 6.64 (d, $J=15.5$ Hz, 1H), 6.36 (dd, $J=16.0, 8.7$ Hz, 1H), 4.55 (q, $J=6.6$ Hz, 1H), 3.51 (dd, $J=17.4, 7.3$ Hz, 1H), 3.06 (dd, $J=17.4, 6.4$ Hz, 1H), 2.23 (s, 3H). ^{13}C NMR (100 MHz, CDCl_3) δ 205.9, 173.3, 153.1, 136.4, 135.3, 133.1, 128.8, 128.6, 127.9, 126.6, 126.0, 124.9, 122.8, 121.6, 47.6, 43.1, 30.7. HR-MS-ESI m/z : $[\text{M}+\text{Na}]$, calculated for $\text{C}_{19}\text{H}_{17}\text{NNaOS}$ 330.09231, found 330.09224. IR (neat): 1716, 1510, 1437, 1360, 1161, 1013, 966, 756, 731, 694 cm^{-1}

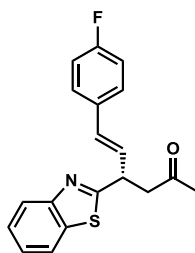
2.5.7.14. Synthesis of (*E*)-4-(benzo[d]thiazol-2-yl)-6-(4-methoxyphenyl)hex-5-en-2-one (122)



See the general procedure for 1,4-conjugate addition reaction above. 3 equivalent of boronic acid was used. The reaction was done at 70°C. The crude reaction mixture was purified via column chromatography with a 10% of ethyl acetate in hexanes as eluent on silica gel. Trial 1: 49.2 mg, 0.146 mmol, 72% yield; 90:10 er (with catalyst **100**, 42h, 41 mg of starting material). Trial 2: 53.4 mg, 0.158 mmol, 82% yield; 88:12 er (with catalyst **100**, 42h, 39 mg of starting material). Trial 3: 53.7 mg, 0.159 mmol, 80% yield; 92:8 er (with catalyst **107**, 7h, 40.4 mg of starting material). Trial 4: 59.4 mg, 0.176 mmol, 90% yield; 93:7 er (with catalyst **107**, 7h, 39.7 mg of starting

material). ^1H NMR (500 MHz, CDCl_3) δ 7.95 (d, J = 8.0 Hz, 1H), 7.81 (d, J = 8.0 Hz, 1H), 7.44 (m, 1H), 7.35-7.28 (m, 3H), 6.85-6.82 (m, 2H), 6.58 (d, J = 15.4 Hz, 1H), 6.21 (dd, J = 15.4, 8.6 Hz, 1H), 4.51 (q, J = 7.4 Hz, 1H), 3.79 (s, 3H), 3.48 (dd, J = 17.4, 6.8 Hz, 1H), 3.04 (dd, J = 17.4, 6.3 Hz, 1H), 2.23 (s, 3H). ^{13}C NMR (125.77 MHz, CDCl_3) δ 206.0, 173.6, 159.5, 153.2, 135.4, 132.5, 129.2, 127.8, 126.6, 125.9, 124.9, 122.8, 121.6, 114.0, 55.3, 47.7, 43.2, 30.7. HR-MS-ESI m/z : $[\text{M}+\text{Na}]$, calculated for $\text{C}_{20}\text{H}_{19}\text{NNaO}_2\text{S}$ 360.10287, found 360.10301. IR (neat): 1709, 1512, 1252, 1176, 1031, 968, 833, 760, 731 cm^{-1} .

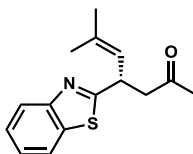
2.5.7.15. Synthesis of (*E*)-4-benzo[d]thiazol-2-yl)-6-phenylhex-5-en-2-one (123)



See the general procedure for 1,4-conjugate addition reaction above. 3 equivalent of boronic acid was used. The reaction was done at 90°C . The crude reaction mixture was purified via column chromatography with a 10% of ethyl acetate in hexanes as eluent on silica gel. Trial 1: 31.3 mg, 0.096 mmol, 48% yield; 65:35 er (with catalyst **100**, 60h, 40.9 mg of starting material). Trial 2: 30.1 mg, 0.092 mmol, 46% yield; 84:16 er (with catalyst **100**, 60h, 40.4 mg of starting material). Trial 3: 53 mg, 0.163 mmol, 82% yield; 88:12 er (with catalyst **107**, 24h, 40.4 mg of starting material). Trial 4: 55.6 mg, 0.170 mmol, 85% yield; 87:13 er (with catalyst **107**, 24h, 40.7 mg of starting material). ^1H NMR (400 MHz, CDCl_3) δ 7.96 (d, J = 8.2 Hz, 1H), 7.82 (dd, J = 8.7, 1.3 Hz, 1H), 7.46-7.42 (m, 1H), 7.36-7.31 (m, 3H), 7.01-6.95 (m, 2H), 6.59 (d, J = 15.5 Hz,

1H), 6.27 (dd, J= 15.5, 8.7 Hz, 1H), 4.56-4.50 (m, 1H), 3.49 (dd, J= 17.4, 6.8 Hz), 3.05 (dd, J= 17.4, 6.8), 2.23 (s, 3H). ¹³C NMR (100 MHz, CDCl₃) δ 205.8, 173.1, 163.7, 161.3, 153.2, 135.3, 132.6, 131.8, 128.6, 128.2, 128.1, 126, 125, 122.8, 121.6, 115.7, 115.4, 47.6, 43.0, 30.6. HR-MS-ESI m/z: [M+Na], calculated for C₁₉H₁₆FNNaOS 348.08288, found 348.08287. IR (neat): 1716, 1508, 1228, 1159, 967, 760, 731 cm⁻¹.

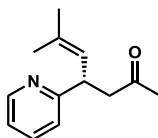
2.5.7.16. Synthesis of 4-(benzo[d]thiazol-2-yl)-6-methylhept-5-en-2-one (**124**)



See the general procedure for 1,4-conjugate addition reaction above. 3 equivalent of boronic acid was used. The reaction was done at 90°C. The crude reaction mixture was purified via column chromatography with a 10% of ethyl acetate in hexanes as eluent on silica gel. Trial 1: 43.3 mg, 0.167 mmol, 84% yield; 82:17 er (with catalyst **100**, 16h, 40.5 mg of starting material). Trial 2: 45.8 mg, 0.176 mmol, 91% yield; 78:22 er (with catalyst **100**, 16h, 39.2 mg of starting material). Trial 3: 51.1 mg, 0.197 mmol, 98% yield; 86:14 er (with catalyst **107**, 4h, 40.5 mg of starting material). Trial 4: 43.7 mg, 0.168 mmol, 84% yield; 86:14 er (with catalyst **107**, 4h, 40.8 mg of starting material). ¹H NMR (400 MHz, CDCl₃) δ 7.92 (d, J= 8.2 Hz, 1H), 7.79 (d, J= 7.8 Hz, 1H), 7.41 (m, 1H), 7.31 (m, 1H), 5.28 (m, 1H), 4.55 (m, 1H), 3.37 (dd, J= 17.4, 6.4 Hz, 1H), 2.86 (dd, J= 17.4, 6.8 Hz, 1H), 2.2 (s, 3H), 1.8 (d, J= 0.92 Hz, 3H), 1.75 (d, J= 0.92 Hz, 3H). ¹³C NMR (100 MHz, CDCl₃) δ 206.4, 174.9, 153.3, 136.3, 135.3, 125.8, 124.7, 124.3, 122.6, 121.5, 48.2, 38.8, 30.6, 25.8, 18.4. HR-MS-ESI m/z: [M+Na], calculated

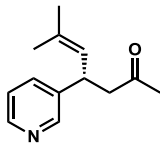
for C₁₅H₁₇NNaOS 282.09231, found 282.09222. IR (neat): 1717, 1437, 1359, 760, 730 cm⁻¹

2.5.7.17. Synthesis of 6-methyl-4-(pyridine-2-yl)hept-5-en-2-one (125)



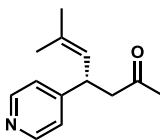
See the general procedure for 1,4-conjugate addition reaction above. The crude reaction mixture was purified via flash column chromatography with a 10 - 20% gradient of ethyl acetate in dichloromethane as eluent on silica gel. HPLC Chiralpak AY-3 (hexane/*i*-PrOH/Et₃N = 50:45.5:0.5, 1.0 mL/min, UV-254 detector). Trial 1: 34.7 mg, 0.174 mmol, 87% yield; 86:14 er (with cat. **100**, 1.3 eq of boronic acid, 115°C, 3h). Trial 2: 36.2 mg, 0.180 mmol, 90% yield; 87:13 er (with cat. **100**, 1.3 eq of boronic acid, 115°C, 3h). Trial 3: 38.9 mg, 0.191 mmol, 96% yield; 94:6 er (with cat. **107**, 1.3 eq of boronic acid, 70°C, 16h). Trial 4: 39.5 mg, 0.194 mmol, 97% yield; 94:6 er (with cat. **107**, 1.3 eq of boronic acid, 70°C, 16h). Trial 5: 37.4 mg, 92% yield; 93:7 er (with cat. **107**, 1.3 eq of boronic acid, 120°C, 75min). Trial 6: 37.5 mg, 92% yield; 93:7 er (with cat. **107**, 1.3 eq of boronic acid, 120°C, 75min). ¹H NMR (400 MHz, CDCl₃) δ 8.48 (d, J=4.1 Hz, 1H), 7.56 (t, J= 7.8 Hz, 1H), 7.18 (d, J= 7.8 Hz, 1H), 7.06 (t, J= 6.9 Hz, 1H), 5.25 (d, J= 9.6 Hz, 1H), 4.23 (q, J= 16.9, 8.7 Hz, 1H), 3.20 (dd, 16.5, 7.8 Hz, 1H), 2.70 (dd, J= 16.5, 6.4, 1H), 2.10 (s, 3H), 1.73 (s, 3H), 1.69 (s, 3H). ¹³C NMR (100 MHz, CDCl₃) δ 208.0, 163.2, 149.1, 136.5, 133.2, 126.1, 122.9, 121.3, 48.5, 41.8, 30.7, 25.9, 18.3. HR-MS-ESI m/z: [M+Na], calculated for C₁₃H₁₇NNaO 226.1202, found 226.1201. IR (neat): 2970, 2924, 1713, 1590, 1434, 992, 764, 603 cm⁻¹

2.5.7.18. Synthesis of 6-methyl-4-(pyridine-3-yl)hept-5-en-2-one (126)



See the general procedure for 1,4-conjugate addition reaction above. The crude reaction mixture was purified via flash column chromatography with a 2% of ethyl acetate in diethyl ether as eluent on silica gel. HPLC Chiralcel OD-H (hexane/i-PrOH = 50:50, 0.75 mL/min, UV-254 detector). Trial 1: 35.3 mg, 0.176 mmol, 88% yield; 98:2 er (with cat. **100**, 1.3 eq of boronic acid). Trial 2: 34.8 mg, 0.174 mmol, 87% yield; 98:2 er (with cat. **100**, 1.3 eq of boronic acid). ^1H NMR (400 MHz, CDCl_3) δ 8.46 (d, $J=2.3$ Hz, 1H), 8.40 (dd, $J= 1.8, 5.0$ Hz, 1H), 7.49 (td, $J= 1.8, 7.8$ Hz, 1H), 7.18 (dd, $J= 7.8, 4.6$ Hz, 1H), 5.19 (td, $J= 9.6, 1.4$ Hz, 1H), 4.08 (dd, $J= 7.3, 6.8$ Hz, 1H), 2.78 (dd, $J= 6.9, 3.2$ Hz, 2H), 2.07 (s, 3H), 1.66 (d, $J= 2.8$ Hz, 6H). ^{13}C NMR (100 MHz, CDCl_3) δ 206.8, 149.1, 147.7, 140.2, 134.8, 133.9, 125.9, 123.5, 50.4, 37.3, 30.8, 25.9, 18.2. HR-MS-ESI m/z : $[\text{M}+\text{Na}]$, calculated for $\text{C}_{13}\text{H}_{17}\text{NNaO}$ 226.1202, found 226.1201. IR (neat): 2924, 1713, 1424, 1162, 1032, 807, 714, 621 cm^{-1}

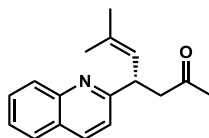
2.5.7.19. Synthesis of 6-methyl-4-(pyridine-4-yl)hept-5-en-2-one (127)



See the general procedure for 1,4-conjugate addition reaction above. The crude reaction mixture was purified via flash column chromatography with a 5% of ethyl acetate in diethyl ether as eluent on silica gel. HPLC Chiralpak AY-3 (hexane/i-PrOH/ Et_3N = 50:45.5:0.5, 1.5 mL/min, UV-254 detector). Trial 1: 37.5 mg, 0.184 mmol,

92% yield; 91:9 er (with cat. **100**, 1.3 eq of boronic acid). Trial 2: 37.3 mg, 0.184 mmol, 92% yield; 91:9 er (with cat. **100**, 1.3 eq of boronic acid). Trial 3: 36.6 mg, 0.180 mmol, 90% yield; 96:4 er (with cat. **107**, 1.3 eq of boronic acid). Trial 4: 37 mg, 0.182 mmol, 91% yield; 95:5 er (with cat. **107**, 1.3 eq of boronic acid). ¹H NMR (400 MHz, CDCl₃) δ 8.46 (dd, J=4.6, 2.3 Hz, 2H), 7.11 (dd, J= 4.6, 1.8 Hz, 2H), 5.15 (td, J= 9.2, 1.4 Hz, 1H), 4.05 (dd, J= 14.6, 7.3 Hz, 1H), 2.72-2.82 (ddd, J= 16.5, 7.3, 6.9 Hz, 2H), 2.08 (s, 3H), 1.67 (d, J= 7.3 Hz, 6H). ¹³C NMR (100 MHz, CDCl₃) δ 206.6, 153.6, 150.1, 134.5, 125.3, 122.7, 49.8, 39.0, 30.8, 25.9, 18.3. HR-MS-ESI m/z: [M+Na], calculated for C₁₃H₁₇NNaO 226.1202, found 226.1202. IR (neat): 2988, 1713, 1600, 1416, 1365, 1157, 1001, 814, 629 cm⁻¹.

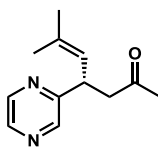
2.5.7.20. Synthesis of 6-methyl-4-(quinolin-2-yl)hept-5-en-2-one (**128**)



See the general procedure for 1,4-conjugate addition reaction above. The crude reaction mixture was purified via flash column chromatography with a 5% gradient of ethyl acetate in hexanes as eluent on silica gel. HPLC Chiralcel OJ-H (hexane/i-PrOH = 90:10 – 70:30, 0.75 mL/min, UV-254 detector). Trial 1: 43.0 mg, 0.170 mmol, 85% yield; 88:12 er (with cat. **100**, 1.3 eq of boronic acid). Trial 2: 43.25 mg, 0.170 mmol, 85% yield; 88:12 er (with cat. **100**, 1.3 eq of boronic acid). Trial 3: 48.5 mg, 0.191 mmol, 96% yield; 95:5 er (with cat. **107**, 1.3 eq of boronic acid). Trial 4: 46.6 mg, 0.186 mmol, 93% yield; 96:4 er (with cat. **107**, 1.3 eq of boronic acid). ¹H NMR (500 MHz, CDCl₃) δ 8.00 (dd, J=8.6, 13.2 Hz, 2H), 7.73 (dd, J= 8.0, 1.2 Hz, 1H), 7.65 (ddd, J= 8.6, 6.9, 1.8

Hz, 1H), 7.45 (dt, J= 6.9, 1.2 Hz, 1H), 7.28 (d, J=8.0, 1H), 5.26 (dm, J=9.7 Hz, 1H), 4.47 (ddd, J= 9.7, 8.6, 6.3 Hz, 1H), 3.44 (dd, J= 16.6, 8.6 Hz, 1H), 2.71 (dd, J= 16.6, 5.7 Hz, 1H), 2.24 (s, 3H), 1.83 (d, J=1.2 Hz, 3H), 1.71 (d, J= 1.7 Hz, 3H). ¹³C NMR (125.77 MHz, CDCl₃) δ 208.3, 163.3, 147.7, 136.2, 133.5, 129.2, 127.5, 127.0, 126.1, 125.8, 121.7, 47.6, 42.6, 30.9, 25.9, 18.4. HR-MS-ESI m/z: [M+H], calculated for C₁₇H₂₀NO 255.1572, found 255.1571. IR (neat): 3064, 2982, 1711, 1599, 1503, 1427, 1142, 827, 756, 622 cm⁻¹.

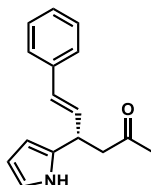
2.5.7.21. Synthesis of 6-methyl-4-(pyrazine-2-yl)hept-5-en-2-one (129)



See the general procedure for 1,4-conjugate addition reaction above. The crude reaction mixture was purified via flash column chromatography with a 5 - 10% gradient of ethyl acetate in hexanes as eluent on silica gel. HPLC Chiralcel OD-H (hexane/*i*-PrOH = 90:10 – 70:30, 0.75 mL/min, UV-254 detector). Trial 1: 38.6 mg, 0.188 mmol, 94% yield; 92:8 er (with cat. **100**, 1.3 eq of boronic acid, 120°C, 4h). Trial 2: 39.0 mg, 0.190 mmol, 95% yield; 92:8 er (with cat. **100**, 1.3 eq of boronic acid, 120°C, 4h). Trial 3: 42.4 mg, 0.198 mmol, 99% yield; 95:5 er (with cat. **107**, 1.3 eq of boronic acid, 70°C, 8h). Trial 4: 42.2 mg, 0.198 mmol, 99% yield; 94:6 er (with cat. **107**, 1.3 eq of boronic acid, 70°C, 8h). ¹H NMR (400 MHz, CDCl₃) δ 8.47 (dd, J= 1.4 Hz, 1H), 8.38 (td, J= 2.7, 1.4 Hz, 1H), 8.32 (d, J=2.7 Hz, 1H), 5.17 (dt (J= 9.6, 1.8 Hz, 1H), 4.27 (ddd, J= 8.7, 8.2, 6.0 Hz, 1H), 3.19 (dd, J= 17.4, 8.2 Hz, 1H), 2.70 (dd, J=17.4, 8.2 Hz, 1H), 2.10 (s, 3H), 1.73 (d, J= 0.9 Hz, 3H), 1.67 (d, J=1.4Hz, 3H). ¹³C NMR (100 MHz, CDCl₃) δ 207.2, 158.9,

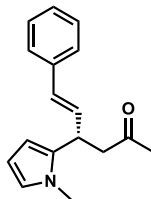
145.1, 143.7, 142.2, 134.2, 125.0, 47.6, 39.1, 30.5, 25.8, 18.3. HR-MS-ESI m/z: [M+Na], calculated for C₁₂H₁₆N₂NaO 227.1155, found 227.1153. IR (neat): 2937, 1711, 1405, 1159, 1019, 652 cm⁻¹.

2.5.7.22. Synthesis of (*E*)-6-phenyl-4-(1*H*-pyrrol-2-yl)hex-5-en-2-one (**130**)



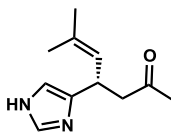
See the general procedure for 1,4-conjugate addition reaction above. 3 equivalent of boronic acid was used. The reaction was done at 70°C in 24h. The crude reaction mixture was purified via column chromatography with a 5-10% gradient of ethyl acetate in hexanes as eluent on silica gel. Trial 1: 9.4 mg, 0.039 mmol, 19% yield; 88:12 er (with catalyst **100**, 27.4 mg of starting material, 48h). Trial 2: 13.8 mg, 0.058 mmol, 28% yield; 96:4 er (with catalyst **100**, 27.4 mg of starting material, 48h). Trial 3: 20.4 mg, 0.085 mmol, 42% yield; 96:4 er (with catalyst **107**, 27.5 mg of starting material). Trial 4: 17.7 mg, 0.074 mmol, 36% yield; 97:3 er (with catalyst **107**, 27.5 mg of starting material). ¹H NMR (500 MHz, CDCl₃) δ 8.42 (s, 1H), 7.35 (d, J= 7.4 Hz, 2H), 7.31-7.28 (m, 2H), 7.24-7.20 (m, 1H), 6.70-6.69 (m, 1H), 6.47 (d, J=16.0, 1H), 6.32 (dd, J= 16.0, 8.0 Hz, 1H), 6.12 (q, J= 2.8 Hz, 1H), 5.94 (m, 1H), 4.09 (q, J= 7.4 Hz, 1H), 3.01 (dd, J= 17.5, 7.4 Hz, 1H), 2.92 (dd, J= 17.5, 5.7 Hz, 1H), 2.17 (s, 3H). ¹³C NMR (125.77 MHz, CDCl₃) δ 208.1, 136.9, 133.2, 130.7, 130.5, 128.6, 127.6, 126.3, 117.2, 108.1, 104.6, 49.0, 36.9, 30.7. HR-MS-ESI m/z: [M+H], calculated for C₁₆H₁₇NNaO 262.12024, found 262.12010. IR (neat): 3284, 1695, 1355, 973, 761, 715, 692 cm⁻¹.

2.5.7.23. Synthesis of (*E*)-4-(1-methyl-1*H*-pyrrol-2-yl)-6-phenylhex-5-en-2-one (131)



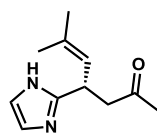
See the general procedure for 1,4-conjugate addition reaction above. 3 equivalent of boronic acid was used. The crude reaction mixture was purified via column chromatography with a 5-10% gradient of ethyl acetate in hexanes as eluent on silica gel. Trial 1: 35.1 mg, 0.138 mmol, 60% yield; 97:3 er (with catalyst **100**, 24h, 34.2 mg of starting material). Trial 2: 37.8 mg, 0.149 mmol, 66% yield; 97:3 er (with catalyst **100**, 24h, 33.8 mg of starting material). Trial 3: 48.1 mg, 0.190 mmol, 90% yield; 97:3 er (with catalyst **107**, 2h, 31.4 mg of starting material). Trial 4: 51.8 mg, 0.204 mmol, 90% yield; 95:5 er (with catalyst **107**, 2h, 33.9 mg of starting material). ¹H NMR (400 MHz, CDCl₃) δ 7.30-7.24 (m, 4H), 7.20-7.17 (m, 1H), 6.56 (appt, J= 2.0 Hz, 1H), 6.25 (d, J= 16.0 Hz, 1H), 6.18 (dd, J= 16.0, 6.4 Hz, 1H), 6.08 (t, J= 3.2 Hz, 1H), 5.95 (dd, J= 3.6, 1.8 Hz, 1H), 4.10 (q, J= 6.4 Hz, 1H), 3.56 (s, 3H), 3.00 (dd, J= 16.9, 6.4 Hz, 1H), 2.9 (dd, J= 16.9, 8.2 Hz, 1H), 2.16 (s, 3H). ¹³C NMR (100 MHz, CDCl₃) δ 206.8, 137.0, 133.5, 131.5, 130.4, 128.5, 127.4, 126.3, 122.0, 106.7, 105.1, 48.3, 35.4, 33.9, 30.9. HR-MS-ESI m/z: [M+Na], calculated for C₁₇H₁₉NNaO 276.13589, found 276.13566. IR (neat): 1715, 1492, 1360, 1089, 968, 747, 710, 694 cm⁻¹

2.5.7.24. Synthesis of 4-(1*H*-imidazol-4-yl)-6-methylhept-5-en-2-one (132)



See the general procedure for 1,4-conjugate addition reaction above. The crude reaction mixture was purified via flash column chromatography with a mixture of 2% methanol, 5% triethyl amine, 46.5% dichloromethane and 46.5% ethyl acetate as eluent on silica gel. HPLC Chiralpak ID (hexane/*i*-PrOH/Et₃N = 70:29.5:0.5, 1.0 mL/min, UV-230 detector). Trial 1: 31.8 mg, 0.166 mmol, 83% yield; 81:19 er (with cat. **100**, 1.3 eq of boronic acid). Trial 2: 32 mg, 0.166 mmol, 83% yield; 81:19 er (with cat. **100**, 1.3 eq of boronic acid). Trial 3: 34.4 mg, 0.178 mmol, 89% yield; 87:13 er (with cat. **107**, 1.3 eq of boronic acid). Trial 4: 33.8 mg, 0.178 mmol, 88% yield; 88:12 er (with cat. **107**, 1.3 eq of boronic acid). ¹H NMR (400 MHz, CDCl₃) δ 7.53 (bs, 1H), 6.73 (bs, 1H), 5.25 (dt, J= 9.6, 1.4 Hz, 1H), 4.08 (dt, J= 9.6, 7.3 Hz, 1H), 2.94 (dd, J= 16.9, 7.3 Hz, 1H), 2.70 (dd, J= 16.9, 6.4 Hz, 1H), 2.11 (s, 3H), 1.69 (d, J= 0.9 Hz, 3H), 1.66 (d, J= 1.4 Hz, 3H). ¹³C NMR (100 MHz, CDCl₃) δ 208.9, 133.3, 125.1, 49.7, 32.3, 30.6, 25.8, 18.1. HR-MS-ESI *m/z*: [M+H], calculated for C₁₁H₁₇N₂O 193.1335, found 193.1334. IR (neat): 3091, 2923, 2873, 1710, 1446, 1361, 1155, 1085, 988, 628 cm⁻¹

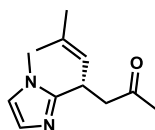
2.5.7.25. Synthesis of 4-(1*H*-imidazol-2-yl)-6-methylhept-5-en-2-one (**133**)



See the general procedure for 1,4-conjugate addition reaction above. The crude reaction mixture was purified via flash column chromatography with a 100% ethyl acetate as eluent on silica gel. HPLC Chiralpak ID (hexane/*i*-PrOH/Et₃N = 70:29.5:0.5, 1.0 mL/min, UV-230 detector). Trial 1: 29.3 mg, 0.152 mmol, 76% yield; 83:17 er (with cat. **100**, 1.3 eq of boronic acid). Trial 2: 29.4 mg, 0.152 mmol, 76% yield; 84:16 er (with cat. **100**, 1.3 eq of boronic acid). Trial 3: 32 mg, 0.166 mmol, 83% yield; 91:9 er (with

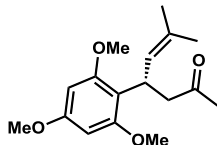
cat. **107**, 1.3 eq of boronic acid). Trial 4: 32 mg, 0.166 mmol, 83% yield; 91:9 er (with cat. **107**, 1.3 eq of boronic acid). ^1H NMR (400 MHz, CDCl_3) δ 9.14 (bs, 1H), 6.92 (s, 2H), 5.36 (dm, $J=9.6$ Hz, 1H), 4.18 (ddd, $J=9.6, 7.3, 5.9$ Hz, 1H), 3.20 (dd, $J=17.8, 7.3$ Hz, 1H), 2.76 (dd, 17.8, 5.5 Hz, 1H), 2.14 (s, 3H), 1.74 (d, $J=1.4$ Hz, 3H), 1.70 (d, $J=1.4$ Hz, 3H). ^{13}C NMR (100 MHz, CDCl_3) δ 208.2, 149.6, 134.8, 123.6, 48.3, 33.4, 30.6, 25.9, 18.2. HR-MS-ESI m/z : $[\text{M}+\text{H}]$, calculated for $\text{C}_{11}\text{H}_{17}\text{N}_2\text{O}$ 193.1335, found 193.1332. IR (neat): 2967, 2888, 2654, 1720, 1566, 1449, 1360, 1097, 757, 732, 648 cm^{-1}

2.5.7.26. Synthesis of 6-methyl-4-(1-methyl-1*H*-imidazol-2-yl)hept-5-en-2-one (**134**)



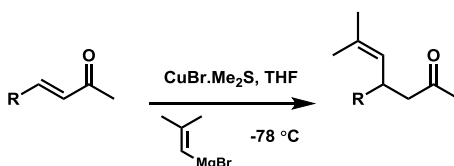
See the general procedure for 1,4-conjugate addition reaction above. The crude reaction mixture was purified via flash column chromatography with a 100% ethyl acetate as eluent on silica gel. HPLC Chiralpak ID (hexane/EtOH/Et₃N = 70:29.5:0.5, 1.0 mL/min, UV-230 detector). Trial 1: 38.8 mg, 0.188 mmol, 94% yield; 96:4 er (with cat. **107**, 1.3 eq of boronic acid). Trial 2: 37 mg, 0.180 mmol, 90% yield; 96:4 er (with cat. **107**, 1.3 eq of boronic acid). ^1H NMR (400 MHz, CDCl_3) δ 6.85 (d, $J=0.92$ Hz, 1H), 6.70 (d, $J=1.5$ Hz, 1H), 5.08 (dm, $J=9.6$, 1H), 4.14 (ddd, $J=10.0, 8.2, 5.9$ Hz, 1H), 3.54 (s, 3H), 3.32 (dd, $J=17.4, 8.2$ Hz, 1H), 2.69 (dd, $J=17.4, 5.5$ Hz, 1H), 2.12 (s, 3H), 1.74 (d, $J=1.4$ Hz, 3H), 1.65 (d, $J=1.4$ Hz, 3H). ^{13}C NMR (100 MHz, CDCl_3) δ 207.6, 149.8, 132.8, 126.9, 124.5, 120.6, 47.6, 32.6, 31.7, 30.8, 25.7, 18.2. HR-MS-ESI m/z : $[\text{M}+\text{H}]$, calculated for $\text{C}_{12}\text{H}_{19}\text{N}_2\text{O}$ 207.1492, found 207.1492. IR (neat) 2976, 2927, 1713, 1492, 1363, 1156, 1133, 726 cm^{-1} .

2.5.7.27. Synthesis of 6-methyl-4-(2,4,6-trimethoxyphenyl)hept-5-en-2-one (136)



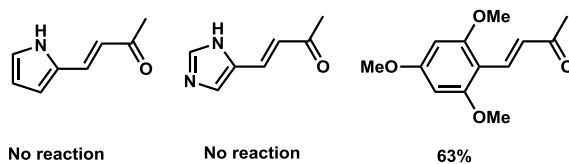
See the general procedure for 1,4-conjugate addition reaction above. 2 equivalent of boronic acid was used. The crude reaction mixture was purified via column chromatography with a 10% ethyl acetate in hexanes as eluent on silica gel. Trial 1: 50.6 mg, 0.173 mmol, 86% yield; 98:2 er (with catalyst **100**, 4h, 47.4 mg of starting material). Trial 2: 44.1 mg, 0.151 mmol, 75% yield; 88:12 er (with catalyst **10d**, 4h, 47.2 mg of starting material). Trial 3: 53.7 mg, 0.184 mmol, 92% yield; 97:3 er (with catalyst **107**, 1h, 47.3 mg of starting material). Trial 4: 58 mg, 0.198 mmol, 99% yield; 99:1 er (with catalyst **10e**, 1h, 47.1 mg of starting material). $^1\text{H NMR}$ (400 MHz, CDCl_3) δ 6.09 (s, 2H), 5.49 (app.d., $J= 9.6$ Hz, 1H), 4.65 (q, $J= 7.8$ Hz, 1H), 3.80 (s, 6H), 3.77 (s, 3H), 2.87 (dd, $J= 15.1, 7.8$ Hz, 1H), 2.78 (dd, $J= 14.6, 6.8$ Hz, 1H), 2.04 (s, 3H), 1.67 (s, 3H), 1.62 (s, 3H). $^{13}\text{C NMR}$ (100 MHz, CDCl_3) δ 209.5, 159.4, 158.6, 131.2, 126.8, 113.0, 91.2, 55.8, 55.3, 48.5, 30.1, 30.0, 25.9, 17.9. IR (neat): 1709, 1605, 1591, 1458, 1418, 1224, 1204, 1149, 1115, 814 cm^{-1}

2.5.8. General procedure for cuprate conjugate addition



To a flame dried flask equipped with stir bar was added $\text{CuBr}\cdot\text{Me}_2\text{S}$ and 4ml THF. The temperature was then cooled down to -78 °C. 2-Methyl-1-propenylmagnesium bromide was added dropwise and the reaction mixture was then allowed to stir at that

temperature for 30 minutes. A solution of enone (2 mmol in 5ml THF) was added via cannula and stirred for 30 minutes. After then, the reaction mixture was warmed up to R.T., quenched with 2N HCl and extracted with Et₂O. The organic layer was dried over MgSO₄ and concentrated via rotary evaporation. The crude product was purified via flash column chromatography on silica gel with appropriate eluents.¹⁰



2.6. References

1. Previously published in Nguyen, T. S.; Le, P. Q.; May, J. A. *Org. Lett.* **2012**, *14*, 6104—6107.
2. Chandraratna; Roshantha A. U.S.Patent 5, *113*, **1995**.
3. (a) Robinson, C. N.; Leonard J. Wiseman, L. J; Slater, C. D. *Tetrahedron* **1989**, *45*, 4103—4112; (b) Benington, F.; Morin, R. D.; Khaled, M. A. *Synthesis* **1984**, *7*, 619—620.
4. Pizzirani, D.; Roberti, M.; Grimaudo, S.; Cristina, A. D.; Pipitone, R. M.; Tolomeo, M.; Recanatini, M. *J. Med. Chem.* **2009**, *52*, 6936—6940.
5. Goldys, A.; McErlean, C. S. P. *Tetrahedron Lett.* **2009**, *50*, 3985—2987.
6. Wu, T. R.; Shen, L.; Chong, J. M. *Org. Lett.* 2004, *6*, 2701—2704.
7. Momiyama, N.; Nishimoto, H.; Terada, M. *Org. Lett.* **2011**, *13*, 2126—2129.
8. Cammidge, A.; Crepy, K. *J. Org. Chem.* **2003**, *68*, 6832—6835.
9. Brown, H. C.; Bhat, N. G.; Srebnik, M. *Tetrahedron Lett.* **1988**, *22*, 2631—2634.

10. Bhat V.; Allan K.M.; Rawal V.H. *J. Am.Chem.Soc.* **2011**, *133*, 5798—5801.

APPENDIX ONE

Spectra relevant to Chapter 2:

BINOL-catalyzed asymmetric of chiral heterocycles

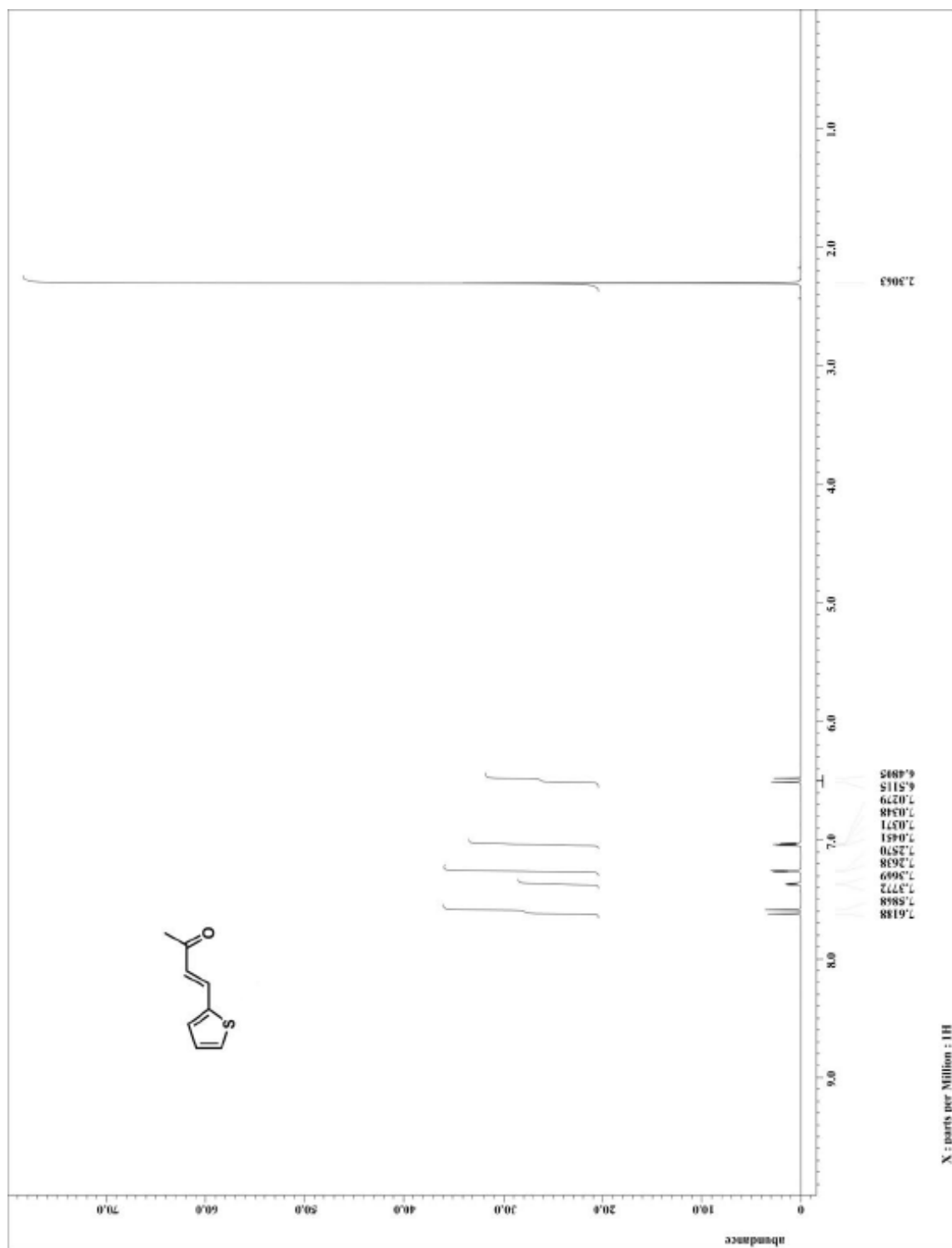


Figure A.1.1. $^1\text{H NMR}$ for compound 102

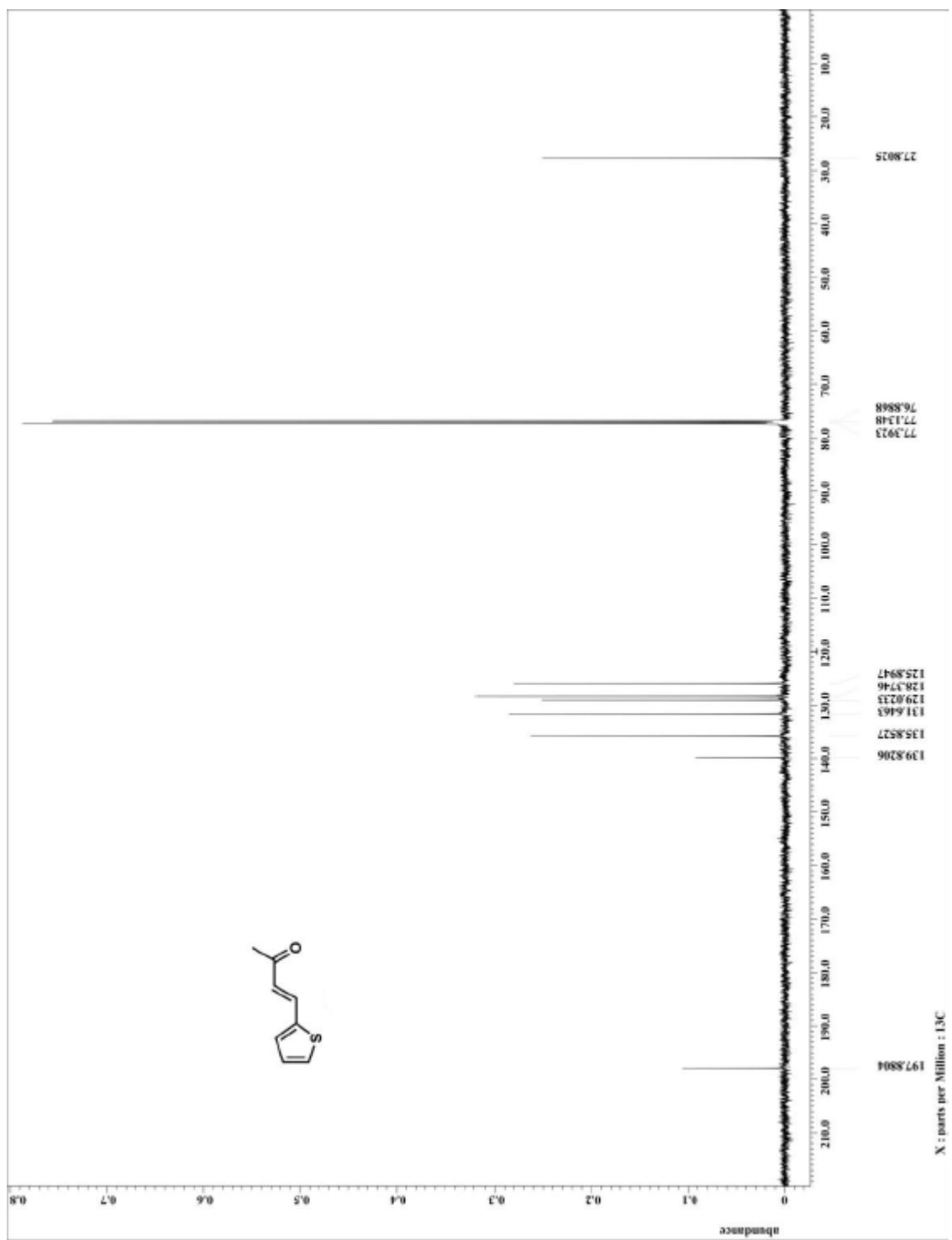


Figure A.1.2. ^{13}C NMR for compound 102

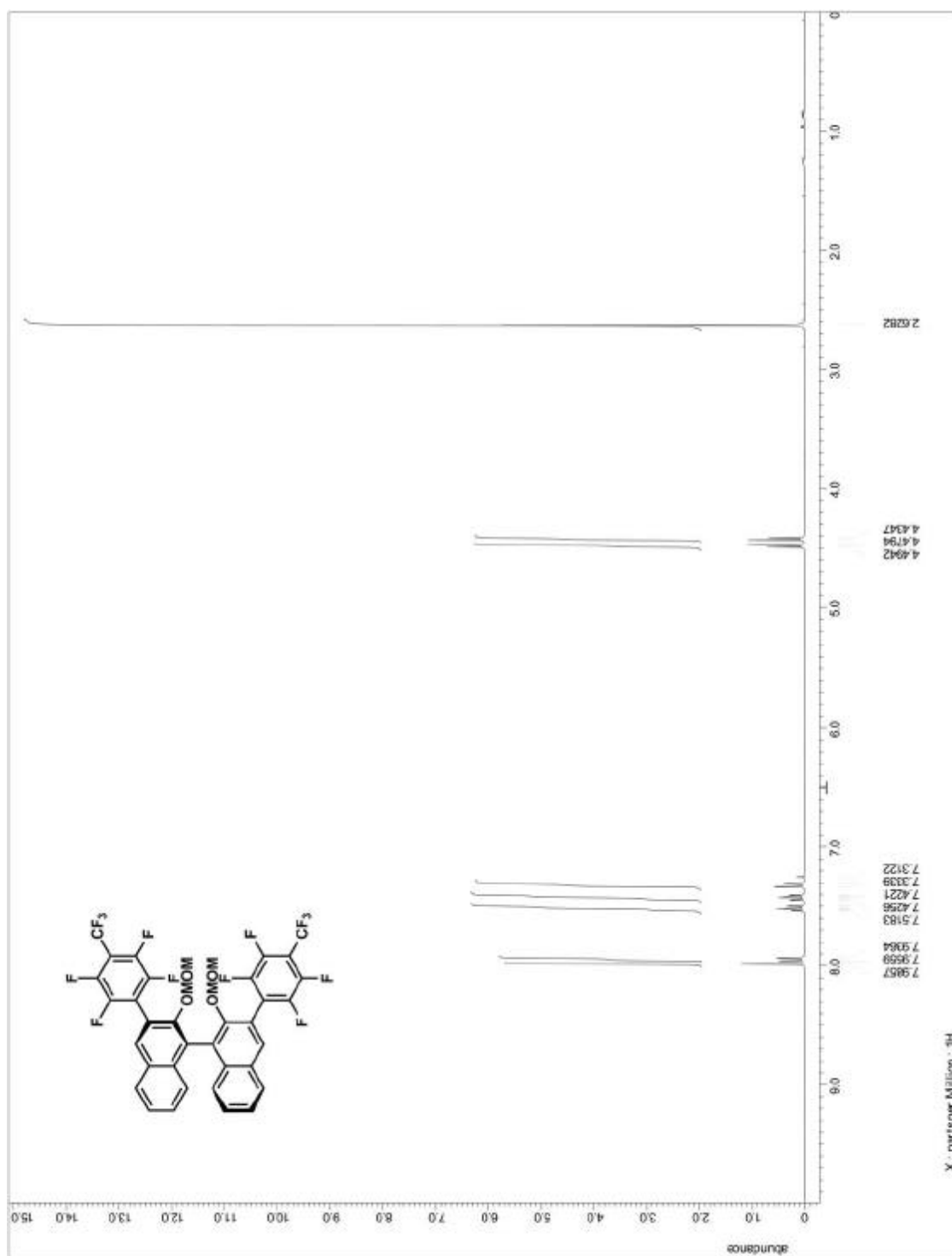


Figure A.1.3. ^1H NMR for precursor to compound 107

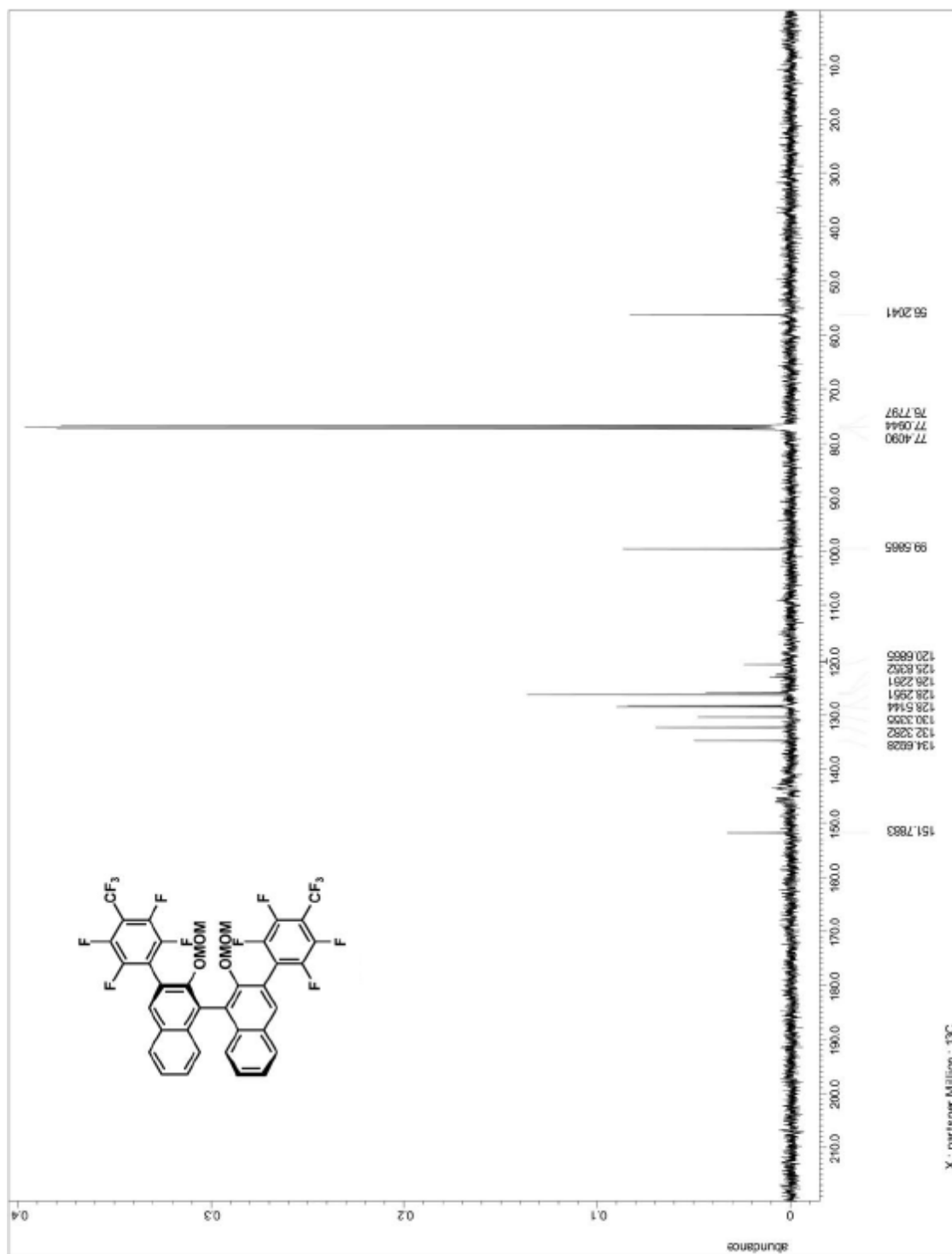


Figure A.1.4. ^{13}C NMR for precursor to compound 107

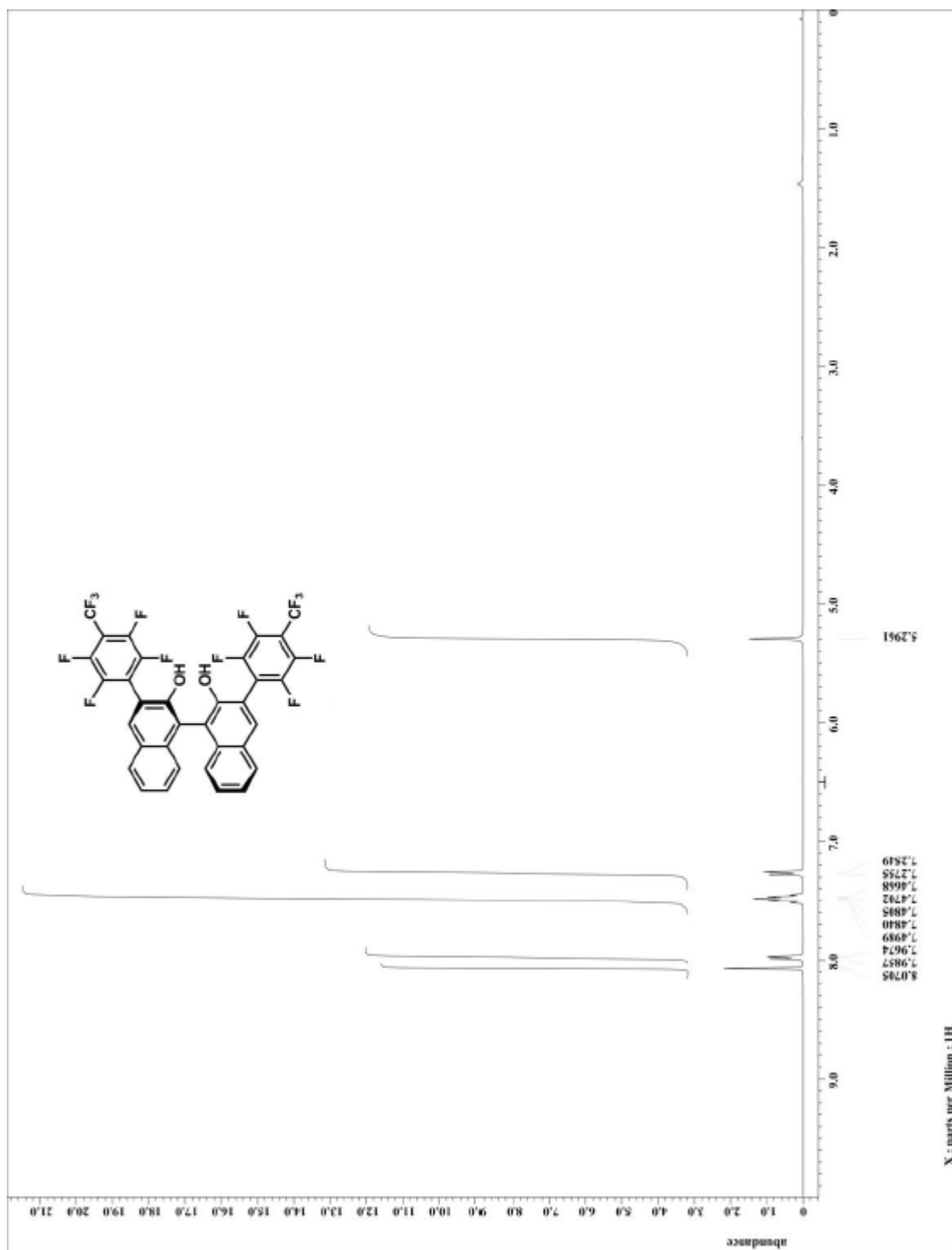


Figure A.1.5. ^1H NMR for compound 107

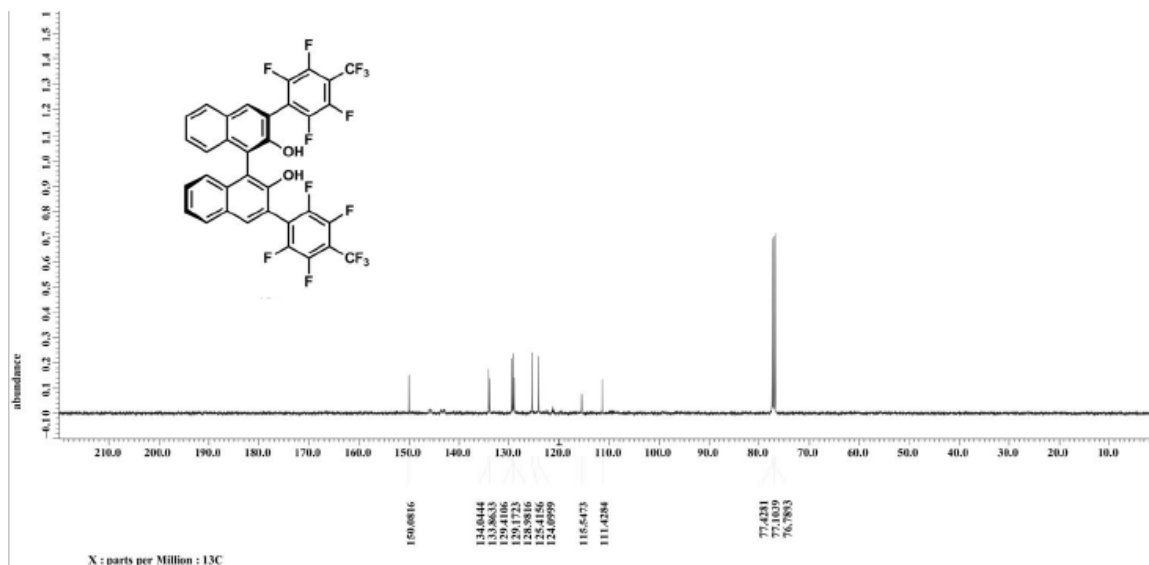


Figure A.1.6. ^{13}C NMR for compound 107

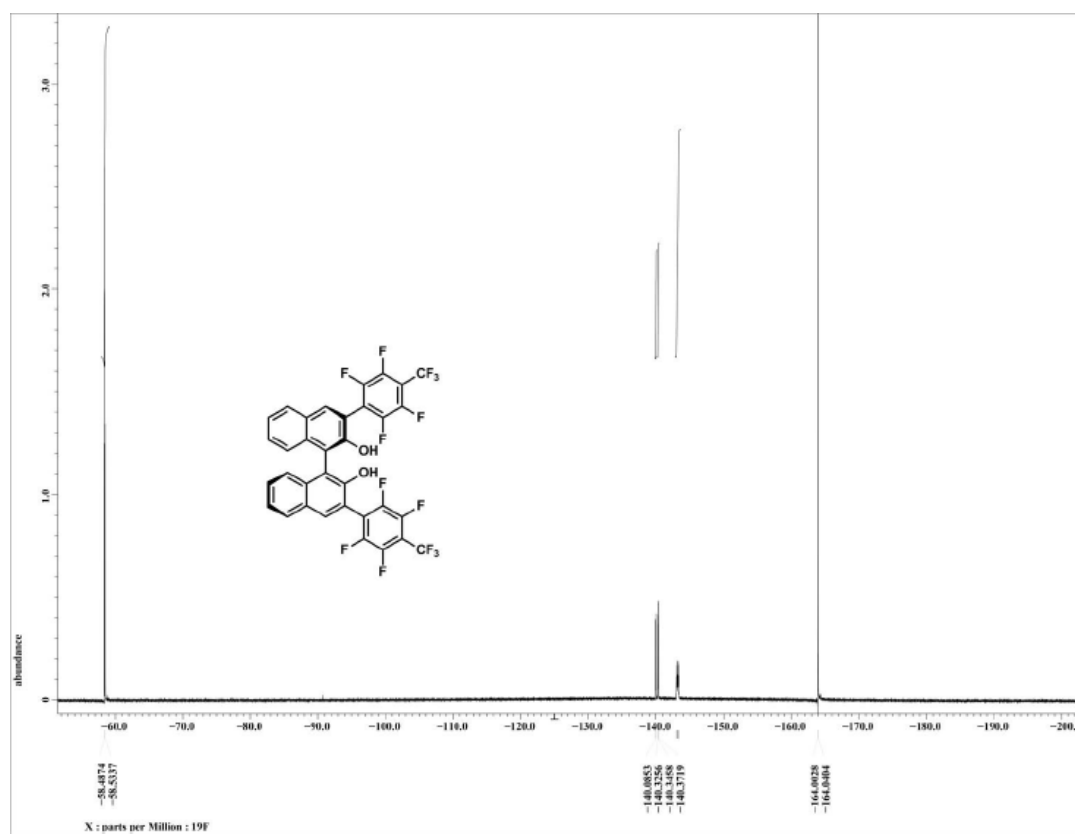


Figure A.1.7. ^{19}F NMR for compound 107

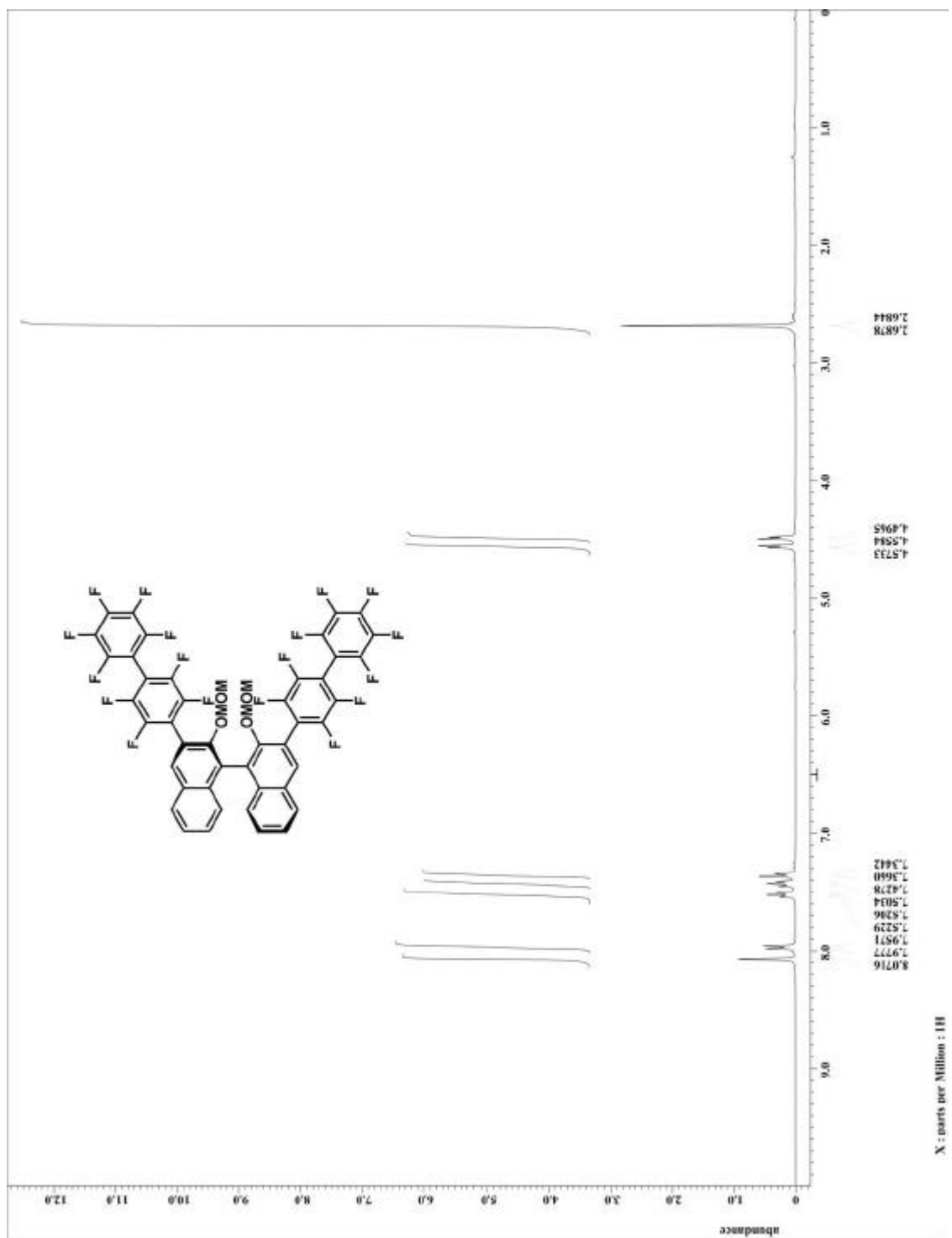


Figure A.1.8. ^1H NMR for precursor to compound 108

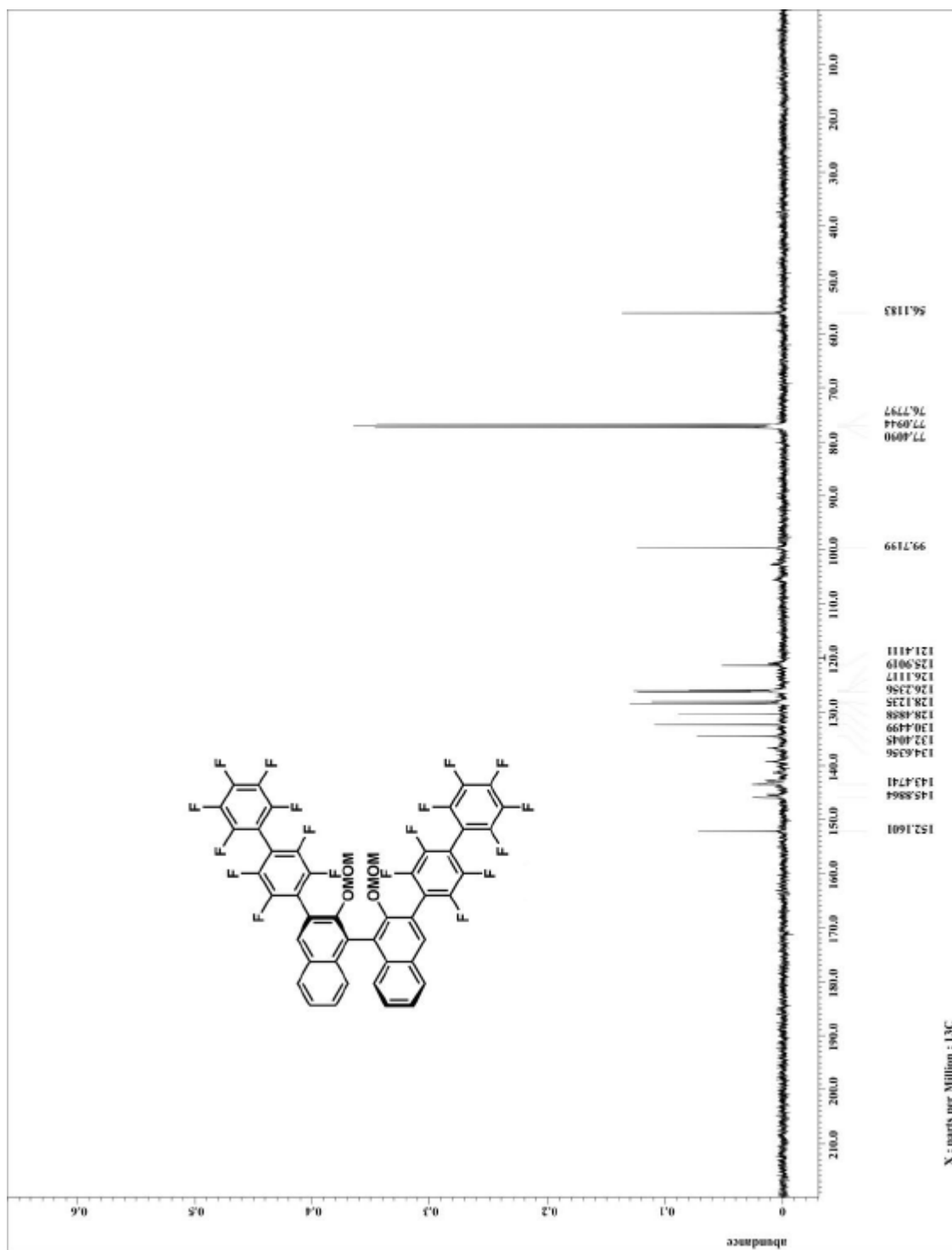


Figure A.1.9. ^{13}C NMR for precursor to compound 108

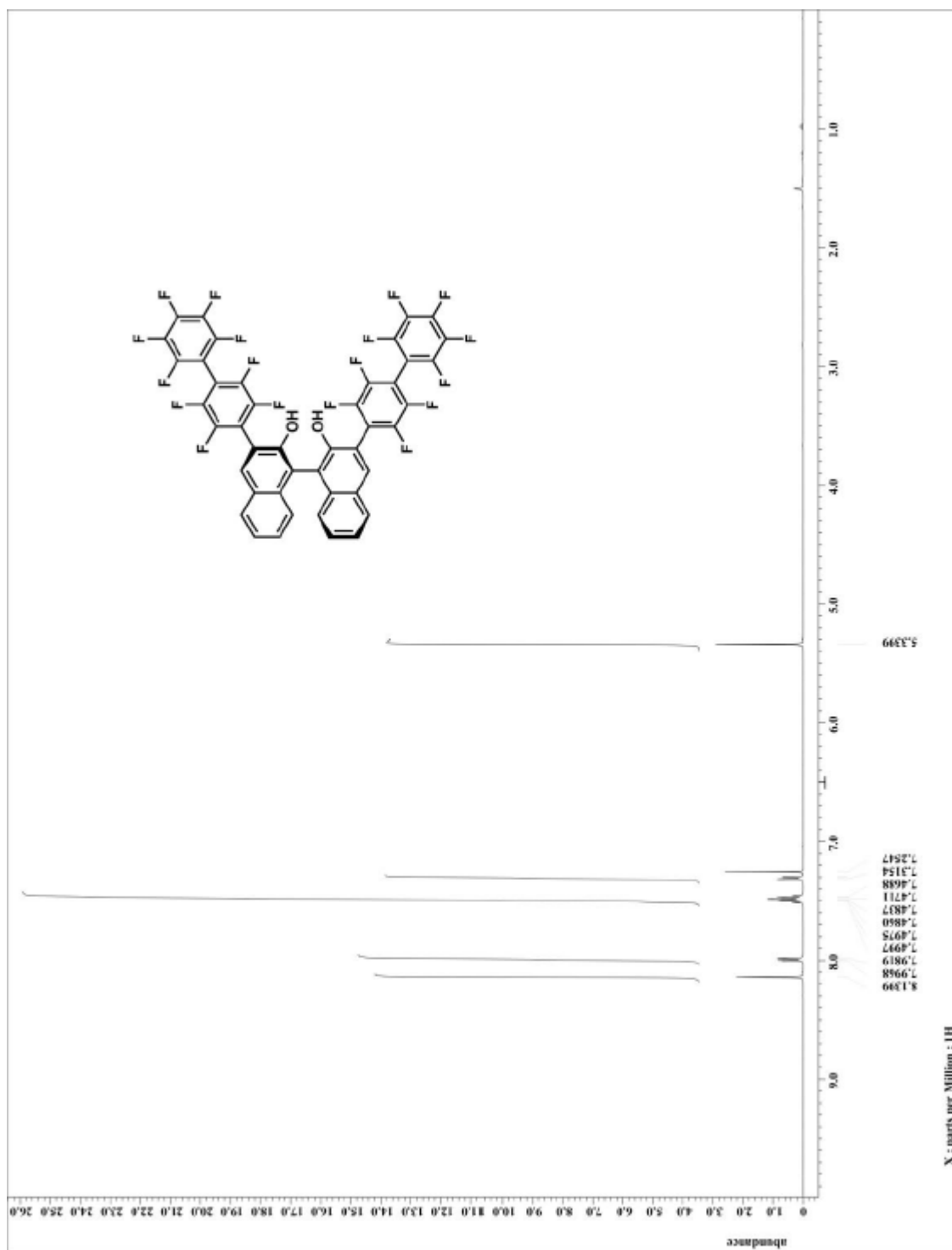


Figure A.1.10. ^1H NMR for compound 108

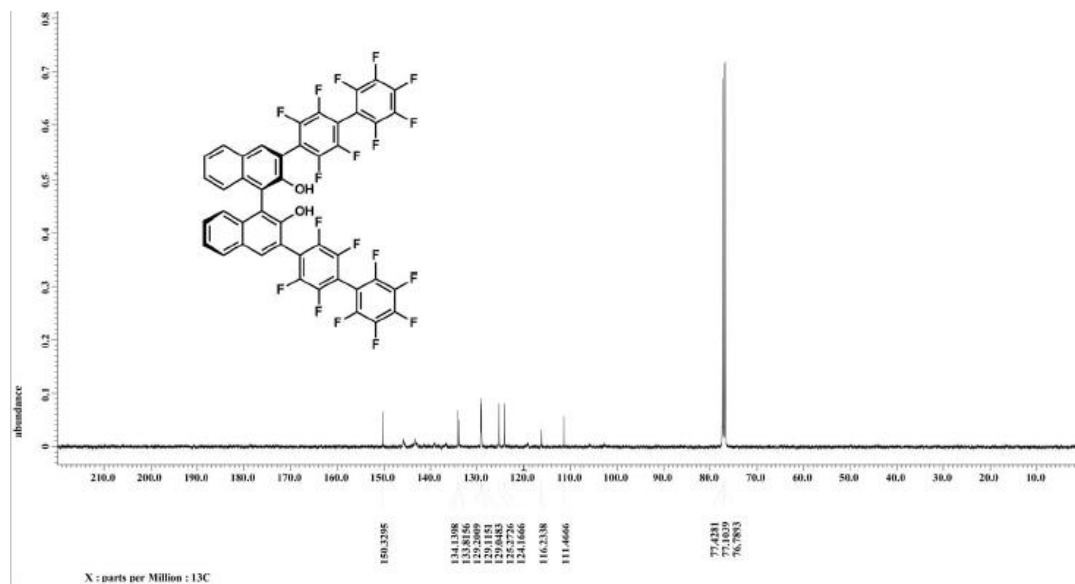


Figure A.1.11. ^{13}C NMR for compound 108

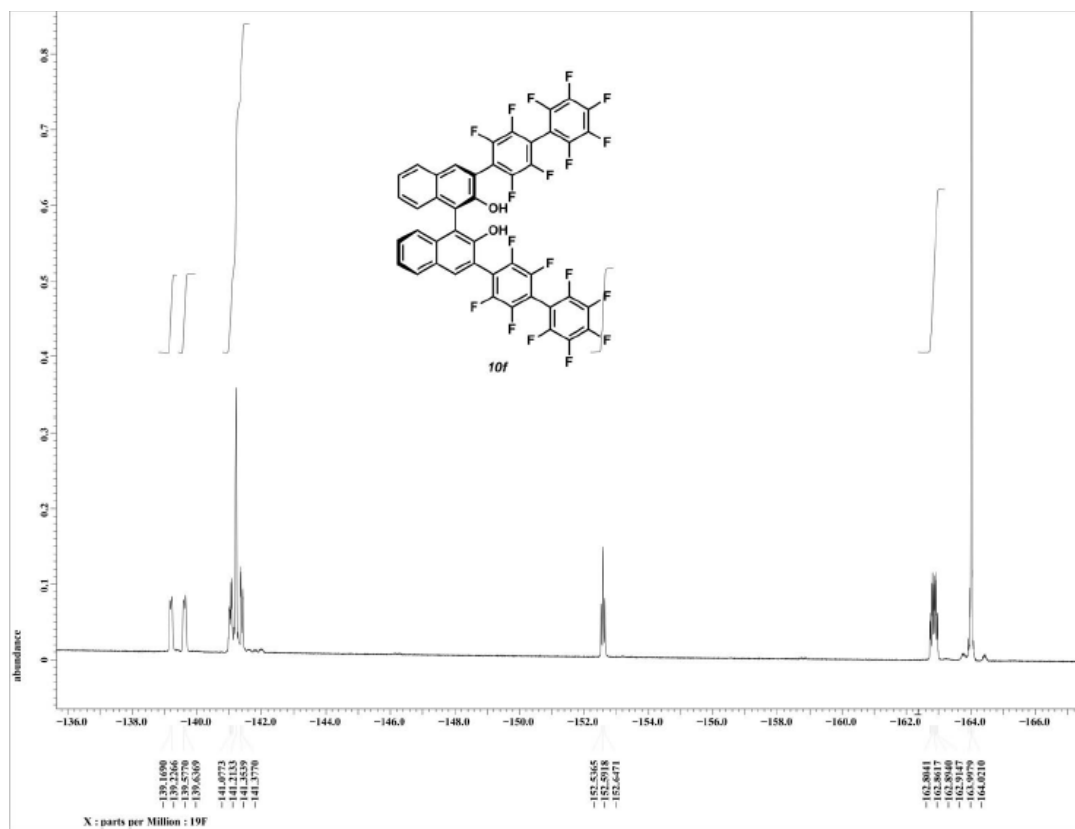


Figure A.1.12. ^{19}F NMR for compound 108

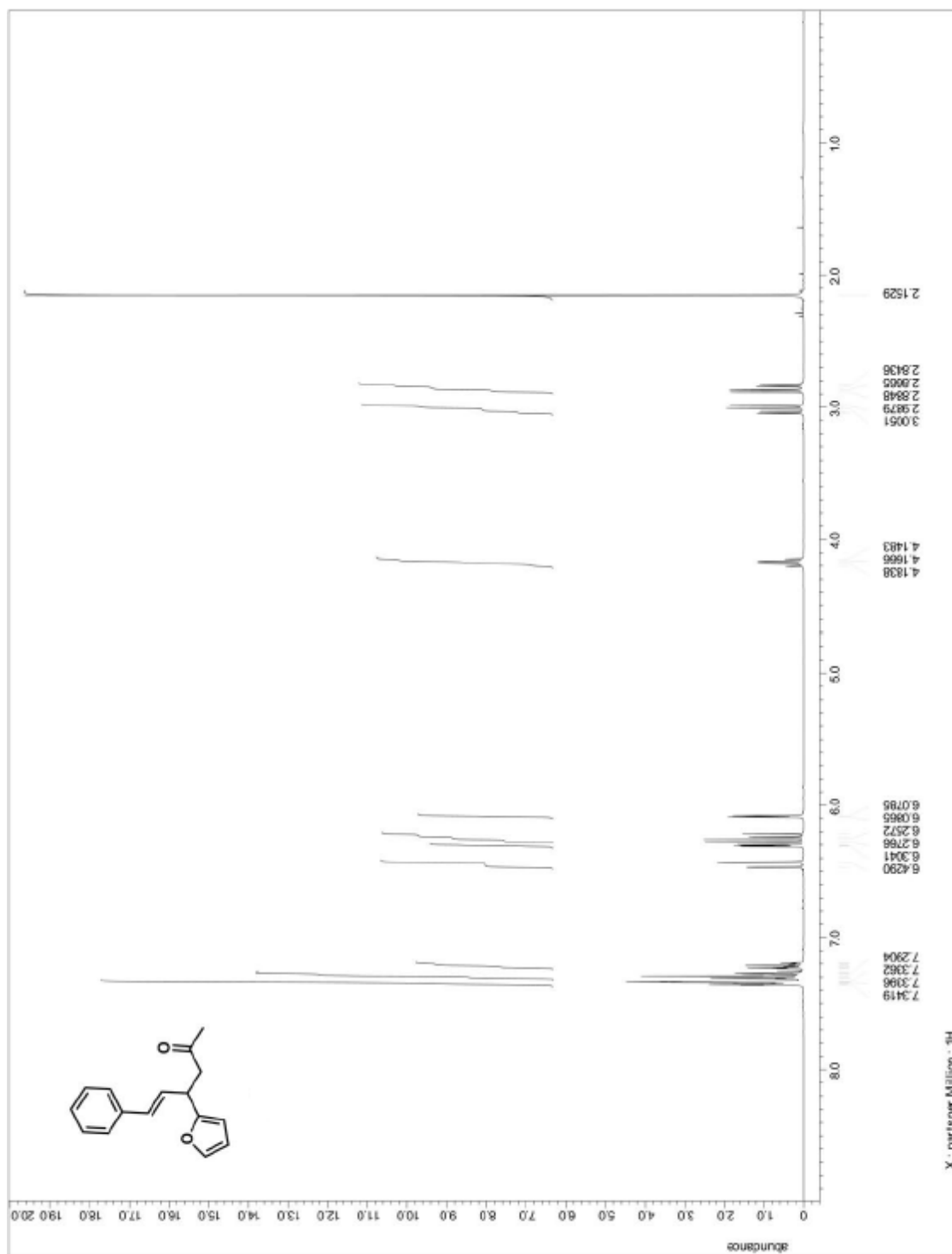


Figure A.1.13. ^1H NMR for compound 109

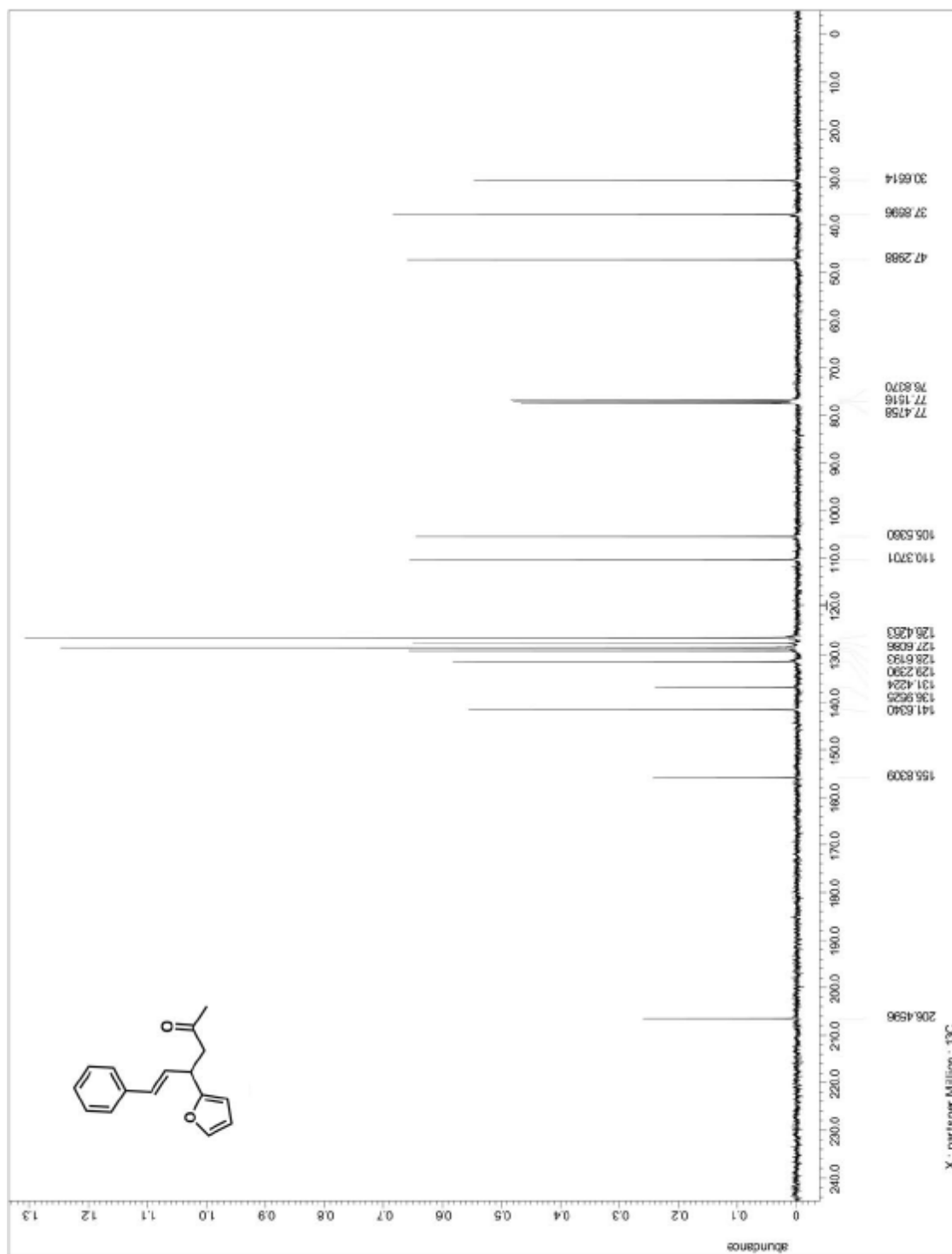
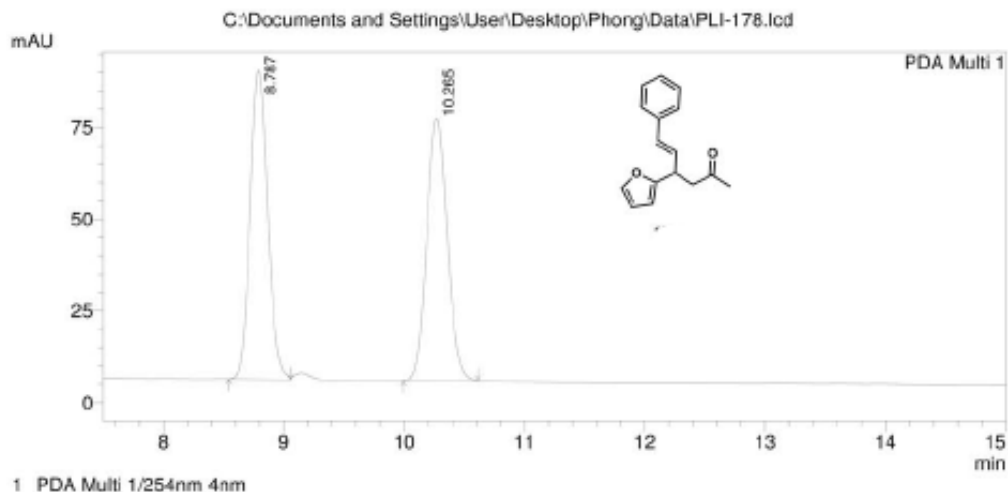


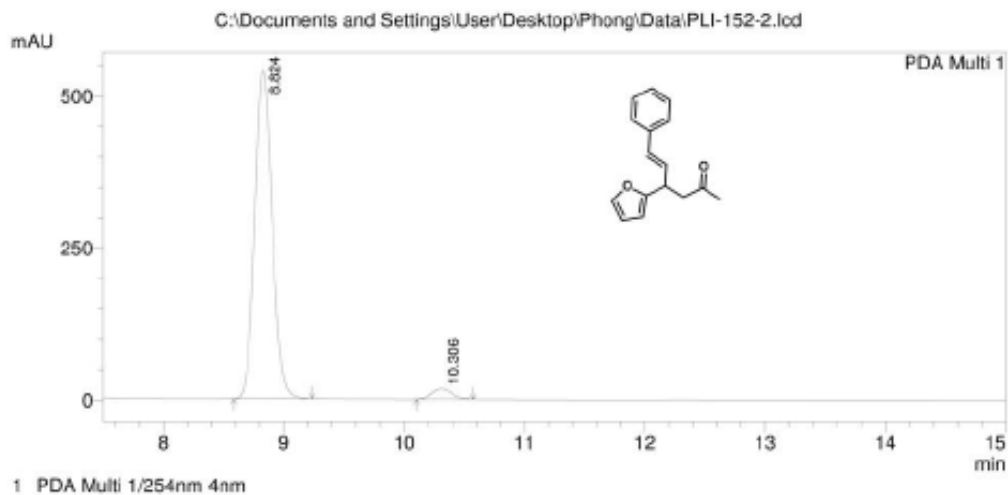
Figure A.1.14. ^{13}C NMR for compound 109



PeakTable

PDA Ch1 254nm 4nm

Peak#	Ret. Time	Area	Height	Area %	Height %
1	8.787	851065	84219	50.158	54.047
2	10.265	845695	71607	49.842	45.953
Total		1696759	155826	100.000	100.000



PeakTable

PDA Ch1 254nm 4nm

Peak#	Ret. Time	Area	Height	Area %	Height %
1	8.824	5392459	538892	96.555	96.940
2	10.306	192389	17012	3.445	3.060
Total		5584848	555904	100.000	100.000

Figure A.1.15. HPLC trace for compound 109

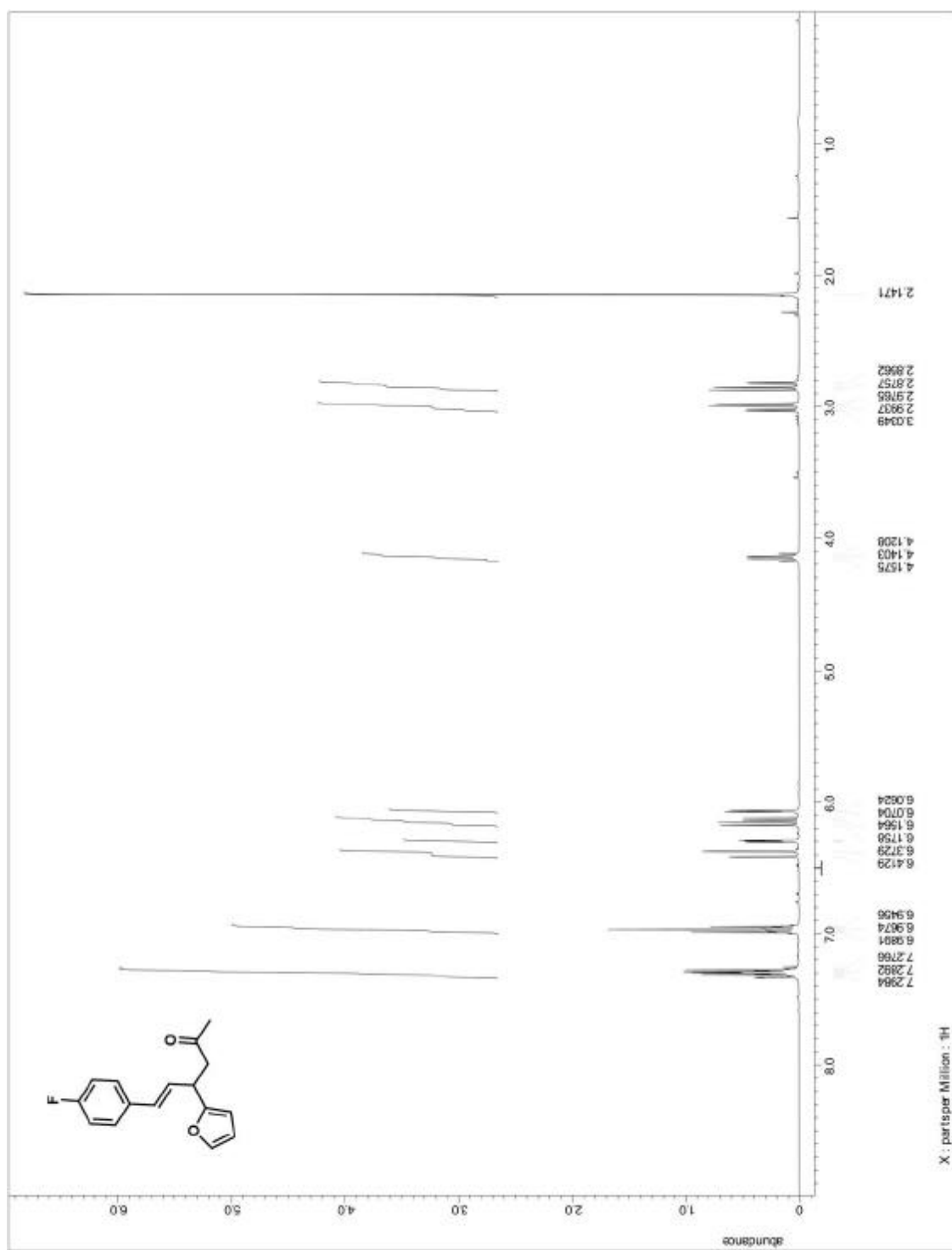


Figure A.1.16. ^1H NMR for compound 110

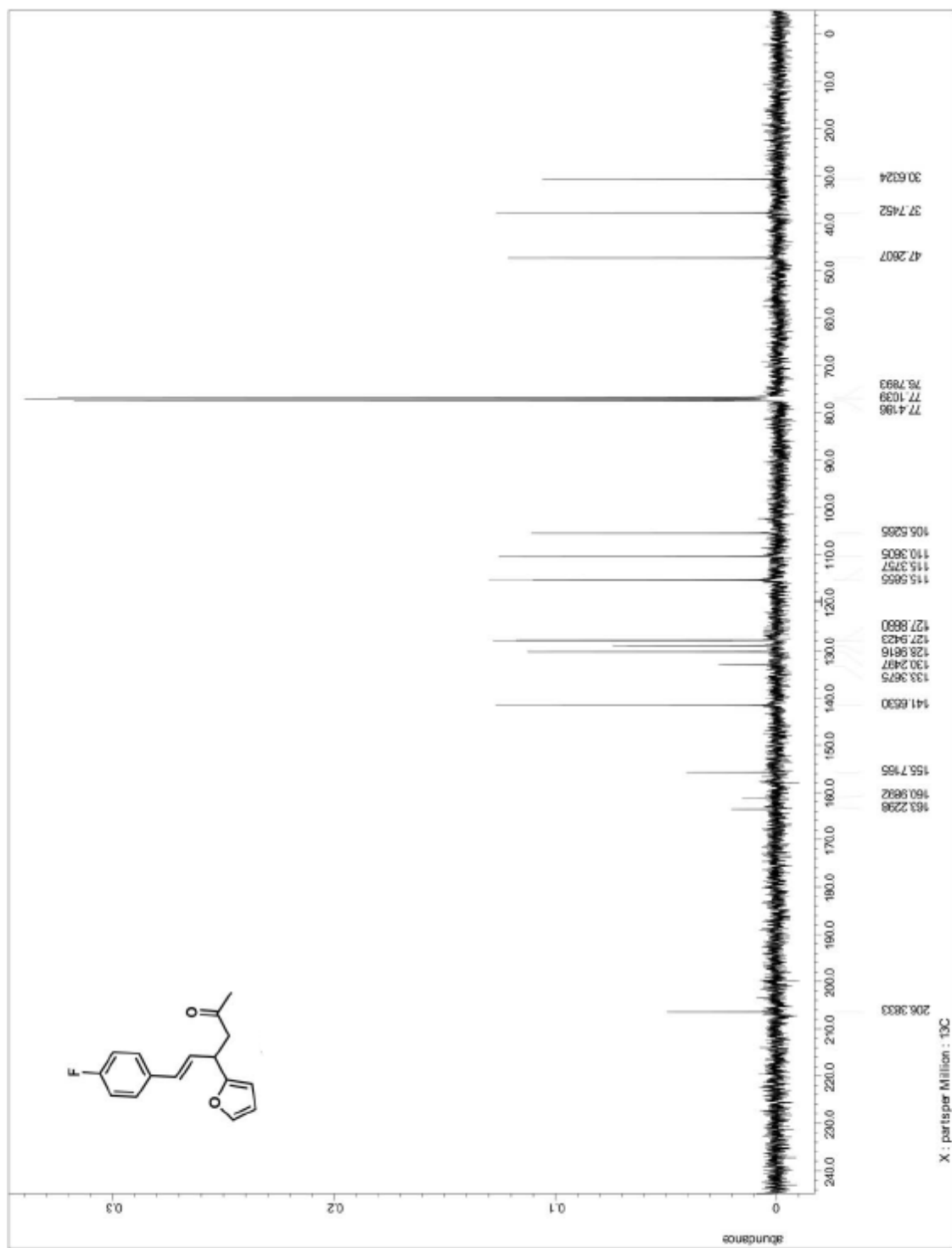
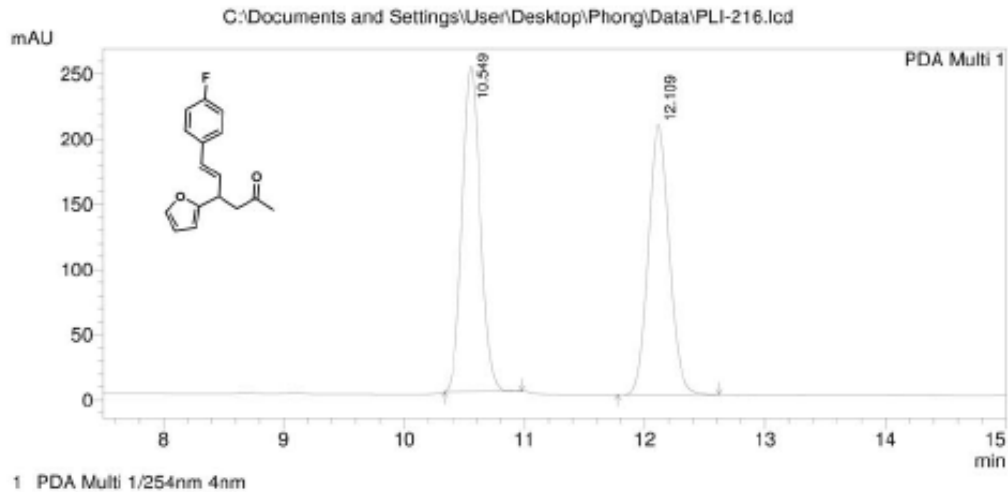
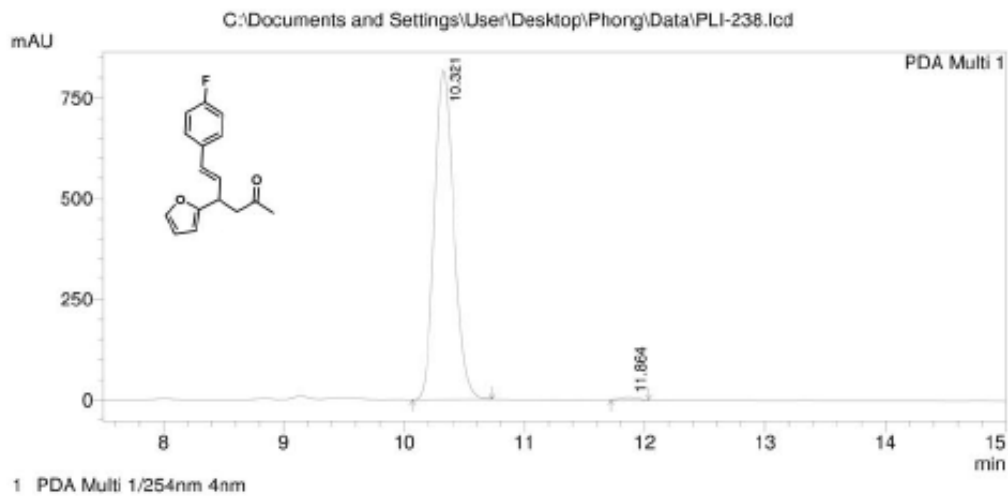


Figure A.1.17. ^{13}C NMR for compound 110



PeakTable

Peak#	Ret. Time	Area	Height	Area %	Height %
1	10.549	2621724	248724	51.083	54.595
2	12.109	2510590	206856	48.917	45.405
Total		5132314	455581	100.000	100.000



PeakTable

Peak#	Ret. Time	Area	Height	Area %	Height %
1	10.321	9134267	816771	99.314	99.197
2	11.864	63084	6609	0.686	0.803
Total		9197351	823380	100.000	100.000

Figure A.1.18. HPLC trace for compound 110

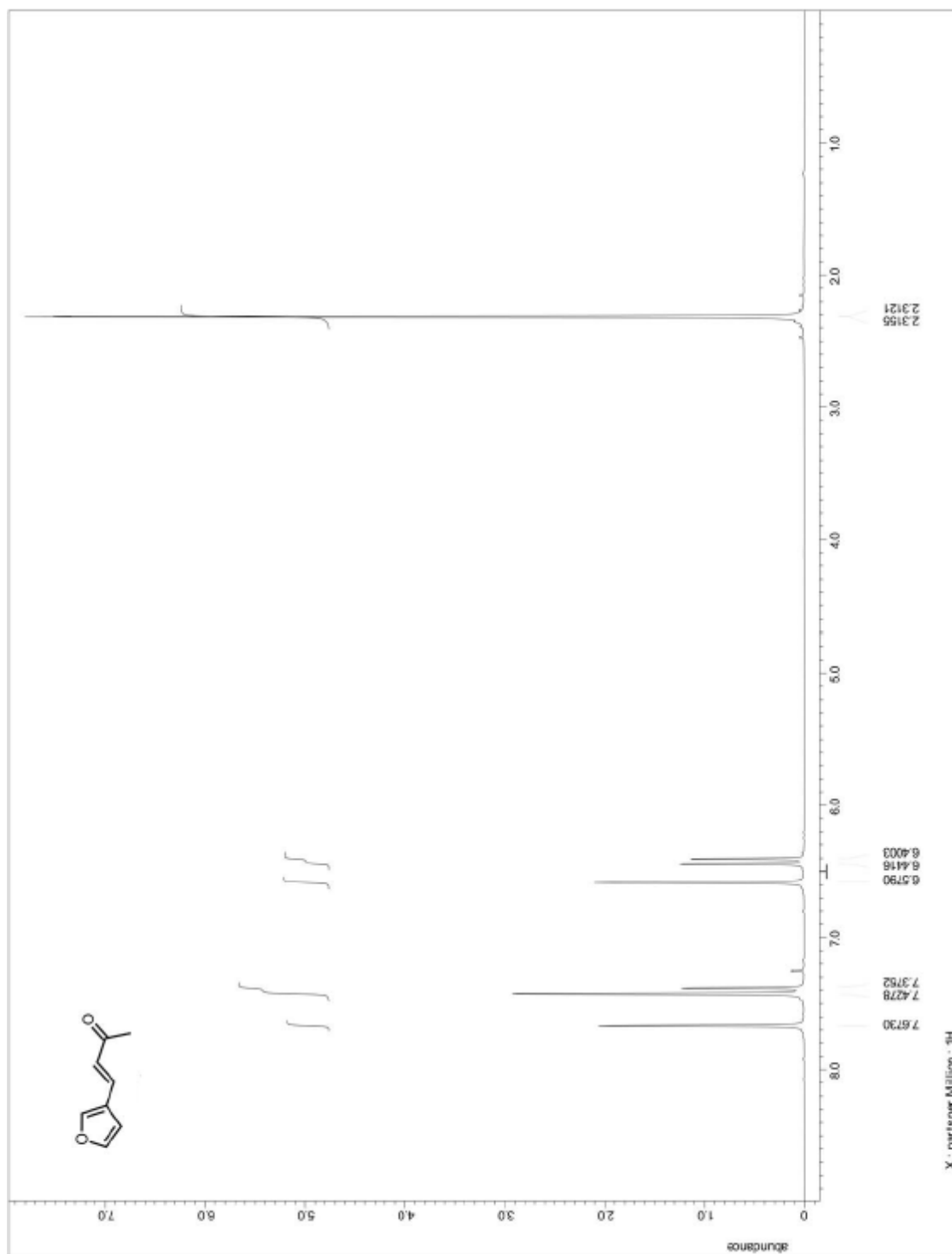


Figure A.1.19. ^1H NMR for precursor to compound 111

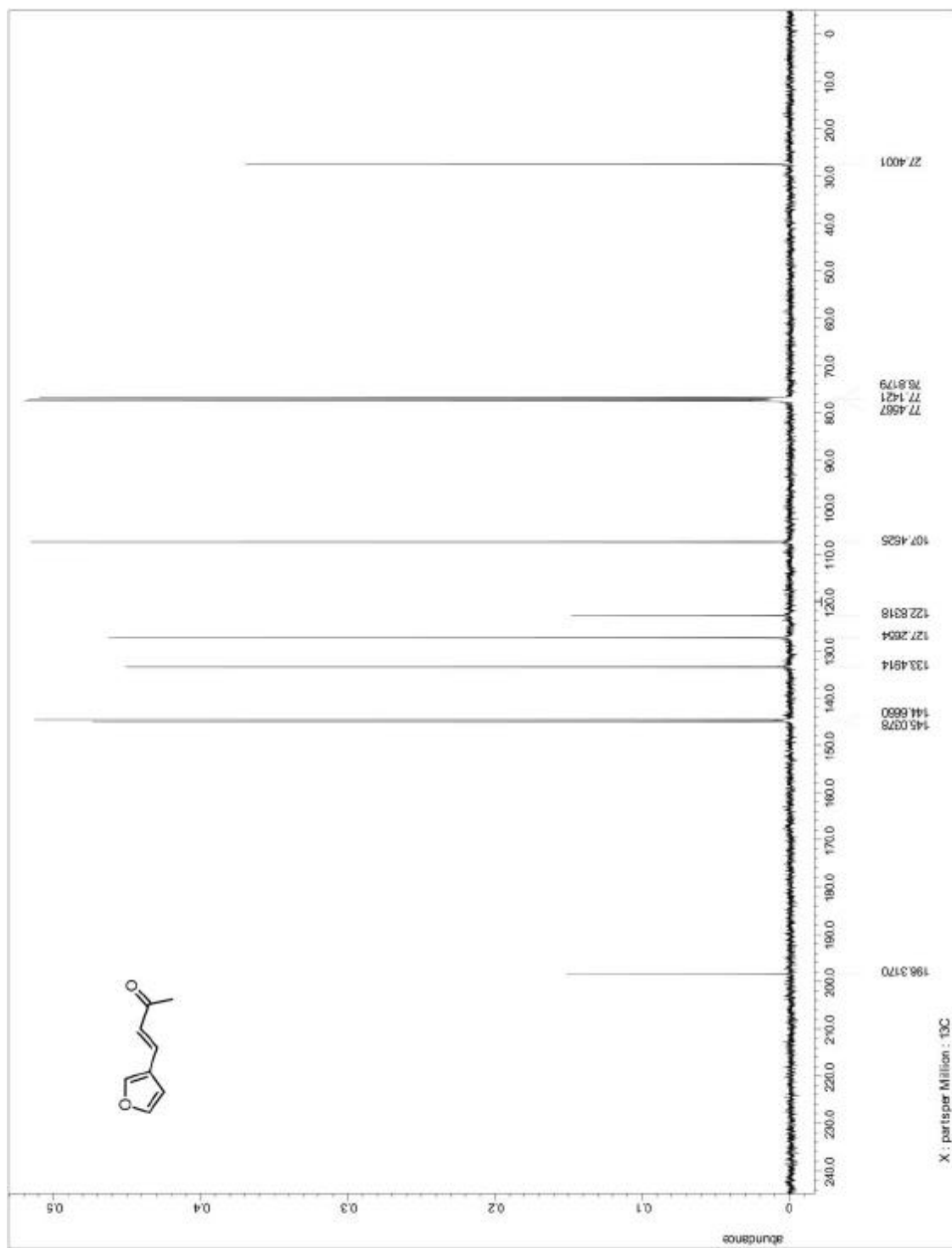


Figure A.1.20. ^{13}C NMR for precursor to compound 111

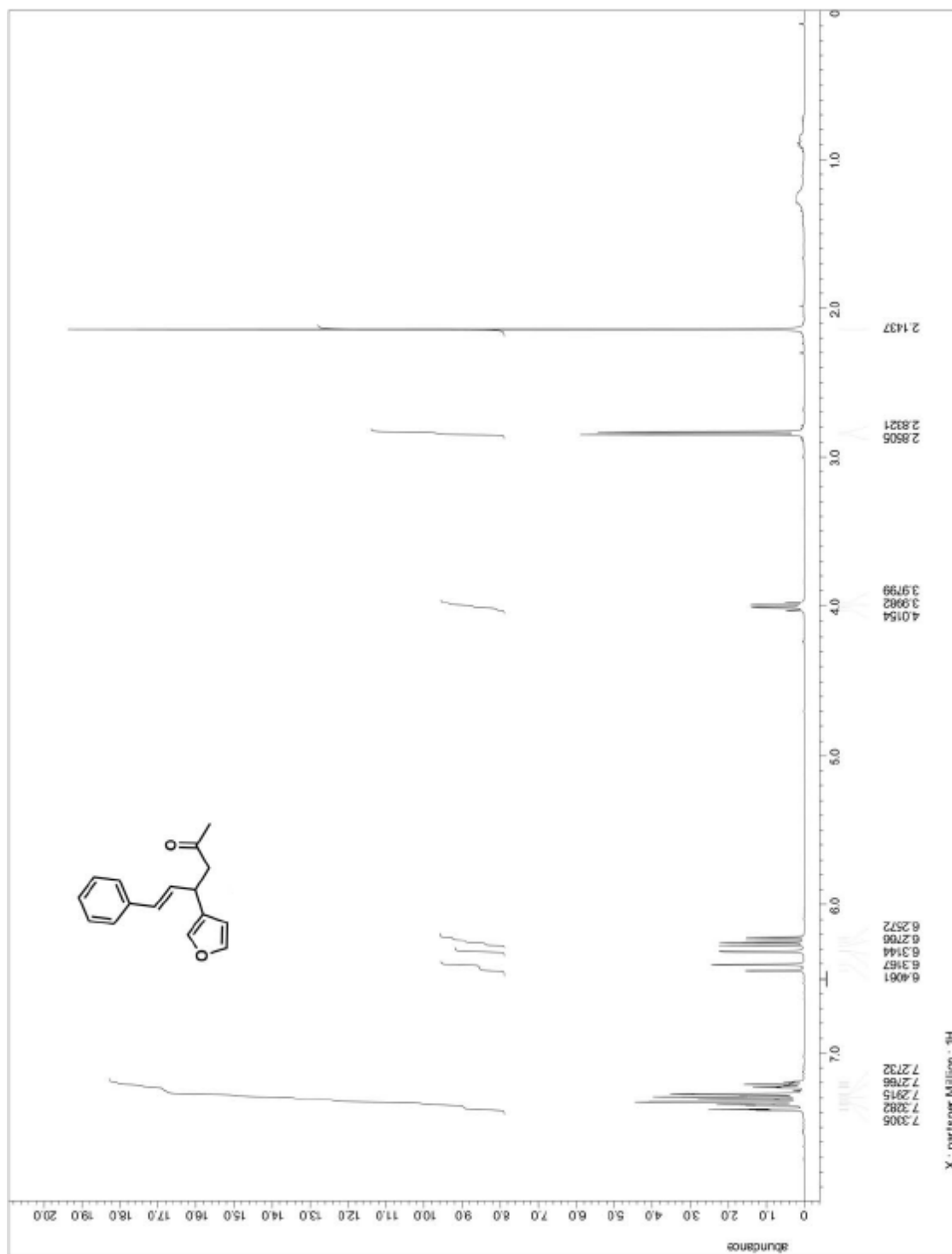


Figure A.1.21. ^1H NMR for compound 111

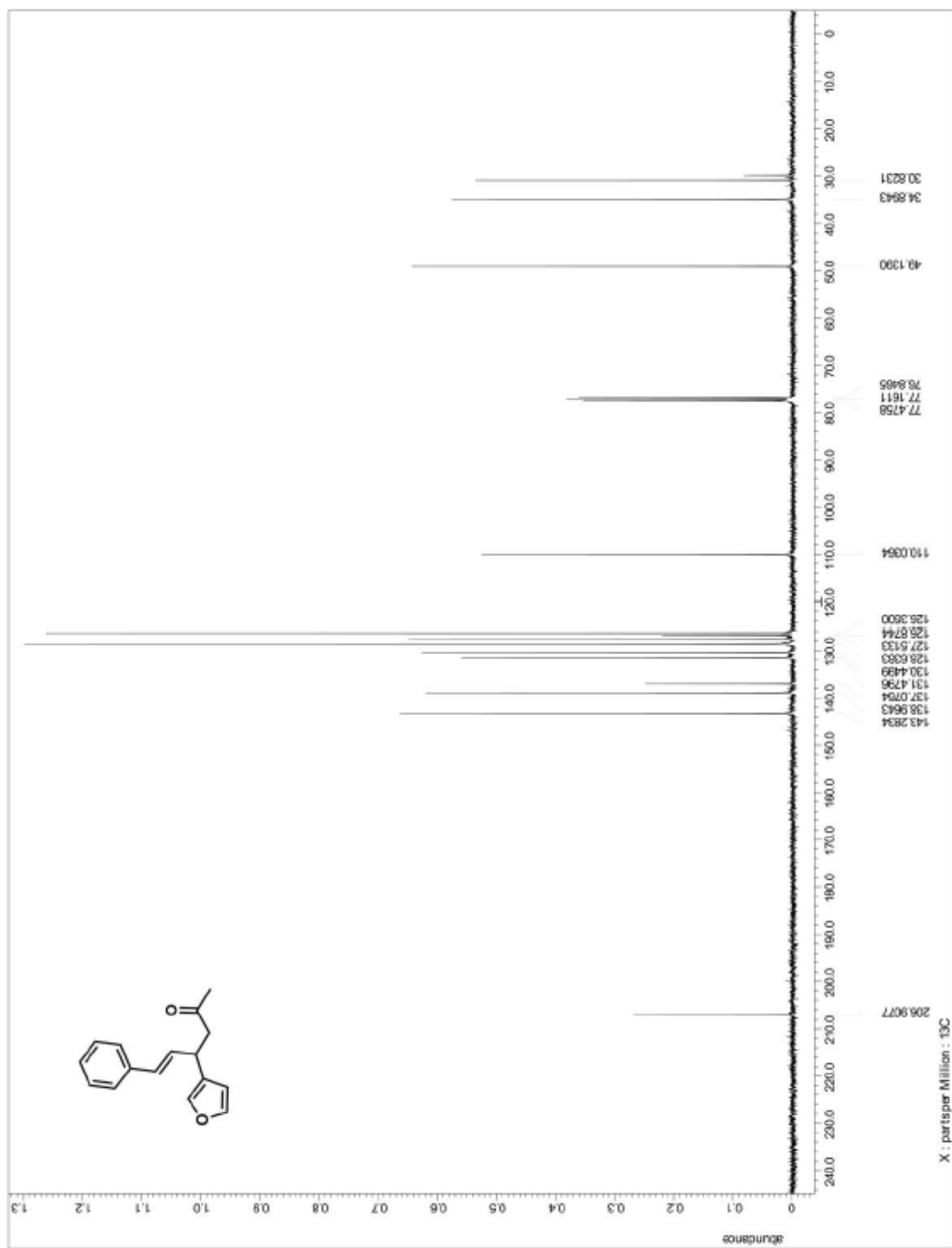
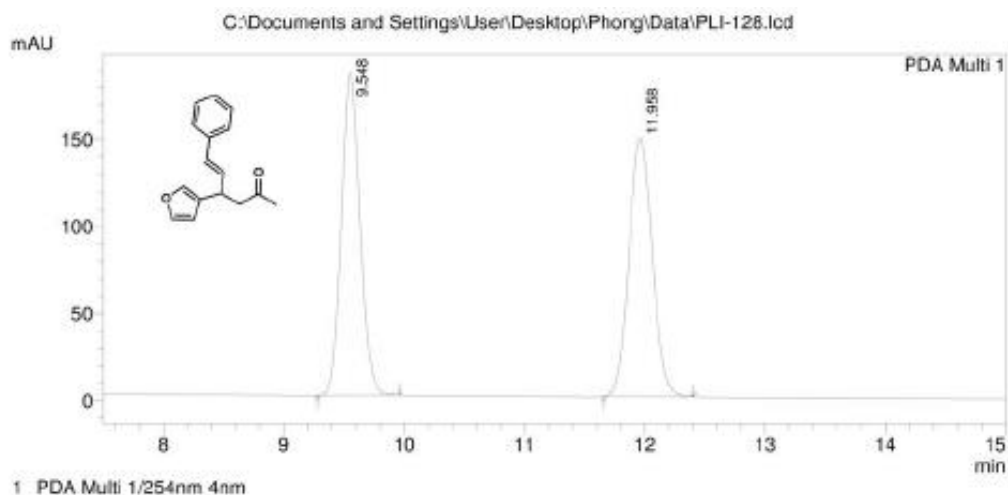
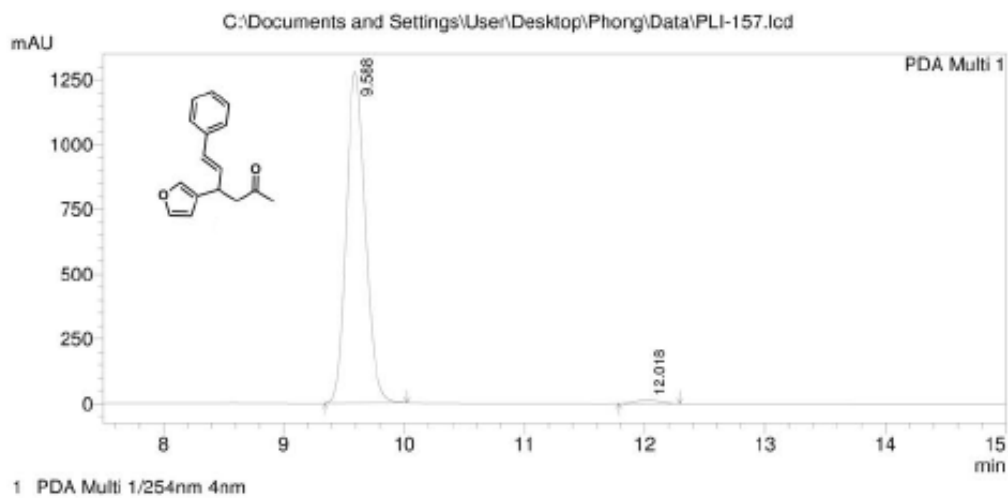


Figure A.1.22. ^{13}C NMR for compound 111



PeakTable

Peak#	Ret. Time	Area	Height	Area %	Height %
1	9.548	2005872	185246	50.054	55.508
2	11.958	2001537	148482	49.946	44.492
Total		4007409	333728	100.000	100.000



PeakTable

Peak#	Ret. Time	Area	Height	Area %	Height %
1	9.588	14092530	1274742	98.753	98.933
2	12.018	178013	13750	1.247	1.067
Total		14270543	1288492	100.000	100.000

Figure A.1.23. HPLC trace for compound 111

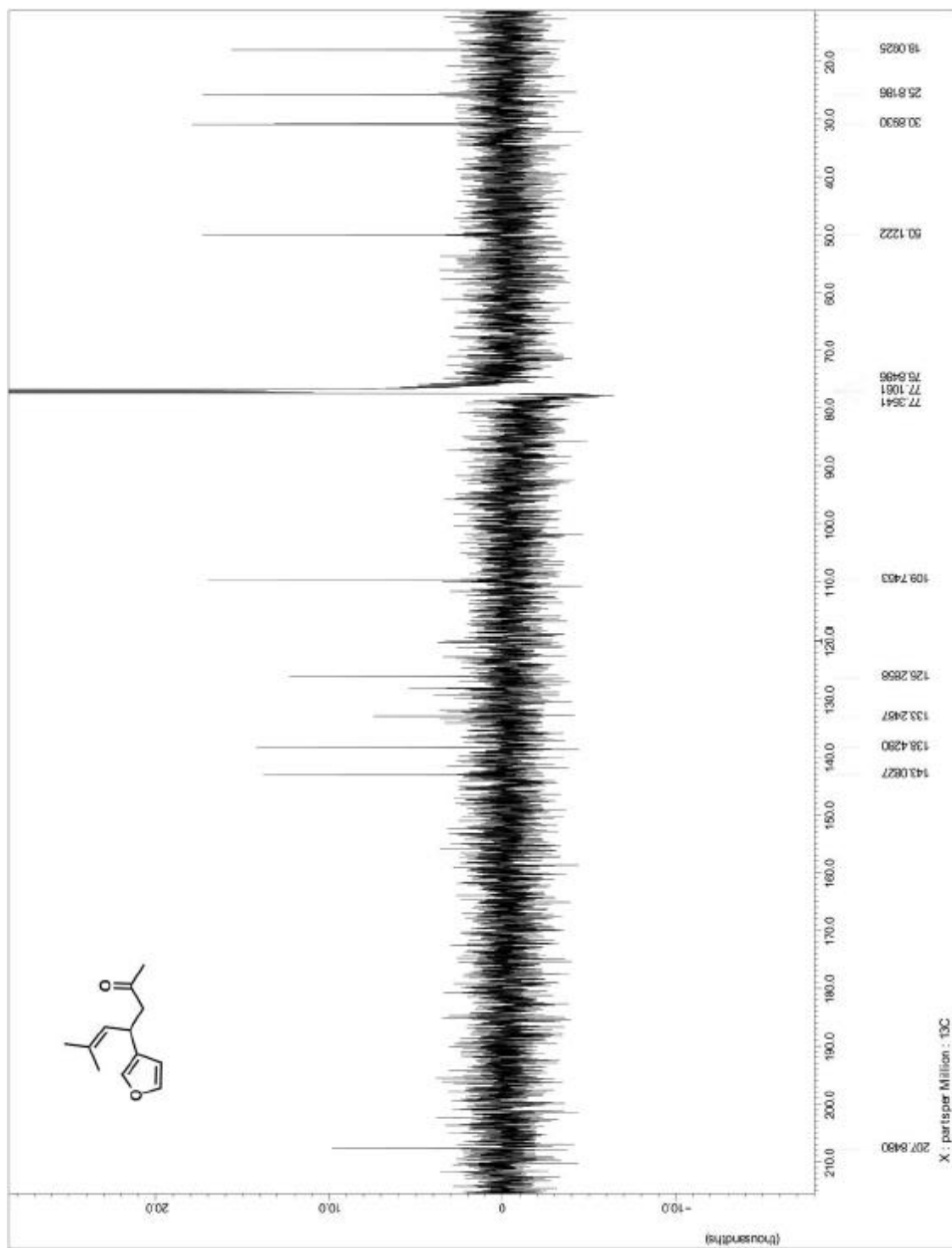
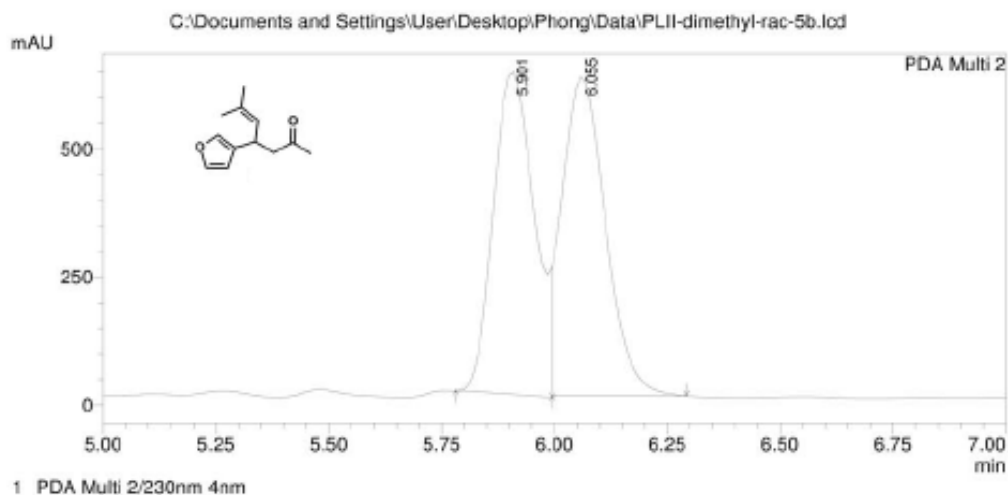
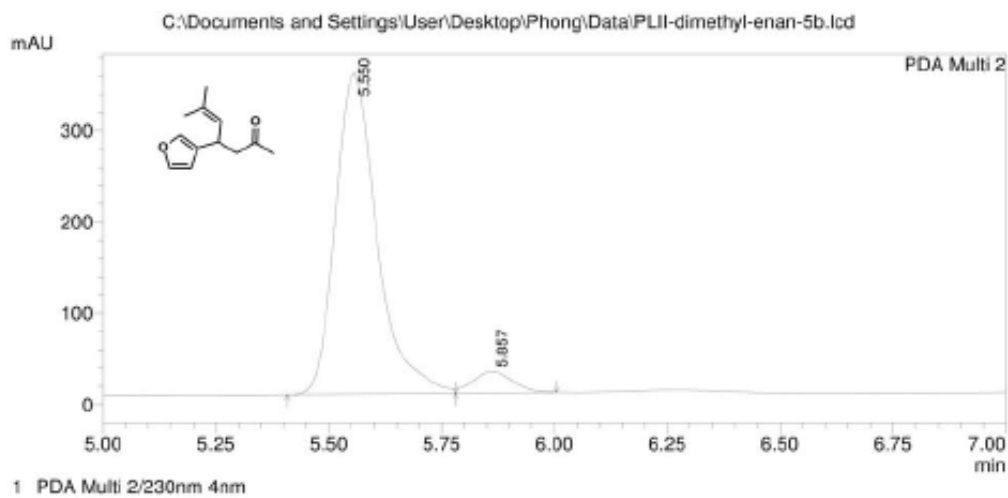


Figure A.1.25. ^{13}C NMR for compound 112



PeakTable

Peak#	Ret. Time	Area	Height	Area %	Height %
1	5.901	4065896	629375	50.001	50.236
2	6.055	4065661	623456	49.999	49.764
Total		8131557	1252831	100.000	100.000



PeakTable

Peak#	Ret. Time	Area	Height	Area %	Height %
1	5.550	2268350	352799	93.917	93.680
2	5.857	146920	23801	6.083	6.320
Total		2415270	376600	100.000	100.000

Figure A.1.26. HPLC trace for compound 112

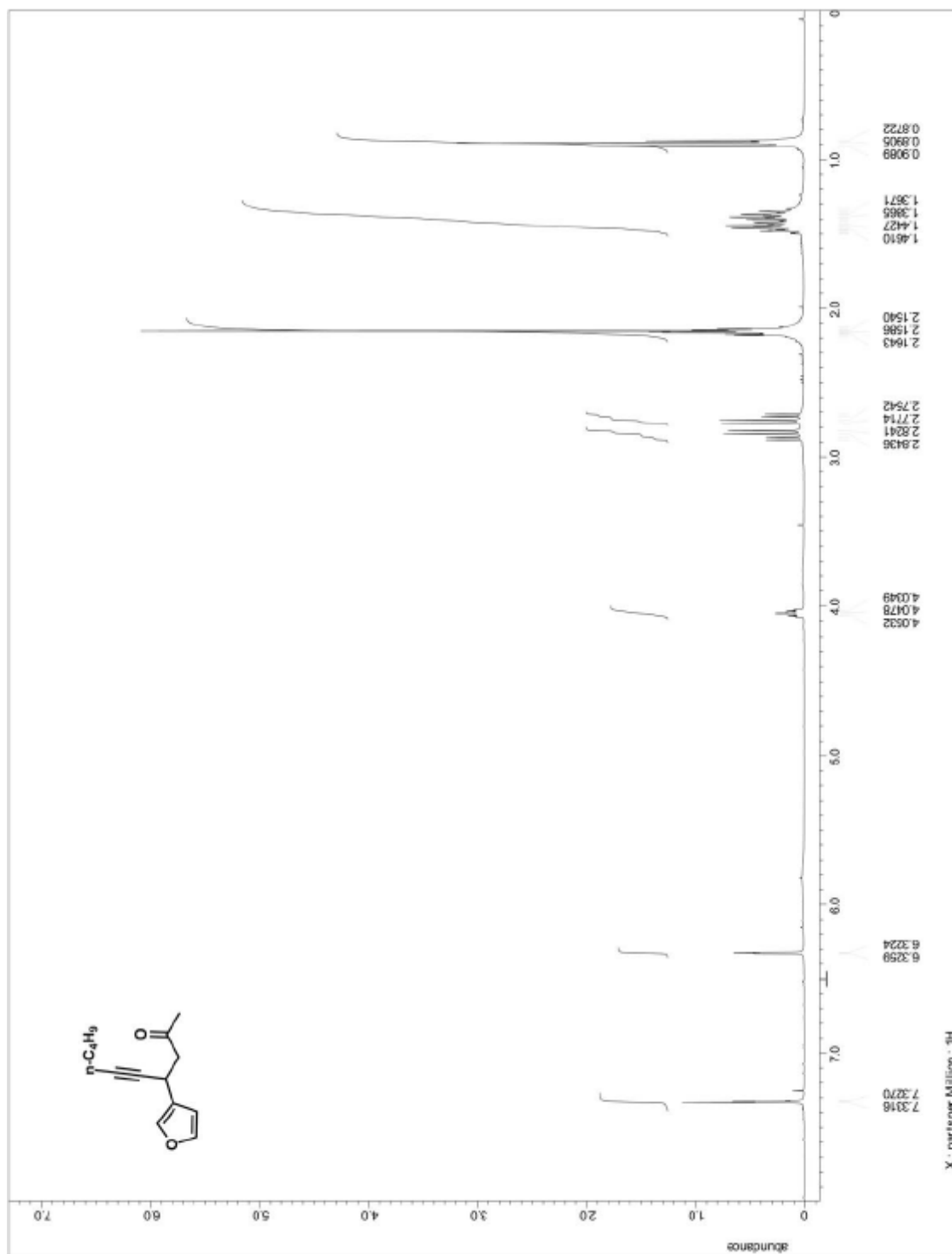


Figure A.1.27. ¹H NMR for compound 113

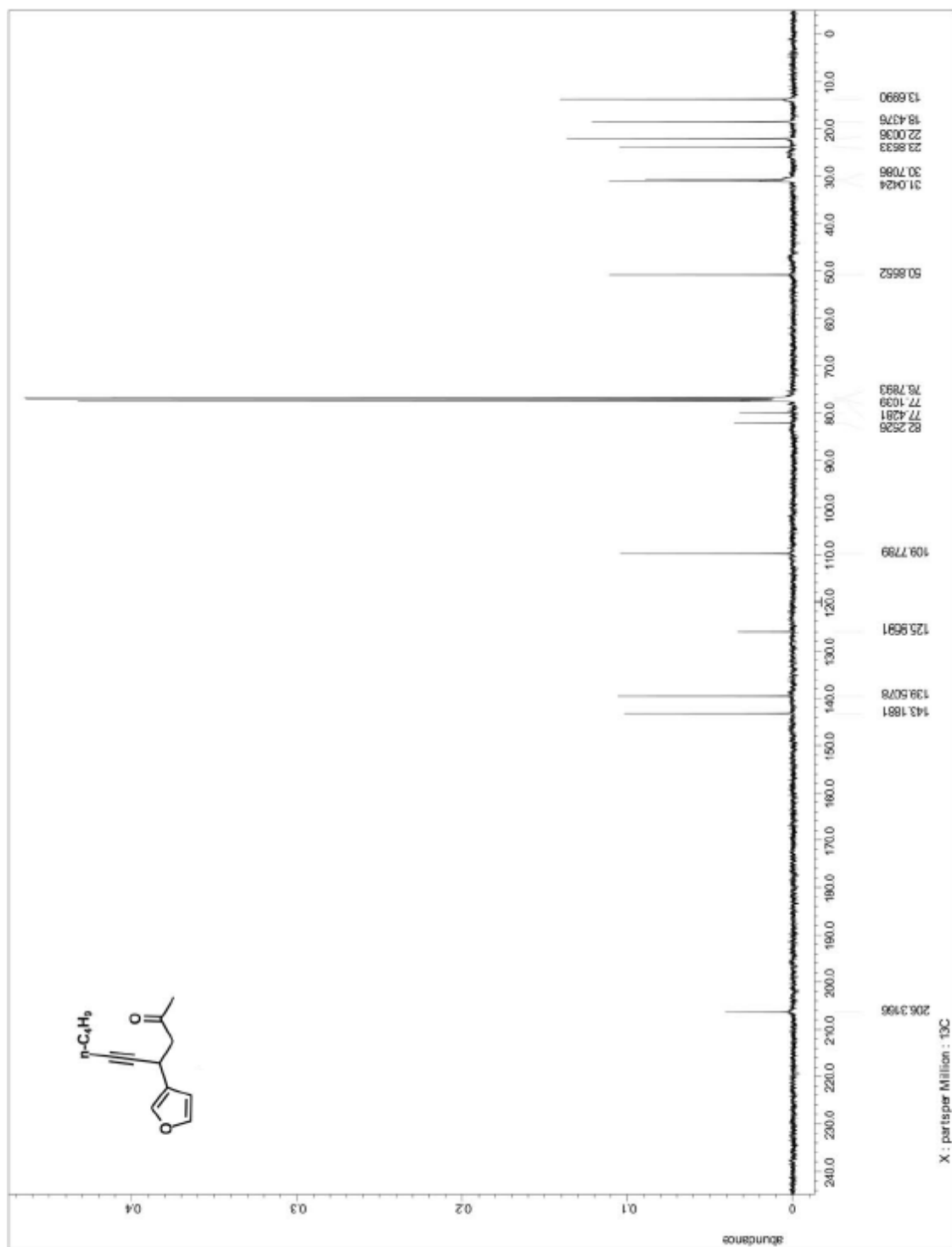
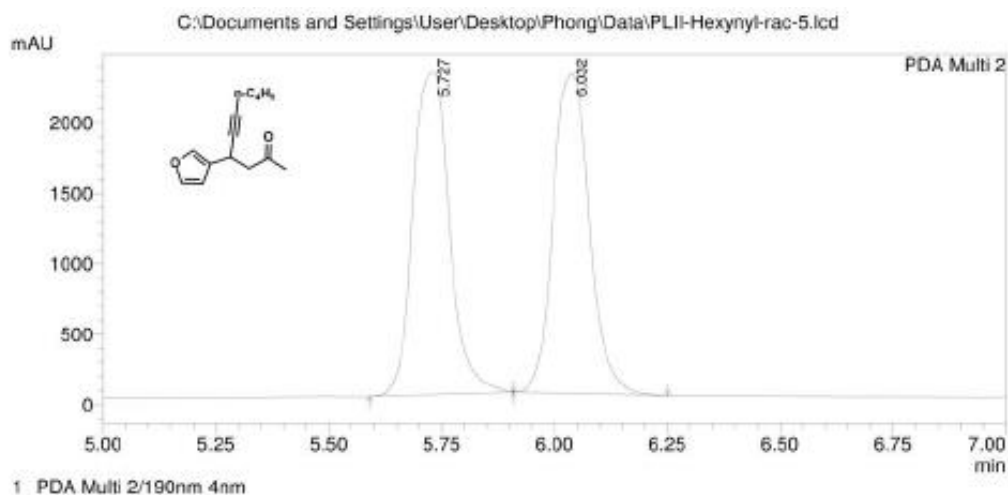
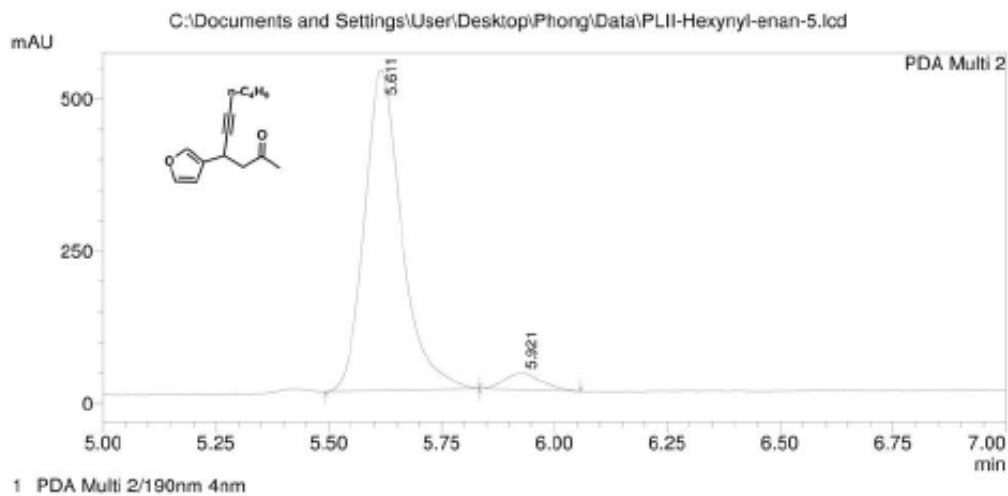


Figure A.1.28. ^{13}C NMR for compound 113



PeakTable

Peak#	Ret. Time	Area	Height	Area %	Height %
1	5.727	12923414	2285599	50.380	50.172
2	6.032	12728306	2269949	49.620	49.828
Total		25651720	4555548	100.000	100.000



PeakTable

Peak#	Ret. Time	Area	Height	Area %	Height %
1	5.611	3025046	523365	95.099	95.044
2	5.921	155901	27293	4.901	4.956
Total		3180947	550658	100.000	100.000

Figure A.1.29. HPLC trace for compound 113

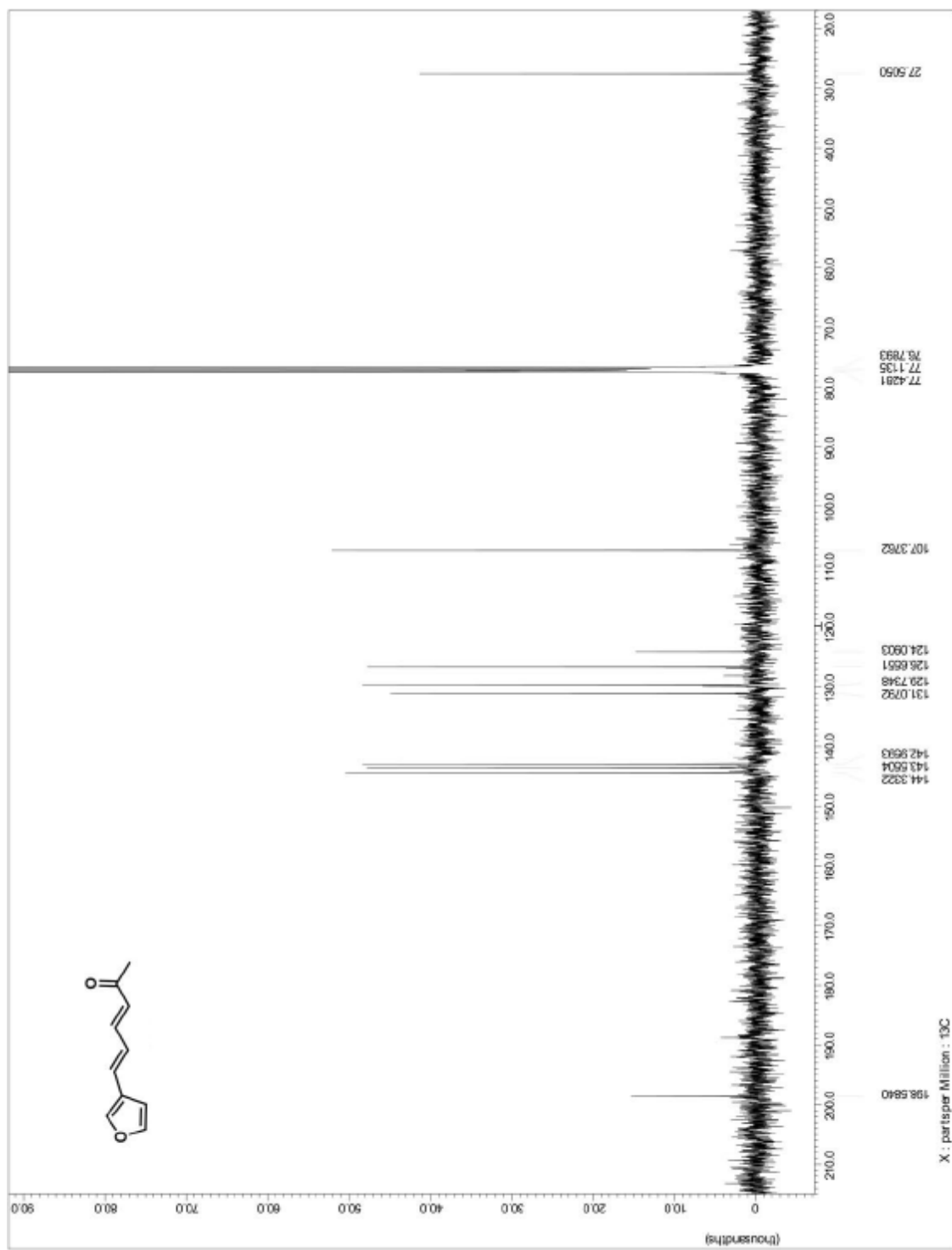


Figure A.1.31. ^{13}C NMR for precursor to compound 114

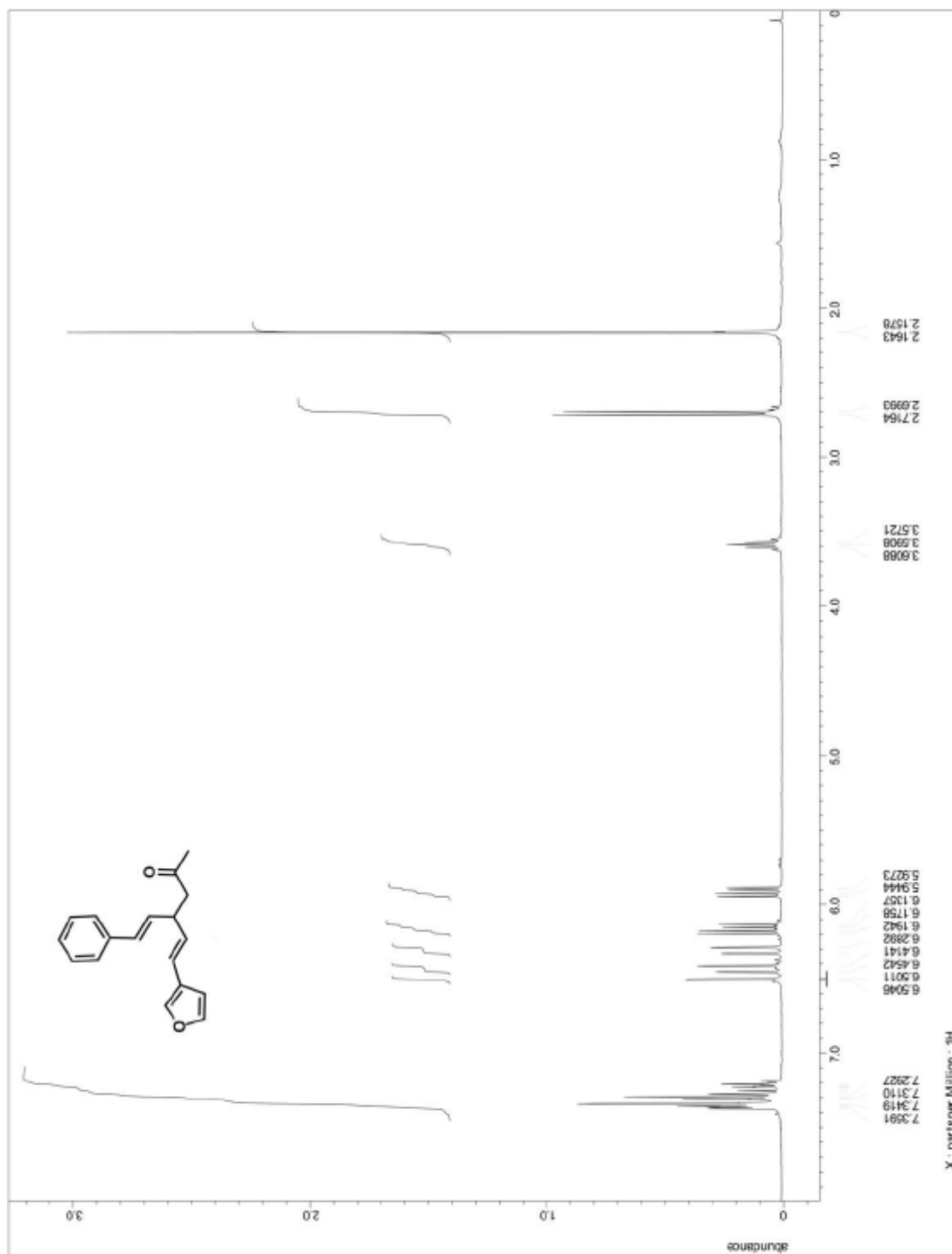


Figure A.1.32. ^1H NMR for compound 114

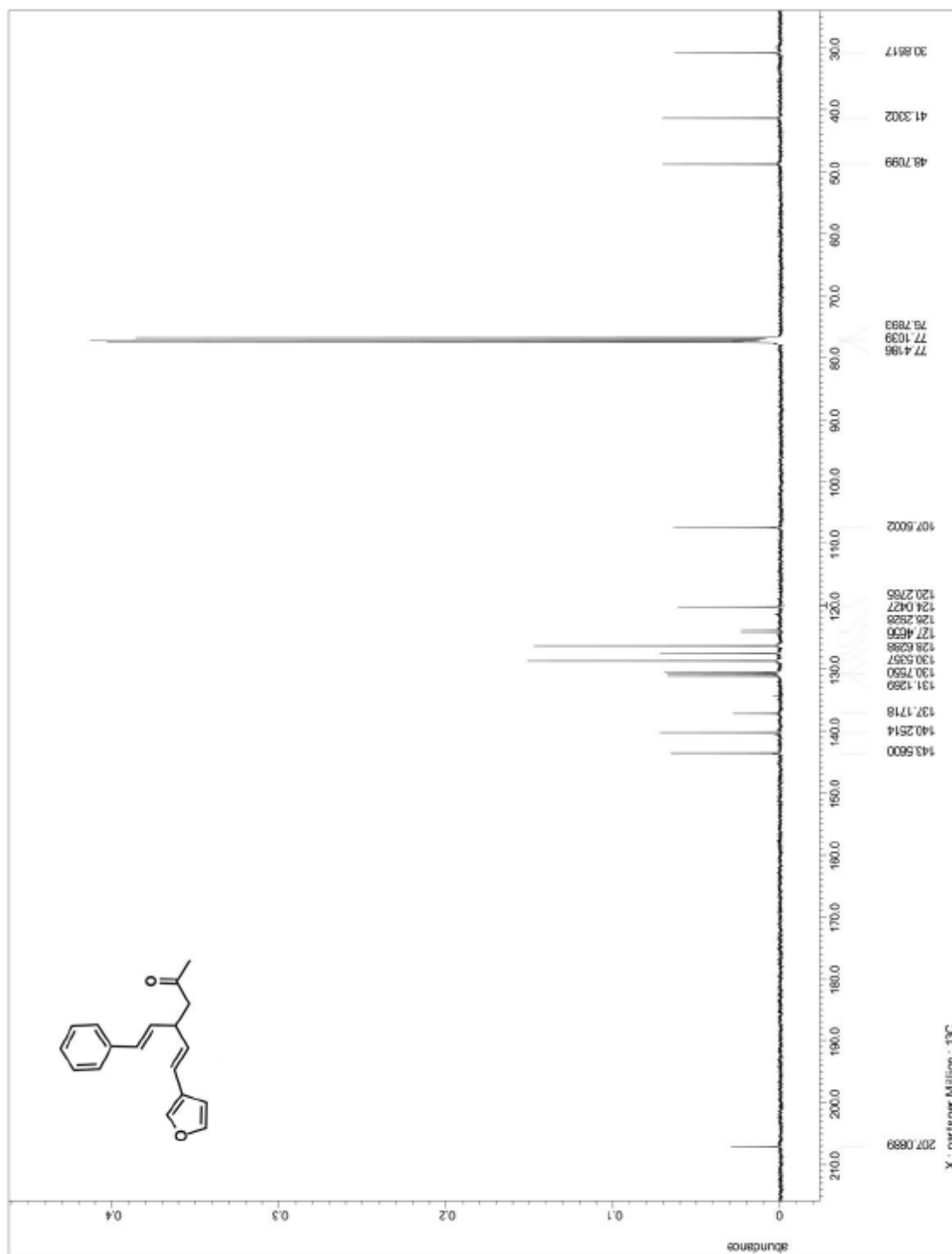
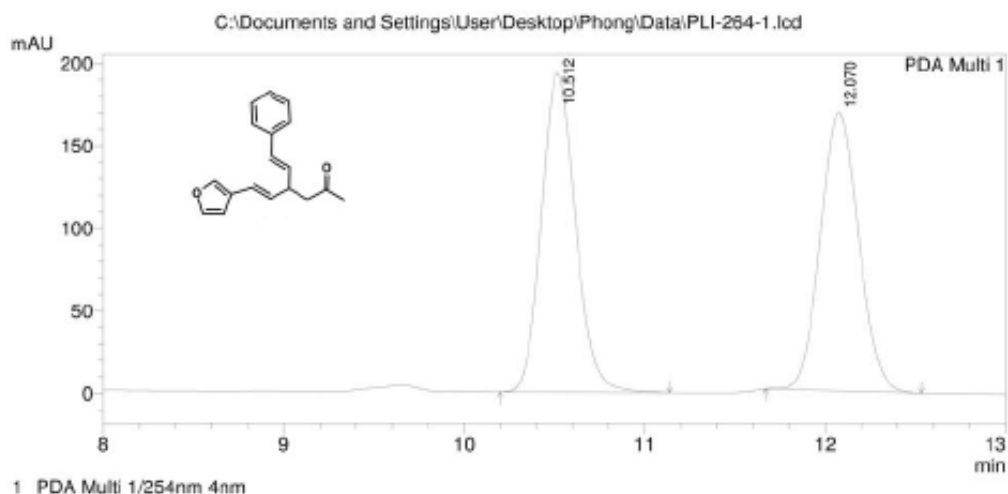
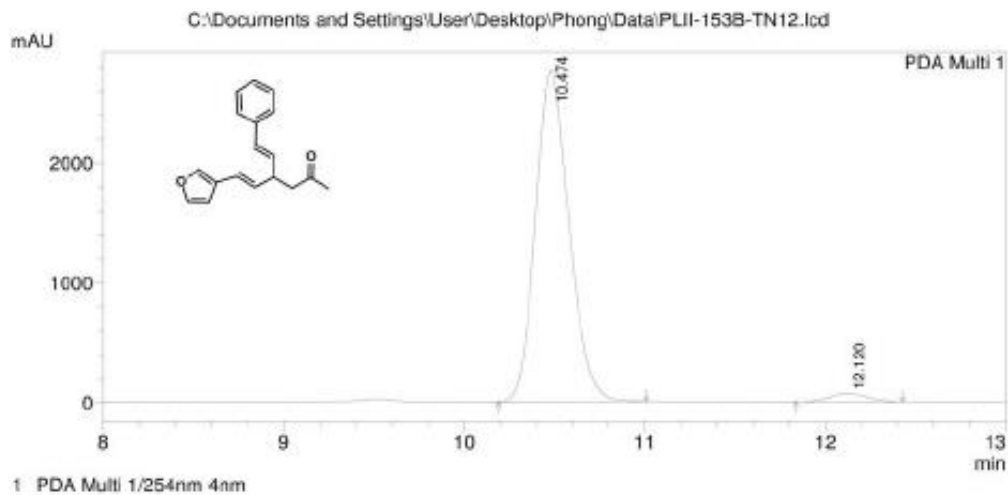


Figure A.1.33. ^{13}C NMR for compound 114



PeakTable

Peak#	Ret. Time	Area	Height	Area %	Height %
1	10.512	2543982	193595	50.508	53.381
2	12.070	2492857	169069	49.492	46.619
Total		5036839	362665	100.000	100.000



PeakTable

Peak#	Ret. Time	Area	Height	Area %	Height %
1	10.474	35648419	2763564	97.378	97.621
2	12.120	960020	67347	2.622	2.379
Total		36608439	2830912	100.000	100.000

Figure A.1.34. HPLC trace for compound 114

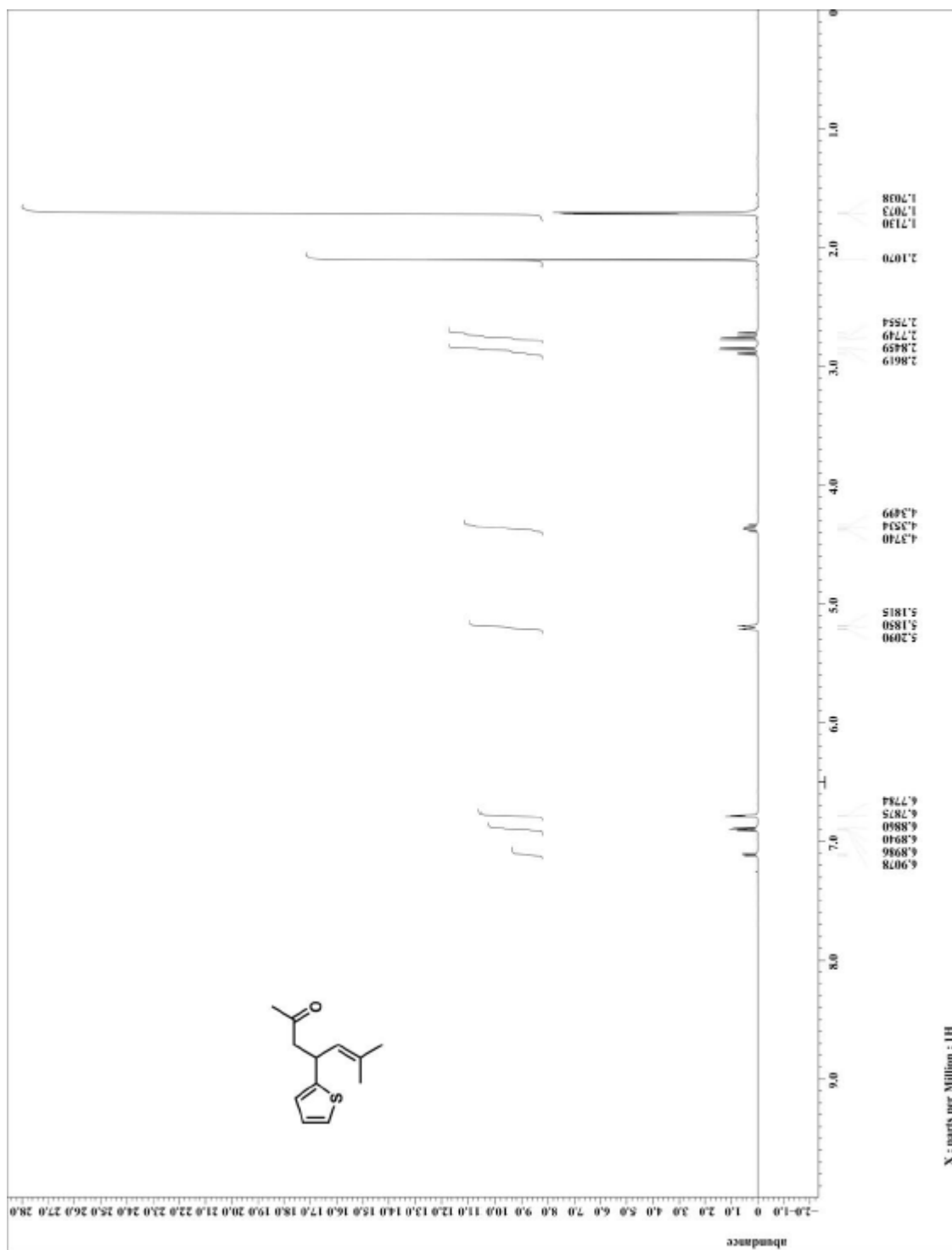


Figure A.1.35. ^1H NMR for compound 115

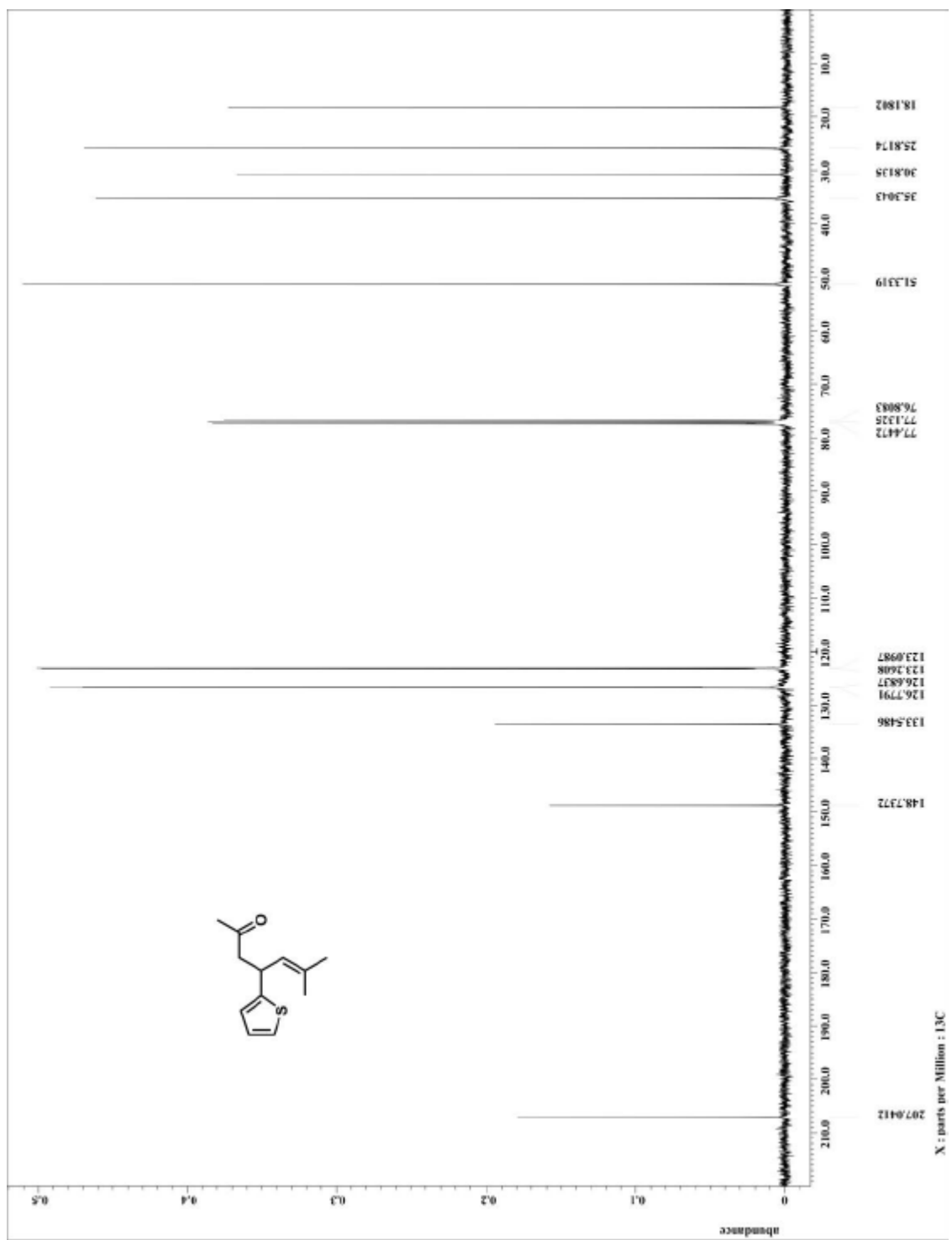
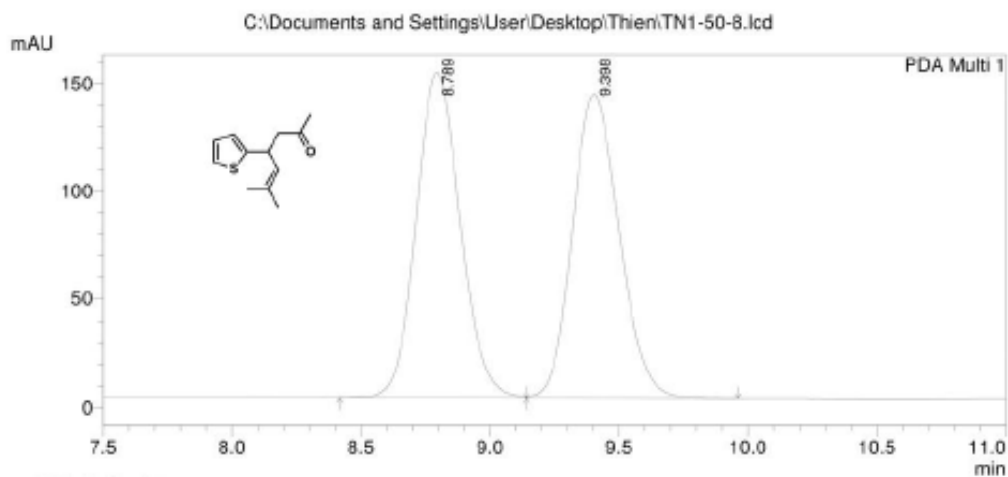
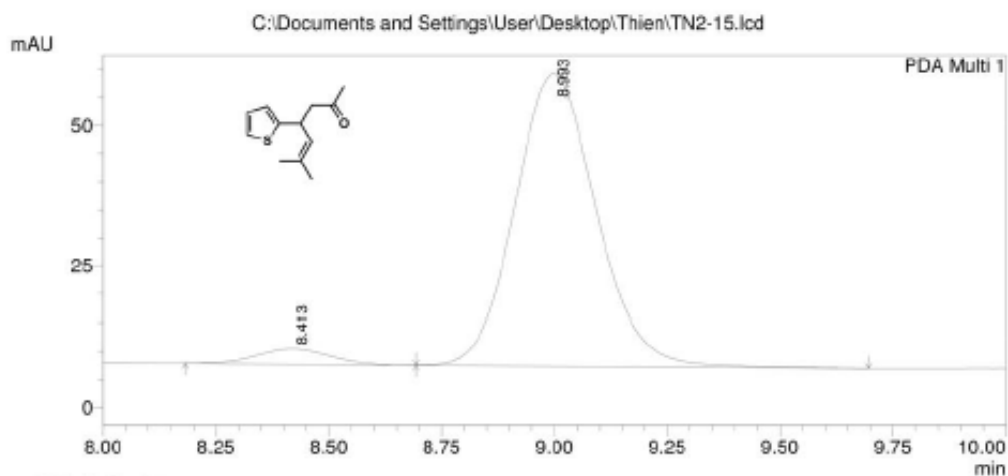


Figure A.1.36. ^{13}C NMR for compound 115



PeakTable

Peak#	Ret. Time	Area	Height	Area %	Height %
1	8.789	1792053	150475	50.236	51.720
2	9.398	1775195	140465	49.764	48.280
Total		3567248	290940	100.000	100.000



PeakTable

Peak#	Ret. Time	Area	Height	Area %	Height %
1	8.413	29748	2653	4.400	4.871
2	8.993	646319	51824	95.600	95.129
Total		676066	54478	100.000	100.000

Figure A.1.37. HPLC trace for compound 115

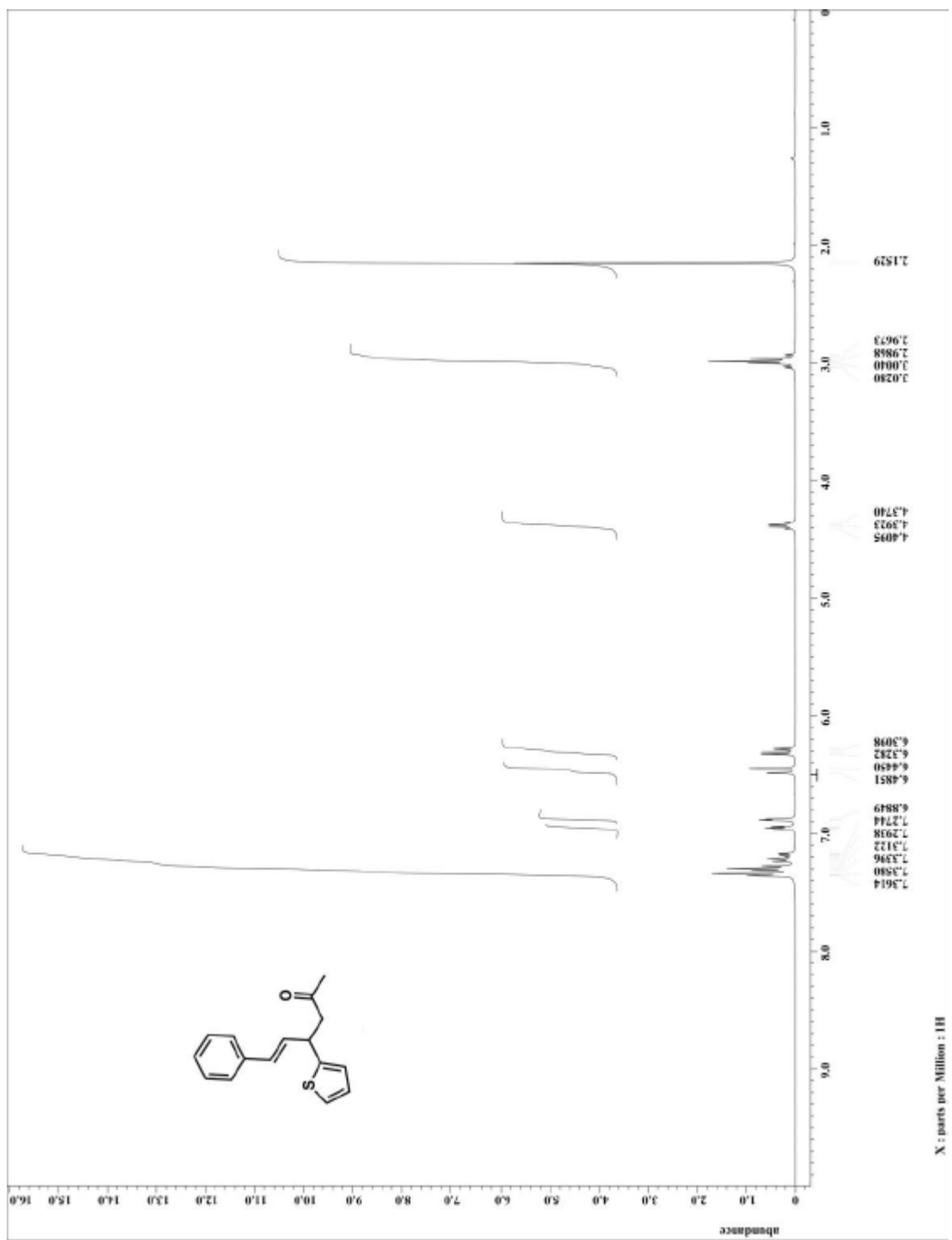


Figure A.1.38. ¹H NMR for compound 116

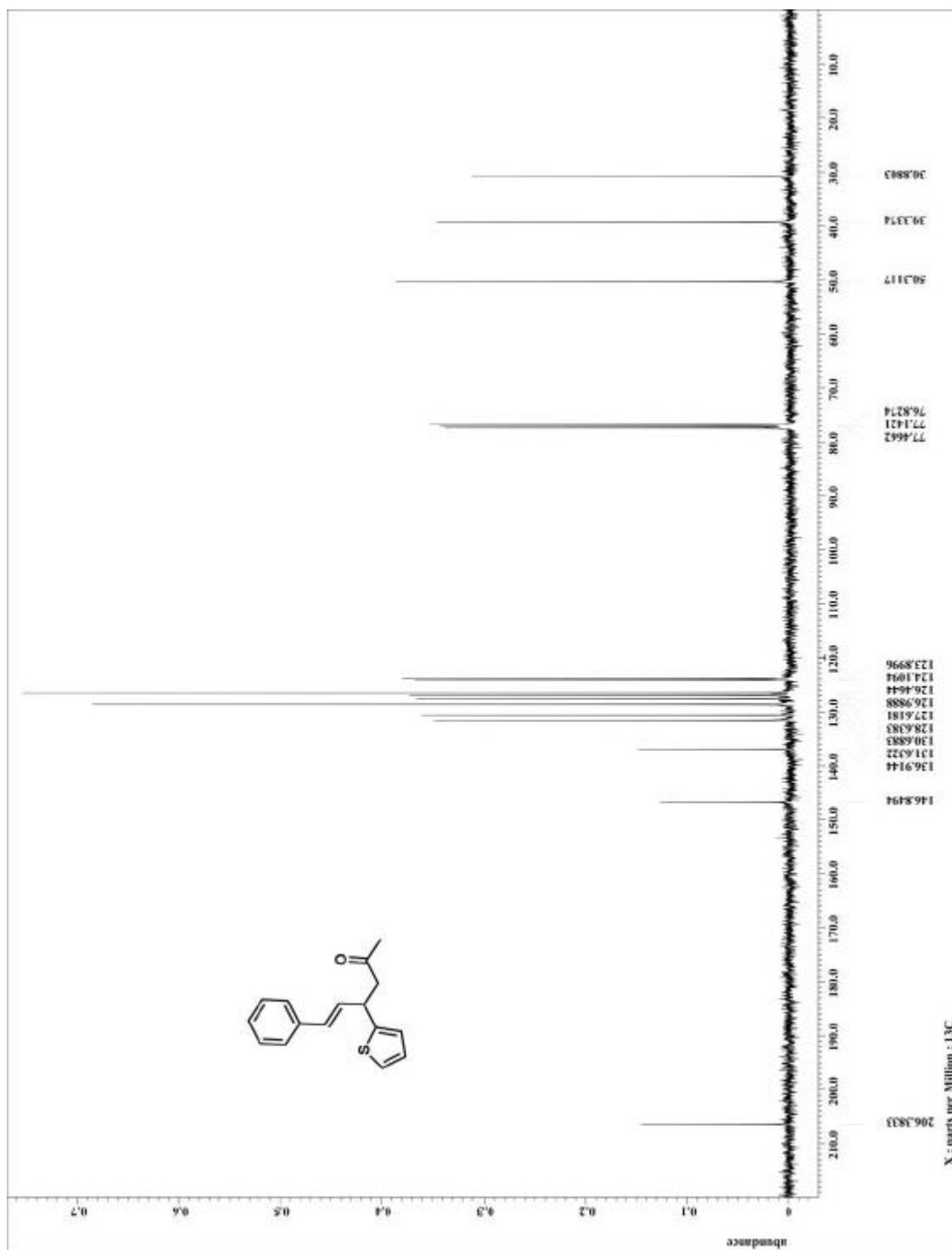
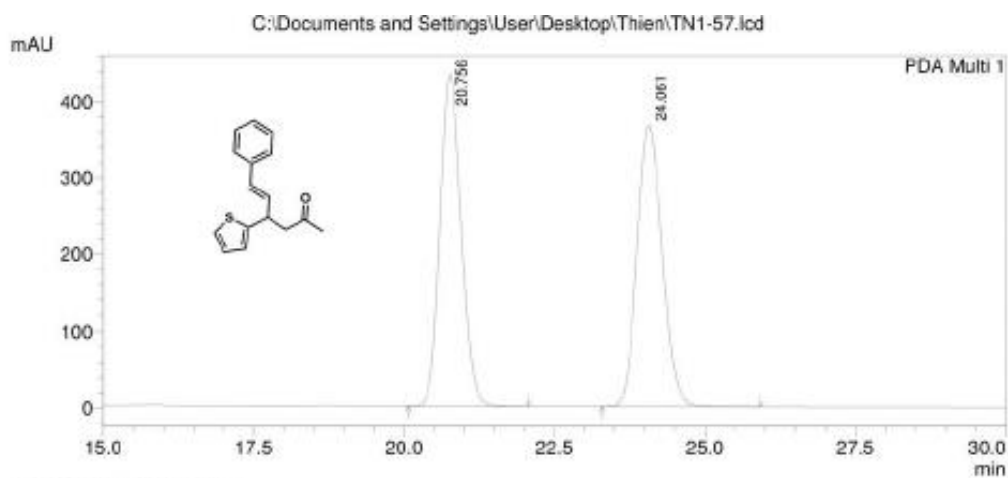
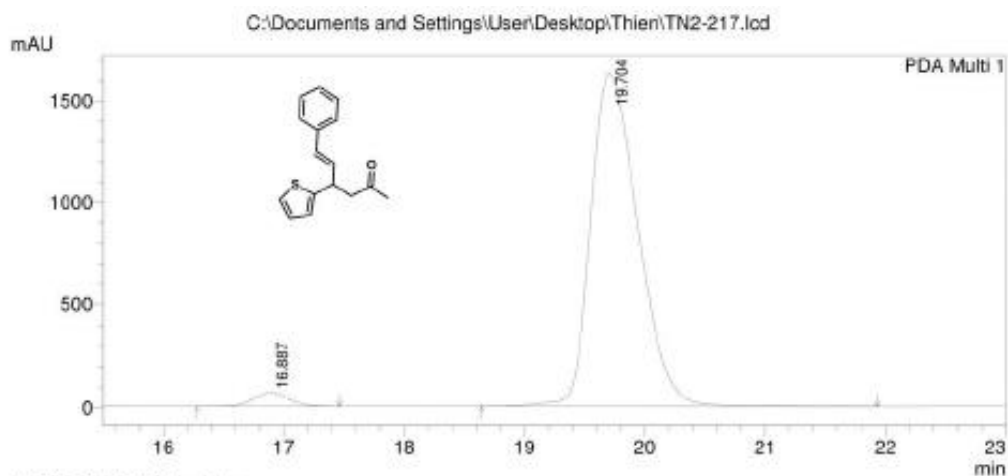


Figure A.1.39. ^{13}C NMR for compound 116



PeakTable

Peak#	Ret. Time	Area	Height	Area %	Height %
1	20.756	10669071	434446	49.946	54.160
2	24.061	10692160	367704	50.054	45.840
Total		21361231	802151	100.000	100.000



PeakTable

Peak#	Ret. Time	Area	Height	Area %	Height %
1	16.887	1376592	67452	2.996	3.975
2	19.704	44566510	1629240	97.004	96.025
Total		45943102	1696692	100.000	100.000

Figure A.1.40. HPLC trace for compound 116

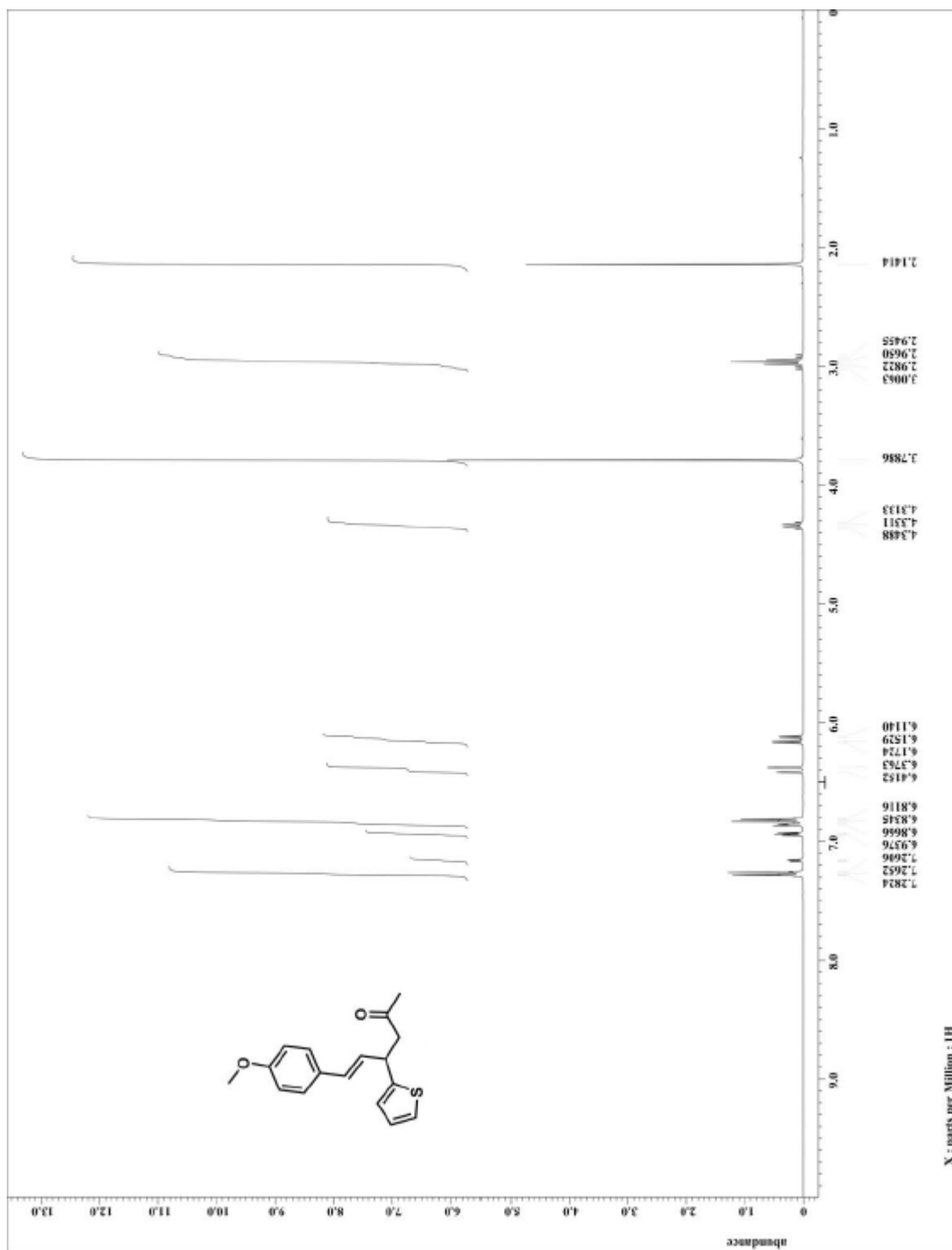


Figure A.1.41. ^1H NMR for compound 117

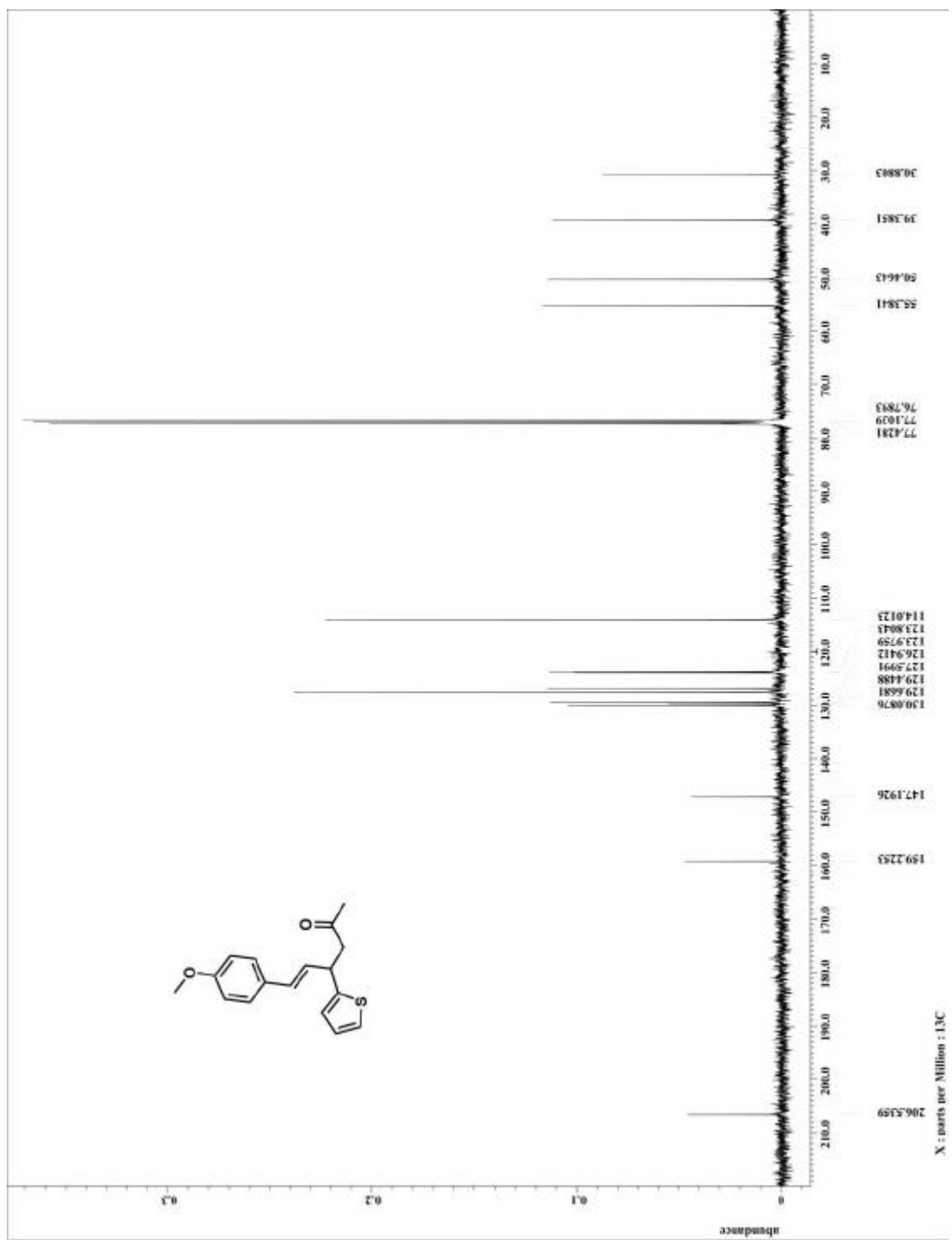
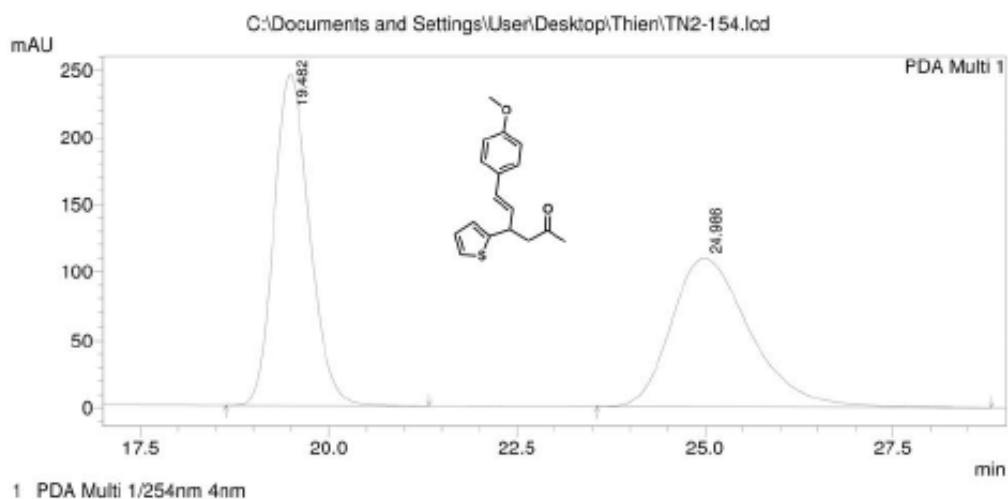
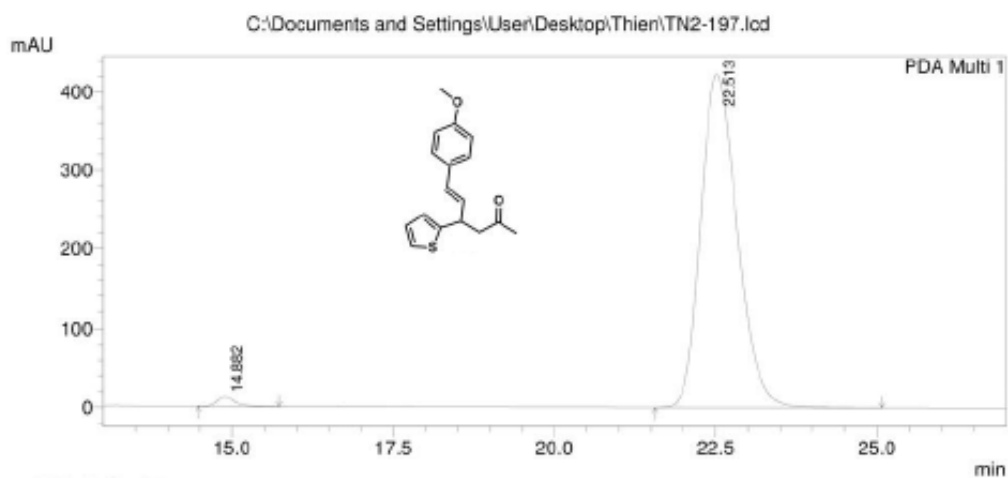


Figure A.1.42. ^{13}C NMR for compound 117



PeakTable

Peak#	Ret. Time	Area	Height	Area %	Height %
1	19.482	8061408	245429	50.211	69.129
2	24.986	7993710	109599	49.789	30.871
Total		16055118	355028	100.000	100.000



PeakTable

Peak#	Ret. Time	Area	Height	Area %	Height %
1	14.882	240746	12914	1.424	2.967
2	22.513	16664916	422361	98.576	97.033
Total		16905662	435275	100.000	100.000

Figure A.1.43. HPLC trace for compound 117

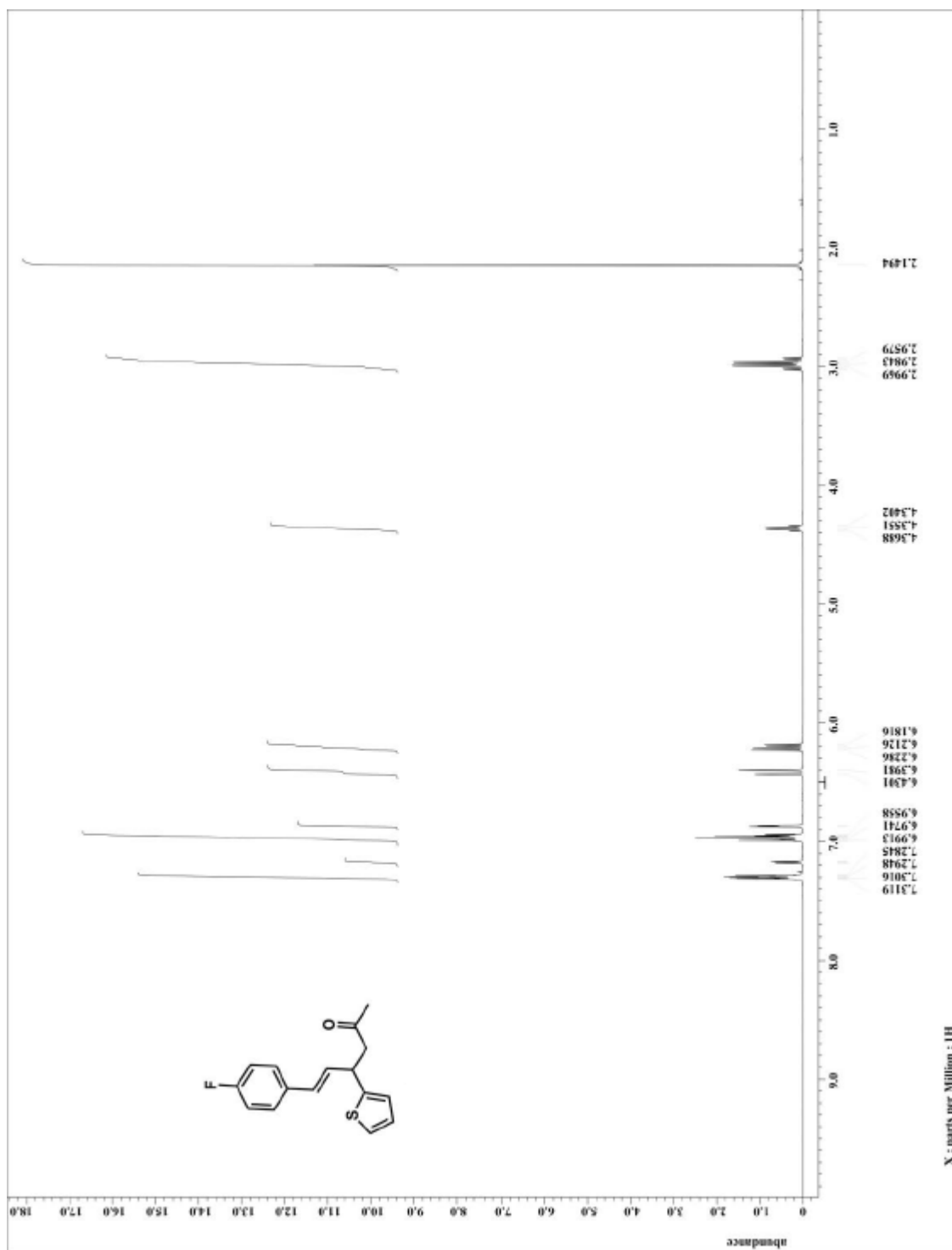


Figure A.1.44. ¹H NMR for compound 118

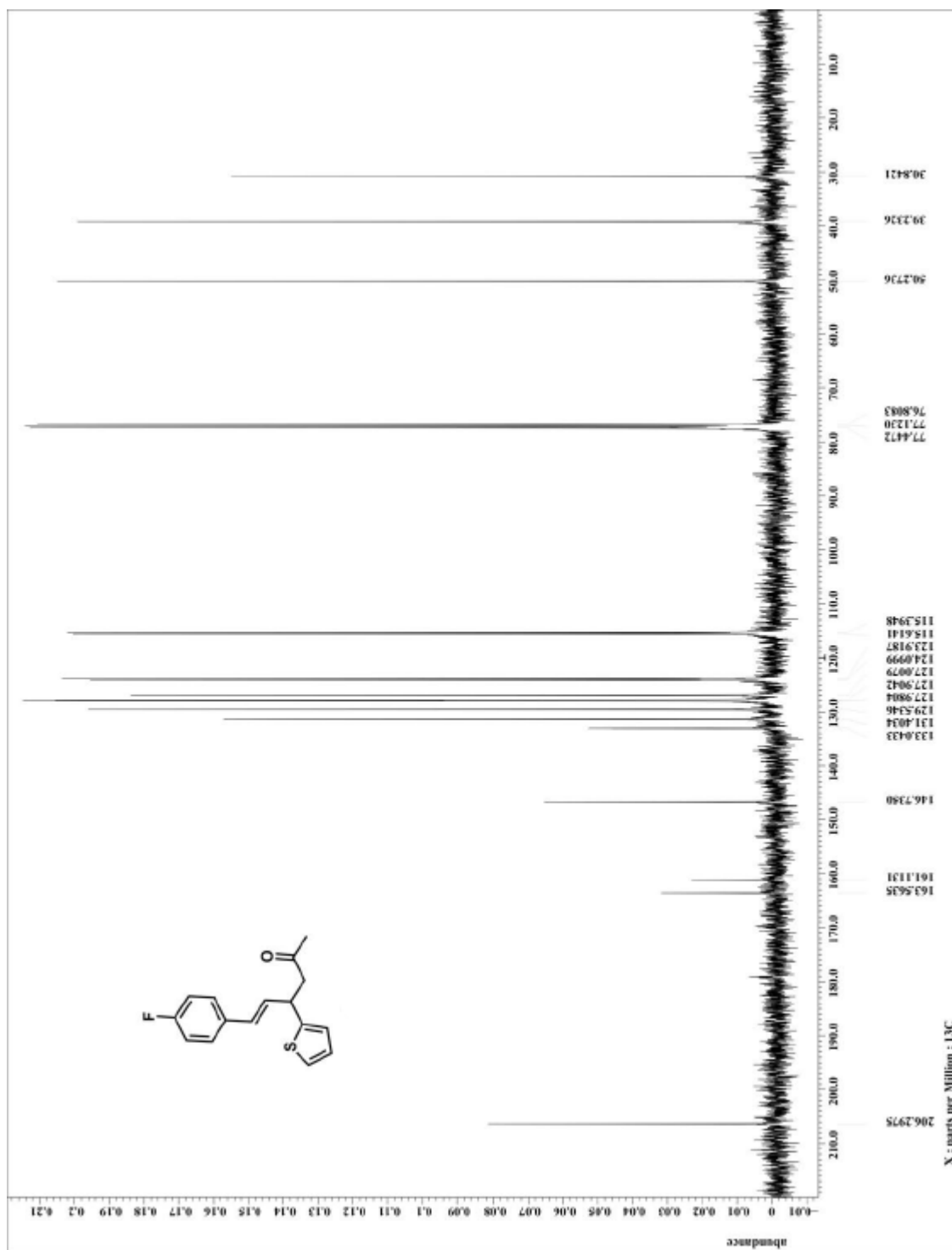
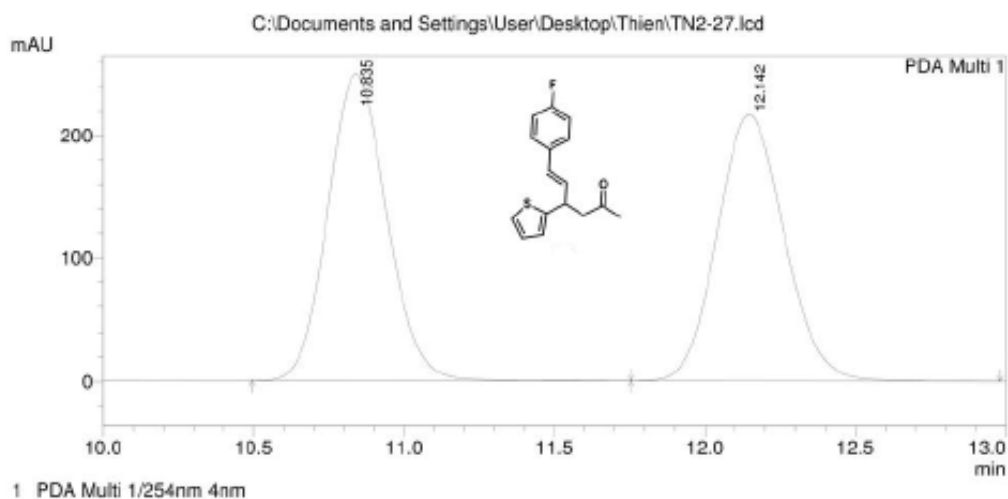
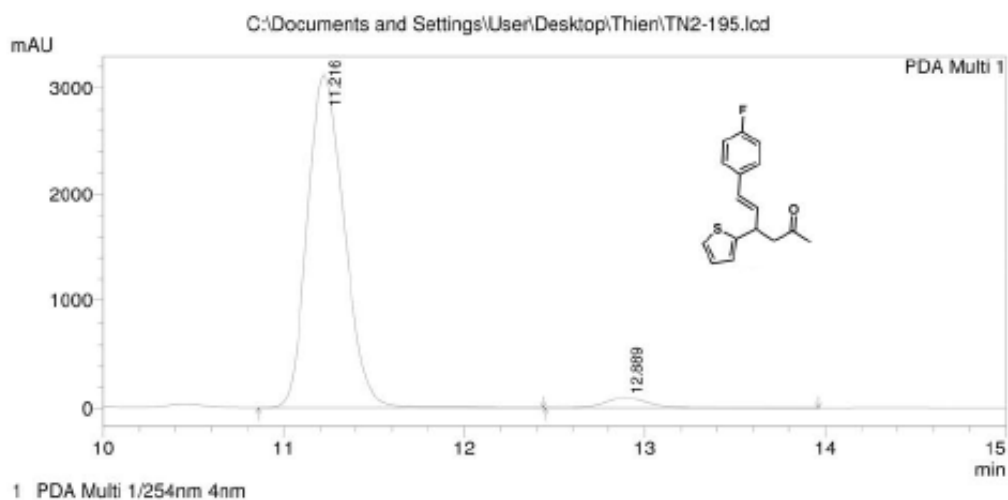


Figure A.1.45. ^{13}C NMR for compound 118



PeakTable

Peak#	Ret. Time	Area	Height	Area %	Height %
1	10.835	3393762	249374	50.317	53.530
2	12.142	3351060	216482	49.683	46.470
Total		6744823	465856	100.000	100.000



PeakTable

Peak#	Ret. Time	Area	Height	Area %	Height %
1	11.216	44001699	3122010	96.702	97.051
2	12.889	1500877	94860	3.298	2.949
Total		45502576	3216870	100.000	100.000

Figure A.1.46. HPLC trace for compound 118

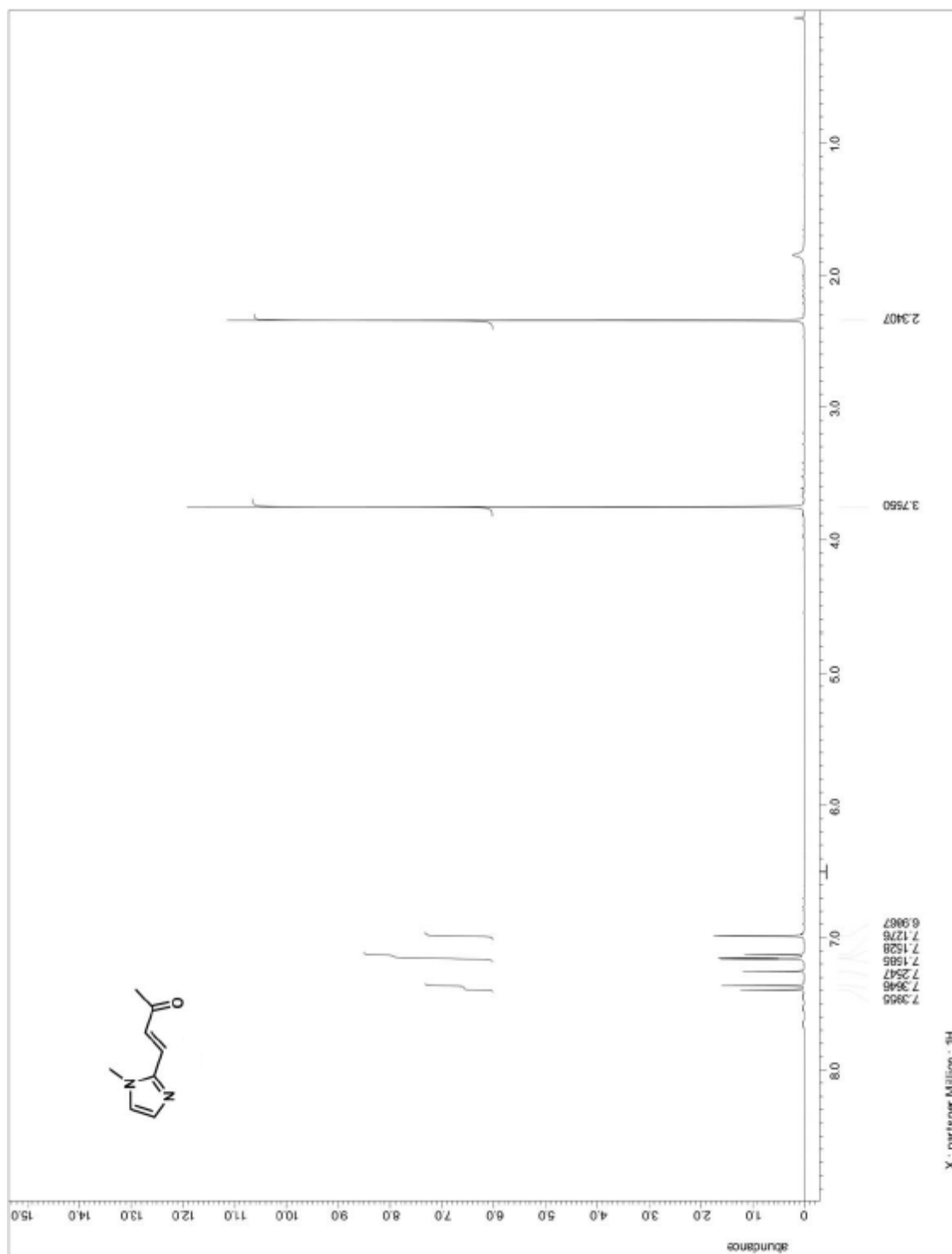


Figure A.1.47. ^1H NMR for precursor to compound 119

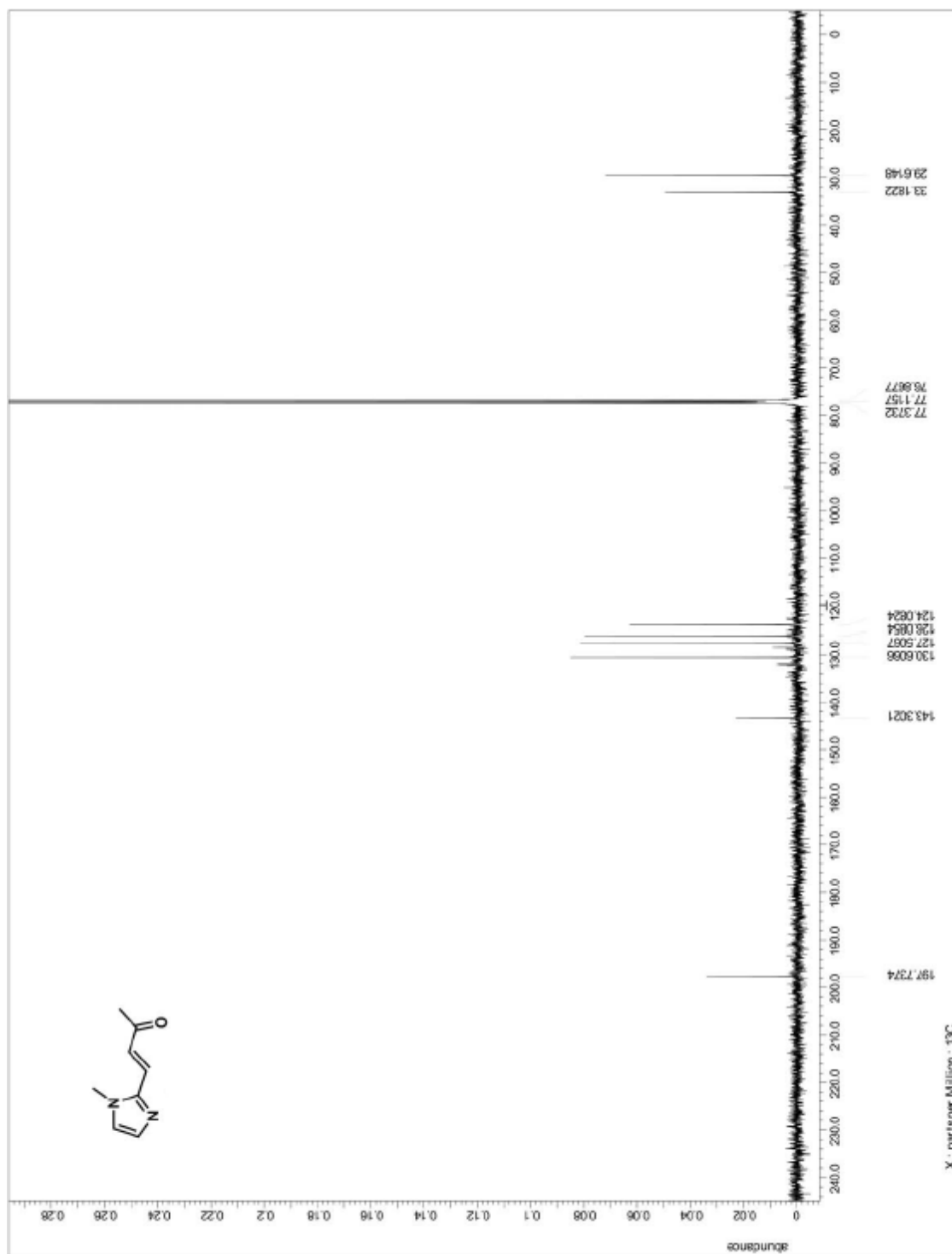


Figure A.1.48. ^{13}C NMR for precursor to compound 119

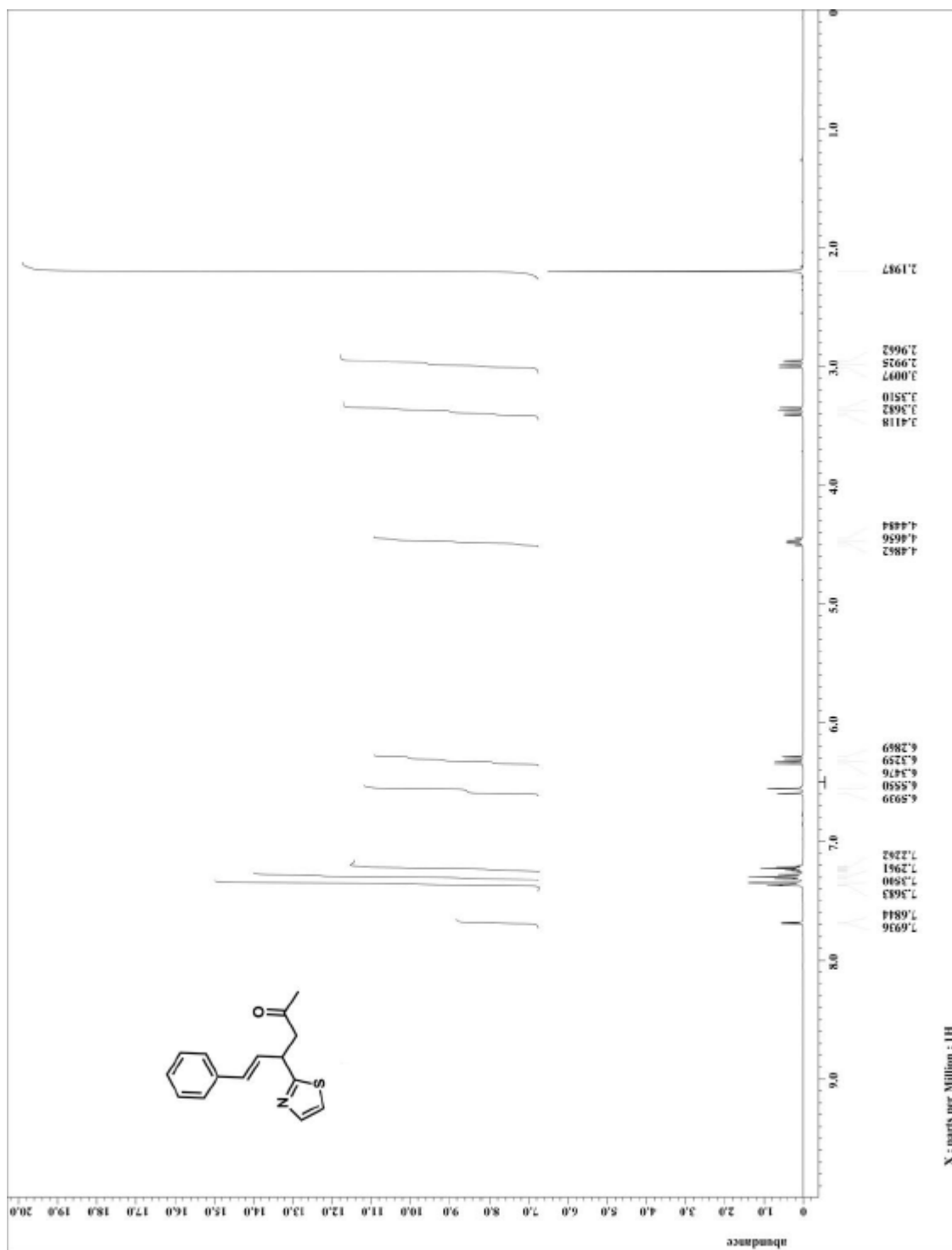


Figure A.1.49. ^1H NMR for compound 119

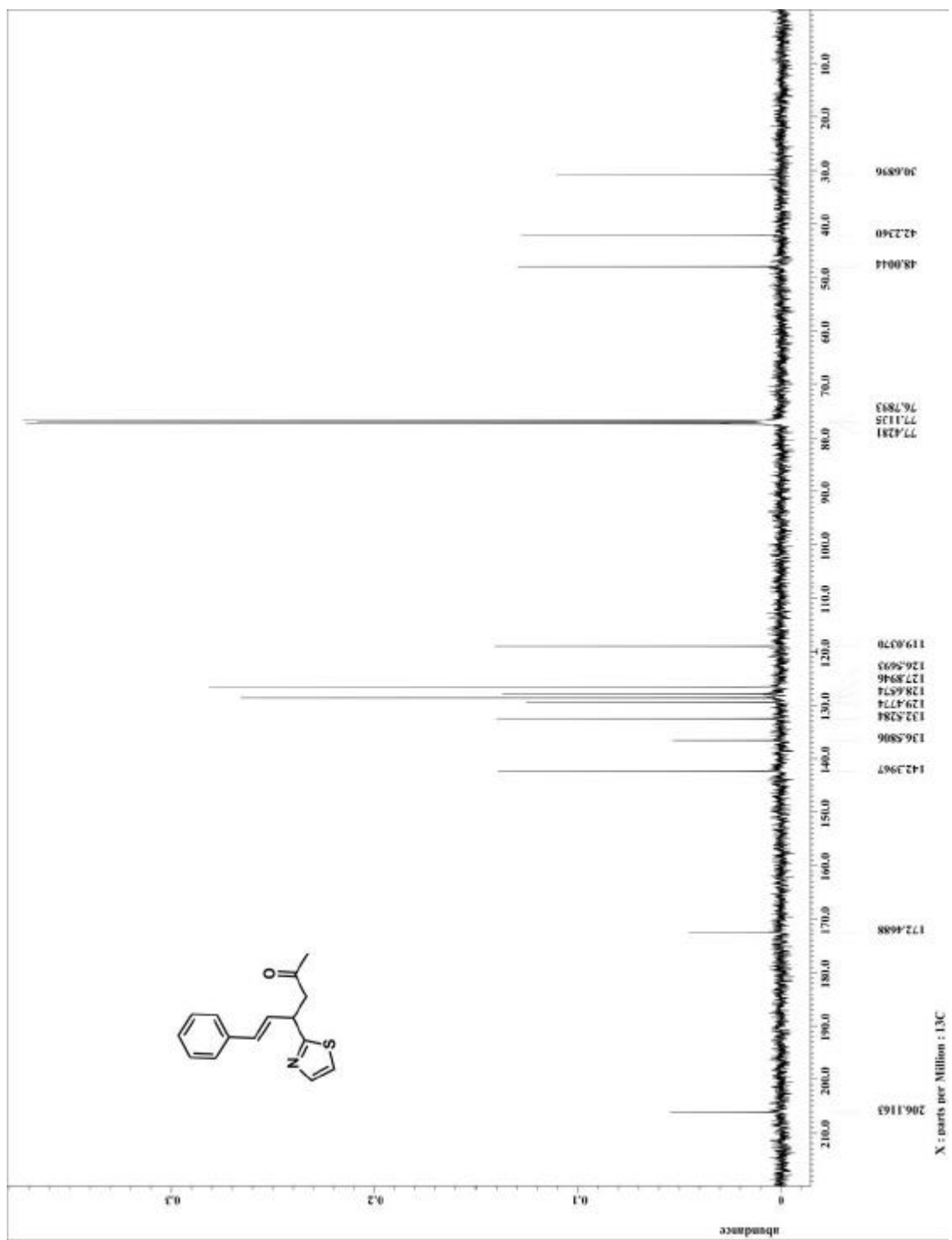
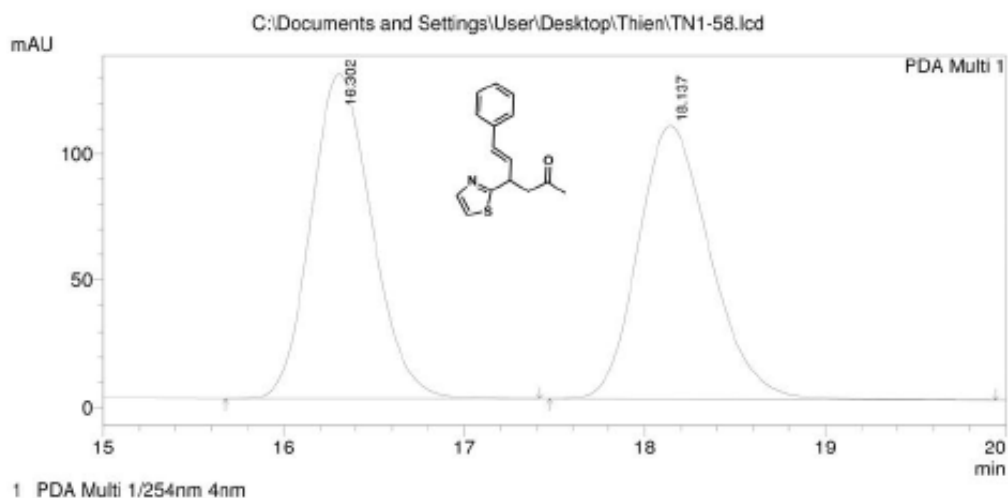
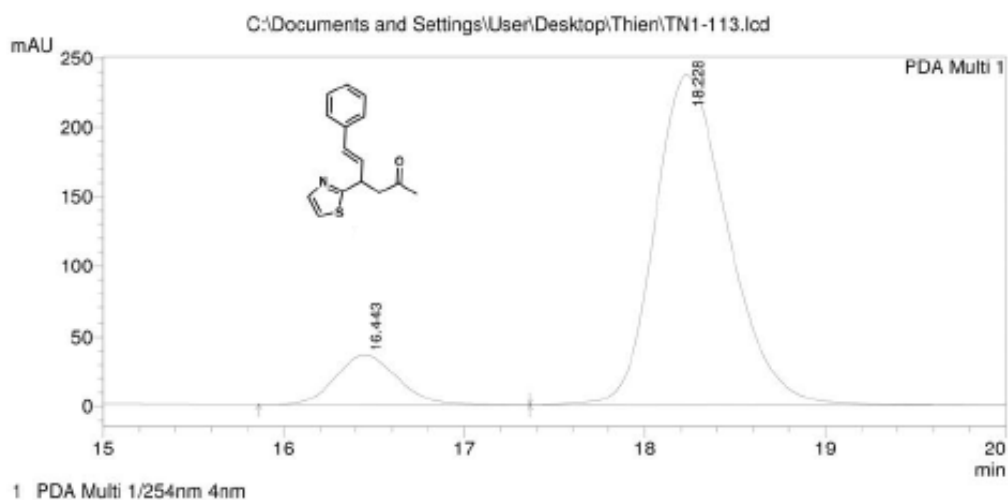


Figure A.1.50. ^{13}C NMR for compound 119



PeakTable

Peak#	Ret. Time	Area	Height	Area %	Height %
1	16.302	3006730	128216	50.024	54.323
2	18.137	3003845	107810	49.976	45.677
Total		6010574	236026	100.000	100.000



PeakTable

Peak#	Ret. Time	Area	Height	Area %	Height %
1	16.443	851838	35768	11.310	13.111
2	18.228	6679880	237040	88.690	86.889
Total		7531718	272808	100.000	100.000

Figure A.1.51. HPLC trace for compound 119

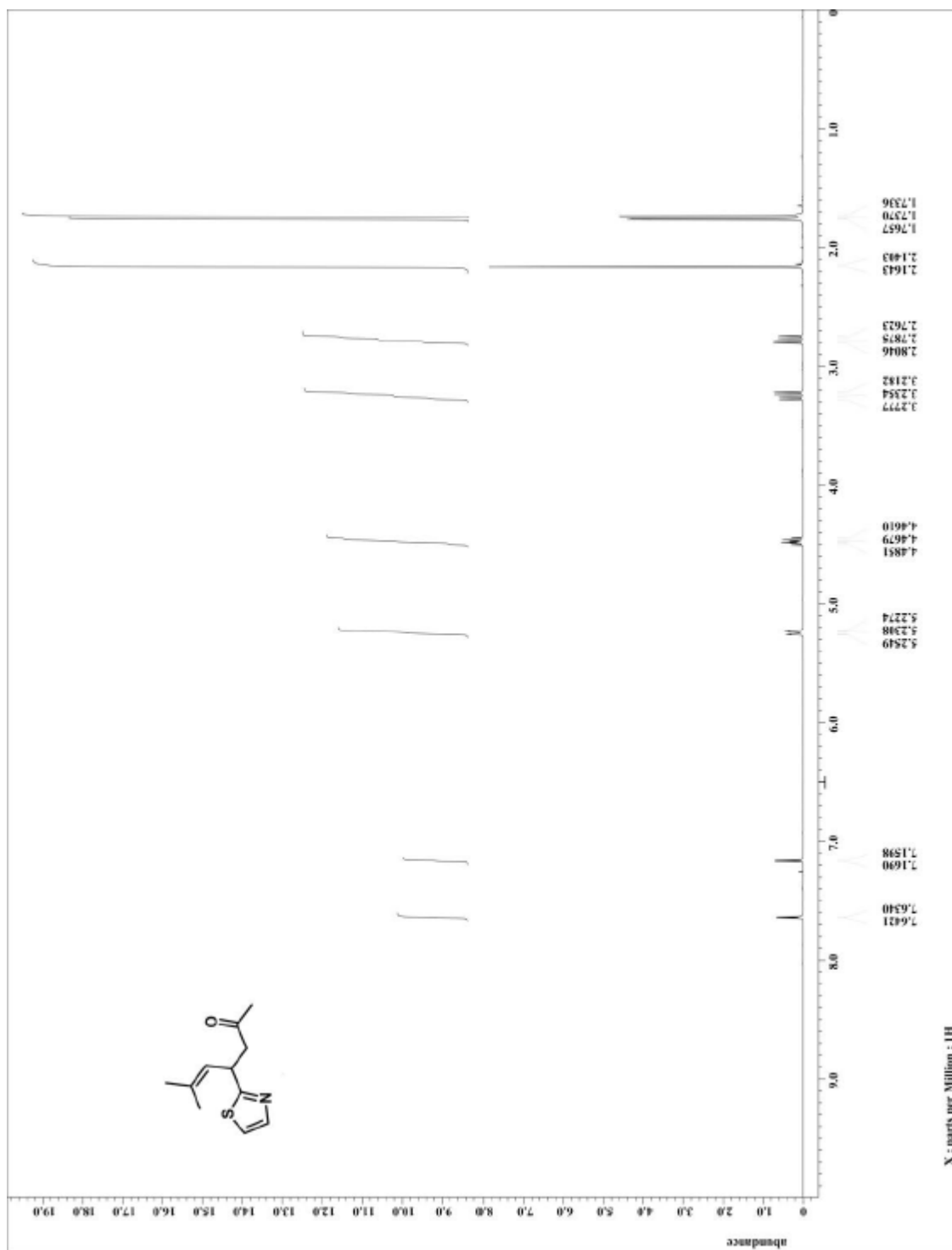


Figure A.1.52. ¹H NMR for compound 120

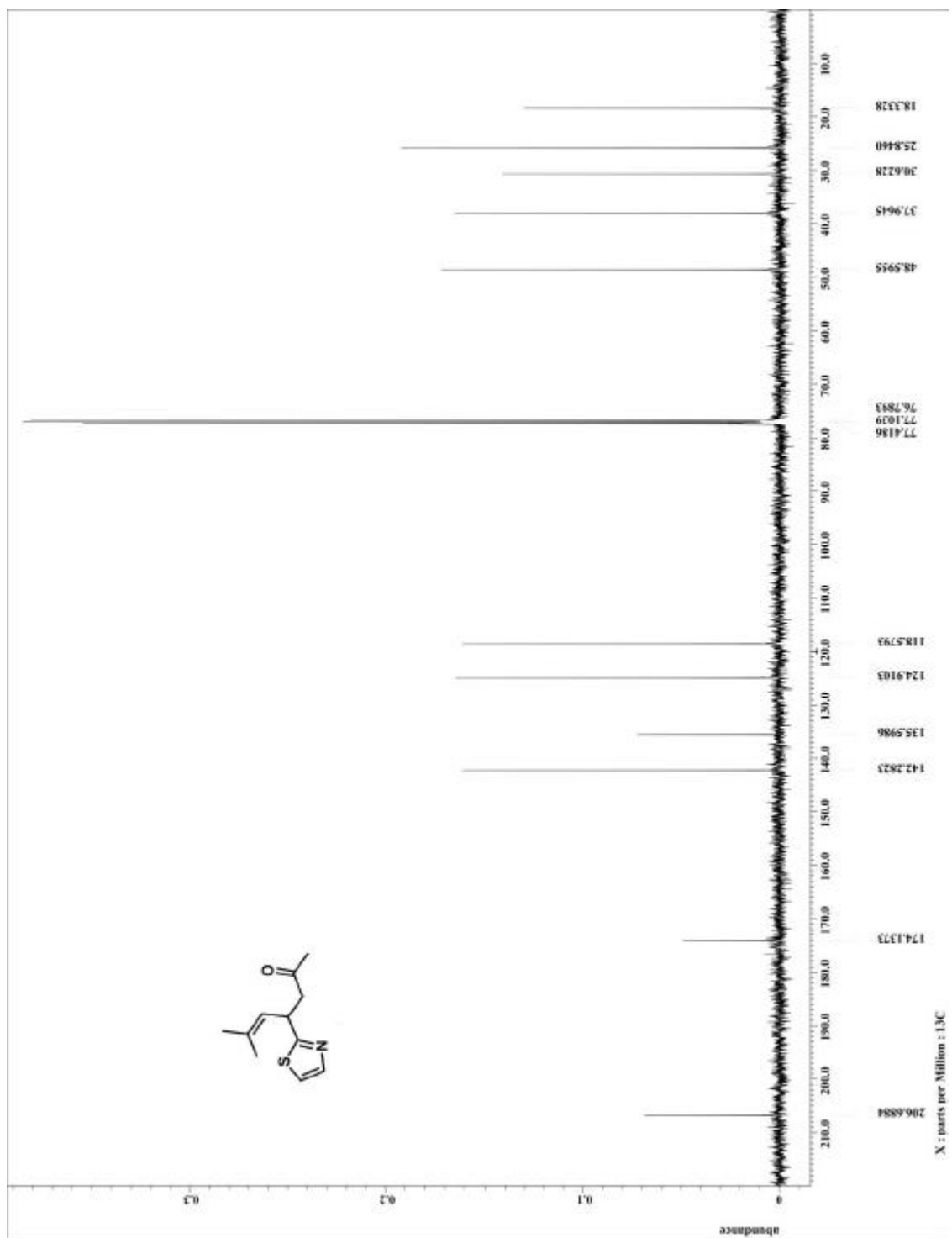
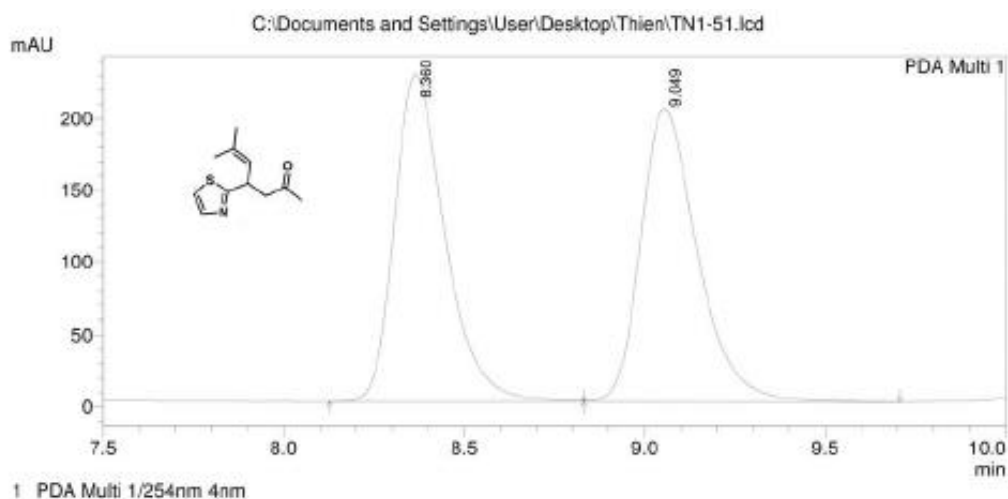
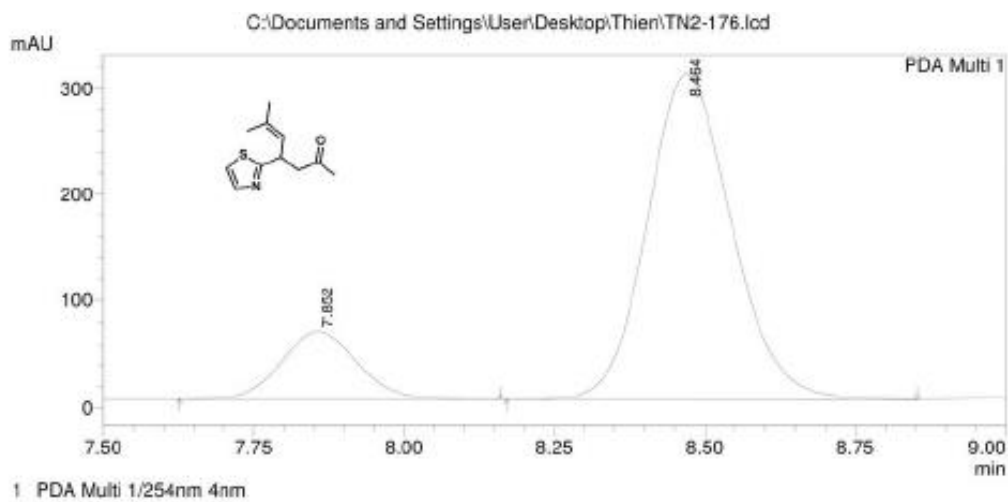


Figure A.1.53. ^{13}C NMR for compound 120



PeakTable

Peak#	Ret. Time	Area	Height	Area %	Height %
1	8.360	2215574	227297	50.010	52.720
2	9.049	2214685	203847	49.990	47.280
Total		4430260	431144	100.000	100.000



PeakTable

Peak#	Ret. Time	Area	Height	Area %	Height %
1	7.852	558450	63811	15.804	17.232
2	8.464	2975096	306490	84.196	82.768
Total		3533546	370302	100.000	100.000

Figure A.1.54. HPLC trace for compound 120

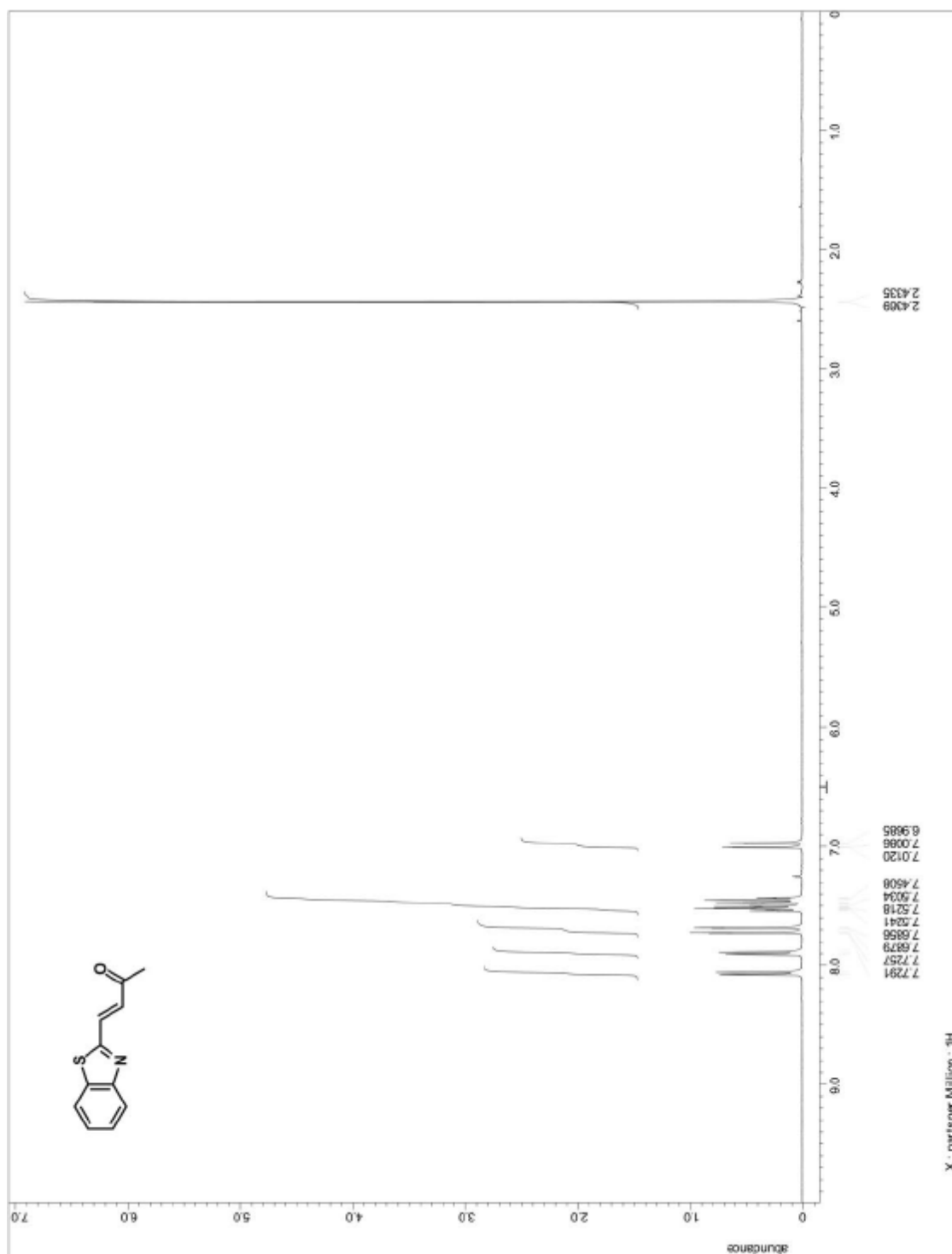


Figure A.1.55. ^1H NMR for precursor to compound 121

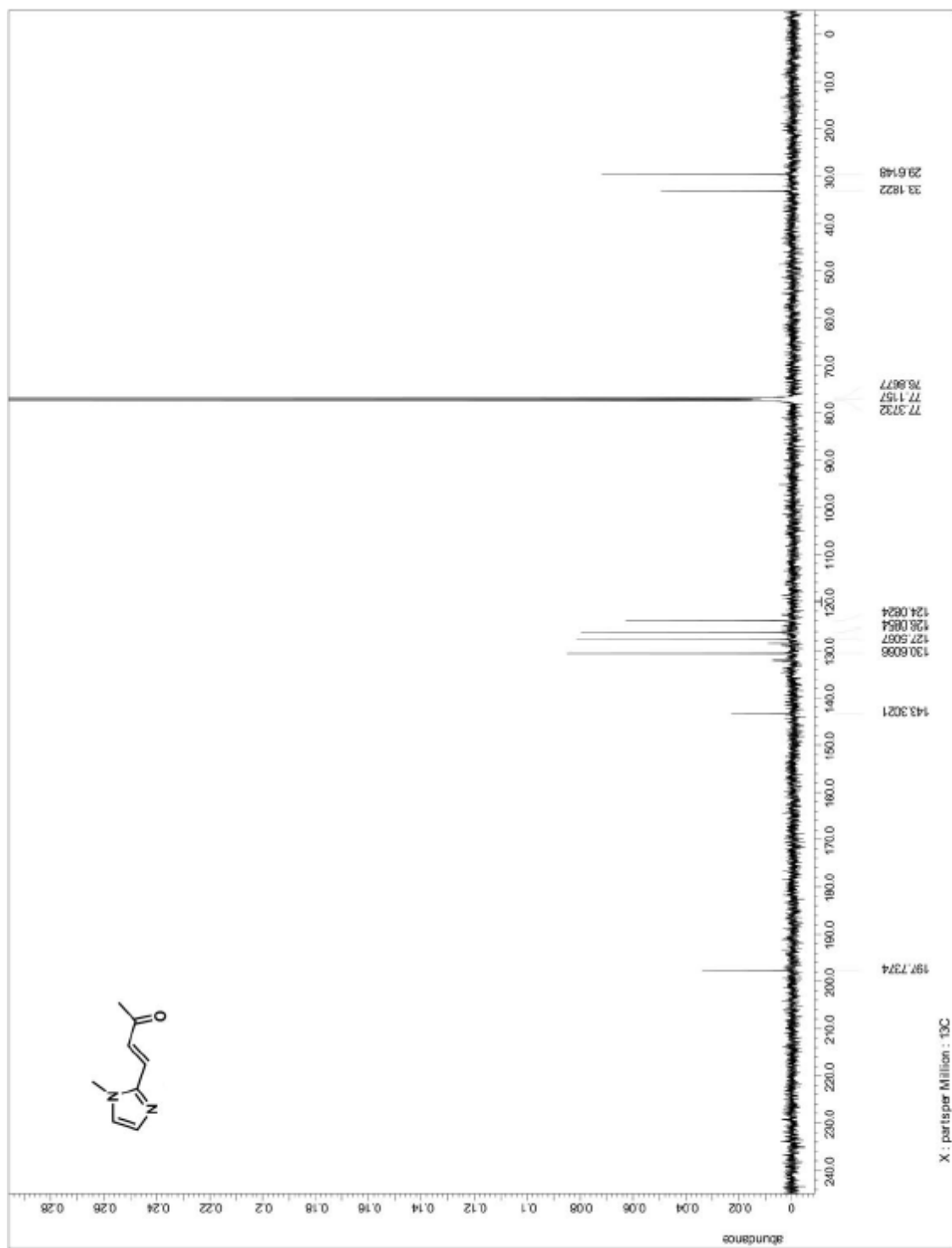


Figure A.1.56. ^{13}C NMR for precursor to compound 121

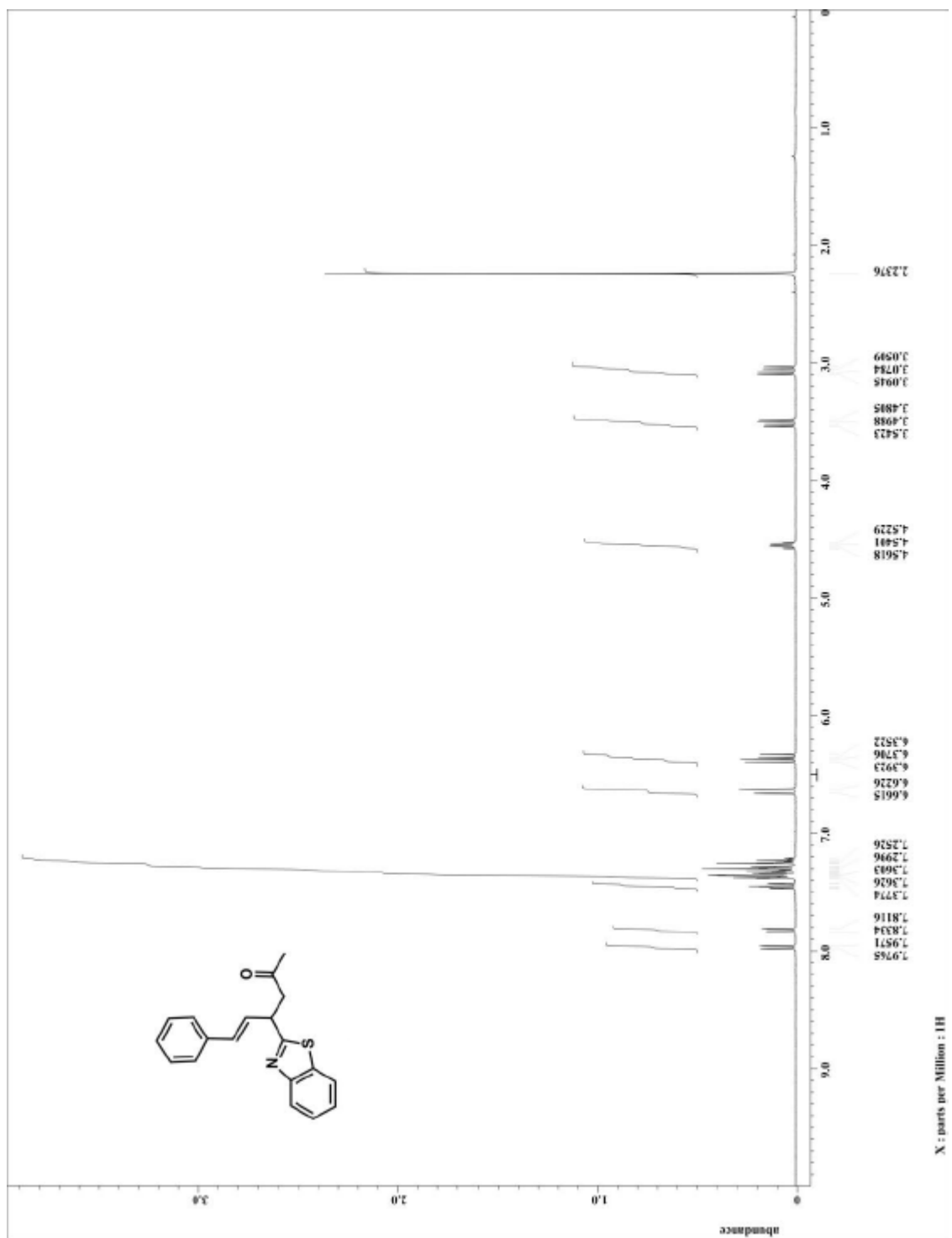
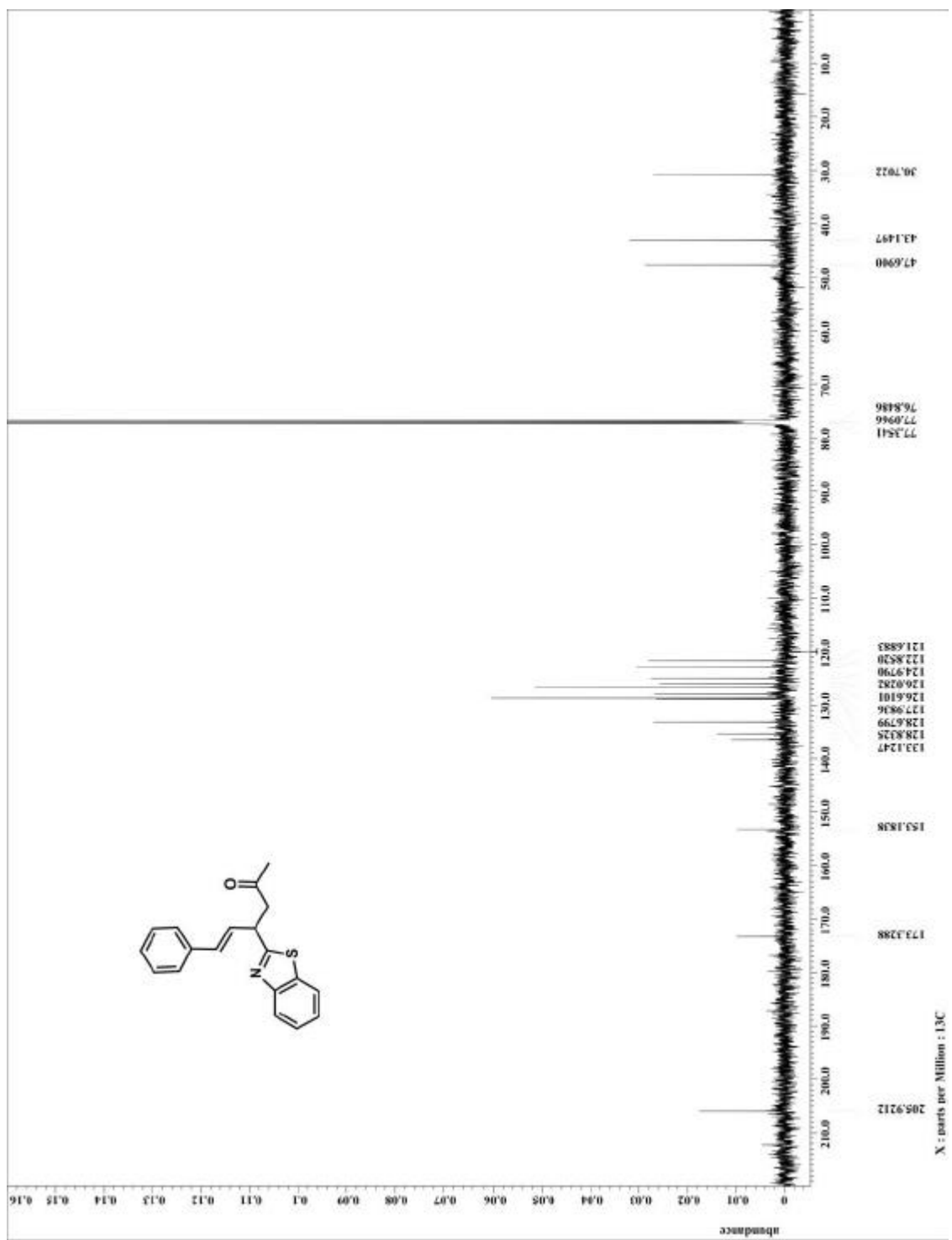
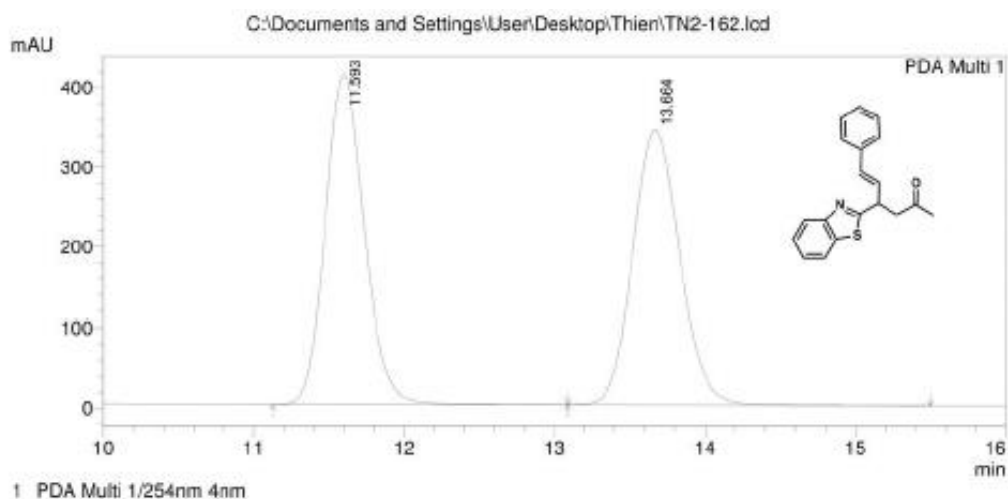


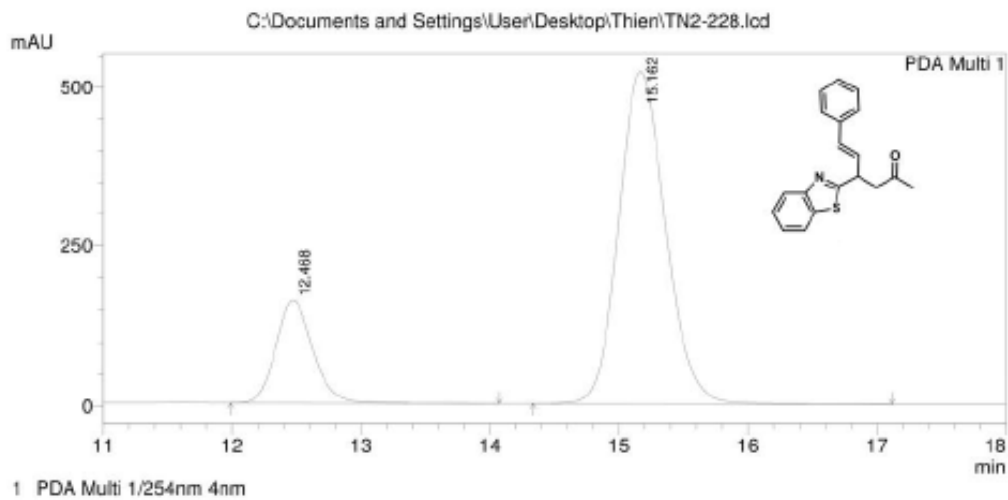
Figure A.1.57. ^1H NMR for compound 121





PeakTable

Peak#	Ret. Time	Area	Height	Area %	Height %
1	11.593	7441353	412047	49.878	54.507
2	13.664	7477804	343906	50.122	45.493
Total		14919157	755953	100.000	100.000



PeakTable

Peak#	Ret. Time	Area	Height	Area %	Height %
1	12.468	3208592	159170	19.679	23.401
2	15.162	13096262	521007	80.321	76.599
Total		16304854	680177	100.000	100.000

Figure A.1.59. HPLC trace for compound 121

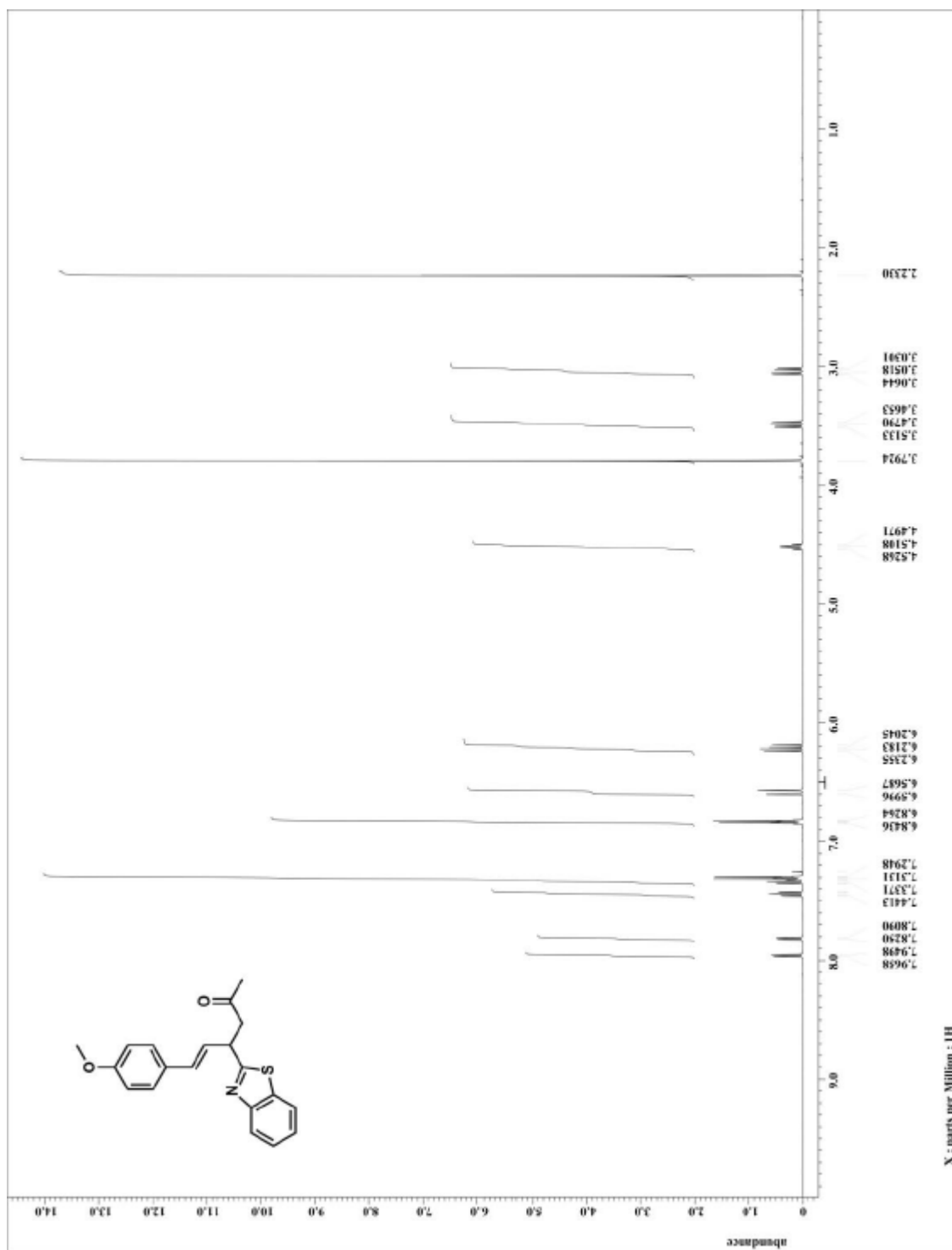


Figure A.1.60. ^1H NMR for compound 122

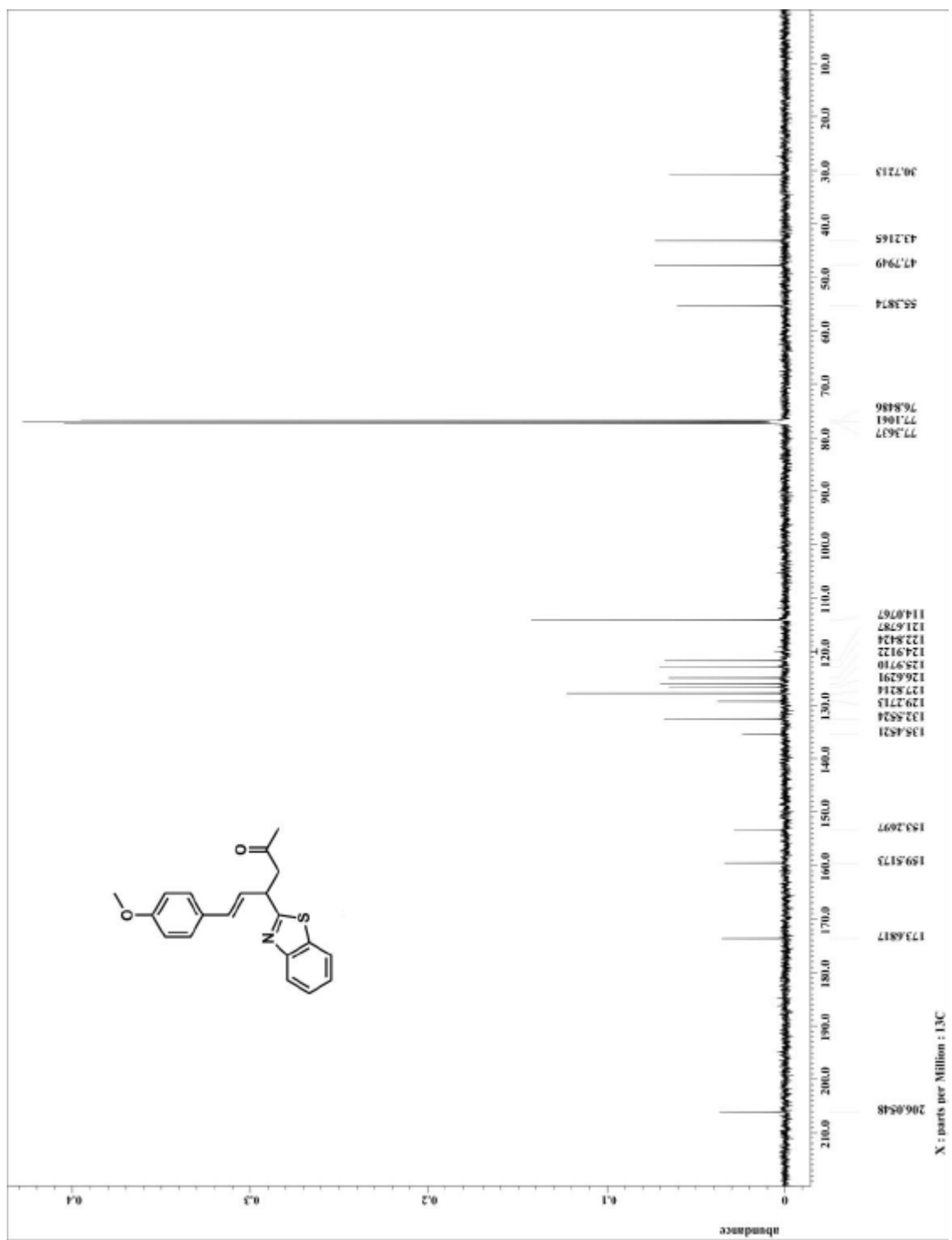
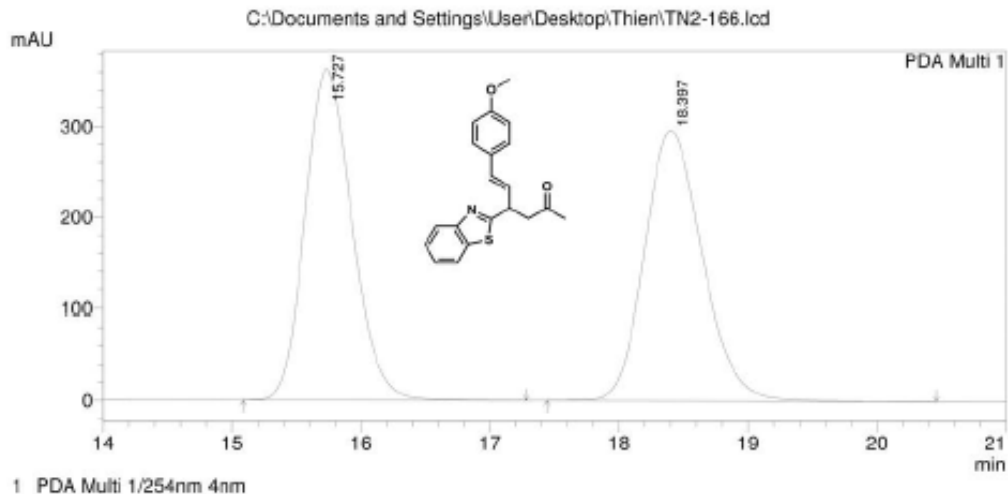
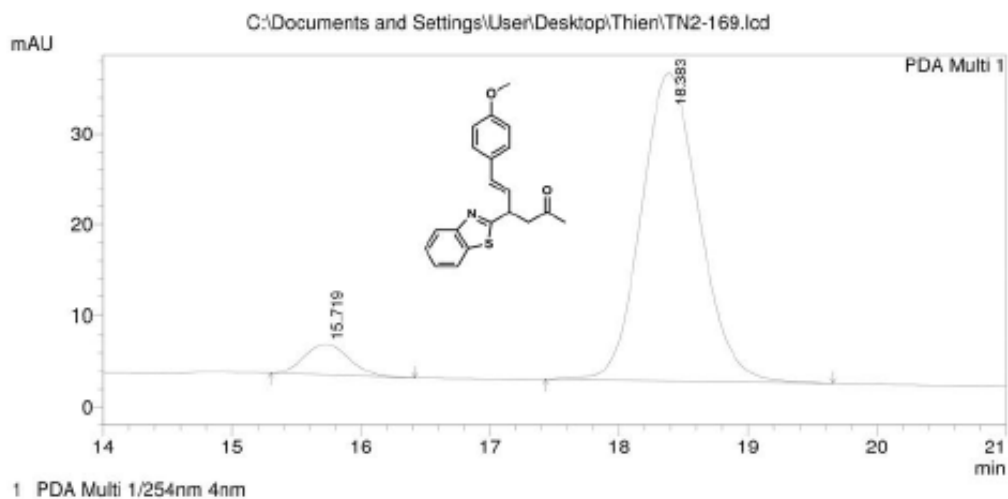


Figure A.1.61. ^{13}C NMR for compound 122



PeakTable

Peak#	Ret. Time	Area	Height	Area %	Height %
1	15.727	9192319	363070	49.936	55.086
2	18.397	9216057	296032	50.064	44.914
Total		18408376	659102	100.000	100.000



PeakTable

Peak#	Ret. Time	Area	Height	Area %	Height %
1	15.719	82302	3428	7.240	9.202
2	18.383	1054384	33818	92.760	90.798
Total		1136685	37246	100.000	100.000

Figure A.1.62. HPLC trace for compound 122

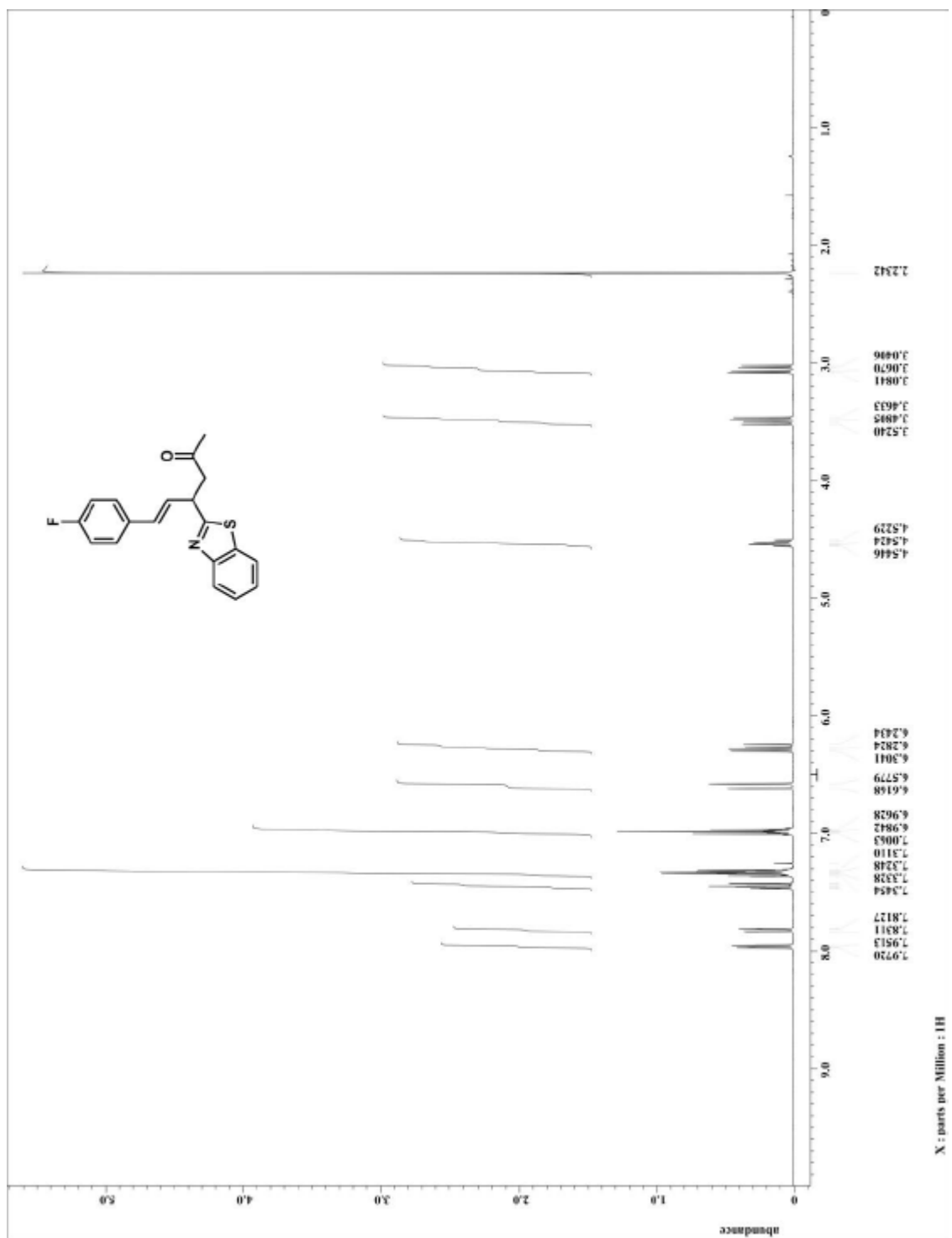


Figure A.1.63. ^1H NMR for compound 123

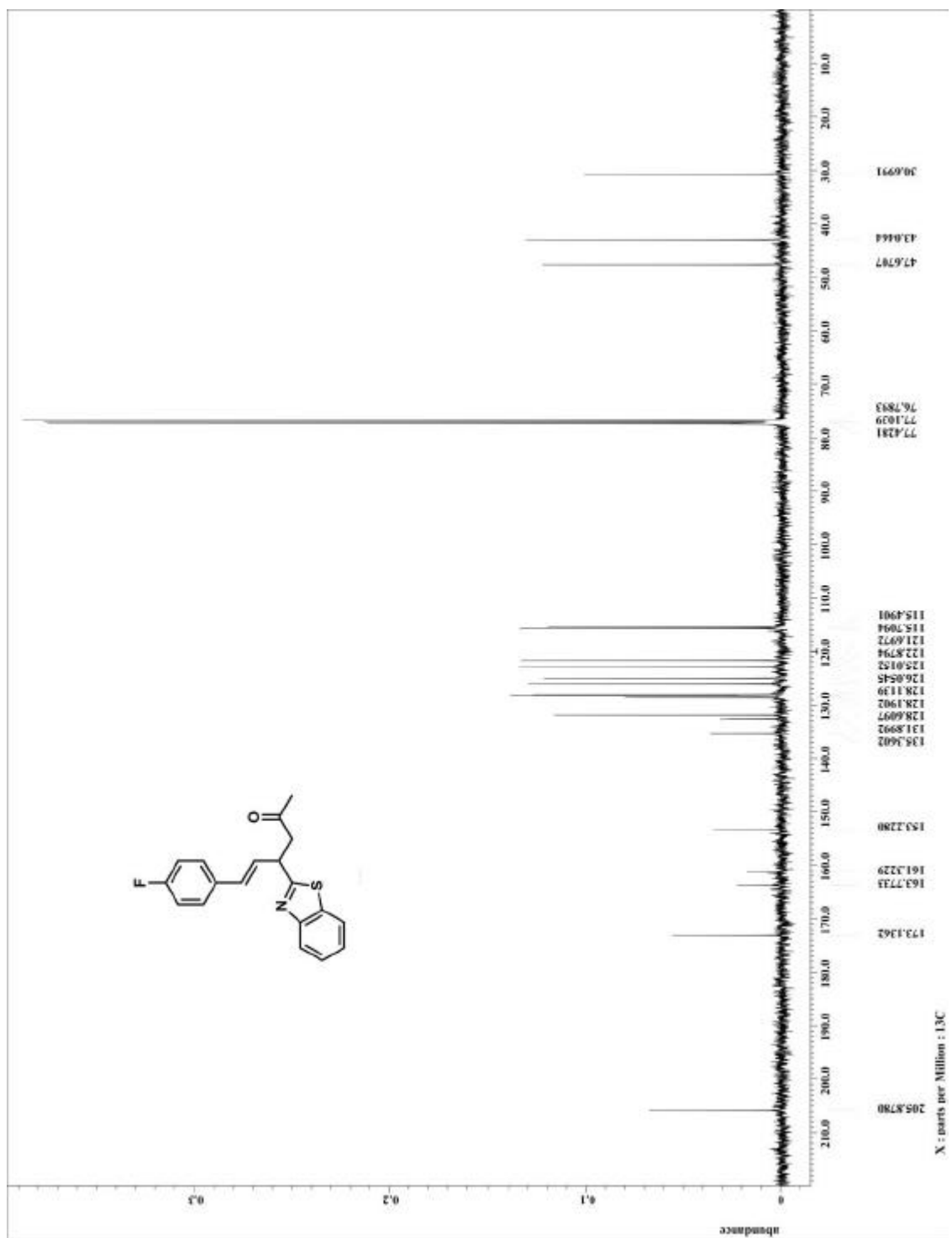
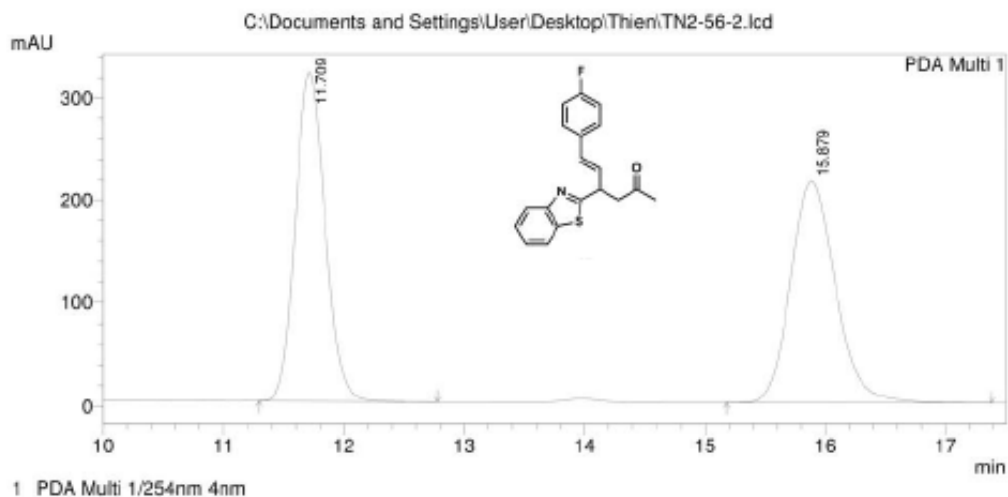
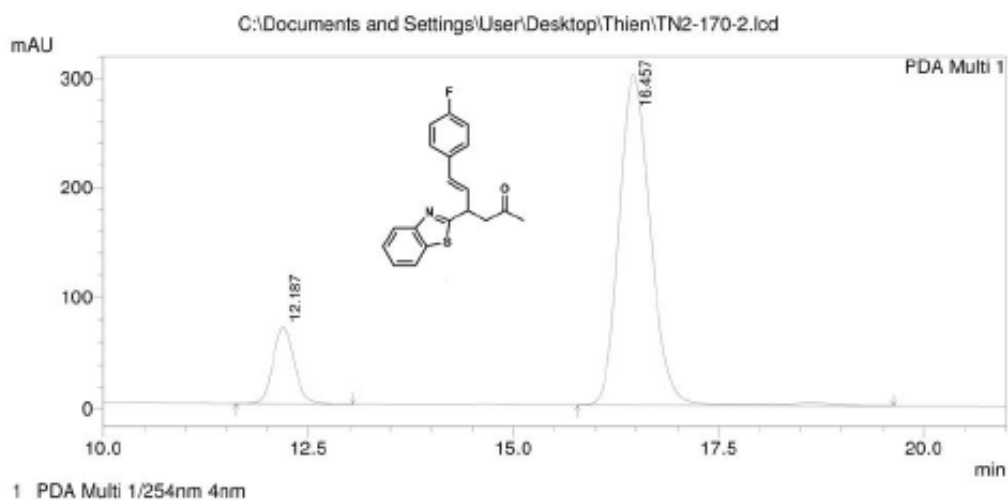


Figure A.1.64. ^{13}C NMR for compound 123



PeakTable

Peak#	Ret. Time	Area	Height	Area %	Height %
1	11.709	5488295	320224	49.608	59.718
2	15.879	5574973	216000	50.392	40.282
Total		11063268	536224	100.000	100.000



PeakTable

Peak#	Ret. Time	Area	Height	Area %	Height %
1	12.187	1269747	70014	13.741	18.910
2	16.457	7970570	300228	86.259	81.090
Total		9240317	370241	100.000	100.000

Figure A.1.65. HPLC trace for compound 123

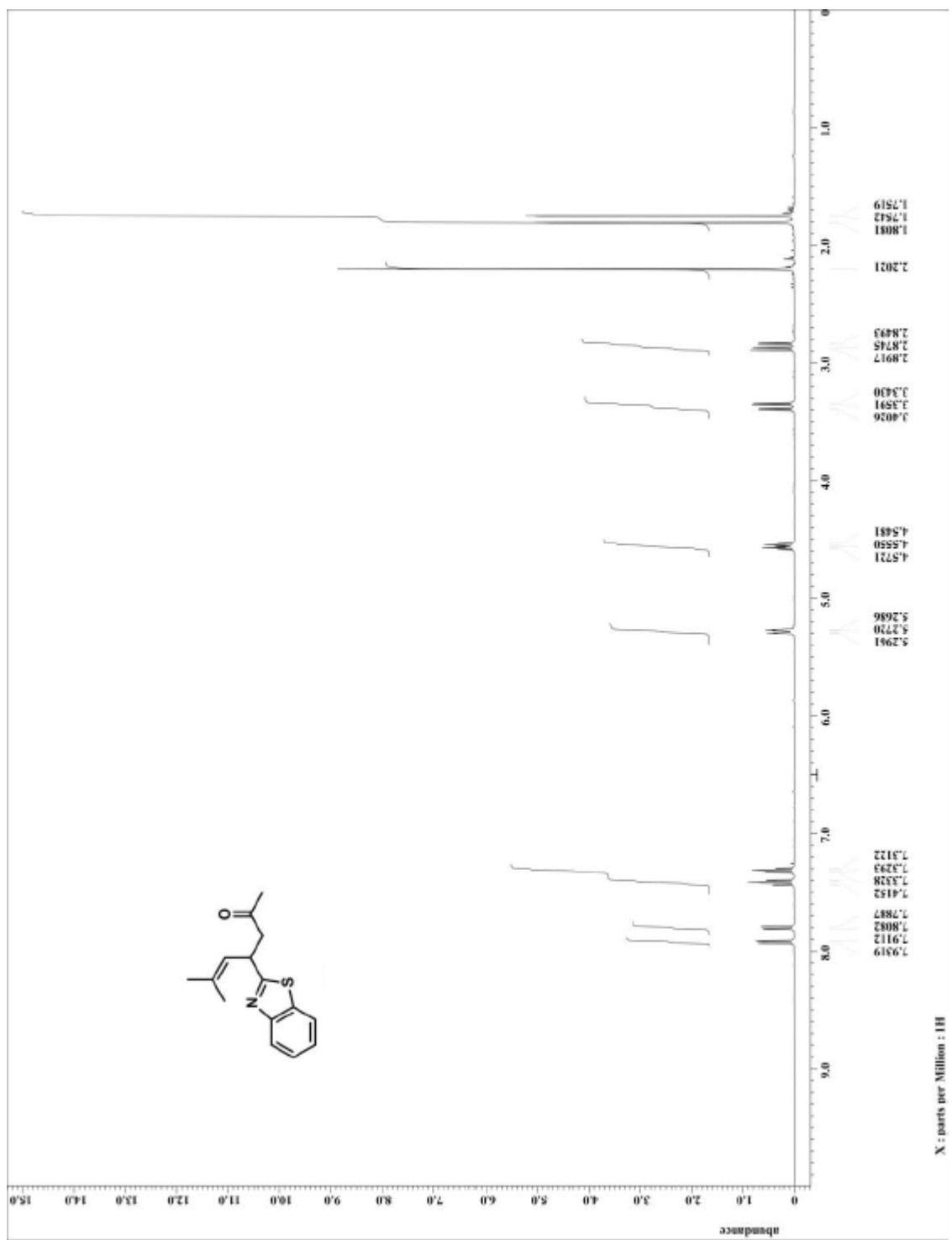


Figure A.1.66. ^1H NMR for compound 124

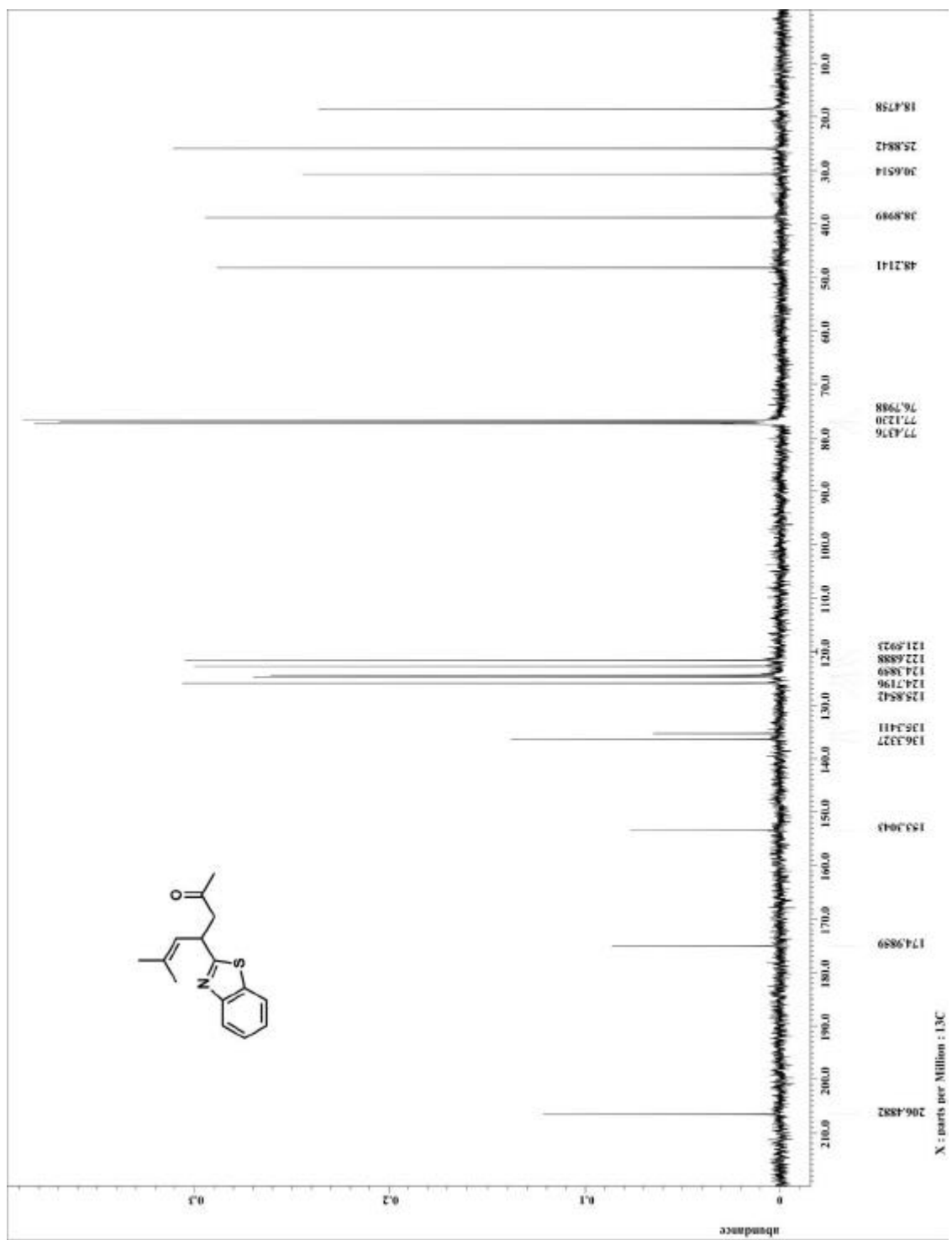
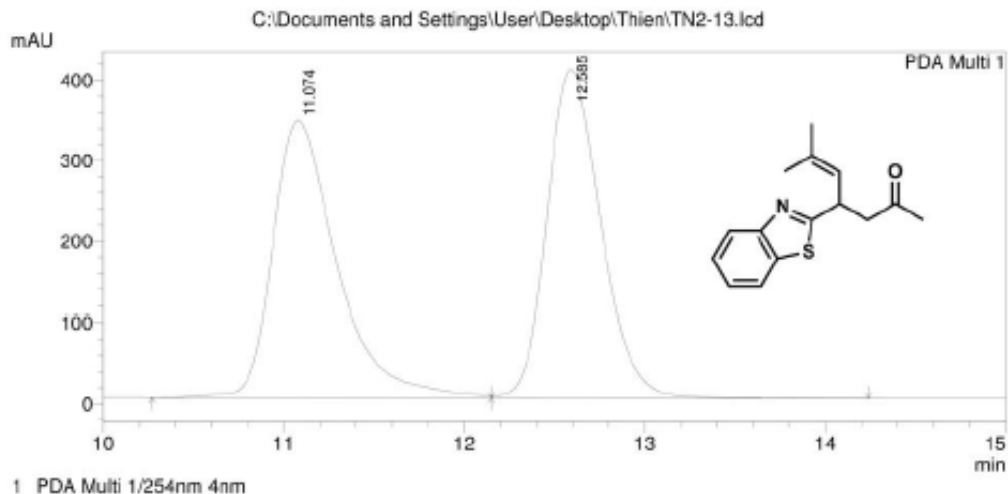
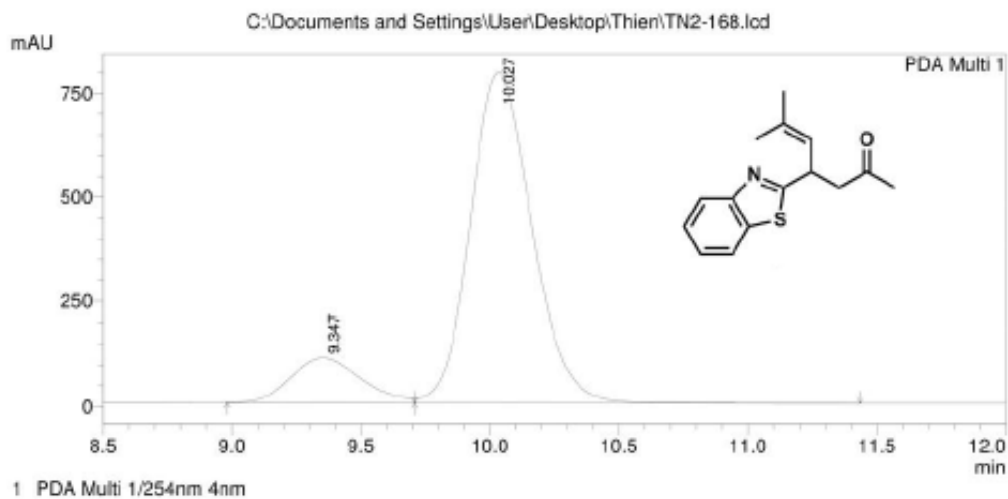


Figure A.1.67. ^{13}C NMR for compound 124



PeakTable

Peak#	Ret. Time	Area	Height	Area %	Height %
1	11.074	8460938	342699	50.115	45.800
2	12.585	8421948	405547	49.885	54.200
Total		16882886	748246	100.000	100.000



PeakTable

Peak#	Ret. Time	Area	Height	Area %	Height %
1	9.347	2054631	108827	13.514	12.067
2	10.027	13148637	793053	86.486	87.933
Total		15203268	901880	100.000	100.000

Figure A.1.68. HPLC trace for compound 124

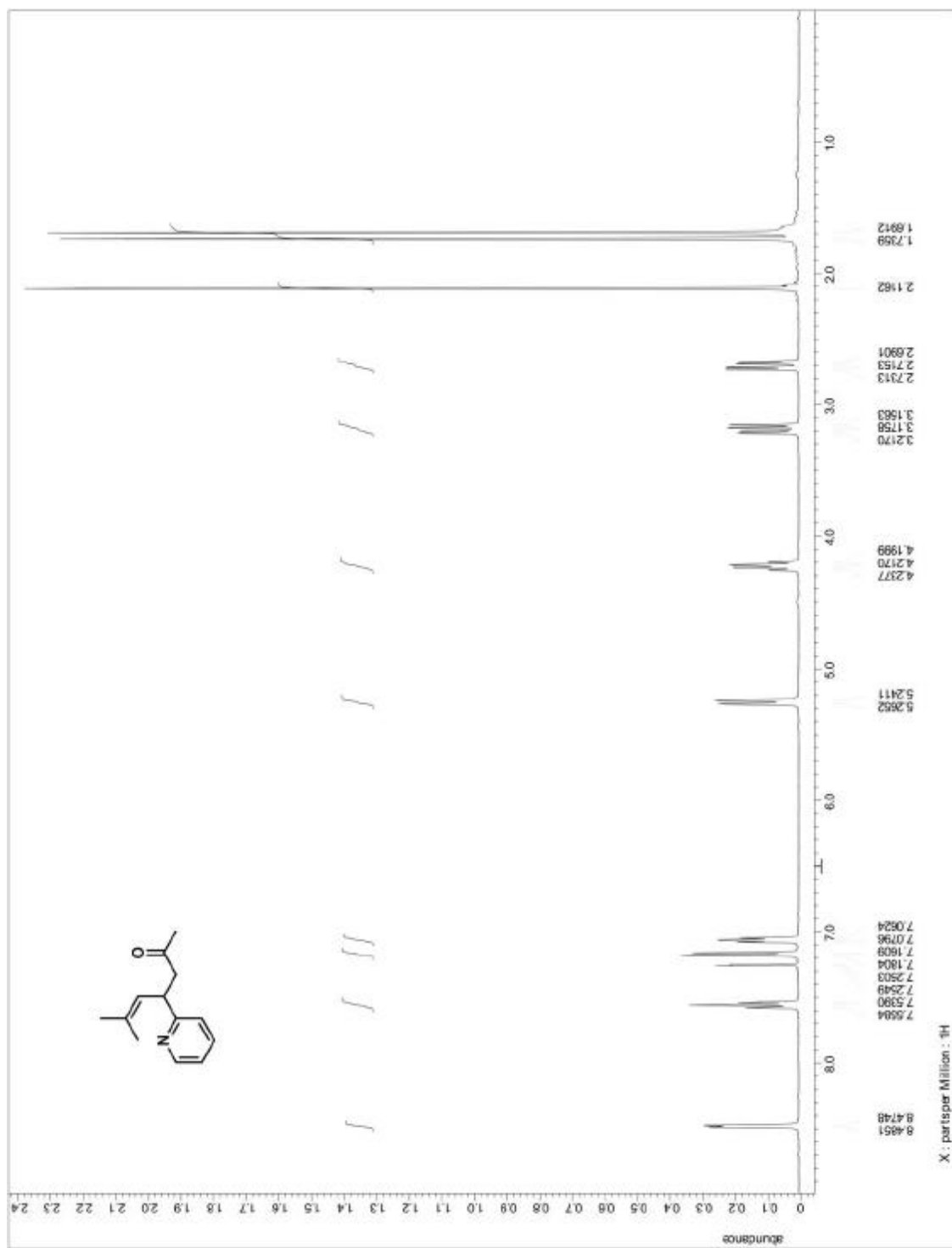


Figure A.1.69. ^1H NMR for compound 125

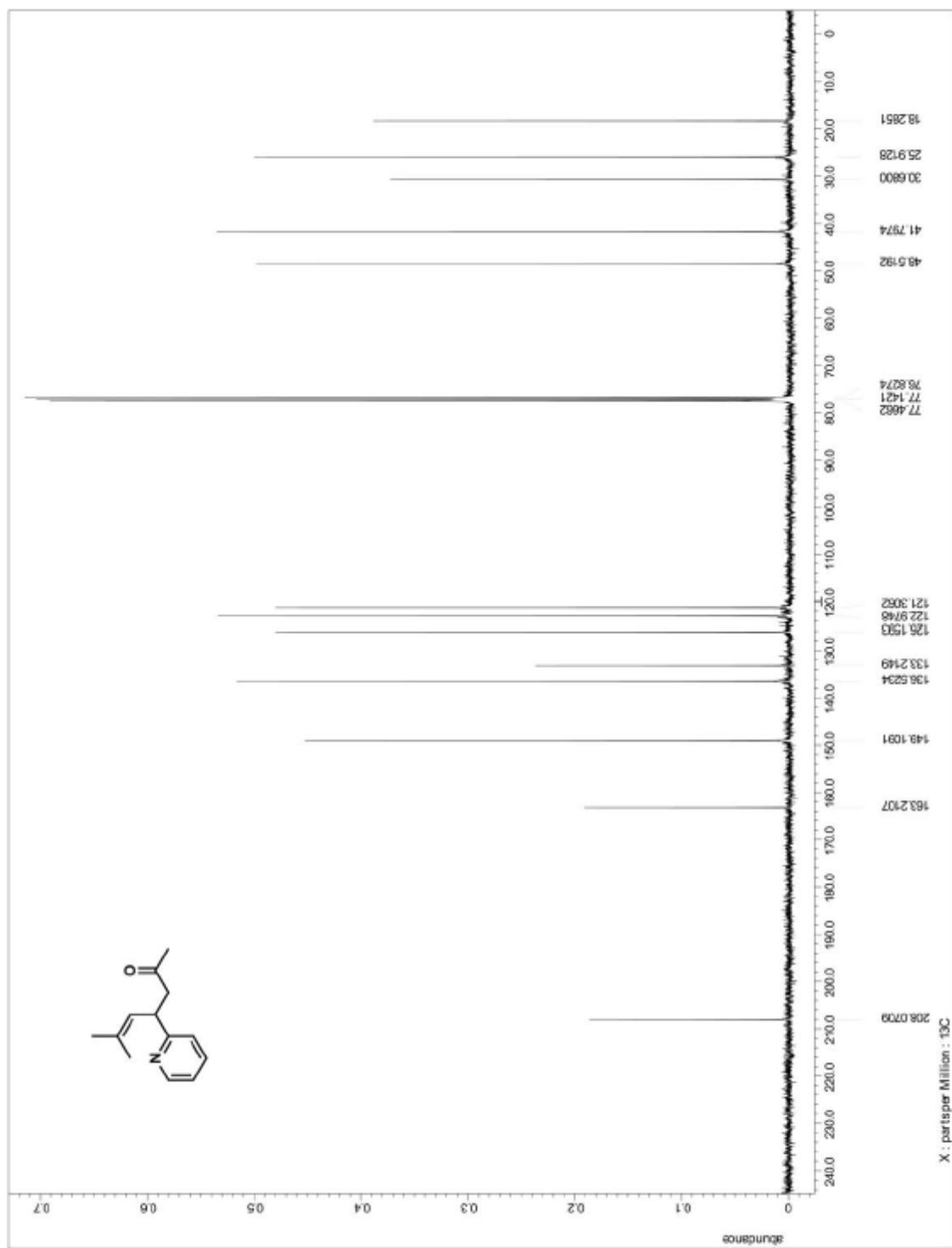
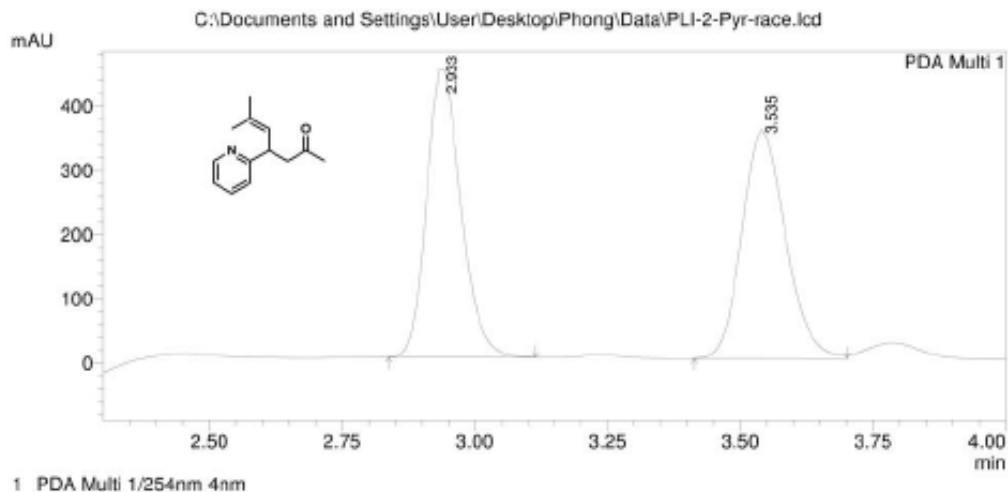


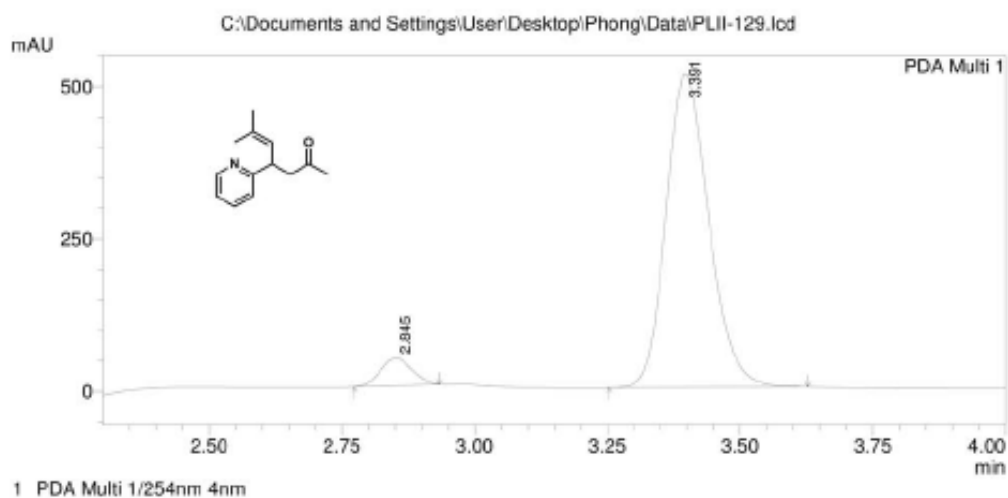
Figure A.1.70. ^{13}C NMR for compound 125



PeakTable

PDA Ch1 254nm 4nm

Peak#	Ret. Time	Area	Height	Area %	Height %
1	2.933	2022257	447091	49.855	55.675
2	3.535	2034011	355949	50.145	44.325
Total		4056268	803041	100.000	100.000



PeakTable

PDA Ch1 254nm 4nm

Peak#	Ret. Time	Area	Height	Area %	Height %
1	2.845	188720	45688	6.132	8.168
2	3.391	2889147	513637	93.868	91.832
Total		3077867	559325	100.000	100.000

Figure A.1.71. HPLC trace for compound 125

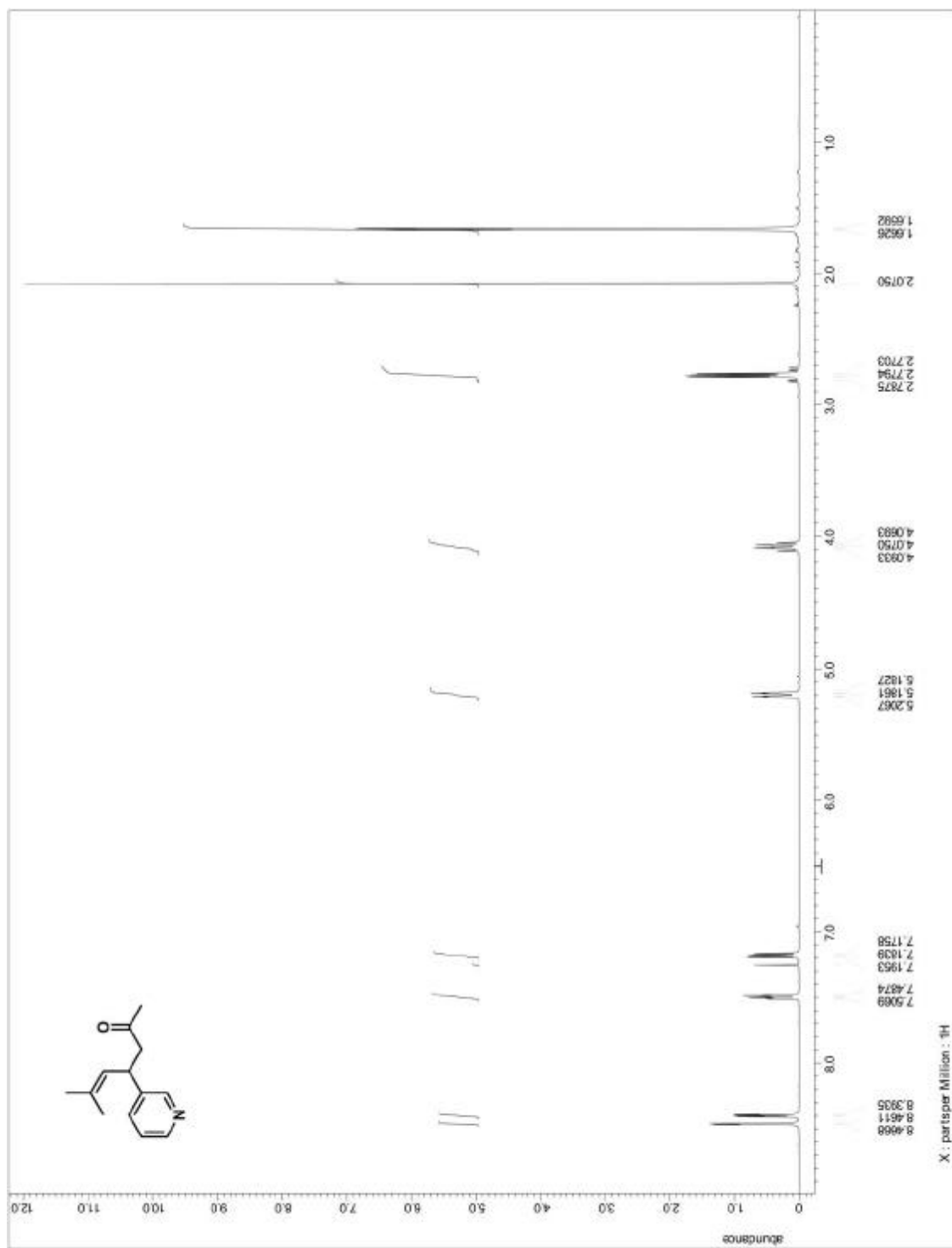


Figure A.1.72. ¹H NMR for compound 126

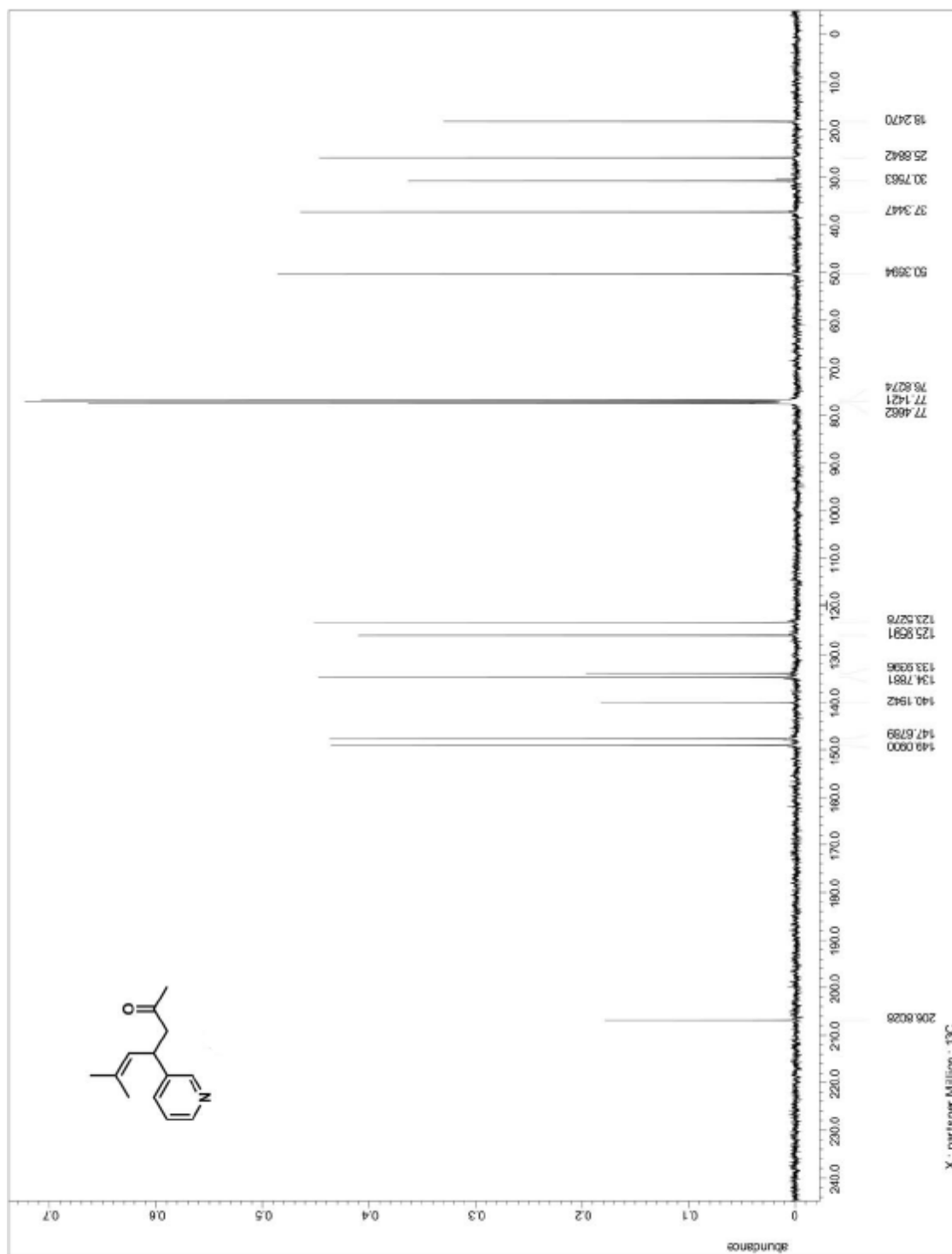
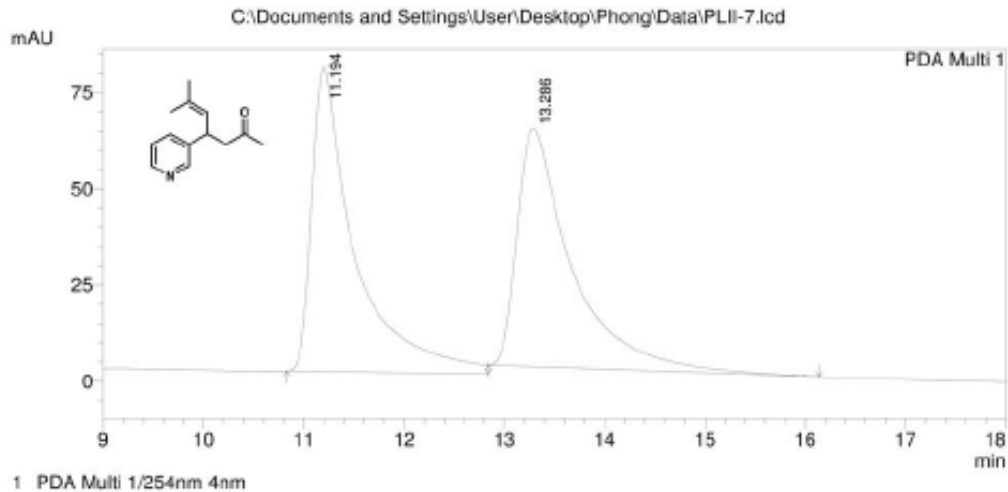


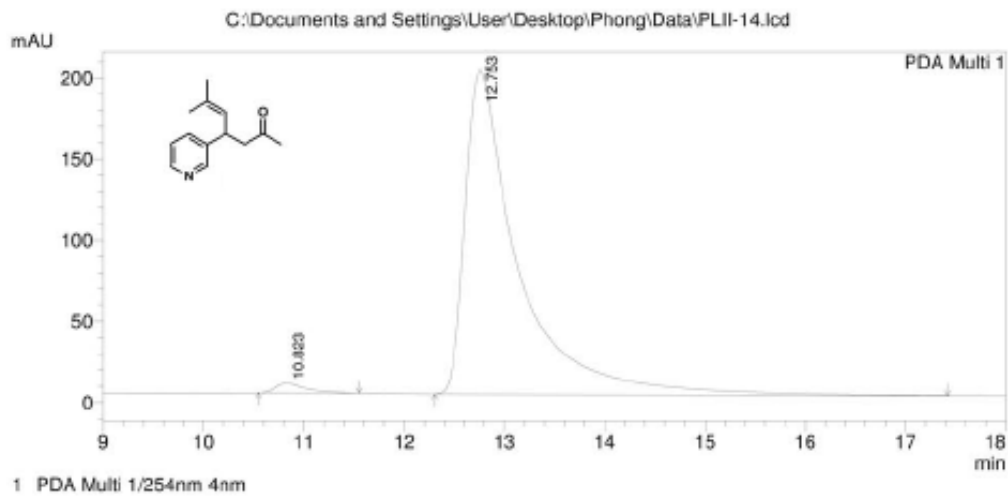
Figure A.1.73. ^{13}C NMR for compound 126



PeakTable

PDA Ch1 254nm 4nm

Peak#	Ret. Time	Area	Height	Area %	Height %
1	11.194	2349716	78928	50.241	56.079
2	13.286	2327219	61818	49.759	43.921
Total		4676935	140746	100.000	100.000



PeakTable

PDA Ch1 254nm 4nm

Peak#	Ret. Time	Area	Height	Area %	Height %
1	10.823	123044	5831	1.639	2.838
2	12.753	7386276	199657	98.361	97.162
Total		7509319	205487	100.000	100.000

Figure A.1.74. HPLC trace for compound 126

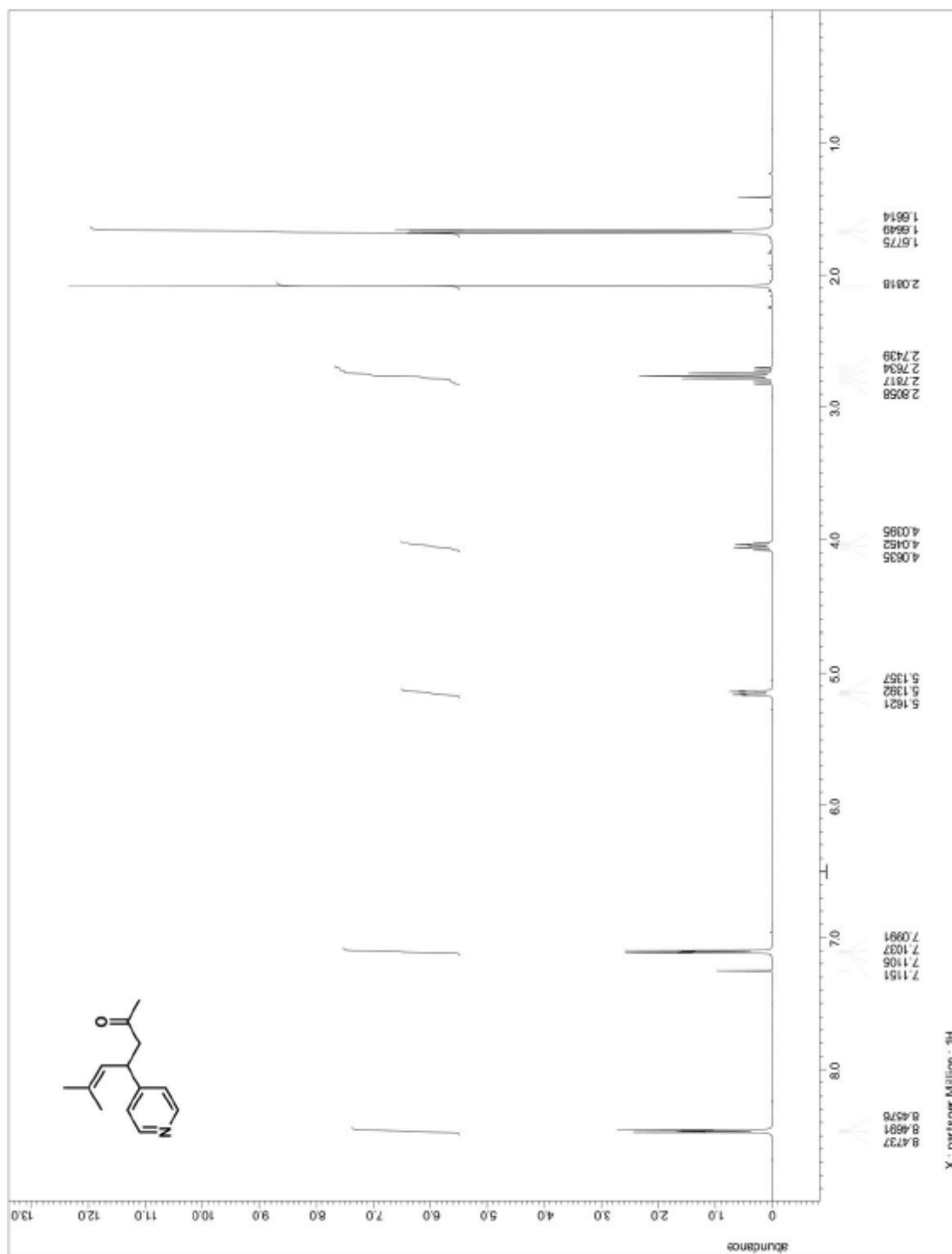


Figure A.1.75. ^1H NMR for compound 127

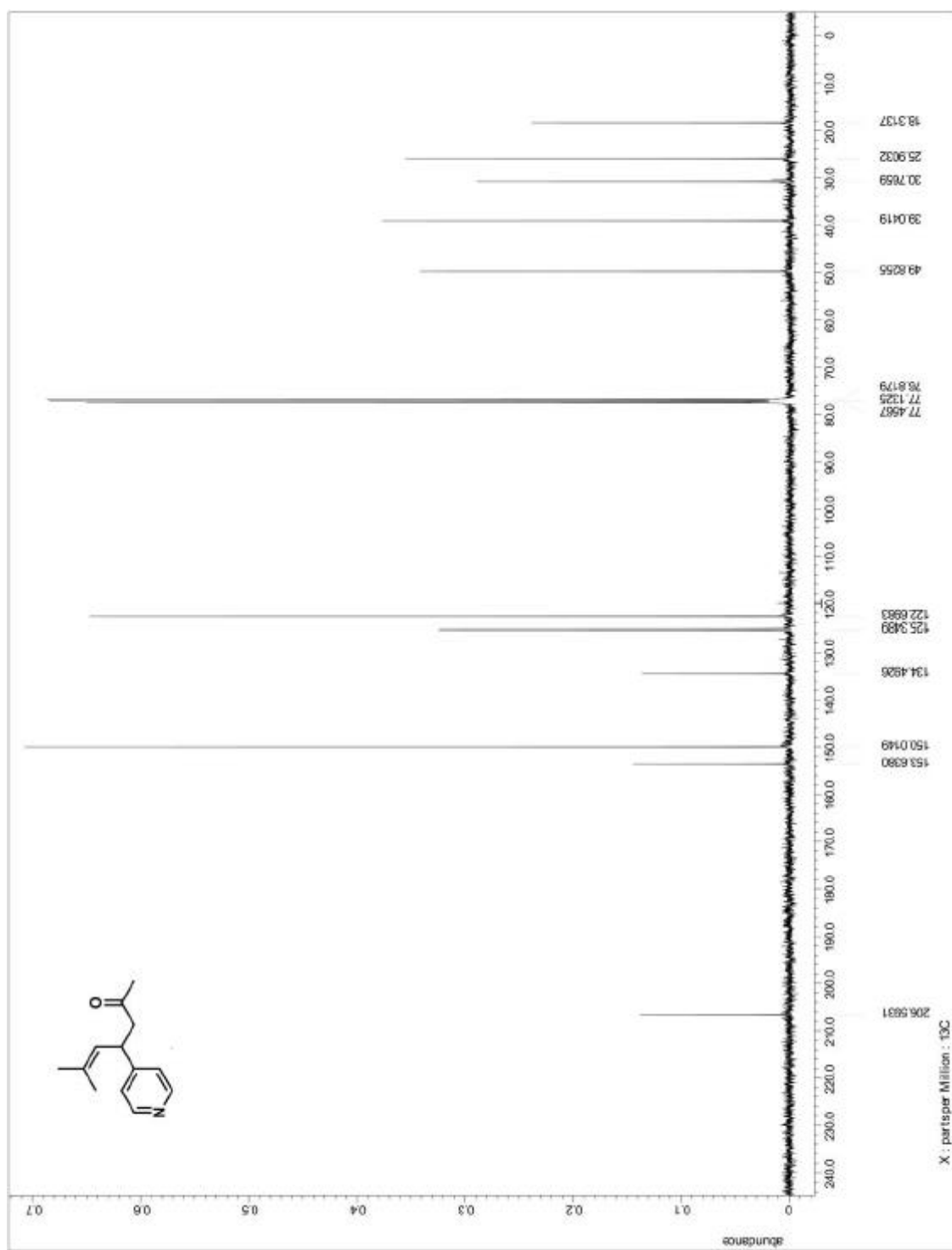
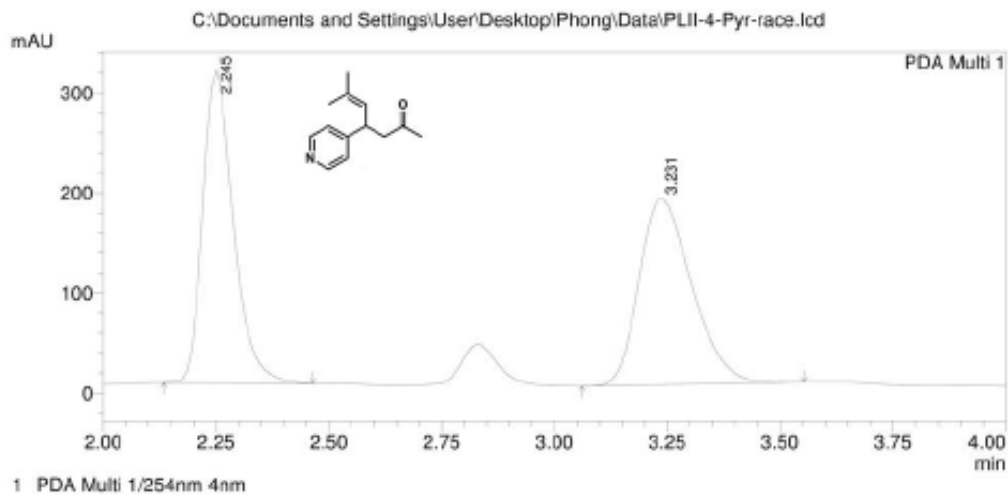
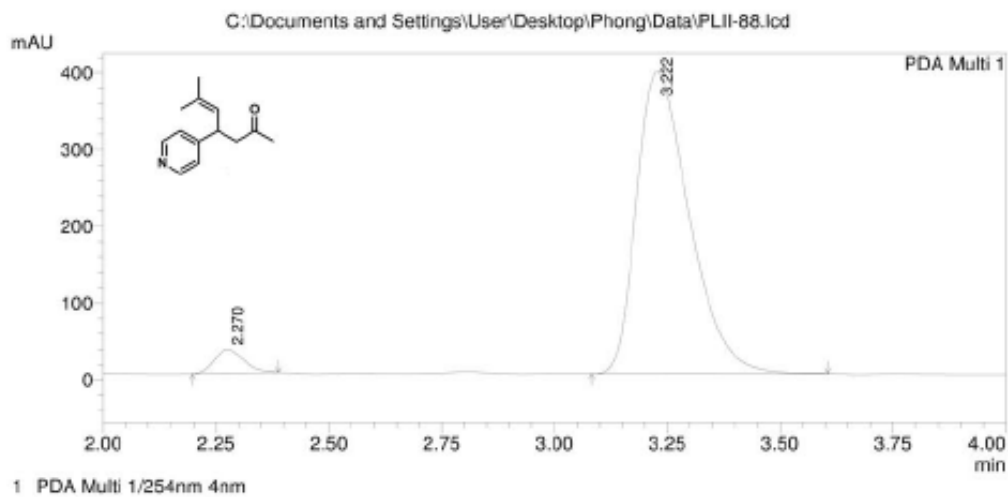


Figure A.1.76. ^{13}C NMR for compound 127



PeakTable

Peak#	Ret. Time	Area	Height	Area %	Height %
1	2.245	1471231	312075	49.401	62.653
2	3.231	1506900	186028	50.599	37.347
Total		2978131	498103	100.000	100.000



PeakTable

Peak#	Ret. Time	Area	Height	Area %	Height %
1	2.270	140357	31342	4.209	7.382
2	3.222	3194561	393231	95.791	92.618
Total		3334918	424573	100.000	100.000

Figure A.1.77. HPLC trace for compound 127

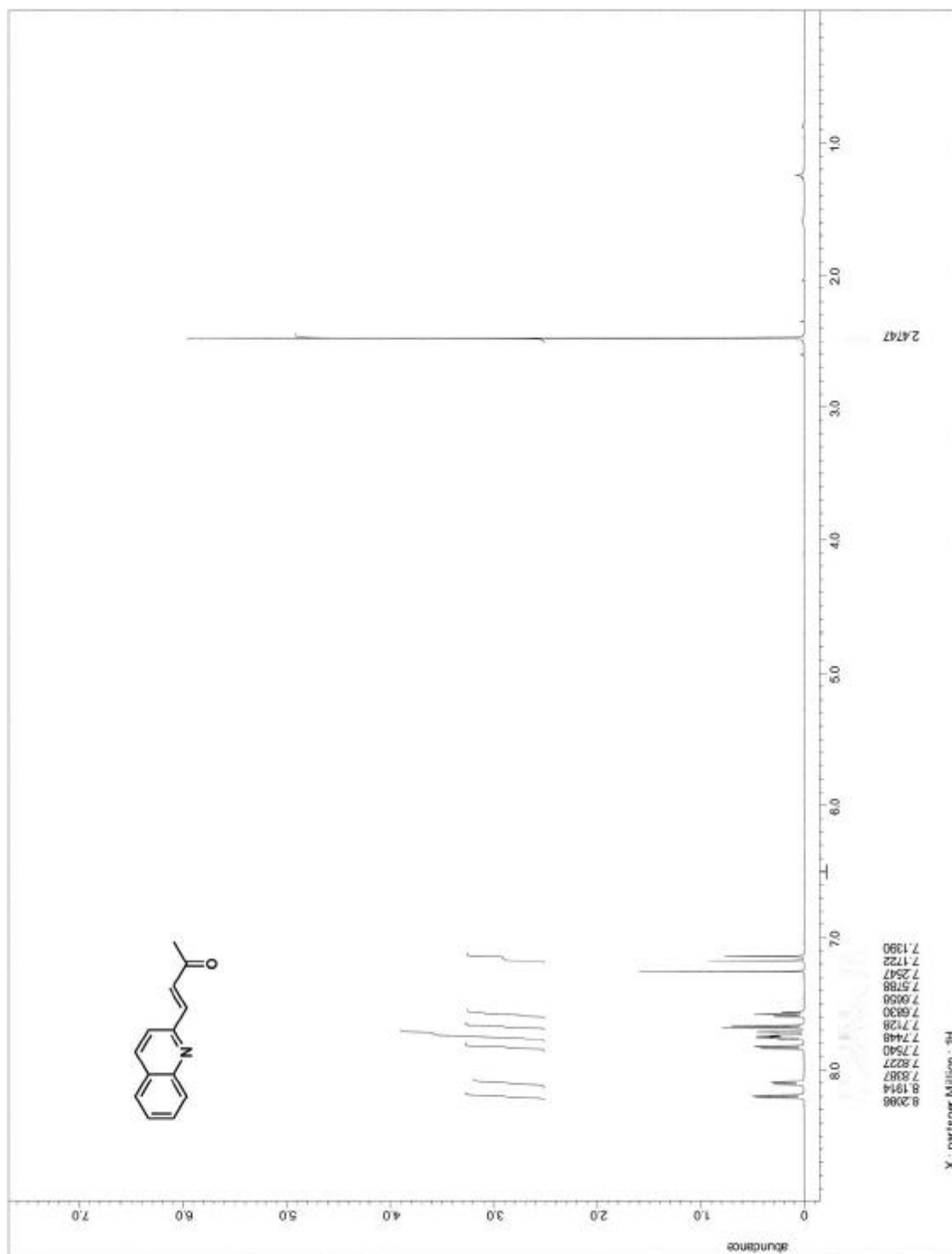


Figure A.1.78. ^1H NMR for precursor to compound 128

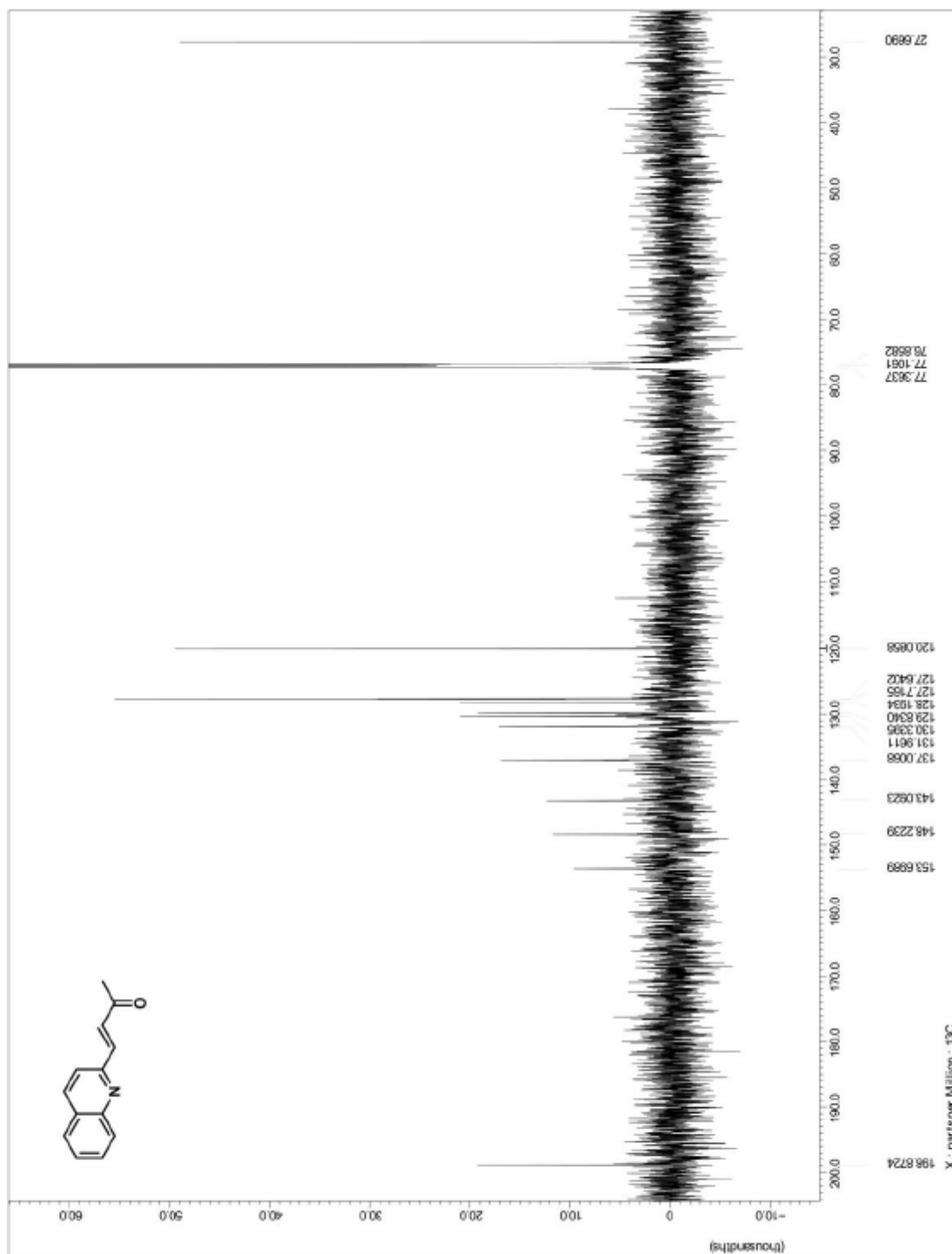


Figure A.1.79. ¹³C NMR for precursor to compound 128

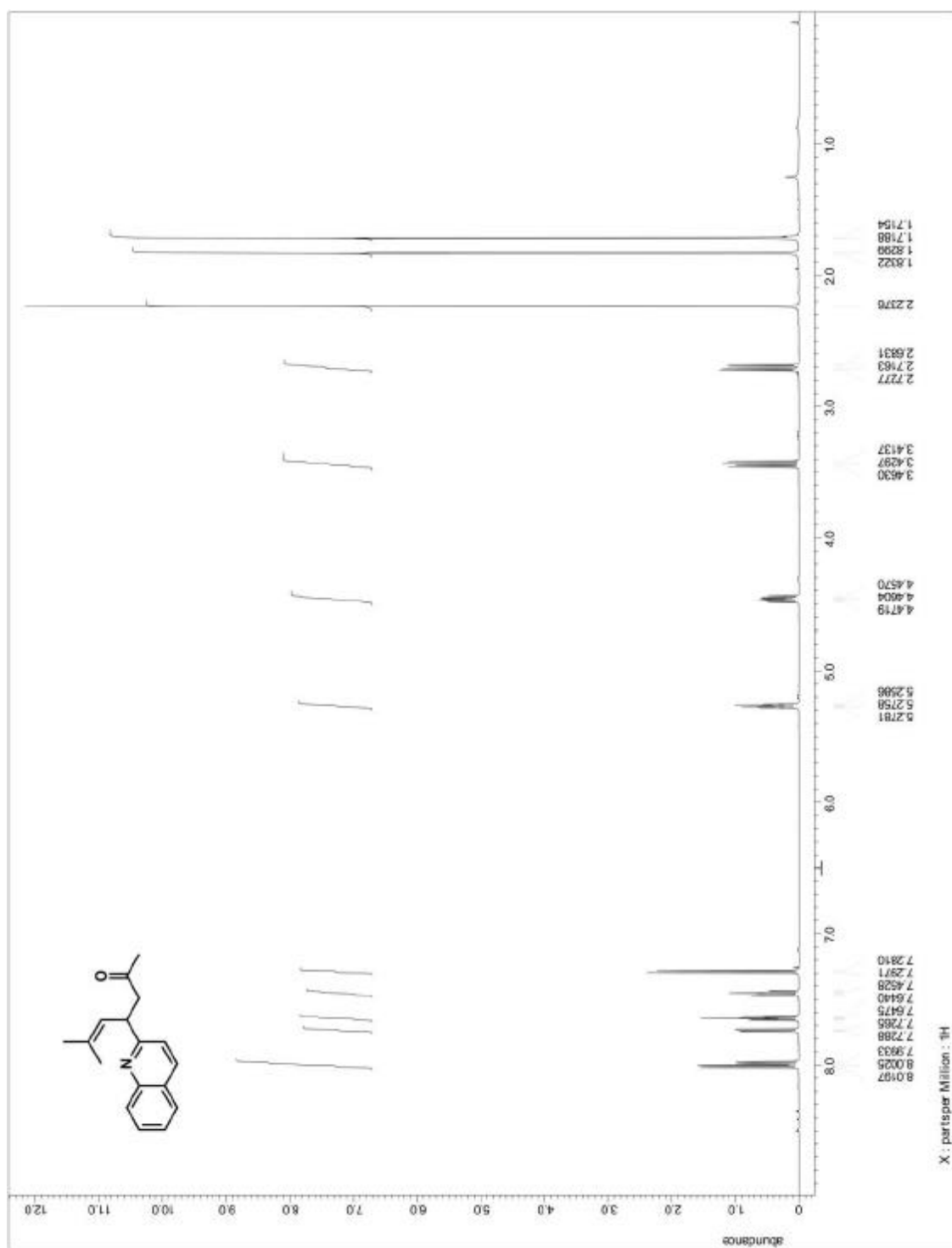


Figure A.1.80. ^1H NMR for compound 128

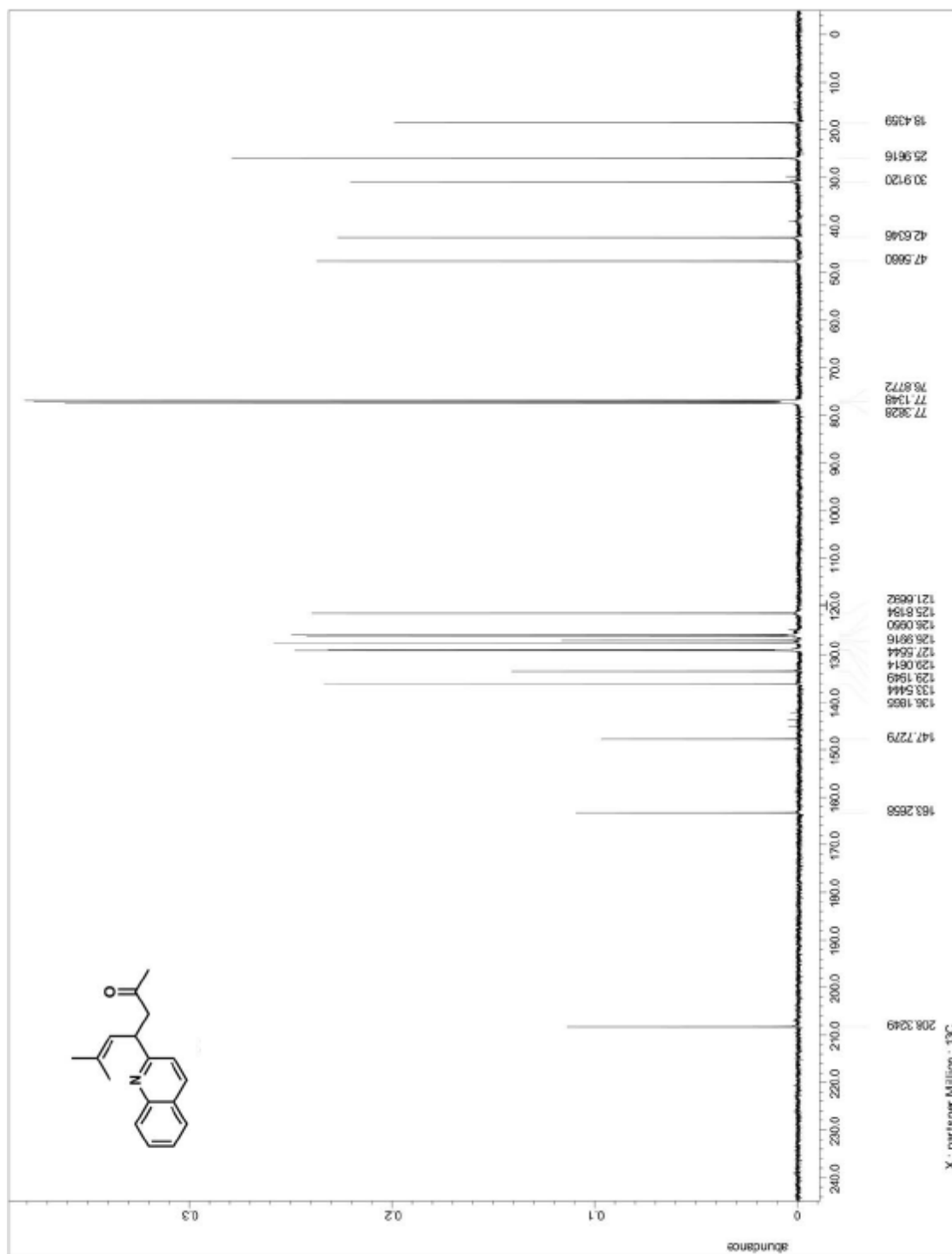
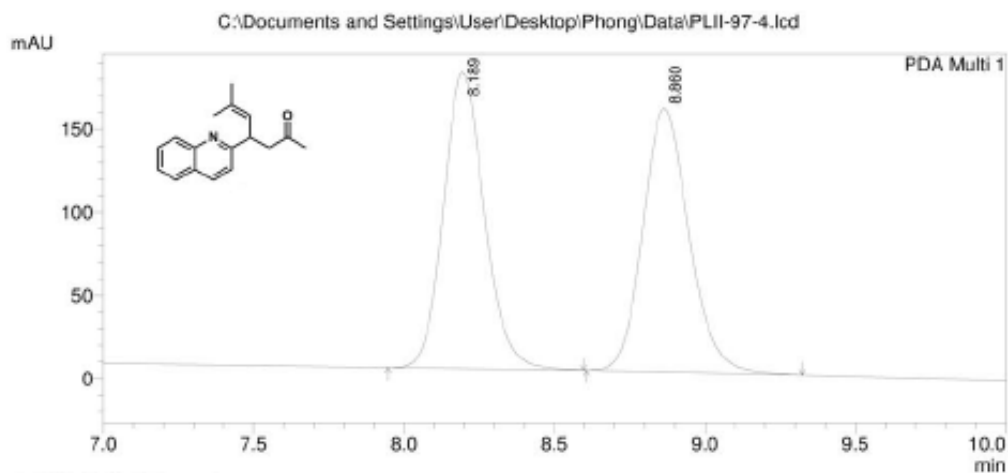
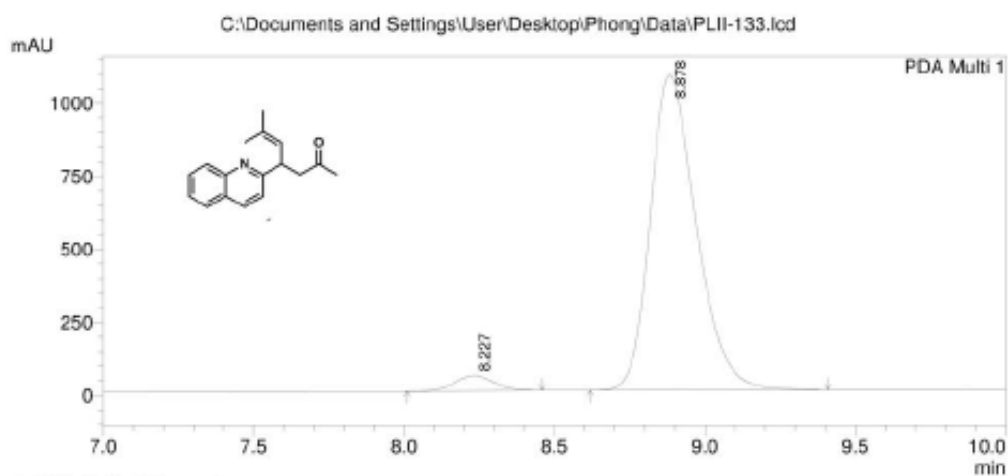


Figure A.1.81. ^{13}C NMR for compound 128



PeakTable

Peak#	Ret. Time	Area	Height	Area %	Height %
1	8.189	1688952	178304	50.045	52.915
2	8.860	1685933	158056	49.955	47.085
Total		3374885	336959	100.000	100.000



PeakTable

Peak#	Ret. Time	Area	Height	Area %	Height %
1	8.227	472476	52538	3.964	4.644
2	8.878	11448049	1078880	96.036	95.356
Total		11920525	1131418	100.000	100.000

Figure A.1.82. HPLC trace for compound 128

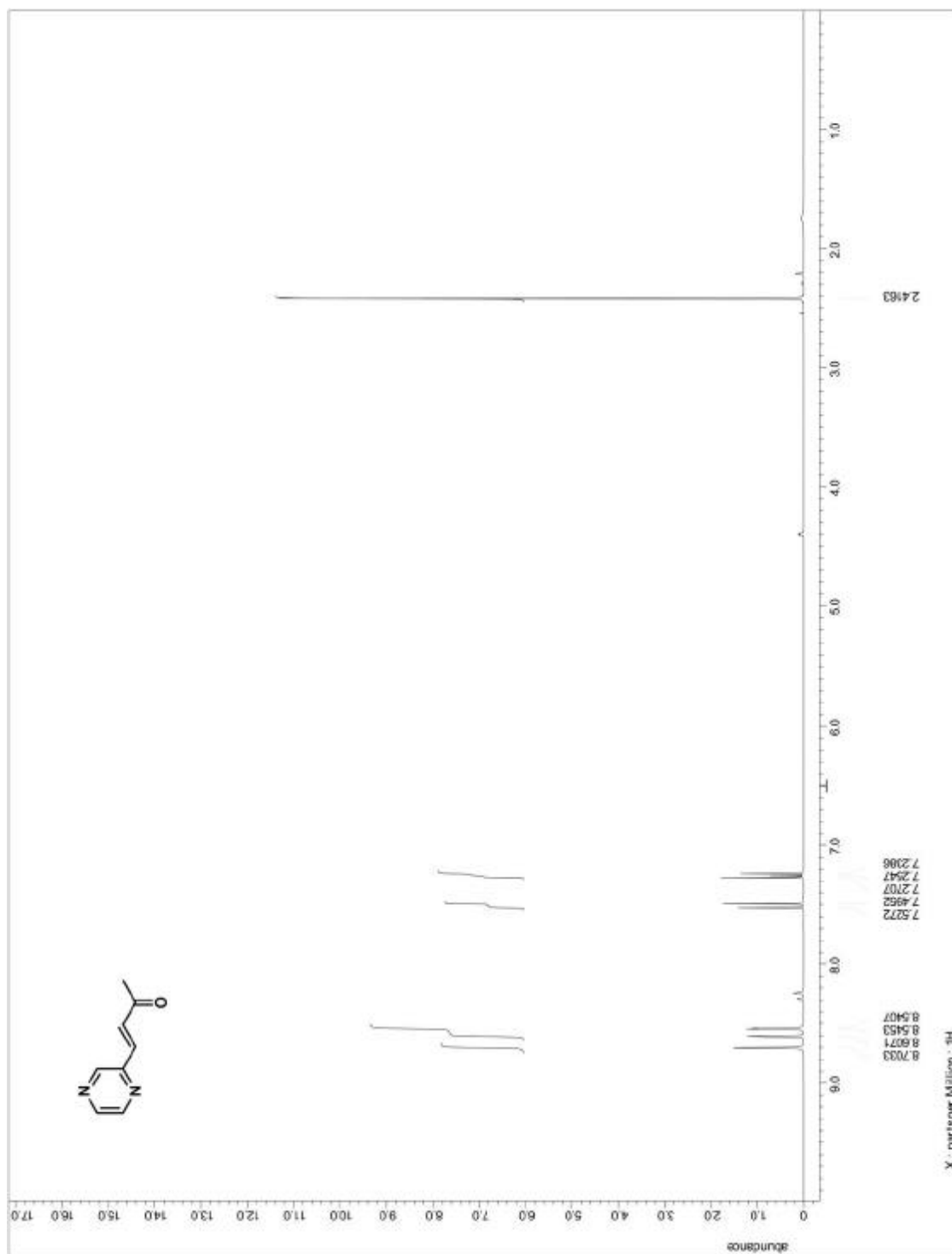


Figure A.1.83. ^1H NMR for precursor to compound 129

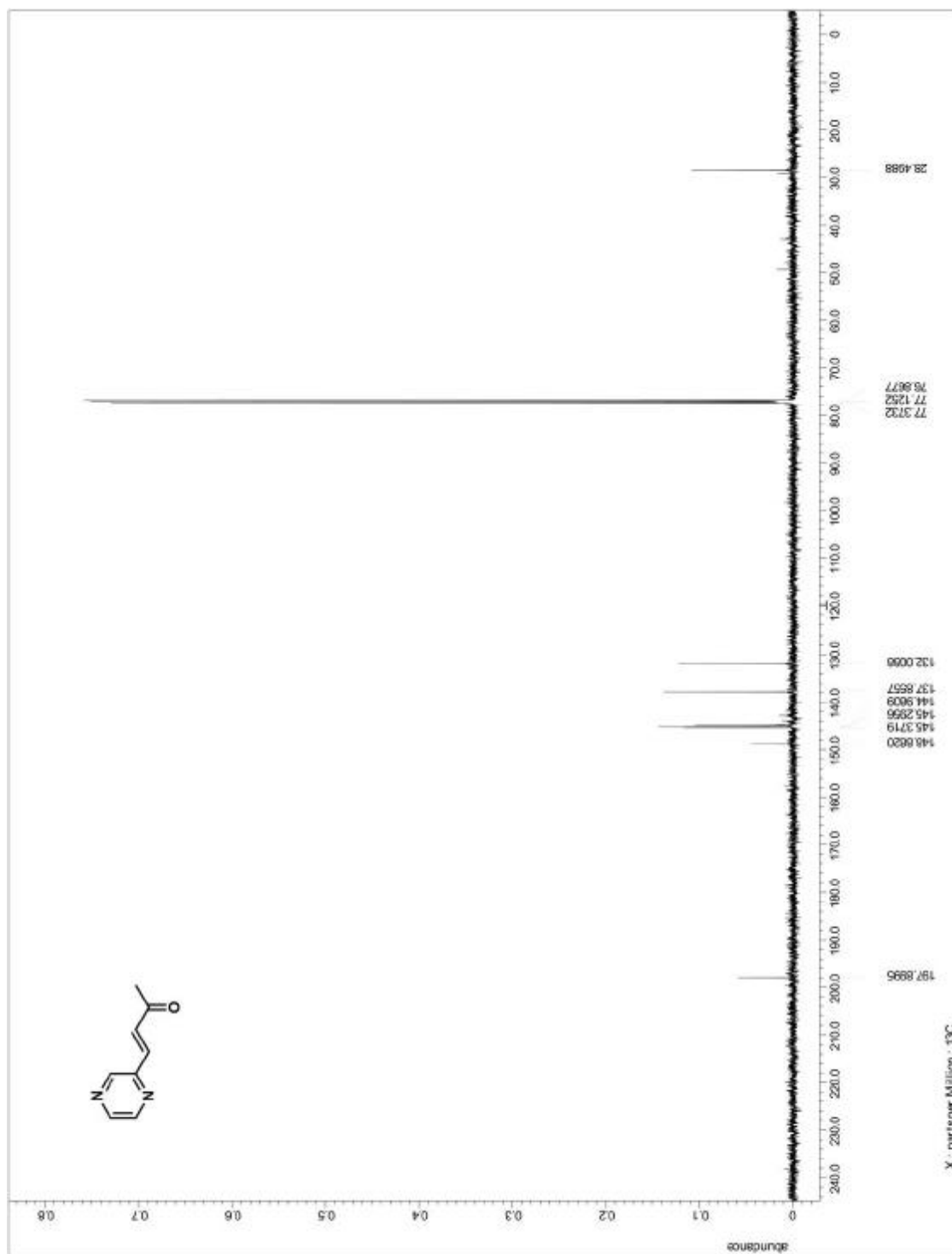


Figure A.1.84. ^{13}C NMR for precursor to compound 129

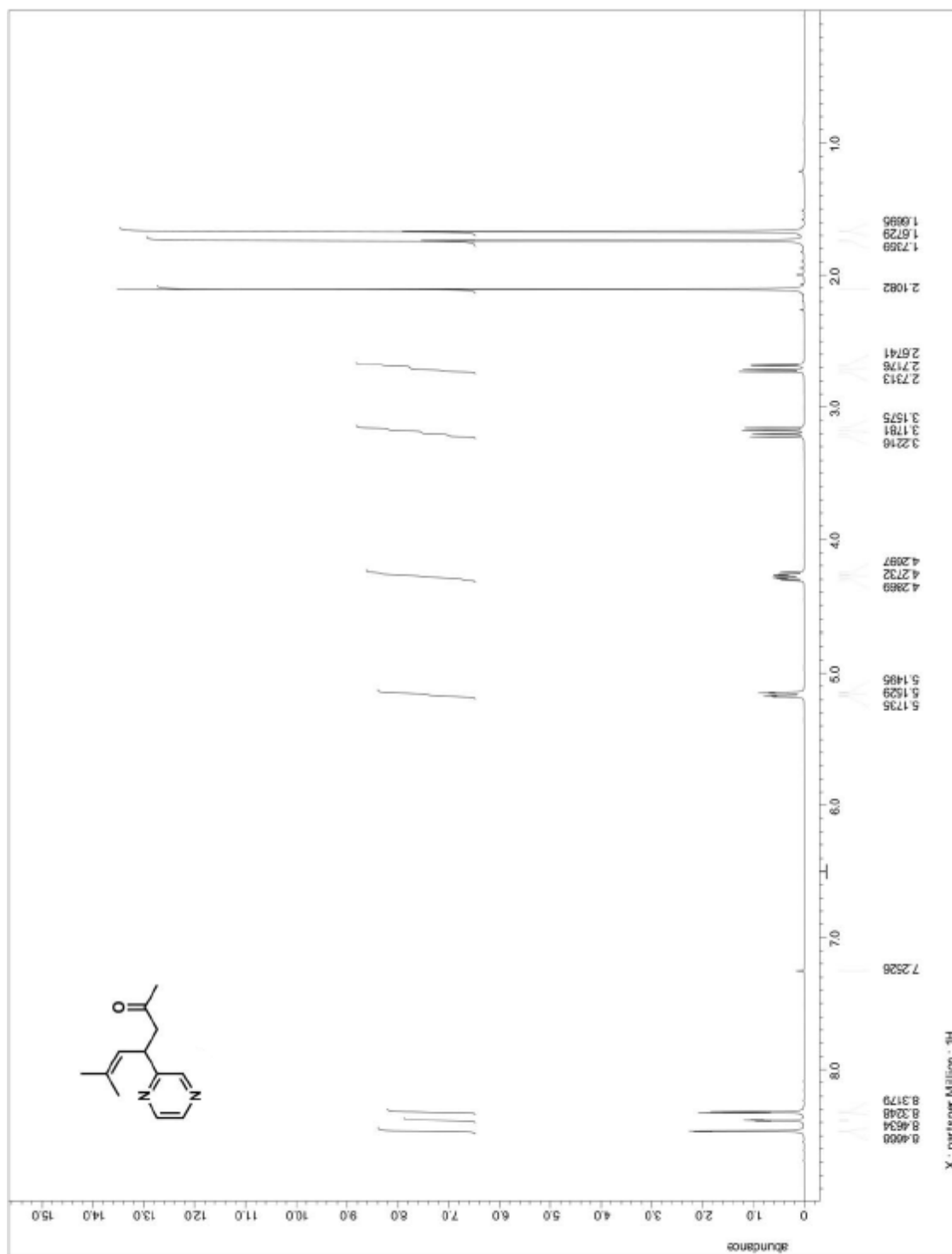


Figure A.1.85. ¹H NMR for compound 129

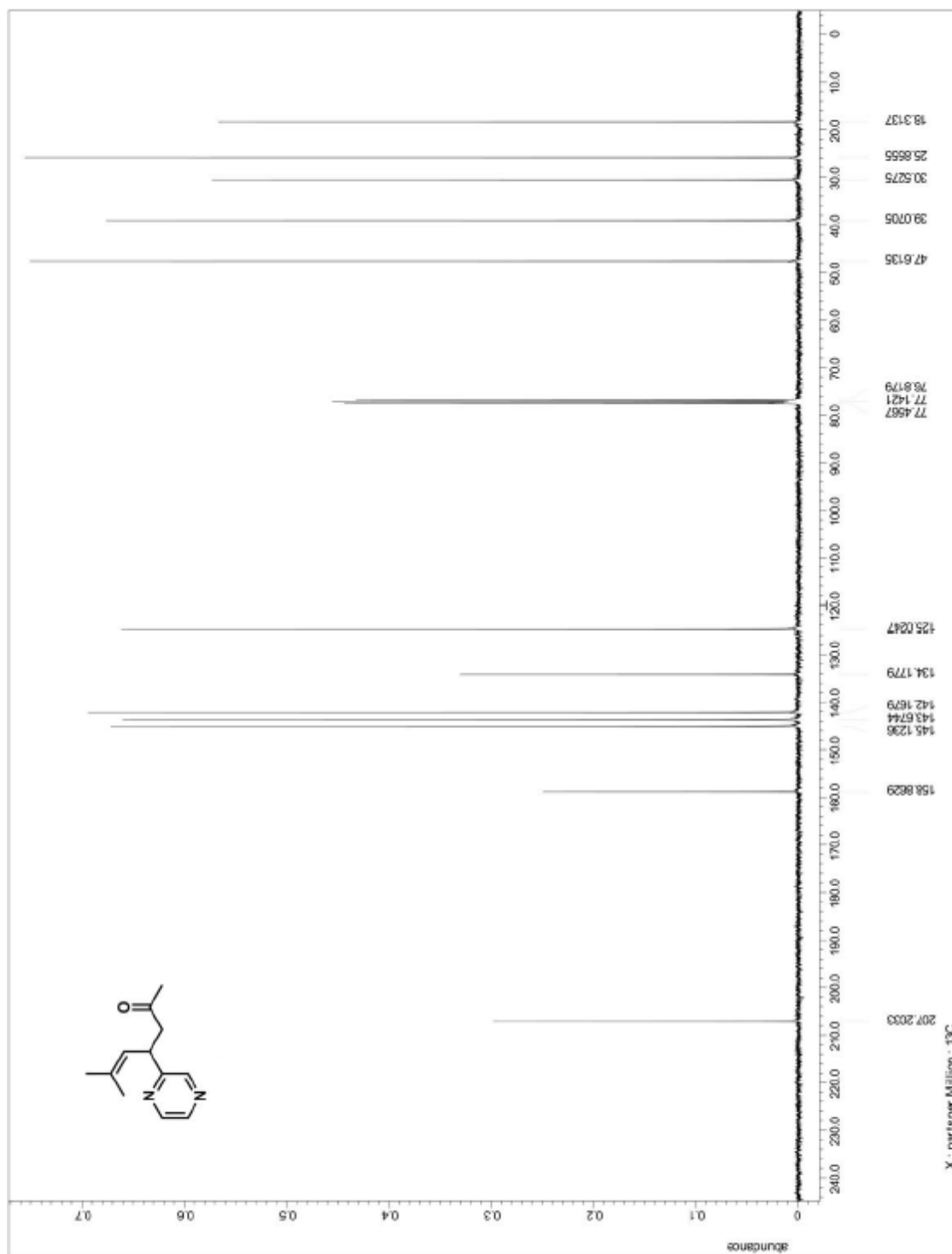
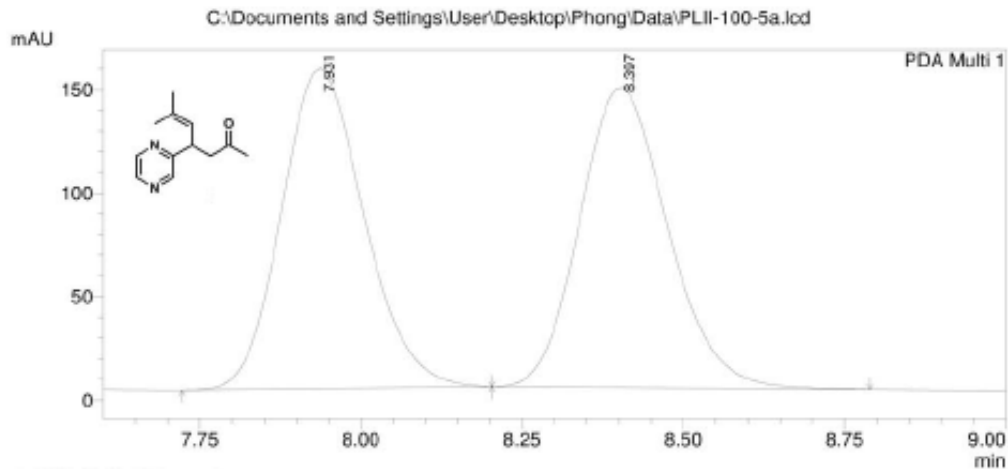
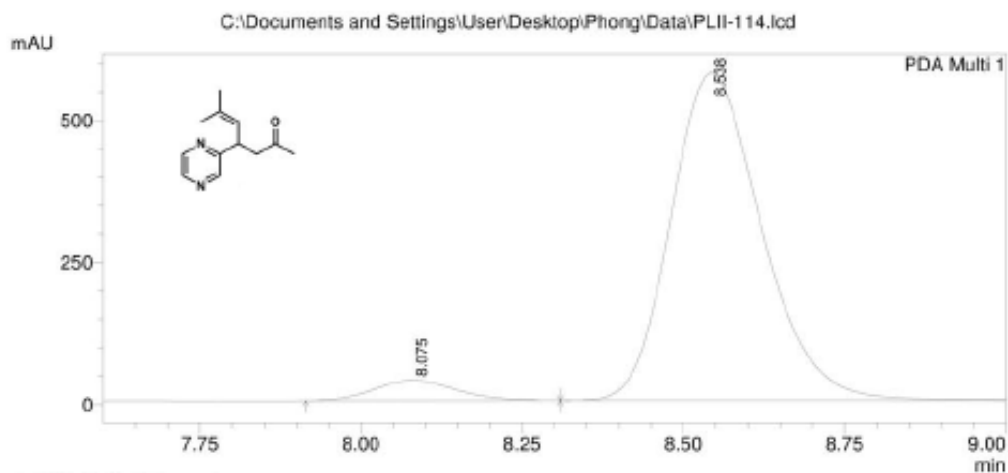


Figure A.1.86. ^{13}C NMR for compound 129



PeakTable

Peak#	Ret. Time	Area	Height	Area %	Height %
1	7.931	1376121	154841	50.010	51.622
2	8.397	1375565	145113	49.990	48.378
Total		2751686	299954	100.000	100.000



PeakTable

Peak#	Ret. Time	Area	Height	Area %	Height %
1	8.075	313935	35725	5.271	5.827
2	8.538	5641998	577402	94.729	94.173
Total		5955932	613127	100.000	100.000

Figure A.1.87. HPLC trace for compound 129

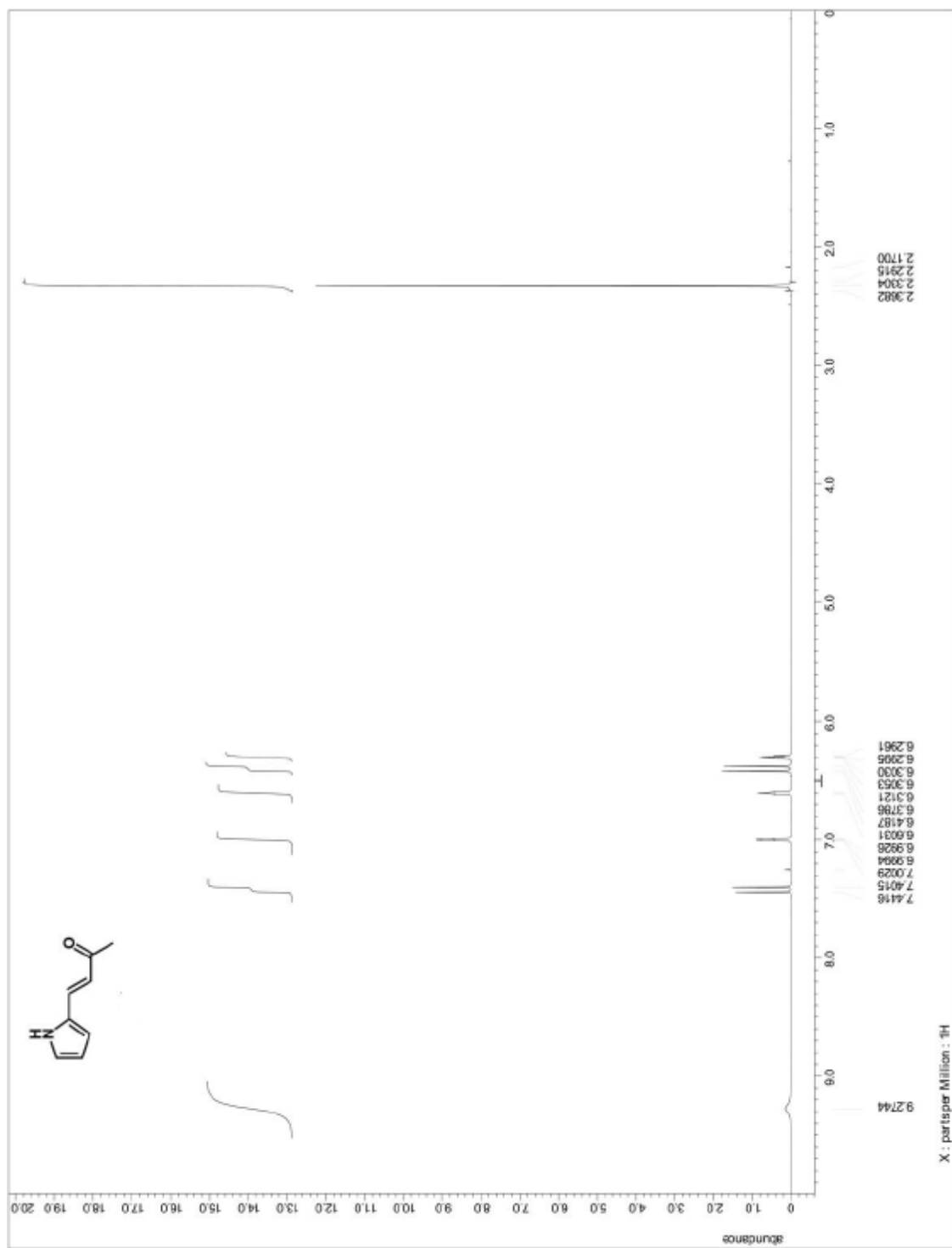


Figure A.1.88. ^1H NMR for precursor to compound 130

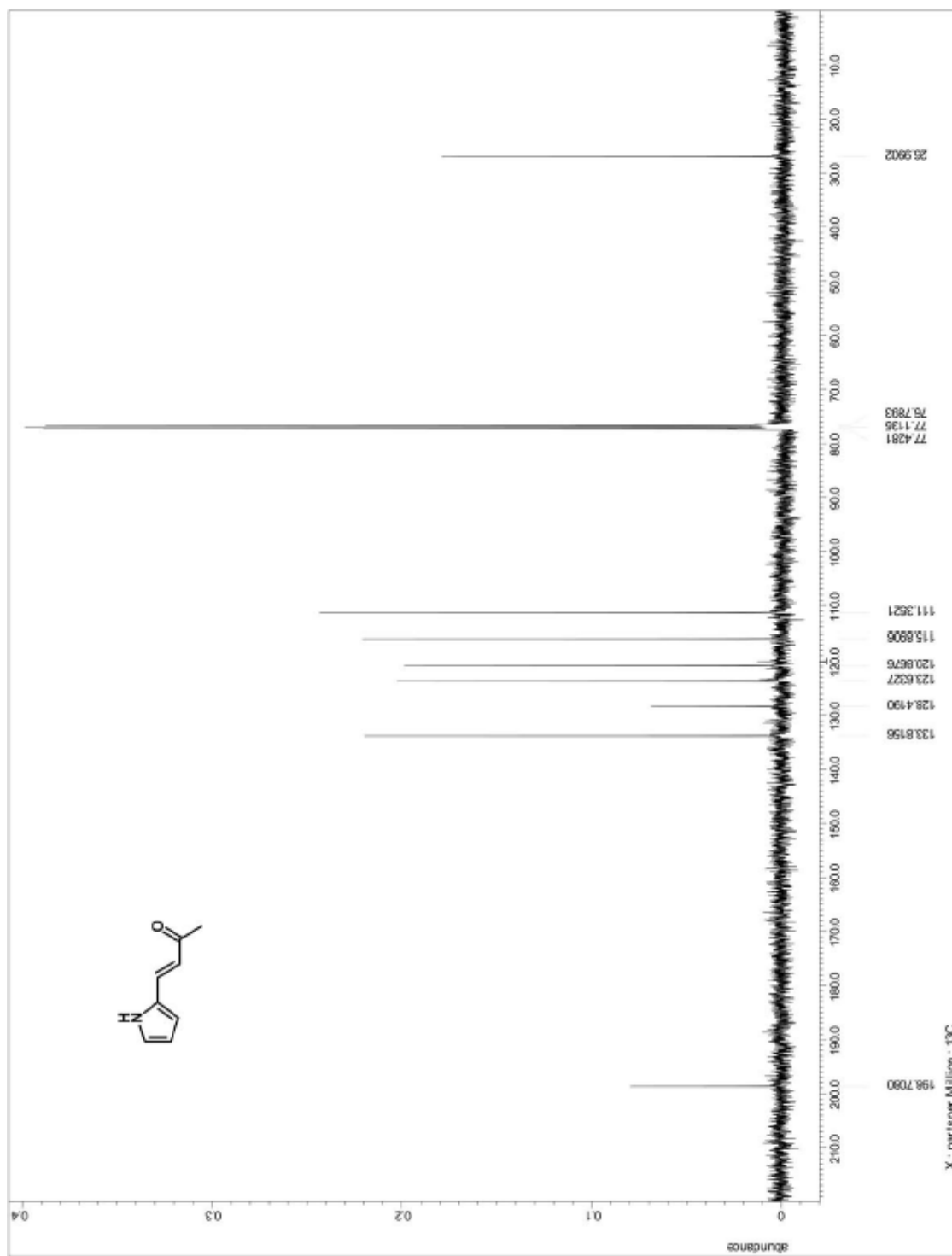


Figure A.1.89. ^{13}C NMR for precursor to compound 130

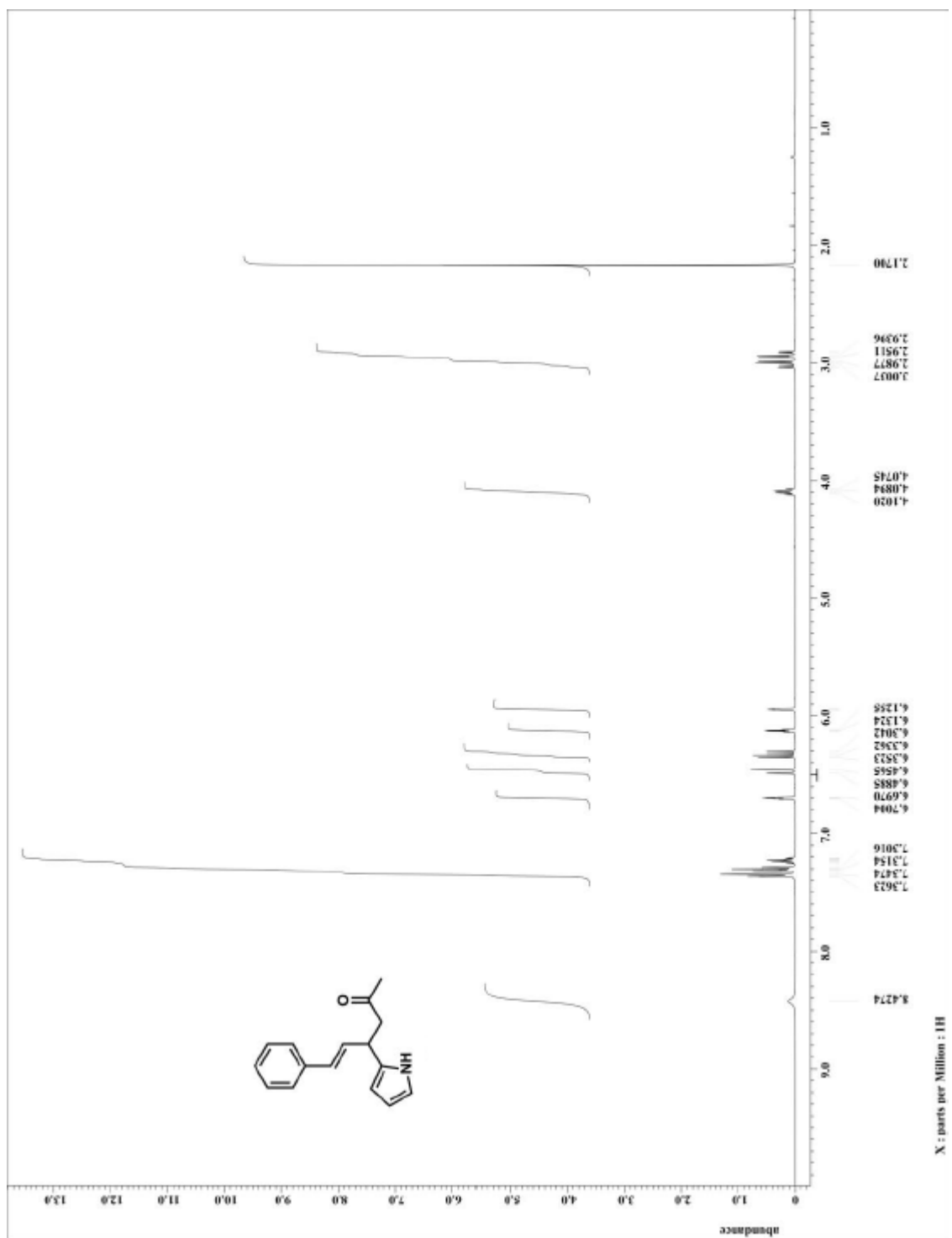


Figure A.1.90. ¹H NMR for compound 130

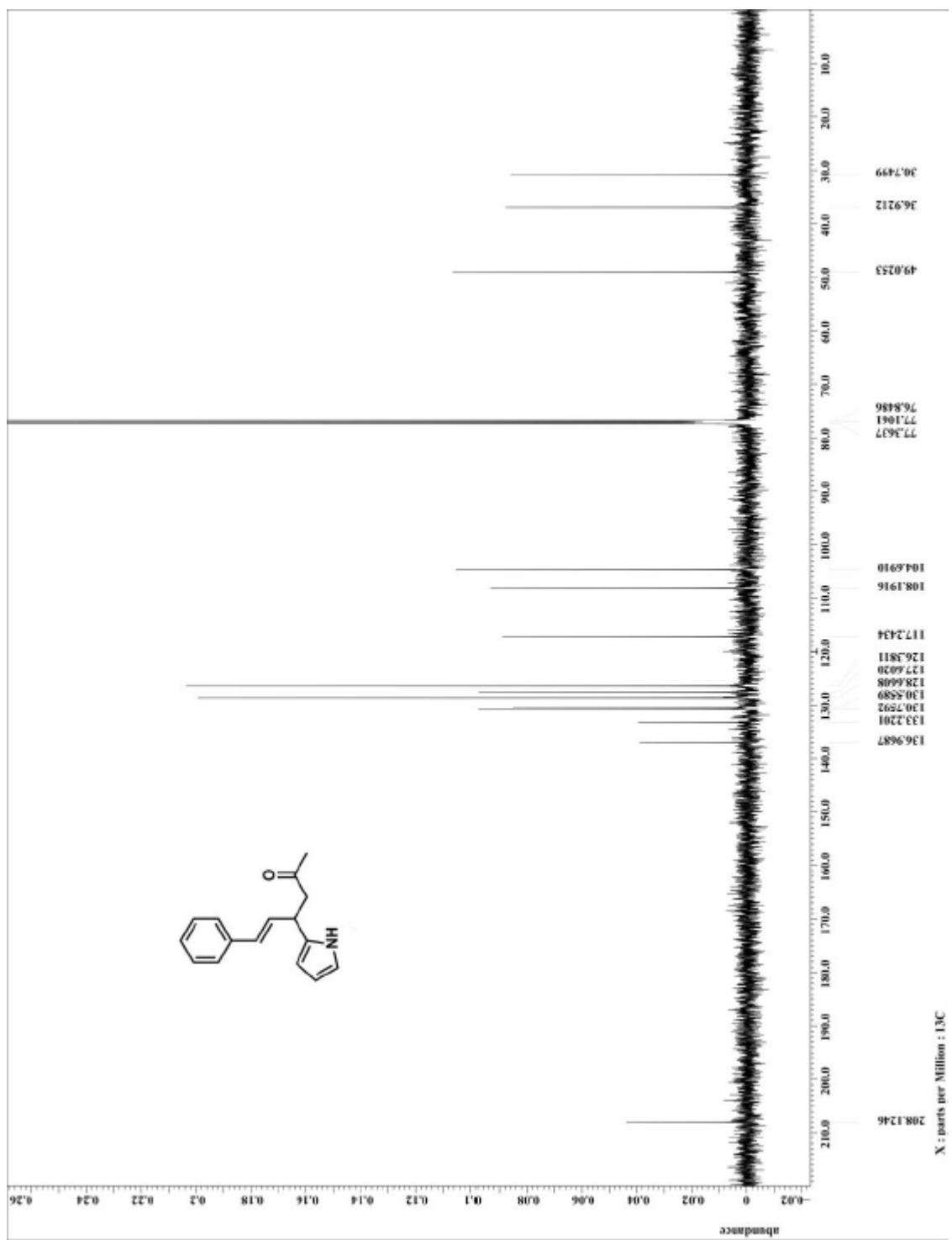
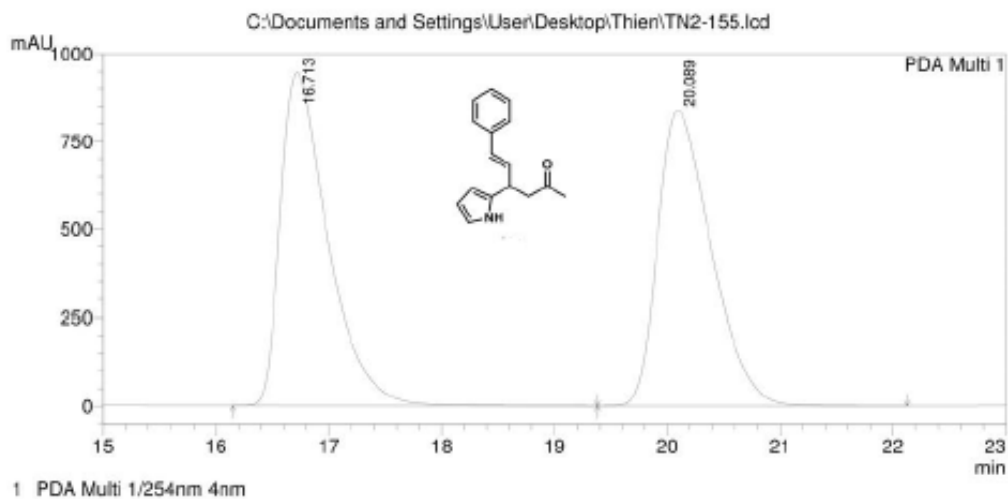
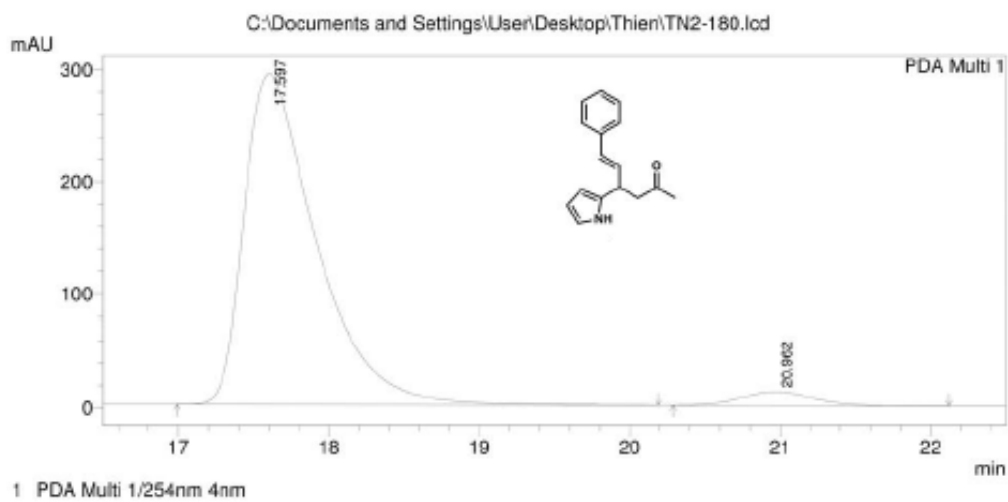


Figure A.1.91. ^{13}C NMR for compound 130



PeakTable

Peak#	Ret. Time	Area	Height	Area %	Height %
1	16.713	27603593	945629	50.093	53.022
2	20.089	27501630	837848	49.907	46.978
Total		55105223	1783477	100.000	100.000



PeakTable

Peak#	Ret. Time	Area	Height	Area %	Height %
1	17.597	9780860	293753	96.121	96.039
2	20.962	394660	12116	3.879	3.961
Total		10175520	305868	100.000	100.000

Figure A.1.92. HPLC trace for compound 130

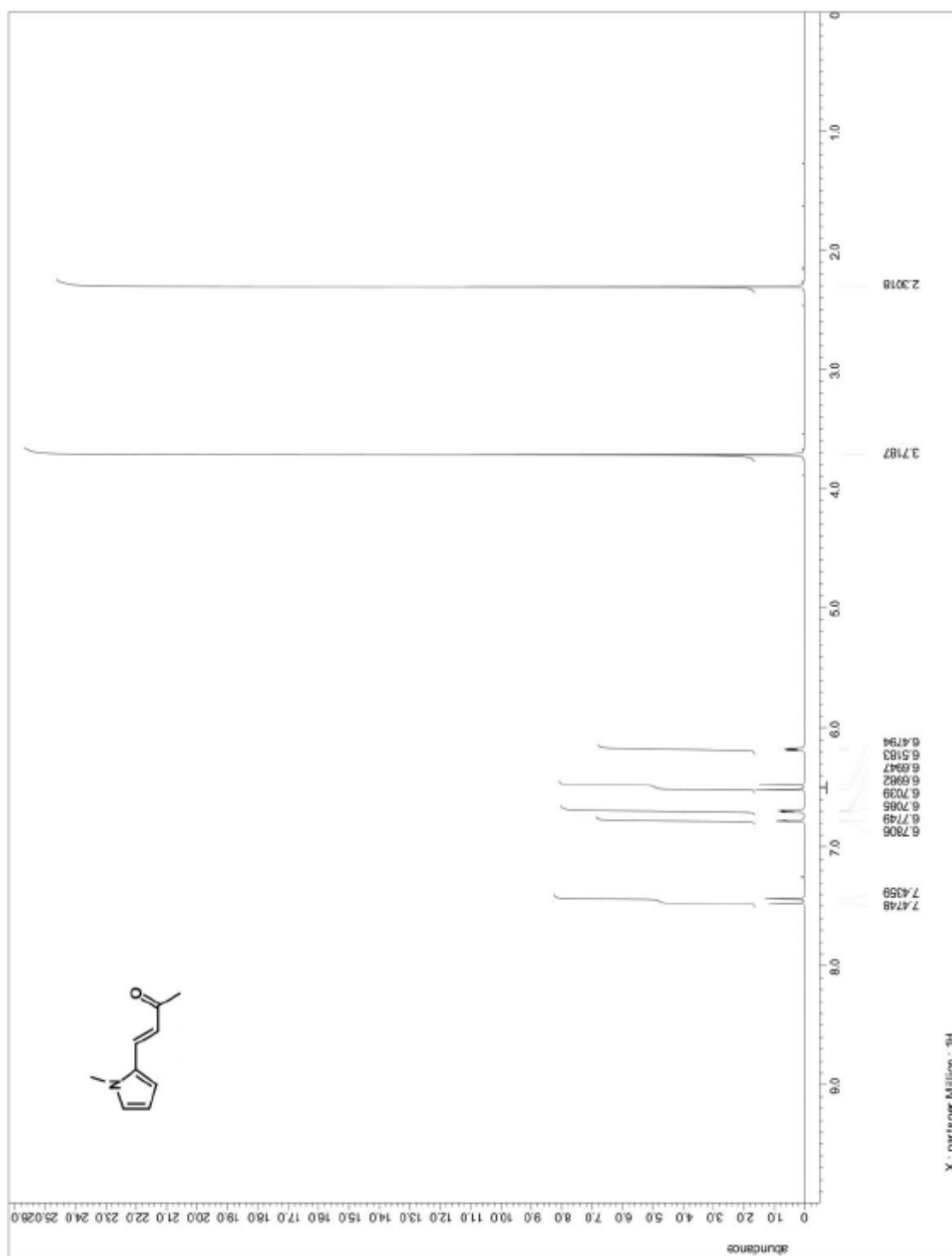


Figure A.1.93. ^1H NMR for precursor to compound 131

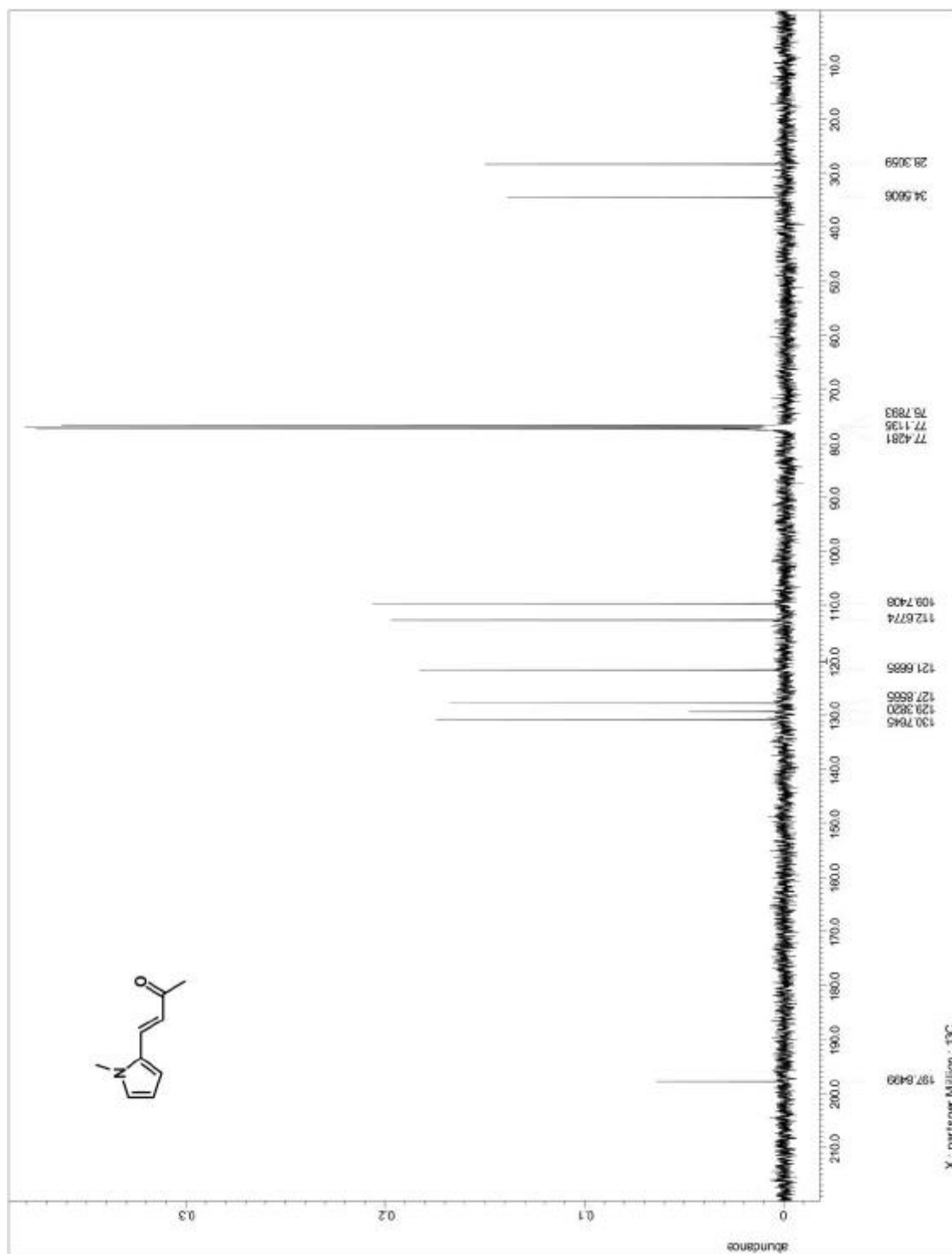


Figure A.1.94. ^{13}C NMR for precursor to compound 131

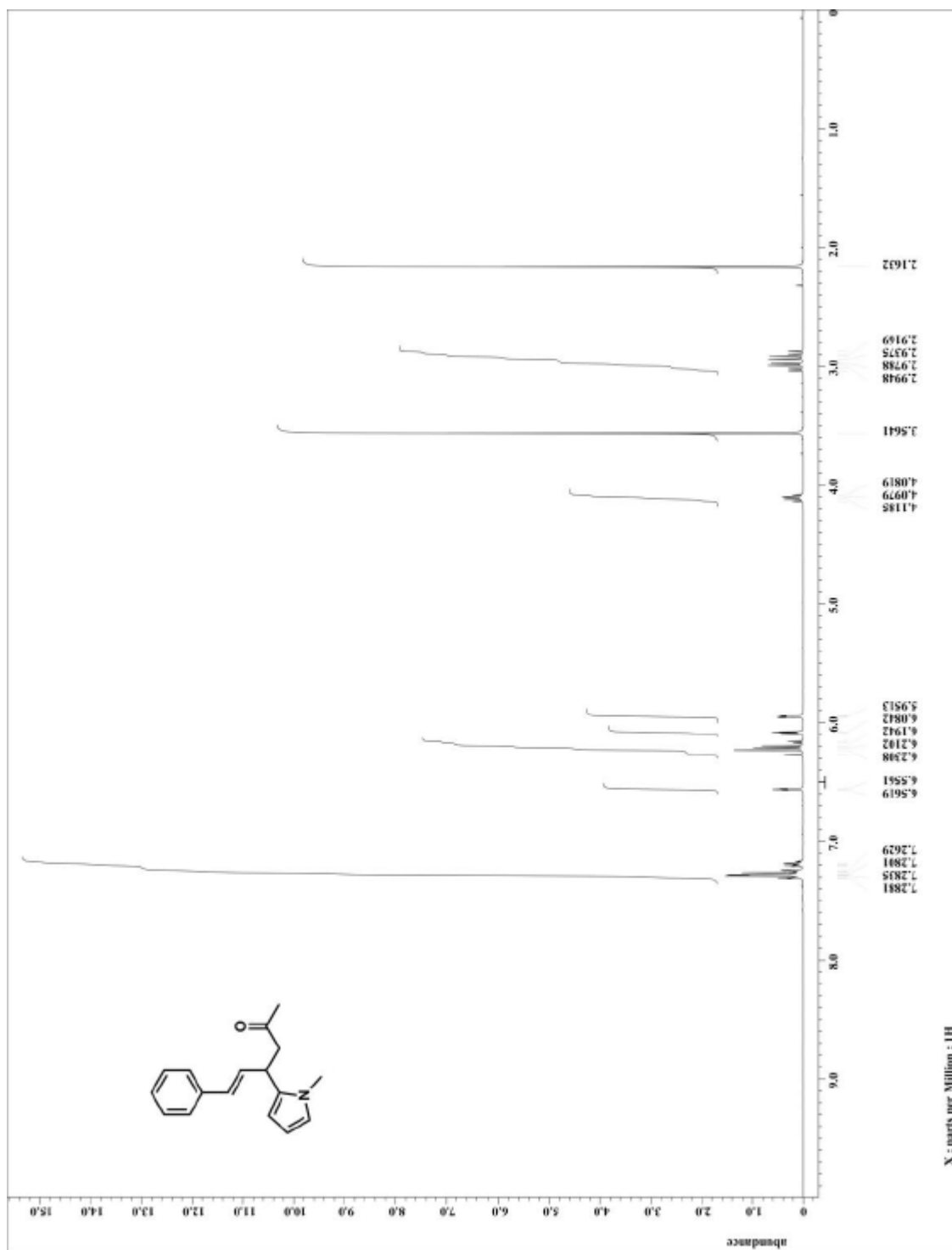


Figure A.1.95. ^1H NMR for compound 131

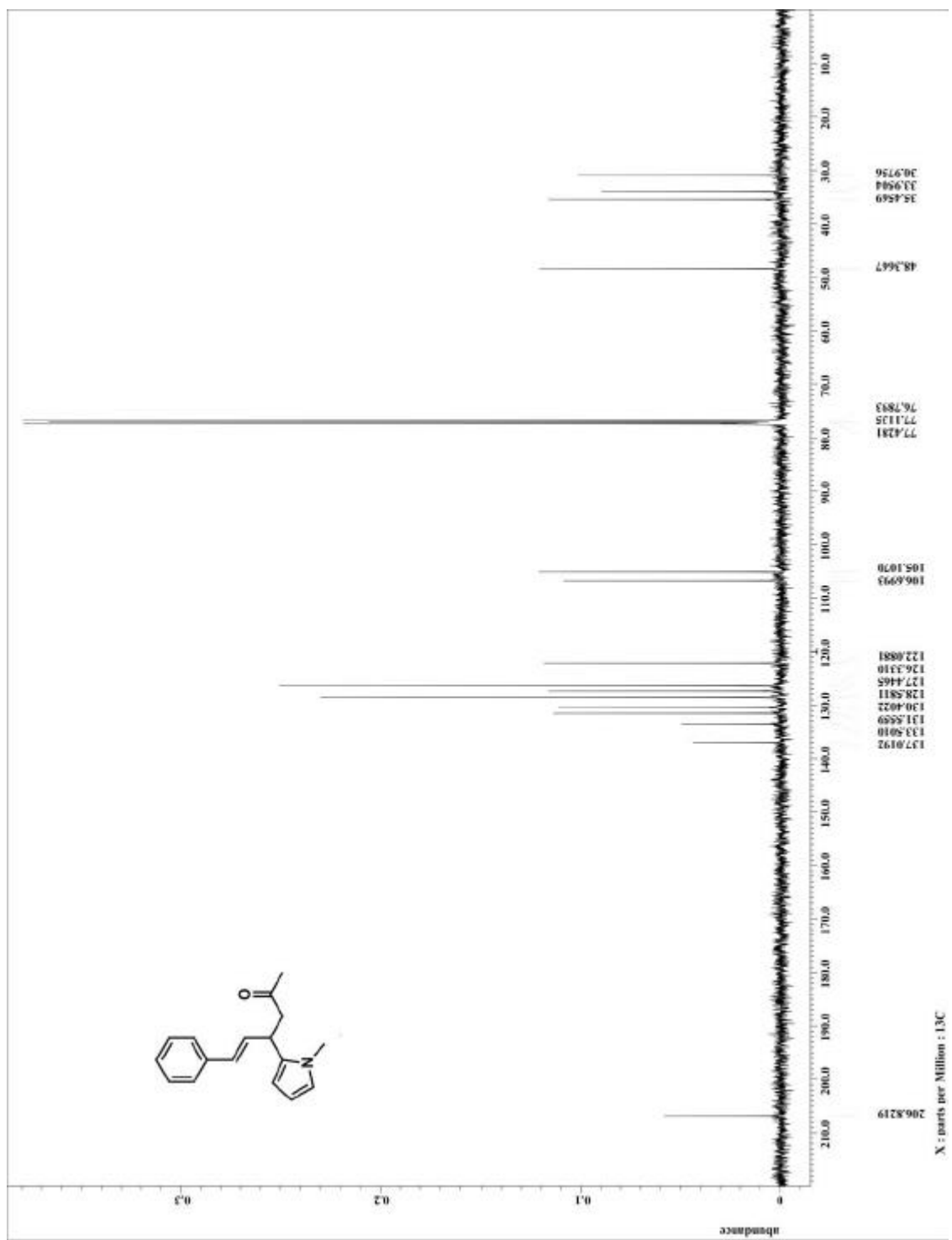
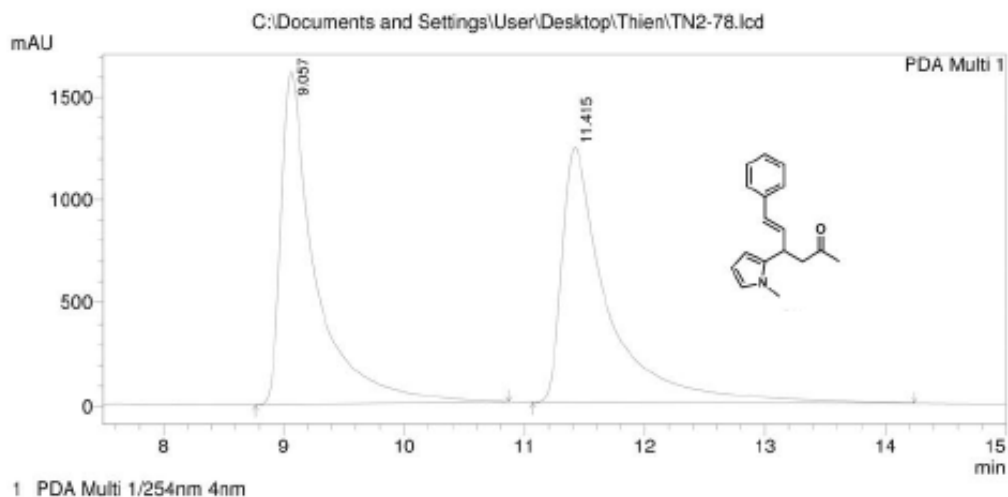
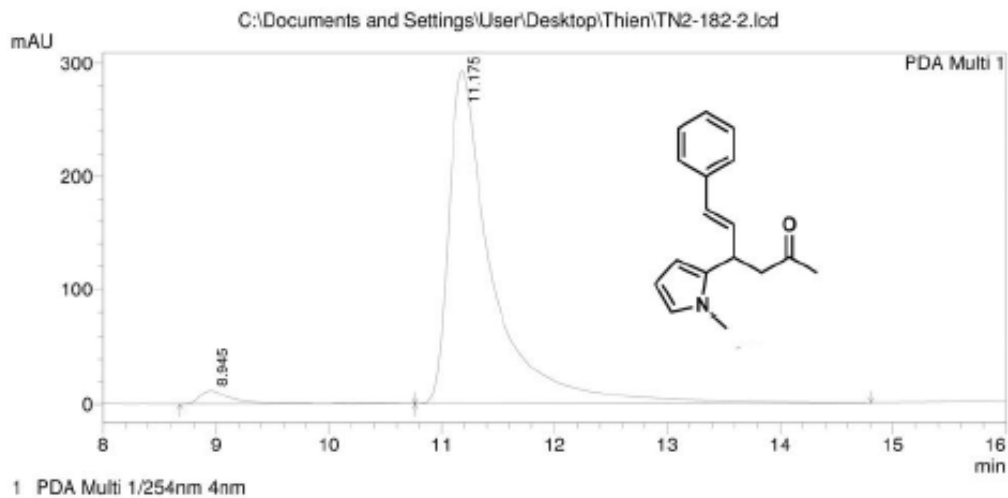


Figure A.1.96. ^{13}C NMR for compound 131



PeakTable

Peak#	Ret. Time	Area	Height	Area %	Height %
1	9.057	32338256	1612769	49.480	56.608
2	11.415	33017688	1236240	50.520	43.392
Total		65355944	2849009	100.000	100.000



PeakTable

Peak#	Ret. Time	Area	Height	Area %	Height %
1	8.945	237026	12026	2.949	3.944
2	11.175	7799758	292861	97.051	96.056
Total		8036784	304887	100.000	100.000

Figure A.1.97. HPLC trace for compound 131

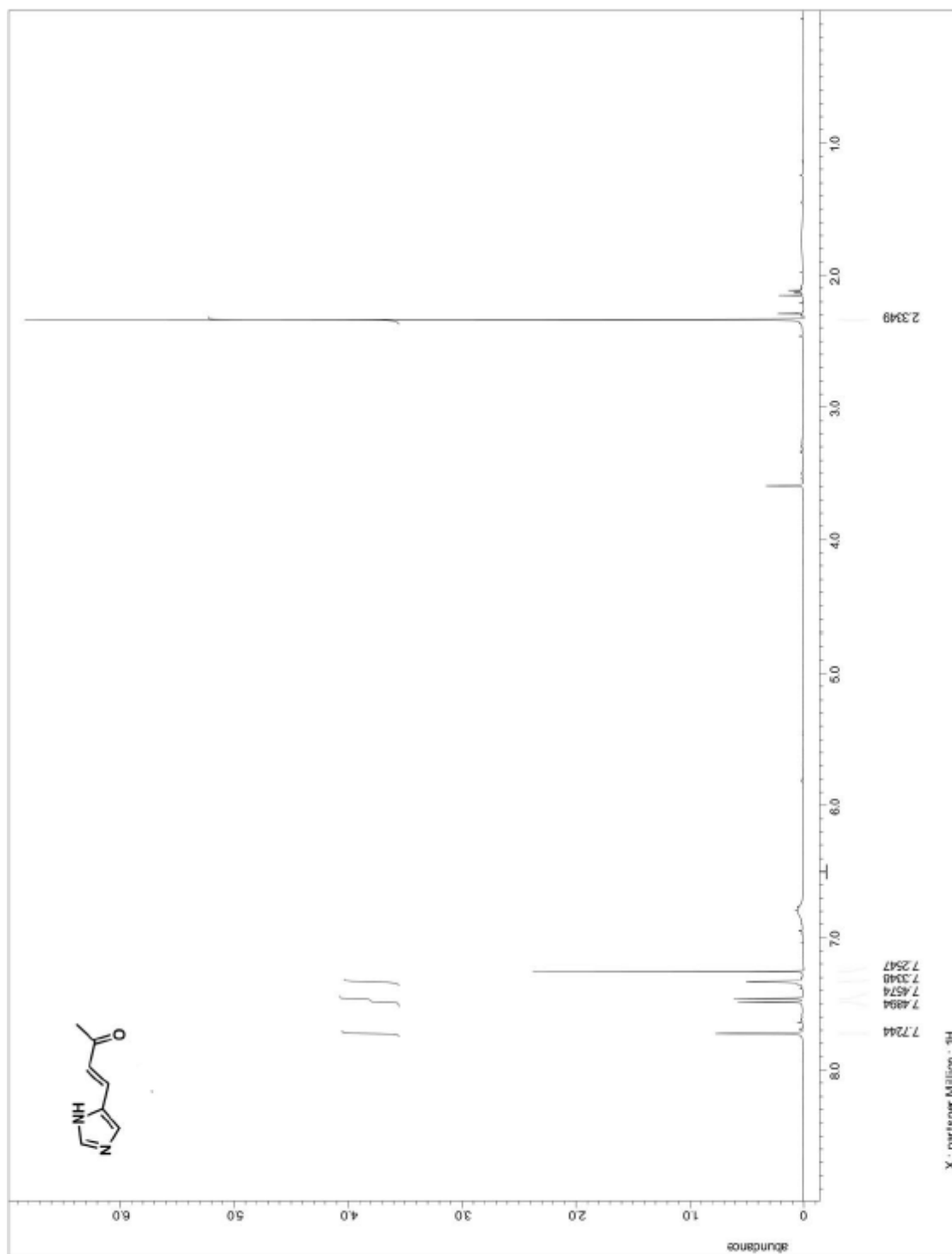


Figure A.1.98. ^1H NMR for precursor to compound 132

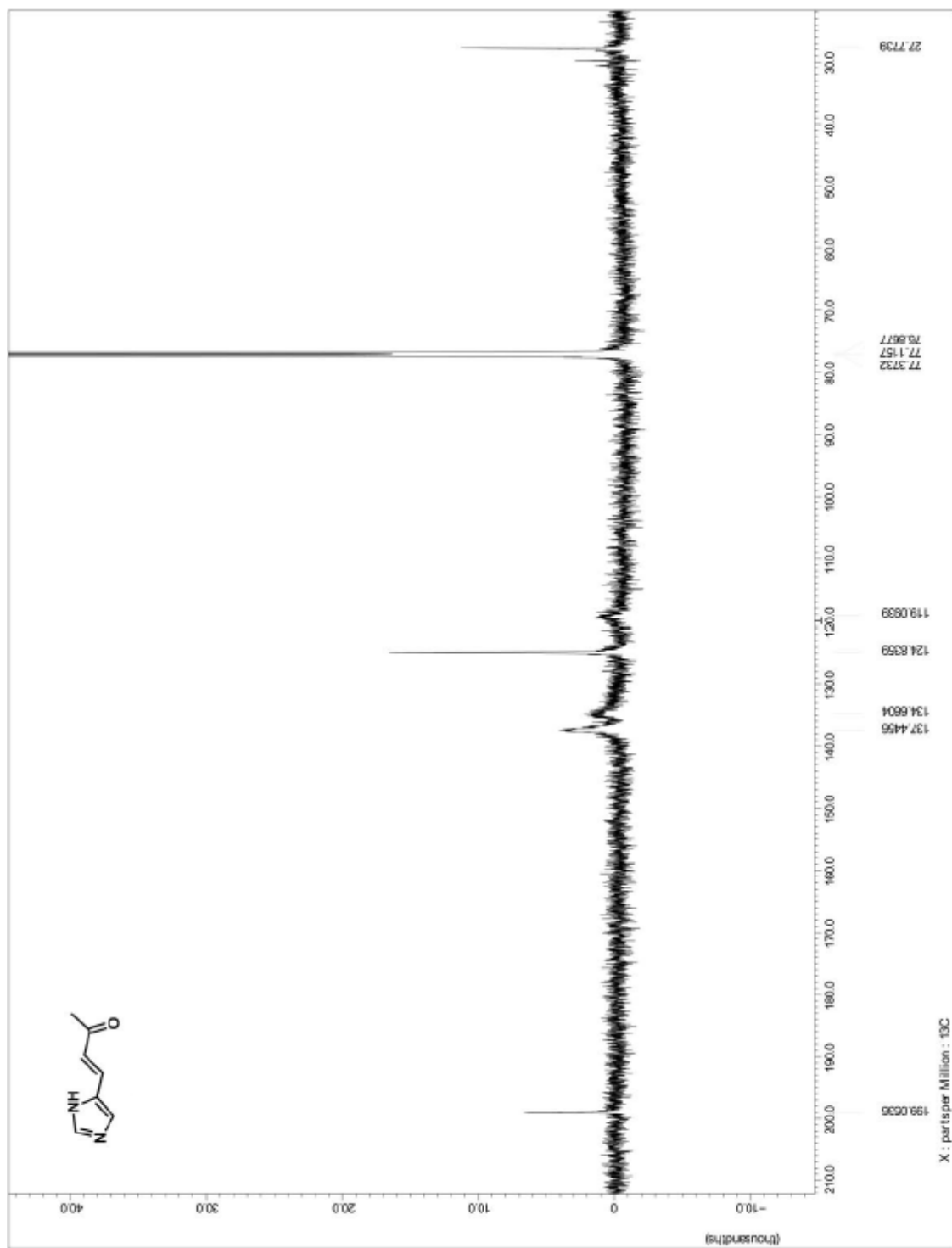


Figure A.1.99. ^{13}C NMR for precursor to compound 132

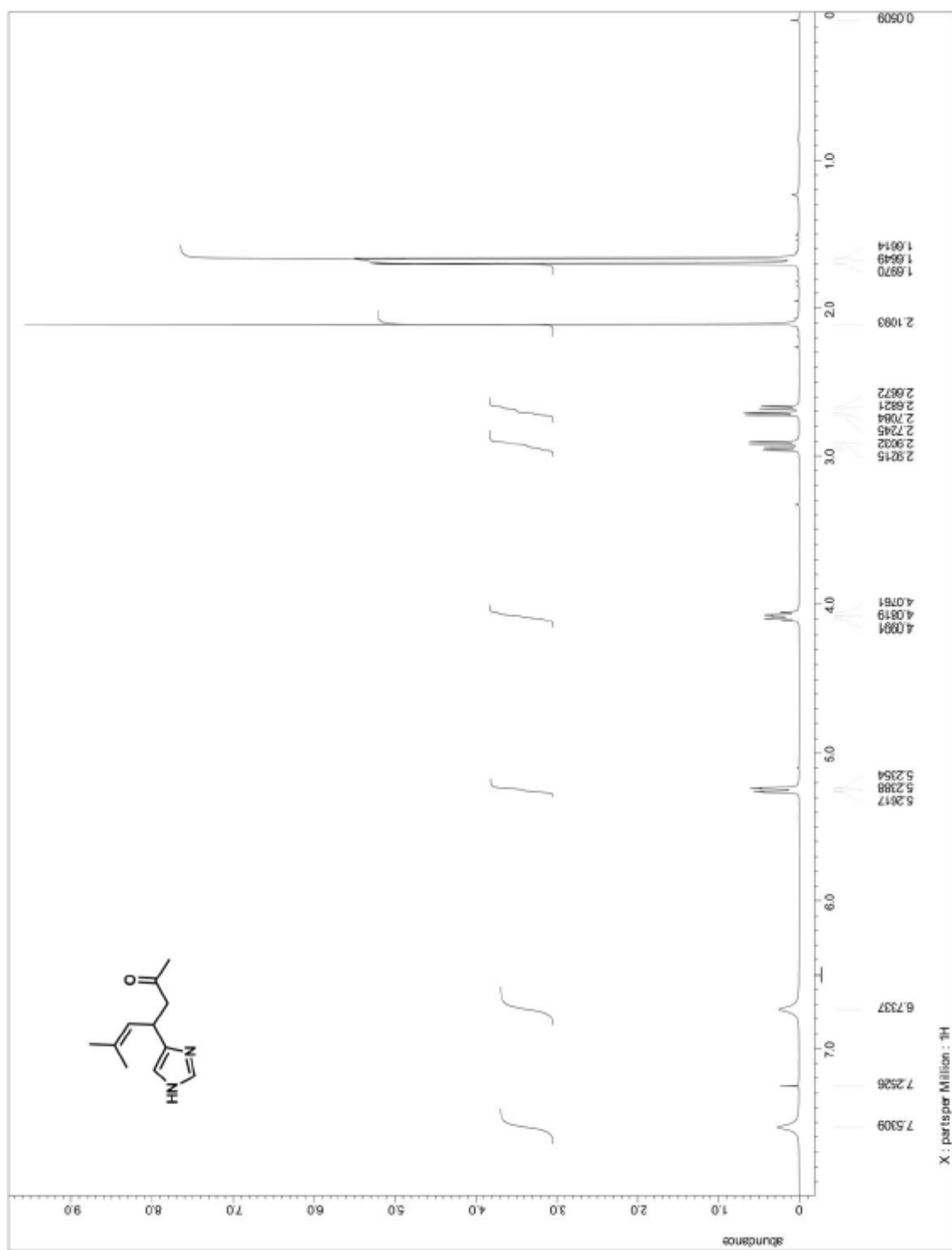


Figure A.1.100. ^1H NMR for compound 132

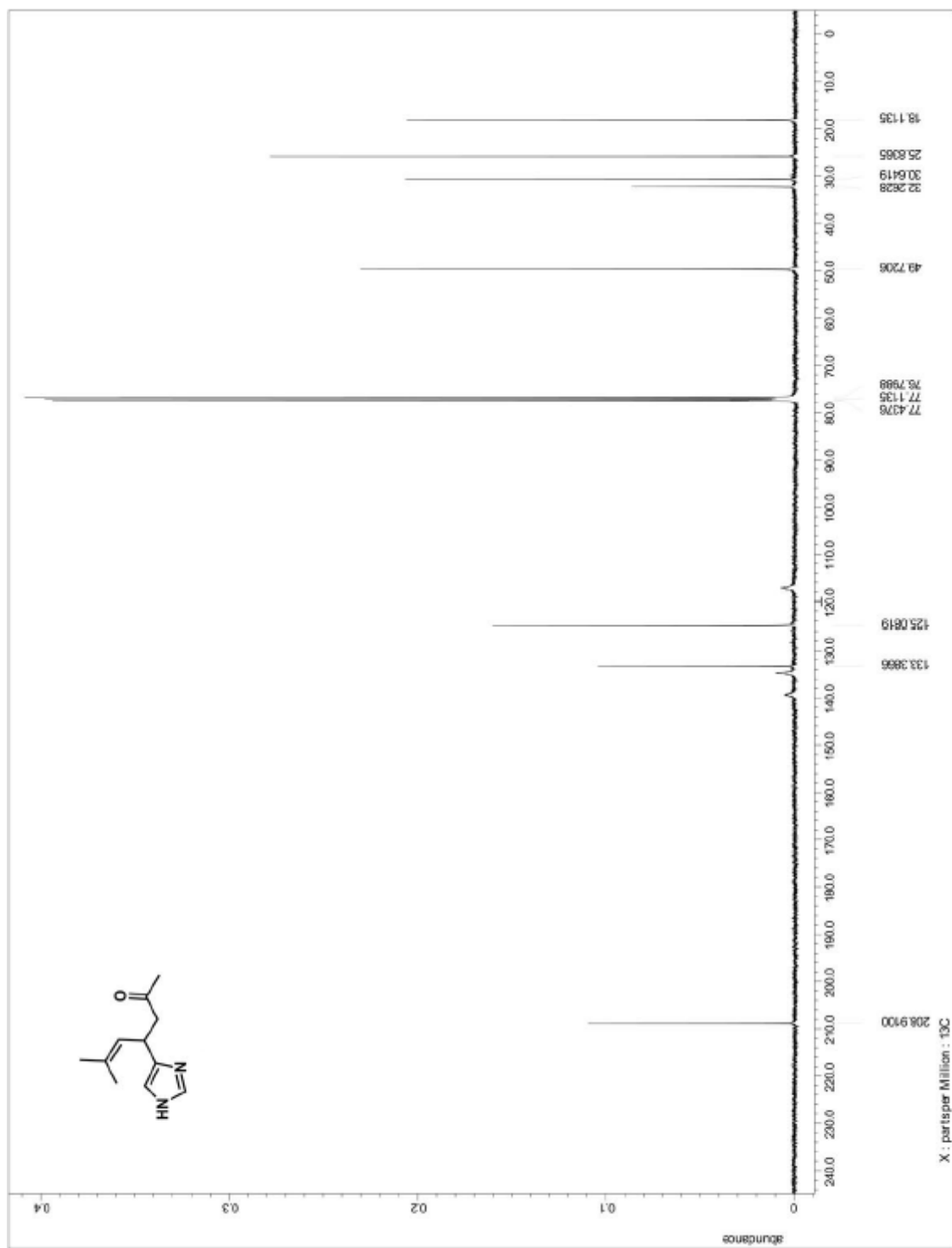
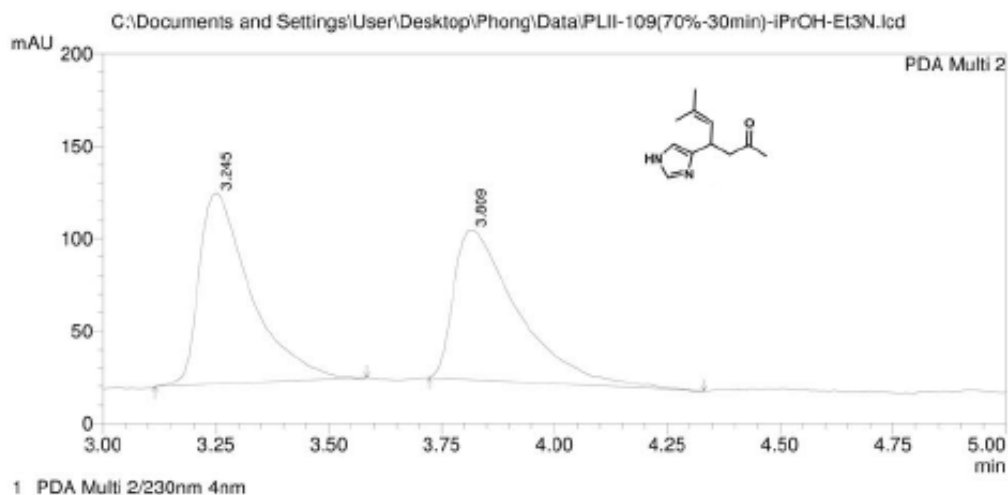
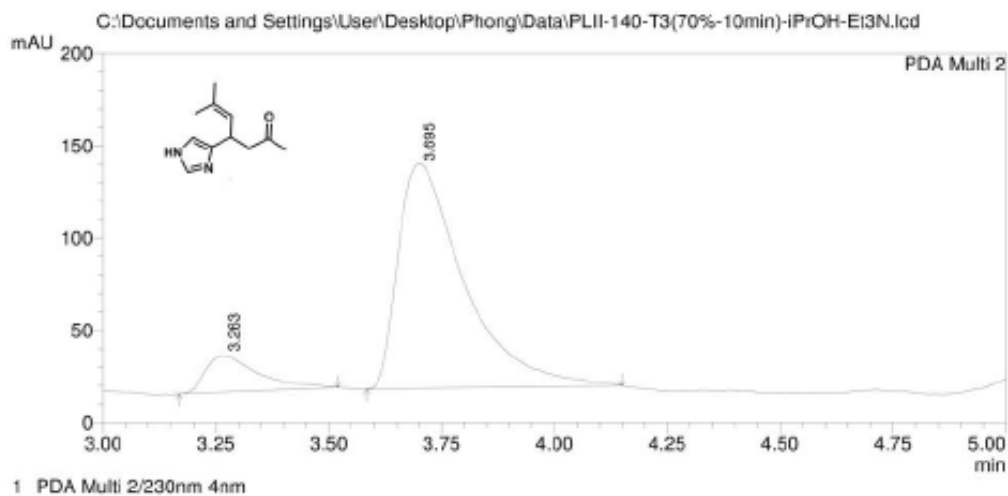


Figure A.1.101. ^{13}C NMR for compound 132



PeakTable

Peak#	Ret. Time	Area	Height	Area %	Height %
1	3.245	822398	103584	50.694	56.237
2	3.809	799880	80608	49.306	43.763
Total		1622278	184192	100.000	100.000



PeakTable

Peak#	Ret. Time	Area	Height	Area %	Height %
1	3.263	162714	19952	11.582	14.014
2	3.695	1242206	122421	88.418	85.986
Total		1404920	142373	100.000	100.000

Figure A.1.102. HPLC trace for compound 132

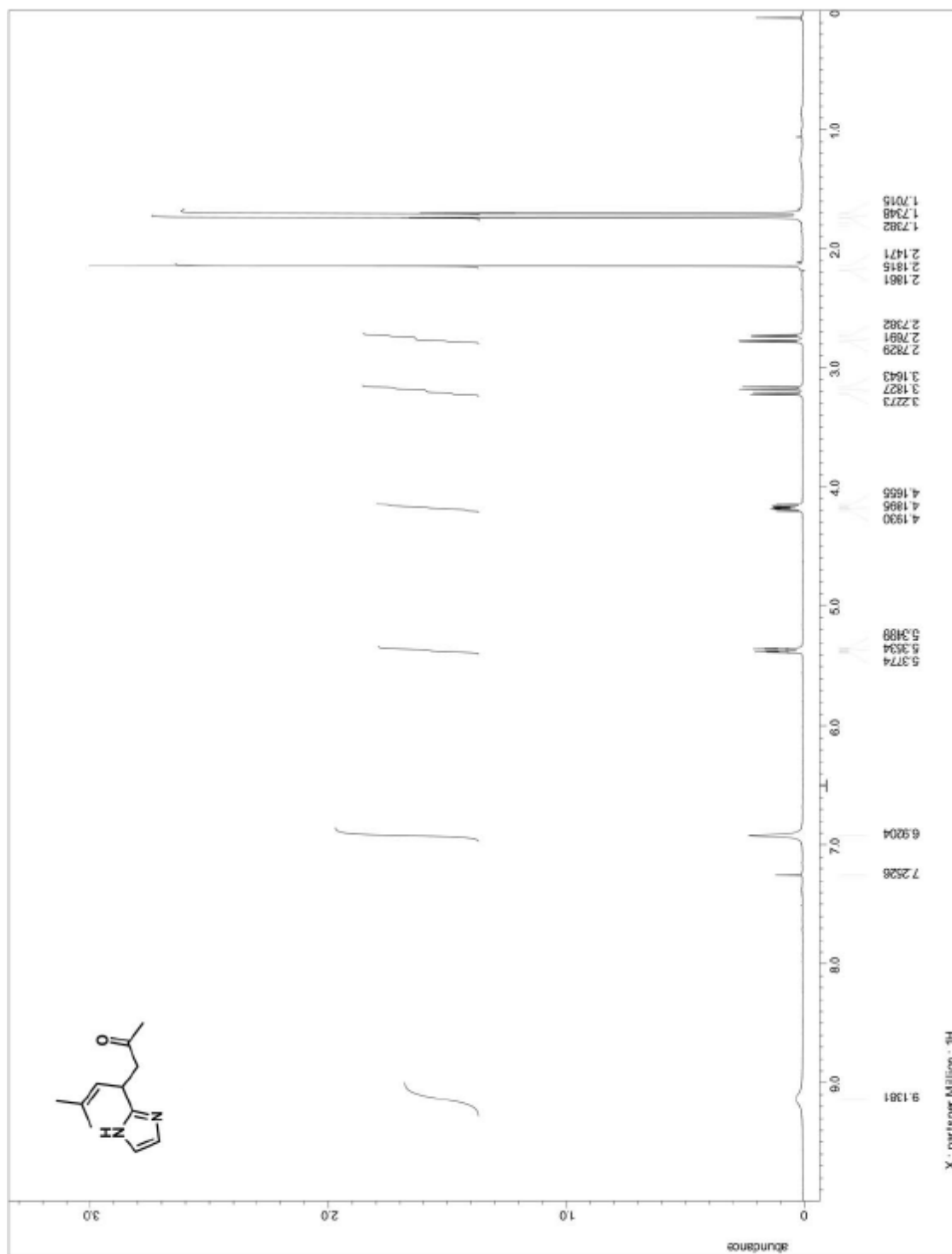


Figure A.1.103. ^1H NMR for compound 133

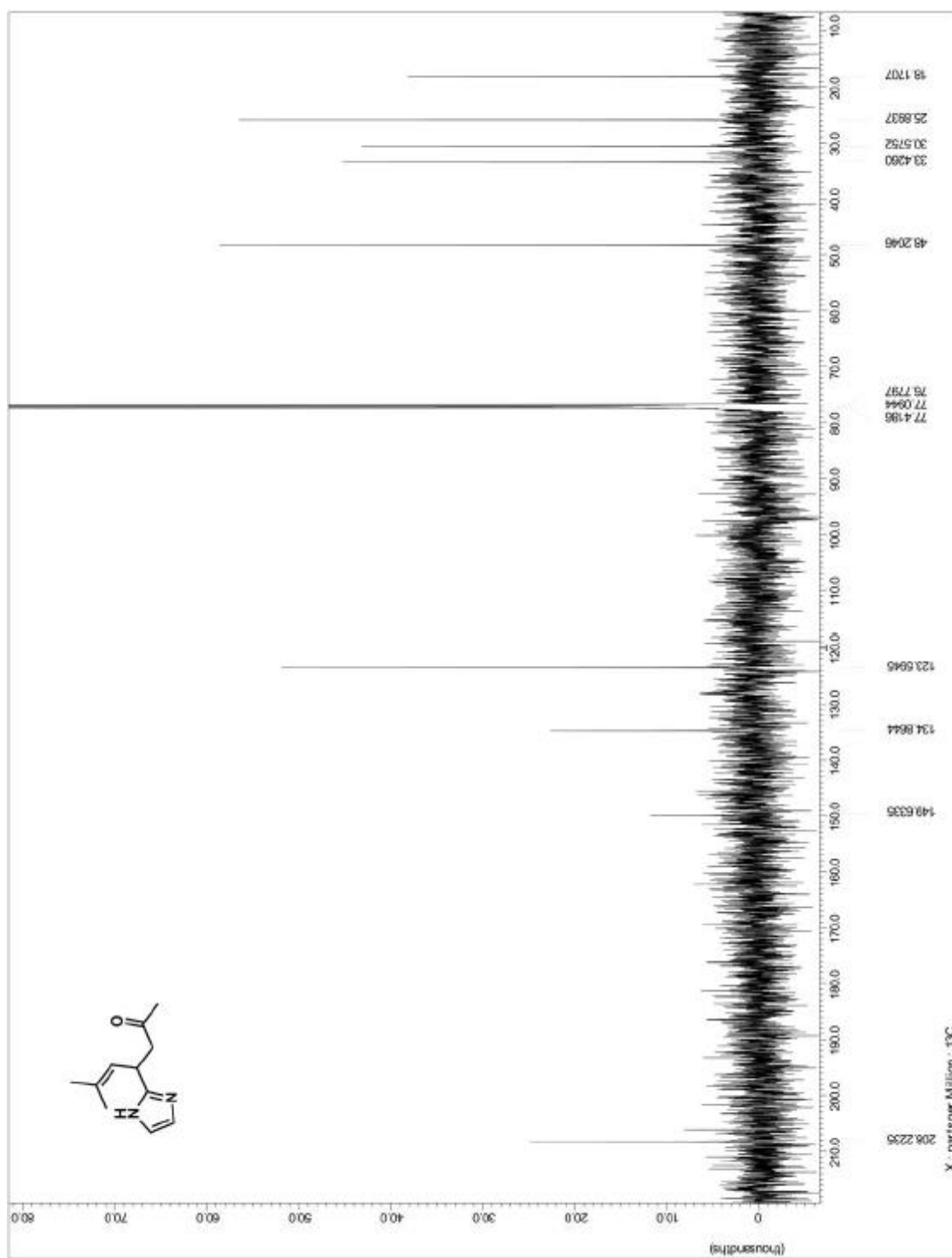
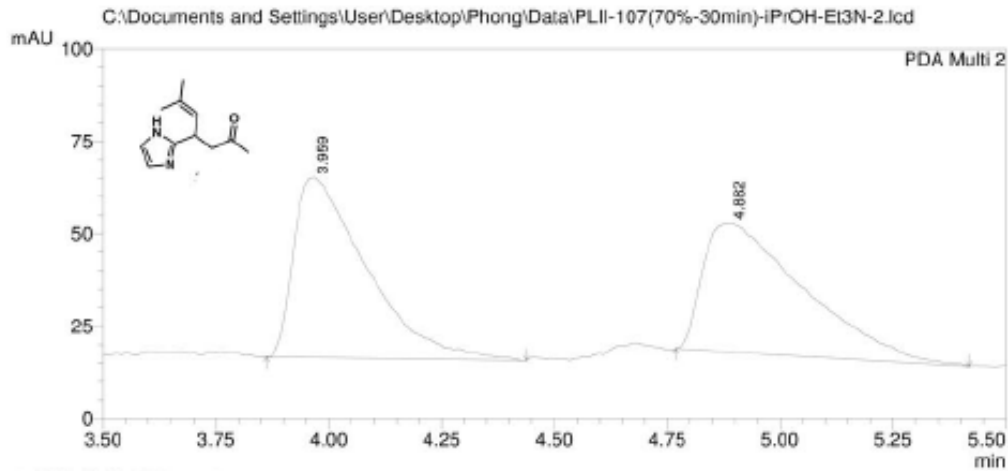


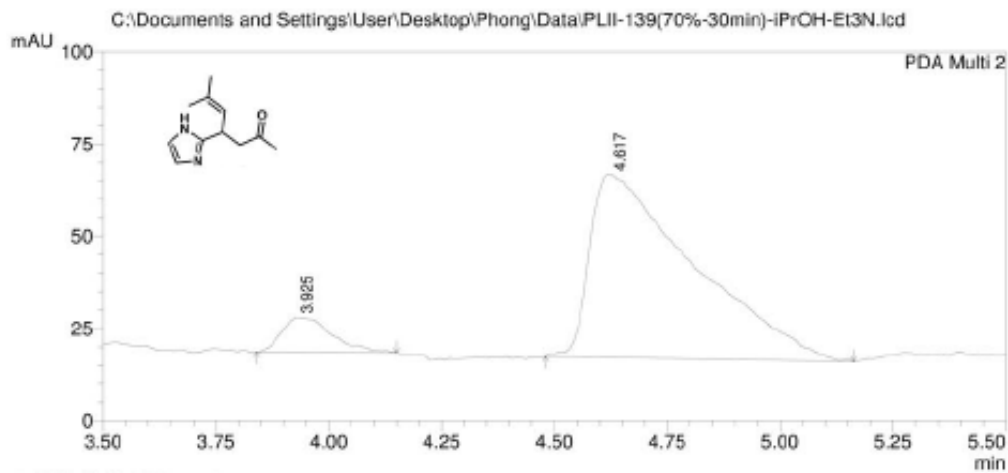
Figure A.1.104. ^{13}C NMR for compound 133



PeakTable

PDA Ch2 230nm 4nm

Peak#	Ret. Time	Area	Height	Area %	Height %
1	3.959	543131	48678	50.203	58.358
2	4.882	538748	34735	49.797	41.642
Total		1081879	83413	100.000	100.000



PeakTable

PDA Ch2 230nm 4nm

Peak#	Ret. Time	Area	Height	Area %	Height %
1	3.925	73570	9471	8.509	16.058
2	4.617	791034	49509	91.491	83.942
Total		864604	58980	100.000	100.000

Figure A.1.105. HPLC trace for compound 133

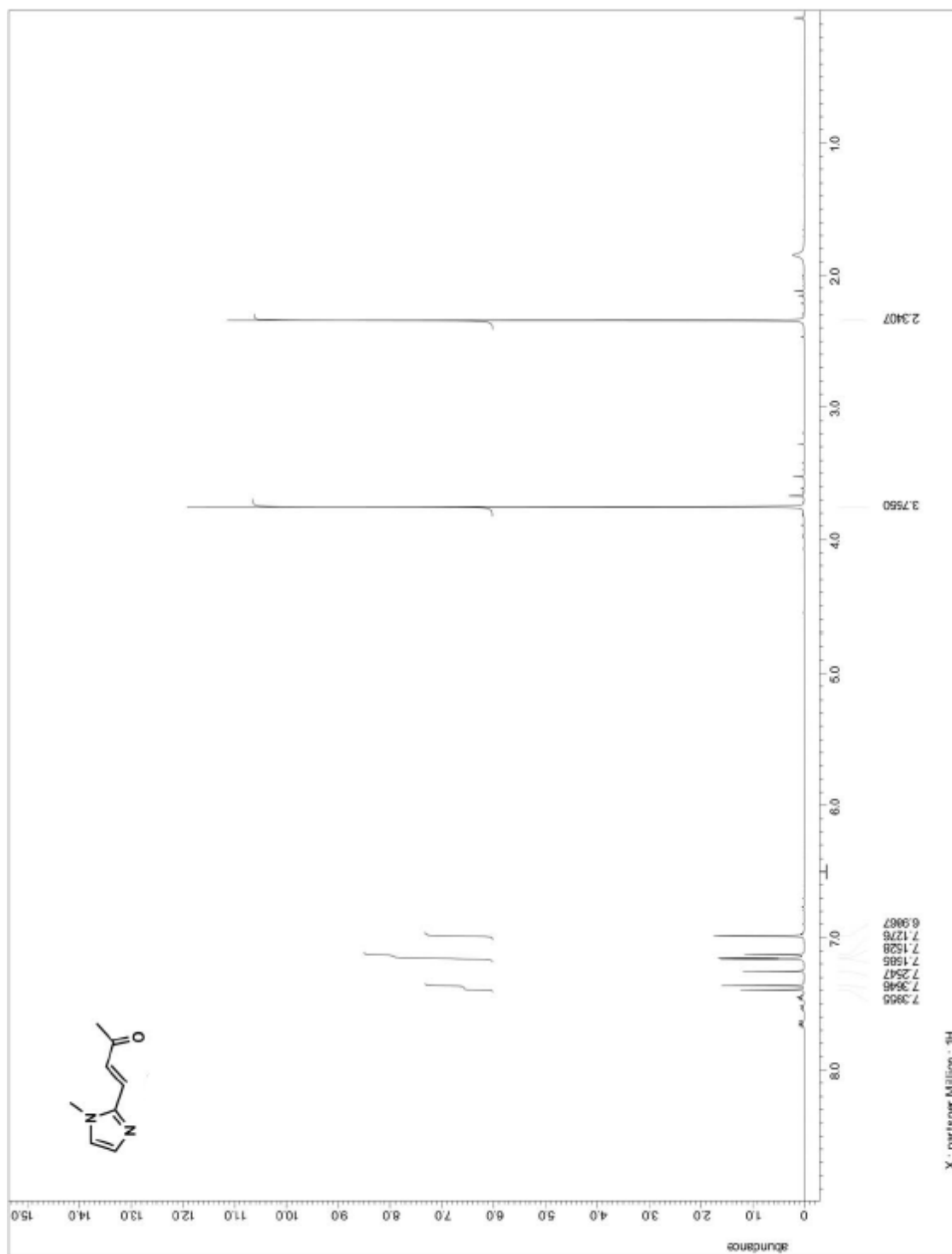


Figure A.1.106. ^1H NMR for precursor to compound 134

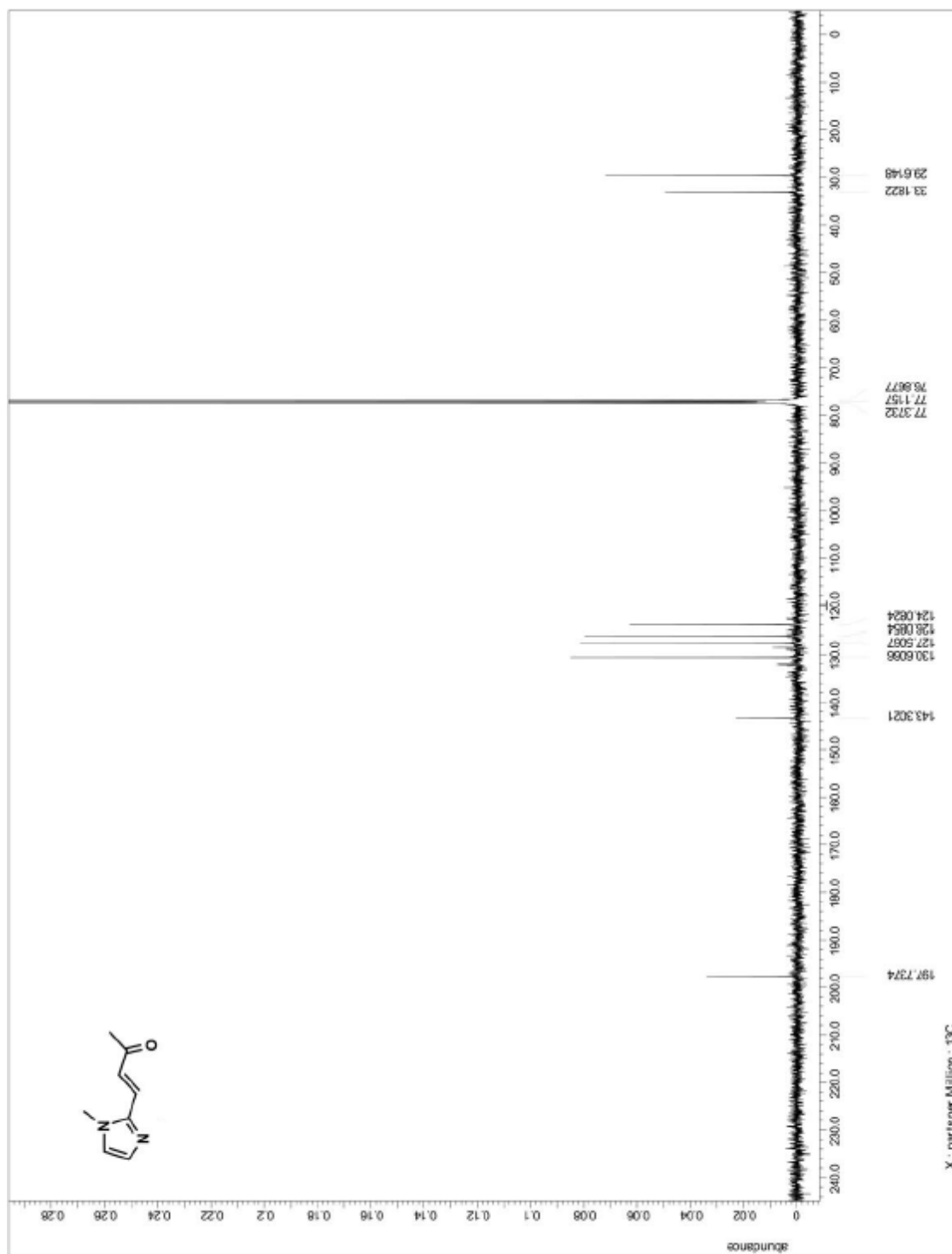


Figure A.1.107. ^{13}C NMR for precursor to compound 134

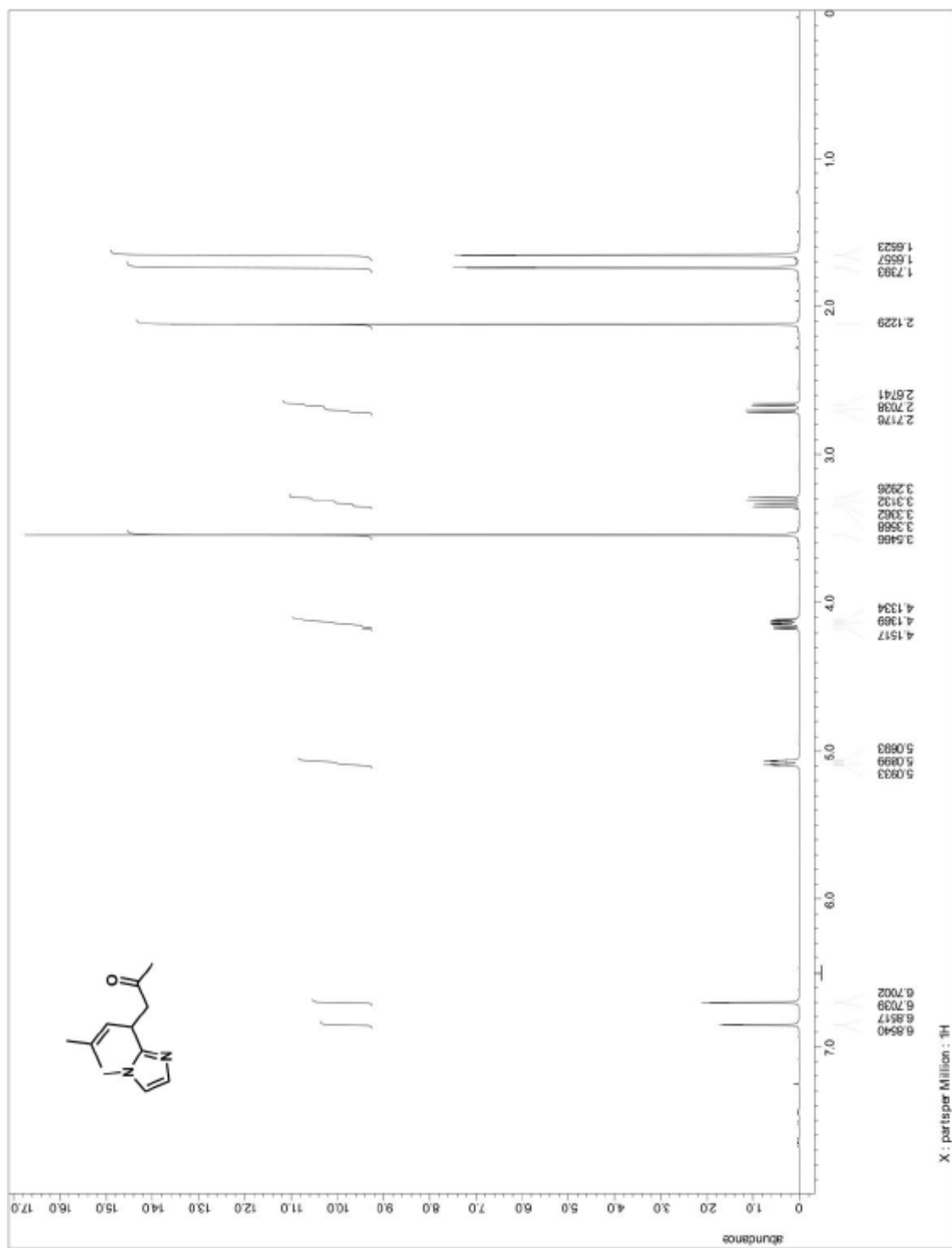


Figure A.1.108. ^1H NMR for compound 134

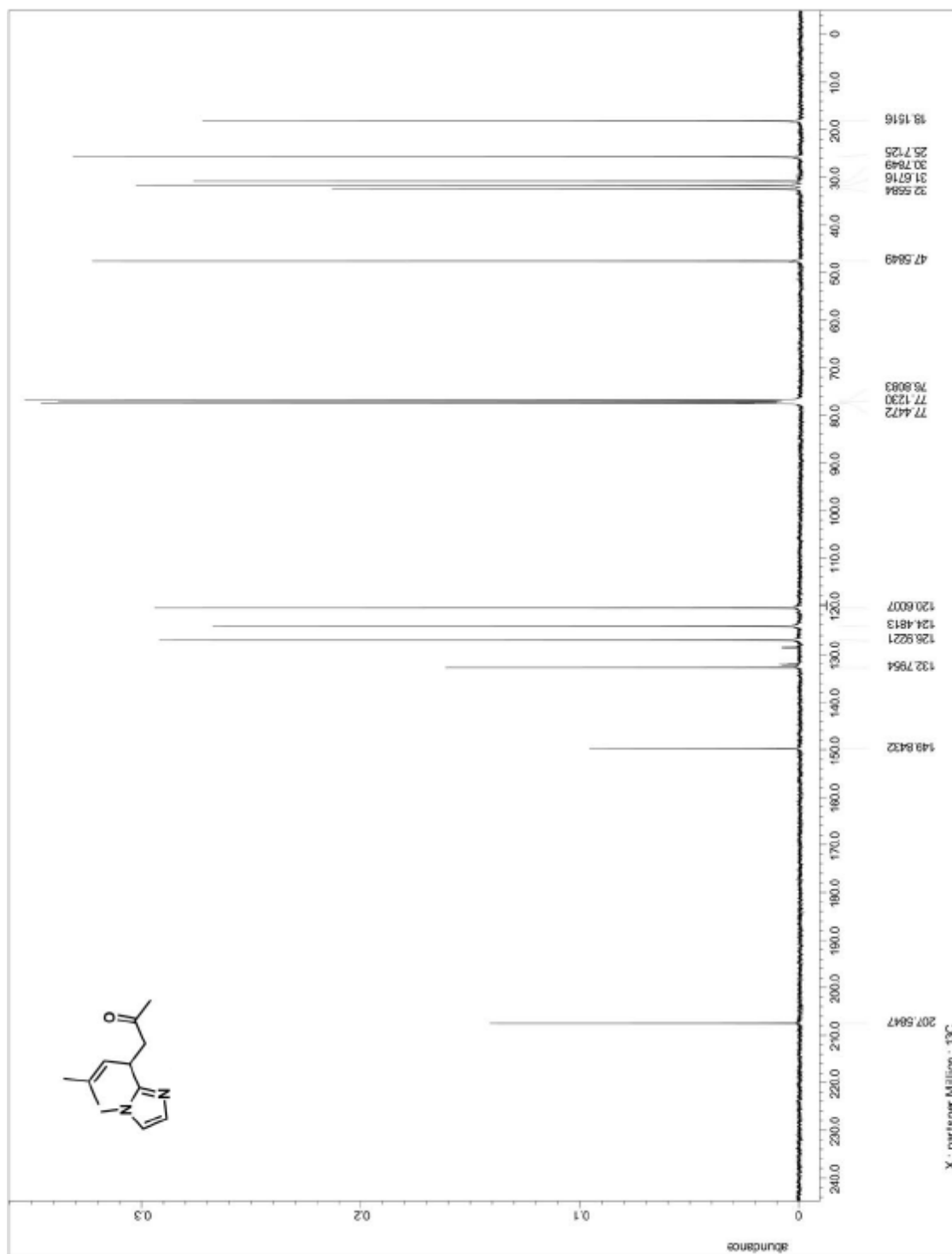
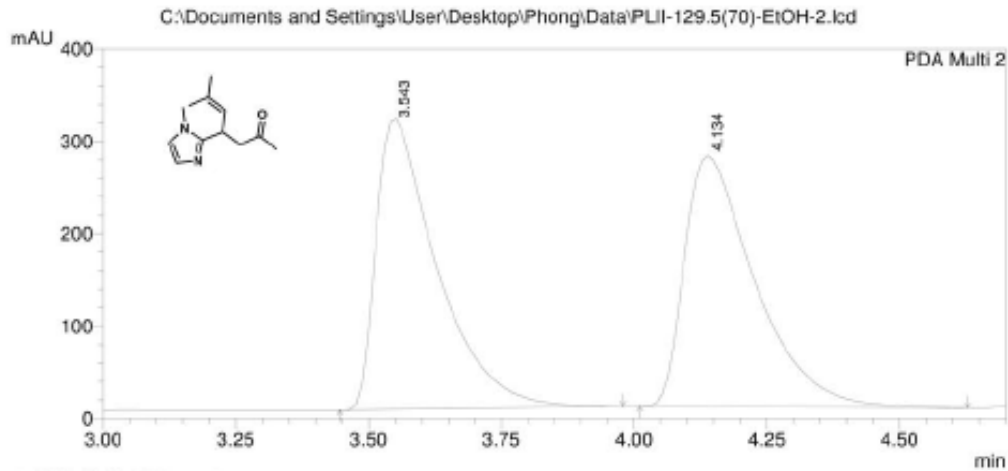


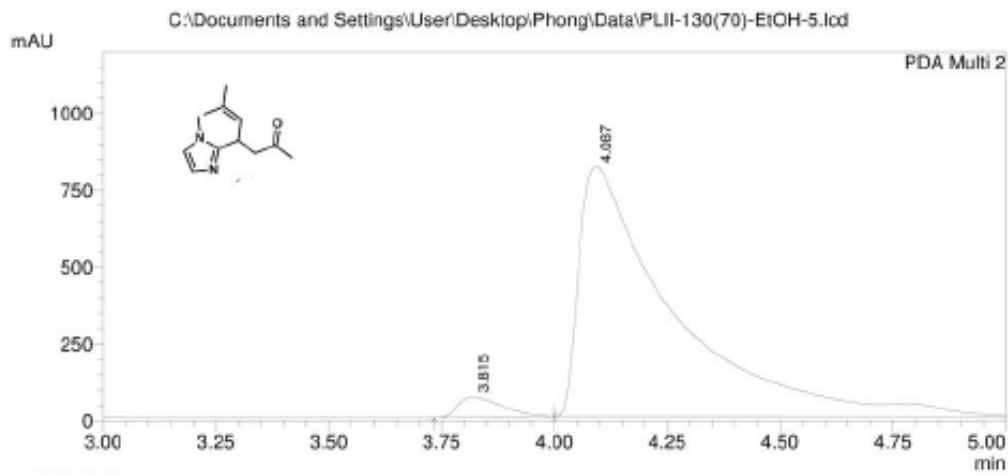
Figure A.1.109. ^{13}C NMR for compound 134



PeakTable

PDA Ch2 230nm 4nm

Peak#	Ret. Time	Area	Height	Area %	Height %
1	3.543	2507726	314225	50.134	53.601
2	4.134	2494341	272001	49.866	46.399
Total		5002067	586227	100.000	100.000



PeakTable

PDA Ch2 230nm 4nm

Peak#	Ret. Time	Area	Height	Area %	Height %
1	3.815	455913	67851	3.687	7.693
2	4.087	11910445	814159	96.313	92.307
Total		12366357	882010	100.000	100.000

Figure A.1.110. HPLC trace for compound 134

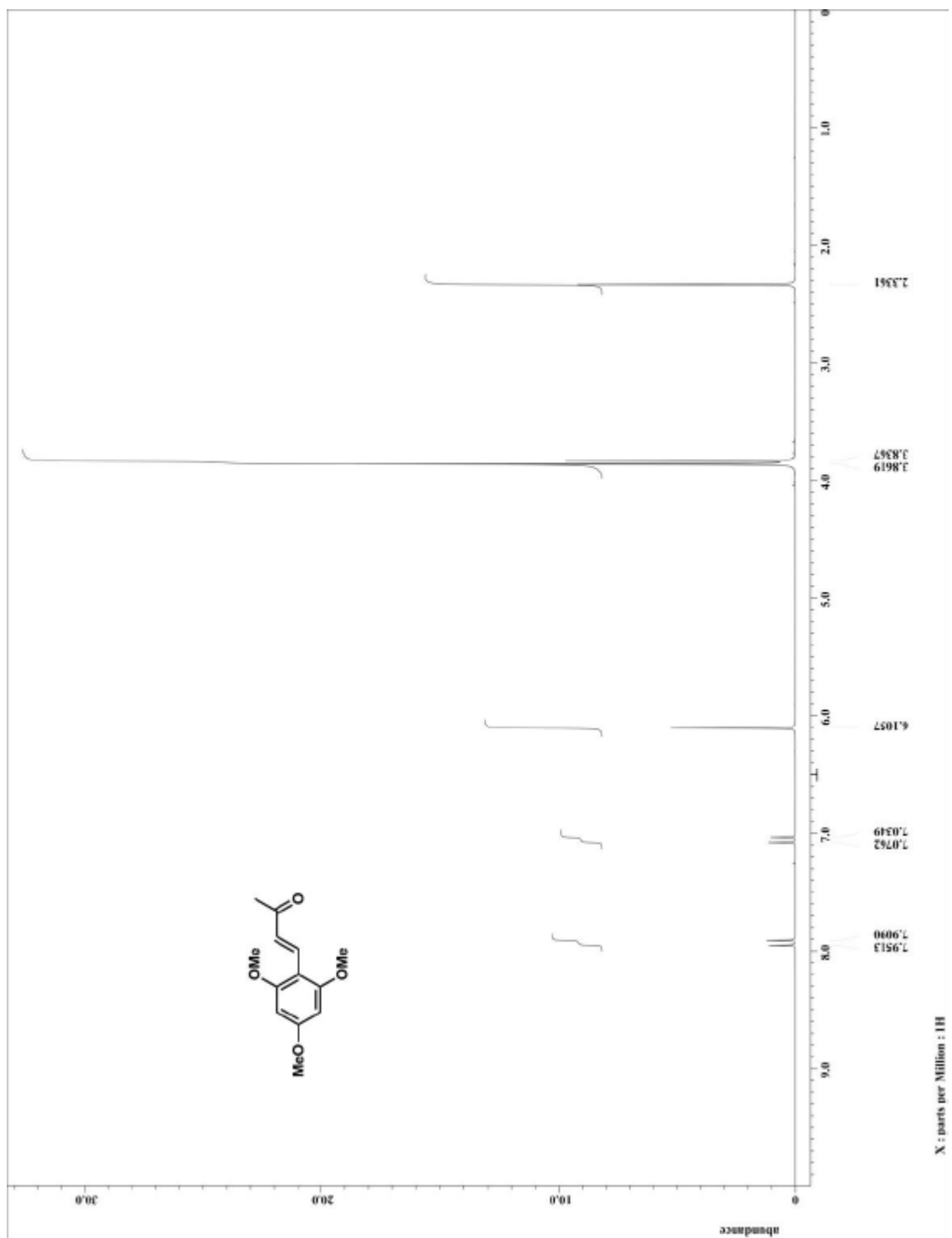


Figure A.1.111. ^1H NMR for compound 135

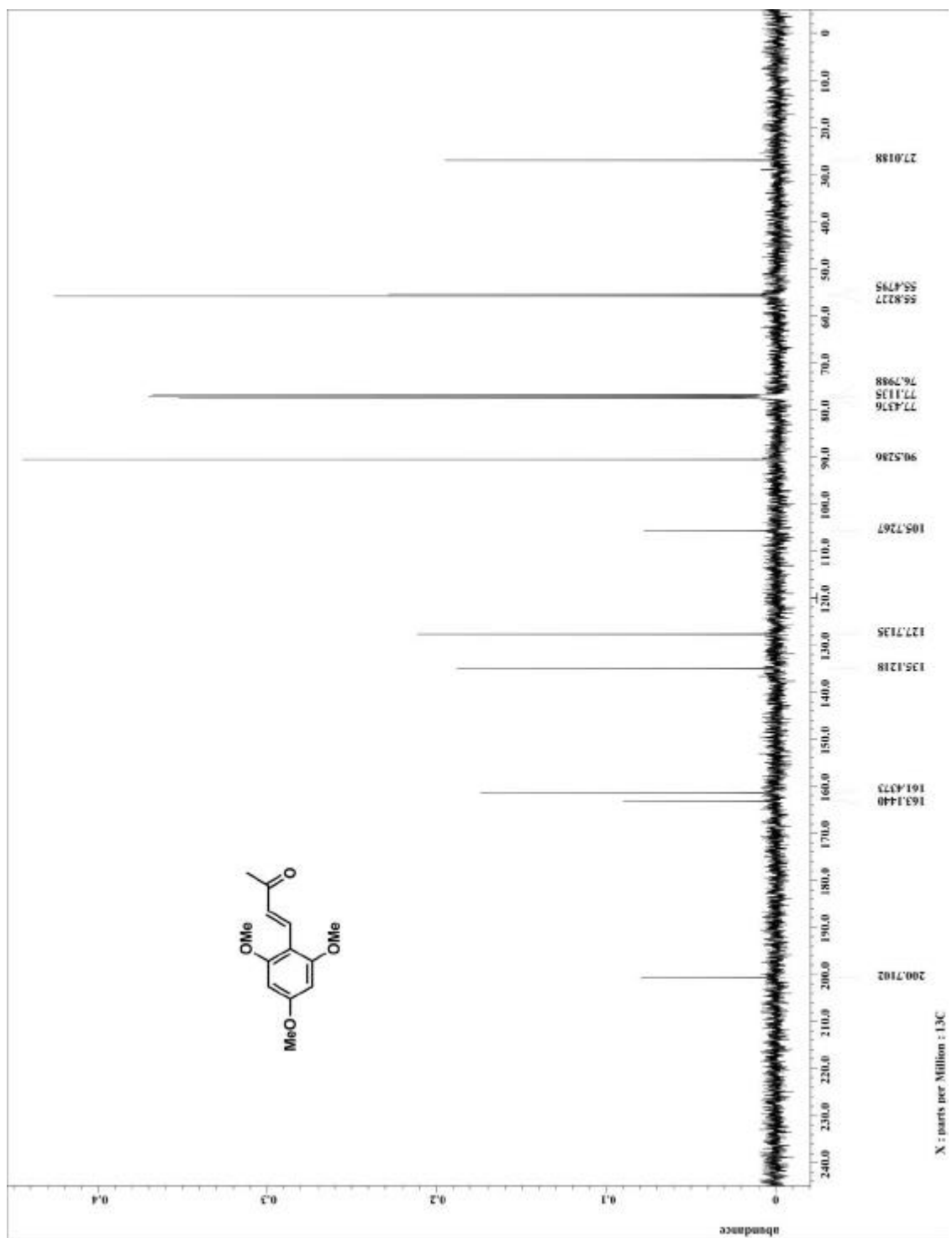


Figure A.1.112. ^{13}C NMR for compound 135

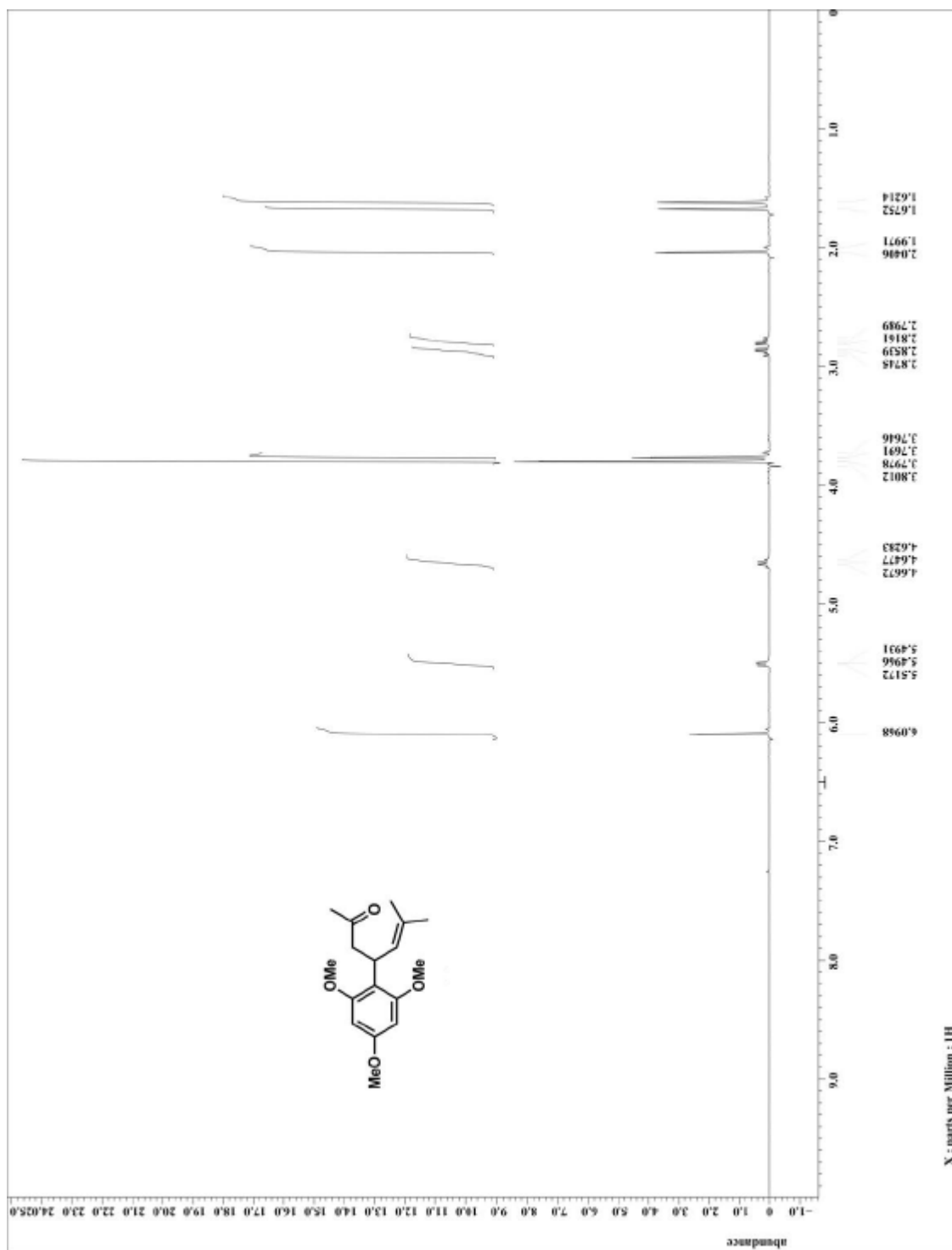


Figure A.1.113. ¹H NMR for compound 136

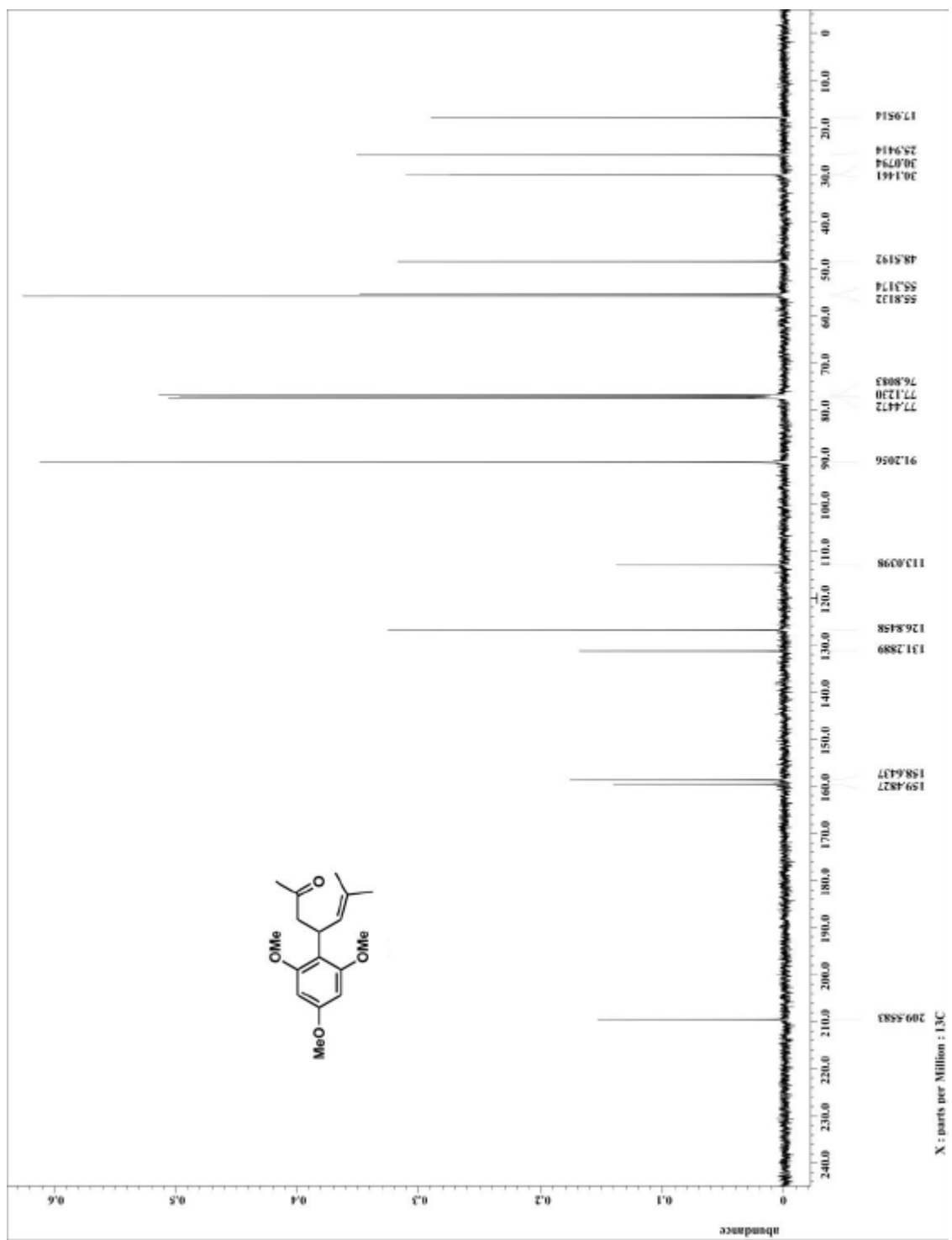
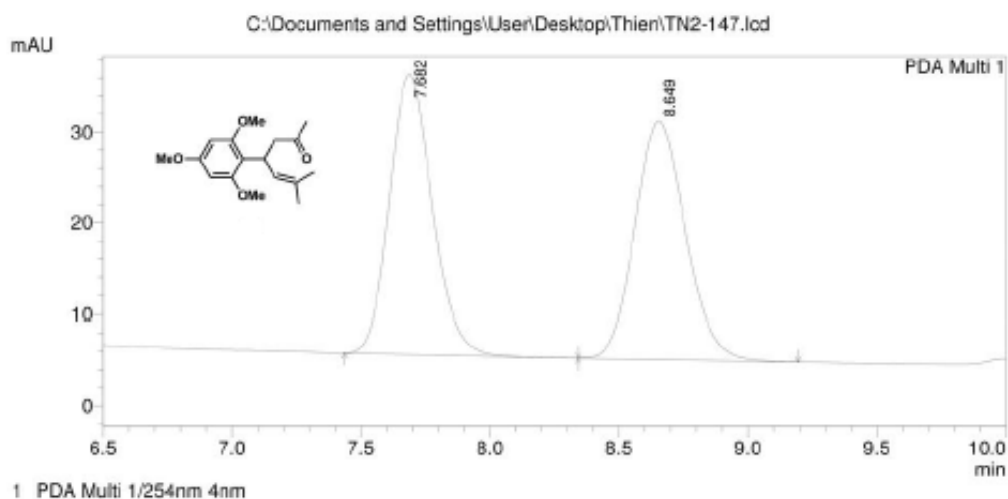
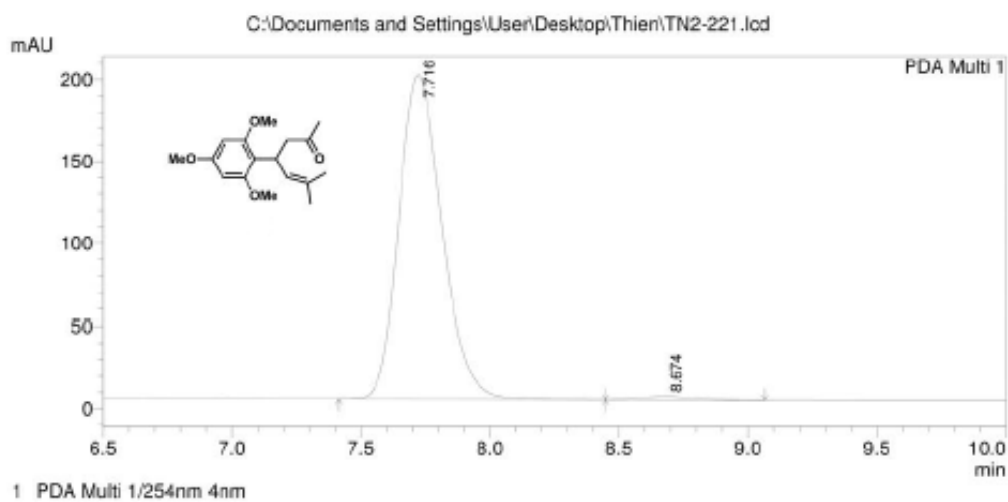


Figure A.1.114. ^{13}C NMR for compound 136



PeakTable

Peak#	Ret. Time	Area	Height	Area %	Height %
1	7.682	352817	30661	49.903	54.038
2	8.649	354192	26078	50.097	45.962
Total		707009	56739	100.000	100.000



PeakTable

Peak#	Ret. Time	Area	Height	Area %	Height %
1	7.716	2293742	197211	98.700	98.862
2	8.674	30209	2271	1.300	1.138
Total		2323950	199481	100.000	100.000

Figure A.1.115. HPLC trace for compound 136

Chapter 3

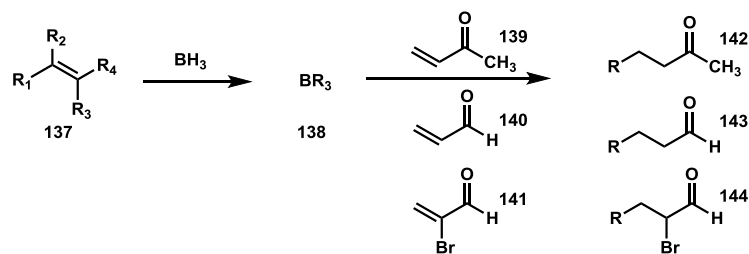
Experimental mechanistic study of the BINOL-catalyzed conjugate addition of vinylboronic acids to enones¹

3.1. Background

In the first chapter, we introduced the seminal work by Chong on the BINOL-catalyzed conjugate addition of boronic esters to enones and in the second our work in developing this chemistry to access different chiral heterocyclic structures. This section will provide a complete historical picture of the mechanistic aspects of this powerful asymmetric strategy.

3.1.1. H.C. Brown's work

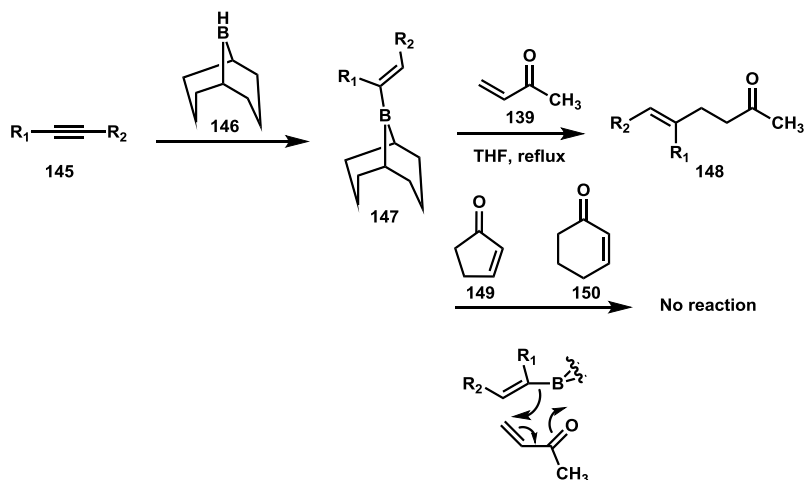
In 1967, Brown and coworkers showed that alkylboranes could undergo a conjugate addition to methyl vinyl ketone² and acrolein³ to generate elongated ketones and aldehydes (Scheme 3.1.1.1). The method was later performed on 2-bromoacrolein⁴ to form different α -bromo carbonyl compounds which were very useful but difficult to obtain considering the state of the art at the time (Scheme 3.1.1.1). This breakthrough allowed for the use of a mild boron nucleophile that was advantageous over the utilization of organometallic reagents that were typically too harsh for 1,4-addition, especially towards enal substrates.



Scheme 3.1.1.1. Conjugate addition of alkylboranes to unsaturated carbonyl compounds

The transformation was subsequently proven to go through a radical process.⁵ Specifically, inhibition was observed with the addition of galvinoxyl, a radical scavenger, to the reaction. To further support this hypothesis, they also carried out the reactions in the presence of peroxide or ultraviolet light⁶ on a number of less reactive substrates, and a great boost in yield was observed under the given conditions. Finally, they showed that the slow addition of external oxygen was sufficient for the efficient formation of the products especially for difficult substrates as mentioned above.⁷

In light of the successfully established method, the Brown group proceeded to investigate the reactivity of vinylboranes to transfer the vinyl group to α,β -unsaturated ketones.⁸ Although attempts to achieve the same free radical transformation were not successful, they found the reactions were highly operative in thermal conditions. An interesting observation was that cyclic enones that could not adopt an *s-cis* conformation gave a complex mixture without any trace of the desired products. This implied a particular cyclic transition state that can transfer the vinyl from boron to carbon with the retention of its stereochemistry (Scheme 3.1.1.2).



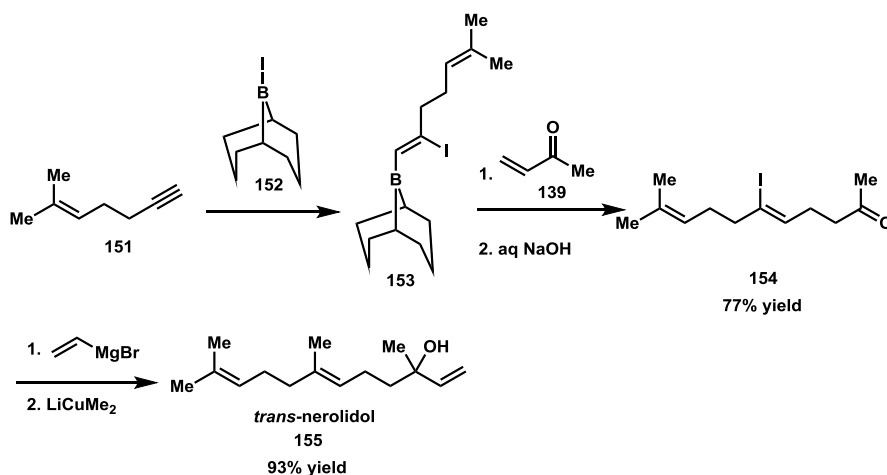
Scheme 3.1.1.2. 1,4-Addition of vinylboranes to unsaturated carbonyl compounds.

These seminal works by H.C. Brown initiated a research trend in developing methods for organoboron in conjugate addition reactions. The following sections describe this chemistry in terms of scope and mechanistic insights.

3.1.2. Suzuki's work

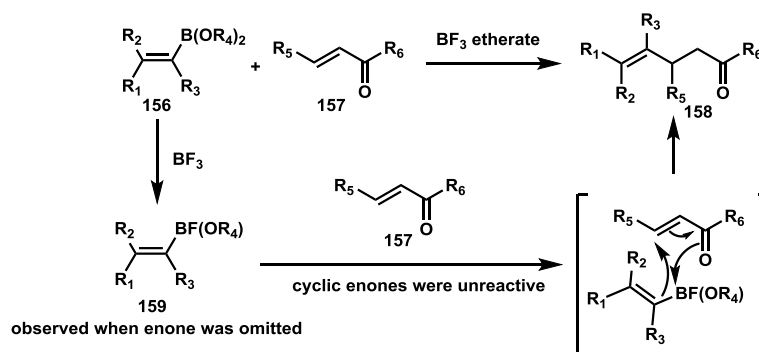
In the vinylation of enones by Brown, the vinylboranes were accessed via the hydroboration of alkynes by 9-BBN, which gave exclusively α,β -disubstituted alkenylboranes (Scheme 3.1.1.2). This restriction set a limitation of the strategy in that highly substituted vinylboranes, especially trisubstituted vinylboranes, were left out of the scope. In 1985, Suzuki *et al.* described their elegant solution for the problem in which haloborations were performed on terminal alkynes followed by the standard conjugate addition to methyl vinyl ketone. The halo group on the addition product was subsequently manipulated by means of some coupling transformations to achieve chemical structures with a highly substituted olefin moiety at the terminal.⁹ The utility of the method was

demonstrated by the synthesis of the terpenoid *trans*-nerolidol in excellent yield and stereoselectivity (Scheme 3.1.2.1).



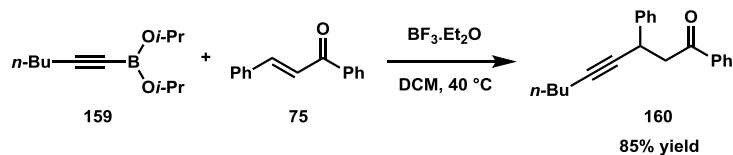
Scheme 3.1.2.1. Application of conjugate addition of halovinylboranes to enones in the synthesis of *trans*-nerolidol.

It is worth noticing that the reactions require an excess of 9-BBN in order to take place smoothly, indicating a Lewis acid promoted mechanism. This was later reaffirmed in a 1990 report of the conjugate addition of vinylboronic esters to enones in which the reactions only proceeded in the presence of stoichiometric BF₃ etherate (Scheme 3.1.2.2).¹⁰ This observation in addition to the inertness of cyclic enones made them believe that the reaction should proceed initially with the activation of the vinylboronic ester by BF₃ etherate to form a stronger Lewis acid **159**, followed by a closed six-membered ring transition state for the C-C bond formation. Although there was not evidence reported for the proposed pathway, they observed the intermediate **159** when carrying out the reaction in the absence of the enone.



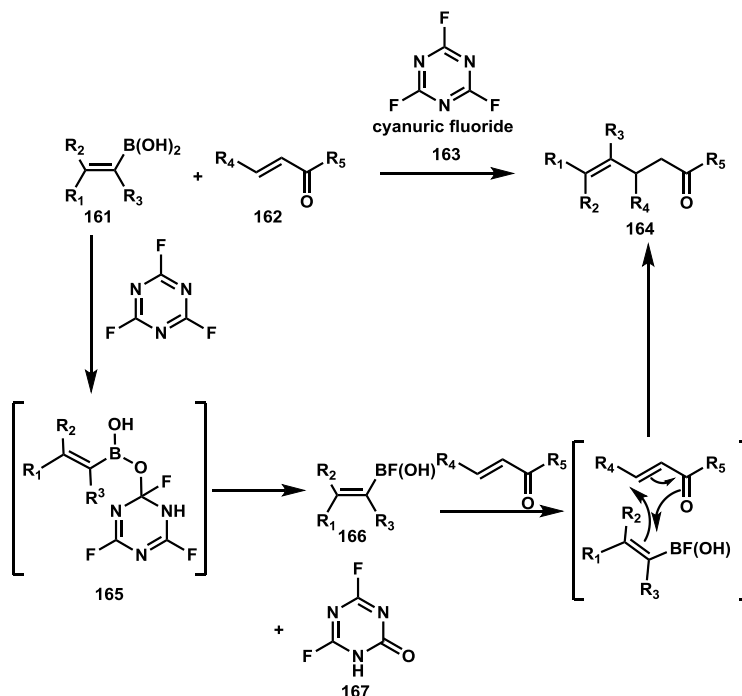
Scheme 3.1.2.2. Conjugate addition of vinyl boronic esters to enones and proposed cyclic transition state.

Taking advantage of the novel method developed by H.C. Brown in 1988¹¹ to prepare alkynylboronic esters, the Suzuki group was able to introduce a number of alkynyl groups to enones (Scheme 3.1.2.3).¹² Unsurprisingly, all the mechanism related observations were in accord with those described in their proceeding publication.



Scheme 3.1.2.3. Conjugate addition of alkynylboronic esters to enones.

Later, they disclosed the extension to the use of different alkenylboronic acids using cyanuric fluoride to activate the boronic acids in the same way as BF_3 does to boronic esters (Scheme 3.1.2.4).¹³ This could be perceived as an improvement since BF_3 etherate could cause undesired side products and boronic acids are generally more stable and easier to handle than the esters.

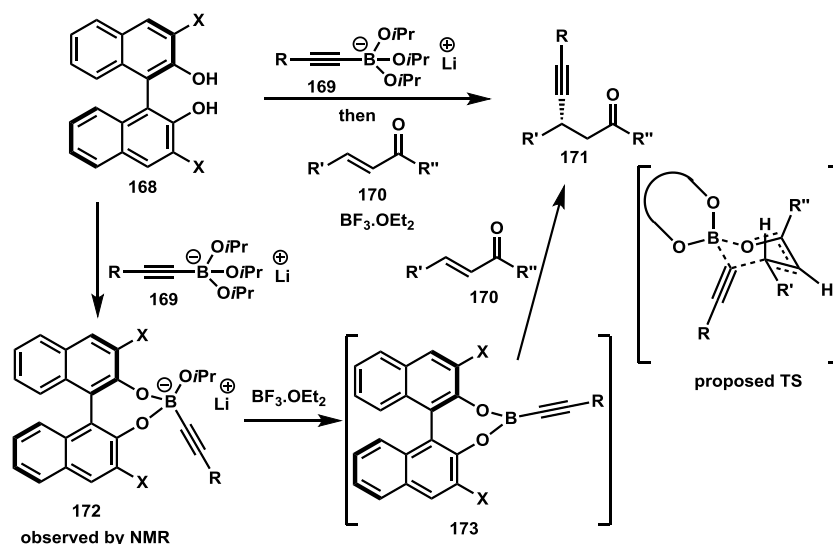


Scheme 3.1.2.4. Conjugate addition of vinylboronic acids to enones facilitated by cyanuric fluoride.

3.1.3. Chong's work and the proposed mechanism

In 2000, two years after Suzuki revealed his work with boronic acids, Chong and coworkers described the employment of stoichiometric BINOL to facilitate the enantioselective conjugate addition of various alkynyl boronate salts to chalcone substrates (Scheme 3.1.3.1).¹⁴ When BINOL was treated with enone and **169** without the $\text{BF}_3 \cdot \text{Et}_2\text{O}$, the reaction did not proceed. With a stoichiometric amount of $\text{BF}_3 \cdot \text{Et}_2\text{O}$, a smooth transformation took place with good yield and great selectivity. It is also noteworthy that cyclic enones such as cyclohexenone are completely unreactive under their standard conditions. This is in agreement with the observations from Brown and Suzuki. With the configuration of the product defined by X-ray analysis and the above

observations, they proposed a transition state that invokes a six-membered ring conformation formed by the trivalent boron species **173** and the enone.

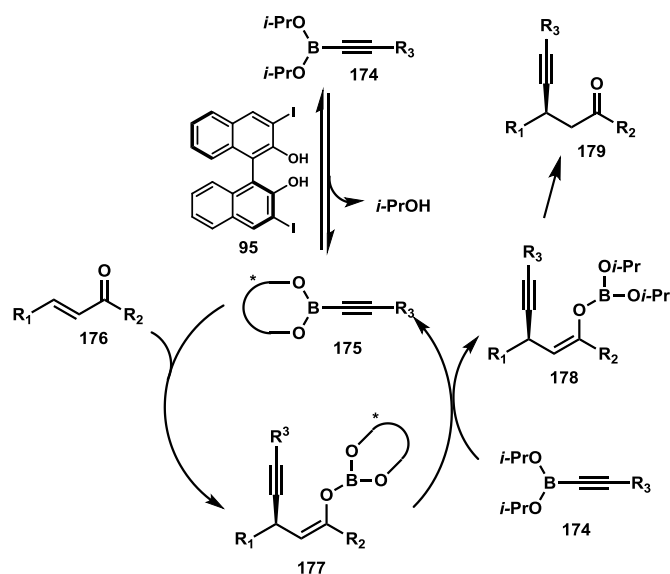


Scheme 3.1.3.1. Asymmetric conjugate addition of alkynylborates to enones and proposed transition state.

In their subsequent reports where they demonstrated the catalytic activity of BINOL in the reaction of alkynyl¹⁵ and vinyl¹⁶ boronic esters, they proposed a similar transition state for the reactions.

A catalytic cycle was also postulated to rationalize the catalytic ability of the I_2 -BINOL (Scheme 3.1.3.2). To begin, a double exchange between the BINOL and the boronic ester occurs to form the trivalent boronate **175** with the concurrent releasing of two alcohol molecules. The newly formed boronate possesses a greater Lewis acidity than the parent boronic ester and will bind to the carbonyl oxygen more strongly. At this point, the carbon-carbon bond formation takes place to form the intermediate **177**, which

engages in the ligand exchange/disproportionation with another alkynylboronic ester to yield intermediate **178**. **178** will then afford the product via protonolysis process.



Scheme 3.1.3.2. Chong's proposed catalytic cycle of the BINOL catalyzed conjugate addition of alkynylboronic esters to enones.

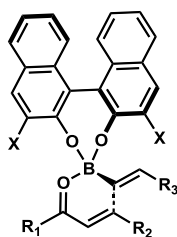
An NMR study was also carried out showing that the equilibrium between boronate **174** and **175** is established quickly at room temperature. This leaves either the addition or the disproportionation step to be rate determining. However, the latter is less likely to be the slowest step due to the dependence of the reaction rate on the aryl groups attached to the β -position of the enones.

3.1.4. Theoretical study

In 2006, Pellegrinet and Goodman carried out a calculational study¹⁷ on the mechanistic pathway proposed by Chong (Scheme 3.1.3.2). The calculation confirmed the catalytic capability of BINOL. Specifically, the energy barrier for the reaction of the enone with the activated trivalent boronate **175** is much lower than that for the enone

with the starting boronic ester. The distance between the boron and the carbonyl oxygen in the transition state of the reaction of the enone and **175** is also shorter than that in the transition state with **174**. This result reaffirmed the higher Lewis acidity of **175** than the boronic ester. In addition, the complexation between **174** and the enone was shown to lower the LUMO of the enone and hence facilitate the addition step. Finally, the facial selectivity was correctly reproduced, with a calculated energy difference between the two diastomeric transition states of $1.18 \text{ kcalmol}^{-1}$ of the model system.

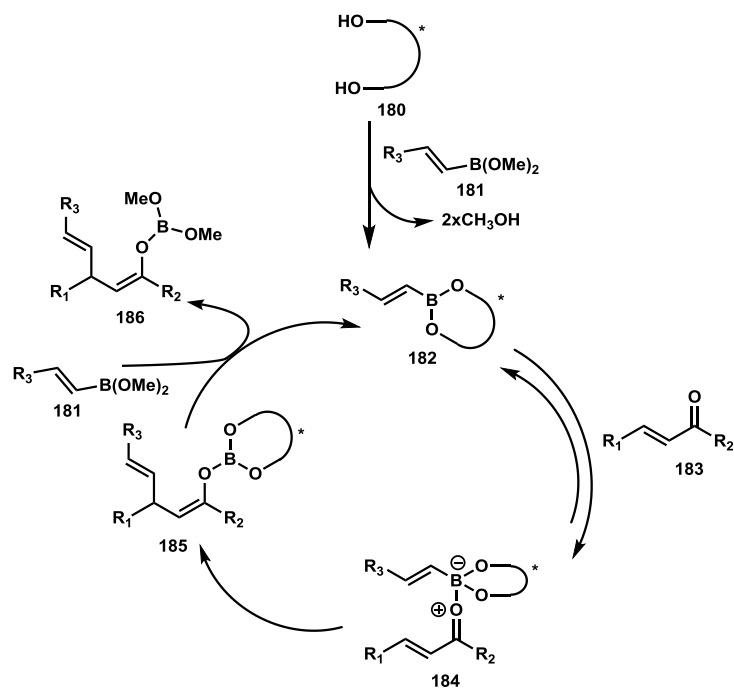
In 2008, they performed the same work on the reaction of alkenylboronic esters. This study gave a thorough computational analysis on both the transition state and the catalytic cycle of the reaction.¹⁸ Contrary to the previously proposed chair-like six-membered ring transition state, the reaction was determined to proceed through a sofa-like conformation in which five atoms of the six-membered ring were actually in the same plane (Scheme 3.1.4.1). Like the previous theoretical study, the computed facial selectivity was in the great agreement with experimental data from Chong's study.



Scheme 2.1.4.1. Calculated sofa-like transition state.

The computational analysis of the reaction coordinates revealed a strong support for the catalytic pathway proposed by Chong with a more detailed mechanism (Scheme

2.1.4.2). The reversible double exchange of methoxy groups with the BINOL that gives rise to the highly acidic boronate species **182** was confirmed to be more favorable than the mono exchange pathway proposed by Schaus and coworkers in their asymmetric allylation of ketones¹⁹ and acyl imines²⁰. The addition process in Chong's cycle was broken into two steps in which the activated boronate **182** coordinated to the enone carbonyl to form the highly bound complex **184**, and this complex in turn engages in carbon-carbon bond formation. Chong's proposal of the addition step being rate-determining was also confirmed by having the highest activation energy. Intrigued by these results on the rate determining step of Chong's work and the theoretical study, we decided to study the mechanism of the transformation by an experimental approach.

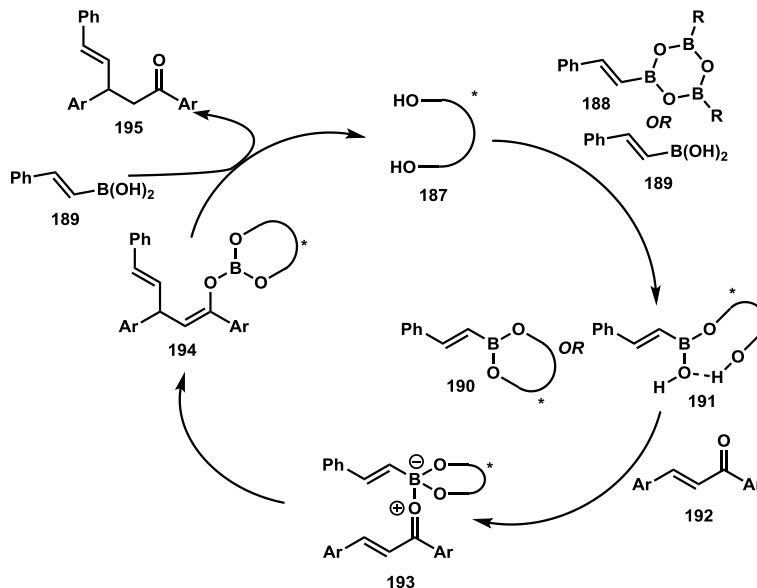


Scheme 2.1.4.2. Detailed catalytic cycle supported by theoretical study.

3.2. Approach

3.2.1. Postulated mechanistic scheme

We anticipated that the use of boronic acids in our methods in place of boronic esters did not alter the mechanism of the reaction. We, therefore, come up with a revised catalytic cycle (Scheme 3.2.1) that accommodates the incorporation of boronic acids in the pathway derived from the theoretical study mentioned above. In addition, the mono-dentate coordination associated with an intramolecular hydrogen bond as proposed by Schaus cannot be excluded. Finally, because boronic acids are in equilibrium with the corresponding boroxines, we cannot rule out the possibility of the generation of activated boronates from boroxine.



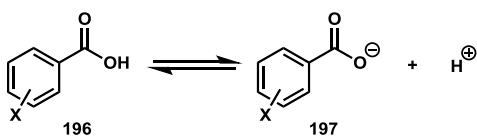
Scheme 3.2.1. Revised scheme for the use of boronic acids.

The fact that the electronic nature of the β -aryl groups have great impact on the reaction rate indicates that the formation of **190** or **191** from BINOL is not the rate

determining step. The same argument can also be applied for the protonolysis being a rapid process since the stability of the boron enolate **194** is not affected by the β -aryl groups. Furthermore, the presence of super-stoichiometric amounts of boronic acid would also accelerate this step. As a consequence, either the formation of complex **193** or the carbon-carbon bond formation for **194** would be the slowest step. In either scenario, the electronic effects from the enone and/or ketone aryl groups would influence the reaction rate. Therefore, we decided to implement a Hammett plot analysis to verify the rate determining step.

3.2.2. Hammett plot

The Hammett plots are generally used for those reactions whose mechanisms express a rate dependence on the electronic nature of the substituents. Hammett established a quantified scale to evaluate the ability of substituents to exert their electronic demand. In order to do that, he measured the acidity constants of different benzoic acids bearing different substituents at meta or para positions (Scheme 3.2.2.1). Ortho substituents were not examined to eliminate any possible steric effects.



Scheme 3.2.2.1. Acid dissociation of substituted benzoic acids.

The acidity of each substituted benzoic acid was then compared with the parent acid via equation 3.2.1. The σ_x value, which is called substituent parameter, reflects quantitatively the capability of each substituent to withdraw or donate the electrons. An

electron withdrawing group will make the acid more acidic, the ratio K_x/K_H will be greater than 1, and consequently a positive σ_x will be obtained. In the opposite sense a negative σ_x is produced by an electron donating group.

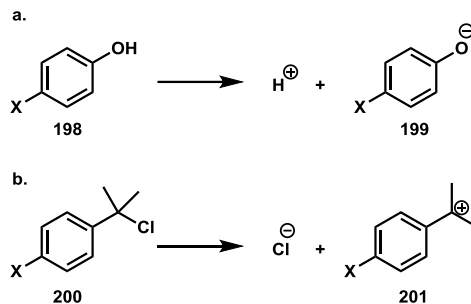
$$\log(K_x/K_H) = \sigma_x \quad (3.2.1)$$

The established set of σ values can then serve to investigate the electronic sensitivity of reactions different from acid dissociation. Specifically, the Hammett relationship given in equation 3.2.2 will be utilized and a plot of $\log(k_x/k_H)$ or $\log k_x$ versus σ_x is made to determine the ρ value, which is the slope of the graph.

$$\log k_x \text{ (or } \log(k_x/k_H)) = \rho\sigma \quad (3.2.2)$$

This ρ value is critical in understanding the electronic change along the progression of the reaction. If ρ is positive, the reaction is accelerated by electron withdrawing groups and a negative charge is building during the reaction. And when ρ has a negative value, electron donating groups will facilitate the reaction and a positive charge is developed during the reaction.

One interesting feature about σ values is that they do not include effects for direct stabilization through resonance. The reason is that σ 's are derived from the dissociation of benzoic acid to benzoate, when the negative charge cannot be delocalized by resonance. Therefore, in many reactions that generate charges that can be significantly stabilized by resonant delocalization, σ^+ or σ^- can be employed. The σ^+ scale was measured by the ionization of para-substituted phenols, and the σ^- scale was collected upon the heterolysis of para-substituted chlorodimethylphenylmethanes (Scheme 3.2.2.2).



Scheme 3.2.2.2. (a) Ionization of substituted phenol for σ^- values; (b) heterolysis of substituted chlorodimethylphenylmethanes for σ^+ values.

3.3. Results and discussion

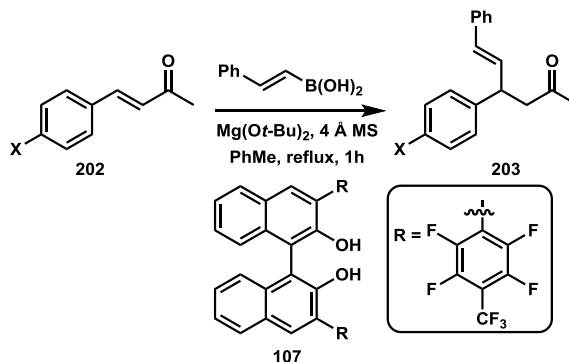
3.3.1. Electronic effect from β -aryl groups

We commenced our study by looking at the electronic effects of different substituents on the aryl ring at the β -position of the enone on the reaction rate. A series of methyl styrenyl ketones were made through Wittig reactions. Their reactions with styrenyl boronic acid catalyzed by BINOL **107** conveniently yielded products without the formation of side products. The reactions were monitored by gas chromatography every five minutes for an hour. The ratio between the integration of the starting enone and that of the corresponding product reflected the percentage of the remaining substrate at a given timepoint. Fortunately, a first order dependence with respect to starting material was observed since the plot of the natural log of the ratio versus the reaction time gave a completely straight line.

The rate constant corresponding to each substituent, which was the slope of the plot, was then determined (Table 3.3.1). With all the rate constants in hand, we could produce a Hammett plot using σ^+ values to define the ρ value (Figure 3.3.1). Indeed, a negative ρ

value was obtained, indicating the acceleration of the reaction by electron donating groups. This observation is relatively unusual since electron rich substrates would typically be considered less electrophilic for a nucleophilic attack. Albeit unusual, we find this unsurprising for it correlates to our experimental observation on the greater reactivity of electron rich enones. At this point, the obtained data showed a consistency with the complex formation as the rate determining step because an electron releasing group can give a stronger binding to the boron center and also stabilize the positive charge at the β carbon. Therefore, a similar Hammett study on the keto aryl ring would be helpful in confirming the actual slow step.

Table 3.3.1. Reaction rate constants of β -aryl substrates



X	σ^+	k (min ⁻¹)	logk
CF ₃	0.61	7.55 x 10 ⁻³	-2.12
Br	0.15	12.1 x 10 ⁻³	-1.92
H	0	15.2 x 10 ⁻³	-1.82
Ph	-0.18	11.9 x 10 ⁻³	-1.93
OCH ₃	-0.78	24.7 x 10 ⁻³	-1.61

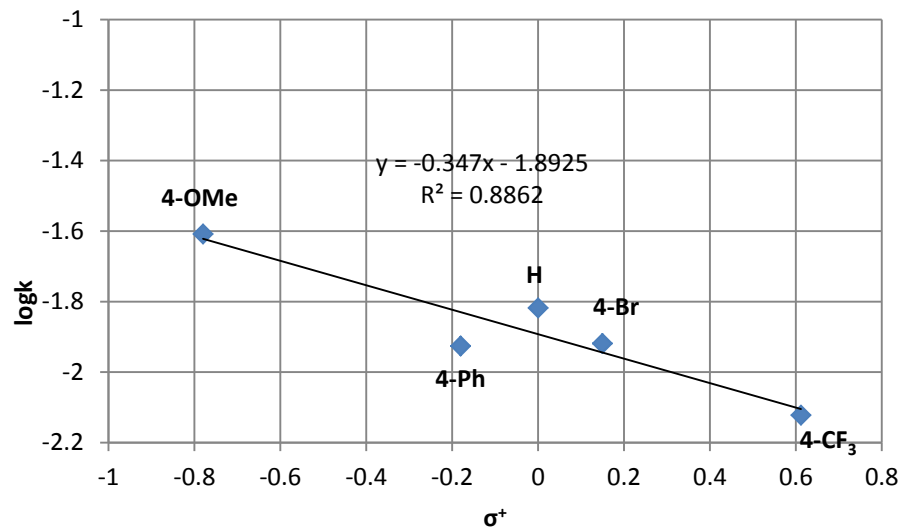
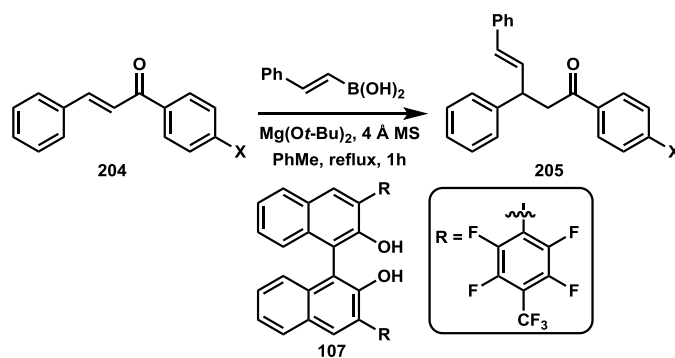


Figure 3.3.1. Hammett plot for β-aryl substitution.

3.3.2. Electronic effect from keto aryl groups

A small library of aryl styrenyl ketones was easily synthesized through a three-step synthesis²¹, and the rate constants were also quickly determined (Table 3.3.2). The Hammett plot was again plotted using σ⁺ values and to our surprise, the opposite result was observed (figure 3.3.2). The plot depicted a straight line with positive slope, expressing a positive rho value and showing that electron donating groups decelerate the reaction. These data are not consistent with the possibility of the complex formation to be rate determining. Thus, the addition step appeared more likely to be rate defining.

Table 3.3.2. Reaction rate constants of keto-aryl substrates



X	σ^+	k (min^{-1})	logk
Br	0.15	9.56×10^{-2}	-1.02
H	0	7.44×10^{-2}	-1.13
F	-0.07	8.40×10^{-2}	-1.08
Ph	-0.18	10.2×10^{-2}	-0.991
Ph	-0.26	6.74×10^{-2}	-1.17
OMe	-0.78	3.32×10^{-2}	-1.48

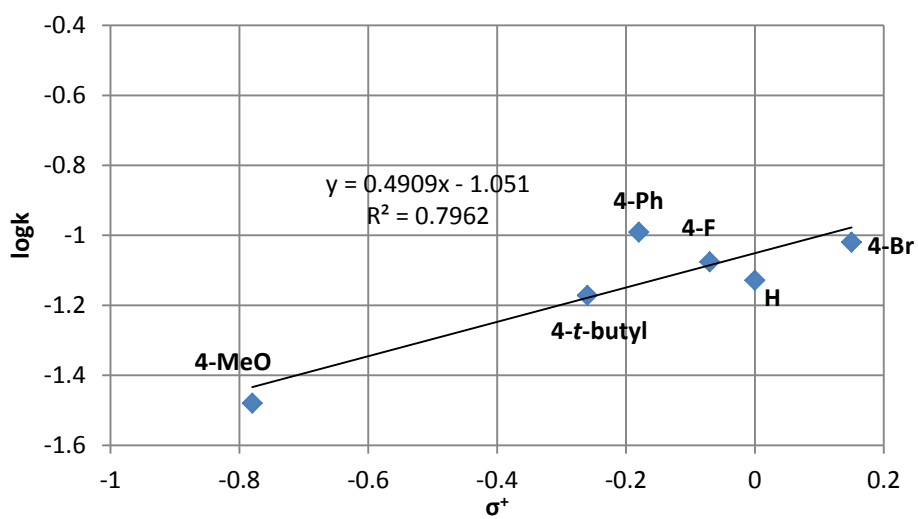
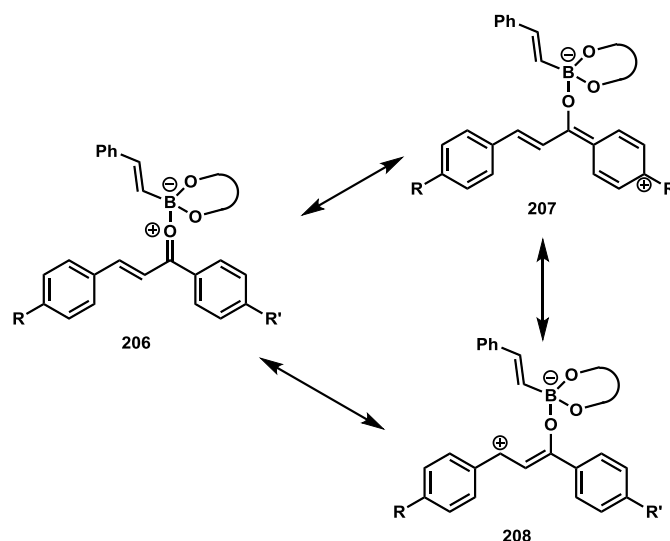


Figure 3.3.2. Hammett plot for keto-aryl substitution.

It appears, from the data obtained above, that the reaction rate is strongly dependent on the localization of the cationic charge on the β -carbon for the carbon-carbon bond formation. In case of the electron donating group on the keto aryl ring, the positive charge on the complex **206** will be delocalized along that ring making the β -carbon less electrophilic because of cross-conjugation and thus causing a slow reaction (Scheme 3.3.2, from **206** to **207**). In addition, when the group on the β -aryl ring becomes more donating, the cationic charge is more likely to reside on the β -carbon (**208**) where the carbon-carbon bond forming occurs, due to stabilization via resonance. Consequently, a faster reaction will be observed.



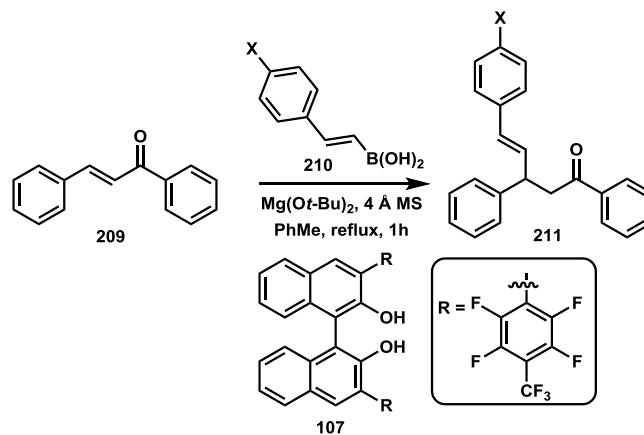
Scheme 3.3.2. Resonance stabilization from aryl groups.

3.3.3. Electronic effect from boronic acids

To have stronger support for our proposal of the carbon-carbon bond formation being rate determining, we also investigated the rate dependence on the electronics of the nucleophiles. We anticipated a positive correlation between the electron donating ability

of the substituent and the reaction rate. In fact, this trend was correctly reproduced with higher rate constants for electron donating groups (Table 3.3.3). As depicted in the Hammett plot (Figure 3.3.3), a clear negative rho value was obtained, confirming the slow step to be carbon-carbon formation.

Table 2.3.3. Reaction rate constants from styrenylboronic acids



X	σ^+	k (min ⁻¹)	logk
CF ₃	0.61	1.42 x 10 ⁻²	-1.85
H	0	7.44 x 10 ⁻²	-1.13
F	-0.07	7.18 x 10 ⁻²	-1.14
Me	-0.31	12.8 x 10 ⁻²	-0.894
OMe	-0.78	30.1 x 10 ⁻²	-0.521

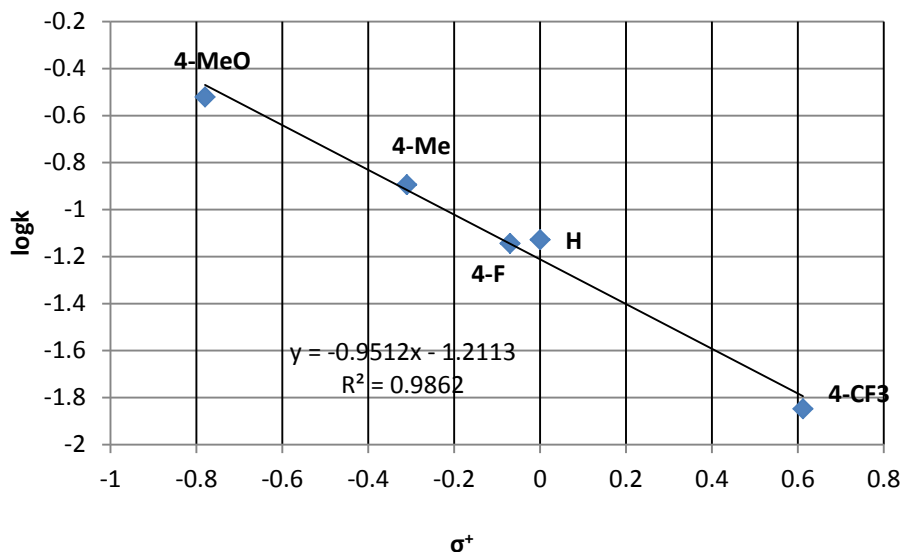


Figure 3.3.3. Hammett plot for boronic acid aryl substitution.

3.4. Conclusion

A deeper insight into the mechanism of the BINOL-catalyzed conjugate addition of alkenylboronic acids to enones was carried out with some success. The work further confirmed the mechanistic pathway proposed by the theoretical study. The Hammett plot analysis on the electronic effects from the β-aryl, keto aryl and the nucleophile aryl groups reveal the behaviors correlating to the scheme. Furthermore, this Hammett study also gave firm evidence for carbon-carbon bond formation as the rate determining step since it demonstrated the rate dependence on the ability of the aryl groups in the enone to accommodate the cationic charge on the β-carbon where the bond would be made.

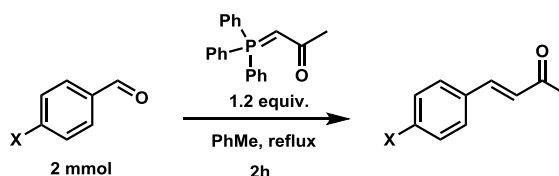
3.5. Experimental section

3.5.1. General consideration

GC data were recorded on an Agilent 7890B GC with an Agilent 5977A MS detector. ¹H-NMR spectra were recorded on a JEOL-500 spectrometer with tetramethylsilane as

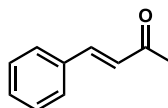
internal standard in CDCl_3 solvent. Chemical shifts were reported in parts per million (ppm, δ) and coupling constants are given in Hertz. Proton coupling patterns are described as singlet (s), doublet (d), triplet (t), and multiplet (m). All reagents were purchased from Sigma-Aldrich and used without further purification. Silica gel (230-400 mesh, Silicycle, Canada) was used for chromatographic separation.

3.5.2. General procedure for the synthesis of (*E*)-4-phenylbut-3-en-2-ones from benzaldehydes and Wittig reagent



A 10 ml round bottom flask equipped with a stir bar and a condenser was flame-dried under vacuum and backfilled with argon three times. Benzaldehyde (2 mmol) was then added followed by the addition of 1-(triphenylphosphoranylidene)-2-propanone (1.2 eq, 764 mg) and toluene (4 ml). The reaction mixture was heated at reflux for two hours. Product was then purified using silica gel column chromatography with proper eluent.

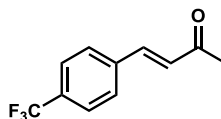
3.5.2.1. Synthesis of (*E*)-4-phenylbut-3-en-2-one (209)



See the general procedure for enone formation above. After silica gel chromatography using 5%-10% ethyl acetate in hexanes as eluent, the title compound was obtained in 98% yield (286 mg) as a white solid. $^1\text{H-NMR}$ (500 MHz, CDCl_3): δ = 7.53 (m, 3H), 7.34 (m, 3H), 6.72 (d, J = 16.6 Hz, 1H), 2.38 (s, 3H). $^{13}\text{C-NMR}$ (125.77 MHz, CDCl_3): δ =

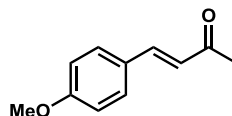
198.6, 143.6, 134.5, 133.6, 129.1, 128.4, 127.2, 27. All spectral properties were identical to those reported in the literature.²²

3.5.2.2. Synthesis of (*E*)-4-(4-(trifluoromethyl)phenyl)but-3-en-2-one (210)



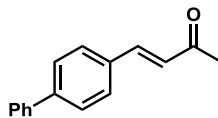
See the general procedure for enone formation above. After silica gel chromatography using 5%-10% ethyl acetate in hexanes as eluent, the title compound was obtained in 62% yield (264 mg) as a white solid. ¹H-NMR (500 MHz, CDCl₃): δ= 7.64 (m, 4H), 7.51 (d, J= 16Hz, 1H), 6.77 (d, J= 16 Hz, 1H), 2.4 (s, 3H). ¹³C-NMR (125.77 MHz, CDCl₃): δ= 198.0, 141.4, 129.2, 128.4, 126.03, 126.0, 27.9. All spectral properties were identical to those reported in the literature.²³

3.5.2.3. Synthesis of (*E*)-4-(4-methoxyphenyl)but-3-en-2-one (211)



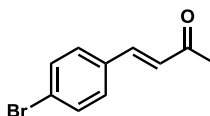
See the general procedure for enone formation above. After silica gel chromatography using 20% ethyl acetate in hexanes as eluent, the title compound was obtained in 81% yield (287 mg) as a white solid. ¹H-NMR (500 MHz, CDCl₃): δ= 7.48 (m, 3H), 6.91 (d, J= 9.2Hz, 2H), 6.6 (d, J= 16Hz, 1H), 3.84 (s, 3H), 2.35 (s, 3H). ¹³C-NMR (125.77 MHz, CDCl₃): δ= 198.5, 161.7, 143.4, 131.1, 127.1, 125.1, 114.5, 55.5, 27.5. All spectral properties were identical to those reported in the literature.²⁴

3.5.2.4. Synthesis of (*E*)-4-(biphenyl-4-yl)but-3-en-2-one (212)



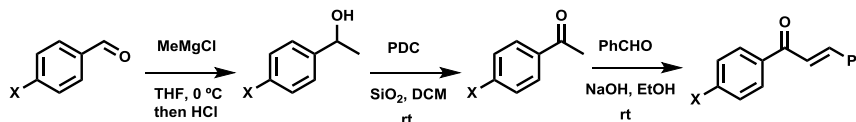
After silica gel chromatography using 5-10% ethyl acetate in hexanes as eluent, the title compound was obtained in 66% yield (296 mg) as a white solid. ¹H-NMR (500 MHz, CDCl₃): δ= 7.63 (m, 6H), 7.55 (d, 16 Hz, 1H), 7.46 (m, 2H), 7.38 (m, 1H), 6.76 (d, 16 Hz, 1H), 2.4 (s, 3H). ¹³C-NMR (125.77 MHz, CDCl₃): δ= 198.5, 143.4, 143.1, 140.2, 133.4, 129.0, 128.9, 128.0, 127.7, 127.1, 127.07, 27.7. All spectral properties were identical to those reported in the literature.²⁵

3.5.2.5. Synthesis of (*E*)-4-(4-bromophenyl)but-3-en-2-one (213)



After silica gel chromatography using 10% ethyl acetate in hexanes as eluent, the title compound was obtained in 74% yield (332 mg) as a white solid. ¹H-NMR (500 MHz, CDCl₃): δ= 7.53 (d, 8.6 Hz, 2H), 7.45-7.39 (m, 3H), 6.69 (d, 16 Hz, 1H), 2.37 (s, 3H). ¹³C-NMR (125.77 MHz, CDCl₃): δ= 198.2, 142.0, 133.4, 132.3, 129.7, 127.6, 124.9, 27.8. All spectral properties were identical to those reported in the literature.²³

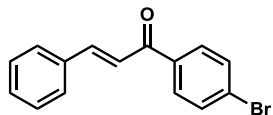
3.5.3. General procedure for the synthesis of (*E*)-chalcones from the corresponding benzaldehydes



A 20 ml round bottom flask equipped with a stir bar was flame-dried under vacuum and backfilled with argon. The flask was then charged with 5 ml of THF and benzaldehyde (5 mmol) and cooled in an ice bath. MeMgCl (3M in THF, 2 equiv., 1.3 ml) was added dropwise to the flask and the reaction was allowed to stir at 0 °C for one hour. 6M HCl (2.5 ml) was then added and the aqueous phase was extracted with ether (2x5 ml). The combined organic extract was dried with MgSO₄ and the solvent was removed to give the crude secondary benzylic alcohol which was subjected to the next reaction without further purification.

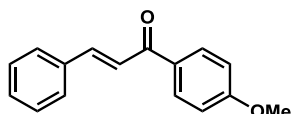
A 50 ml round bottom flask equipped with a stir bar was charged with 2g silica gel. The flask was then flame-dried under vacuum and backfilled with argon. Pyridinium dichromate (2 equiv., 3.76 g) was added followed by the addition of 5 ml DCM. A solution of the crude alcohol obtained from previous step in 5 ml DCM was added to the flask and the reaction was allowed to stir for 16h. The reaction mixture was next passed through a silica gel plug and rinsed with ethyl acetate. The solvent was then removed and the corresponding ketone was purified by column chromatography using appropriate eluent. The product was collected into a 20 ml vial (4 dram) and 5 ml of ethanol was added followed by the addition of benzaldehyde (1 equiv) and a stir bar. 2.5 M NaOH (1.2 equiv) was added dropwise to the vial with stirring. The reaction was allowed to stir for one hour and water was then added. The mixture was extracted with DCM (3x5 ml). The organic extracts were combined and dried under MgSO₄. The solvent was removed and the crude mixture was recrystallized from ethanol to give the pure product.

3.5.3.1. Synthesis of (*E*)-1-(4-bromophenyl)-3-phenylprop-2-ene-1-one (214)



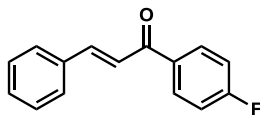
See the general procedure for chalcone formation above. The title compound was obtained in 40% yield (580 mg) over 3 steps as a bright yellow solid. $^1\text{H-NMR}$ (500 MHz, CDCl_3): δ = 7.88 (d, J = 8.6 Hz, 2H), 7.82 (d, J = 16 Hz, 1H), 7.64 (m, 4H), 7.49-7.42 (m, 4H). $^{13}\text{C-NMR}$ (125.77 MHz, CDCl_3): δ = 189.5, 145.5, 137, 134.8, 132.0, 130.9, 130.1, 129.1, 128.6, 128.0, 121.5. All spectral properties were identical to those reported in the literature.²⁶

3.5.3.2. Synthesis of (*E*)-1-(4-methoxyphenyl)-3-phenylprop-2-ene-1-one (215)



See the general procedure for chalcone formation above. The title compound was obtained in 40% yield (475 mg) over 3 steps as a white solid. $^1\text{H-NMR}$ (500 MHz, CDCl_3): δ = 8.04 (d, J = 9.2 Hz, 2H), 7.8 (d, J = 15.5 Hz, 1 H), 7.64 (m, 2H), 7.55 (d, J = 16 Hz, 1H), 7.4 (m, 3H), 6.98 (d, J = 8.8 Hz, 2H), 3.88 (s, 3H). $^{13}\text{C-NMR}$ (125.77 MHz, CDCl_3): δ = 188.8, 163.5, 144.1, 135.2, 131.2, 130.9, 130.4, 129.0, 128.5, 121.9, 113.9, 55.6. All spectral properties were identical to those reported in the literature.²⁷

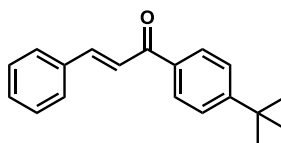
3.5.3.3. Synthesis of (*E*)-1-(4-bromophenyl)-3-phenylprop-2-ene-1-one (216)



See the general procedure for chalcone formation above. The title compound was obtained in 23% yield (257 mg) over 3 steps as a white solid. $^1\text{H-NMR}$ (500 MHz,

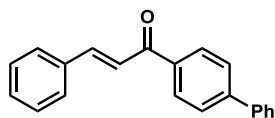
CDCl₃): δ = 8.06 (dd, J= 8.6 Hz; 5.2 Hz, 2H), 7.82 (d, J= 15.5 Hz, 1H), 7.64 (m, 2H), 7.51 (d, J= 15.5 Hz, 1H), 7.42 (m, 3H), 7.17 (t, J= 8.6 Hz, 2H). ¹³C-NMR (125.77 MHz, CDCl₃): δ = 188.9, 166.7, 164.7, 147.2, 134.8, 134.6, 131.23, 131.16, 130.8, 129.1, 128.6, 121.6, 115.9, 115.8. All spectral properties were identical to those reported in the literature.²⁸

3.5.3.4. Synthesis of (*E*)-1-(4-*tert*-butylphenyl)-3-phenylprop-2-ene-1-one (217)



See the general procedure for chalcone formation above. The title compound was obtained in 24% (320 mg) over 3 steps as a white solid. ¹H-NMR (500 MHz, CDCl₃): δ = 7.98 (d, J= 8.6 Hz, 2H), 7.81 (d, J= 16 Hz, 1H), 7.65 (m, 2H), 7.56-7.52 (m, 3H), 7.42-7.41 (m, 3H), 1.36 (s, 9H). ¹³C-NMR (125.77 MHz, CDCl₃): δ = 190.2, 156.7, 144.5, 135.7, 135.1, 130.5, 129.0, 128.6, 128.5, 125.7, 122.2, 35.2, 31.2. All spectral properties were identical to those reported in the literature.²⁸

3.5.3.5. Synthesis of (*E*)-1-(biphenyl-4-yl)-3-phenylprop-2-ene-1-one (218)



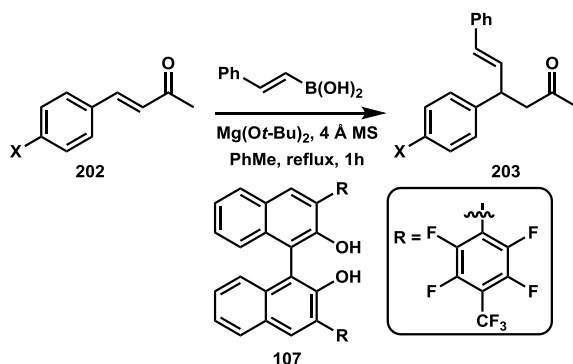
The title compound was obtained in 51% (732 mg) over 3 steps as a yellow solid. ¹H-NMR (500 MHz, CDCl₃): δ = 8.21 (d, J= 8.6 Hz, 2H), 7.87 (d, J= 16 Hz, 1H), 7.73 (d, J= 8.6 Hz, 2H), 7.68-7.65 (m, 4H), 7.60 (d, J=16 Hz, 1H), 7.50-7.40 (m, 6H). ¹³C-NMR (125.77 MHz, CDCl₃): δ = 190.0, 145.6, 144.8, 140.0, 137.0, 135.0, 130.7, 129.3, 129.1,

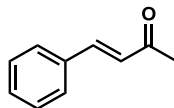
128.6, 128.4, 127.4, 122.1. All spectral properties were identical to those reported in the literature.²⁹

3.5.4. General procedure for the Hammett plot study

The reactions were conducted in 2 dram vials equipped with a stir bar and 100 mg of 4 Å molecular sieves: after the vial was charged with the molecular sieves, it was flame-dried and backfilled with argon 3 times. The enone (0.2 mmol), BINOL **107** (0.2 equiv., 28.7 mg), styrenylboronic acid (3 equiv., 88.8 mg), and Mg(*Or*-Bu)₂ (0.1 equiv., 3.4 mg) were then added followed by the addition of 4 ml toluene. The reaction was allowed to heat at reflux for one hour. 0.2 ml of the reaction solution was extracted via syringe every 5 minutes for GC analysis. The extracted reaction mixture was passed through a short silica gel column (Pasteur pipet) using 1:1 mixture of hexanes and ethyl acetate as the eluent. The collected eluent was then transferred to a GC sample vial and *trans*-stilbene or (*E*)-4-phenylbut-3-en-2-one was added as internal standard. The percent of the enone at different time points were calculated from the integration of the peaks for the substrate and the product recorded by the GC.

3.5.4.1. Reactions of β-aryl substrates





Time (min)	Area of substrate	Area of product	[A] _t /[A] ₀	ln([A] _t /[A] ₀)
5	1024027862	56209913	0.94796524	-0.053437444
10	493685549	42012655	0.921574023	-0.081672176
15	353654167	41224243	0.895602693	-0.110258387
20	517766670	117471331	0.815075089	-0.204475037
25	363672643	111039948	0.766090157	-0.266455418
30	290449130	141008850	0.673180574	-0.395741673
35	308385367	169148996	0.645786756	-0.437285929
40	303297857	227491153	0.571409452	-0.559649247
45	489678933	430080161	0.532399121	-0.630361843
50	249014278	283422433	0.467688033	-0.7599538
55	356990293	433706041	0.45148849	-0.7952054
60	232399972	369868218	0.385874559	-0.95224294

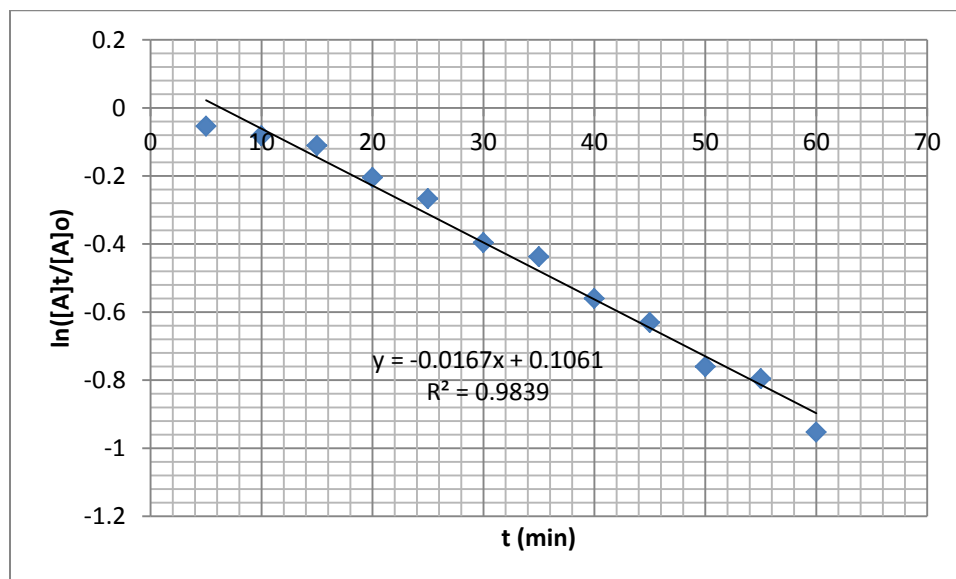


Figure 3.5.4.1.1. A plot of natural log of fraction of enone **209** versus time (first trial)

Time (min)	Area of substrate	Area of product	[A] _t /[A] _o	ln([A] _t /[A] _o)
5	387754323	7693641	0.980544493	-0.019647257
10	413010473	31674845	0.928770204	-0.073893929
15	323428383	51739545	0.862089634	-0.14839603
20	298686171	73859692	0.801743358	-0.220966725
25	319002498	103607716	0.754838589	-0.281251342
30	363144498	165652671	0.686736842	-0.375804114
35	268163380	144516140	0.649810245	-0.43107489
40	235329497	146060034	0.617031873	-0.482834599
45	272345674	190131046	0.588885153	-0.529524101
50	249648793	231835065	0.51849878	-0.656817605
55	278475335	271796616	0.506068562	-0.68108312
60	235942179	278779223	0.458388127	-0.780039015

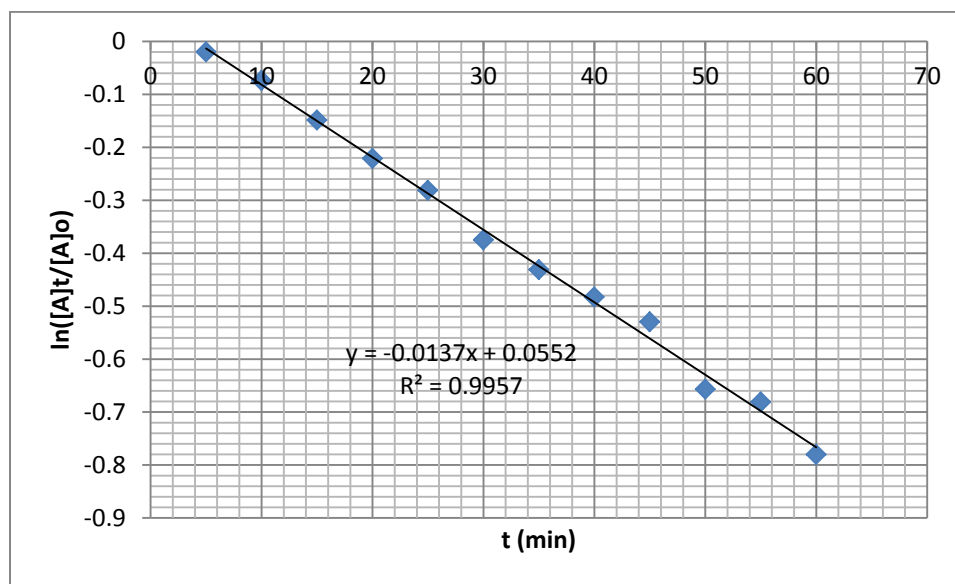
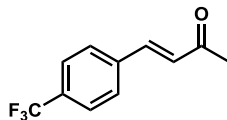


Figure 3.5.4.1.2. A plot of natural log of fraction of enone **209** versus time (second trial)

$$k_{\text{average}} = (0.0167 + 0.0137)/2 = 0.0152$$



Time (min)	Area of substrate	Area of product	[A] _t /[A] _o	ln([A] _t /[A] _o)
10	573802074	9498832	0.983715382	-0.016418669
15	661268880	25810220	0.962434864	-0.038288889
20	591557977	41667022	0.93419871	-0.068066112
25	725034457	75253373	0.905967116	-0.098752269
30	611350083	88908253	0.873035067	-0.135779556
35	630660893	112060610	0.84912163	-0.16355284
40	499264610	115834889	0.811681054	-0.208647806
45	399276033	107589666	0.787735359	-0.238593084
50	573795676	167271096	0.774283368	-0.255817364
55	526711027	206379739	0.718479964	-0.330617459
60	638951435	275495371	0.698730002	-0.358490875

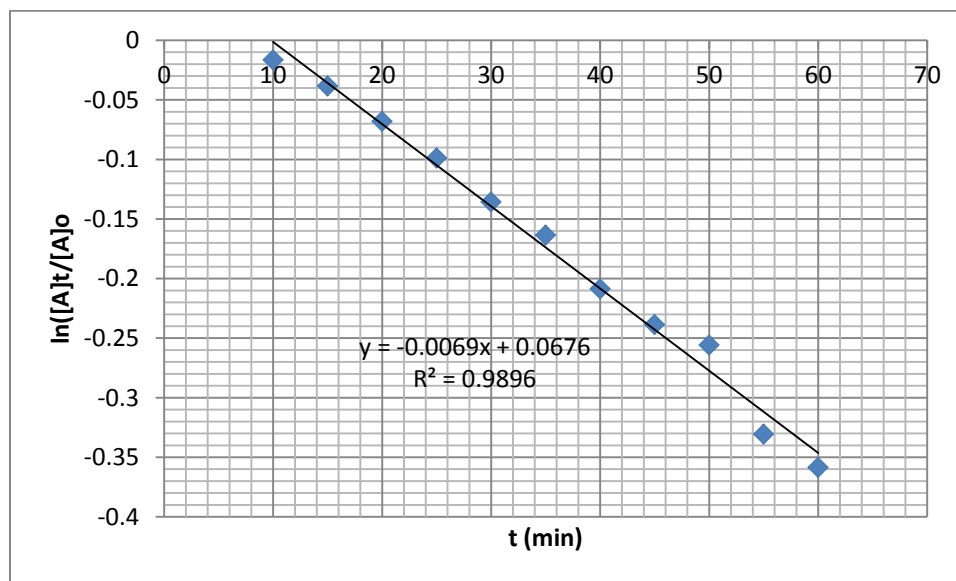


Figure 3.5.4.1.3. A plot of natural log of fraction of enone **210** versus time (first trial)

Time (min)	Area of substrate	Area of product	[A] _t /[A] _o	ln([A] _t /[A] _o)
5	328501912	2427319	0.992665141	-0.007361891
10	217571227	5000242	0.977534216	-0.022721984
20	158626465	6756129	0.95914849	-0.041709378
30	141555259	18742784	0.883075405	-0.124344686
35	145659935	25718216	0.849932937	-0.162597831
40	145451400	39865399	0.784879777	-0.242224723
45	185379364	64546155	0.741738438	-0.298758607
55	188203184	86637974	0.684770742	-0.378671179
60	149973235	85114767	0.637945083	-0.449503076

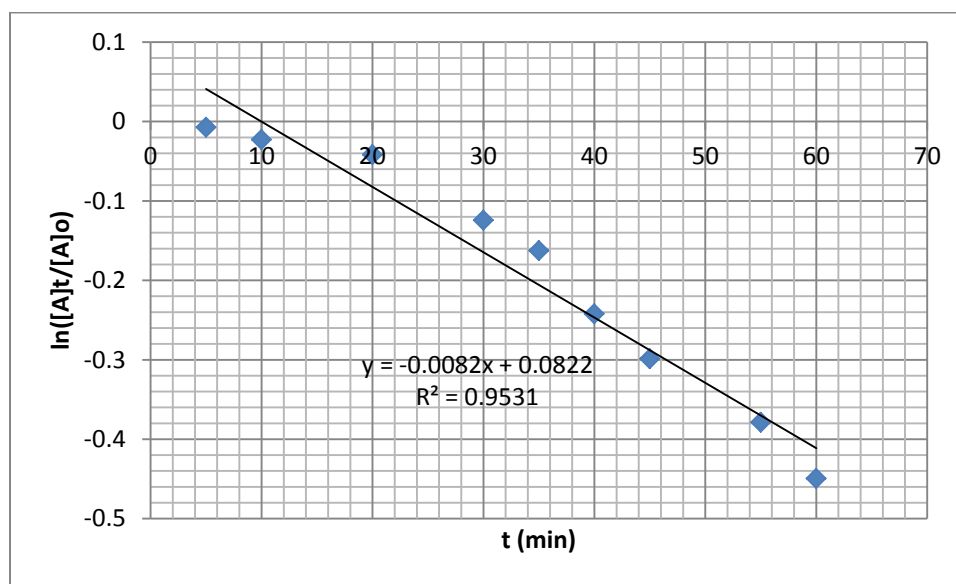
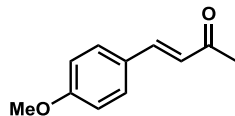


Figure 3.5.4.1.4. A plot of natural log of fraction of enone **210** versus time (second trial)

$$k_{\text{average}} = (0.0069 + 0.0082)/2 = 0.00755$$



Time (min)	Area of substrate	Area of product	[A] _t /[A] ₀	ln([A] _t /[A] ₀)
5	658898107	119065151	0.846952732	-0.166110392
10	380263509	126372571	0.750565394	-0.286928498
15	412072082	204490077	0.668338262	-0.402960853
20	348236932	237464118	0.594564296	-0.519926417
25	377053135	334754767	0.529711927	-0.635421955
30	434509856	483529699	0.473301889	-0.748021851
35	351000718	492228926	0.416257564	-0.876451067
40	385283841	651629525	0.371568015	-0.990023349
45	332400425	649013862	0.338695319	-1.08265434
50	302998039	721932450	0.295627891	-1.218653742
55	324742034	878725025	0.269838739	-1.30993076
60	197690085	718236833	0.21583609	-1.533236003

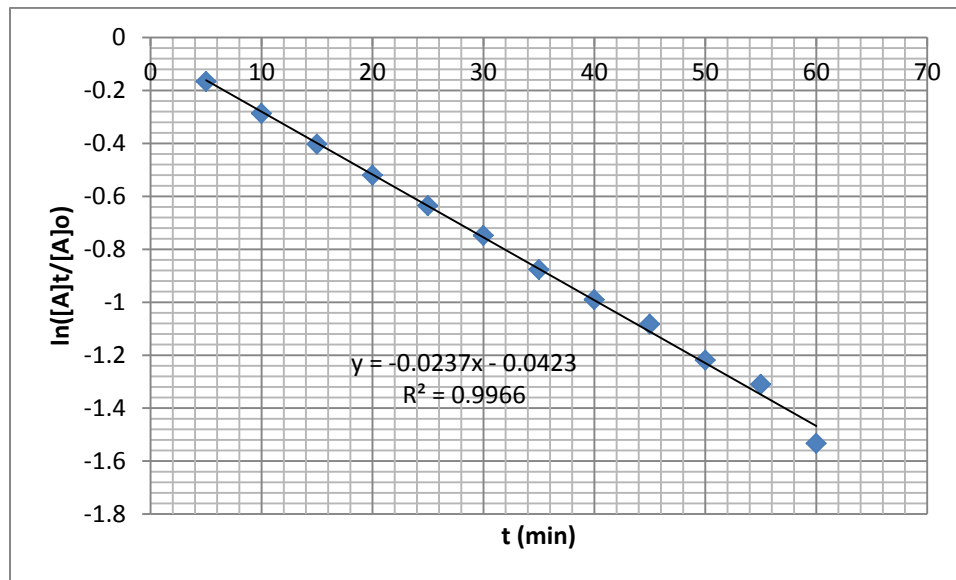


Figure 3.5.4.1.5. A plot of natural log of fraction of enone **211** versus time (first trial)

Time (min)	Area of substrate	Area of product	[A] _t /[A] _o	ln([A] _t /[A] _o)
5	94544996	27430637	0.7751138	-0.254745421
10	63432223	31329639	0.669385573	-0.401395042
15	118916356	75558412	0.611474472	-0.491882071
20	81381576	60381767	0.574066431	-0.555010155
30	54446711	78119871	0.410712187	-0.889862584
40	39498255	89869720	0.305317101	-1.186404368
45	35467489	99548588	0.262690858	-1.336777383
50	34295795	92213307	0.27166921	-1.303170091
60	44034578	187430220	0.190243087	-1.659452622

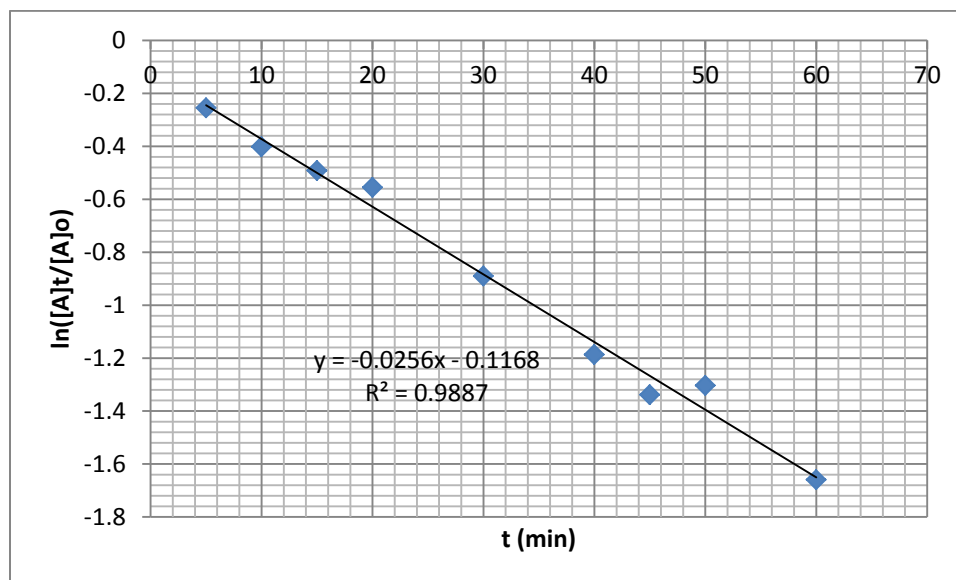
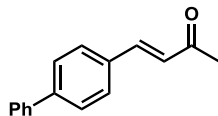


Figure 3.5.4.1.6. A plot of natural log of fraction of enone **211** versus time (second trial)

$$k_{\text{average}} = (0.0237 + 0.0256)/2 = 0.02465$$



Time (min)	Area of substrate	Area of product	[A] _t /[A] ₀	ln([A] _t /[A] ₀)
5	1239144484	382436965	0.764158029	-0.268980667
10	1045526656	382170339	0.732316913	-0.311541918
15	865582281	329228709	0.724451221	-0.322340847
20	850121377	377586994	0.692445696	-0.367525461
25	782071678	422297511	0.649362077	-0.431764819
30	909388110	623588440	0.593217235	-0.522194615
35	759253538	520637694	0.565611216	-0.569848334
40	799719453	735149061	0.521034503	-0.651939015
45	806744874	824615272	0.494522853	-0.704161916
50	611545946	720564310	0.459080578	-0.778529534
55	641948728	841007346	0.43288452	-0.837284285
60	611363656	959179276	0.389268987	-0.943484692

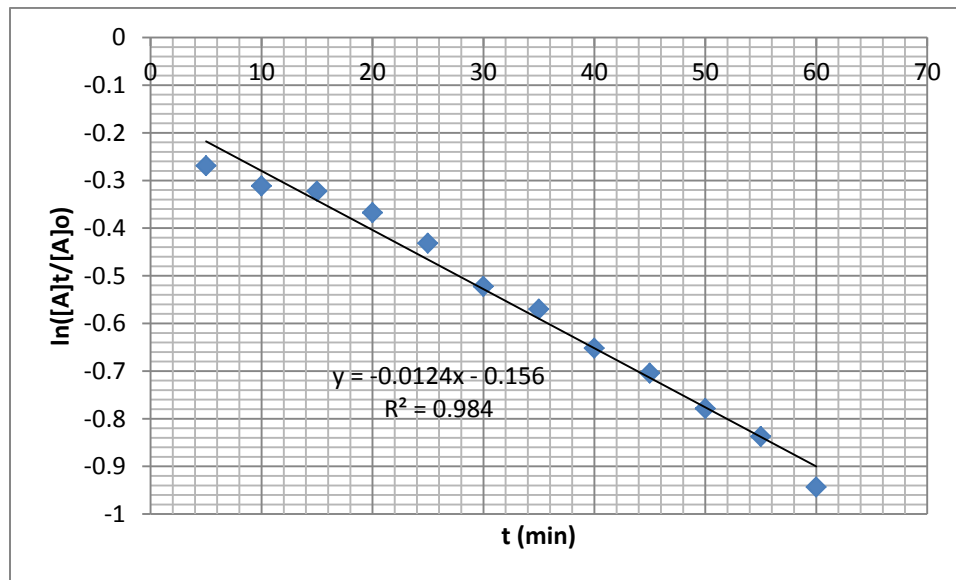


Figure 3.5.4.1.7. A plot of natural log of fraction of enone **212** versus time (first trial)

Time (min)	Area of substrate	Area of product	[A] _t /[A] _o	ln([A] _t /[A] _o)
5	208688291	36675662	0.850525469	-0.161900922
10	339591666	129482592	0.72396142	-0.323017175
15	256408207	105441296	0.708604557	-0.344457656
20	321292516	162724516	0.663804153	-0.409768124
30	222801420	135817238	0.621276711	-0.475978707
35	267244144	216847896	0.552052342	-0.594112415
45	145107346	133505304	0.520821096	-0.652348683
50	212927354	216090433	0.496313581	-0.700547333
60	206743381	279372177	0.425296778	-0.854968054

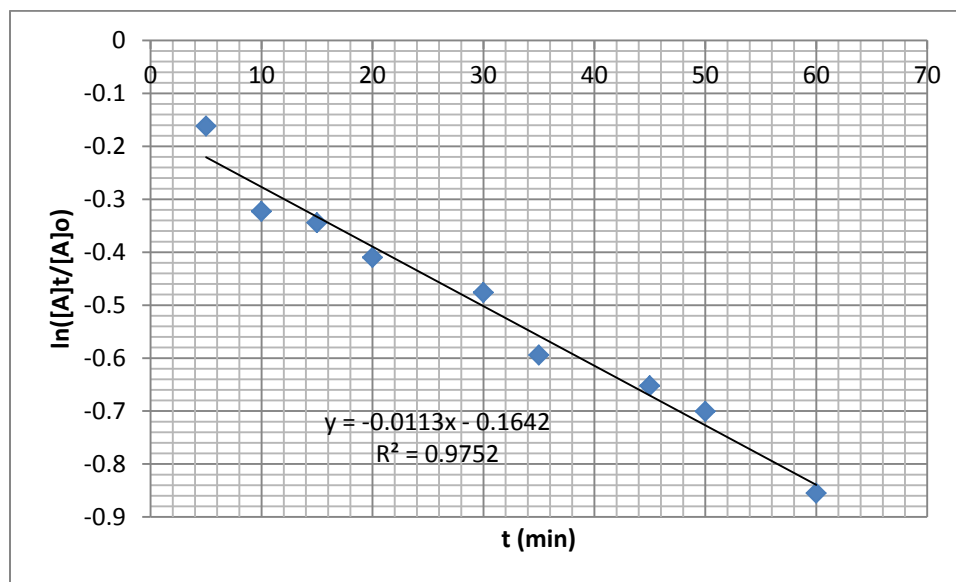
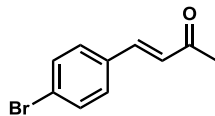


Figure 3.5.4.1.8. A plot of natural log of fraction of enone **212** versus time (second trial)

$$k_{\text{average}} = (0.0124 + 0.0113)/2 = 0.01185$$



Time (min)	Area of substrate	Area of product	[A] _t /[A] ₀	ln([A] _t /[A] ₀)
5	469619560	20593184	0.957991333	-0.042916548
10	497040596	39520682	0.926344513	-0.076509069
15	418761076	57287436	0.879660508	-0.128219232
20	375455839	71625541	0.839793057	-0.174599778
25	464905438	97725100	0.826306798	-0.190789149
30	435414872	143959841	0.751525502	-0.285650135
35	440334304	183198938	0.706192187	-0.347867859
40	377238280	170028166	0.689313739	-0.372058758
45	381438539	211717675	0.643065907	-0.441508061
50	341928264	251227950	0.604989002	-0.502545
55	303385688	217926541	0.581965415	-0.541344258
60	310182617	253648141	0.55013426	-0.597592921

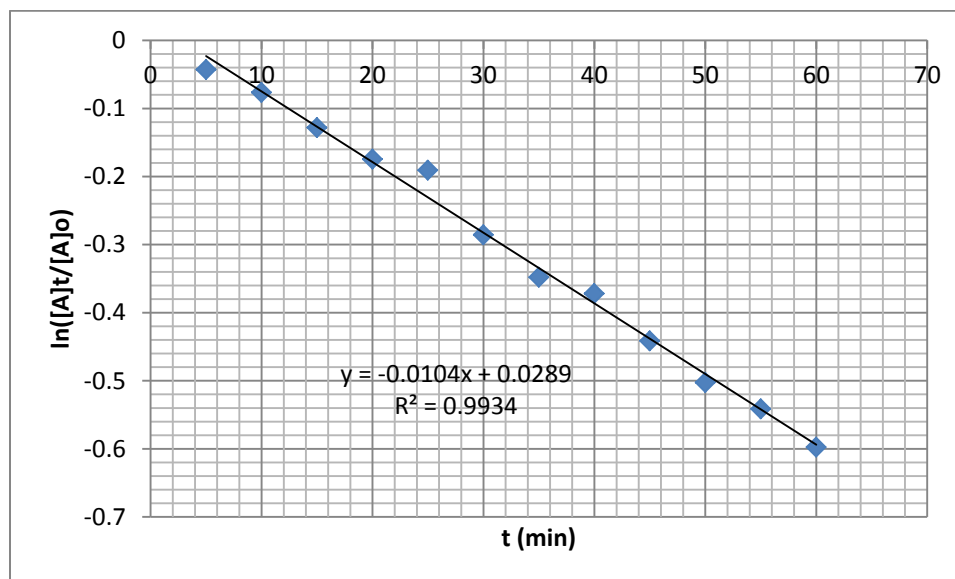


Figure 3.5.4.1.9. A plot of natural log of fraction of enone **213** versus time (first trial)

Time (min)	Area of substrate	Area of product	[A] _t /[A] _o	ln([A] _t /[A] _o)
5	235846511	7018990	0.971099272	-0.02932658
10	474554394	83045024	0.851066874	-0.161264571
15	252036974	55361541	0.819903029	-0.198569203
20	236738581	84253809	0.737520853	-0.304460916
25	199410062	85465492	0.69999008	-0.356689115
30	263650387	137813603	0.656722381	-0.420493905
35	184677037	123230950	0.599779951	-0.511192439
40	326865178	221973505	0.595557835	-0.518256775
45	255528412	226278235	0.530354684	-0.634209281
50	177390011	185289194	0.489109958	-0.715167952
55	178950123	195568755	0.477813358	-0.738535088
60	226056571	282672274	0.444355717	-0.811129873

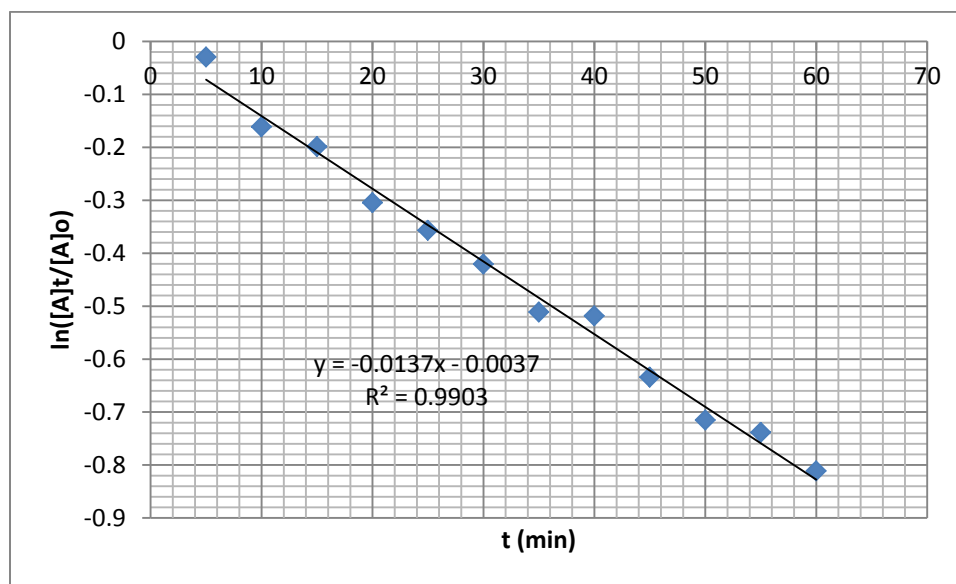
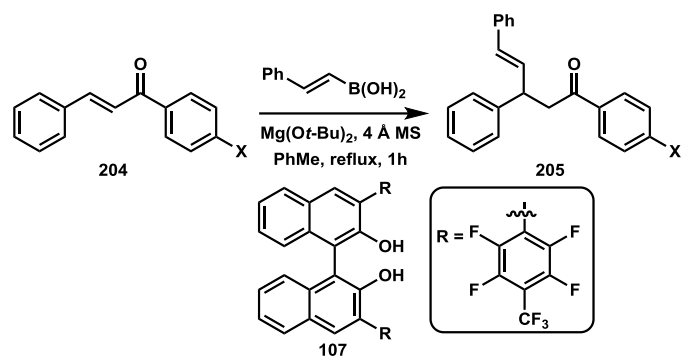
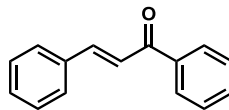


Figure 3.5.4.1.10. A plot of natural log of fraction of enone **213** versus time (second trial)

$$k_{\text{average}} = (0.0104 + 0.0137)/2 = 0.01205$$

3.5.4.2. Reactions of keto-aryl substrates





Time (min)	Area of substrate	Area of product	[A] _t /[A] _o	ln([A] _t /[A] _o)
5	777375089	1023501727	0.431664777	-0.840105972
10	385363837	766387689	0.334589387	-1.094851209
15	260364862	851412935	0.234187859	-1.451631668
20	211225775	1036202221	0.169329032	-1.775911523
25	142205784	1043336296	0.11995001	-2.120680205
30	125564553	1269601002	0.089999751	-2.40794837
35	74926046	1250170754	0.056543828	-2.872739216
40	45057907	1142647205	0.037936948	-3.271829754
45	27548549	1275513495	0.021141395	-3.856522308
50	23589807	1323044970	0.017517598	-4.044549303

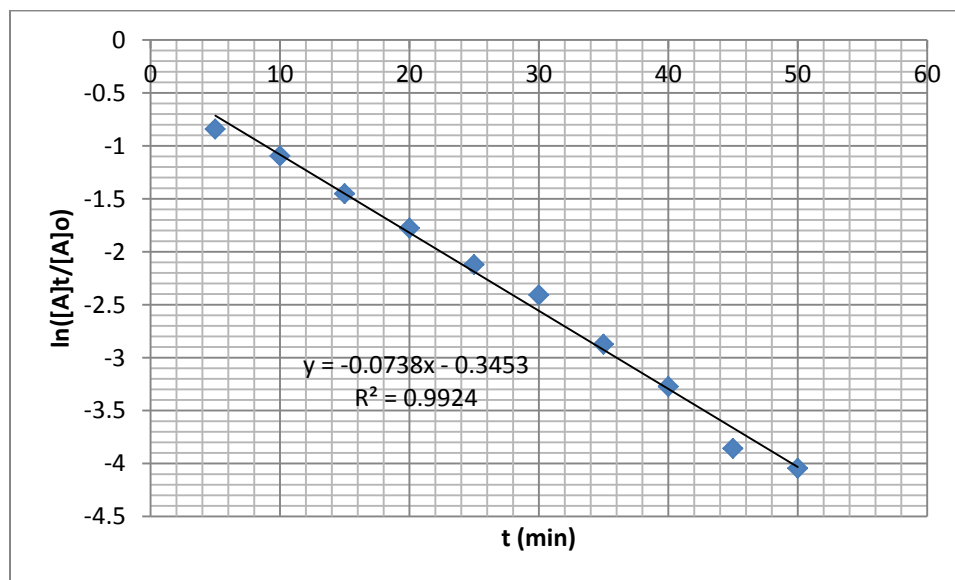


Figure 3.5.4.2.1. A plot of natural log of fraction of (*E*)-chalcone versus time (first trial)

Time (min)	Area of substrate	Area of product	[A] _t /[A] _o	ln([A] _t /[A] _o)
5	311370998	622119157	0.333555738	-1.097945297
15	55221187	217957164	0.202143349	-1.598778186
20	54786535	106936406	0.118656732	-2.131520564
25	26878274	391842533	0.064191399	-2.745886051
30	17663738	415813231	0.040748965	-3.200324829
35	22915488	377440102	0.057237838	-2.860540092
40	11199925	370141117	0.029369838	-3.527787051
45	6106179	373129963	0.016101259	-4.128857791
50	4623800	406271980	0.011252976	-4.487122692

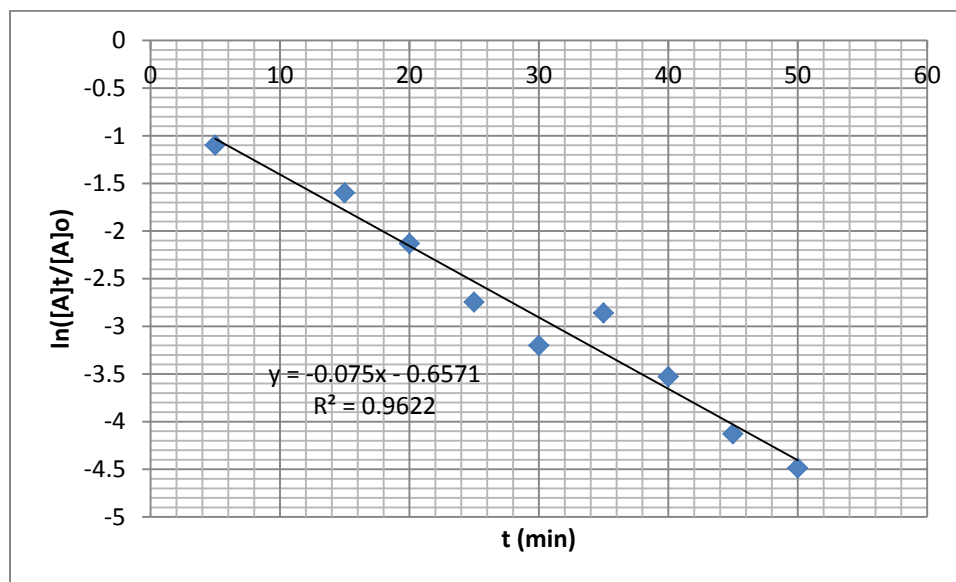
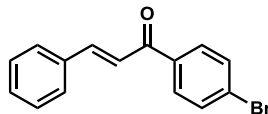


Figure 3.5.4.2.2. A plot of natural log of fraction of (*E*)-chalcone versus time (second trial)

$$k \text{ average} = (0.0738 + 0.075) / 2 = 0.0744$$



Time (min)	Area of substrate	Area of product	[A] _t /[A] ₀	ln([A] _t /[A] ₀)
5	371379007	552588784	0.401939343	-0.911454089
10	285150803	627108617	0.312576441	-1.16290623
15	259243713	942461945	0.215729793	-1.533728615
20	184290929	1104282204	0.143019379	-1.944775141
25	115651416	1104177735	0.09480952	-2.355885458
30	74914503	1085436220	0.064561948	-2.74013008
35	50142042	1198757334	0.040148985	-3.215158117
40	33783262	1256194673	0.026189023	-3.642414918
45	10250907	1159794323	0.008761112	-4.737432445
50	6736146	1372859590	0.004882696	-5.322057711
55	4386590	1336080771	0.003272433	-5.722221512

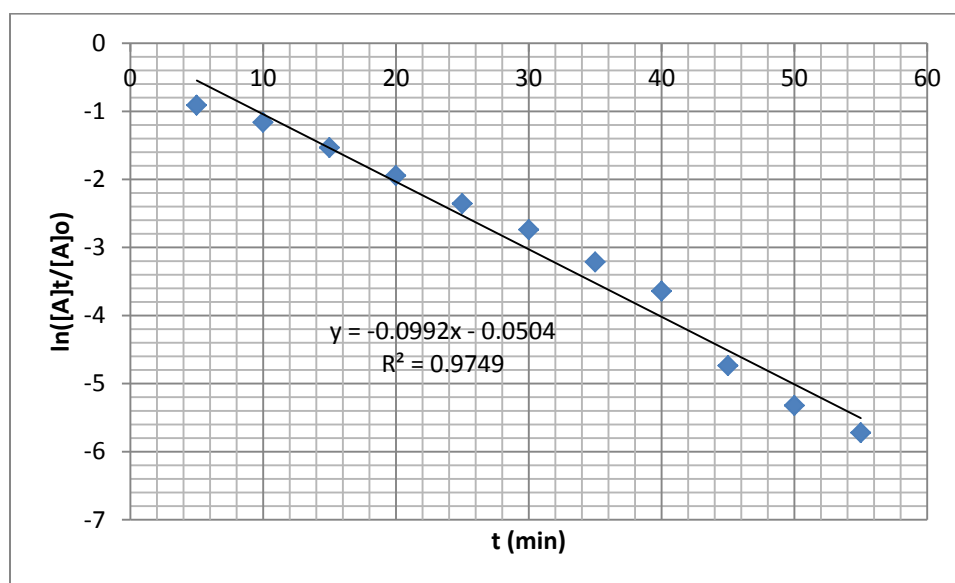


Figure 3.5.4.2.3. A plot of natural log of fraction of enone **214** versus time (first trial)

Time (min)	Area of substrate	Area of product	[A]t/[A]o	ln([A]t/[A]o)
5	155706523	321037921	0.326603749	-1.119007621
10	101991333	251449537	0.288566892	-1.242828359
15	65400878	299404962	0.179275852	-1.718829585
20	41585215	337891801	0.109585597	-2.211049332
25	40356892	321631437	0.111486721	-2.193849789
30	25337034	453070233	0.052961224	-2.938195254
35	14209117	452162259	0.030467387	-3.491098441
40	7193468	464814194	0.015240152	-4.183821729
45	6922994	535436506	0.012764586	-4.361080694
50	2552614	484458744	0.005241385	-5.251169531

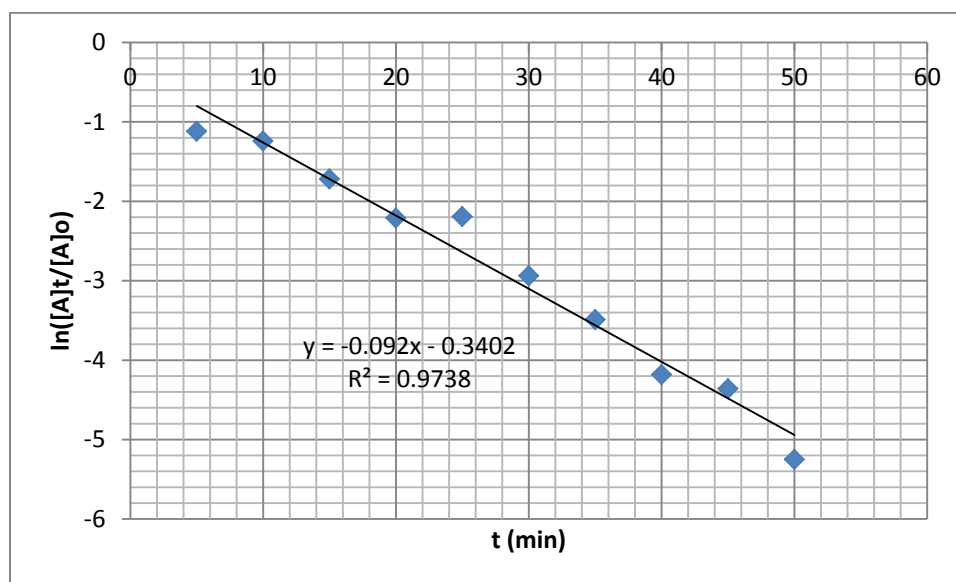
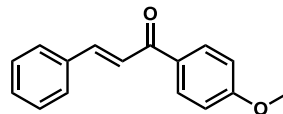


Figure 3.5.4.2.4. A plot of natural log of fraction of enone **214** versus time (second trial)

$$k \text{ average} = (0.092 + 0.0992) / 2 = 0.0956$$



Time (min)	Area of substrate	Area of product	[A] _t /[A] ₀	ln([A] _t /[A] ₀)
5	356834928	665353896	0.349089052	-1.052428227
10	303729930	787973005	0.278216647	-1.279355162
15	245524144	844967662	0.225149921	-1.490988784
20	189238584	720026915	0.208122473	-1.569628561
25	206176036	945778946	0.178979248	-1.720485413
30	151768003	921862598	0.14135961	-1.95644821
35	104889973	819113584	0.11351685	-2.175803997
40	120462123	1035628149	0.104197852	-2.261463769
45	103420240	1050067378	0.089658734	-2.411744659
50	113154460	1208152374	0.085638292	-2.457622763
55	72650503	1049952693	0.064716102	-2.737745236
60	70725956	1013734592	0.065217639	-2.730025303

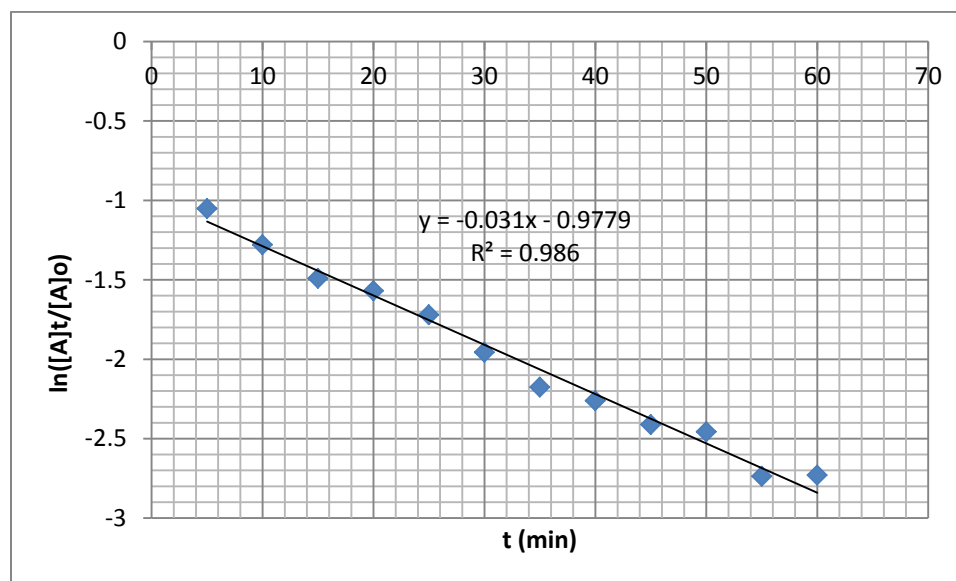


Figure 3.5.4.2.5. A plot of natural log of fraction of enone **215** versus time (first trial)

Time (min)	Area of substrate	Area of product	[A] _t /[A] ₀	ln([A] _t /[A] ₀)
5	97547205	204726403	0.322711618	-1.130996178
10	115895882	327793960	0.261209229	-1.34243355
15	112430924	375092482	0.230616463	-1.466999284
20	74019576	287756165	0.204600716	-1.586694924
25	82143167	421729641	0.163023615	-1.813860211
30	56317580	281424722	0.166747192	-1.791276436
35	43198491	371883025	0.104072307	-2.262669359
40	53144886	536650476	0.090107331	-2.406753754
45	29740399	417987945	0.066425097	-2.711680333
50	39833890	693185528	0.054342203	-2.91245414
55	22805791	360353041	0.059520463	-2.821435115
60	24768222	358390610	0.056621262	-2.871370707

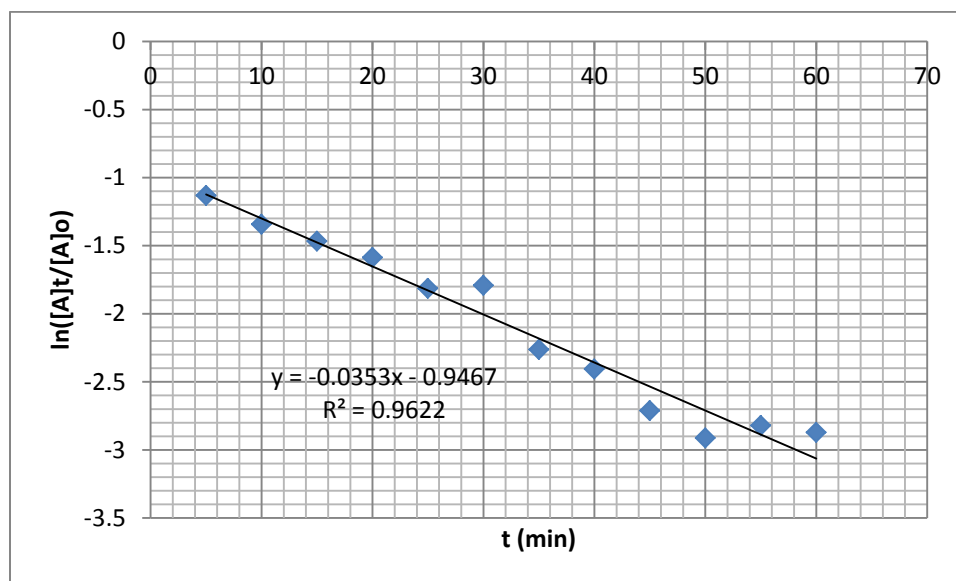
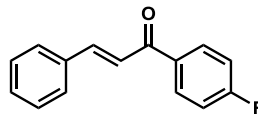


Figure 3.5.4.2.6. A plot of natural log of fraction of enone **215** versus time (second trial)

$$k \text{ average} = (0.0353 + 0.031) / 2 = 0.03315$$



Time (min)	Area of substrate	Area of product	[A] _t /[A] ₀	ln([A] _t /[A] ₀)
5	1461176838	1336473237	0.522287205	-0.649537642
10	531163805	1012166247	0.344167344	-1.066627276
15	296897789	901498814	0.247745853	-1.395351844
20	259599271	1138892968	0.185627967	-1.684010788
25	192904557	1226934932	0.135863637	-1.996103562
30	111904203	1069338752	0.094734282	-2.356679339
35	99171935	1388323051	0.066670433	-2.707993702
40	56959165	1344738995	0.040635828	-3.20310513
45	32817111	1312310954	0.024397016	-3.713294455
50	16339850	1319647890	0.012230539	-4.403819293
55	10877581	1449388764	0.007449039	-4.899670207

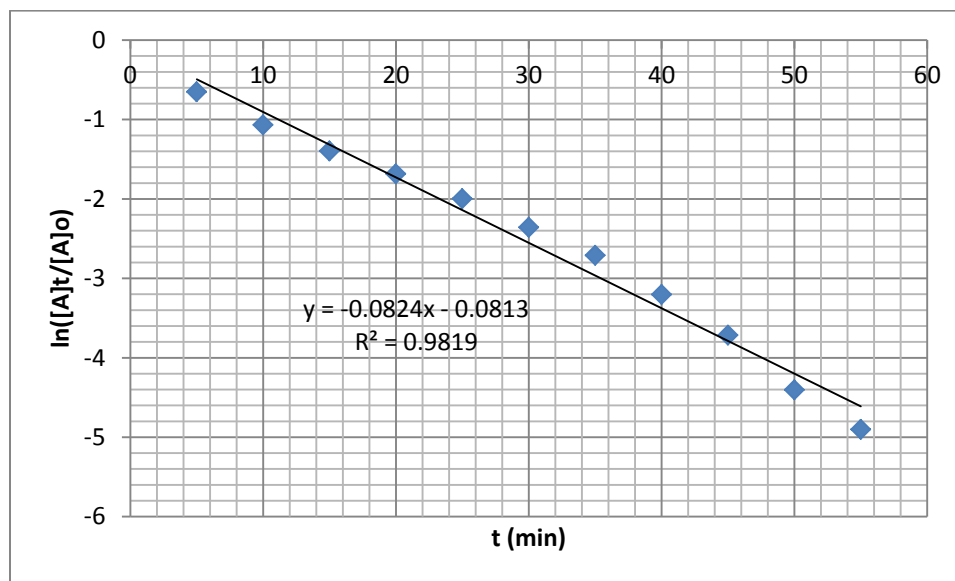


Figure 3.5.4.2.7. A plot of natural log of fraction of enone **216** versus time (first trial)

Time (min)	Area of substrate	Area of product	[A] _t /[A] ₀	ln([A] _t /[A] ₀)
5	173087870	220458448	0.439815752	-0.821399385
10	143108740	268282494	0.347865313	-1.055939907
15	111968191	309479691	0.26567506	-1.325481298
20	62491759	275109132	0.185105432	-1.686829713
25	58063978	390991897	0.129302345	-2.045601857
30	38759252	362321566	0.096637012	-2.336793465
35	34742140	385557392	0.082660429	-2.49301428
40	22365643	398242291	0.053174563	-2.934175127
45	21671048	542952674	0.038381398	-3.26018236

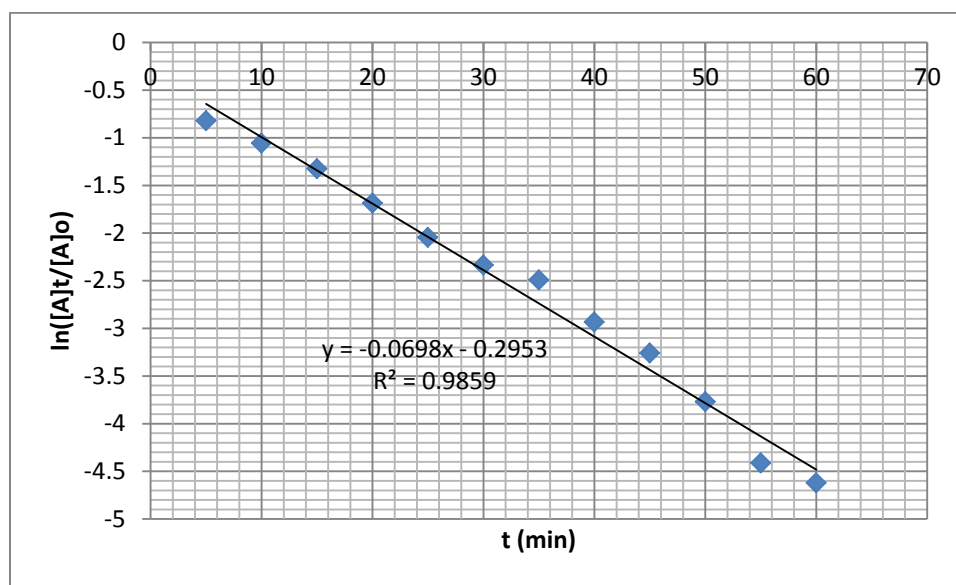
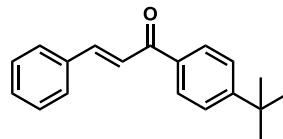


Figure 3.5.4.2.8. A plot of natural log of fraction of enone **216** versus time (second trial)

$$k \text{ average} = (0.0856 + 0.0824) / 2 = 0.0840$$



Time (min)	Area of substrate	Area of product	[A] _t /[A] ₀	ln([A] _t /[A] ₀)
5	146586694	181893150	0.446257804	-0.806858458
10	114749999	310504737	0.269838263	-1.309932524
15	101160966	327955469	0.235742464	-1.445015324
20	72666332	412205488	0.149867096	-1.898006402
25	50152677	301386562	0.142665942	-1.947249454
30	42654115	454282071	0.08583419	-2.45533787
35	40611133	601802676	0.063216469	-2.761190434
40	18081729	464731132	0.037450802	-3.284727146
45	25715660	610311002	0.040431732	-3.208140354
50	12669304	648314246	0.019167352	-3.954546886
55	16184776	703148340	0.022499696	-3.794253483
60	13814097	704299931	0.019236635	-3.950938745

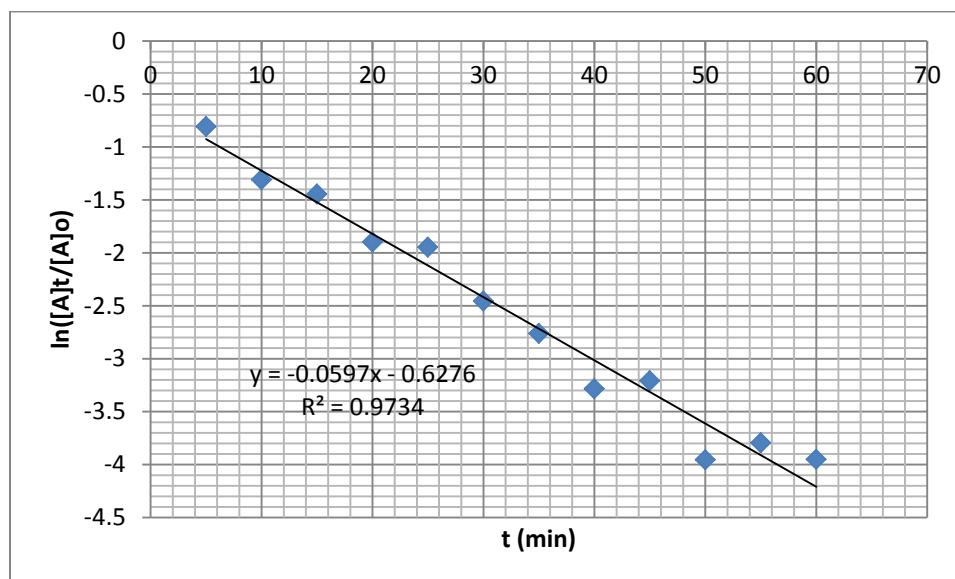


Figure 3.5.4.2.9. A plot of natural log of fraction of enone **217** versus time (first trial)

Time (min)	Area of substrate	Area of product	[A] _t /[A] _o	ln([A] _t /[A] _o)
5	205130397	496564549	0.292335577	-1.229852899
10	117648021	447989103	0.207992043	-1.570255457
15	91613637	482353558	0.159614761	-1.834992108
20	68098481	596282138	0.102499199	-2.277900292
25	29710473	413270082	0.067069474	-2.702026269
30	25100222	471835964	0.050509951	-2.985584905
35	25611612	316802197	0.039867779	-3.222186819
40	17657676	465155185	0.036572506	-3.308458516
45	11449012	624577650	0.018000836	-4.017337061
50	4517846	699937243	0.006413249	-5.049389329

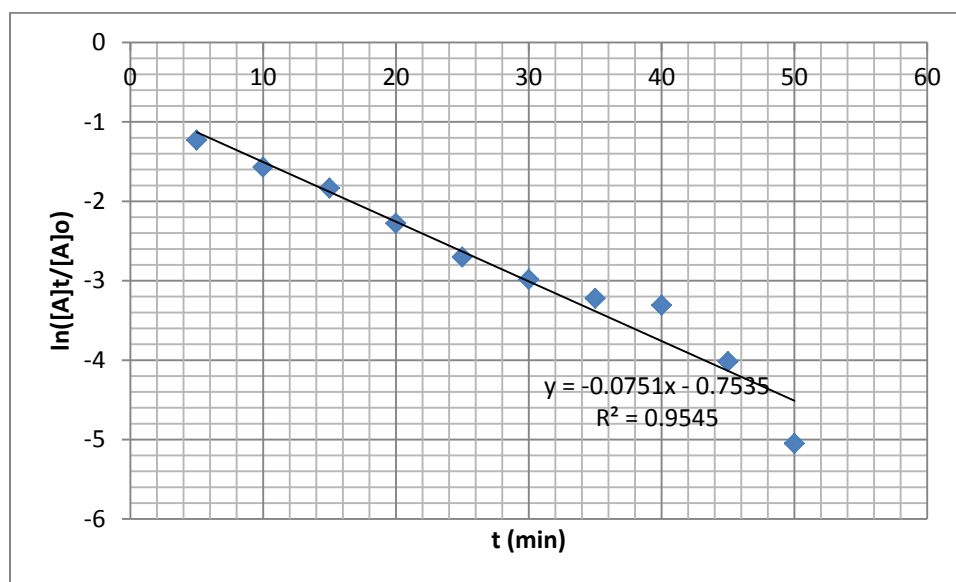
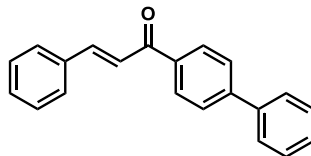


Figure 3.5.4.2.10. A plot of natural log of fraction of enone **217** versus time (second trial)

$$k \text{ average} = (0.0751 + 0.0597) / 2 = 0.0674$$



Time (min)	Area of substrate	Area of product	[A] _t /[A] _o	ln([A] _t /[A] _o)
10	313101344	807822165	0.279324451	-1.275381265
15	260805654	1249028701	0.172737925	-1.755979719
20	174112802	1353627232	0.113967559	-2.17184144
25	103662420	1365465302	0.070560523	-2.651284462
30	57278346	1277663391	0.042907001	-3.148720282
35	39866211	1411364734	0.027470618	-3.59463829
40	29146189	1647830745	0.017380197	-4.052423845
45	159750638	1695229590	0.008611986	-4.754600382
50	11920534	2170203532	0.005462812	-5.209791647

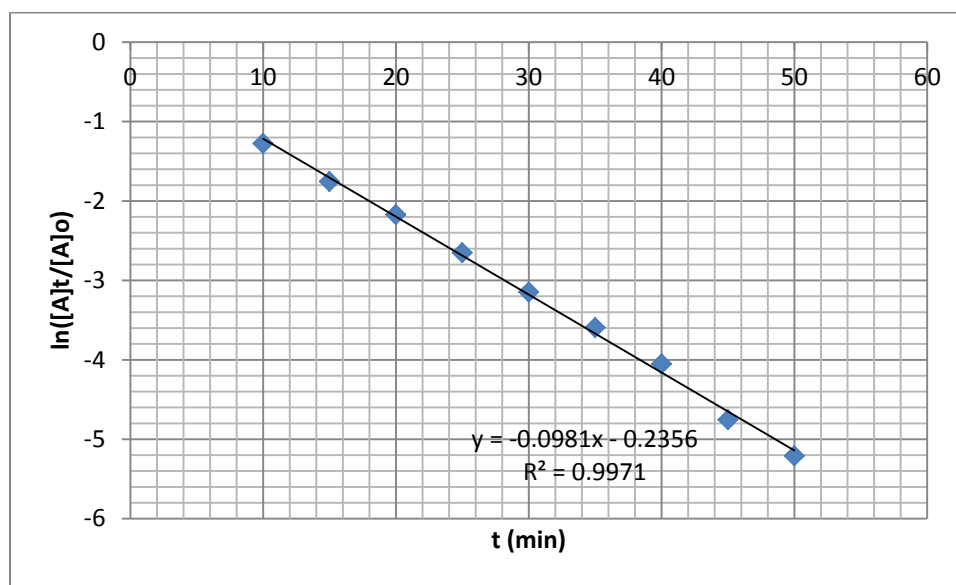


Figure 3.5.4.2.11. A plot of natural log of fraction of enone **218** versus time (first trial)

Time (min)	Area of substrate	Area of product	[A] _t /[A] _o	ln([A] _t /[A] _o)
5	415596084	1721154707	0.19449909	-1.637327794
10	207369496	1737045636	0.106648777	-2.238214303
15	124618612	1049110133	0.106173264	-2.242682955
20	75815826	1228359025	0.058133176	-2.845018758
25	47422935	1338351819	0.034221243	-3.374908685
30	20304830	1288599082	0.01551285	-4.166086553
35	16295911	2232216098	0.00724742	-4.927109707

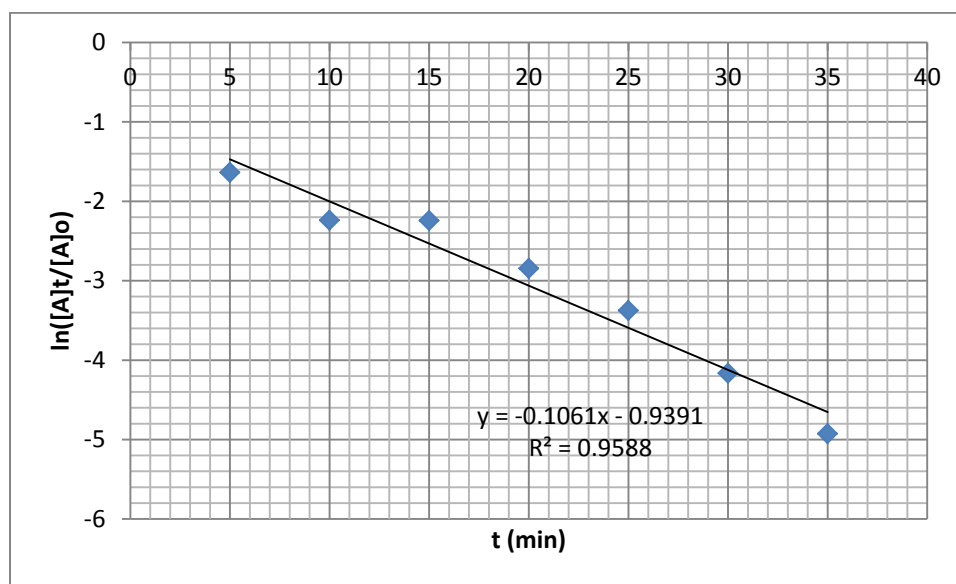
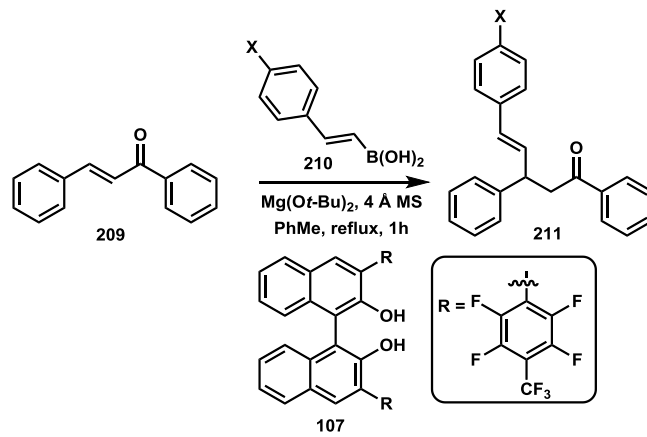
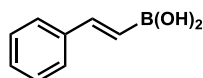


Figure 3.5.4.2.12. A plot of natural log of fraction of enone **218** versus time (second trial)

$$k \text{ average} = (0.0981 + 0.1061) / 2 = 0.1021$$

3.5.4.3. Reactions of boronic acids





Time (min)	Area of substrate	Area of product	[A] _t /[A] ₀	ln([A] _t /[A] ₀)
5	777375089	1023501727	0.431664777	-0.840105972
10	385363837	766387689	0.334589387	-1.094851209
15	260364862	851412935	0.234187859	-1.451631668
20	211225775	1036202221	0.169329032	-1.775911523
25	142205784	1043336296	0.11995001	-2.120680205
30	125564553	1269601002	0.089999751	-2.40794837
35	74926046	1250170754	0.056543828	-2.872739216
40	45057907	1142647205	0.037936948	-3.271829754
45	27548549	1275513495	0.021141395	-3.856522308
50	23589807	1323044970	0.017517598	-4.044549303

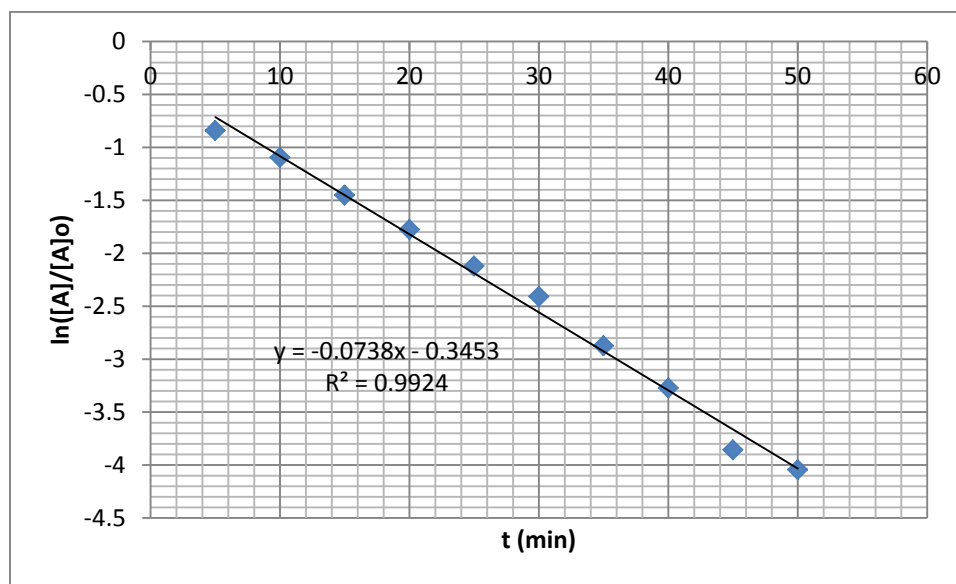


Figure 3.5.4.3.1. A plot of natural log of fraction of (*E*)-chalcone in the reaction with styrenylboronic acid versus time (first trial)

Time (min)	Area of substrate	Area of product	[A] _t /[A] _o	ln([A] _t /[A] _o)
5	311370998	622119157	0.333555738	-1.097945297
15	55221187	217957164	0.202143349	-1.598778186
20	54786535	106936406	0.118656732	-2.131520564
25	26878274	391842533	0.064191399	-2.745886051
30	17663738	415813231	0.040748965	-3.200324829
35	22915488	377440102	0.057237838	-2.860540092
40	11199925	370141117	0.029369838	-3.527787051
45	6106179	373129963	0.016101259	-4.128857791
50	4623800	406271980	0.011252976	-4.487122692

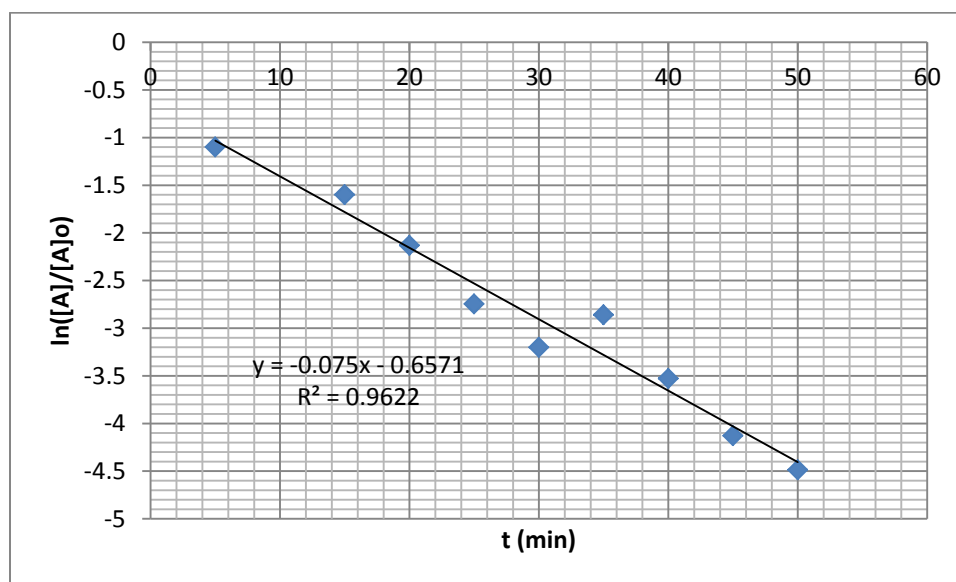
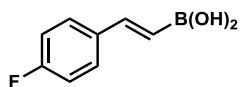


Figure 3.5.4.3.2. A plot of natural log of fraction of (*E*)-chalcone in the reaction with styrenylboronic acid versus time (second trial)

$$k \text{ average} = (0.0738 + 0.075) / 2 = 0.0744$$



Time	Area of substrate	Area of product	[A]/[A] ₀	ln([A]/[A] ₀)
5	283815268	356312073	0.443373138	-0.813343565
10	149094619	226668012	0.396778729	-0.924376512
15	154445619	318508396	0.326555255	-1.11915611
20	116727511	386854625	0.231794384	-1.461904576
25	83147191	420523256	0.165082529	-1.801309756
30	55527453	428949314	0.114613242	-2.166191931
35	40063180	443649525	0.082824329	-2.491033438
40	35243905	528550879	0.062511939	-2.772397721
45	20204102	561880323	0.034709917	-3.360729844
50	21197463	741761790	0.027783218	-3.583323122
55	9529268	554861019	0.016884181	-4.081378106

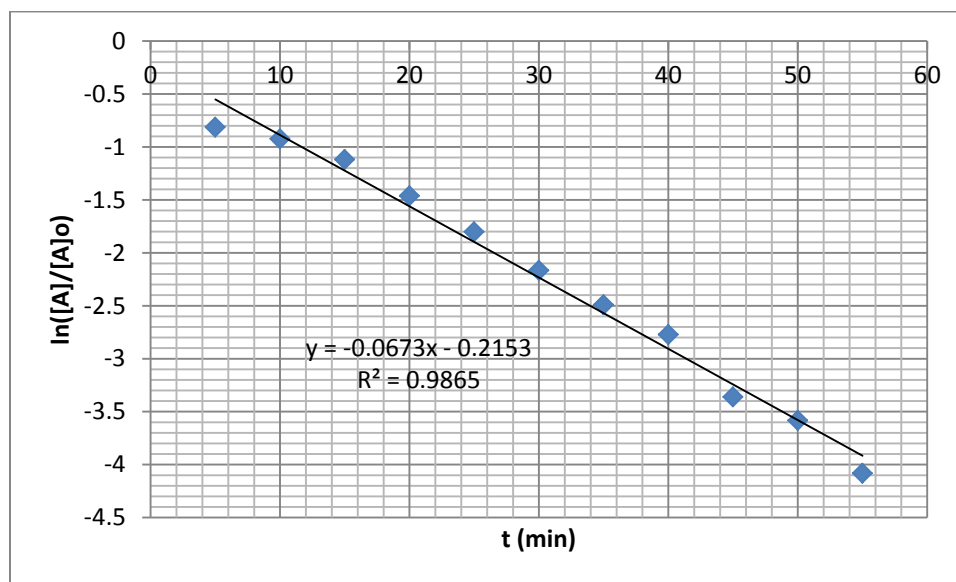


Figure 3.5.4.3.3. A plot of natural log of fraction of (*E*)-chalcone in the reaction with (*E*)-2-(4-fluorophenyl)vinylboronic acid versus time (first trial)

Time	Area of substrate	Area of product	[A]/[A] ₀	ln([A]/[A] ₀)
5	170469484	156438489	0.52146016	-0.651122402
10	144507413	254005725	0.362616434	-1.014409659
15	101393159	342917315	0.228203396	-1.47751796
20	84837164	372897700	0.185341277	-1.685556416
25	54716040	451467937	0.108095164	-2.224743292
30	65222637	567488681	0.103084353	-2.272207663
35	26344386	516724263	0.048510232	-3.02598054
40	16692027	486047359	0.033202147	-3.405140736
45	16488882	667169877	0.024118585	-3.724772567
50	12550324	682508306	0.018056497	-4.01424972

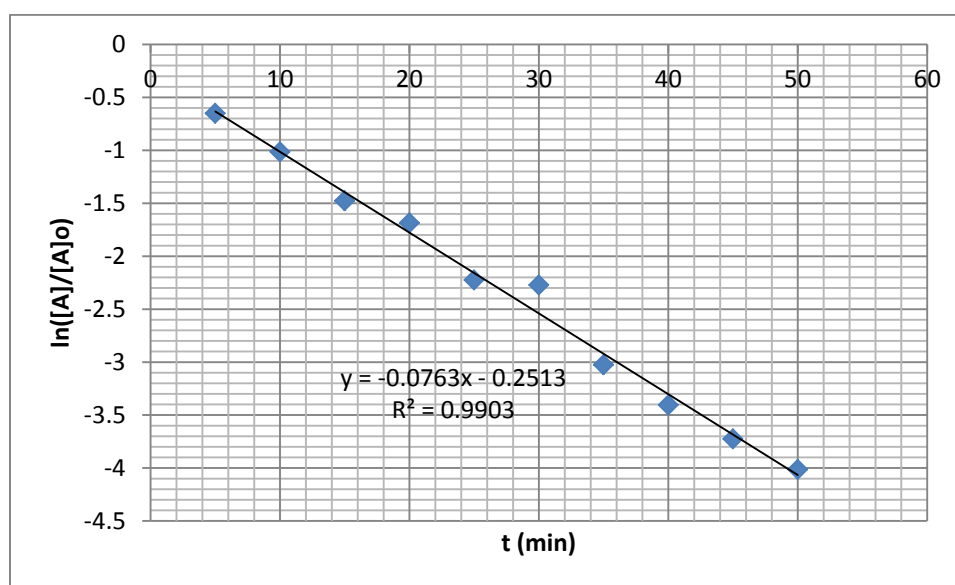
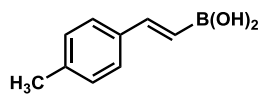


Figure 3.5.4.3.4. A plot of natural log of fraction of (*E*)-chalcone in the reaction with (*E*)-2-(4-fluorophenyl)vinylboronic acid versus time (second trial)

$$k \text{ average} = (0.0763 + 0.0673) / 2 = 0.0718$$



Time	Area of substrate	Area of product	[A]/[A] _o	ln([A]/[A] _o)
5	131014926	172710011	0.431360452	-0.840811224
10	116058175	243882886	0.322436609	-1.131848725
15	85721503	322205066	0.210139544	-1.559983476
20	53937033	331470416	0.139948081	-1.966483773
25	34600889	486318856	0.066422687	-2.711716614
30	25057631	497778263	0.047926379	-3.038089225
35	11223036	464491638	0.023591948	-3.746849798
40	10109635	673682483	0.014784662	-4.214165021
45	2955433	586610401	0.005012897	-5.29574122

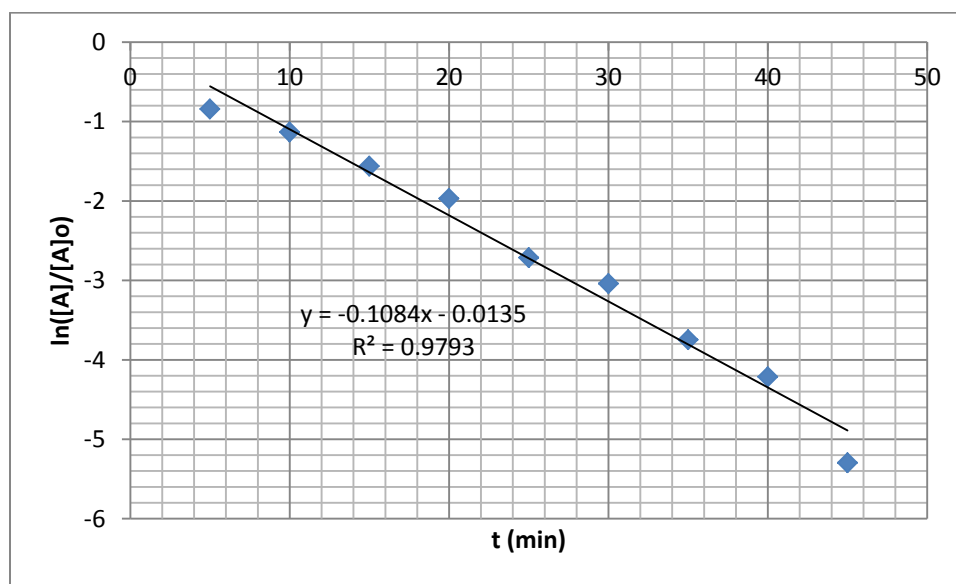


Figure 3.5.4.3.5. A plot of natural log of fraction of (*E*)-chalcone in the reaction with (*E*)-2-(4-methylphenyl)vinylboronic acid versus time (first trial)

Time	Area of substrate	Area of product	[A]/[A] ₀	ln([A]/[A] ₀)
5	139967719	163505571	0.461219236	-0.773881783
10	109147837	378042084	0.224035499	-1.495950762
15	63780693	442296645	0.126029538	-2.071238973
20	22861130	670873535	0.032953709	-3.412651472
25	9871090	579259630	0.016755348	-4.089037811
30	6128790	520084974	0.011646959	-4.452710185
35	3551929	510240339	0.006913162	-4.9743282

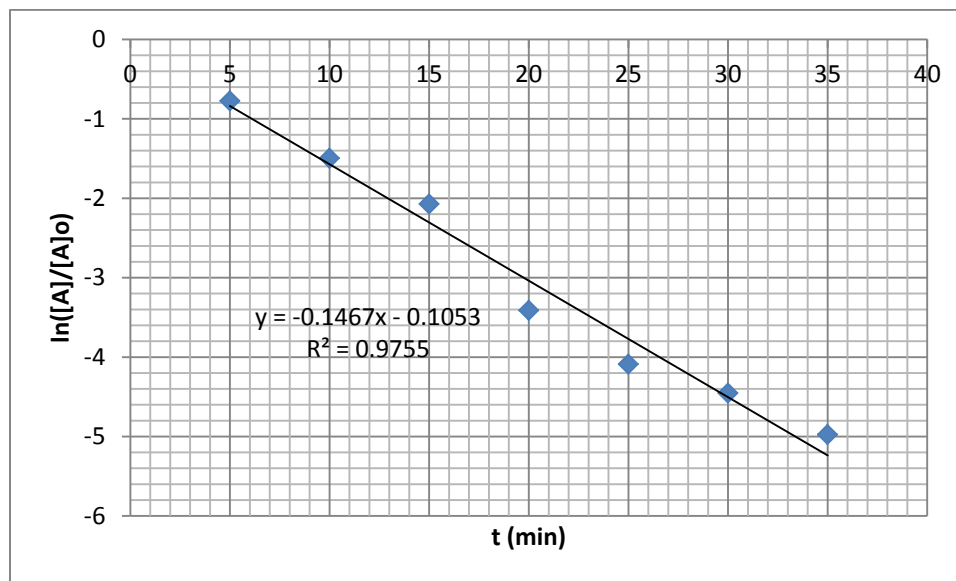
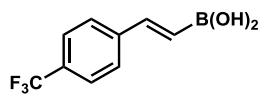


Figure 3.5.4.3.6. A plot of natural log of fraction of (*E*)-chalcone in the reaction with (*E*)-2-(4-methylphenyl)vinylboronic acid versus time (second trial)

$$k \text{ average} = (0.1084 + 0.1467) / 2 = 0.1276$$



Time	Area of substrate	Area of product	[A]/[A] ₀	ln([A]/[A] ₀)
5	229609679	27513609	0.892994488	-0.11317487
10	346932410	107938786	0.762704724	-0.270884316
15	294625245	119463465	0.711502724	-0.340376033
20	235610681	93135458	0.716694899	-0.333105053
30	259269473	147767763	0.636967457	-0.451036713
35	224412354	151267770	0.597349553	-0.515252822
40	226910101	182370302	0.554412328	-0.589846595
45	237081959	233925887	0.503350339	-0.686468852
50	179169727	206295918	0.464813737	-0.766118519
55	185686689	250575888	0.425630569	-0.854183517
60	173877937	289277424	0.375420327	-0.979709009

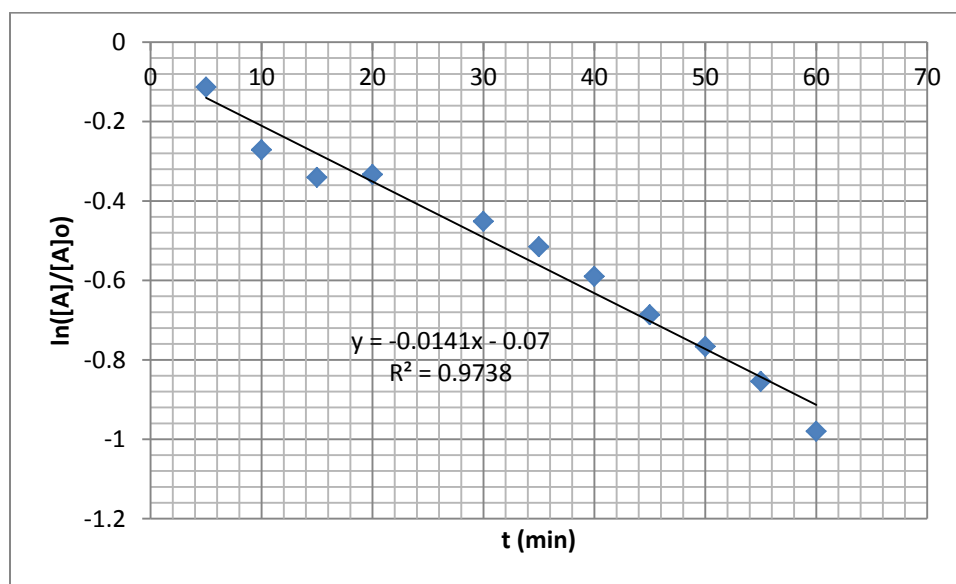


Figure 3.5.4.3.7. A plot of natural log of fraction of (*E*)-chalcone in the reaction with (*E*)-2-(4-trifluoromethylphenyl)vinylboronic acid versus time (first trial)

Time	Area of substrate	Area of product	[A]/[A] ₀	ln([A]/[A] ₀)
5	283651416	95906882	0.74731976	-0.291262127
10	261855037	92979099	0.737964616	-0.303859401
15	225163767	89197775	0.716257356	-0.33371574
20	227261278	110114168	0.673615347	-0.395096033
25	211893796	149895282	0.585683231	-0.534976198
30	240478319	189564060	0.559196793	-0.581253824
35	264760164	215238889	0.551584763	-0.594959756
40	212567604	212909721	0.499597961	-0.693951582
45	195755447	219819151	0.471047672	-0.752795975
50	225000040	312328268	0.418738482	-0.870508702
55	164693261	262442292	0.385576101	-0.953016698
60	111773355	213544559	0.343581925	-1.068329696

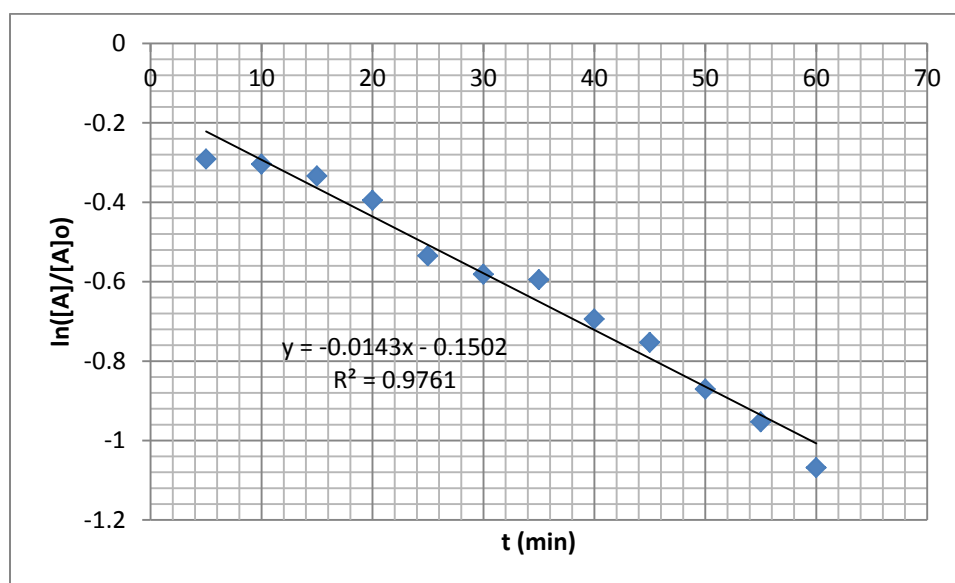
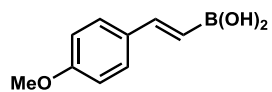


Figure 3.5.4.3.8. A plot of natural log of fraction of (*E*)-chalcone in the reaction with (*E*)-2-(4-trifluoromethylphenyl)vinylboronic acid versus time (second trial)

$$k \text{ average} = (0.0141 + 0.0143) / 2 = 0.0142$$



Time	Area of substrate	Area of product	[A]/[A] ₀	ln([A]/[A] ₀)
5	143414437	179541038	0.444068759	-0.811775866
10	71685646	378313708	0.159301664	-1.836955615
15	17225879	467883413	0.035509274	-3.337961364
20	3368420	516133654	0.006483939	-5.038427011

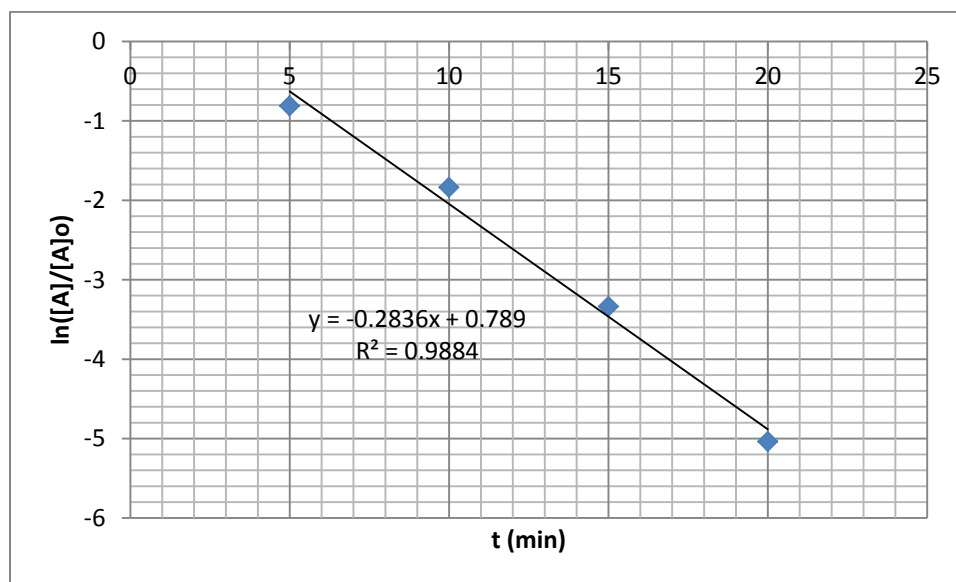


Figure 3.5.4.3.9. A plot of natural log of fraction of (*E*)-chalcone in the reaction with (*E*)-2-(4-methoxyphenyl)vinylboronic acid versus time (first trial)

Time	Area of substrate	Area of product	[A]/[A] ₀	ln([A]/[A] ₀)
5	83974687	223082403	0.273482325	-1.296518283
10	27928324	318808374	0.080546202	-2.518924326
15	4687671	411990017	0.011250113	-4.487377122

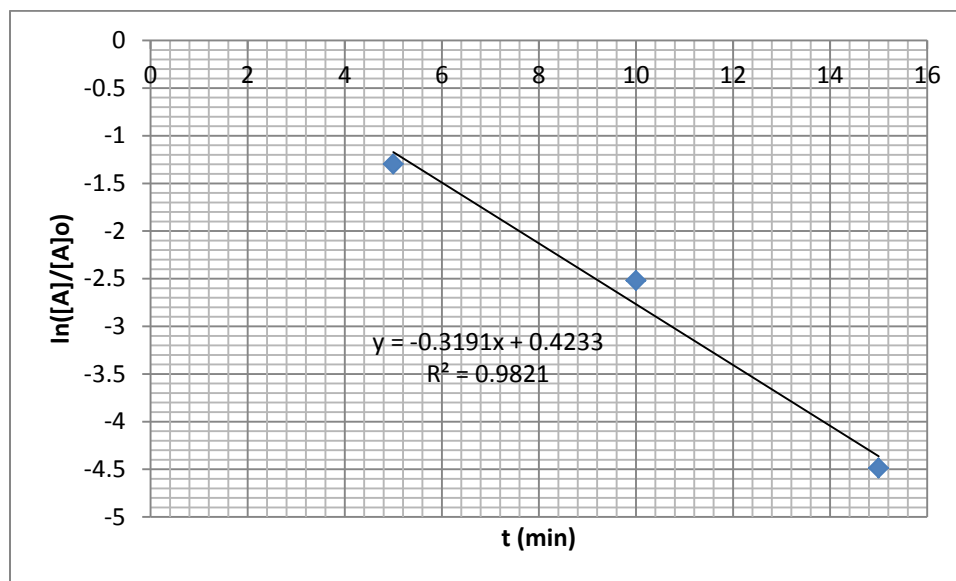


Figure 3.5.4.3.10. A plot of natural log of fraction of (*E*)-chalcone in the reaction with (*E*)-2-(4-methoxyphenyl)vinyboronic acid versus time (second trial)

$$k \text{ average} = (0.2836 + 0.3191) / 2 = 0.3014$$

3.6. References

1. Previously published in Nguyen, T. S.; Yang, M. S.; May, J. A. *Tetrahedron Lett* **2015**, In Press. doi: 10.1016/j.tetlet.2015.01.166.
2. Suzuki, A.; Arase, A.; Matsumoto, H.; Itoh, M.; Brown, H. C.; Rogic, M. M.; Rathke, M. W. *J. Am. Chem. Soc.* **1967**, *89*, 5708—5709.
3. Brown, H. C.; Rogic, M. M.; Rathke, M. W.; Kabalka, G. W. *J. Am. Chem. Soc.* **1967**, *89*, 5709—5710.
4. Brown, H. C.; Kabalka, G. W.; Rathke, M. W.; Rogic, M. M. *J. Am. Chem. Soc.* **1968**, *90*, 4165—4166.
5. Kabalka, G. W.; Brown, H. C.; Suzuki, A.; Honma, S.; Arase, A.; Itoh, M. *J. Am. Chem. Soc.* **1970**, *92*, 710—712.
6. Brown, H. C.; Kabalka, G. W. *J. Am. Chem. Soc.* **1970**, *92*, 712—714.
7. Brown, H. C.; Kabalka, G. W. *J. Am. Chem. Soc.* **1970**, *92*, 714—716.
8. Jacob, P., III; Brown, H. C. *J. Am. Chem. Soc.* **1976**, *98*, 7832—7833.
9. Satoh, Y.; Serizawa, H.; Hara, S.; Suzuki, A. *J. Am. Chem. Soc.* **1985**, *107*, 5225—5228.
10. Hara, S.; Hyuga, S.; Aoyama, M.; Sato, M.; Suzuki, A. *Tetrahedron Lett.* **1990**, *31*, 247—250.
11. Brown, H. C.; Bhat, N. G.; Srenik, M. *Tetrahedron Lett.* **1988**, *29*, 2631—2634.
12. Fujishima, H.; Takada, E.; Hara, S.; Suzuki, A. *Chem. Lett.* **1992**, 695—698.
13. (a) Hara, S.; Ishimura, S.; Suzuki, A. *Synlett.* **1996**, 993—994; (b) Hara, S.; Shudoh, H.; Ishimura, S.; Suzuki, A. *Bull. Chem. Soc. Jpn.* **1998**, *71*, 2403—2408.

14. Chong, J. M.; Shen, L.; Taylor, N. J. *J. Am. Chem. Soc.* **2000**, *122*, 1822—1823.
15. Wu, T. R.; Chong, J. M. *J. Am. Chem. Soc.* **2005**, *127*, 3244—3245.
16. Wu, T. R.; Chong, J. M. *J. Am. Chem. Soc.* **2007**, *129*, 4908—4909.
17. Pellegrinet, S. C.; Goodman, J. M. *J. Am. Chem. Soc.* **2006**, *128*, 3116—3117.
18. Paton, R. S.; Goodman, J. M.; Pellegrinet, S. C. *J. Org. Chem.* **2008**, *73*, 5078—5089.
19. (a) Lou, S.; Moquist, P. N.; Schaus, S. E. *J. Am. Chem. Soc.* **2006**, *128*, 12660—12661; (b) Barnett, D. S.; Moquist, P. N.; Schaus, S. E. *Angew. Chem., Int. Ed.* **2009**, *48*, 8679—8682.
20. (a) Lou, S.; Moquist, P. N.; Schaus, S. E. *J. Am. Chem. Soc.* **2007**, *129*, 15398—15404; (b) Bishop, J. A.; Lou, S.; Schaus, S. E. *Angew. Chem., Int. Ed.* **2009**, *48*, 4337—4340.
21. See experimental section for detail procedure
22. Gottumukkala, A. L.; Teichert, J. F.; Heijnen, D.; Eisink, N.; van Dijk, S.; Ferrer, C.; van den Hoogenband, A.; Minnaard, A. J. *J. Org. Chem.* **2011**, *76*, 3498—3501.
23. Bigi, M. A.; White, C. M. *J. Am. Chem. Soc.* **2013**, *135*, 7831—7834.
24. Chen, X.; Zhou, H.; Zhang, K.; Li, J.; Huang, H. *Org. Lett.* **2014**, *16*, 3912—3915.
25. Kerr, W. J.; Mudd, R. J.; Paterson, L. C.; Brown, J. A. *Chem. Eur. J.* **2014**, *20*, 14604—14607.
26. Yao, M.-L.; Kabalka, G. W.; Blevins, D. W.; Reddy, M. S.; Yong, Li. *Tetrahedron* **2012**, *68*, 3738—3743.
27. Kobayashi, S.; Xu, P.; Endo, T.; Ueno, M.; Kitanosono, T. *Angew. Chem., Int. Ed.* **2012**, *51*, 12763—12766.

28. Wu, X.-F.; Neumann, H.; Spannenberg, A.; Schulz, T.; Jiao, H.; Beller, M. *J. Am. Chem. Soc.* **2010**, *132*, 14596—14602.
29. Schmink, J. R.; Holcomb, J. L.; Leadbeater, N. E. *Org. Lett.* **2009**, *11*, 365—368.

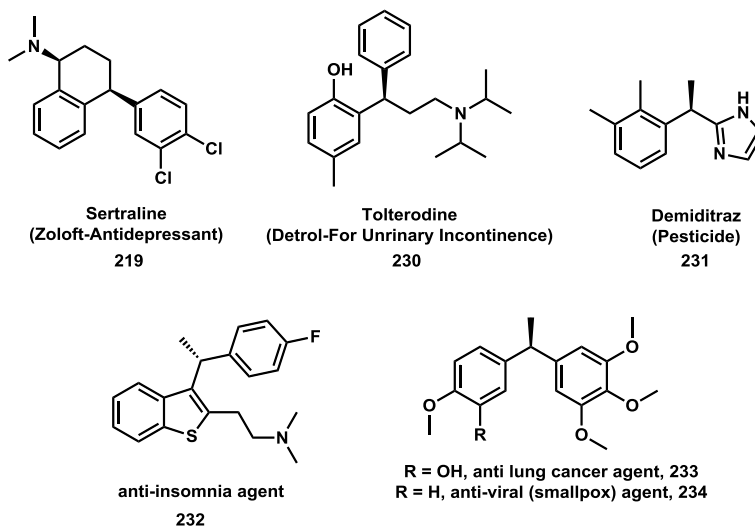
Chapter 4

Enantioselective synthesis of diarylalkane compounds via BINOL-catalyzed conjugate addition

4.1. Background

4.1.1. Introduction

Like chiral heterocycles, chiral diarylalkane structures have been found in many biologically active natural products. Many of them are also in important pharmaceuticals such as Detrol and Zoloft (Scheme 4.1.1). Some others possess interesting activities that may be applied in the potential treatment of a number of diseases.



Scheme 4.1.1. Important diarylalkanes

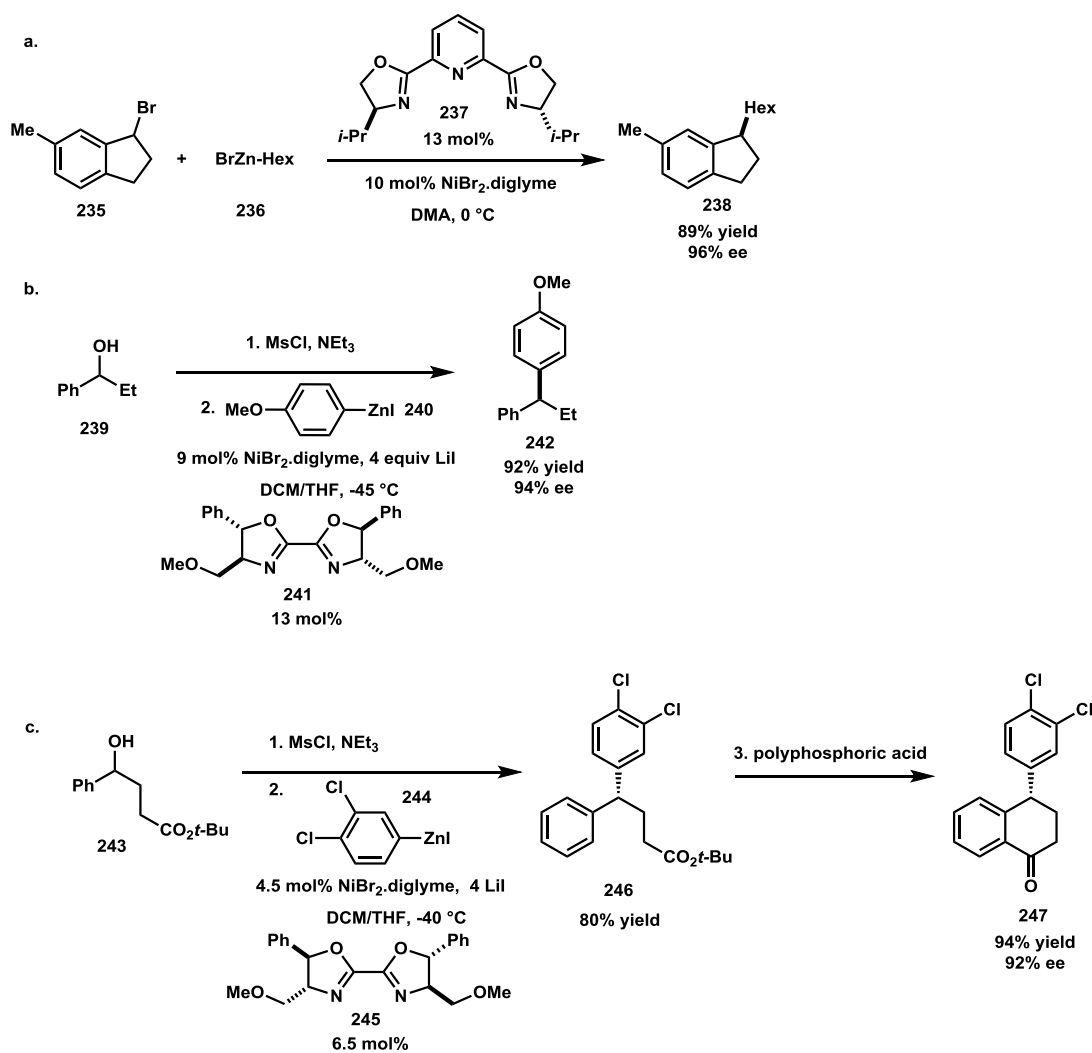
Such important biological activity of bis-aryl compounds has made them a hot topic of many synthetic efforts. In light of the BINOL-catalyzed conjugate addition method that we had established so far, we opted to employ it for the synthesis of different chiral

diarylmethine stereocenters. Therefore, this chapter will discuss the success in using the BINOL chemistry for such goal. It is noteworthy that the method will provide a complementary tool to a wide range of many other methods in the same theme. The next section will cover recent advances for access to chiral diarylalkane compounds, and the literature scope will be limited to carbon-carbon bond formations.

4.1.2. Method towards chiral diarylalkanes

4.1.2.1. Organometallic transformations

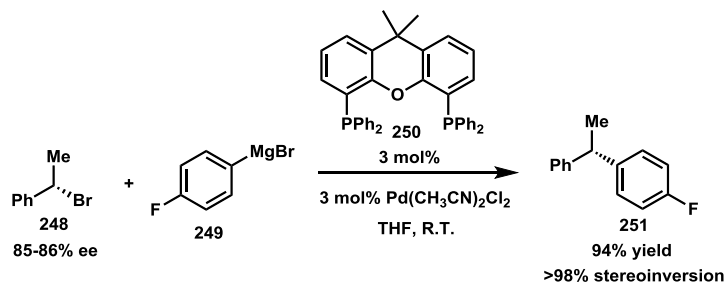
A direct entry to enantioenriched chiral diaryl compounds can be achieved efficiently via the metal-catalyzed coupling of a benzylic electrophile and an organometallic reagent. One prominent method came from the Fu group. In 2005, they reported the nickel catalyzed enantioselective Negishi reaction on racemic secondary benzylic halides using organozinc reagents to obtain alkylated products in good yield and with impressive ee's (Scheme 4.1.2.1.1a).¹ This work established a strong base for their extension to the use of arylzinc reagents in the synthesis of an array of chiral bis-aryl compounds (Scheme 4.1.2.1.1b).² The great utility of the method was also demonstrated by the preparation of (*S*)-sertraline tetralone, a precursor of Zoloft, a medicine for the treatment of mental disorders (Scheme 4.1.2.1.1c).



Scheme 4.1.2.1.1. Nickel catalyzed coupling reactions between (a) alkylzinc and (b) arylzinc reagents to benzylic electrophiles and (c) application to the synthesis of (*S*)-setraline tetralone **247**.

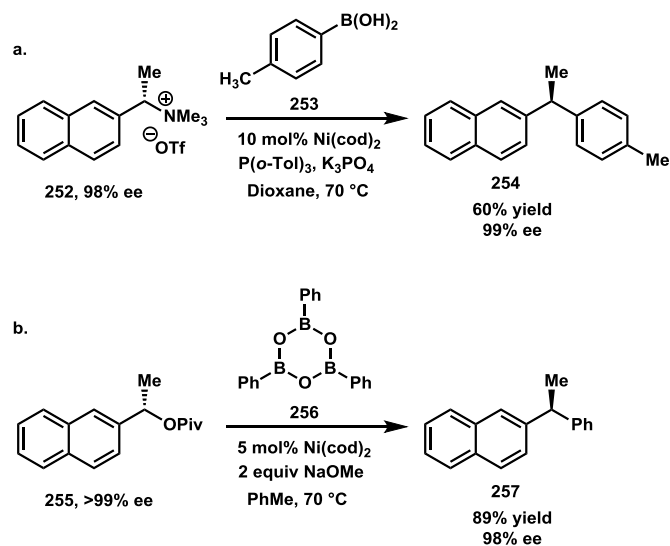
In 2009, Adrio and Carretero performed the arylation and vinylation of secondary benzyl bromides by means of Kumada-Corriu coupling to generate various bis-aryl and vinyl-aryl products.³ Although the strategy was primarily non-asymmetric, the reaction executed on enantioenriched substrates showed a high degree of chirality transfer with

over 98% stereoinversion observed, giving highly optically pure diaryl products (Scheme 4.1.2.1.2).



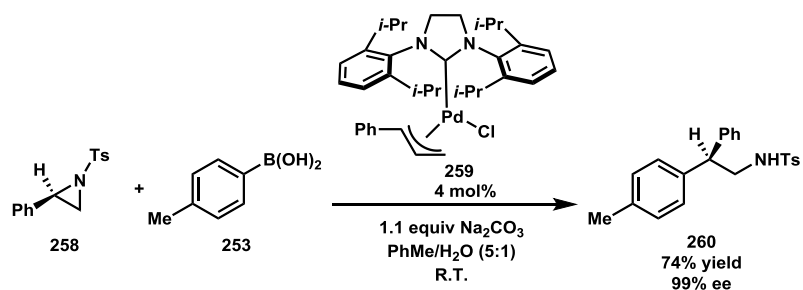
Scheme 4.1.2.1.2. Palladium catalyzed coupling between an aryl-Grignard reagent and enantioenriched benzylbromide.

In a similar communication on the use of enantioenriched benzylic starting materials for coupling reactions, Watson *et al.* demonstrated a nickel catalyzed replacement of ammonium⁴ and pivalate groups by a number of aryl entities (Scheme 4.1.2.1.3).⁵ This method allows the utilization of arylboronic acids and arylboroxines as milder nucleophiles than Grignard and organozinc reagents. Because of this fact, the transformation expresses a great functional group tolerance, including ether, amino, fluoro, chloro and acetal groups. The reactions were also proven to occur with overall inversion of configuration.



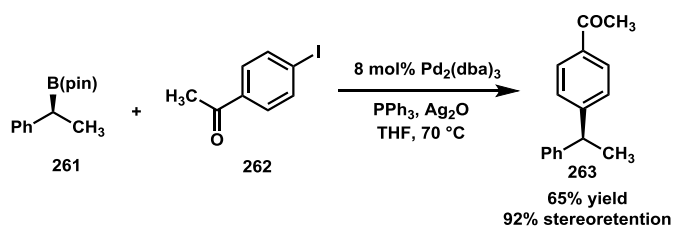
Scheme 4.1.2.1.3. Nickel catalyzed coupling reaction of (a) enantioenriched benzylammonium and arylboronic acid; (b) enantioenriched benzylpivalate and arylboroxine

The utility of boronate nucleophiles was later re-affirmed by Tekada and Minakata in 2014.⁶ In this communication, they carried out the coupling of arylboronic acids and enantiopure arylaziridines leading to the opening of the ring and the installment of a new aryl group at the benzylic position (Scheme 4.1.2.1.4). The strategy employed an efficient palladium/NHC catalytic system to construct a variety of configurationally defined 2-arylphenethylamines, which are difficult targets under traditional routes. Configurational inversion was again observed in all cases tested.



Scheme 4.1.2.1.4. Palladium catalyzed coupling of arylboronic acids and enantioenriched benzylarizidines.

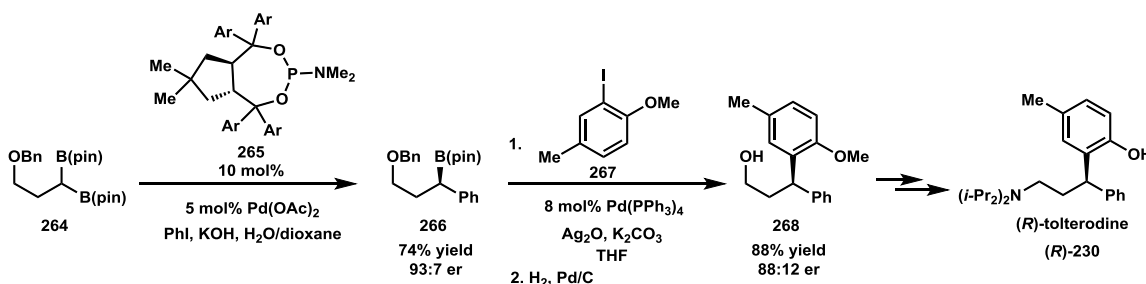
Above were highlighted the methods of the SN-like transformations using aryl nucleophiles and benzylic electrophiles. In the opposite scenario, a coupling between a benzylic nucleophile and an aryl electrophile also provides a powerful tool for the construction of highly configurationally pure bis-aryl structures. An early example is the Suzuki-Miyaura coupling between optically pure secondary benzyl boronic esters and aryl iodides by Crudden and coworkers in 2009.⁷ The reactions proceeded with great chirality transfer and with a retention of configuration (Scheme 4.1.2.1.5).



Scheme 4.1.2.1.5. Suzuki coupling of enantioenriched benzylboronates and aryl iodides.

Intrigued by the versatility of enantioenriched organoboronates in coupling reactions, the Morken group developed an elegant method to prepare enantiopure benzylboronates

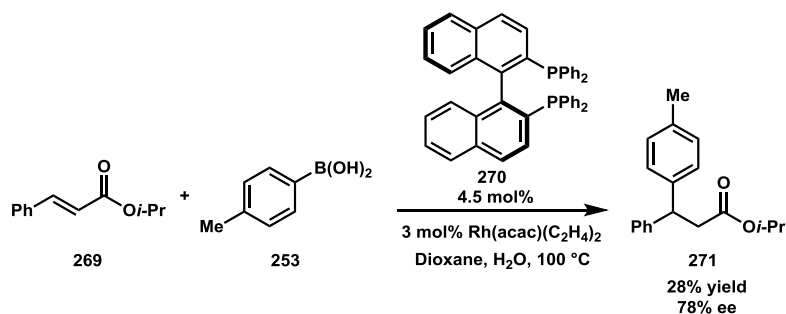
from racemic geminal bis-boronates.⁸ In the presence of a chiral monodentate taddol-derived phosphoramidite ligand, an enantiotopic group selective Suzuki coupling was obtained with inversion in stereochemistry as determined by labelled boron experiments. The reactions advanced in greater yields with aryl iodides than with the bromides, generating highly enantiopure benzylic boronates. The utility of the method was then demonstrated in the synthesis of the pharmaceutical (*R*)-tolterodine (Detrol LA), a chiral bis-aryl compound used for the treatment of urinary incontinence (Scheme 4.1.2.1.6).



Scheme 4.1.2.1.6. Application of enantiotopic group selective Suzuki reaction in the synthesis of (*R*)-tolterodine **230**.

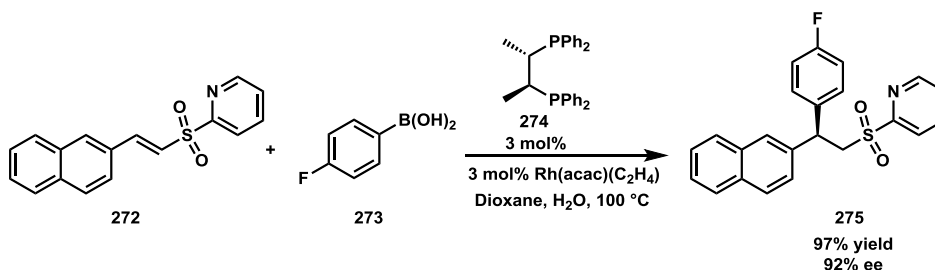
One of the traditional ways to construct carbon carbon bonds is the 1,4-addition reaction. In the context of the synthesis of bis-aryl structures, the rhodium catalyzed conjugate addition of arylboronic acids has also had several major contributions. Since first introduced by Miyaura in 1997, the transformation has developed to a high level of both conversion and selectivity.⁹ However, a literature search reveals fewer examples of acyclic arylenones. An early representative, also by Miyaura, was the enantioselective addition to α,β -unsaturated esters using (*S*)-BINAP as the chiral ligand for rhodium complex.¹⁰ A variety of enone substrates were examined giving moderate to high yields

and good selectivities. Nevertheless, aryl enones were shown to perform poorly with lower enantiomeric excesses than alkyl enones (Scheme 4.1.2.1.7).



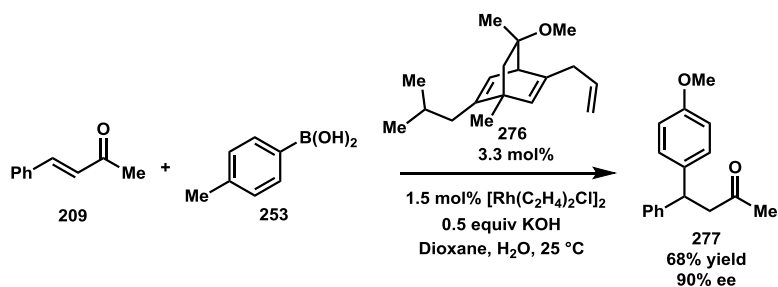
Scheme 4.1.2.1.7. Rhodium catalyzed asymmetric conjugate addition of arylboronic acid to β -aryl α,β -unsaturated esters.

An improvement came from the use of α,β -unsaturated sulfones. The work was done by Carretero and coworkers in 2004.¹¹ The pyridyl sulfone group on the substrates was believed to cause a metal-chelating effect that improved the reactivity. In fact, under their standard conditions, the reactions of styrenyl sulfone substrates with arylboronic acids happened smoothly with good yields and selectivities (Scheme 4.1.2.1.8).



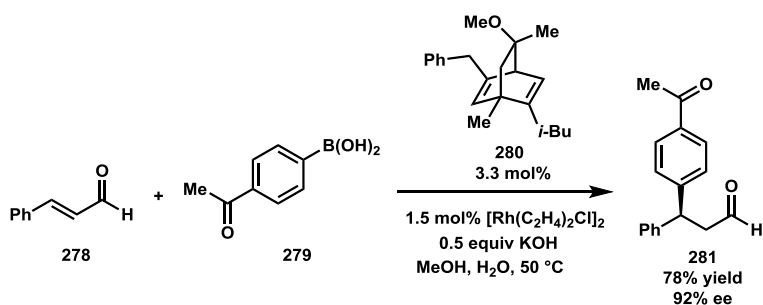
Scheme 4.1.2.1.8. Rhodium catalyzed asymmetric conjugate addition of arylboronic acids to β -aryl α,β -unsaturated sulfones.

In the same year, in an effort to design an efficient [2.2.2]-diene ligand for the Rh(I)-catalyzed conjugate addition reactions of the substrates that were not widely examined at the time, Carreira *et al.* were able to obtain the addition of an arylboronic acid to phenyl-enone with moderate yield and good selectivity (Scheme 4.1.2.1.9).¹² This result, albeit being the only example, demonstrated the applicability of rhodium catalyzed 1,4-addition to produce chiral diaryl compounds from acyclic aryl-enones.



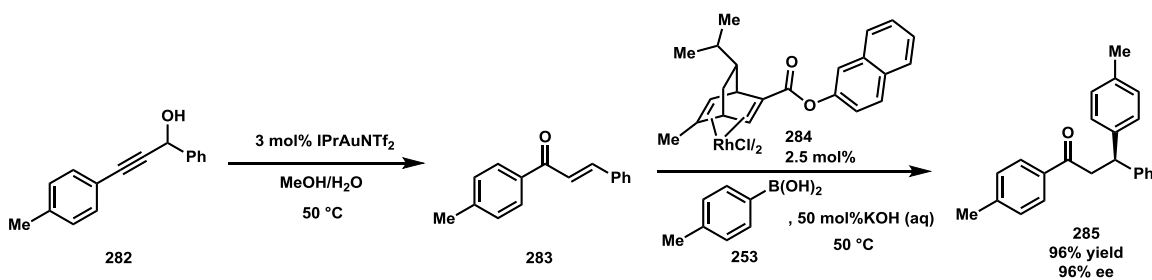
Scheme 4.1.2.1.9. Rhodium catalyzed asymmetric conjugate addition of arylboronic acid to acyclic β -aryl enone.

One year later, in 2005, the Carreira group documented an enantioselective addition of arylboronic acids to aryl-enal substrates using their diene ligand.¹³ It is worth mentioning that this strategy allows the use of strongly electron deficient arylboronic acids in high yielding reactions with great enantioselectivities (Scheme 4.1.2.1.10).



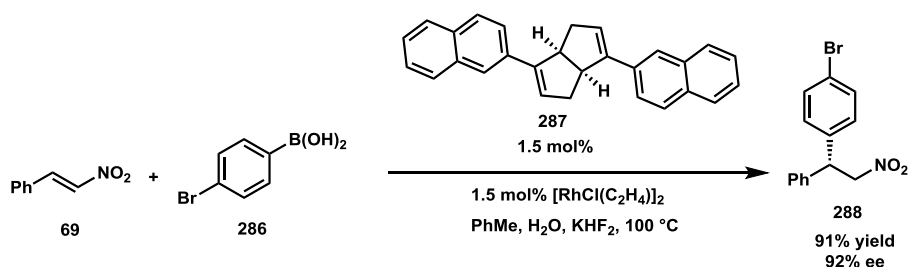
Scheme 4.1.2.1.10. Rhodium catalyzed asymmetric conjugate addition of arylboronic acids to β -aryl enals.

In terms of aryl-enone reactivity, it is worth highlighting the work of Lautens and coworkers in 2013.¹⁴ In this communication, they developed a tandem one-pot procedure to synthesize nonracemic chiral β -disubstituted ketones, including diaryl compounds. The transformation goes through the sequence of gold-catalyzed Meyer-Schuster rearrangement of a starting propargylic alcohol and enantioselective rhodium catalyzed conjugate addition of boronic acids to the newly formed enones. The reactions proceeded nicely with yields up to 97% over two steps and enantiomeric excesses up to 96% (Scheme 4.1.2.1.11).



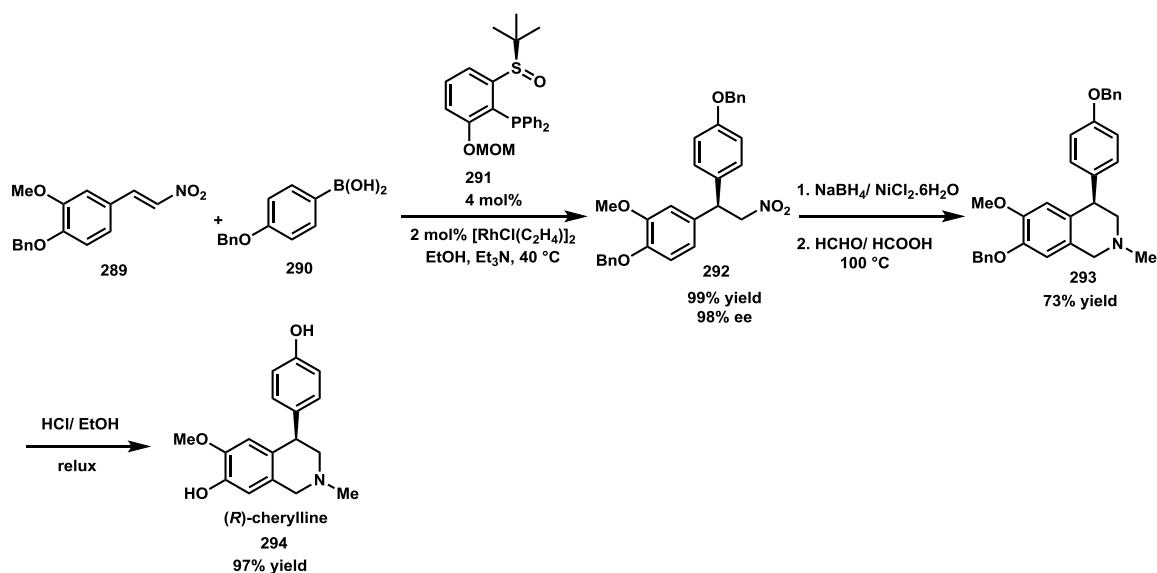
Scheme 4.1.2.1.11. Tandem one-pot synthesis of diaryl ketones.

One of the challenging substrates in terms of stereoselectivity for this type of chemistry is the nitroalkenes. In fact, the Hayashi group were able to obtain high selectivities for the asymmetric addition of boronic acids to cyclic aliphatic enones in 2000.¹⁵ In many reports after, low levels of enantiomeric enrichment were observed with acyclic β -aryl nitroalkene substrates.¹⁶ It was not until 2010 when Lin and coworkers made use of their C_2 -symmetric chiral bicyclo[3.3.0] ligand **287** that a considerable improvement could be achieved.¹⁷ It is noteworthy that the employment of KHF_2 in conjunction with arylboronic acids is crucial for the desired selectivity (Scheme 4.1.2.1.12).



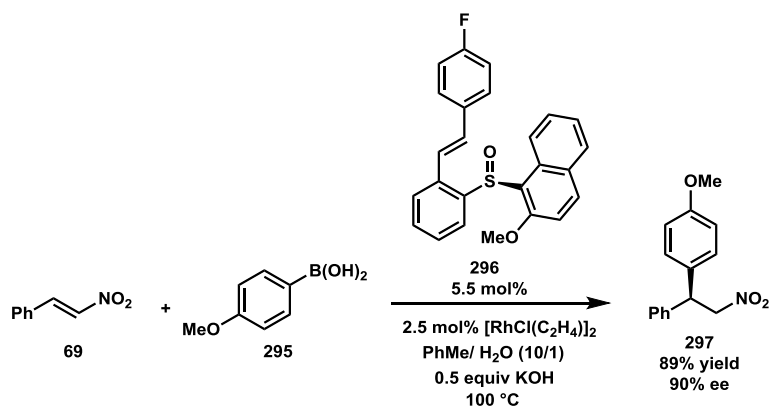
Scheme 4.1.2.1.12. Rhodium catalyzed conjugate addition of arylboronic acids to 2-arylnitroalkenes.

Shortly after, in 2011, Liao *et al.* introduced their *tert*-butanesulfinylphosphine structure **291** as an excellent ligand to obtain the same level of selectivity as Lin's system.¹⁸ The synthesis of (*R*)-cherylline **294** was also disclosed to demonstrate the synthetic applicability of the method (Scheme 4.1.2.1.13).



Scheme 4.1.2.1.13. *tert*-butanesulfinylphosphine ligand in rhodium catalyzed conjugate addition of arylboronic acids to nitroalkenes and application in the synthesis of (*R*)-cherylline **294**.

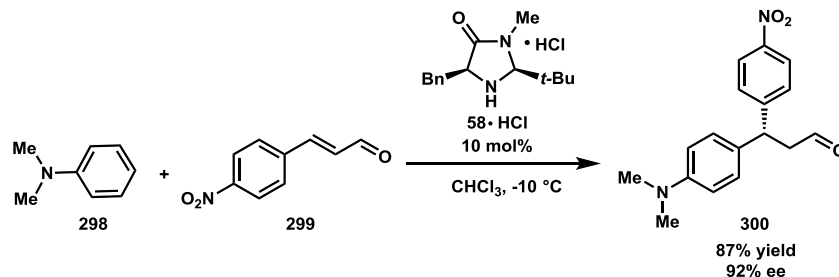
An additional ligand system is the olefin-sulfone ligands introduced by the Wan group in 2012.¹⁹ With this new type of ligand, they were able to obtain a broad scope of substrates including aryl, alkyl and heteroaryl nitroalkenes with good yields and selectivities (Scheme 3.1.2.1.14).



Scheme 3.1.2.1.14. Olefin-sulfoxide ligand for rhodium catalyzed conjugate addition of arylboronic acids to nitroalkenes.

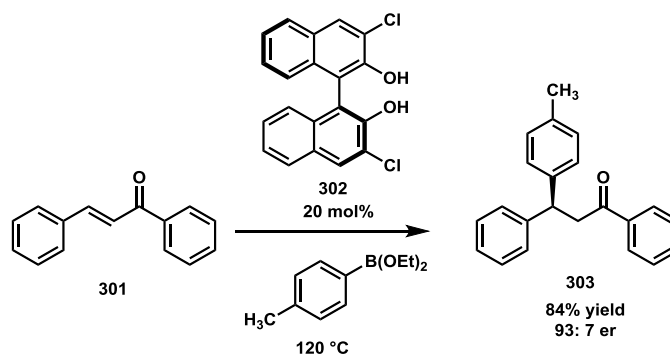
4.1.2.2. Organocatalytic methods

Organocatalysts allow the use of mild reagents which are helpful to achieve a broad functional group tolerance. However, it is because of such mildness that those reagents sometimes do not possess enough reactivity for the targets of interest. The iminium activation strategy, employed by MacMillan group, was shown to facilitate the Friedel-Crafts alkylation of arenes by electron-deficient olefins to form different enantioenriched diarylalkanes with good yield and great ee's.²⁰ Nonetheless, only electron rich aromatic compounds could be used (Scheme 4.1.2.2.1).



Scheme 4.1.2.2.1. Iminium catalysis in the conjugate addition of electron-rich benzenes to α,β -unsaturated aldehydes.

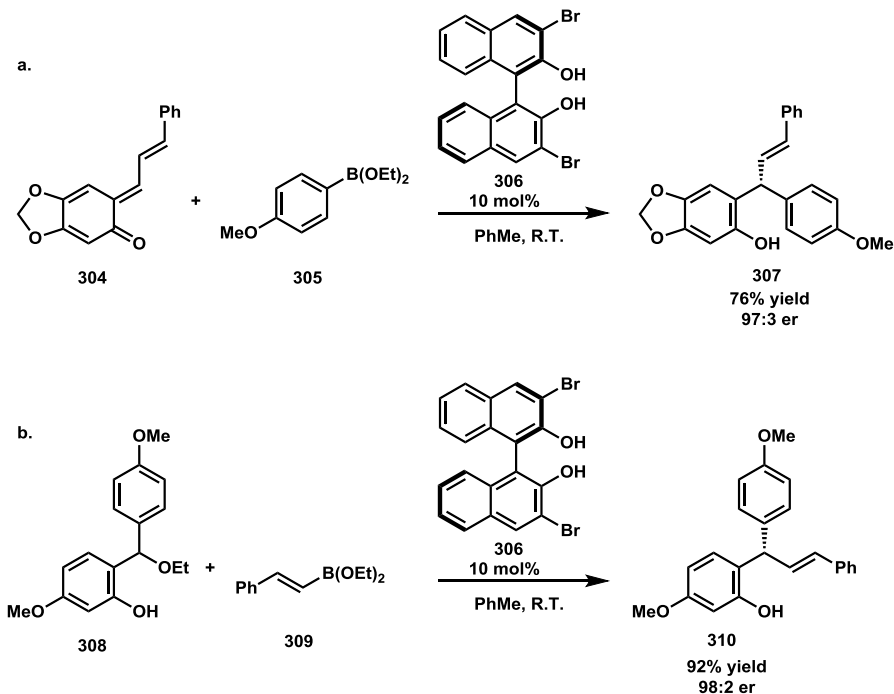
The low reactivity of neutral reagents can be compensated for by applying harsh conditions, typically via elevated temperature. Chong's arylation of aromatic enones using a BINOL-based catalyst required the reactions to operate at 120 °C in the presence of excess arylboronic ester, which also functioned as the solvent.²¹ The high temperature provided enough energy for the transformation to occur. However, it decreased the selectivity to some extent (Scheme 4.1.2.2.2). In addition, the necessity of liquid arylboronic esters greatly narrows the scope of the nucleophile.



Scheme 4.1.2.2.2. BINOL-catalyzed conjugate addition of arylboronic esters to chalcones.

An additional solution for the insufficient reactivity of neutral systems can come from the use of high energy substrates, as an alternative to the employment of reactive nucleophiles by MacMillan described above. In 2012, Schaus and coworkers documented their usage of *o*-quinone methides as the electrophilic counterpart for the addition of aryl and akenylboronic esters to afford a variety of optically pure diarylmethine products (Scheme 4.1.2.2.3a).²² It is the strong propensity of the *o*-quinone methides to rearomatize that plays as the driving force for a smooth transformation under mild

conditions. The Schaus group also showed the application of hydroxybenzyl ethyl ether substrates, which can generate *o*-quinone methides in situ that in turn will be trapped by the addition of boronates (Scheme 4.1.2.2.3b). This is considered to be a solution to access a wider range of *o*-quinone methides that are difficult to isolate. A limitation is the requirement of an ortho hydroxyl group on the aryl ring.

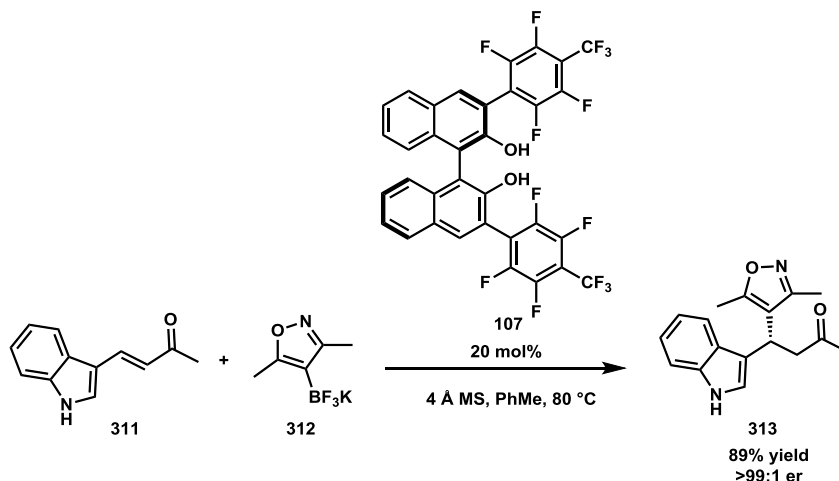


Scheme 4.1.2.2.3. BINOL-catalysis in (a) conjugate addition of arylboronic esters to vinyl *o*-quinone methides and (b) alkenylation of hydroxybenzyl alcohols.

4.2. Approach

In an effort to develop a method for the synthesis of chiral bis-heterocycles, Jiun-le Shih in the May lab was able to acquire efficient conditions in which potassium trifluoroborates were used in place of boronic acids and the reactions could proceed without the presence of any additive (Scheme 4.2.1). Trifluoroborates are known for their

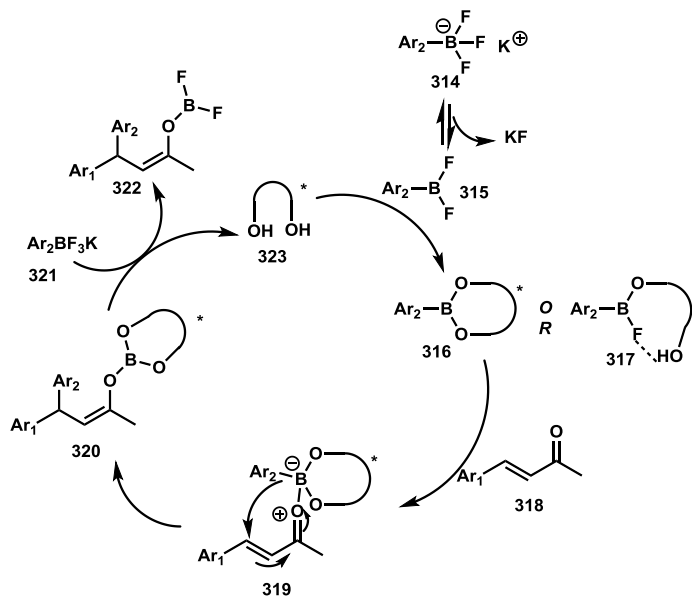
great stability and ease of handling. Furthermore, they exhibited greater reactivity and consistency than the corresponding boronic acids. In light of this accomplishment, we envisaged that aryltrifluoroborate salts would be efficient for obtaining bis-aryl structures.



Scheme 4.2.1. BINOL-catalyzed conjugate addition of heteroaryltrifluoroborates to β -aryl-enones.

It is engrossing to understand how the trifluoroborate salts can work in conjunction with BINOL catalysts for the asymmetric conjugate addition to enones. Another valuable fact from Shih's work is that the stereochemistry of the products, which were elucidated by X-ray analysis, is in great agreement with the enantiomeric induction that has been established so far for the use of boronic esters and acids. From this, we believe that trifluoroborates should go through a similar process which initially involves the formation of an activated trivalent BINOL-derived boronate species. In order for the trifluoroborate to have such interaction with BINOL, we postulate that a fluoride must dissociate from the parent trifluoroborate to form the trivalent difluoroboronate **315**,

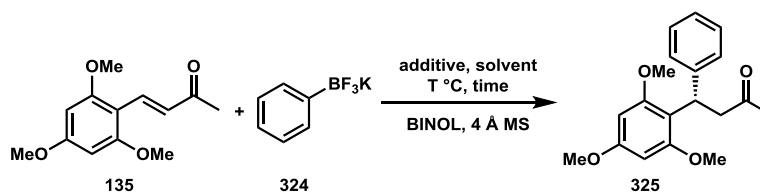
which in turn condenses with the BINOL catalyst to give rise to the active species **316** or **317** (Scheme 4.2.2). This postulate was supported by experimental evidence obtained by Shih.



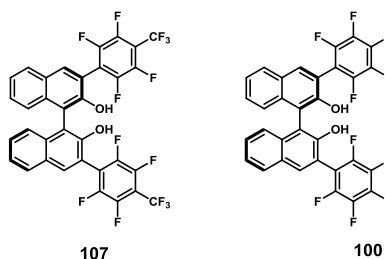
Scheme 4.2.2. Proposed mechanism of the BINOL-catalyzed conjugate addition of aryltrifluoroborates to enones.

4.3. Reaction optimization

Our starting point was to test the potential of the transformation. Therefore, with the use of potassium phenyltrifluoroborate we chose the highly electron rich substrate **135**, which was believed to have great reactivity. Table 4.3.1 summarizes our attempts to enhance the reaction outcome.

Table 4.3.1. Reaction development with potassium phenyltrifluoroborate

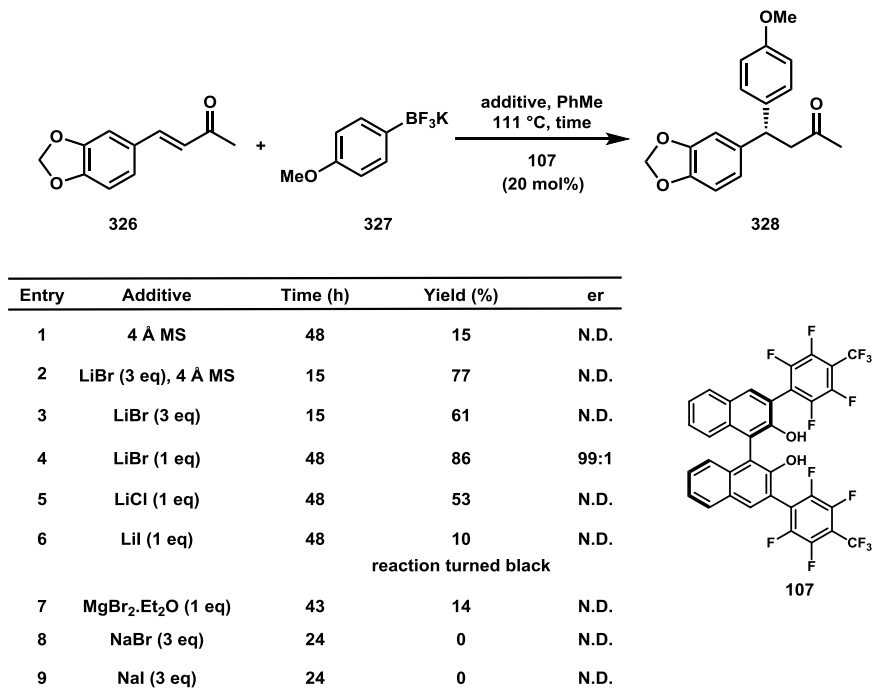
Entry	BINOL (20 mol%)	Additive	Solvent	T °C	Time (h)	Yield (%)	er
1	107	4 Å MS	PhMe	111	40	0	N.D.
2	100	Mg(O <i>t</i> -Bu) ₂ (0.1 eq)	PhMe	111	40	0	N.D.
3	100	Na <i>Ot</i> -Bu (1 eq)	PhMe	111	43	4	N.D.
4	107	Na <i>Ot</i> -Bu (1 eq)	PhMe	111	43	7	N.D.
5	107	NaOMe (1 eq)	PhMe	111	43	12	N.D.
6	107	NaOMe (1 eq)	PhCl	132	43	20	98:2
7	107	MgBr ₂ .Et ₂ O (1 eq)	PhCl	132	43	14	N.D.



As illustrated in the table, Shih's conditions that work so excellently in the bis-heterocyclic stereocenter synthesis give no reaction (entry 1). Different parameters, including the catalyst, additive, solvent and temperature, were examined, with the best yield at 20% (entry 6). Despite the low conversion, the outstanding enantiomeric ratio (98:2 er) indicated a potential highly selective transformation. At this point, we decided to turn our attention to more electron rich nucleophiles with the hope to gain greater reactivity. At the same time, we switched to substrate **326**, which is a more practical structure since the methylenedioxybenzene moiety is present in a number of bioactive

molecules. To begin, we opted to use potassium 4-methoxyphenyltrifluoroborate to serve for the reaction optimization (Table 4.3.2).

Table 4.3.2. Reaction development with 4-methoxyphenyltrifluoroborate



The bis-heterocycle conditions were again tested, giving a 15% yield after 48 hours (entry 1). It is noteworthy that all the heterocyclic nucleophiles employed in that work are electron rich, and mechanistically we believe that the fluoride dissociation occurs more spontaneously in those reagents than in aryltrifluoroborates. Therefore, a stronger fluoride dissociating agent than molecular sieves was sought to help increase the concentration of the trivalent difluoroarylboronate, which is more active toward BINOL. To our delight, the addition of 3 equivalents of LiBr proved to accelerate the reaction, and the yield was boosted to 77% in only 15 hours (entry 2). This phenomenon is understandable, since fluoride dissociation would form LiF, which is thermodynamically

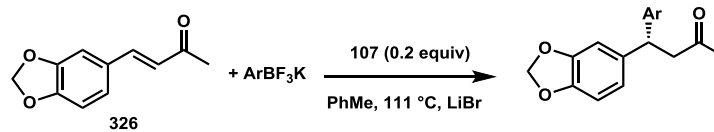
more favored than that of KF^{23} and can drive the equilibrium forward. As it turned out, the molecular sieves could be omitted when LiBr is in use (entry 3) although with a lower yield due to the formation of side products. This problem can be alleviated by decreasing the amount of LiBr to 1 equivalent (entry 4). The reaction proceeds more slowly but affords more of the desired product in 86%. Excellent enantioselectivity (99:1 er) was also achieved. LiCl appeared to be less effective (entry 5). The use of LiI caused serious decomposition presumably, due to the in situ formation of reactive iodine (entry 6). Magnesium and sodium salts were demonstrated to be not as effective as lithium additives. With optimal conditions in hand (entry 4), we carried the study on the scope of the reaction.

4.4. Reaction scope

4.4.1. Aryltrifluoroborate scope

Using the substrate from the optimization process, we examined a variety of electron rich aryltrifluoroborate salts (Table 4.4.1). To our delight, all the nucleophiles under examination gave high yields with excellent selectivities.

Table 4.4.1. Reactions of electron rich aryltrifluoroborates



entry	Ar	product	time	equiv LiBr	yield	er
1		328	48 h	1.0	86%	95:05
2		329	46 h	1.0	75%	99:01
3		330	3 h	N/A ^a	94%	98:02
4		R ₁ OMe H 331	9 h	1.0	88%	99:01
5		SMe H 332	15 h	1.0	97%	98:02
6		OMe OMe 333	24 h	1.0	85%	>99:01
7		OPh H 334	39 h	1.0	83%	94:06
8		OBn H 335	17 h	1.0	92%	99:01
9		O <i>i</i> -Pr H 336	4 h	2.0	89%	98:02
10		Me Me 337	48 h	1.0	76%	99:01
11		338	20 h	2.0	98%	95:05

^a 4 Å MS used instead of LiBr

It is noteworthy that a *para*-amino group is electronically sufficient for the fluoride dissociation, so the reaction requires only molecular sieves to proceed (entry 3). An interesting feature is that the reagents bearing *ortho* donating groups react more rapidly than the *para*-substituted reagents (entry 1 vs. entry 4; entry 2 vs. entry 5). This implies a possible proximal electronic stabilization of the transition state by the *ortho* donating group. Other *ortho* substituted aryltrifluoroborates react smoothly under the given conditions (entry 4-11). These results show the advantage of the strategy over the typical Friedel-Crafts reactions, which rarely get functionalized at the *ortho* position, especially

with bulky substituents. It is worth mentioning that the presence of an additional electron withdrawing group beside an electron donating one does not have a negative effect on the reaction outcome (entry 11). Finally, methyl groups provide adequate electron density to afford an efficient reaction (entry 10).

4.4.2. Aryl enone scope

With the success of expanding the scope of nucleophiles, we continued to different aromatic enones. To serve this purpose, we chose the potassium 2-benzyloxyphenyltrifluoroborate **339** as the nucleophile because of its availability as well as of the removability of the benzyl group (Table 4.4.2). As expected, a wide range of enones possessing different electronic natures were shown to be compatible.

Table 4.4.2. Scope of aryl enones

entry	Ar	product	time	yield	er	entry	Ar	product	time	yield	er
1		340	23 h	88%	>99:01	7		346	48 h	81%	95:05
2		341	16 h	89%	>99:01	8		347	15 h	83%	>99:01
3		342	15 h	83%	95:05	9		348	22 h	83%	>99:01
4		343	46 h	86%	>99:01	10		349	15 h	91%	99:01
5		344	20 h	81%	97:03	11		350	24 h	50%	>99:01
6		345	20 h	81%	97:03						

It is interesting that not only do the electron rich substrates give good results (entry 7-8), but the electron deficient enones do also (entry 2-6; entry 9). The high reactivities of the halogenated substrates (entry 2-6) are important, for those groups are well known for their great functionalizability. A phenolic substrate also proved compatible to give a considerably selective reaction albeit in moderate yield (entry 11).

4.5. Conclusion

A highly enantioselective conjugate addition of potassium aryltrifluoroborates to β -aryl-enones was established to obtain a broad collection of optically pure bis-aryl compounds. The reactions require the aid of LiBr to effectively dissociate one fluoride from the trifluoroborate in order to be operable in BINOL catalysis. It is important that the nucleophiles be electron rich. That requirement, however, is inapplicable to the electrophiles since enones of all electronic nature are demonstrated to react under the standard conditions.

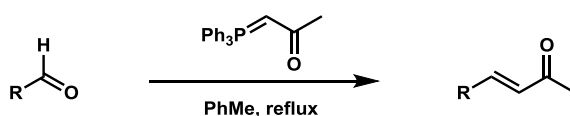
4.6. Experimental section

4.6.1. General consideration

All reactions were carried out in flame- or oven-dried glassware. THF, toluene and CH_2Cl_2 were purged with argon and dried over activated alumina columns. Flash chromatography was performed on 60Å silica gel (EMD Chemicals Inc). Preparative plate chromatography was performed on EMD silica gel plates, 60Å, with UV-254 indicator. Chemical names were generated using Cambridge Soft ChemBioDraw Ultra 12.0. Analysis by HPLC was performed on a Shimadzu Prominence LC (LC-20AB) equipped with a SPD-20A UV-Vis detector and a Chiralpak or Chiralcel (250 mm x 4.6 mm) column (see below for column details). Analytical thin layer chromatography was

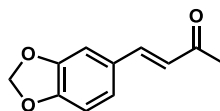
performed on EMD silica gel/TLC plates with fluorescent detector 254 nm. The ^1H , ^{13}C and ^{19}F NMR spectra were recorded on a JEOL ECA-500 or ECX-400P spectrometer using residual solvent peak as an internal standard (CDCl_3 : 7.24 ppm for ^1H NMR and 77.00 ppm for ^{13}C NMR). Hexafluorobenzene ($\delta = -164.9$ ppm) was employed as an external standard in ^{19}F NMR spectra. HRMS analyses were performed under contract by UT Austin's mass spectrometric facility via ESI method and a US10252005 instrument.

4.6.2. General procedure for the synthesis of starting material (enone)



To a flask equipped with a stir bar and a condenser was added carboxaldehyde (2 mmol), 1-(triphenylphosphoranylidene)-2-propanone (1.2 equiv, 764 mg), and toluene (4 ml). The reaction mixture was refluxed for 1-2 h. After completion, the reaction mixture was concentrated via rotary evaporation. The crude mixture was purified via flash column chromatography with an appropriate eluent on silica gel.

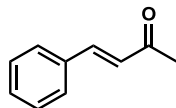
4.6.2.1. Synthesis of (*E*)-4-(benzo[*d*][1,3]dioxol-5-yl)but-3-en-2-one (326)



See general procedure for enone formation above. 5 mmol of corresponding aldehyde was used. After silica gel chromatography using 10%-20% ethyl acetate in hexanes as eluent, the title compound was obtained in 95% yield (364 mg) as a white solid. ^1H NMR (500 MHz, CDCl_3): $\delta = 7.41$ (d, $J = 16.6$ Hz, 1H), 7.03-7.00 (m, 2H), 6.81 (d, $J = 8.0$ Hz, 1H), 6.54 (d, $J = 16.0$ Hz, 1H), 6.00 (s, 2H), 2.34 (s, 3H). ^{13}C NMR (125.77 MHz,

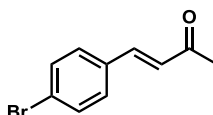
CDCl₃): δ = 198.2, 149.8, 148.4, 143.1, 128.7, 125.2, 124.8, 108.5, 106.4, 101.5, 27.5. All spectral properties were identical to those reported in the literature.²⁴

4.6.2.2. Synthesis of (*E*)-4-phenylbut-3-en-2-one (209)



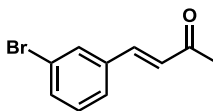
See section 2.5.2.1, chapter 2 for detail.

4.6.2.3. Synthesis of (*E*)-4-(4-bromophenyl)but-3-en-2-one (213)



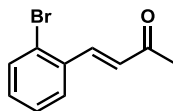
See section 2.5.2.5, chapter 2 for detail.

4.6.2.4. Synthesis of (*E*)-4-(3-bromophenyl)but-3-en-2-one, precursor to 342



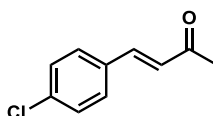
See general procedure for enone formation above. After silica gel chromatography using 10% ethyl acetate in hexanes as eluent, the title compound was obtained in 99% yield (445 mg) as a white solid. ¹H NMR (500 MHz, CDCl₃): δ = 7.66 (dd, *J* = 2.3 Hz; 1.7 Hz, 1H), 7.49 (ddd, *J* = 8 Hz; 2.5 Hz; 1 Hz, 1H), 7.44 (d, *J* = 7.4 Hz, 1H), 7.4 (d, *J* = 16 Hz, 1H), 7.25 (t, *J* = 8 Hz, 1H), 6.68 (d, *J* = 16 Hz, 1H), 2.36 (s, 3H). ¹³C NMR (125.77 MHz, CDCl₃): δ = 197.8, 141.4, 136.4, 133.1, 130.8, 130.4, 128.0, 126.7, 123.0, 27.7.

4.6.2.5. Synthesis of (*E*)-4-(2-bromophenyl)but-3-en-2-one, precursor to 343



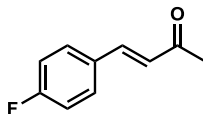
See general procedure for enone formation above. After silica gel chromatography using 10% ethyl acetate in hexanes as eluent, the title compound was obtained in 90% yield (406 mg) as a white solid. ^1H NMR (500 MHz, CDCl_3): δ = 7.81 (d, J = 16 Hz, 1H), 7.54 (m, 2H), 7.27 (dd, J = 8 Hz; 6.8 Hz, 1H), 7.16 (td, J = 8 Hz; 1.7 Hz, 1H), 6.55 (d, J = 16 Hz, 1H), 2.35 (s, 3H). ^{13}C NMR (125.77 MHz, CDCl_3): δ = 197.9, 141.5, 134.1, 133.2, 131.2, 129.5, 127.6, 127.5, 125.3, 27.0. All spectral properties were identical to those reported in the literature.²⁴

4.6.2.6. Synthesis of (*E*)-4-(4-chlorophenyl)but-3-en-2-one, precursor to 344



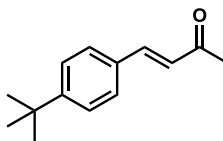
See general procedure for enone formation above. After silica gel chromatography using 10% ethyl acetate in hexanes as eluent, the title compound was obtained in 93% yield (336 mg) as a white solid. ^1H NMR (500 MHz, CDCl_3): δ = 7.47-7.43 (m, 3H), 7.36 (d, J = 8.6 Hz, 2H), 6.67 (d, J = 16.6 Hz, 1H), 2.36 (s, 3H). ^{13}C NMR (125.77 MHz, CDCl_3): δ = 198.0, 141.8, 136.3, 132.8, 129.3, 129.2, 127.4, 27.6. All spectral properties were identical to those reported in the literature.²⁴

4.6.2.7. Synthesis of (*E*)-4-(4-fluorophenyl)but-3-en-2-one, precursor to 345



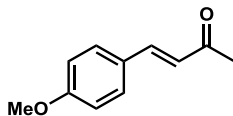
See general procedure for enone formation above. After silica gel chromatography using 10% ethyl acetate in hexanes as eluent, the title compound was obtained in 99% yield (325 mg) as a colorless liquid. ^1H NMR (500 MHz, CDCl_3): δ = 7.51 (m, 2H), 7.45 (d, J = 16 Hz, 1H), 7.06 (m, 2H), 6.62 (dd, J = 16 Hz; 2.6 Hz, 1H), 2.35 (s, 3H). ^{13}C NMR (125.77 MHz, CDCl_3): δ = 198.1, 164.9, 162.9, 142.0, 130.6, 130.5, 130.1, 130.0, 126.7, 116.1, 116.0, 27.5. ^{19}F NMR (470.6 MHz, CDCl_3): δ = -112.3. All spectral properties were identical to those reported in the literature.²⁵

4.6.2.8. Synthesis of (*E*)-4-(4-*t*-butylphenyl)but-3-en-2-one, precursor to 346



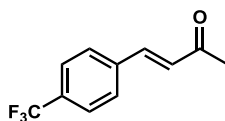
See general procedure for enone formation above. After silica gel chromatography using 10% ethyl acetate in hexanes as eluent, the title compound was obtained in 90% yield (364 mg) as a white solid. ^1H NMR (500 MHz, CDCl_3): δ = 7.51-7.47 (m, 3H), 7.41 (d, J = 8.6 Hz, 2H), 6.69 (d, J = 16 Hz, 1H), 2.37 (s, 3H), 1.32 (s, 9H). ^{13}C NMR (125.77 MHz, CDCl_3): δ = 198.5, 154.1, 143.4, 131.5, 128.0, 126.4, 125.9, 34.8, 31.1, 27.3. All spectral properties were identical to those reported in the literature.²⁶

4.6.2.9. Synthesis of (*E*)-4-(4-methoxyphenyl)but-3-en-2-one (211)



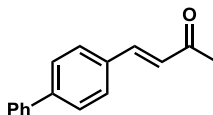
See section 2.5.2.3, chapter 2 for detail.

4.6.2.10. Synthesis of (*E*)-4-(4-(trifluoromethyl)phenyl)but-3-en-2-one (210)



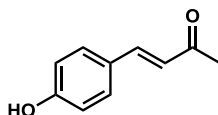
See section 2.5.2.2, chapter 2 for detail.

4.6.2.11. Synthesis of (*E*)-4-(biphenyl-4-yl)but-3-en-2-one (312)



See section 2.5.2.4, chapter 2 for detail.

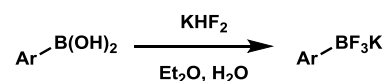
4.6.2.12. Synthesis of (*E*)-4-(4-hydroxyphenyl)but-3-en-2-one, precursor to 350



See general procedure for enone formation above 2.4 equivalents of Wittig reagent were employed. After silica gel chromatography using 20% ethyl acetate in hexanes as eluent, the title compound was obtained in 86% yield (281 mg) as a yellow solid. ^1H

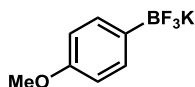
NMR (500 MHz, CDCl₃): δ = 7.51 (d, J =16.0 Hz, 1H), 7.44 (d, J = 8.6 Hz, 2H), 7.39 (OH), 6.91 (d, J = 8.6 Hz, 2H), 6.6 (d, J = 16.6 Hz, 1H), 2.39 (s, 3H). ¹³C NMR (125.77 MHz, CDCl₃): δ = 200.1, 158.9, 144.8, 130.4, 126.4, 124.2, 116.1, 27.1. All spectral properties were identical to those reported in the literature.²⁷

4.6.3. General procedure for potassium aryltrifluoroborate synthesis



Following a procedure by Molander and coworkers,²⁸ arylboronic acid (5 mmol) was added to a reaction flask containing 10 ml diethyl ether at room temperature. The potassium hydrogendifluoride (2.8 equiv, 1.09 g) was then added to the suspension followed by the addition of water (4.5 ml) over 30 minutes. The reaction was allowed to stir vigorously in 3 hours. After 3 hours, the reaction mixture was concentrated and dissolved in hot acetone. The solution was then filtered and concentrated. The residue was again dissolved in hot acetone and the product was then precipitated upon the addition of diethyl ether. Finally, the pure product was collected by suction filtration.

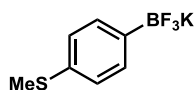
4.6.3.1. Synthesis of potassium (4-methoxyphenyl)trifluoroborate, precursor to 328



See general procedure for trifluoroborate formation above. The title compound was obtained in 98% yield (1.0569 g) as a white solid. ¹H NMR (400 MHz, DMSO-d₆): δ = 7.18 (d, J = 8.2 Hz, 2H), 6.60 (d, J = 8.2 Hz, 2H), 3.59 (s, 3H). ¹³C NMR (100 MHz,

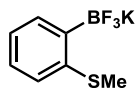
DMSO- d_6): δ = 157.3, 132.3, 111.9, 54.6. ^{19}F NMR (470.6 MHz, DMSO- d_6): δ = -140.5. ^{11}B -NMR (160.4 MHz, DMSO- d_6): δ = 2.30. HRMS (ESI) m/z : calculated for $\text{C}_7\text{H}_7\text{BF}_3\text{O}$ 175.0549, found 175.0547. All spectral properties were identical to those reported in the literature.²⁹

4.6.3.2. Synthesis of potassium (4-methylthiophenyl)trifluoroborate, precursor to 329



See general procedure for trifluoroborate formation above. The title compound was obtained in 90% yield (1.0326 g) as a white solid. ^1H NMR (500 MHz, DMSO- d_6): δ = 7.27 (d, J = 8.0 Hz, 2H), 7.03 (d, J = 8.0 Hz, 2H), 2.40 (s, 3H). ^{13}C NMR (125.77 MHz, DMSO- d_6): δ = 133.3, 132.0, 125.1, 15.4. ^{19}F NMR (470.6 MHz, DMSO- d_6): δ = -141.3. ^{11}B NMR (160.4 MHz, DMSO- d_6): δ = 2.29. HRMS (ESI) m/z : calculated for $\text{C}_7\text{H}_7\text{BF}_3\text{S}$ 191.0320, found 191.0317. All spectral properties were identical to those reported in the literature.³⁰

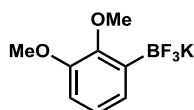
4.6.3.3. Synthesis of potassium (2-methylthiophenyl)trifluoroborate, precursor to 332



See general procedure for trifluoroborate formation above. 6 mmol of the corresponding boronic acid was used. The title compound was obtained in 65% yield

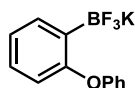
(897.7 mg) as a white solid. ^1H NMR (500 MHz, DMSO- d_6): δ = 7.34 (d, J = 6.3 Hz, 1H), 7.05 (d, J = 7.4 Hz, 1H), 6.96 (d, J = 7.4 Hz, 1H), 6.87 (t, J = 7.4 Hz, 1H), 2.27 (s, 3H). ^{13}C NMR (125.77 MHz, DMSO- d_6): δ = 141.5, 132.07, 132.05, 126.2, 122.5, 122.4, 14.8. ^{19}F NMR (470.6 MHz, DMSO- d_6): δ = -139.4. ^{11}B NMR (160.4 MHz, DMSO- d_6): δ = 6.75. HRMS (ESI) m/z : calculated for $\text{C}_7\text{H}_7\text{BF}_3\text{S}$ 191.0320, found 191.0319

4.6.3.4. Synthesis of potassium (2,3-dimethoxyphenyl)trifluoroborate, precursor to 333



See general procedure for trifluoroborate formation above. The title compound was obtained in 96% yield (1.1706 g) as a white solid. ^1H NMR (400 MHz, DMSO- d_6): δ = 6.93 (d, J = 7.3 Hz, 1H), 6.80 (t, J = 7.3 Hz, 1H), 6.72 (d, J = 7.3 Hz, 1H), 3.70 (s, 3H), 3.60 (s, 3H). ^{13}C NMR (100 MHz, DMSO- d_6): δ = 151.8, 151.6, 125.5, 122.5, 110.5, 59.8, 55.2. ^{19}F NMR (470.6 MHz, DMSO- d_6): δ = -138.7. ^{11}B NMR (160.4 MHz, DMSO- d_6): δ = 2.21. HR MS (ESI) m/z : calculated for $\text{C}_8\text{H}_9\text{BF}_3\text{O}_2$ 205.0655, found 205.0652

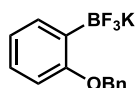
4.6.3.5. Synthesis of potassium (2-phenoxyphenyl)trifluoroborate, precursor to 334



See general procedure for trifluoroborate formation above. 4.67 mmol of the corresponding boronic acid was used. The title compound was obtained in 81% yield (930.1 mg) as a white solid. ^1H NMR (500 MHz, DMSO- d_6): δ = 7.48 (dd, J = 7.4 Hz;

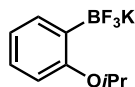
1.7 Hz, 1H), 7.23 (m, 2H), 7.07 (td, $J = 7.4$ Hz; 1.7 Hz, 1H), 6.93 (m, 2H), 6.78 (d, $J = 8.0$ Hz, 2H), 6.62 (d, $J = 7.4$ Hz, 1H). ^{13}C NMR (125.77 MHz, DMSO- d_6): $\delta = 159.7$, 158.9, 134.2, 129.1, 127.0, 122.6, 120.7, 119.2, 117.5. ^{19}F NMR (470.6 MHz, DMSO- d_6): $\delta = -139.3$. ^{11}B NMR (160.4 MHz, DMSO- d_6): $\delta = 1.96$. HRMS (ESI) m/z : calculated for $\text{C}_{12}\text{H}_9\text{BF}_3\text{O}$ 237.0706, found 237.0709

4.6.3.6. Potassium (2-benzyloxyphenyl)trifluoroborate, precursor to 335



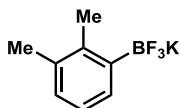
See general procedure for trifluoroborate formation above. The title compound was obtained in 85% yield (1.2321 g) as a white solid. ^1H NMR (400 MHz, DMSO- d_6): $\delta = 7.54$ (d, $J = 7.3$ Hz, 2H), 7.35 (m, 3H), 7.26 (t, $J = 7.3$ Hz, 1H), 7.00 (td, $J = 7.3$ Hz; 1.8 Hz, 1H), 6.72 (m, 2H), 5.02 (s, 2H). ^{13}C NMR (100 MHz, DMSO- d_6): $\delta = 161.4$, 138.9, 133.4, 128.0, 126.9, 126.8, 126.5, 119.5, 111.6, 68.7. ^{19}F NMR (470.6 MHz, DMSO- d_6): $\delta = -139.2$. ^{11}B NMR (160.4 MHz, DMSO- d_6): $\delta = 2.23$. HRMS (ESI) m/z : calculated for $\text{C}_{13}\text{H}_{11}\text{BF}_3\text{O}$ 251.0863, found 251.0860. All spectral properties were identical to those reported in the literature.³¹

4.6.3.7. Synthesis of potassium (2-isopropoxyphenyl)trifluoroborate, precursor to 336



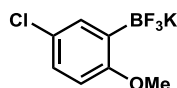
See general procedure for trifluoroborate formation above. 6.15 mmol of the corresponding boronic acid was used. The title compound was obtained in 97% yield (1.452 g) as a white solid. ^1H NMR (400 MHz, DMSO- d_6): δ = 7.33 (d, J = 5.9 Hz, 1H), 6.99 (m, 1H), 6.69 (m, 2H), 4.41 (sep, J = 5.9 Hz, 1H), 1.19 (d, J = 5.9 Hz, 6H). ^{13}C NMR (100 MHz, DMSO- d_6): δ = 161.0, 133.87, 133.84, 126.4, 119.6, 115.0, 69.8, 22.4. ^{19}F NMR (470.6 MHz, DMSO- d_6): δ = -138.7. ^{11}B NMR (160.4 MHz, DMSO- d_6): δ = 2.11. HRMS (ESI) m/z : calculated for $\text{C}_9\text{H}_{11}\text{BF}_3\text{O}$ 203.0862, found 203.0865

4.6.3.8. Synthesis of potassium (2,3-dimethylphenyl)trifluoroborate, precursor to 337



See general procedure for trifluoroborate formation above. The title compound was obtained in 99% yield (1.05 g) as a white solid. ^1H NMR (500 MHz, DMSO- d_6): δ = 7.18 (dd, J = 6.5 Hz; 1.4 Hz, 1H), 6.81-6.76 (m, 2H), 2.20 (s, 3H), 2.12 (s, 3H). ^{13}C NMR (125.77 MHz, DMSO- d_6): δ = 139.0, 133.8, 129.6, 126.7, 123.3, 20.3, 17.9. ^{19}F NMR (470.6 MHz, DMSO- d_6): δ = -138.4. ^{11}B NMR (160.4 MHz, DMSO- d_6): δ = 2.3. HRMS (ESI) m/z : calculated for $\text{C}_8\text{H}_9\text{BF}_3$ 173.0756, found 173.0750

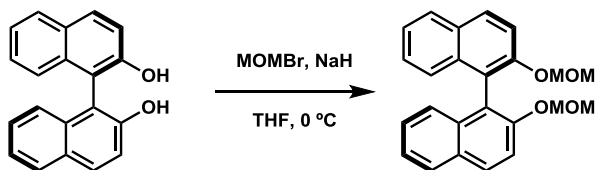
4.6.3.9. Synthesis of potassium (2-methoxy-5-chlorophenyl)trifluoroborate, precursor to 338



See general procedure for trifluoroborate formation above. The title compound was obtained in 97% yield (1.2079 g) as a white solid. ^1H NMR (500 MHz, DMSO-d_6): δ = 7.20 (d, J = 2.8 Hz, 1H), 7.03 (dd, J = 8.6 Hz; 3.4 Hz, 1H), 6.69 (d, J = 8.6 Hz, 1H), 3.61 (s, 3H). ^{13}C NMR (125.77 MHz, DMSO-d_6): δ = 161.1, 132.63, 132.61, 125.9, 123.4, 111.3, 55.0. ^{19}F NMR (470.6 MHz, DMSO-d_6): δ = -140.1. ^{11}B NMR (160.4 MHz, DMSO-d_6): δ = 1.29. HRMS (ESI) m/z : calculated for $\text{C}_7\text{H}_6\text{BCIF}_3\text{O}$ 209.0159, found 209.0159

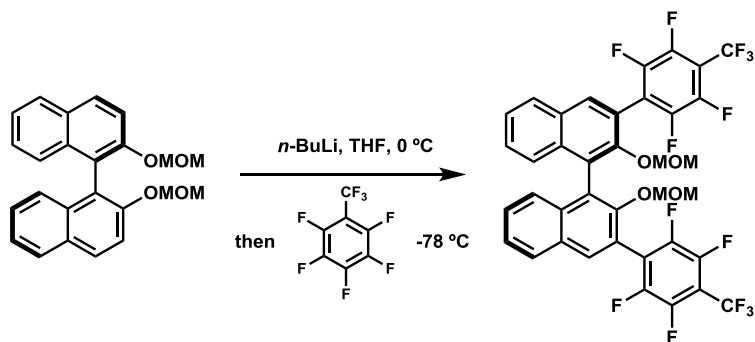
4.6.4. Procedure for catalyst synthesis

4.6.4.1. Synthesis of (*R*)-2,2'-bis(methoxymethoxy)-1,1'-binaphthyl



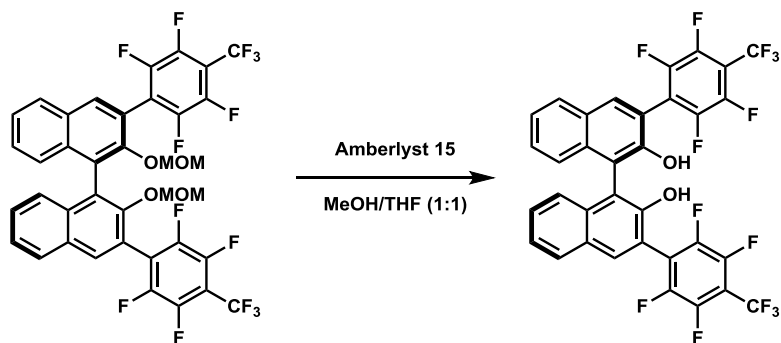
See chapter 1 for detail

4.6.4.2. Synthesis of (*R*)-2,2'-bis(methoxymethoxy)-3,3'-bis(2,3,5,6-tetrafluoro-4-(trifluoromethyl)phenyl)-1,1'-binaphthyl



Title compound was prepared following the procedure previously described in the literature with modifications.³² To a flame-dried flask equipped with a magnetic stirbar was added (*R*)-2,2'-bis(methoxymethoxy)-1,1'-binaphthyl (1.1091g, 2.96 mmol, 1 equiv) and 24ml THF. The reaction mixture was then cooled down to 0 °C followed by the addition of 2.5M *n*-BuLi (3.6 ml, 8.88 mmol, 3 equiv) and allowed to stir in 2 hours. The reaction temperature was decreased to -78 °C and perfluorotoluene (2.9 ml, 20.72 mmol, 7 equiv) was added dropwise via syringe. The reaction mixture was then warmed up to R.T. and stirred at this temperature for 12h. After completion, the reaction was quenched with saturated aq. NH₄Cl, extracted with Et₂O, and wash with brine. After the removal of solvents via rotary evaporation, the reaction mixture was purified by column chromatography on silica gel using 2-5% ethyl acetate in hexanes as eluent. The product was obtained as a white solid (2.0971 g, 2.6 mmol, 88% yield) and the spectral data agreed with the reported data.

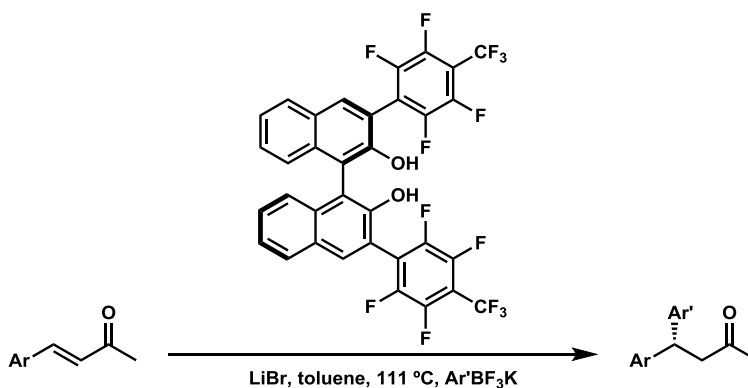
4.6.4.3. Synthesis of (*R*)-3,3'-bis(2,3,5,6-tetrafluoro-4-(trifluoromethyl)phenyl)-1,1'-binaphthyl-2,2'-diol (107)



To MOM-protected BINOL (2.0971 g, 2.6 mmol) was added MeOH (8 mL) and THF (8 mL). Amberlyst 15 resin (4 g) was then added and reaction allowed to reflux at 65 °C

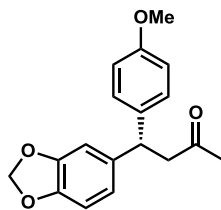
for 12h. After completion, the resin was filtered off and the organic layer concentrated to reduce solvent amount. The organic layer was then passed through a silica plug with 2-5% ethyl acetate in hexanes as eluent to afford the hydrolyzed product. (1.774 g, 2.47 mmol, 95% yield) and the spectral data agreed with the reported data.³²

4.6.5. General procedure for the BINOL-catalyzed conjugate addition of potassium aryltrifluoroborate to (*E*)-4-aryl-3-buten-2-one



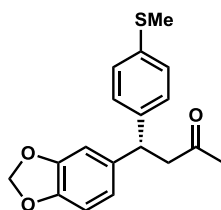
To a 2 dram vial equipped with a stir bar was added LiBr (1 equiv, 8.7 mg) and the flask was flamed-dried under high vacuum. The flask was then back-filled with Argon. The aryl-enone (0.1 mmol, 1.0 equiv), potassium aryltrifluoroborate (3 equiv), and (*R*)-3,3'-(C_7F_7)₂-BINOL **107** (0.02 mmol, 0.2 equiv, 14.3 mg) were then added. Freshly dried toluene (4 mL) was added and the reaction was heated to 111°C and allowed to stir at this temperature (see each product for specific reaction times). After completion, the crude reaction mixture was then loaded onto silica gel and purified via flash column chromatography on silica gel with appropriate eluents. (See each product for specific eluent)

4.6.5.1. Synthesis of 4-(benzo[*d*][1,3]dioxo-5-yl)-4-(4-methoxyphenyl)butan-2-one
(328)



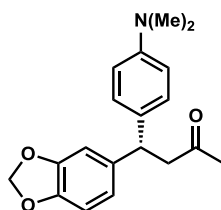
See general procedure for conjugate addition reaction above. The crude reaction mixture was purified via flash column chromatography with 100% dichloromethane as the eluent. HPLC Chiralpak ID (hexane/*i*-PrOH = 90:10, 0.75 mL/min, UV-254 detector). Trial 1: 25.5 mg, 0.085 mmol, 82% yield; 99:1 er (48h, 19.7 mg of starting material). Trial 2: 26.8 mg, 0.089 mmol, 89% yield; 99:1 er (48h, 19.2 mg of starting material). ^1H NMR (400 MHz, CDCl_3) δ = 7.11 (d, J = 8.7 Hz, 2H), 6.81 (d, J = 8.7 Hz, 2H), 6.68 (m, 3H), 5.88 (s, 2H), 4.44 (t, J = 7.8 Hz, 1H), 3.75 (s, 3H), 3.08 (app. d, J = 7.8 Hz, 2H), 2.07 (s, 3H). ^{13}C NMR (100 MHz, CDCl_3) δ = 207.0, 158.0, 147.7, 145.9, 138.1, 136.0, 128.4, 120.3, 113.9, 108.15, 108.12, 100.8, 55.1, 49.9, 44.9, 30.6. IR (neat): 2899, 1712, 1608, 1509, 1484, 1438, 1358, 1243, 1177, 1033, 923, 806 cm^{-1} . HRMS (CI) m/z : calculated for $\text{C}_{18}\text{H}_{18}\text{O}_4$ 298.1205, found 298.1206

4.6.5.2. Synthesis of 4-(benzo[*d*][1,3]dioxo-5-yl)-4-(4-methylthiophenyl)butan-2-one
(329)



See general procedure for conjugate addition reaction above. The crude reaction mixture was purified via flash column chromatography with 100% dichloromethane as the eluent. HPLC Chiralpak ID (hexane/*i*-PrOH = 90:10, 0.75 mL/min, UV-254 detector). Trial 1: 24.7 mg, 0.078 mmol, 77% yield; 99:1 er (46h, 19.5 mg of starting material). Trial 2: 23.3 mg, 0.074 mmol, 72% yield; 99:1 er (46h, 19.5 mg of starting material). ^1H NMR (400 MHz, CDCl_3) δ = 7.16 (dd, J = 6.4 Hz; 1.8 Hz, 2H), 7.11 (dd, J = 6.6 Hz; 1.8 Hz, 2H), 6.68 (m, 3H), 5.89 (s, 2H), 4.45 (t, J = 7.3 Hz, 1H), 3.09 (app. d, J = 7.3 Hz, 2H), 2.43 (s, 3H), 2.08 (s, 3H). ^{13}C NMR (100 MHz, CDCl_3) δ = 206.7, 147.7, 146.0, 140.8, 137.6, 136.2, 127.9, 126.9, 120.4, 108.2, 108.1, 100.9, 49.6, 45.0, 30.6, 15.9. **IR (neat):** 2919, 1712, 1598, 1485, 1438, 1357, 1227, 1158, 1094, 1035, 1014, 924, 805 cm^{-1} . HRMS (CI) m/z : calculated for $\text{C}_{18}\text{H}_{18}\text{O}_3\text{S}$ 314.0977, found 314.0976.

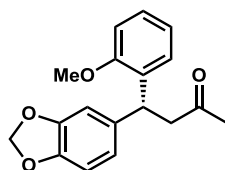
4.6.5.3. Synthesis of 4-(benzo[*d*][1,3]dioxo-5-yl)-4-(4-dimethylaminophenyl)butan-2-one



See general procedure for conjugate addition reaction above. The crude reaction mixture was purified via flash column chromatography with 20% ethyl acetate in hexanes as the eluent. HPLC Chiralpak ID (hexane/*i*-PrOH = 95:5, 0.75 mL/min, UV-254 detector). Trial 1: 31.1 mg, 0.099 mmol, 94% yield; 98:2 er (3h, 20.3 mg of starting material, 50 mg of 4 Å molecular sieves was used in place of LiBr). Trial 2: 29.4 mg,

0.094 mmol, 93% yield; 97:3 er (3h, 19.3 mg of starting material, 50 mg of 4 Å molecular sieves was used in place of LiBr). ¹H NMR (400 MHz, CDCl₃) δ = 7.06 (d, *J* = 9.1 Hz, 2H), 6.69-6.63 (m, 5H), 5.88 (s, 2H), 4.40 (t, *J* = 7.8 Hz, 1H), 3.08 (app. d, *J* = 7.8 Hz, 2H), 2.89 (s, 6H), 2.07 (s, 3H). ¹³C NMR (100 MHz, CDCl₃) δ = 207.8, 149.1, 147.6, 145.7, 138.6, 131.7, 128.0, 120.3, 112.7, 108.1, 108.0, 100.8, 50.0, 44.9, 40.6, 30.6. IR (neat): 2884, 1710, 1608, 1519, 1481, 1434, 1342, 1242, 1193, 1163, 1123, 938, 829, 812 cm⁻¹. HRMS (CI) *m/z*: calculated for C₁₉H₂₁NO₃ 311.1521, found 311.1515

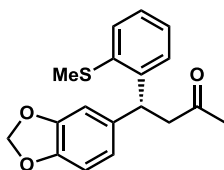
4.6.5.4. Synthesis of 4-(benzo[*d*][1,3]dioxo-5-yl)-4-(2-methoxyphenyl)butan-2-one (331)



See general procedure for conjugate addition reaction above. The crude reaction mixture was purified via flash column chromatography with 10-20% ethyl acetate in hexanes as the eluent. HPLC Chiralcel OD-H (hexane/*i*-PrOH = 90:10, 0.75 mL/min, UV-254 detector). Trial 1: 29.4 mg, 0.098 mmol, 92% yield (15h, 20.3 mg of starting material). Trial 2: 25.7 mg, 0.086 mmol, 86% yield; 99:1 er (15h, 19.0 mg of starting material). Trial 3: 27.6 mg, 0.092 mmol, 92% yield; 99:1 er (15h, 19.1 mg of starting material). ¹H NMR (400 MHz, CDCl₃) δ = 7.17 (td, *J* = 7.8 Hz; 1.8 Hz, 1H), 7.08 (dd, *J* = 7.8 Hz; 1.8 Hz, 1H), 6.88 (td, *J* = 7.8 Hz; 0.9 Hz, 1H), 6.83 (d, *J* = 8.2 Hz, 1H), 6.71 (m, 3H), 5.88 (s, 2H), 4.89 (t, *J* = 7.8 Hz, 1H), 3.80 (s, 3H), 3.12 (dd, *J* = 16.0 Hz; 8.2 Hz, 1H), 3.05 (dd, *J* = 16.0 Hz; 7.3 Hz, 1H), 2.09 (s, 3H). ¹³C NMR (100 MHz, CDCl₃) δ =

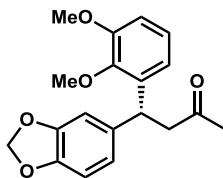
207.3, 156.5, 147.4, 145.7, 137.3, 132.1, 127.58, 127.55, 120.7, 120.5, 110.7, 108.5, 108.0, 100.7, 55.3, 49.0, 39.0, 30.2. IR (neat): 2921, 1712, 1598, 1485, 1437, 1356, 1240, 1159, 1111, 1034, 923, 808, 751 cm^{-1} . HRMS (CI) m/z : calculated for $\text{C}_{18}\text{H}_{18}\text{O}_4$ 298.1205, found 298.1206.

4.6.5.5. Synthesis of 4-(benzo[*d*][1,3]dioxo-5-yl)-4-(2-methylthiophenyl)butan-2-one (332)



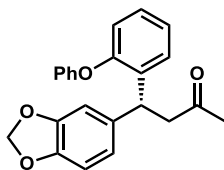
See general procedure for conjugate addition reaction above. The crude reaction mixture was purified via flash column chromatography with 100% dichloromethane as the eluent. HPLC Chiralcel OD-H (hexane/*i*-PrOH = 90:10, 0.75 mL/min, UV-254 detector). Trial 1: 30.4 mg, 0.097 mmol, 96% yield (15h, 19.2 mg of starting material). Trial 2: 30.9 mg, 0.098 mmol, 97% yield; 98:2 er (15h, 19.3 mg of starting material). Trial 3: 30.3 mg, 0.096 mmol, 96% yield; 98:2 er (15h, 19.1 mg of starting material). ^1H NMR (400 MHz, CDCl_3) δ = 7.22-7.11 (m, 4H), 6.71 (m, 3H), 5.88 (m, 2H), 4.99 (t, J = 7.8 Hz, 1H), 3.09 (app. d, J = 7.3 Hz, 2H), 2.43 (s, 3H), 2.10 (s, 3H). ^{13}C NMR (100 MHz, CDCl_3) δ = 206.6, 147.6, 145.9, 141.4, 137.3, 136.5, 127.1, 126.7, 126.2, 125.0, 121.0, 108.6, 108.0, 100.8, 49.8, 41.9, 30.1, 16.1. IR (neat): 2919, 1713, 1484, 1437, 1358, 1234, 1155, 1035, 923, 809, 744 cm^{-1} . HRMS (CI) m/z : calculated for $\text{C}_{18}\text{H}_{18}\text{O}_3\text{S}$ 314.0977, found 314.0977

4.6.5.6. Synthesis of 4-(benzo[*d*][1,3]dioxo-5-yl)-4-(2,3-dimethoxyphenyl)butan-2-one (333)



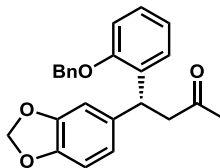
See general procedure for conjugate addition reaction above. The crude reaction mixture was purified via flash column chromatography with 100% dichloromethane as the eluent. HPLC Chiralpak ID (hexane/*i*-PrOH = 90:10, 0.75 mL/min, UV-254 detector). Trial 1: 31.9 mg, 0.097 mmol, 95% yield (24h, 19.5 mg of starting material). Trial 2: 28.6 mg, 0.087 mmol, 86% yield; 99.5:0.5 er (24h, 19.3 mg of starting material). Trial 3: 27.6 mg, 0.084 mmol, 83% yield; 99.5:0.5 er (24h, 19.2 mg of starting material). ^1H NMR (400 MHz, CDCl_3) δ = 6.99 (t, J = 8.0 Hz, 1H), 6.77 (d, J = 7.3 Hz, 2H), 6.73-6.67 (m, 3H), 5.87 (s, 2H), 4.89 (t, J = 7.8 Hz, 1H), 3.82 (s, 3H), 3.70 (s, 3H), 3.09 (app. d, J = 7.3 Hz, 2H), 2.09 (s, 3H). ^{13}C NMR (100 MHz, CDCl_3) δ = 206.9, 152.8, 147.5, 146.4, 145.7, 137.6, 137.5, 123.8, 120.6, 119.2, 110.6, 108.3, 108.0, 100.8, 60.4, 55.5, 49.2, 39.1, 30.3. IR (neat): 2934, 2834, 1712, 1583, 1475, 1439, 1358, 1273, 1223, 1165, 1087, 1036, 1003, 928, 804, 747 cm^{-1} . HRMS (CI) m/z : calculated for $\text{C}_{19}\text{H}_{20}\text{O}_5$ 328.1311, found 328.1312.

4.6.5.7. Synthesis of 4-(benzo[*d*][1,3]dioxo-5-yl)-4-(2-phenoxyphenyl)butan-2-one
(334)



See general procedure for conjugate addition reaction above. The crude reaction mixture was purified via flash column chromatography with 100% dichloromethane as the eluent. HPLC Chiralpak ID (hexane/*i*-PrOH = 90:10, 0.75 mL/min, UV-254 detector). Trial 1: 24.6 mg, 0.068 mmol, 66% yield (39h, 19.5 mg of starting material). Trial 2: 31 mg, 0.086 mmol, 85% yield; 93:7 er (39h, 19.3 mg of starting material). Trial 3: 29.9 mg, 0.083 mmol, 80% yield; 95:5 er (39h, 19.8 mg of starting material). ^1H NMR (400 MHz, CDCl_3) δ = 7.31-7.24 (m, 3H), 7.14 (td, J = 7.3 Hz; 1.8 Hz, 1H), 7.09-7.03 (m, 2H), 6.88-6.82 (m, 3H), 6.70-6.64 (m, 3H), 5.87 (s, 2H), 4.88 (t, J = 7.8 Hz, 1H), 3.14 (m, 2H), 2.07 (s, 3H). ^{13}C NMR (100 MHz, CDCl_3) δ = 206.7, 157.4, 154.1, 147.5, 145.8, 136.8, 135.1, 129.6, 128.1, 127.7, 123.8, 122.8, 120.8, 119.5, 118.1, 108.4, 108.0, 100.8, 48.9, 39.5, 30.1. IR (neat): 2891, 1714, 1578, 1501, 1482, 1440, 1357, 1225, 1159, 1036, 925, 872, 802, 748, 691 cm^{-1} . HRMS (CI) m/z : calculated for $\text{C}_{23}\text{H}_{20}\text{O}_4$ 360.1362, found 360.1367

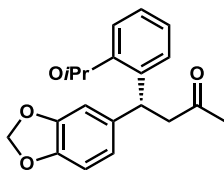
4.6.5.8. Synthesis of 4-(benzo[*d*][1,3]dioxo-5-yl)-4-(2-benzyloxyphenyl)butan-2-one
(335)



See general procedure for conjugate addition reaction above. The crude reaction mixture was purified via flash column chromatography with 100% dichloromethane as the eluent. HPLC Chiralpak ID (hexane/*i*-PrOH = 90:10, 0.75 mL/min, UV-254 detector). Trial 1: 34.3 mg, 0.092 mmol, 90% yield (17h, 19.5 mg of starting material). Trial 2: 34.8 mg, 0.093 mmol, 92% yield; 99:1 er (17h, 19.1 mg of starting material). Trial 3: 34.9 mg, 0.093 mmol, 91% yield; 99:1 er (17h, 19.4 mg of starting material). ¹H NMR (400 MHz, CDCl₃) δ = 7.38-7.30 (m, 5H), 7.18-7.13 (m, 2H), 6.93-6.88 (m, 2H), 6.69 (s, 1H), 6.68 (s, 2H), 5.89 (s, 2H), 5.04 (s, 2H), 4.93 (t, *J* = 7.3 Hz, 1H), 3.10 (m, 2H), 2.04 (s, 3H). ¹³C NMR (100 MHz, CDCl₃) δ = 207.2, 155.6, 147.4, 145.7, 137.2, 136.9, 132.3, 128.4, 127.8, 127.6, 127.5, 127.3, 120.9, 120.7, 111.9, 108.6, 107.9, 100.7, 48.9, 39.4, 30.1. IR (neat): 3031, 2866, 2772, 1703, 1596, 1484, 1449, 1442, 1358, 1244, 1232, 1116, 1039, 1017, 938, 809, 749, 697 cm⁻¹. HRMS (CI) *m/z*: calculated for C₂₄H₂₂O₄ 374.1518, found 374.1519.

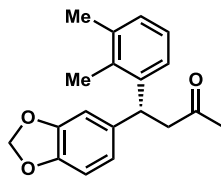
4.6.5.9. Synthesis of 4-(benzo[*d*][1,3]dioxo-5-yl)-4-(2-isopropoxyphenyl)butan-2-one

(336)



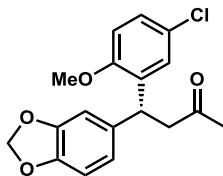
See general procedure for conjugate addition reaction above. The crude reaction mixture was purified via flash column chromatography with 100% dichloromethane as the eluent. HPLC Chiralpak ID (hexane/*i*-PrOH = 90:10, 0.75 mL/min, UV-254 detector). Trial 1: 31.7 mg, 0.085 mmol, 83% yield (4h, 19.3 mg of starting material, 2 equiv of LiBr). Trial 2: 33.5 mg, 0.089 mmol, 90% yield; 98:2 er (4h, 19.0 mg of starting material, 2 equiv of LiBr). Trial 3: 33.9 mg, 0.090 mmol, 88% yield; 98:2 er (4h, 19.5 mg of starting material, 2 equiv of LiBr). ¹H NMR (400 MHz, CDCl₃) δ = 7.15-7.08 (m, 2H), 6.86-6.80 (m, 2H), 6.72-6.67 (m, 3H), 5.88 (dd, *J* = 2.7 Hz; 1.4 Hz, 2H), 4.85 (t, *J* = 7.8 Hz, 1H), 4.55 (sep, *J* = 5.9 Hz, 1H), 3.08 (app. d, *J* = 7.8 Hz, 2H), 2.08 (s, 3H), 1.32 (d, *J* = 5.9 Hz, 3H), 1.23 (d, *J* = 5.9 Hz, 3H). ¹³C NMR (100 MHz, CDCl₃) δ = 207.4, 154.7, 147.3, 145.6, 137.4, 132.9, 127.6, 127.3, 120.9, 120.0, 112.6, 108.7, 107.8, 100.7, 69.5, 48.8, 39.5, 30.1, 22.0, 21.9. IR (neat): 2974, 2898, 1713, 1484, 1451, 1439, 1234, 1116, 1036, 935, 808, 749 cm⁻¹. HRMS (CI) *m/z*: calculated for C₂₀H₂₂O₄ 326.1518, found 326.1522.

4.6.5.10. Synthesis of 4-(benzo[*d*][1,3]dioxo-5-yl)-4-(2,3-dimethylphenyl)butan-2-one
(337)



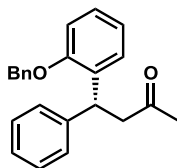
See general procedure for conjugate addition reaction above. The crude reaction mixture was purified via flash column chromatography with 100% dichloromethane as the eluent. HPLC Chiralcel OD-H (hexane/*i*-PrOH = 90:10, 0.75 mL/min, UV-254 detector). Trial 1: 21.9 mg, 0.074 mmol, 73% yield (48h, 19.2 mg of starting material). Trial 2: 21.0 mg, 0.071 mmol, 71% yield; 99:1 er (48h, 19.0 mg of starting material). Trial 3: 25.1 mg, 0.085 mmol, 80% yield; 99:1 er (48h, 20.0 mg of starting material). ¹H NMR (400 MHz, CDCl₃) δ = 7.08-7.01 (m, 3H), 6.69-6.63 (m, 3H), 5.88 (dd, *J* = 5.8 Hz; 1.3 Hz, 2H), 4.76 (t, *J* = 7.3 Hz, 1H), 3.08 (app. d, *J* = 7.3 Hz, 2H), 2.25 (s, 3H), 2.18 (s, 3H), 2.08 (s, 3H). ¹³C NMR (100 MHz, CDCl₃) δ = 207.0, 147.6, 145.7, 141.3, 137.7, 137.2, 134.7, 128.2, 125.3, 123.9, 120.9, 108.4, 108.0, 100.8, 50.3, 41.8, 30.7, 21.0, 15.0. IR (neat): 2919, 1713, 1502, 1484, 1438, 1356, 1239, 1157, 1036, 926, 809, 786 cm⁻¹. HRMS (CI) *m/z*: calculated for C₁₉H₂₀O₃ 296.1412, found 296.1416

4.6.5.11. Synthesis of 4-(benzo[*d*][1,3]dioxo-5-yl)-4-(2-methoxy-5-chlorophenyl)butan-2-one (338)



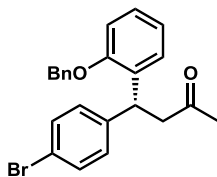
The crude reaction mixture was purified via flash column chromatography with 100% dichloromethane as the eluent. HPLC Chiralpak ID (hexane/*i*-PrOH = 90:10, 0.75 mL/min, UV-254 detector). Trial 1: 26.1 mg, 0.078 mmol, 77% yield (15h, 19.3 mg of starting material, 2 equiv of LiBr). Trial 2: 32.4 mg, 0.097 mmol, 96% yield; 94:6 er (15h, 19.3 mg of starting material, 2 equiv of LiBr). Trial 3: 32.8 mg, 0.098 mmol, 96% yield; 96:4 er (15h, 19.5 mg of starting material, 2 equiv of LiBr). ^1H NMR (400 MHz, CDCl_3) δ = 7.11 (dd, J = 8.7 Hz; 2.7 Hz, 1H), 7.02 (d, J = 2.7 Hz, 1H), 6.74 (d, J = 8.7 Hz, 1H), 6.70 (m, 3H), 5.90 (s, 2H), 4.85 (dd, J = 8.2 Hz; 6.7 Hz, 1H), 3.78 (s, 3H), 3.06 (m, 2H), 2.10 (s, 3H). ^{13}C NMR (100 MHz, CDCl_3) δ = 206.6, 155.2, 147.6, 146.0, 136.4, 134.2, 127.5, 127.1, 125.4, 120.7, 111.9, 108.5, 108.1, 100.8, 55.7, 48.6, 38.7, 30.3. IR (neat): 2900, 1712, 1484, 1439, 1241, 1126, 1034, 925, 807 cm^{-1} . HRMS (CI) m/z : calculated for $\text{C}_{18}\text{H}_{17}\text{O}_4^{35}\text{Cl}$ 332.0815, found 332.0816; calculated for $\text{C}_{18}\text{H}_{17}\text{O}_4^{37}\text{Cl}$ 334.0786, found 334.0788

4.6.5.12. Synthesis of 4-(2-benzyloxyphenyl)-4-phenylbutan-2-one (340)



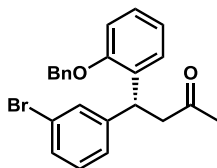
See general procedure for conjugate addition reaction above. The crude reaction mixture was purified via flash column chromatography with 100% dichloromethane as the eluent. HPLC Chiralcel OD-H (hexane/i-PrOH = 90:10, 0.75 mL/min, UV-254 detector). Trial 1: 31.2 mg, 0.094 mmol, 95% yield (23h, 14.5 mg of starting material). Trial 2: 29.1 mg, 0.088 mmol, 87% yield; 99.5:0.5 er (23h, 14.7 mg of starting material). Trial 3: 29.8 mg, 0.090 mmol, 88% yield; 99.5:0.5 er (23h, 14.9 mg of starting material). ^1H NMR (400 MHz, CDCl_3) δ = 7.37-7.14 (m, 12H), 6.93-6.87 (m, 2H), 5.03 (m, 3H), 3.21-3.09 (m, 2H), 2.04 (s, 3H). ^{13}C NMR (100 MHz, CDCl_3) δ = 207.3, 155.7, 143.3, 136.9, 132.2, 128.4, 128.2, 128.0, 127.8, 127.7, 127.5, 127.3, 126.1, 120.7, 111.9, 69.9, 48.8, 39.8, 30.1. IR (neat): 3060, 2904, 2862, 1708, 1599, 1490, 1449, 1353, 1251, 1236, 1160, 1117, 1024, 746, 695 cm^{-1} . HRMS (CI) m/z : calculated for $\text{C}_{23}\text{H}_{22}\text{O}_2$ 330.1620, found 330.1617

4.6.5.13. Synthesis of 4-(2-benzyloxyphenyl)-4-(4-bromophenyl)butan-2-one (341)



See general procedure for conjugate addition reaction above. The crude reaction mixture was purified via flash column chromatography with 100% dichloromethane as the eluent. HPLC Chiralcel OD-H (hexane/*i*-PrOH = 90:10, 0.75 mL/min, UV-254 detector). Trial 1: 39 mg, 0.095 mmol, 96% yield (16h, 22.3 mg of starting material). Trial 2: 36 mg, 0.088 mmol, 88% yield; 99.5:0.5:2 er (16h, 22.5 mg of starting material). Trial 3: 36.5 mg, 0.089 mmol, 90% yield; 99:1 er (16h, 22.4 mg of starting material). ^1H NMR (500 MHz, CDCl_3) δ = 7.38-7.32 (m, 5H), 7.25 (m, 2H), 7.16 (td, J = 7.4 Hz; 1.7 Hz, 2H), 7.06 (d, J = 8.0 Hz, 2H), 6.91 (td, J = 7.4 Hz; 1.1 Hz, 2H), 5.03 (d, J = 11.7 Hz, 1H), 5.00 (d, J = 11.7 Hz, 1H), 4.93 (t, J = 7.7 Hz, 1H), 3.13 (m, 2H), 2.05 (s, 3H). ^{13}C NMR (125.77 MHz, CDCl_3) δ = 206.7, 155.7, 142.5, 136.7, 131.6, 131.2, 129.8, 128.4, 127.89, 127.81, 127.6, 127.4, 120.7, 119.8, 111.9, 69.9, 48.4, 39.3, 30.2. IR (neat): 3057, 3034, 2910, 2885, 1709, 1597, 1584, 1484, 1450, 1410, 1381, 1247, 1224, 1009, 814, 712 cm^{-1} . HRMS (CI) m/z : calculated for $\text{C}_{23}\text{H}_{21}\text{O}_2^{79}\text{Br}$ 408.0725, found 408.0714; calculated for $\text{C}_{23}\text{H}_{21}\text{O}_2^{81}\text{Br}$ 410.0704, found 410.0693

4.6.5.14. Synthesis of 4-(2-benzyloxyphenyl)-4-(3-bromophenyl)butan-2-one (342)



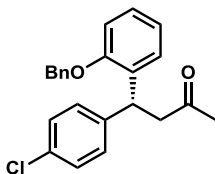
See general procedure for conjugate addition reaction above. The crude reaction mixture was purified via flash column chromatography with 100% dichloromethane as the eluent. HPLC Chiralpak ID (hexane/*i*-PrOH = 90:10, 0.75 mL/min, UV-254 detector). Trial 1: 34.9 mg, 0.085 mmol, 86% yield (15h, 22.2 mg of starting material). Trial 2: 34.9 mg, 0.085 mmol, 86% yield; 93:7 er (15h, 22.2 mg of starting material). Trial 3: 33.4 mg, 0.082 mmol, 80% yield; 96:4 er (15h, 22.9 mg of starting material). ^1H NMR (400 MHz, CDCl_3) δ = 7.40-7.25 (m, 7H), 7.21-7.06 (m, 4H), 6.95-6.88 (m, 2H), 5.01 (s, 2H), 4.94 (t, J = 7.5 Hz, 1H), 3.14 (m, 2H), 2.06 (s, 3H). ^{13}C NMR (100 MHz, CDCl_3) δ = 206.6, 155.7, 145.9, 136.7, 131.4, 131.0, 129.7, 129.2, 128.5, 127.8, 127.7, 127.4, 126.7, 122.36, 122.30, 120.8, 111.9, 48.3, 39.5, 30.2. IR (neat): 3031, 2917, 1714, 1596, 1567, 1449, 1426, 1246, 1234, 1169, 1022, 850, 749, 738, 694 cm^{-1} . HRMS (CI) m/z : calculated for $\text{C}_{23}\text{H}_{21}\text{O}_2^{79}\text{Br}$ 408.0725, found 408.0719; calculated for $\text{C}_{23}\text{H}_{21}\text{O}_2^{81}\text{Br}$ 410.0704, found 410.0698.

4.6.5.15. Synthesis of 4-(2-benzyloxyphenyl)-4-(2-bromophenyl)butan-2-one (343)



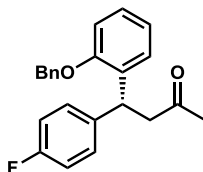
See general procedure for conjugate addition reaction above. The crude reaction mixture was purified via flash column chromatography with 100% dichloromethane as the eluent. HPLC Chiralpak ID (hexane/i-PrOH = 90:10, 0.75 mL/min, UV-254 detector). Trial 1: 36.4 mg, 0.089 mmol, 83% yield (46h, 24.2 mg of starting material). Trial 2: 38.5 mg, 0.094 mmol, 89% yield; 99:1 er (46h, 23.7 mg of starting material). Trial 3: 35.2 mg, 0.086 mmol, 83% yield; 99.5:0.5 er (46h, 23.4 mg of starting material). ^1H NMR (500 MHz, CDCl_3) δ = 7.54 (dd, J = 8.6 Hz,; 1.1 Hz, 1H), 7.33-7.17 (m, 7H), 7.06 (t, J = 7.4 Hz, 3H), 6.91 (m, 2H), 5.39 (dd, J = 8.6 Hz; 6.8 Hz, 1H), 5.07 (d, J = 12.0 Hz, 1H), 5.00 (d, J = 12.0 Hz, 1H), 3.11 (dd, J = 16.0 Hz; 8.8 Hz, 1H), 3.01 (dd, J = 16.0 Hz; 6.9 Hz, 1H), 2.08 (s, 3H). ^{13}C NMR (125.77 MHz, CDCl_3) δ = 206.9, 156.0, 142.4, 136.9, 133.0, 130.3, 128.8, 128.3, 127.9, 127.86, 127.83, 127.7, 127.3, 127.2, 120.6, 111.9, 48.0, 39.8, 29.2. IR (neat): 3031, 2916, 1710, 1598, 1488, 1450, 1354, 1291, 1234, 1156, 1019, 747 cm^{-1} . HRMS (CI) m/z : calculated for $\text{C}_{23}\text{H}_{21}\text{O}_2^{79}\text{Br}$ 408.0725, found 408.0715; calculated for $\text{C}_{23}\text{H}_{21}\text{O}_2^{81}\text{Br}$ 410.0704, found 410.0718.

4.6.5.16. Synthesis of 4-(2-benzyloxyphenyl)-4-(4-chlorophenyl)butan-2-one (344)



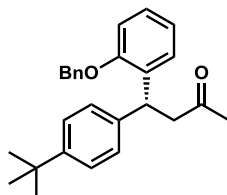
See general procedure for conjugate addition reaction above. The crude reaction mixture was purified via flash column chromatography with 100% dichloromethane as the eluent. HPLC Chiralpak ID (hexane/i-PrOH = 90:10, 0.75 mL/min, UV-254 detector). Trial 1: 34.8 mg, 0.095 mmol, 95% yield (20h, 18 mg of starting material). Trial 2: 28.9 mg, 0.079 mmol, 79% yield; 97:3 er (20h, 18 mg of starting material). Trial 3: 30.2 mg, 0.083 mmol, 82% yield; 97:3 er (20h, 18.3 mg of starting material). ^1H NMR (400 MHz, CDCl_3) δ = 7.38-7.30 (m, 3H), 7.25 (m, 2H), 7.20-7.09 (m, 6H), 6.93 (dd, J = 7.3 Hz; 0.9 Hz, 1H), 6.88 (d, J = 8.2Hz, 1H), 5.03 (d, J = 11.6 Hz, 1H), 4.99 (d, J = 11.6 Hz, 1H), 4.94 (t, J = 7.8 Hz, 1H), 3.13 (m, 2H), 2.05 (s, 3H). ^{13}C NMR (100 MHz, CDCl_3) δ = 206.8, 155.7, 142.0, 136.8, 131.7, 129.4, 128.4, 128.2, 127.9, 127.8, 127.6, 127.4, 120.7, 111.9, 48.5, 39.3, 30.2. IR (neat): 3058, 3035, 2860, 1709, 1596, 1487, 1450, 1412, 1295, 1248, 1225, 1170, 1159, 916, 754, 744 cm^{-1} . HRMS (CI) m/z : calculated for $\text{C}_{23}\text{H}_{20}\text{O}_2\text{Cl}$ 363.1152, found 363.1159.

4.6.5.17. Synthesis of 4-(2-benzyloxyphenyl)-4-(4-fluorophenyl)butan-2-one (345)



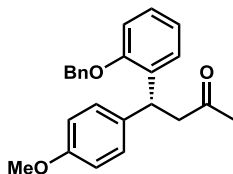
See general procedure for conjugate addition reaction above. The crude reaction mixture was purified via flash column chromatography with 100% dichloromethane as the eluent. HPLC Chiralpak ID (hexane/i-PrOH = 90:10, 0.75 mL/min, UV-254 detector). Trial 1: 33.9 mg, 0.097 mmol, 98% yield (20h, 16.2 mg of starting material). Trial 2: 30 mg, 0.086 mmol, 85% yield; 97:3 er (20h, 16.6 mg of starting material). Trial 3: 26.9 mg, 0.077 mmol, 77% yield; 97:3 er (20h, 16.5 mg of starting material). ^1H NMR (400 MHz, CDCl_3) δ = 7.39-7.26 (m, 5H), 7.21-7.14 (m, 4H), 6.95-6.89 (m, 4H), 5.07-4.97 (m, 3H), 3.14 (m, 2H), 2.06 (s, 3H). ^{13}C NMR (100 MHz, CDCl_3) δ = 206.9, 162.4, 160.0, 155.7, 136.8, 132.0, 129.5, 129.4, 128.4, 127.8, 127.68, 127.61, 127.3, 120.7, 115.0, 114.8, 111.9, 69.9, 48.7, 39.1, 30.1. ^{19}F NMR (376.17 MHz, DMSO-d_6): δ = -120.3. IR (neat): 3061, 3037, 2922, 2860, 1706, 1597, 1508, 1494, 1457, 1354, 1319, 1297, 1249, 1156, 1118, 1021, 815, 750 cm^{-1} . HRMS (CI) m/z: calculated for $\text{C}_{23}\text{H}_{20}\text{O}_2\text{F}$ 347.1447, found 347.1452

4.6.5.18. Synthesis of 4-(2-benzyloxyphenyl)-4-(4-*t*-butylphenyl)butan-2-one (346)



See general procedure for conjugate addition reaction above. The crude reaction mixture was purified via flash column chromatography with 100% dichloromethane as the eluent. HPLC Chiralpak ID (hexane/*i*-PrOH = 90:10, 0.75 mL/min, UV-254 detector). Trial 1: 22.1 mg, 0.057 mmol, 57% yield (48h, 20.3 mg of starting material). Trial 2: 31.5 mg, 0.081 mmol, 78% yield; 97:3 er (48h, 21 mg of starting material). Trial 3: 31.7 mg, 0.082 mmol, 83% yield; 93:7 er (48h, 20 mg of starting material). ^1H NMR (500 MHz, CDCl_3) δ = 7.35-7.30 (m, 2H), 7.27-7.24 (m, 4H), 7.18-7.12 (m, 5H), 6.93-6.87 (m, 2H), 5.06 (d, J = 12.0 Hz, 1H), 5.03 (d, J = 12.0 Hz, 1H), 5.00 (t, J = 7.7 Hz, 1H), 3.18 (dd, J = 16.0 Hz; 7.4 Hz, 1H), 3.12 (dd, J = 16.6 Hz; 8.0 Hz, 1H), 2.05 (s, 3H), 1.29 (s, 9H). ^{13}C NMR (125.77 MHz, CDCl_3) δ = 207.4, 155.7, 148.7, 140.2, 137.0, 132.5, 128.4, 127.9, 127.7, 127.5, 127.4, 127.3, 125.1, 120.7, 112.0, 48.9, 39.3, 34.3, 31.3, 30.0. IR (neat): 3030, 2959, 2866, 1713, 1597, 1585, 1488, 1450, 1414, 1360, 1237, 1157, 1109, 1015, 828, 749, 695 cm^{-1} . HRMS (CI) m/z : calculated for $\text{C}_{27}\text{H}_{29}\text{O}_2$ 385.2168, found 385.2171.

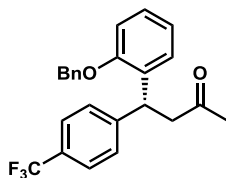
4.6.5.19. Synthesis of 4-(2-benzyloxyphenyl)-4-(4-methoxyphenyl)butan-2-one (347)



See general procedure for conjugate addition reaction above. The crude reaction mixture was purified via flash column chromatography with 100% dichloromethane as the eluent. HPLC Chiralpak ID (hexane/i-PrOH = 90:10, 0.75 mL/min, UV-254 detector). Trial 1: 34.3 mg, 0.095 mmol, 95% yield (15h, 17.7 mg of starting material). Trial 2: 31.1 mg, 0.086 mmol, 85% yield; 99.7:0.3 er (15h, 17.8 mg of starting material). Trial 3: 29 mg, 0.080 mmol, 80% yield; 99.8:0.2 er (15h, 17.8 mg of starting material). ^1H NMR (400 MHz, CDCl_3) δ = 7.38-7.31 (m, 5H), 7.18-7.12 (m, 4H), 6.93-6.88 (m, 2H), 6.79 (d, J = 8.7 Hz, 2H), 5.04 (s, 2H), 4.97 (t, J = 7.5 Hz, 1H), 3.76 (s, 3H), 3.12 (m, 2H), 2.04 (s, 3H). ^{13}C NMR (100 MHz, CDCl_3) δ = 207.4, 157.8, 155.6, 137.0, 135.3, 132.6, 129.0, 128.4, 127.79, 127.74, 127.4, 127.3, 120.7, 113.6, 111.9, 69.9, 55.1, 49.0, 39.0, 30.0. IR (neat): 3060, 3002, 2927, 2875, 1708, 1597, 1510, 1449, 1316, 1280, 1245, 1116, 1037, 821, 785, 755, 698 cm^{-1} . HRMS (CI) m/z : calculated for $\text{C}_{24}\text{H}_{24}\text{O}_3$ 360.1725, found 360.1710.

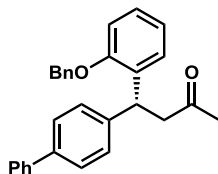
4.6.5.20. Synthesis of 4-(2-benzyloxyphenyl)-4-(4-trifluoromethylphenyl)butan-2-one

(348)



See general procedure for conjugate addition reaction above. The crude reaction mixture was purified via flash column chromatography with 100% dichloromethane as the eluent. HPLC Chiralpak ID (hexane/i-PrOH = 90:10, 0.75 mL/min, UV-254 detector). Trial 1: 38.6 mg, 0.097 mmol, 99% yield (22h, 21.0 mg of starting material). Trial 2: 37.6 mg, 0.094 mmol, 94% yield; 99.5:0.5 er (22h, 21.4 mg of starting material). Trial 3: 37.5 mg, 0.094 mmol, 95% yield; 99:1 er (22h, 21.2 mg of starting material). ^1H NMR (400 MHz, CDCl_3) δ = 7.46 (d, J = 8.2 Hz, 2H), 7.35-7.27 (m, 5H), 7.22-7.17 (m, 4H), 6.69-6.88 (m, 2H), 5.03-4.97 (m, 3H), 3.18 (m, 2H), 2.08 (s, 3H). ^{13}C NMR (100 MHz, CDCl_3) δ = 206.5, 155.8, 147.7, 136.6, 131.2, 128.4, 128.3, 127.99, 127.94, 127.7, 127.4, 125.1, 120.8, 112.0, 69.9, 48.1, 39.7, 30.2. ^{19}F NMR (376.17 MHz, DMSO-d_6): δ = -65.5. IR (neat): 3057, 3034, 2910, 2884, 1709, 1596, 1484, 1450, 1293, 1247, 1224, 1158, 1117, 1010, 754, 744 cm^{-1} . HRMS (CI) m/z : calculated for $\text{C}_{24}\text{H}_{21}\text{O}_2\text{F}_3$ 398.1494, found 398.1483

4.6.5.21. Synthesis of 4-(2-benzyloxyphenyl)-4-(biphenyl-4-yl)butan-2-one (349)



See general procedure for conjugate addition reaction above. The crude reaction mixture was purified via flash column chromatography with 100% dichloromethane as the eluent. HPLC Chiralpak ID (hexane/*i*-PrOH = 90:10, 0.75 mL/min, UV-254 detector). Trial 1: 37.1 mg, 0.091 mmol, 89% yield (15h, 22.6 mg of starting material). Trial 2: 37.1 mg, 0.091 mmol, 89% yield; 99.8:0.2 er (15h, 22.6 mg of starting material). Trial 3: 37.3 mg, 0.092 mmol, 93% yield; 99.8:0.2 er (15h, 22.0 mg of starting material). ^1H NMR (400 MHz, CDCl_3) δ = 7.56 (d, J = 8.2 Hz, 2H), 7.49-7.40 (m, 4H), 7.37-7.27 (m, 8H), 7.23-7.16 (m, 2H), 6.96-6.90 (m, 2H), 5.08-5.04 (m, 3H), 3.76 (s, 3H), 3.21 (m, 2H), 2.08 (s, 3H). ^{13}C NMR (100 MHz, CDCl_3) δ = 207.2, 155.7, 142.5, 136.9, 132.2, 128.6, 128.4, 127.86, 127.81, 127.6, 127.3, 127.0, 126.9, 120.7, 112.0, 69.9, 48.7, 39.5, 30.1. IR (neat): 3028, 2923, 1712, 1597, 1486, 1449, 1354, 1236, 1157, 1116, 1007, 835, 750, 695 cm^{-1} . HRMS (CI) m/z : calculated for $\text{C}_{29}\text{H}_{25}\text{O}_2$ 405.1855, found 405.1852.

4.6.5.22. Synthesis of 4-(2-benzyloxyphenyl)-4-(4-hydroxyphenyl)butan-2-one (350)



See general procedure for conjugate addition reaction above. The crude reaction mixture was purified via flash column chromatography with 20-30% ethyl acetate in hexanes as the eluent. HPLC Chiralpak ID (hexane/*i*-PrOH = 90:10 - 60:40, 0.75 mL/min, UV-254 detector). Trial 1: 18.1 mg, 0.052 mmol, 52% yield (24h, 16.4 mg of starting material). Trial 2: 16.1 mg, 0.046 mmol, 46% yield; 99.5:0.5 er (24h, 16.5 mg of starting material). Trial 3: 18.9 mg, 0.054 mmol, 53% yield; 99.5:0.5 er (24h, 16.6 mg of starting material). ¹H NMR (400 MHz, CDCl₃) δ = 7.38-7.29 (m, 5H), 7.17-7.09 (m, 2H), 7.04 (d, *J* = 8.2 Hz, 2H), 6.89 (m, 2H), 6.65 (dd, *J* = 8.2 Hz; 1.8 Hz, 2H), 5.28 (OH), 5.05 (d, *J* = 12.3 Hz, 1H), 5.02 (d, *J* = 12.3 Hz, 1H), 4.93 (t, *J* = 7.5 Hz, 1H), 3.10 (m, 2H), 2.04 (s, 3H). ¹³C NMR (100 MHz, CDCl₃) δ = 208.6, 155.6, 154.1, 136.9, 134.8, 132.6, 129.2, 128.4, 127.84, 127.82, 127.4, 127.3, 120.7, 115.1, 111.9, 70.0, 49.0, 39.1, 29.9. IR (neat): 3355, 3030, 2923, 1698, 1612, 1596, 1512, 1488, 1449, 1355, 1223, 1172, 1112, 1012, 831, 749 cm⁻¹. HRMS (CI) *m/z*: calculated for C₂₃H₂₁O₃ 345.1491, found 345.1495

4.7. References

1. Arp, F. O.; Fu, G. C. *J. Am. Chem. Soc.* **2005**, *127*, 10482—10483.
2. Do, H.-Q.; Chandrashekar, E. R. R. *J. Am. Chem. Soc.* **2013**, *135*, 16288—16291.
3. Lopez-Perez, A.; Adrio, J.; Carretero, J. C. *Org. Lett.* **2009**, *11*, 5514—5517.

4. Maity, P.; Shacklady-McAtee, D. M.; Yap, G. P. A.; Sirianni, E. R.; Watson, M. P.; *J. Am. Chem. Soc.* **2013**, *135*, 280—285.
5. Zhou, Q.; Srinivas, H. D.; Dasgupta, S.; Watson, M. P. *J. Am. Chem. Soc.* **2013**, *135*, 3307—3310.
6. Takeda, Y.; Ikeda, Y.; Kuroda, A.; Tanaka, S.; Minakata, S. *J. Am. Chem. Soc.* **2014**, *136*, 8544—8547.
7. Imao, D.; Glasspoole, B. W.; Laberge, V. S.; Crudden, C. M. *J. Am. Chem. Soc.* **2009**, *131*, 5024—5025.
8. Sun, C.; Potter, B.; Morken, J. P. *J. Am. Chem. Soc.* **2014**, *136*, 6534—6537.
9. Hayashi, T.; Yamasaki, K. *Chem. Rev.* **2003**, *103*, 2829—2844.
10. Sakuma, S.; Sakai, M.; Itooka, R.; Miyaura, N. *J. Org. Chem.* **2000**, *65*, 5951—5955.
11. Mauleon, P.; Carretero, J. C. *Org. Lett.* **2004**, *6*, 3195—3198.
12. Defieber, C.; Paquin, J.-F.; Carreira, E. M. *Org. Lett.* **2004**, *6*, 3873—3876.
13. Paquin, J.-F.; Defieber, C.; Stepheson, C. R. J., Carreira, E. M. *J. Am. Chem. Soc.* **2005**, *127*, 10850—10851.
14. Hansmann, M. M.; Hasmi, A. S. K.; Lautens, M. *Org. Lett.* **2013**, *15*, 3226—3229.
15. Hayashi, T.; Senda, T.; Ogasawara, M. *J. Am. Chem. Soc.* **2000**, *122*, 10716—10717.
16. (a) Boiteau, J.-G.; Imbos, R.; Minnaard, A. J.; Feringa, B. L. *Org. Lett.* **2003**, *5*, 681—684; (b) Duursma, A., Hoen, R.; Schuppan, J.; Hulst, R., Minnaard, A. J.; Feringa, B. L. *Org. Lett.* **2003**, *5*, 3111—3113; (c) Duursma, A.; Pena, D.; Minnaard, A. J.; Feringa, B. L. *Tetrahedron: Asymmetry* **2005**, *16*, 1901—1904.

17. Wang, Z.-Q.; Feng, C.-G.; Zhang, S.-S.; Xu, M.-H.; Lin, G.-Q. *Angew. Chem., Int. Ed.* **2010**, *49*, 5780
18. Lang, F.; Chen, G.; Li, C.; Xing, J.; Han, F.; Cun, L.; Liao, J. *Chem. Eur. J.* **2011**, *17*, 5242—5245.
19. Xue, F.; Wang, D.; Li, X.; Wan, B. *J. Org. Chem.* **2012**, *77*, 3071—3081.
20. Paras, N.; MacMillan, D. W. C. *J. Am. Chem. Soc.* **2002**, *124*, 7894—7895.
21. Turner, H. M.; Patel, J.; Niljianskul, N.; Chong, J. M. *Org. Lett.* **2011**, *13*, 5796—5799.
22. Luan, Y.; Schaus, S. E. *J. Am. Chem. Soc.* **2012**, *134*, 19965—19968.
23. Lide, D. R.; Kehiaian, H. V. *CRC Handbook of Thermophysical and Thermochemical Data*; CRC Press: Ann Arbor, 1994.
24. Leung, P. S.-W.; Teng, Y.; Toy, P. H. *Org. Lett.* **2010**, *12*, 4996—4999.
25. Wang, Y.-F.; Gao, Y.-R.; Mao, Shuai, Zhang Y.-L.; Guo, D.-D.; Yan, Z.-L.; Guo, S.-H.; Wang, Y.-Q. *Org. Lett.* **2014**, *16*, 1610—1613.
26. Luo, T.; Zhang, R.; Zhang, W.; Shen, X.; Umemoto, T.; Hu, J. *Org. Lett.* **2014**, *16*, 888—891.
27. Chuprajob, T.; Changtam, C.; Chokchaisiri, R.; Chunglok, W.; Sornkaew, N.; Suksamrarn, A. *Bioorg. Med. Chem. Lett.* **2014**, *24*, 2839—2844.
28. Molander, G. A.; Bernardi, C. R. *J. Org. Chem.* **2002**, *67*, 8424—8429.
29. Molander, C.A.; Biolatto, B. *Org. Lett.* **2002**, *4*, 1867—1870.
30. Wilson, P. G.; Percy, J. M.; Redmond, J. M.; McCarter, A. W. *J. Org. Chem.* **2012**, *77*, 6384—6393.

31. Presset, M. ; Oehrich, D. ; Rombouts, F. ; Molander, G. A. *J. Org. Chem.* **2013**, *78*, 12837—12843.
32. Le, P. Q.; Nguyen T. S.; May, J. A. *Org. Lett.* **2012**, *14*, 6104—6107.

APPENDIX TWO

Spectra relevant to Chapter 4:

**Enantioselective synthesis of diarylalkane compounds via BINOL-catalyzed
conjugate addition**

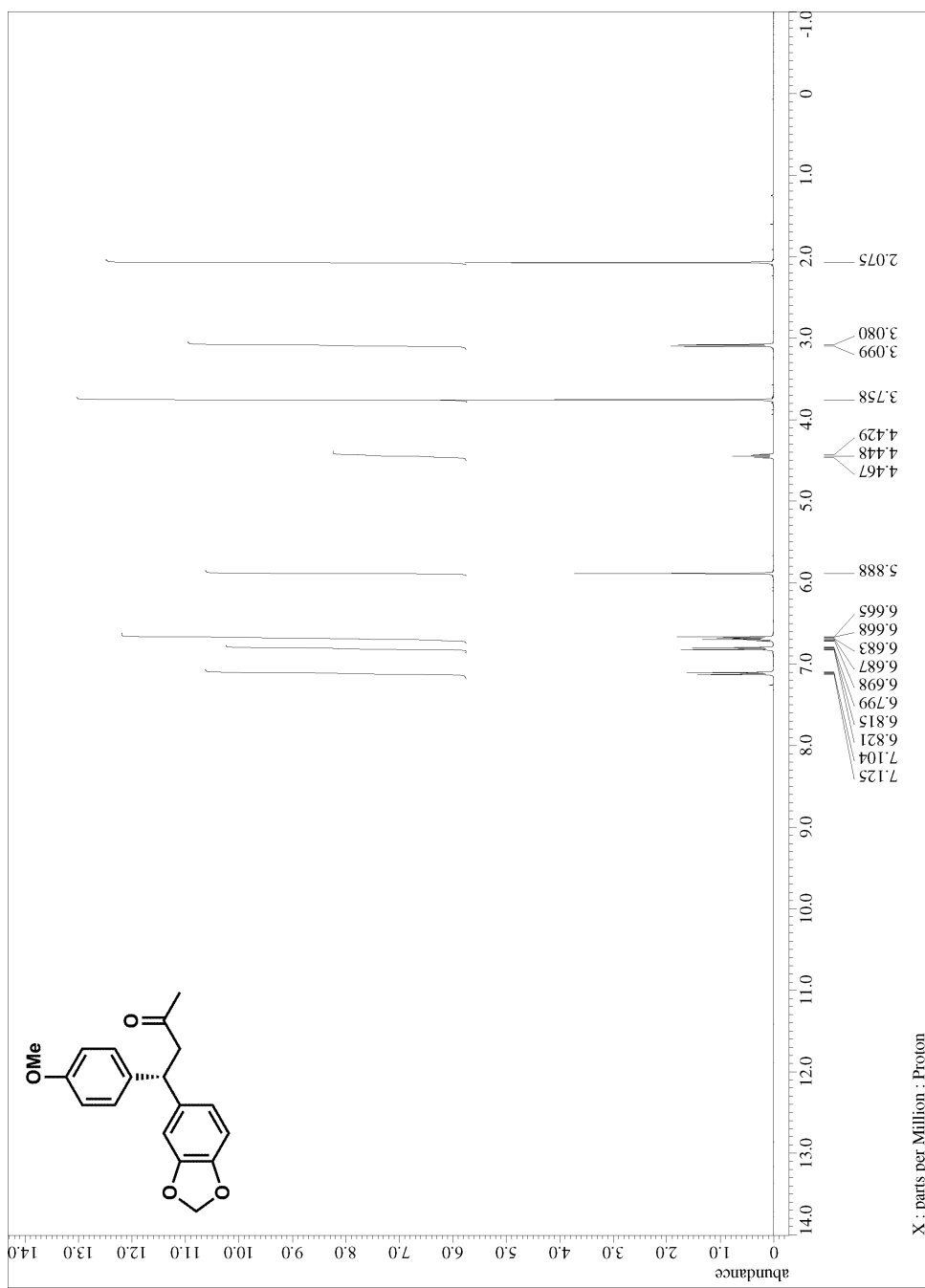


Figure A.2.1. ^1H NMR for compound 328

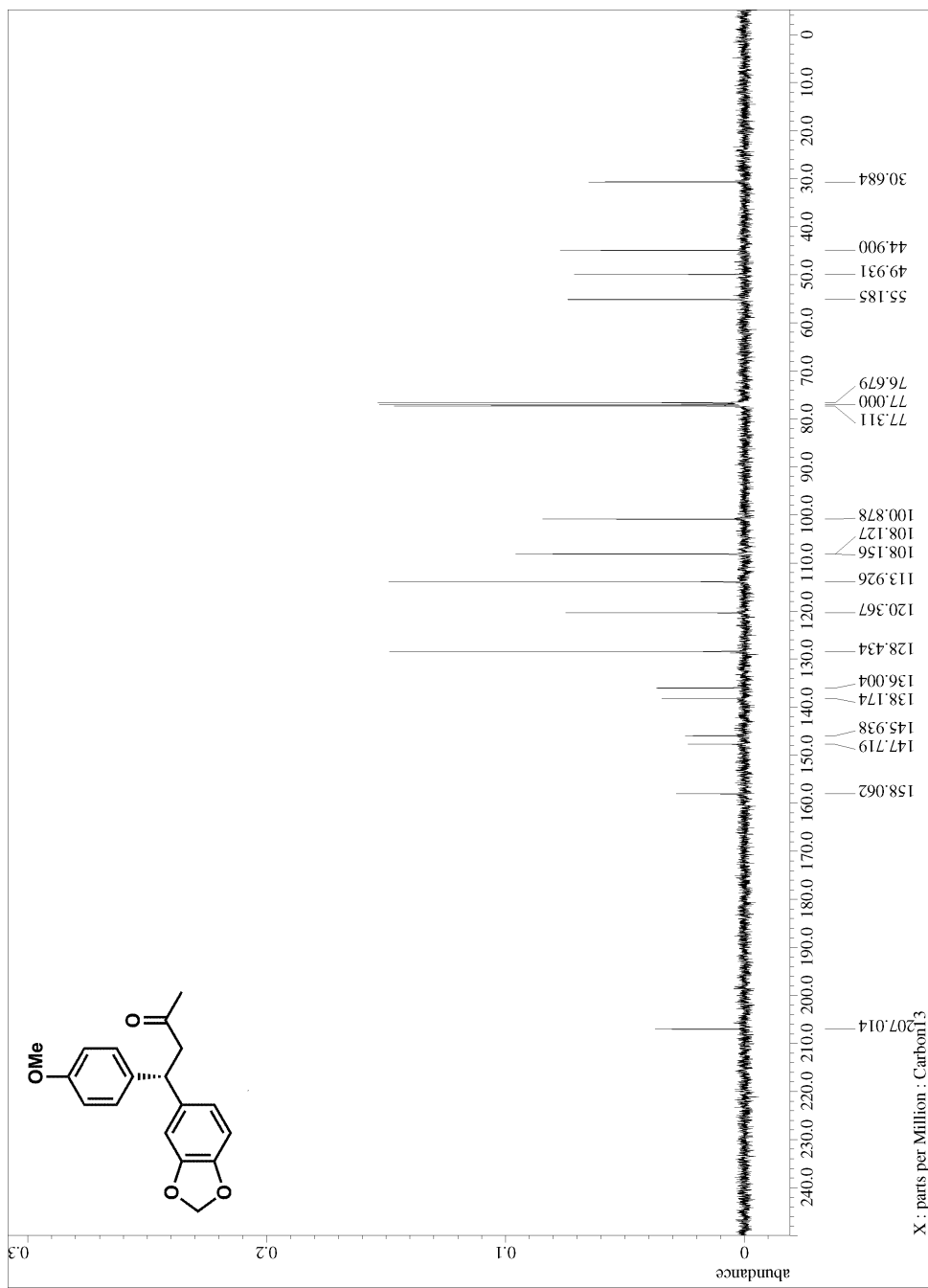
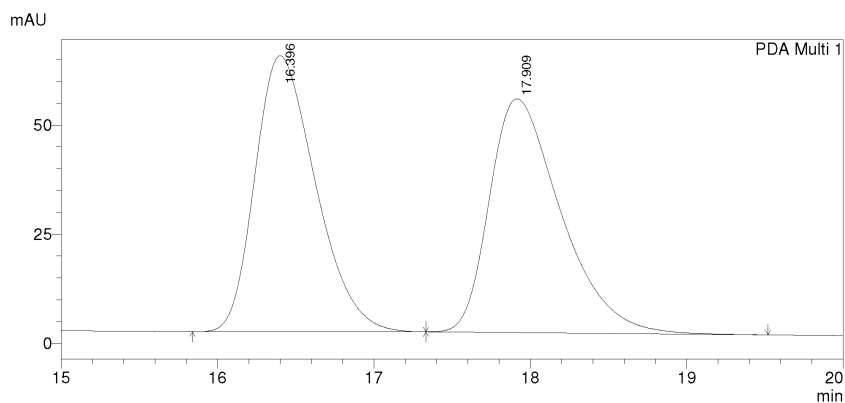


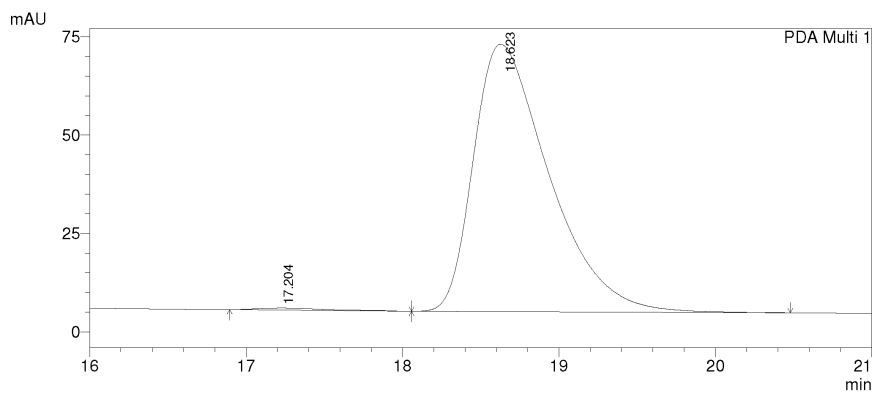
Figure A.2.2. ^{13}C NMR for compound 328



1 PDA Multi 1/254nm 4nm

PeakTable

Peak#	Ret. Time	Area	Height	Area %	Height %
1	16.396	1702075	63255	49.969	54.134
2	17.909	1704173	53595	50.031	45.866
Total		3406247	116850	100.000	100.000



1 PDA Multi 1/254nm 4nm

PeakTable

Peak#	Ret. Time	Area	Height	Area %	Height %
1	17.204	15184	504	0.661	0.736
2	18.623	2281600	67999	99.339	99.264
Total		2296784	68504	100.000	100.000

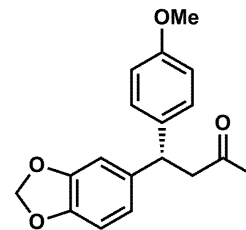


Figure A.2.3. HPLC trace for compound 328

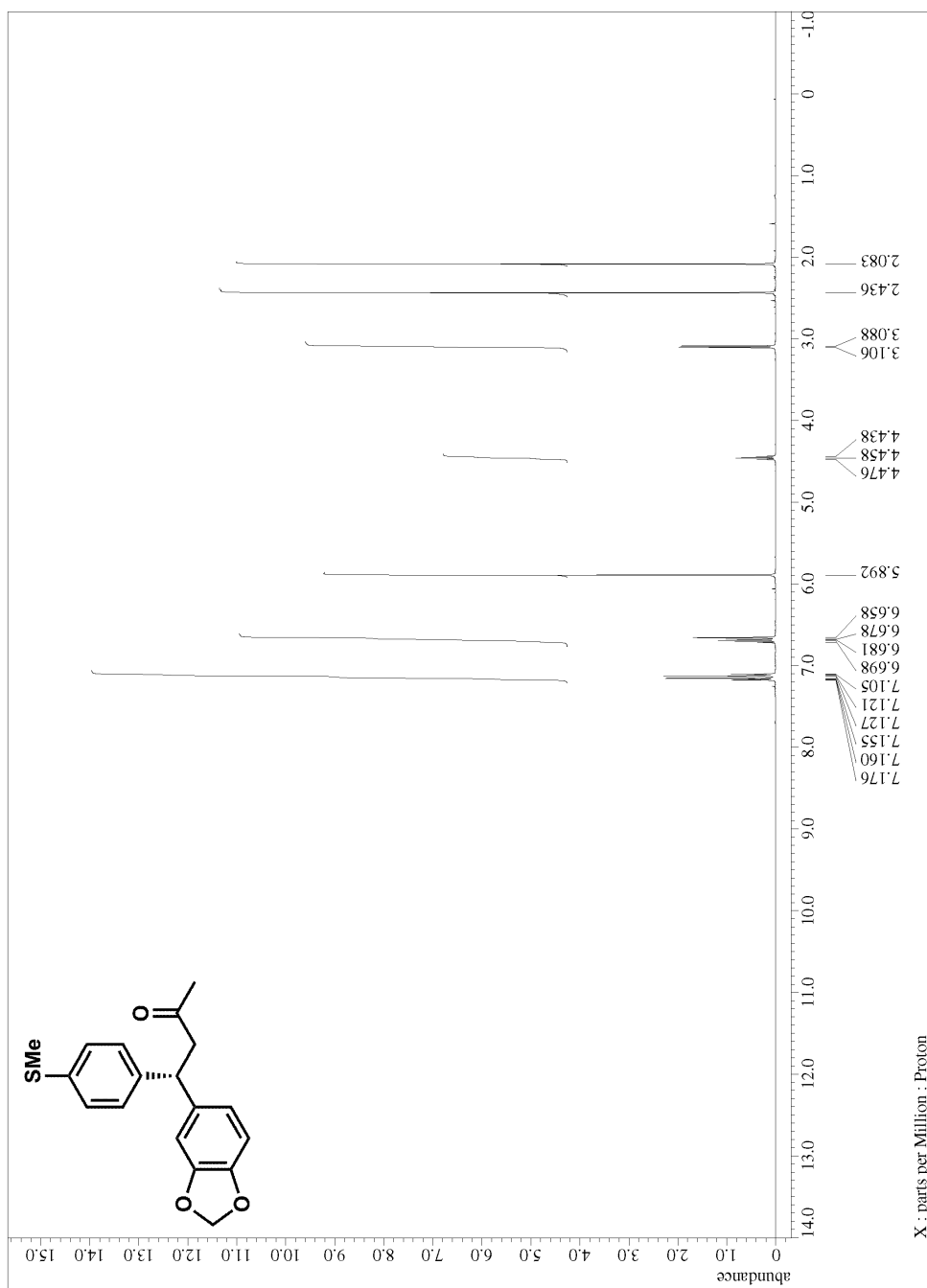


Figure A.2.4. ^1H NMR for compound **329**

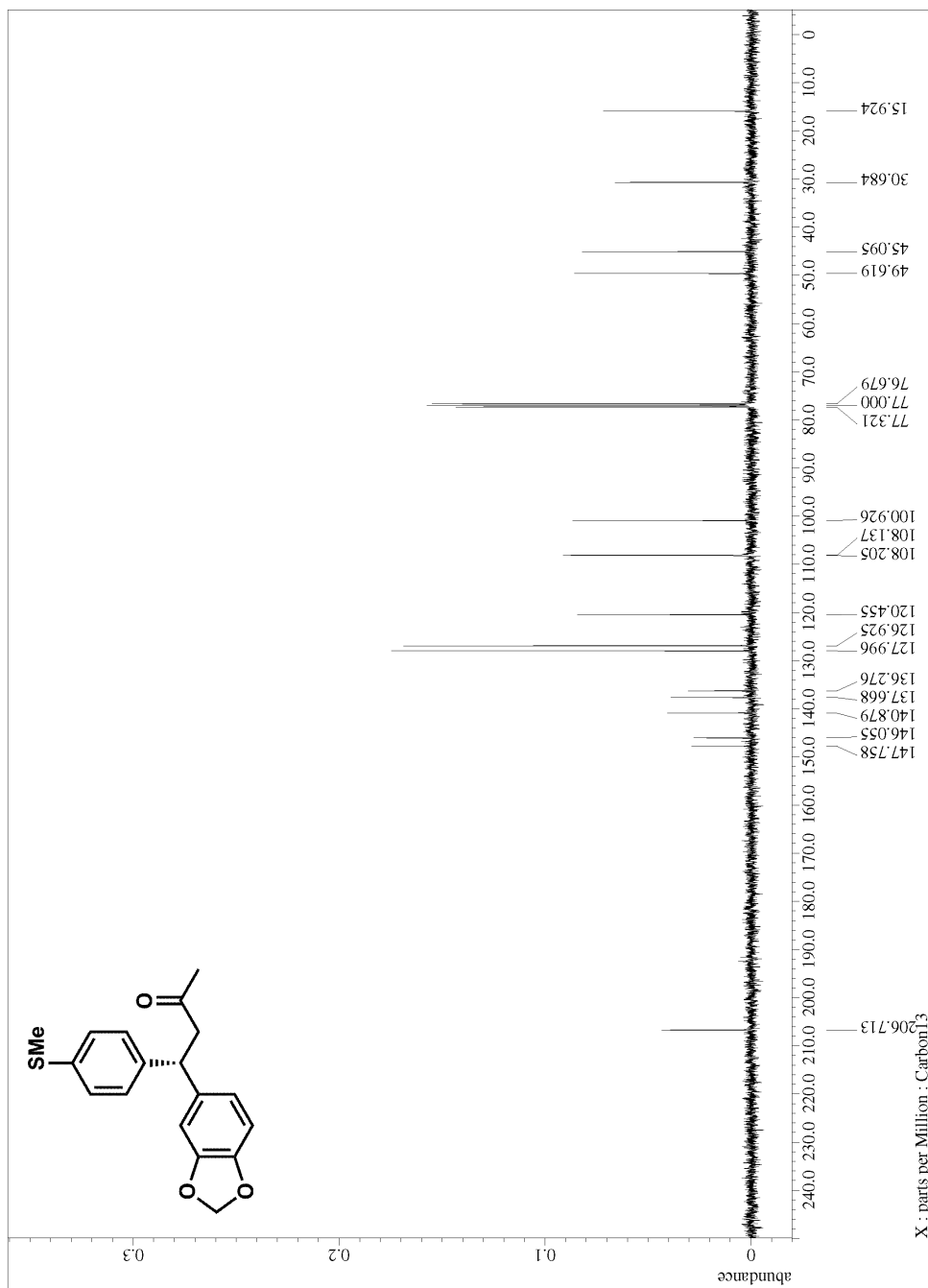
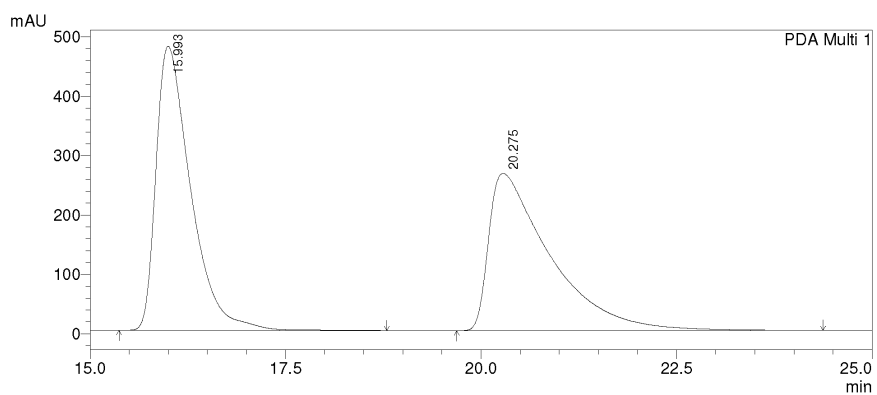


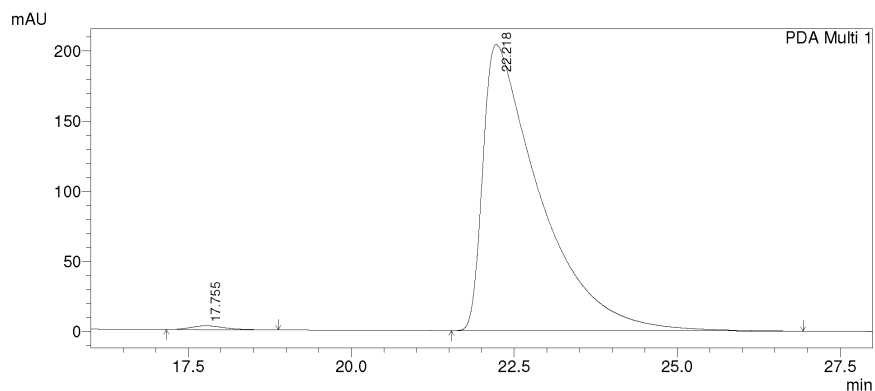
Figure A.2.5. ^{13}C NMR for compound 329



1 PDA Multi 1/254nm 4nm

PeakTable

Peak#	Ret. Time	Area	Height	Area %	Height %
1	15.993	14736504	478433	50.505	64.358
2	20.275	14441804	264963	49.495	35.642
Total		29178309	743396	100.000	100.000



1 PDA Multi 1/254nm 4nm

PeakTable

Peak#	Ret. Time	Area	Height	Area %	Height %
1	17.755	96155	2735	0.769	1.324
2	22.218	12412818	203775	99.231	98.676
Total		12508973	206510	100.000	100.000

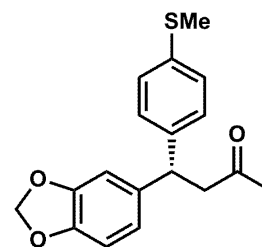


Figure A.2.6. HPLC trace for compound 329

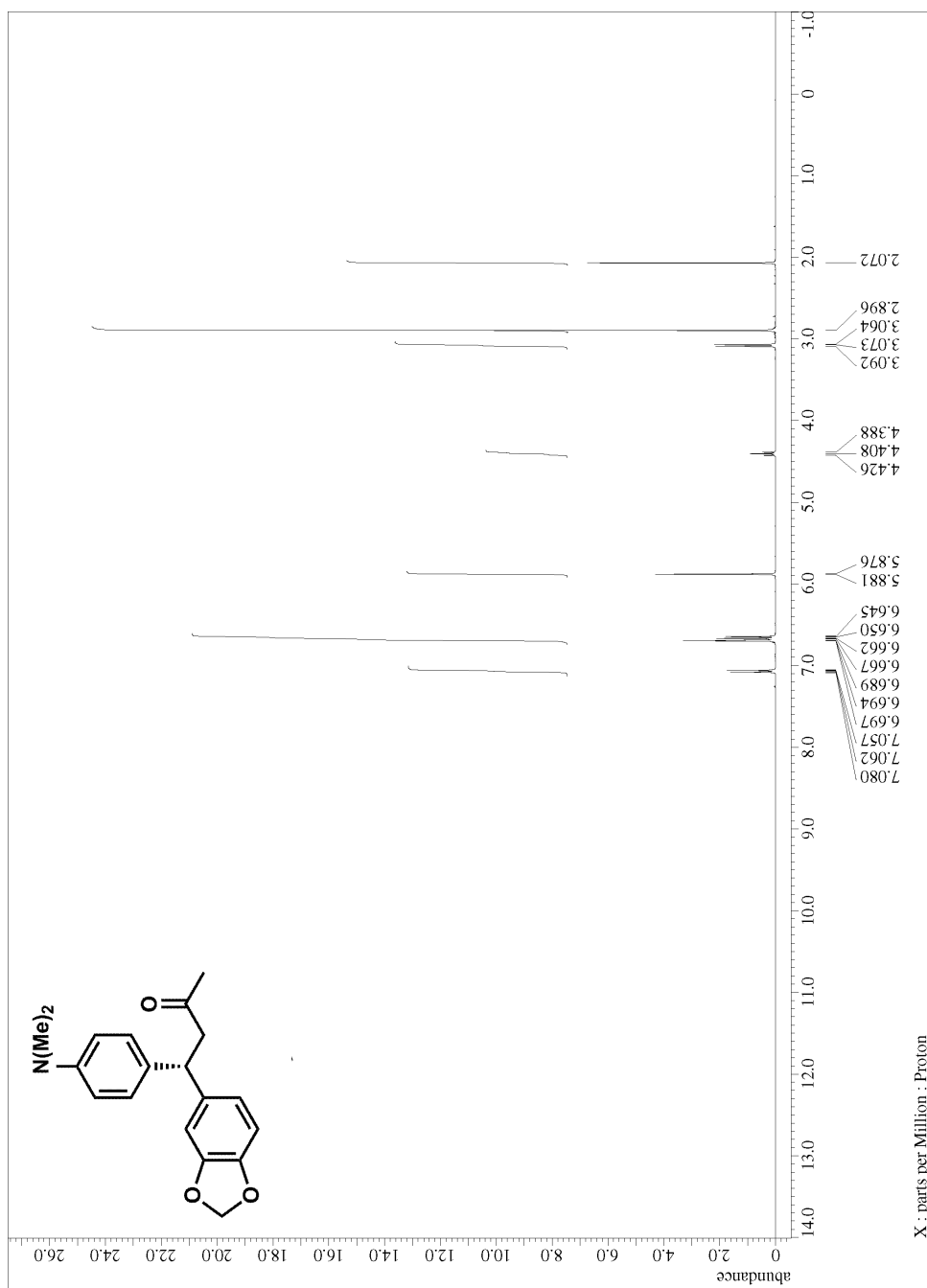


Figure A.2.7. ^1H NMR for compound 330

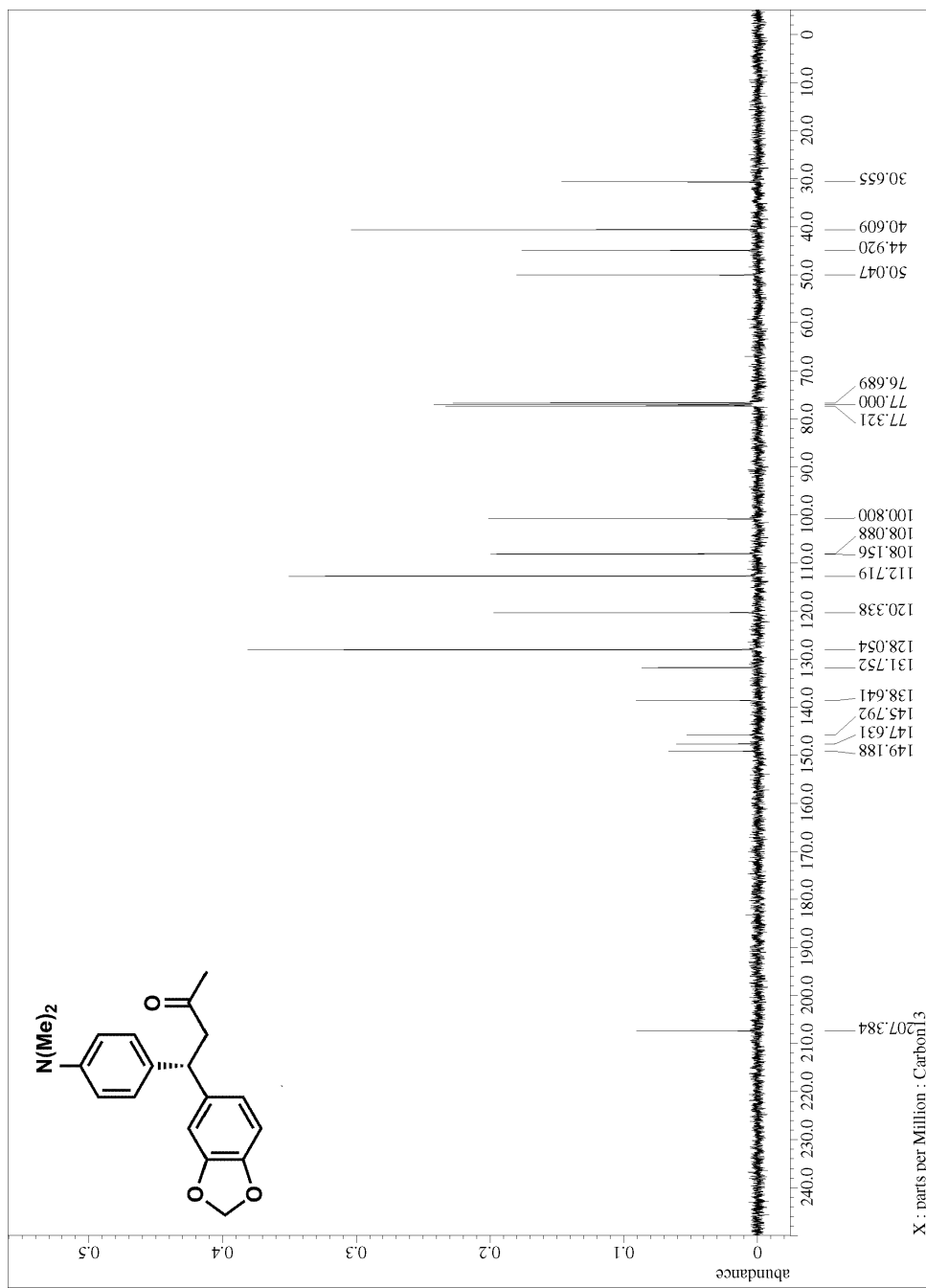
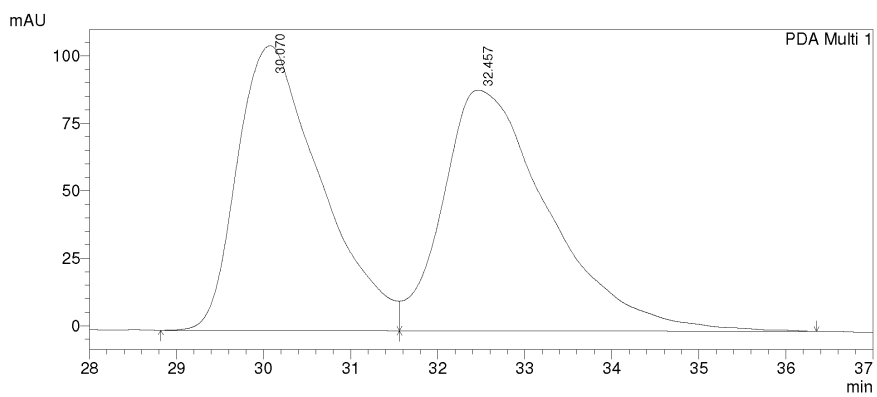


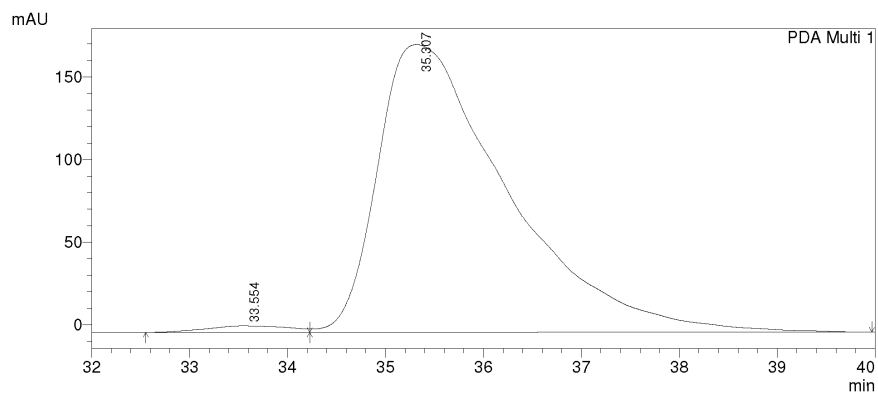
Figure A.2.8. ^{13}C NMR for compound 330



1 PDA Multi 1/254nm 4nm

PeakTable

Peak#	Ret. Time	Area	Height	Area %	Height %
1	30.070	7032428	105419	48.232	54.192
2	32.457	7548019	89109	51.768	45.808
Total		14580447	194527	100.000	100.000



1 PDA Multi 1/254nm 4nm

PeakTable

Peak#	Ret. Time	Area	Height	Area %	Height %
1	33.554	229700	3883	1.408	2.181
2	35.307	16084202	174156	98.592	97.819
Total		16313902	178038	100.000	100.000

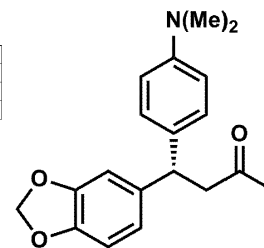


Figure A.2.9. HPLC trace for compound 330

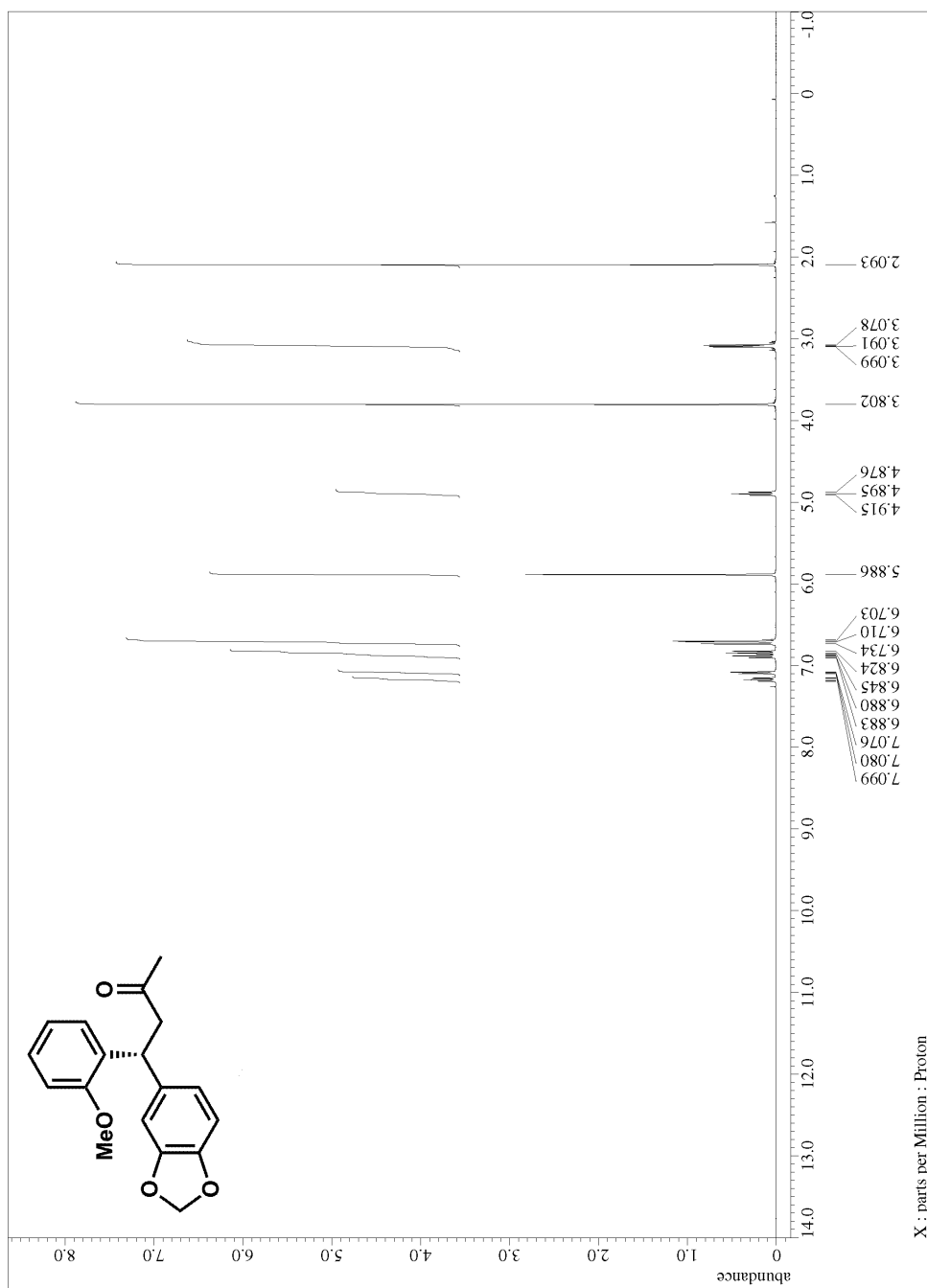


Figure A.2.10. ^1H NMR for compound 331

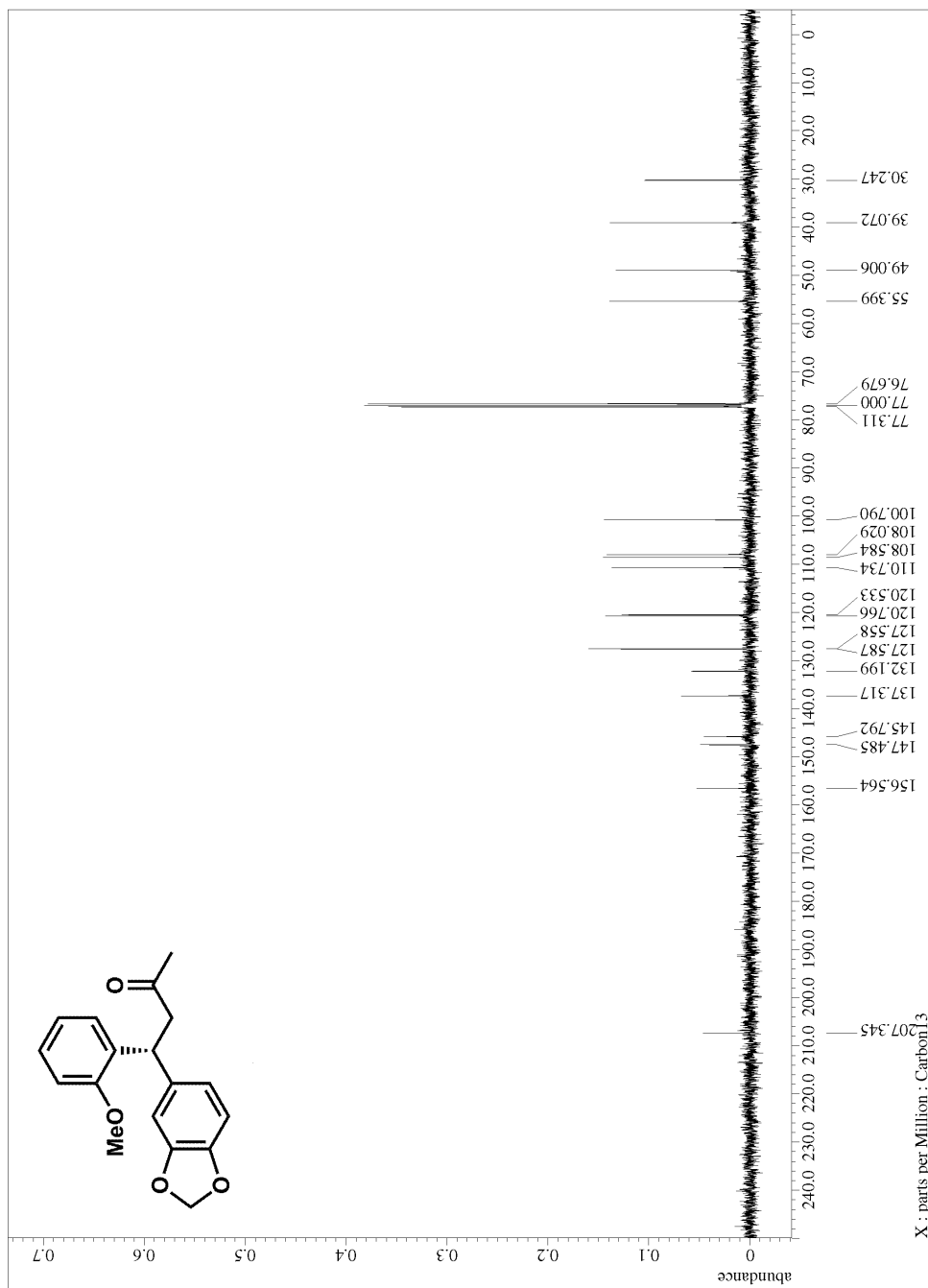
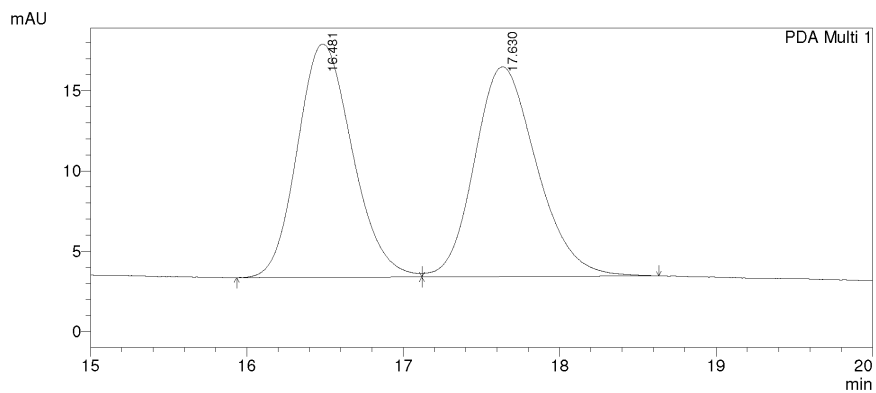
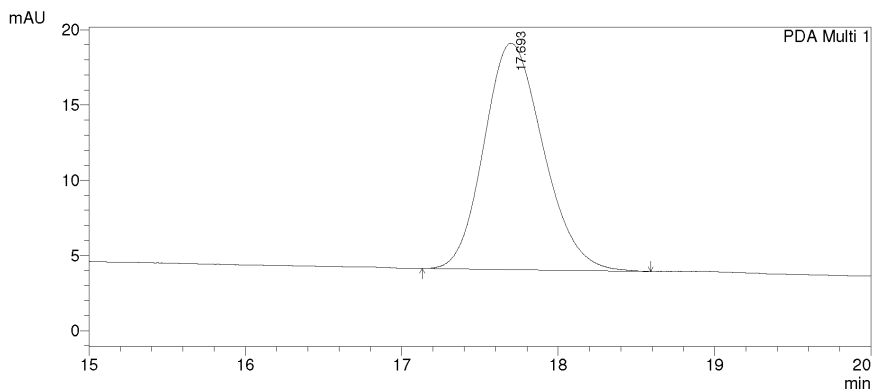


Figure A.2.11. ¹³C NMR for compound 331



PDA Ch1 254nm 4nm

Peak#	Ret. Time	Area	Height	Area %	Height %
1	16.481	354580	14540	49.594	52.657
2	17.630	360384	13073	50.406	47.343
Total		714963	27613	100.000	100.000



PDA Ch1 254nm 4nm

Peak#	Ret. Time	Area	Height	Area %	Height %
1	17.693	395104	15044	100.000	100.000
Total		395104	15044	100.000	100.000

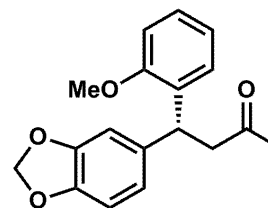


Figure A.2.12. HPLC trace for compound 331

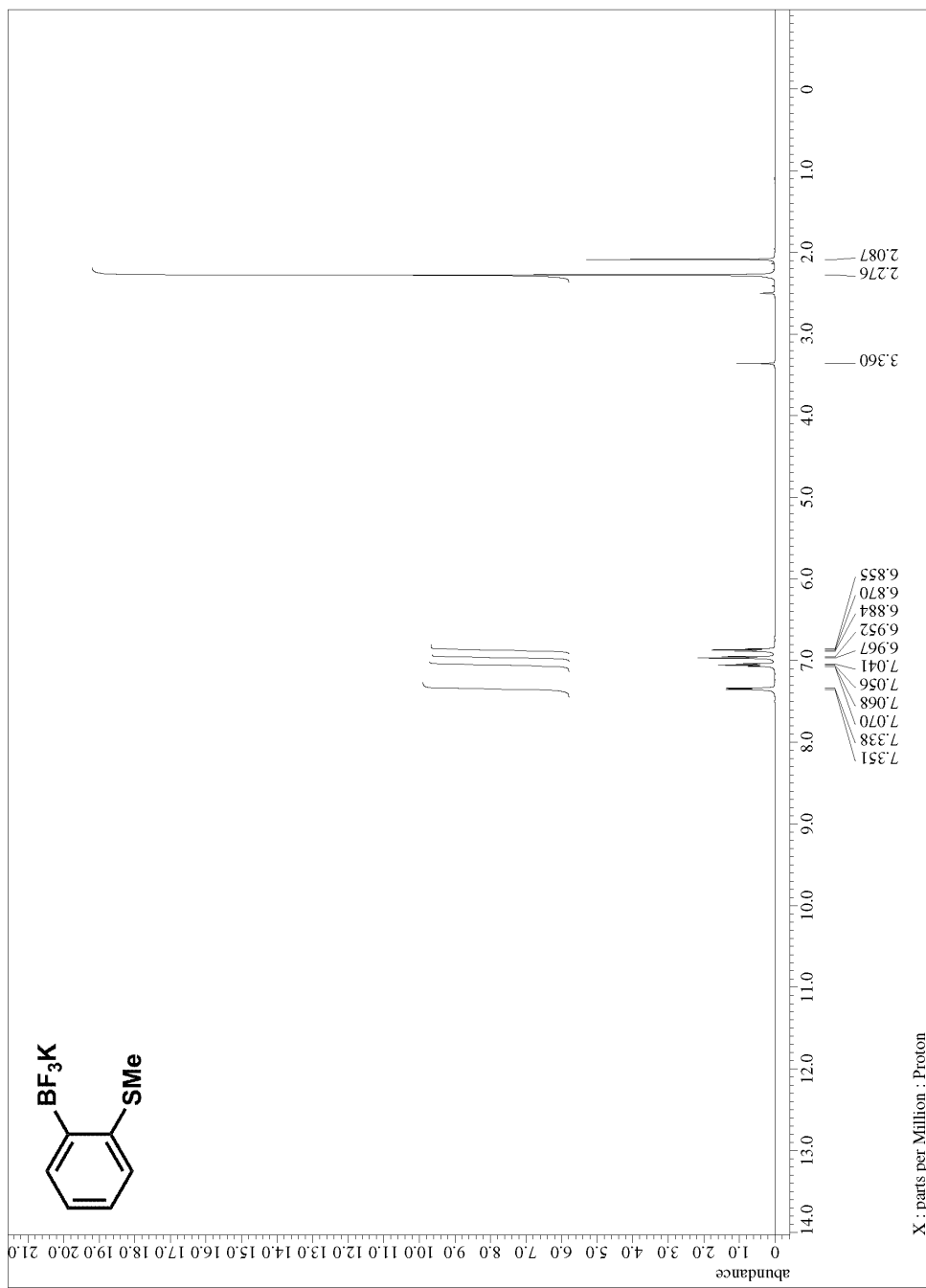


Figure A.2.13. ^1H NMR for precursor to compound 332

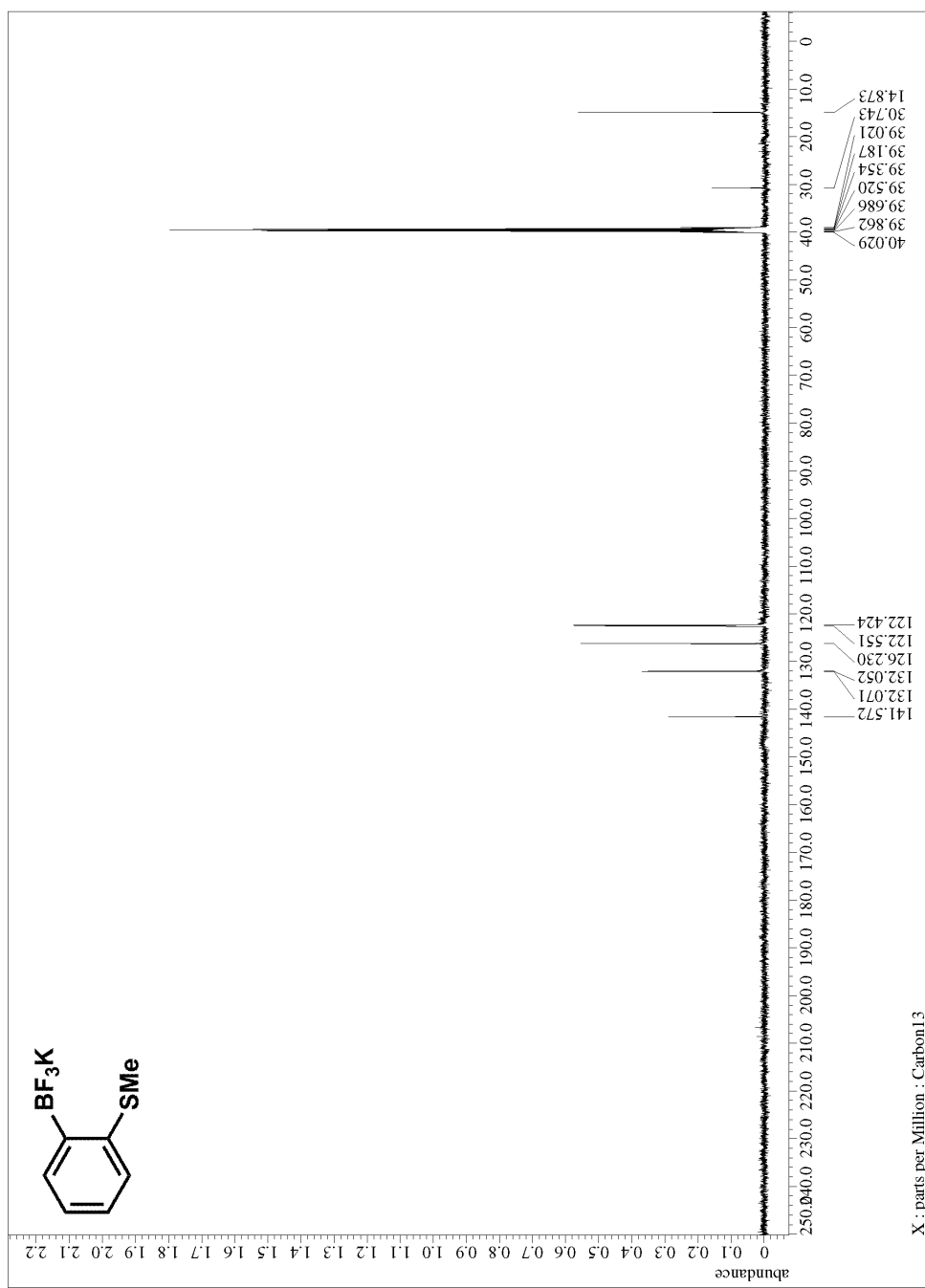


Figure A.2.14. ^{13}C NMR for precursor to compound 332

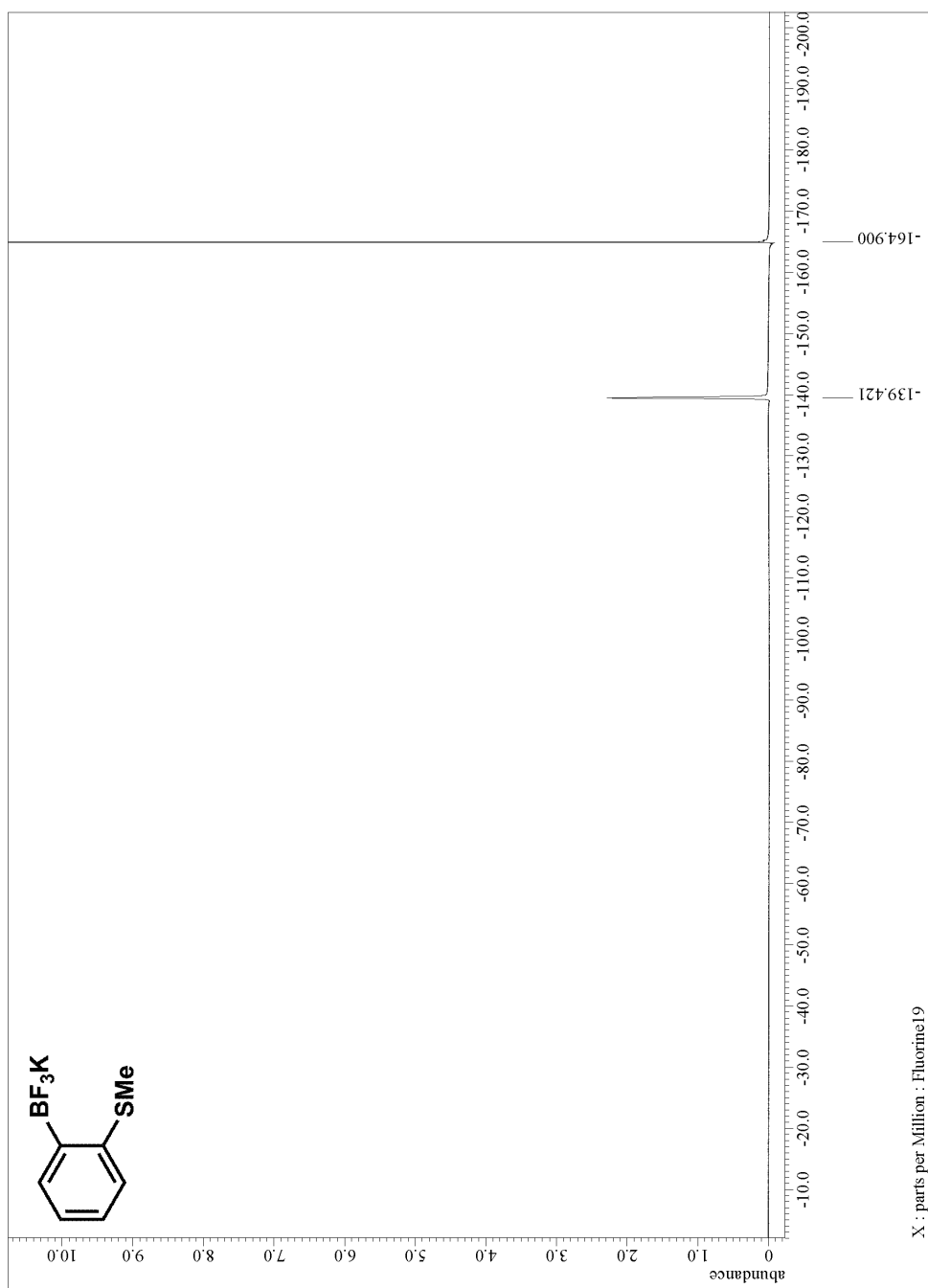


Figure A.2.15. ^{19}F NMR for precursor to compound 332

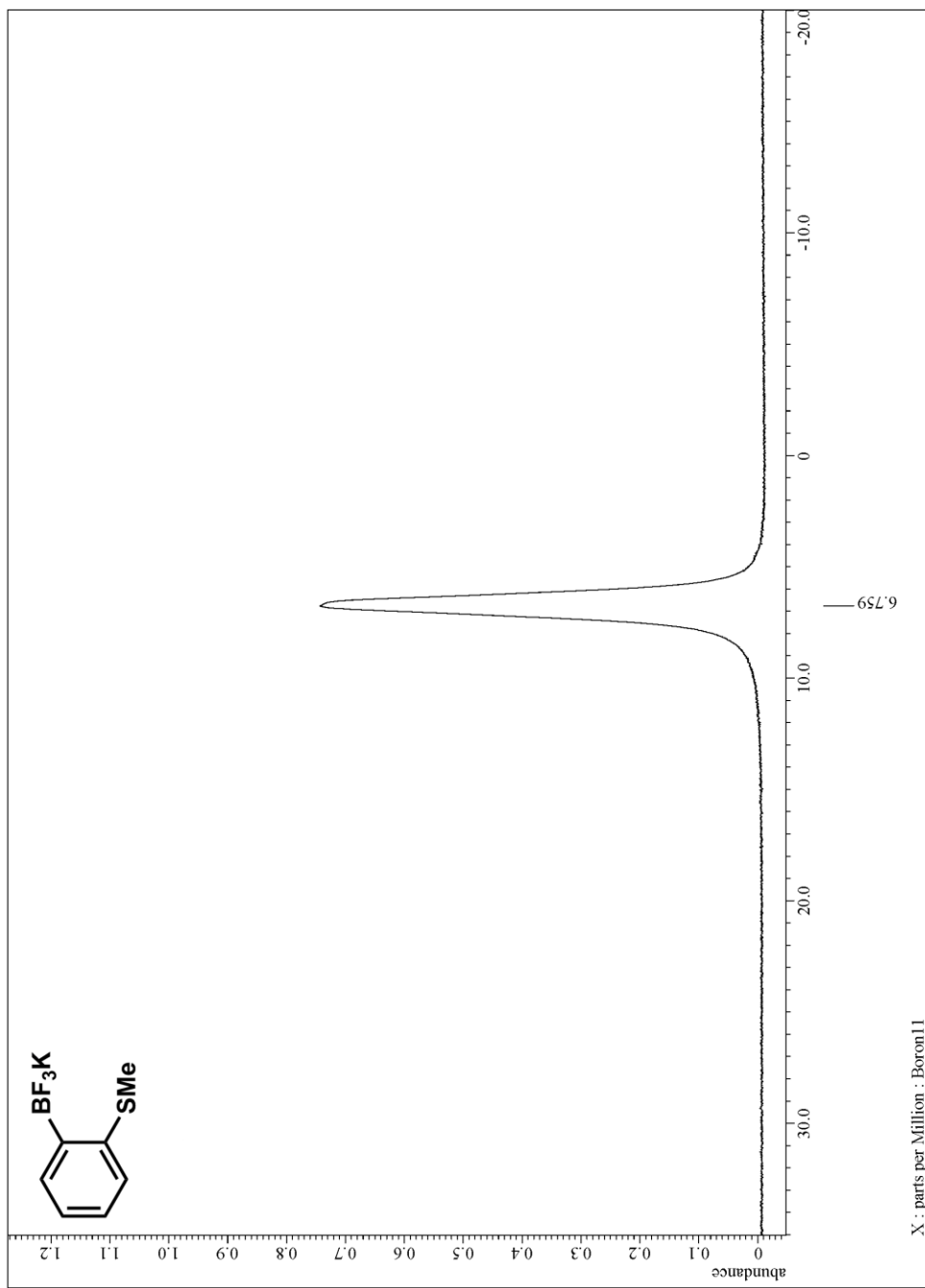


Figure A.2.16. ^{11}B NMR for precursor to compound **332**

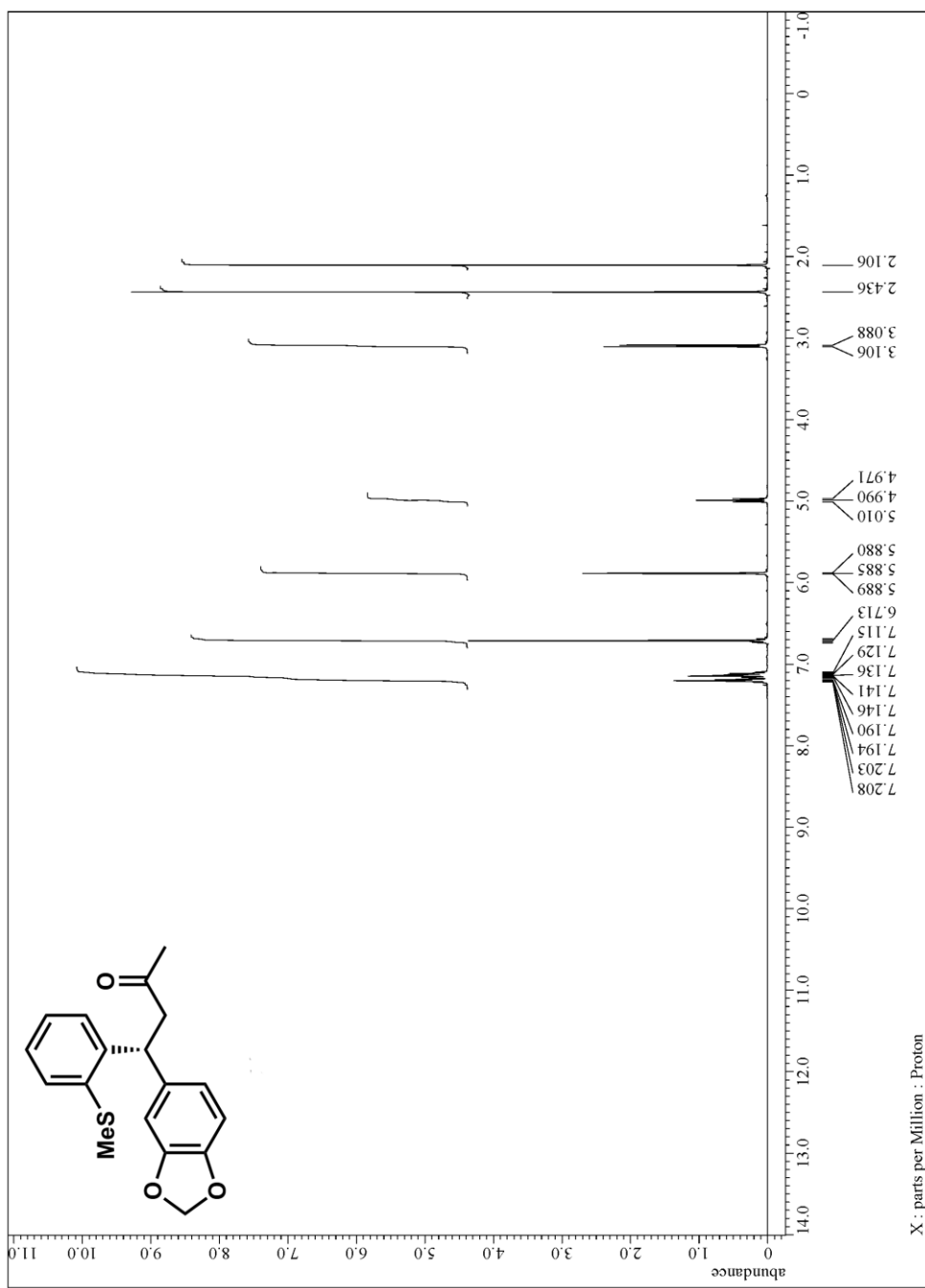


Figure A.2.17. ¹H NMR for compound 332

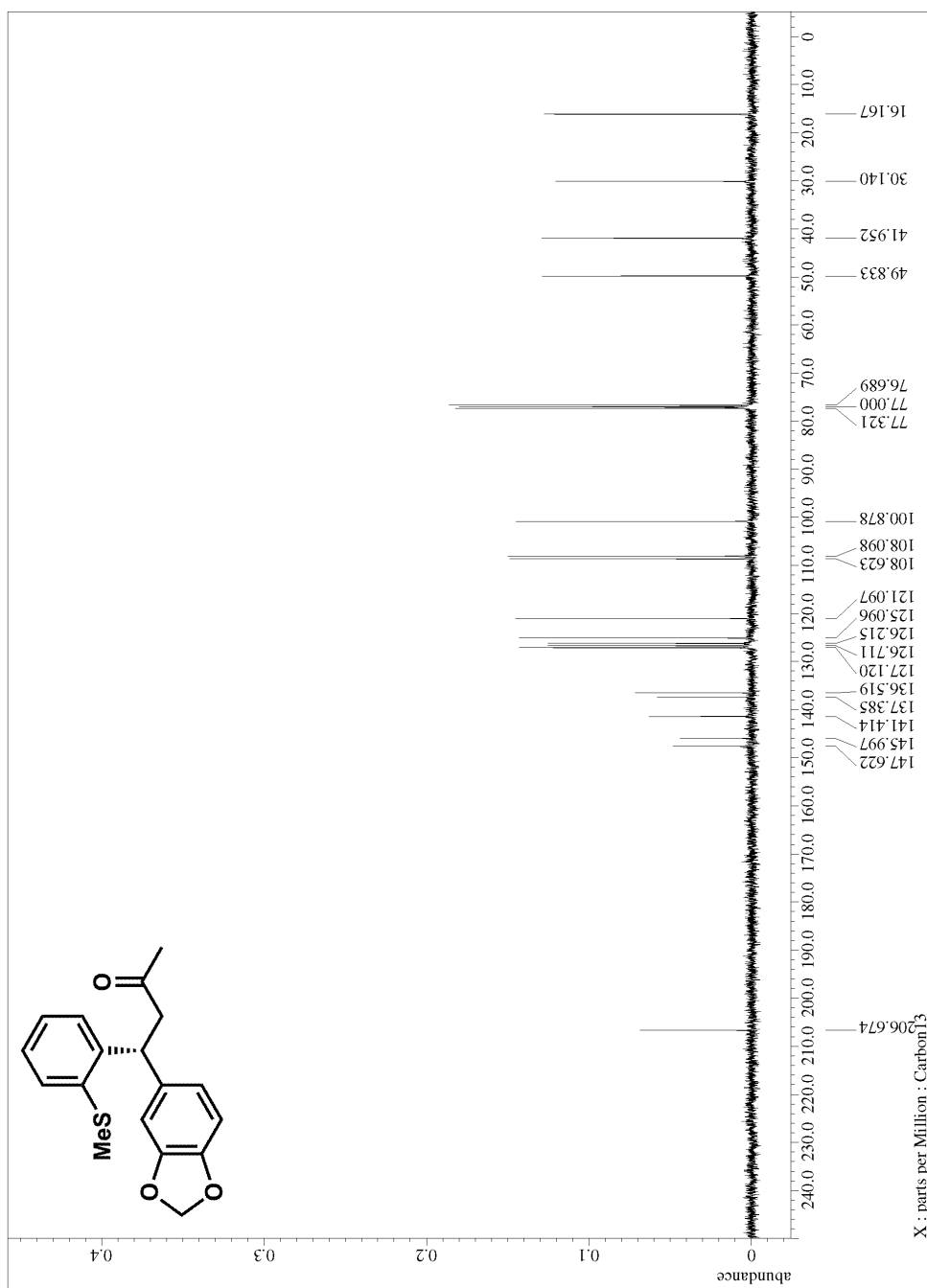
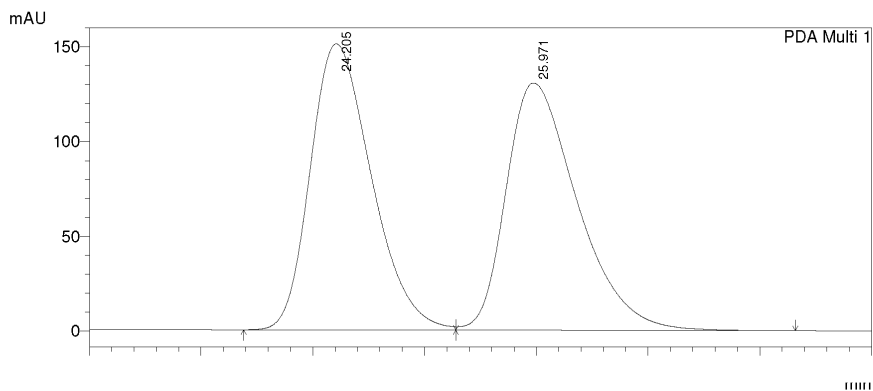


Figure A.2.18. ^{13}C NMR for compound 332

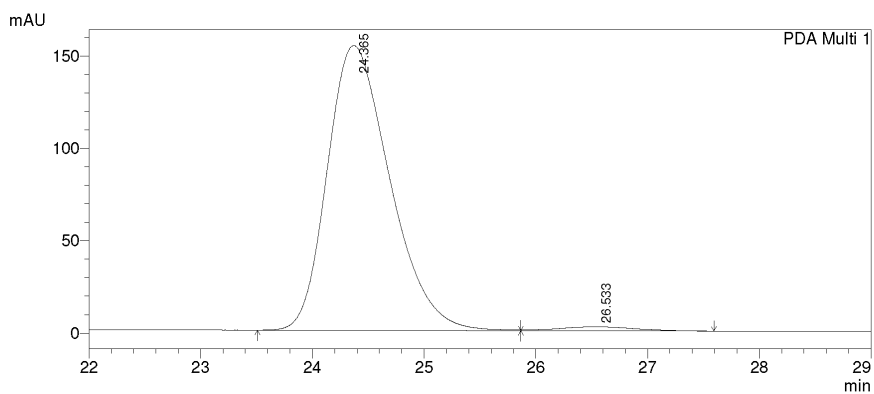


1 PDA Multi 1/254nm 4nm

PeakTable

PDA Ch1 254nm 4nm

Peak#	Ret. Time	Area	Height	Area %	Height %
1	24.205	5737859	150918	49.880	53.638
2	25.971	5765541	130446	50.120	46.362
Total		11503400	281364	100.000	100.000



1 PDA Multi 1/254nm 4nm

PeakTable

PDA Ch1 254nm 4nm

Peak#	Ret. Time	Area	Height	Area %	Height %
1	24.365	5994970	154245	98.327	98.586
2	26.533	102028	2213	1.673	1.414
Total		6096998	156458	100.000	100.000

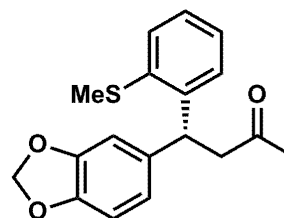


Figure A.2.19. HPLC trace for compound 332

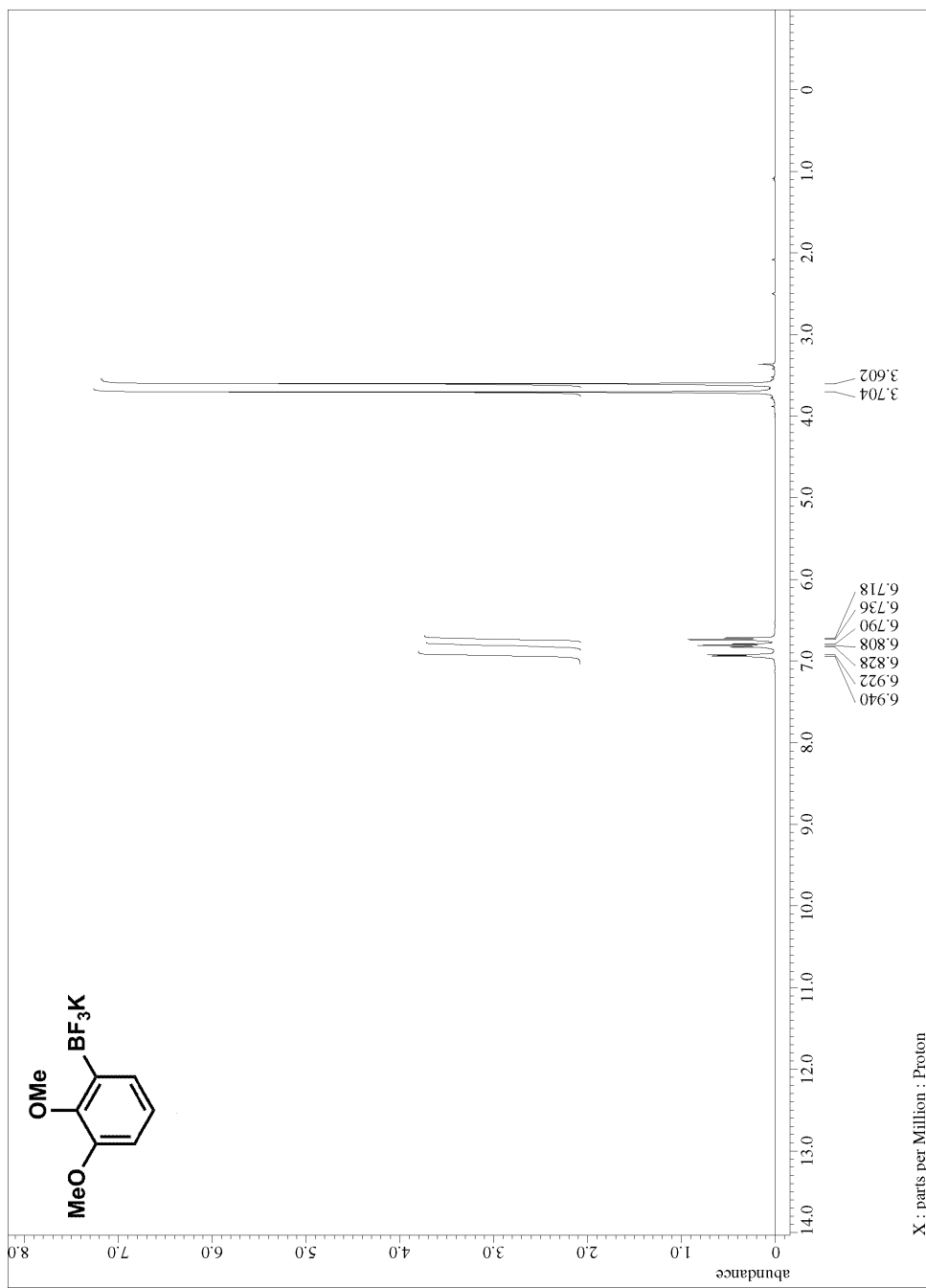


Figure A.2.20. ^1H NMR for precursor to compound 333

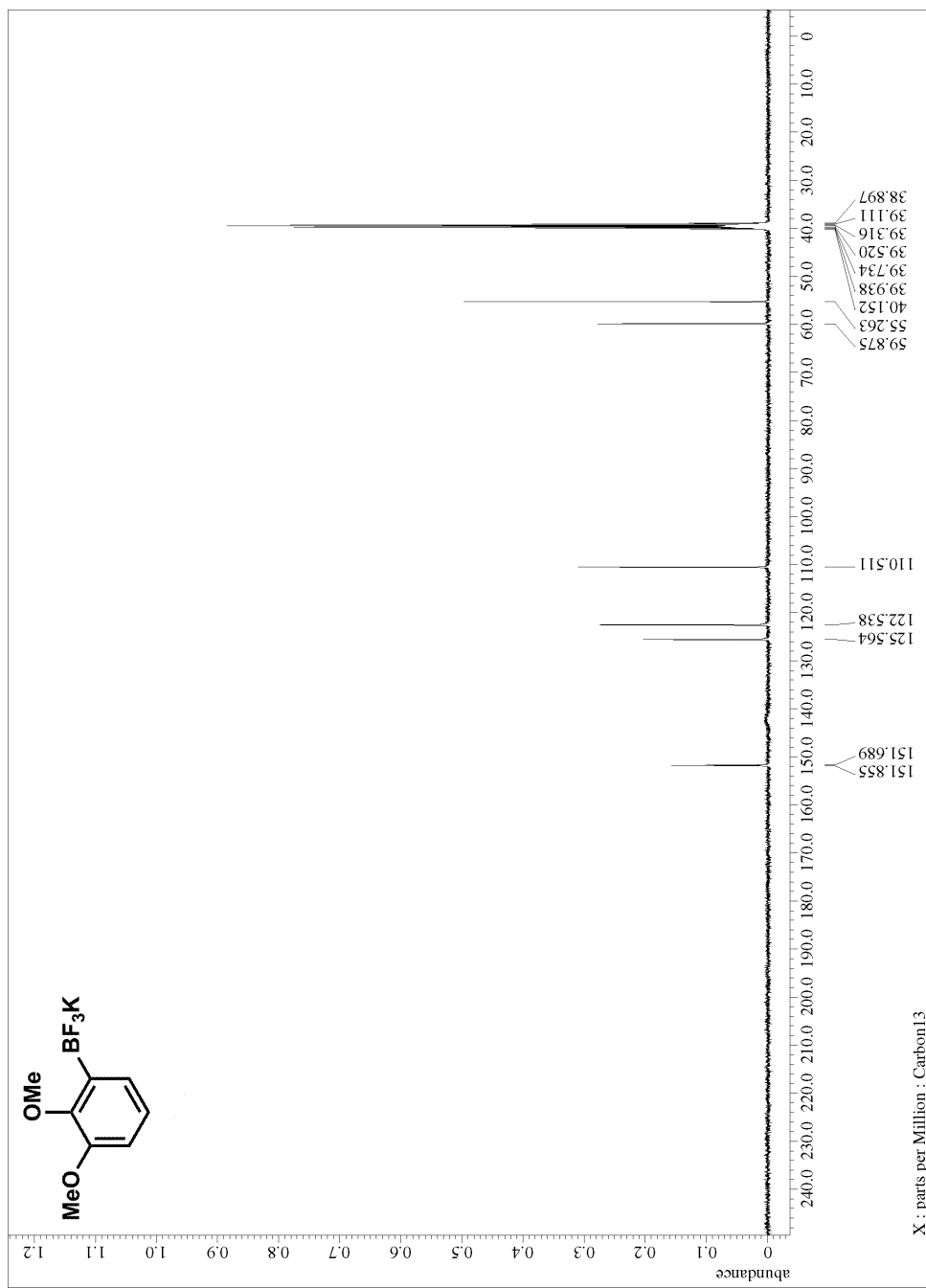


Figure A.2.21. ^{13}C NMR for precursor to compound 333

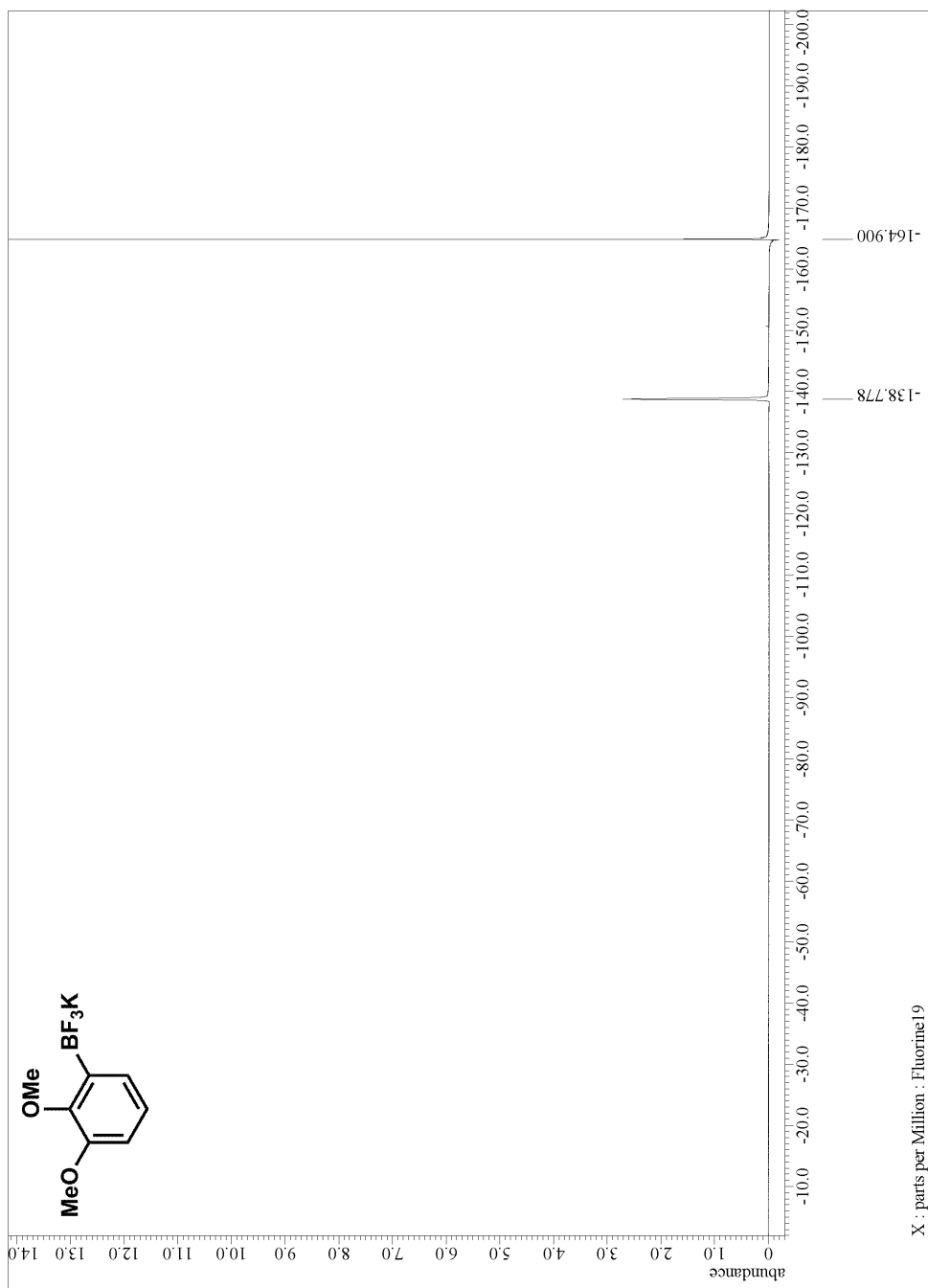


Figure A.2.22. ^{19}F NMR for precursor to compound 333

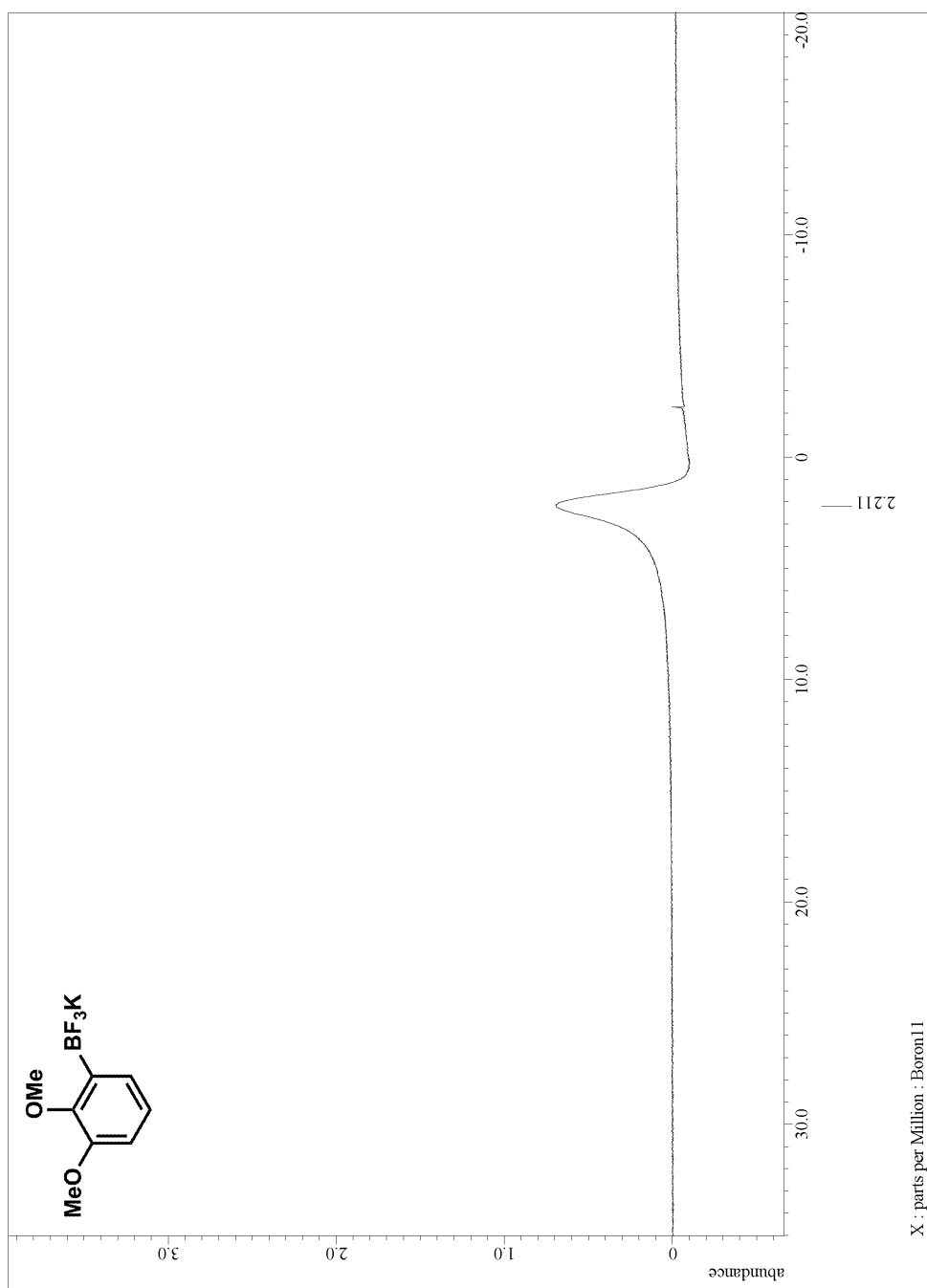


Figure A.2.23. ^{11}B NMR for precursor to compound 333

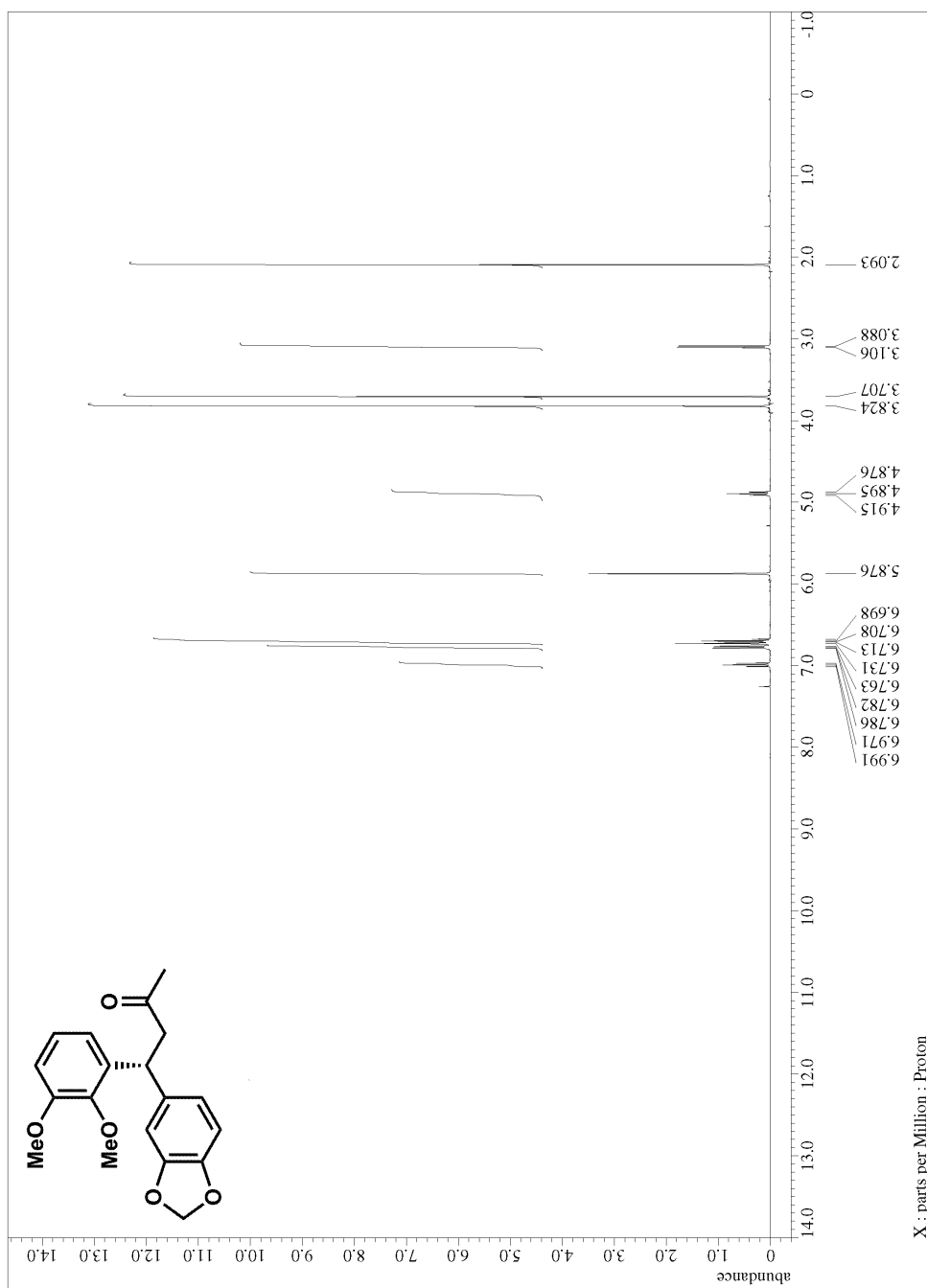


Figure A.2.24. ^1H NMR for compound 333

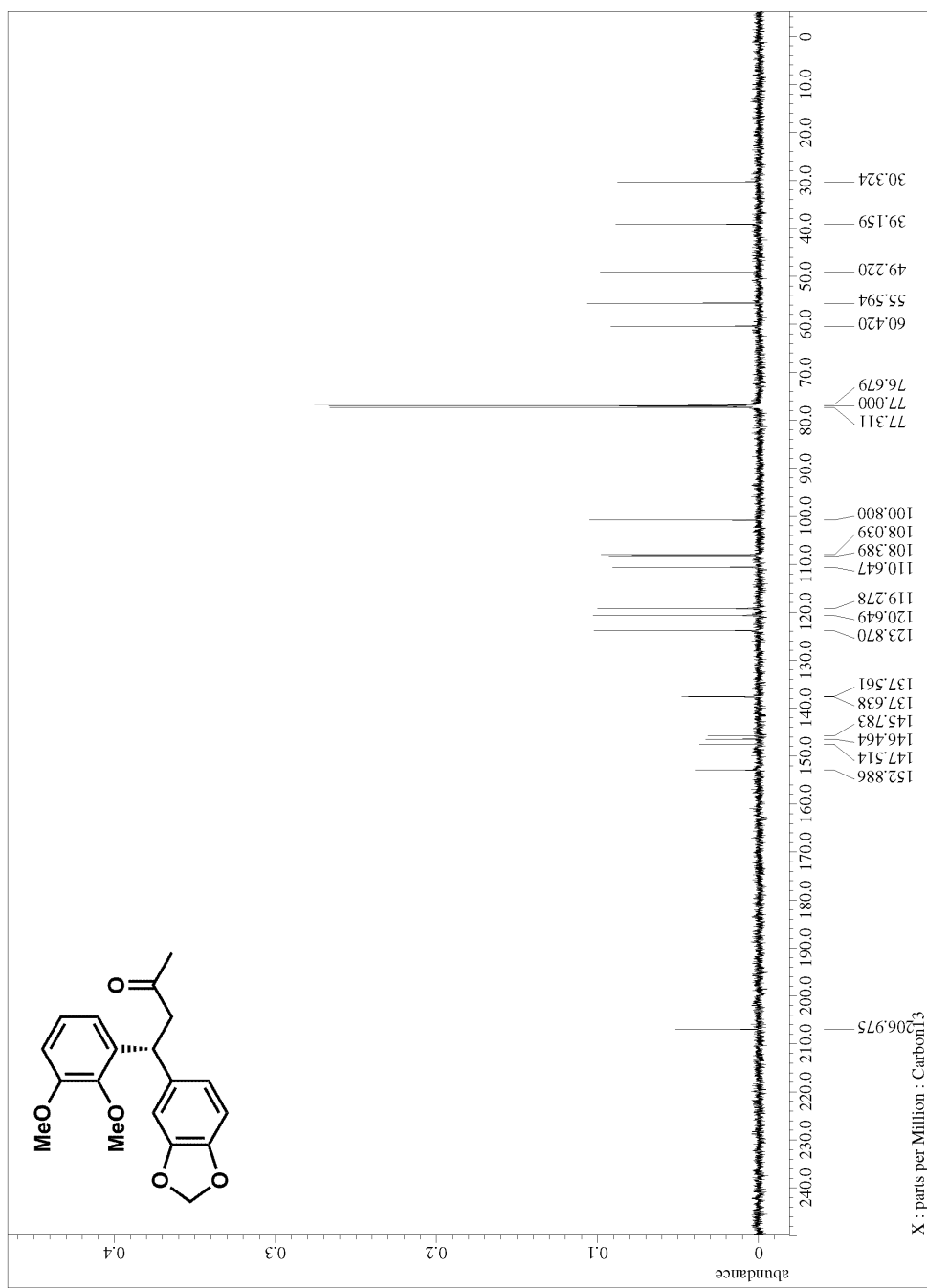
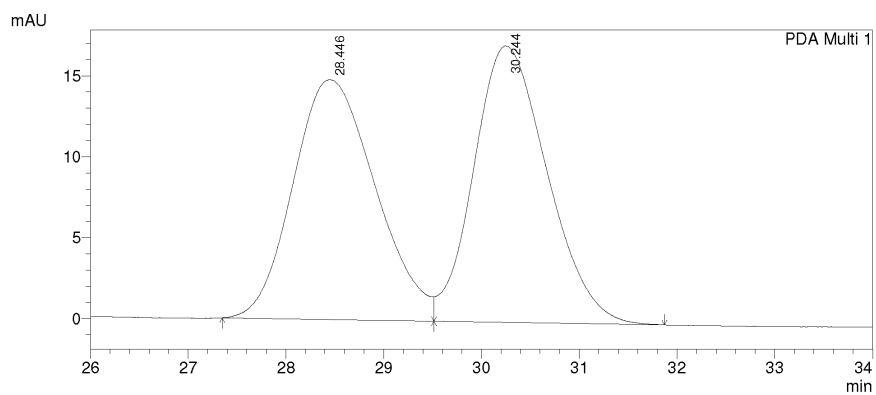


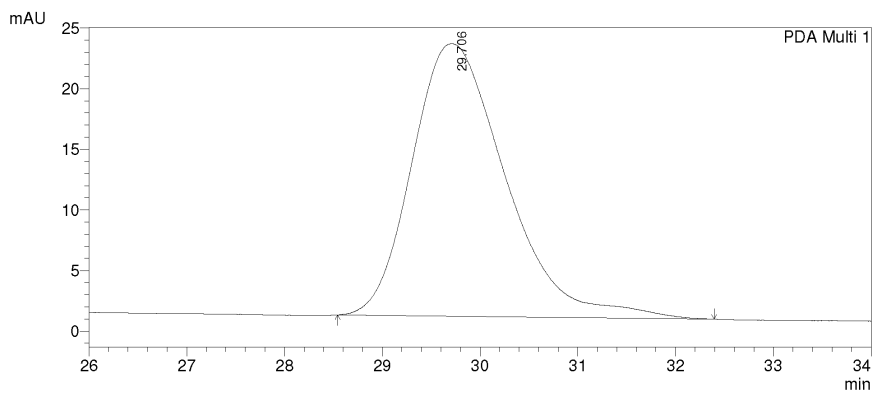
Figure A.2.25. ^{13}C NMR for compound **333**



1 PDA Multi 1/254nm 4nm

PeakTable

Peak#	Ret. Time	Area	Height	Area %	Height %
1	28.446	866806	14828	49.337	46.465
2	30.244	890107	17085	50.663	53.535
Total		1756913	31913	100.000	100.000



1 PDA Multi 1/254nm 4nm

PeakTable

Peak#	Ret. Time	Area	Height	Area %	Height %
1	29.706	1491722	22481	100.000	100.000
Total		1491722	22481	100.000	100.000

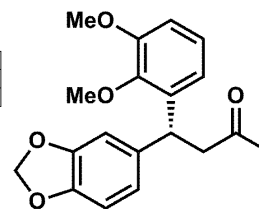


Figure A.2.26. HPLC trace for compound 333

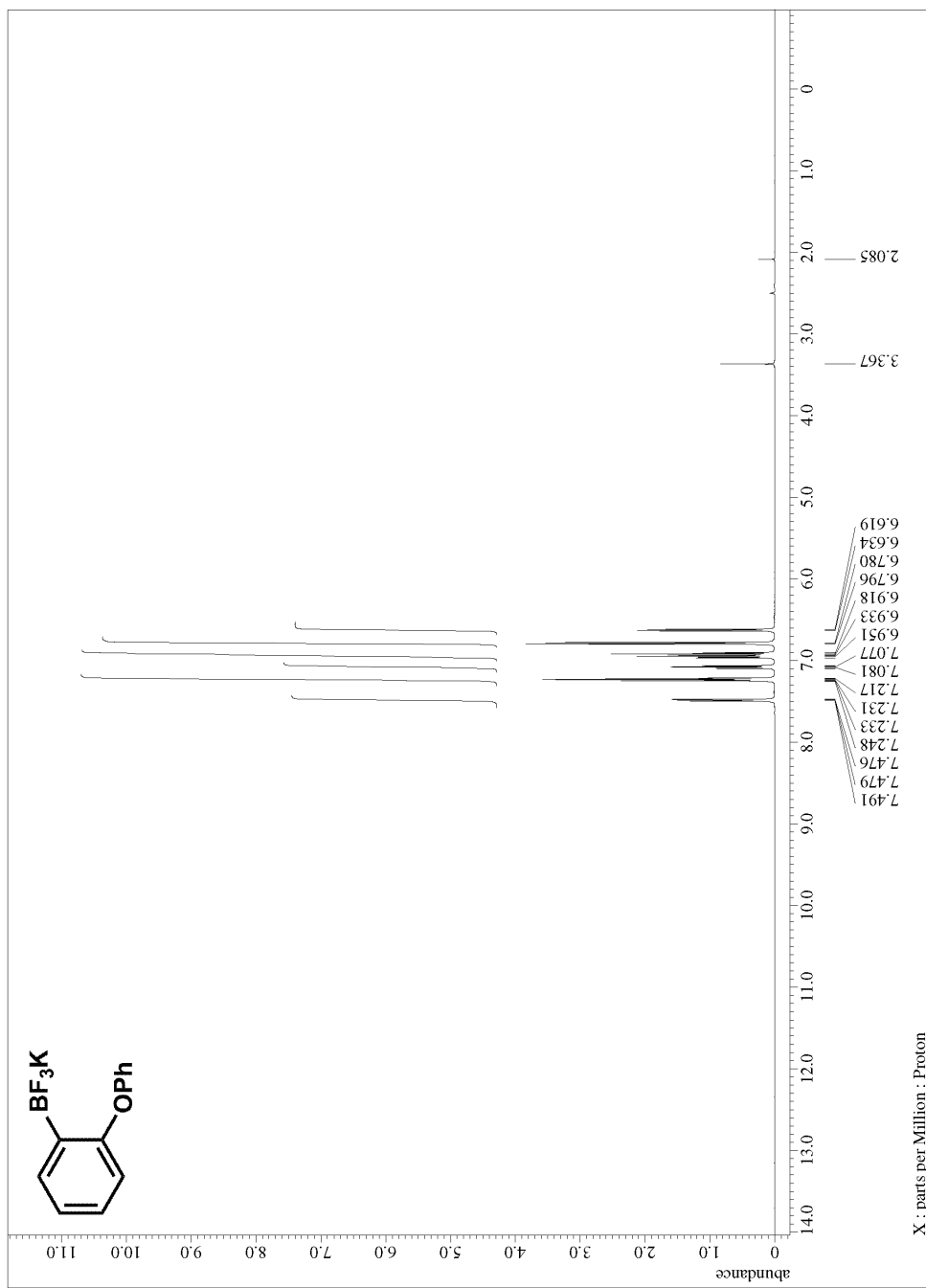


Figure A.2.27. ^1H NMR for precursor to compound 334

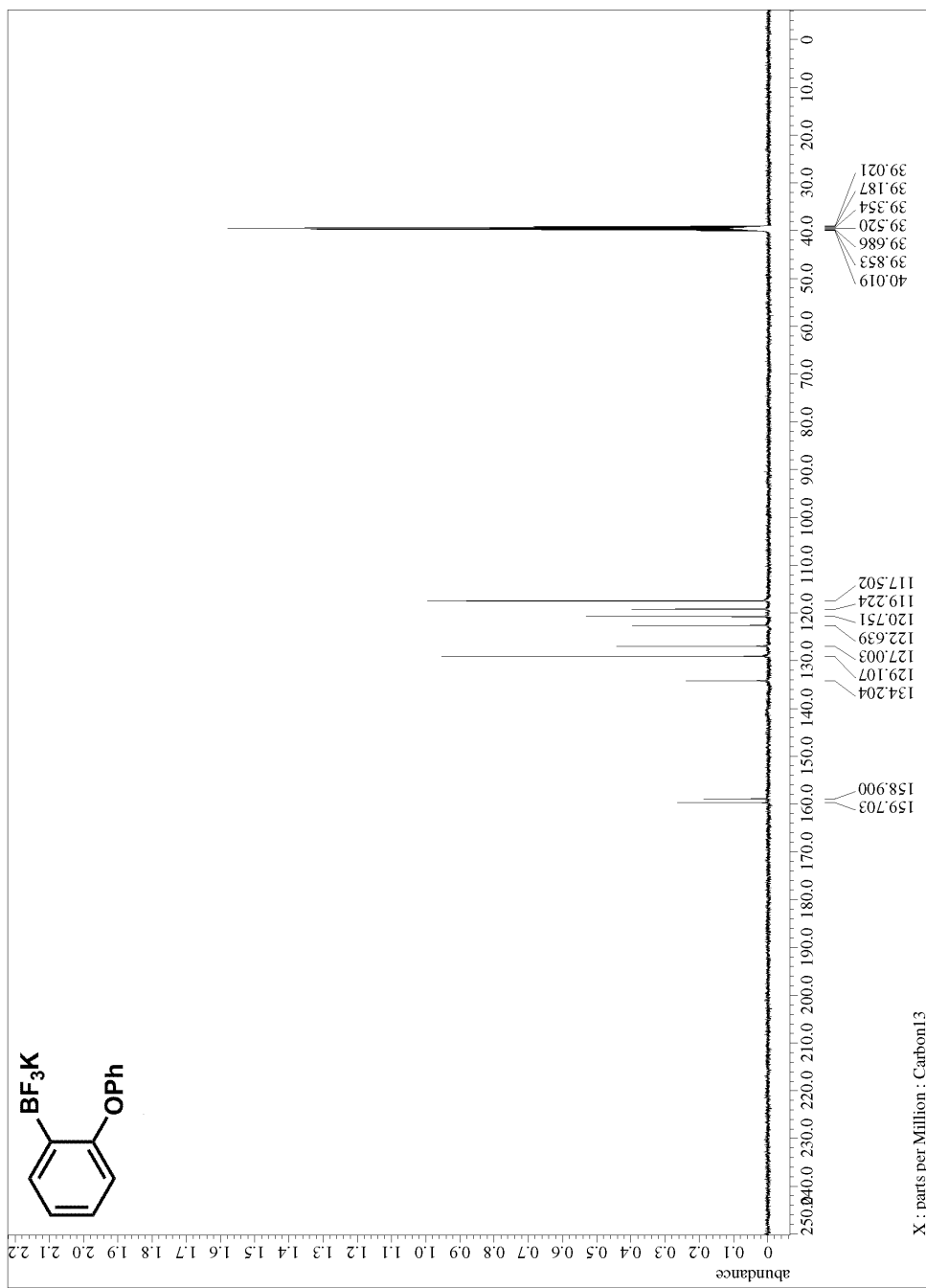


Figure A.2.28. ^{13}C NMR for precursor to compound 334

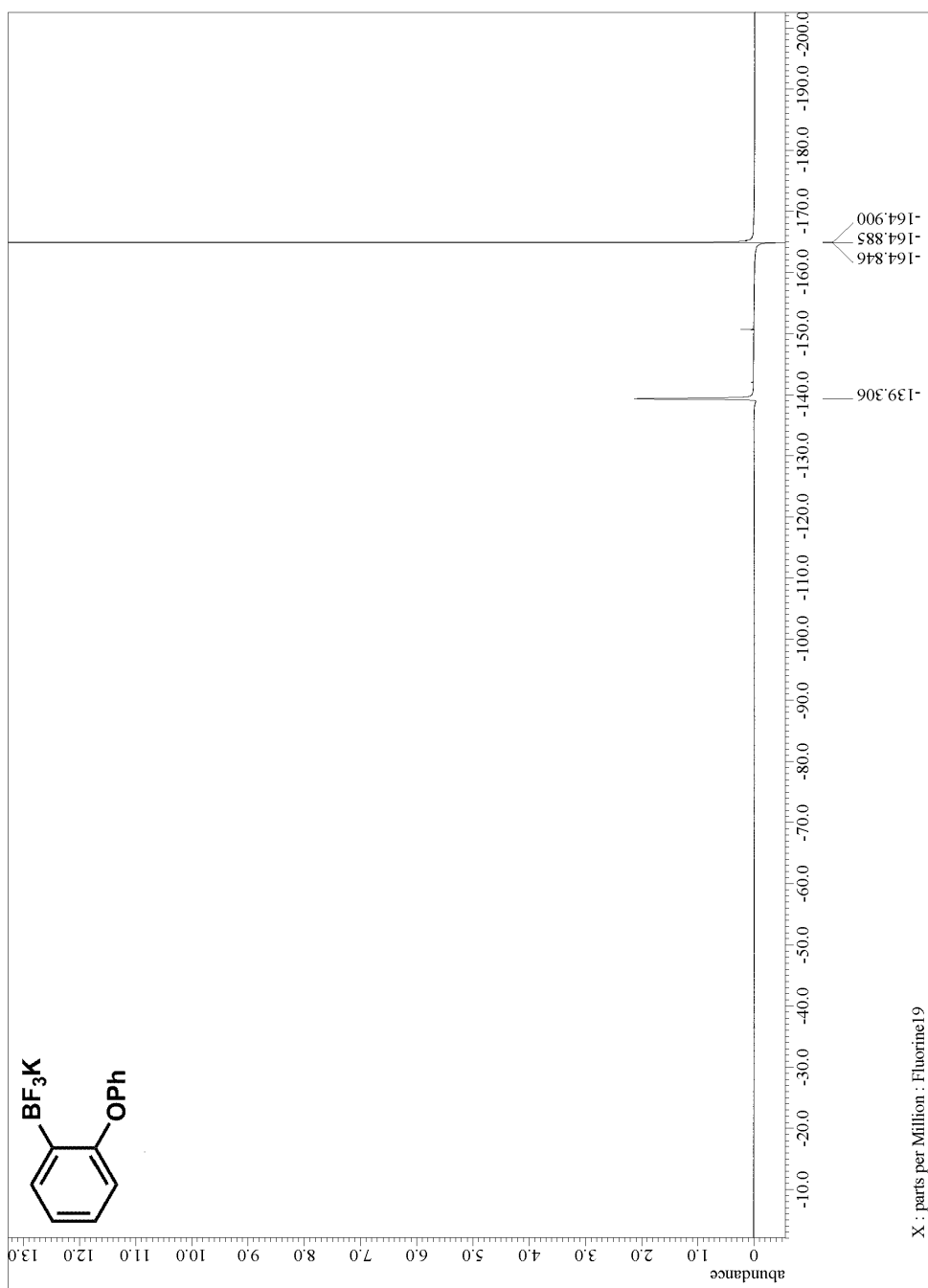


Figure A.2.29. ^{19}F NMR for precursor to compound 334

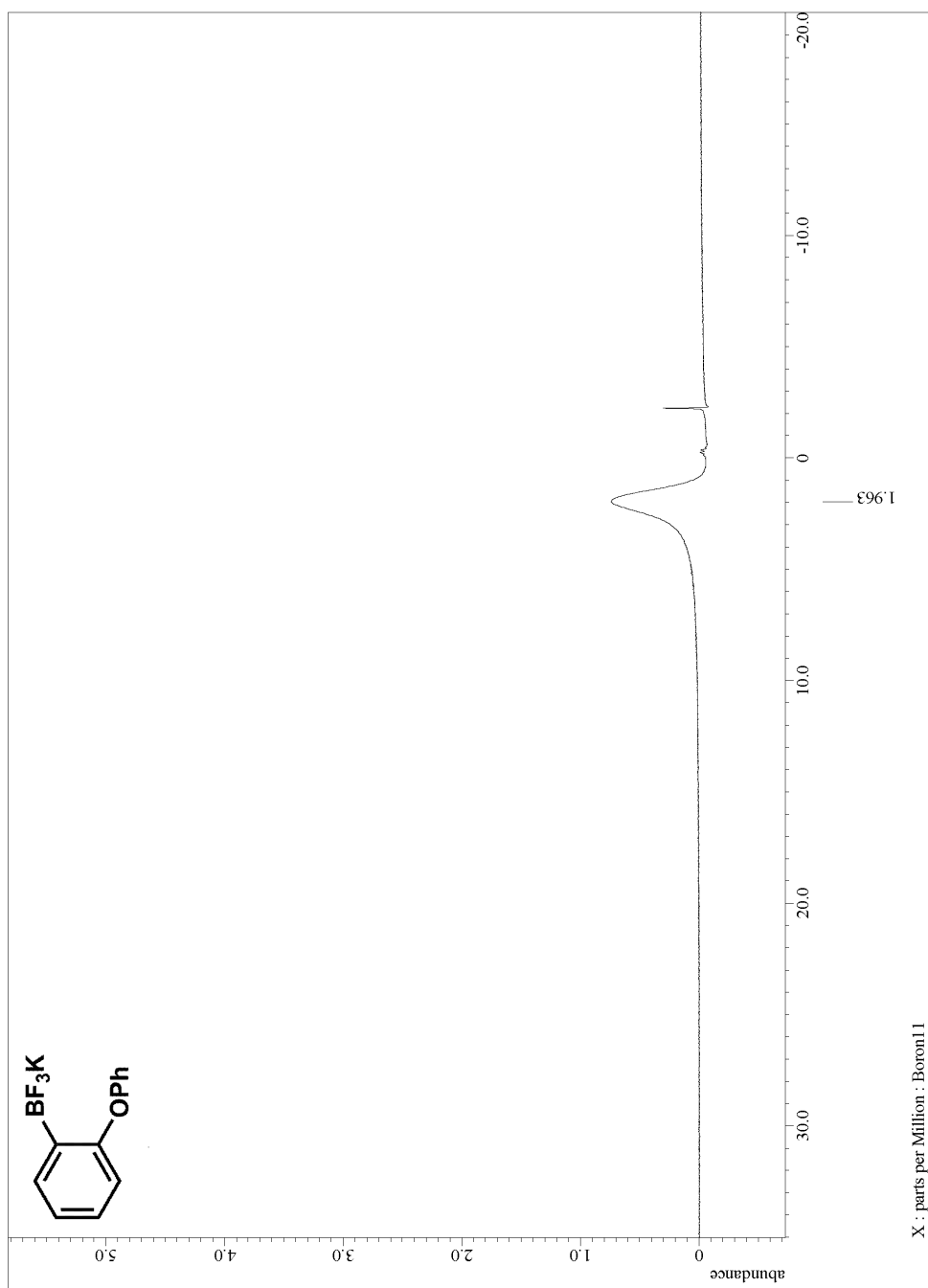


Figure A.2.30. ^{11}B NMR for precursor to compound 334

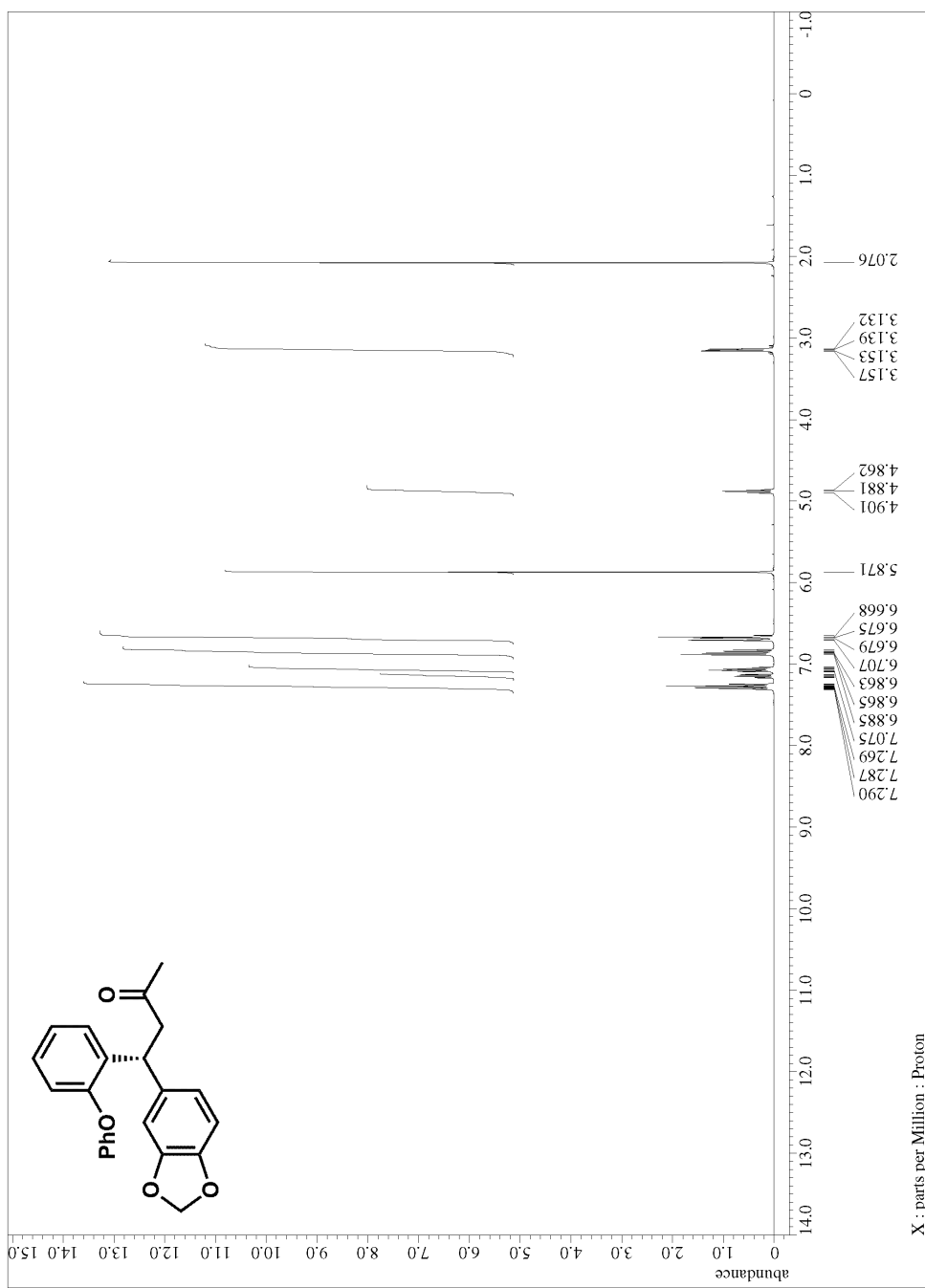


Figure A.2.31. ^1H NMR for compound 334

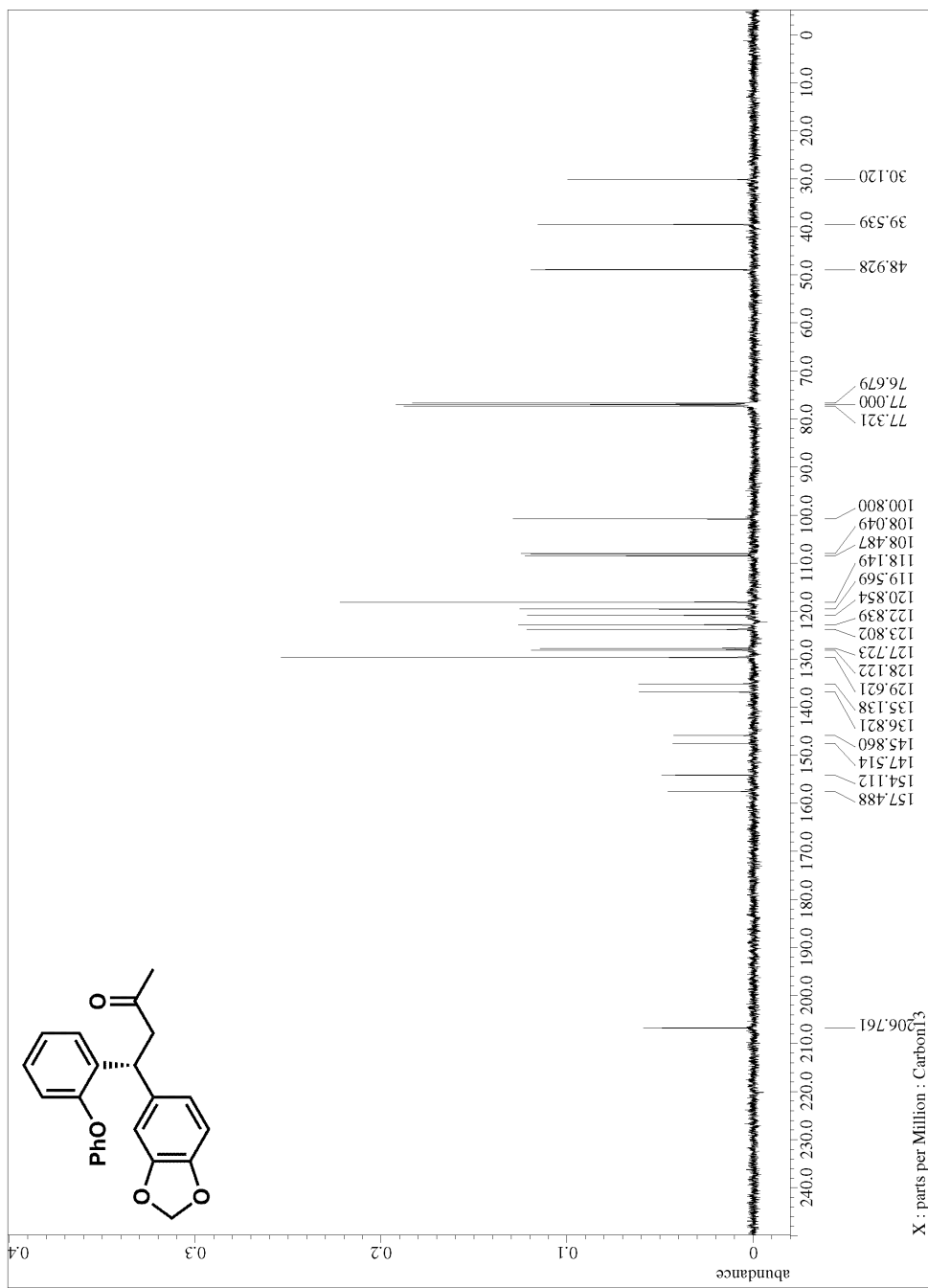
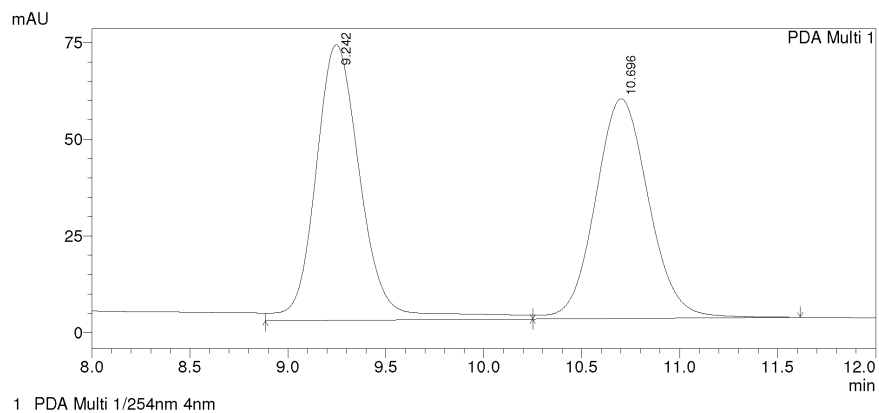


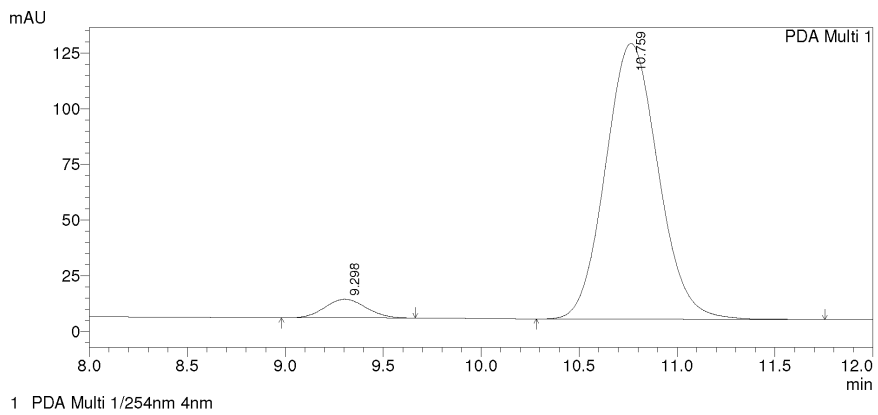
Figure A.2.32. ^{13}C NMR for compound 334



PeakTable

PDA Ch1 254nm 4nm

Peak#	Ret. Time	Area	Height	Area %	Height %
1	9.242	1153477	71350	51.767	55.674
2	10.696	1074717	56807	48.233	44.326
Total		2228194	128157	100.000	100.000



PeakTable

PDA Ch1 254nm 4nm

Peak#	Ret. Time	Area	Height	Area %	Height %
1	9.298	120959	8333	4.972	6.309
2	10.759	2311835	123742	95.028	93.691
Total		2432793	132074	100.000	100.000

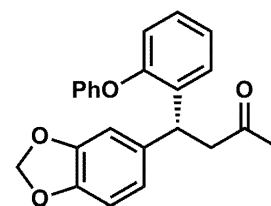


Figure A.2.33. HPLC trace for compound 334

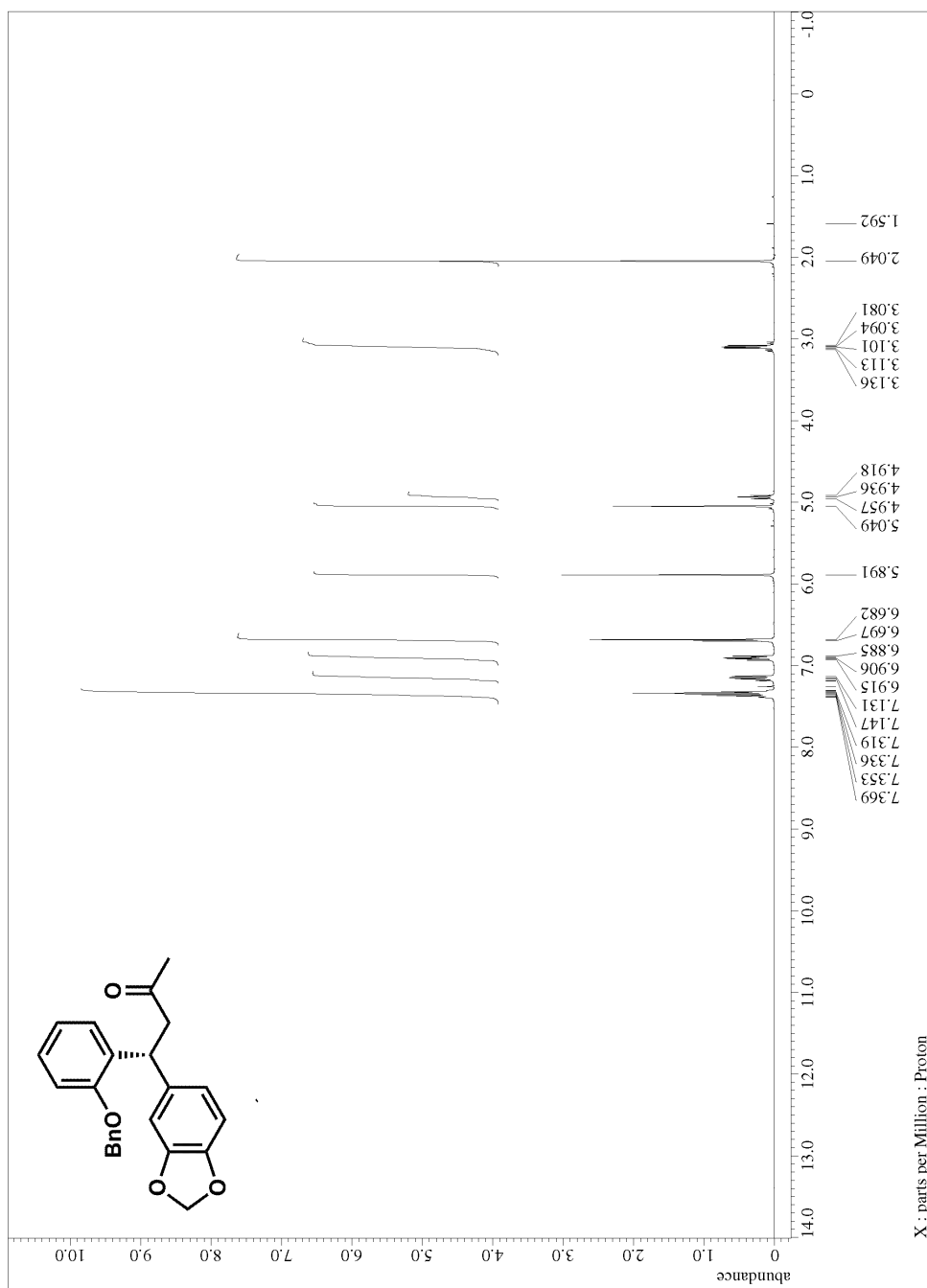


Figure A.2.34. ¹H NMR for compound 335

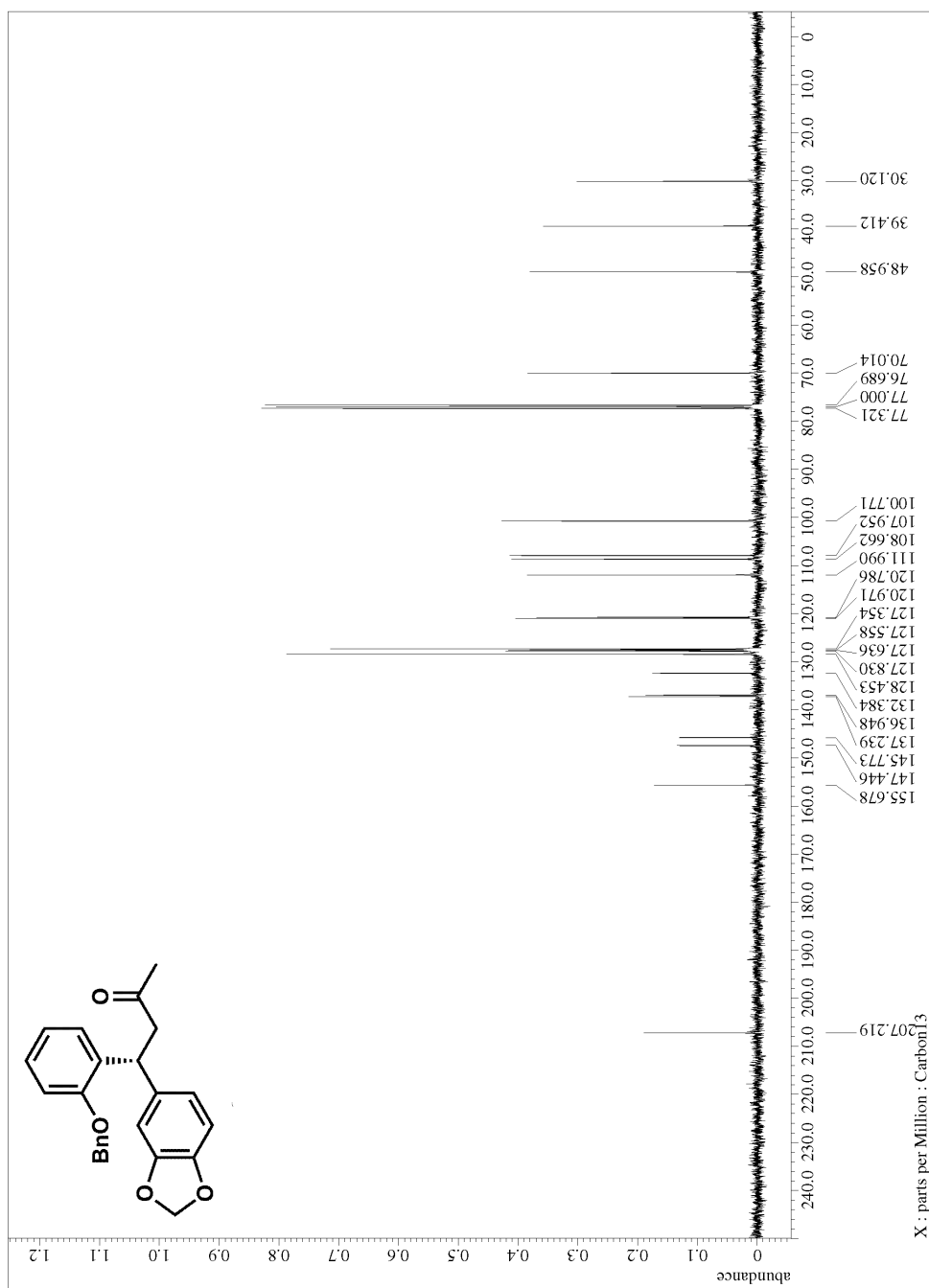
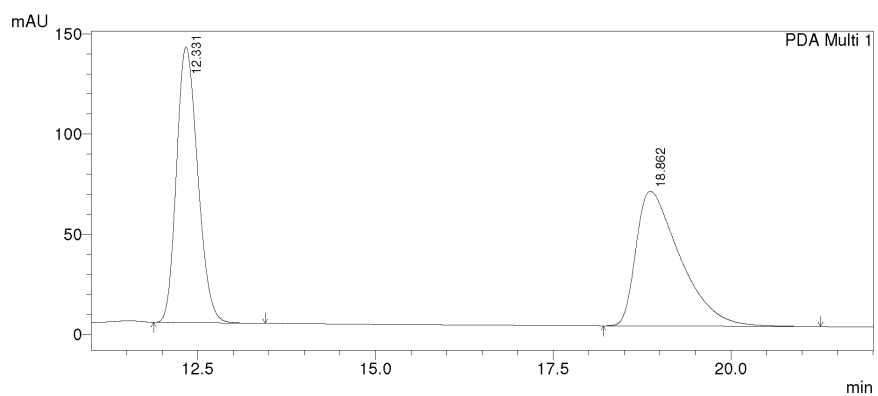


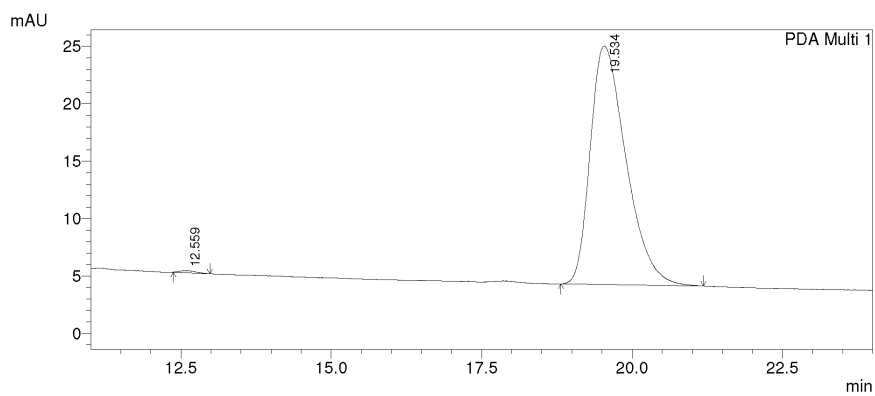
Figure A.2.35. ^{13}C NMR for compound 335



1 PDA Multi 1/254nm 4nm

PeakTable

Peak#	Ret. Time	Area	Height	Area %	Height %
1	12.331	2856006	137520	49.678	67.174
2	18.862	2893076	67202	50.322	32.826
Total		5749082	204721	100.000	100.000



1 PDA Multi 1/254nm 4nm

PeakTable

Peak#	Ret. Time	Area	Height	Area %	Height %
1	12.559	3261	176	0.378	0.841
2	19.534	859659	20774	99.622	99.159
Total		862920	20950	100.000	100.000

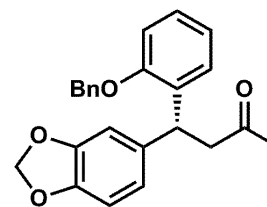


Figure A.2.36. HPLC trace for compound 335

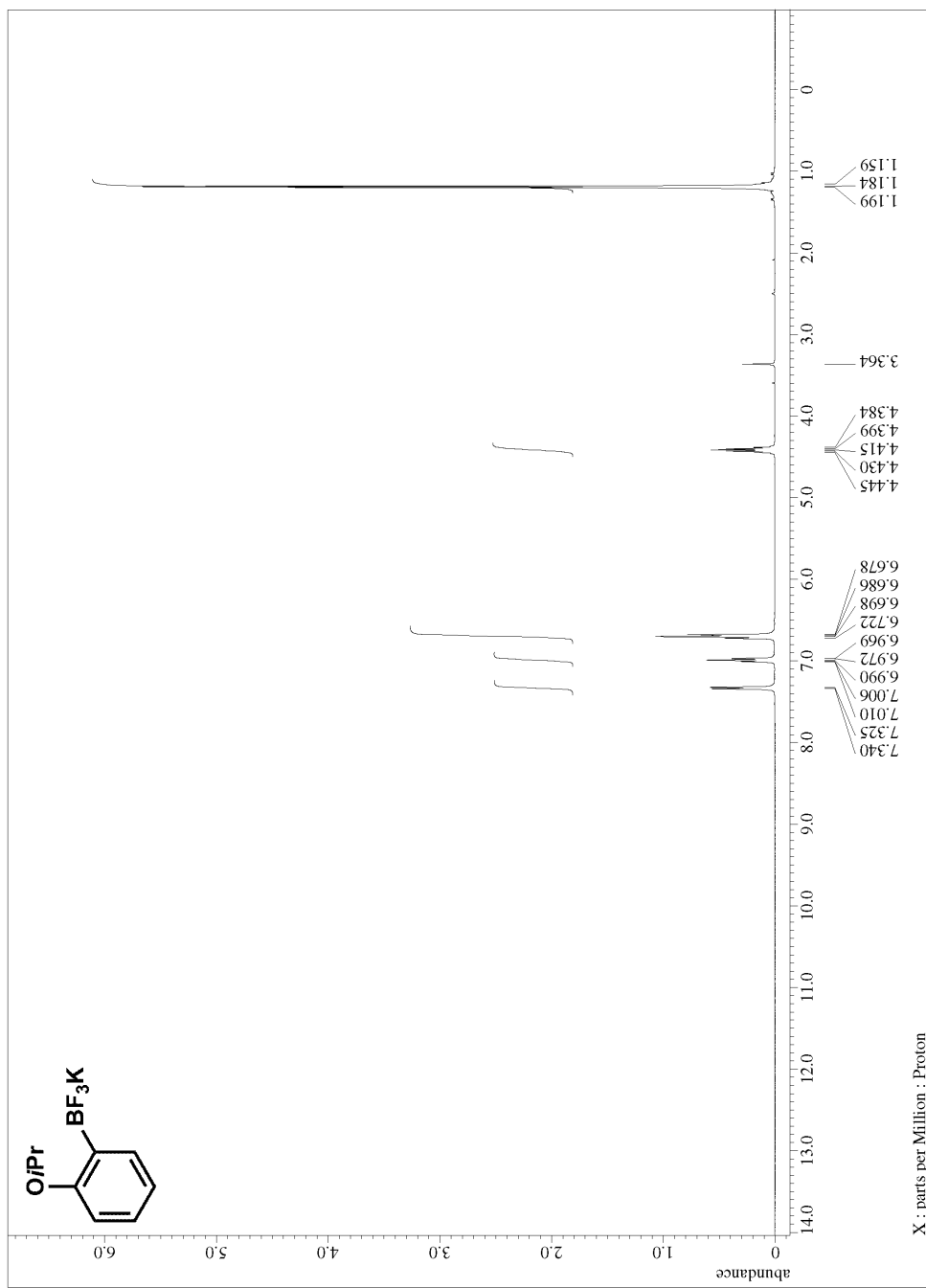


Figure A.2.37. ¹H NMR for precursor to compound 336

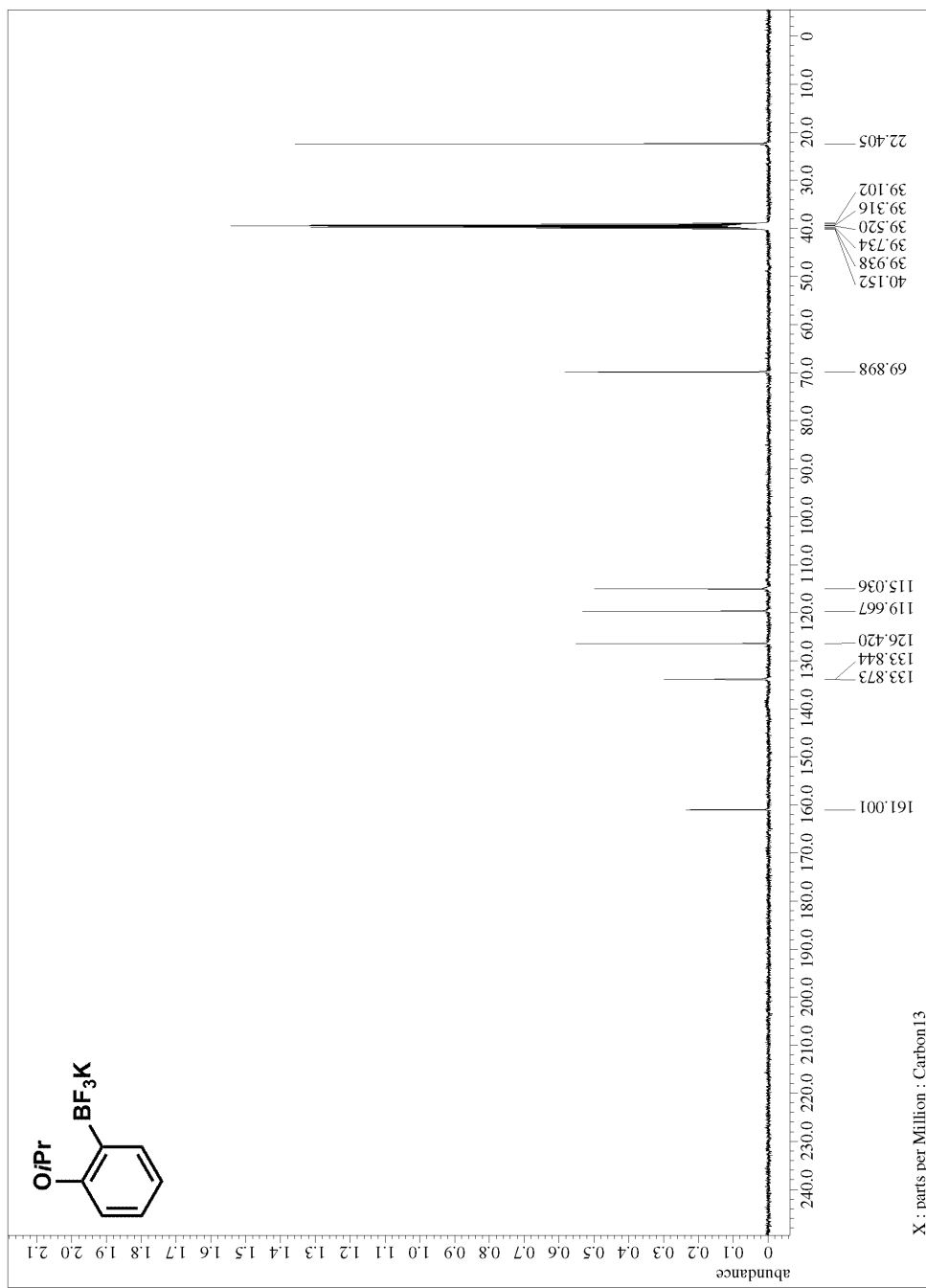


Figure A.2.38. ^{13}C NMR for precursor to compound 336

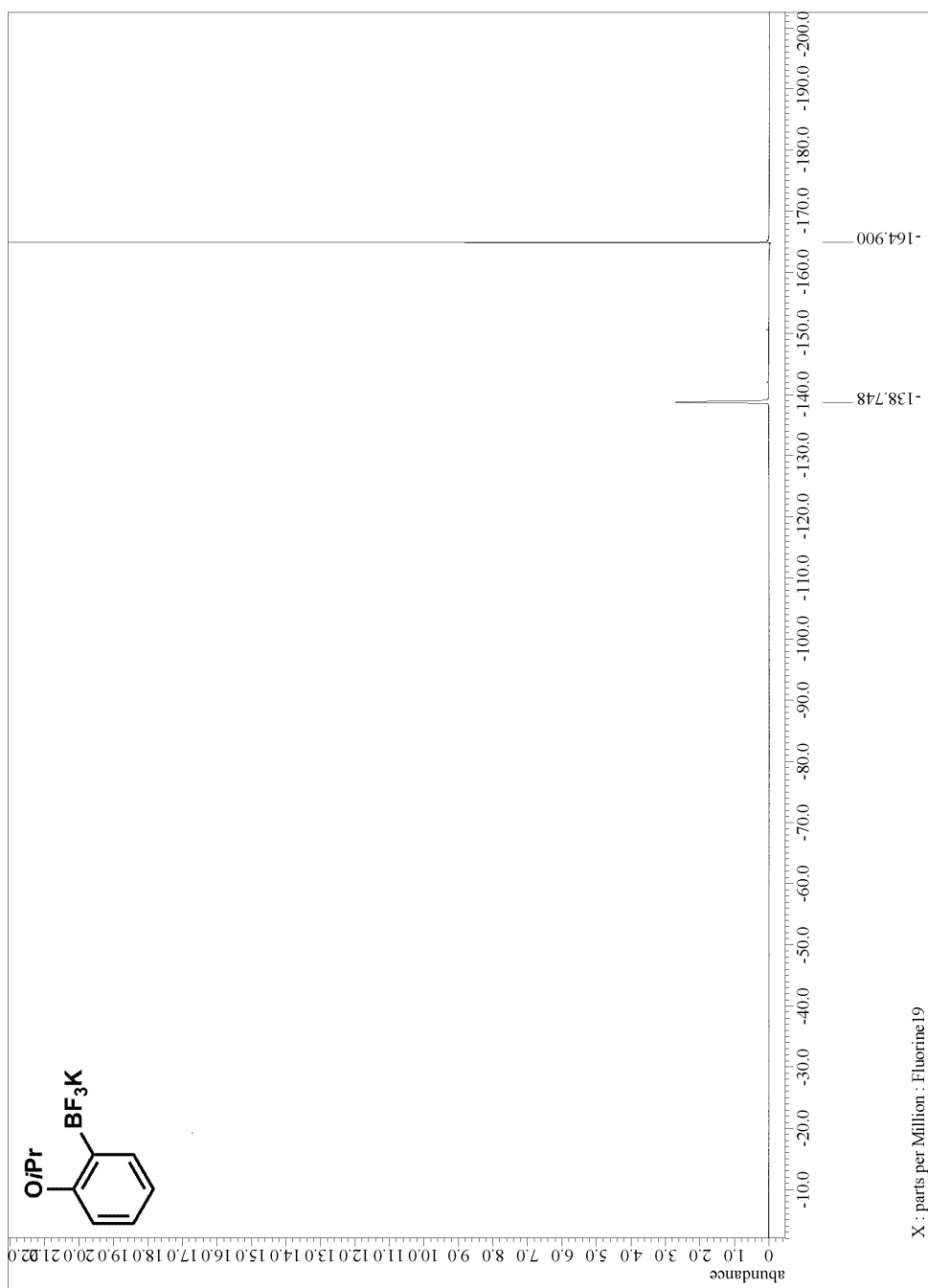


Figure A.2.39. ^{19}F NMR for precursor to compound **336**

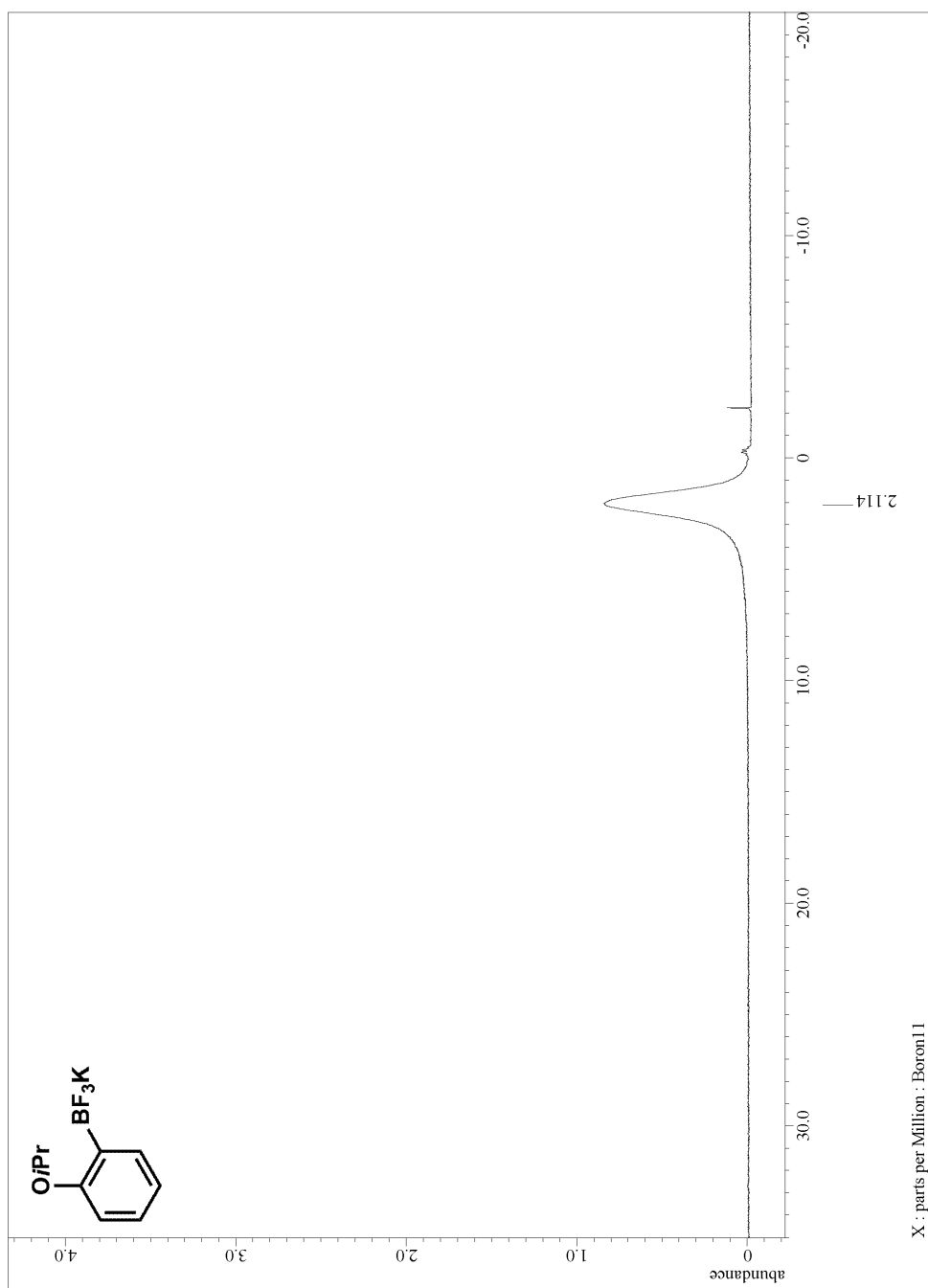


Figure A.2.40. ^{11}B NMR for precursor to compound **336**

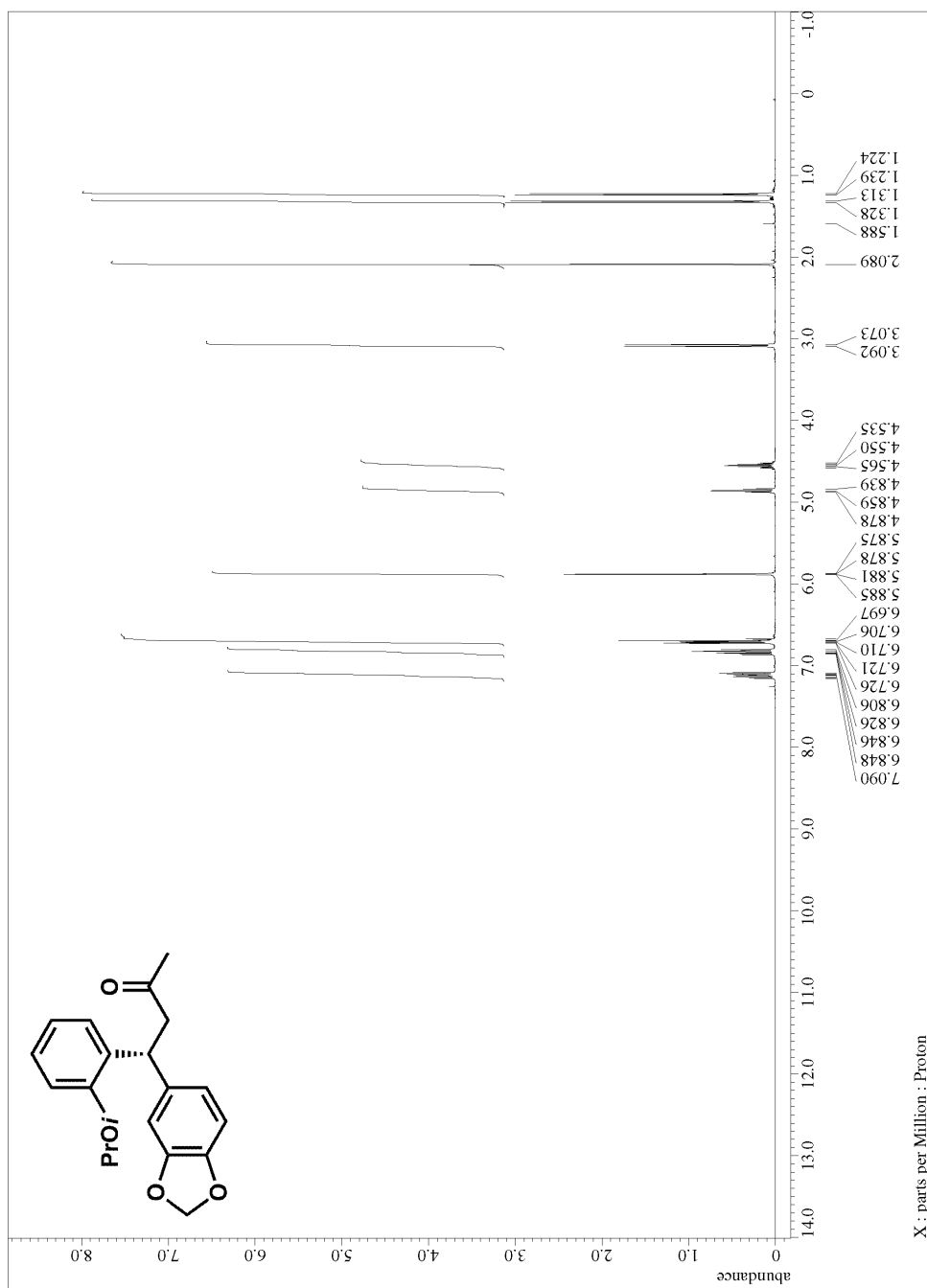


Figure A.2.41. ^1H NMR for compound 336

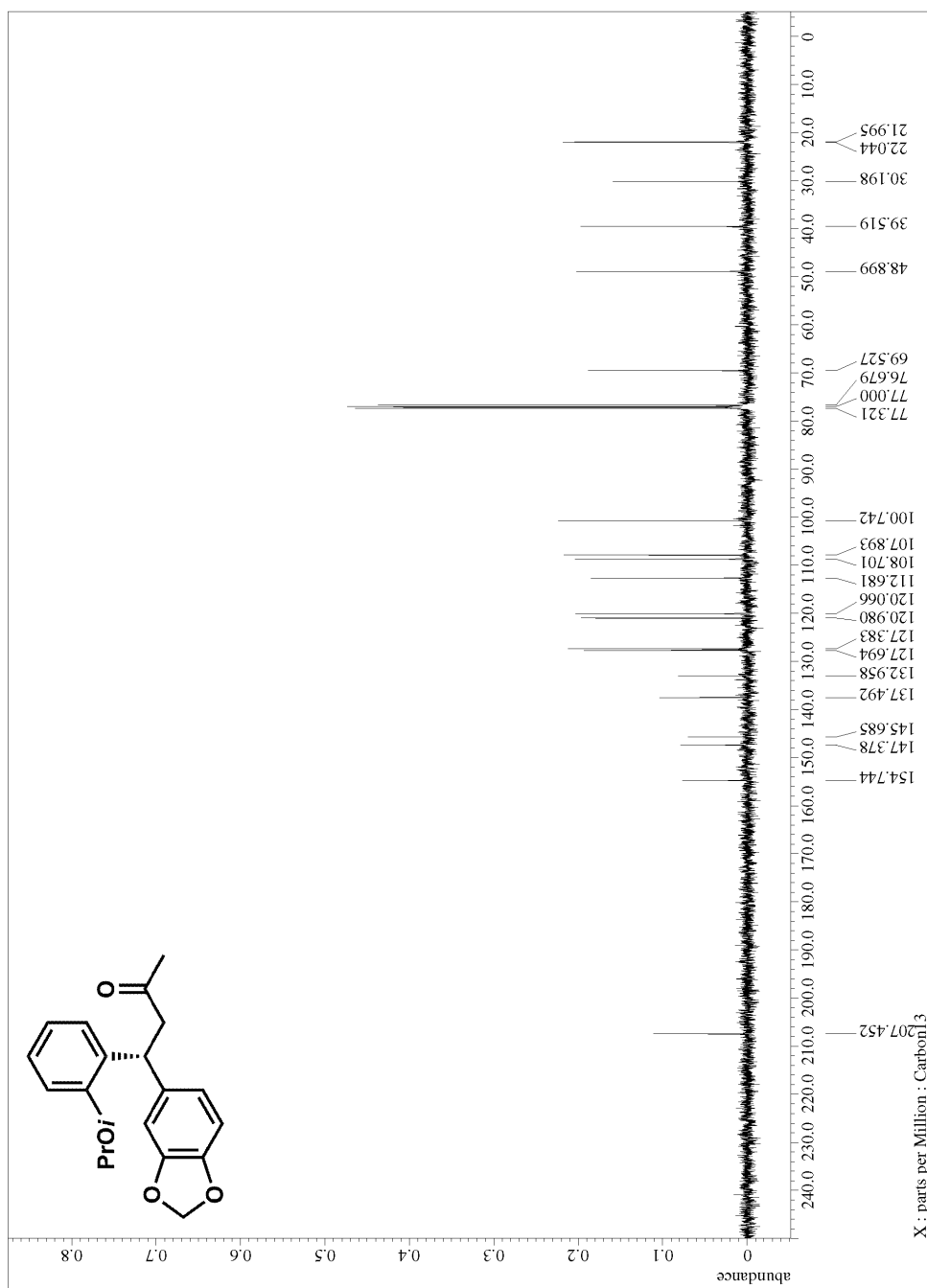
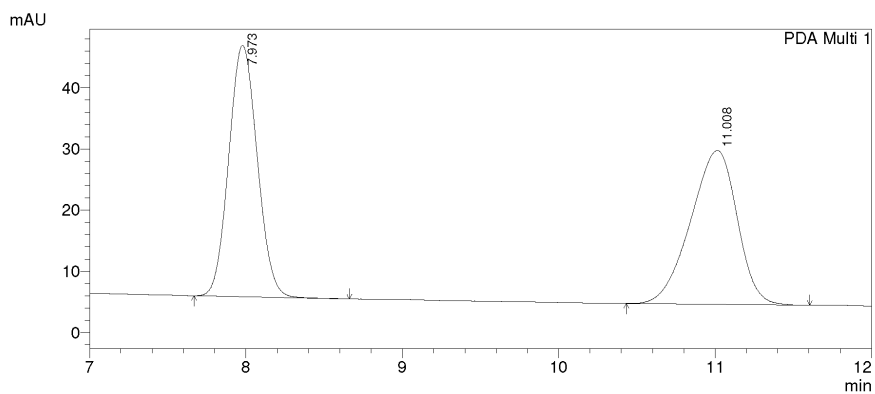


Figure A.2.42. ^{13}C NMR for compound 336

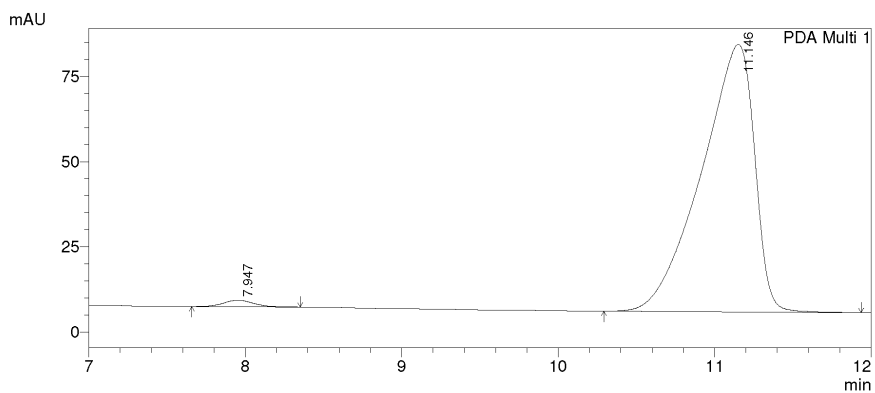


1 PDA Multi 1/254nm 4nm

PeakTable

PDA Ch1 254nm 4nm

Peak#	Ret. Time	Area	Height	Area %	Height %
1	7.973	519604	41115	49.970	62.053
2	11.008	520233	25143	50.030	37.947
Total		1039837	66257	100.000	100.000



1 PDA Multi 1/254nm 4nm

PeakTable

PDA Ch1 254nm 4nm

Peak#	Ret. Time	Area	Height	Area %	Height %
1	7.947	24974	1878	1.334	2.339
2	11.146	1846688	78418	98.666	97.661
Total		1871663	80296	100.000	100.000

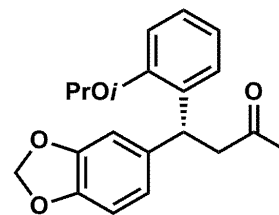


Figure A.2.43. HPLC trace for compound 336

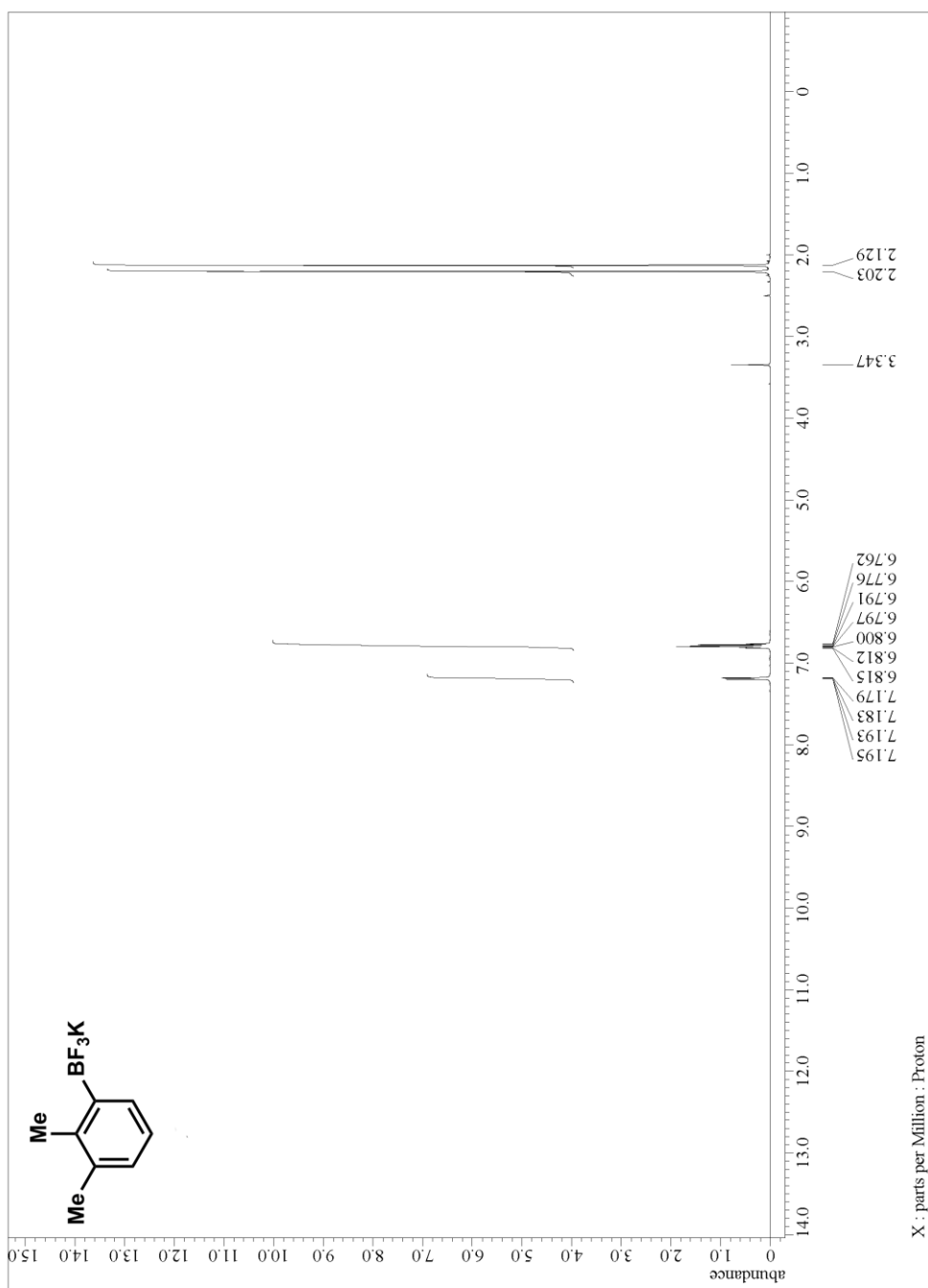


Figure A.2.44. ^1H NMR for precursor to compound 337

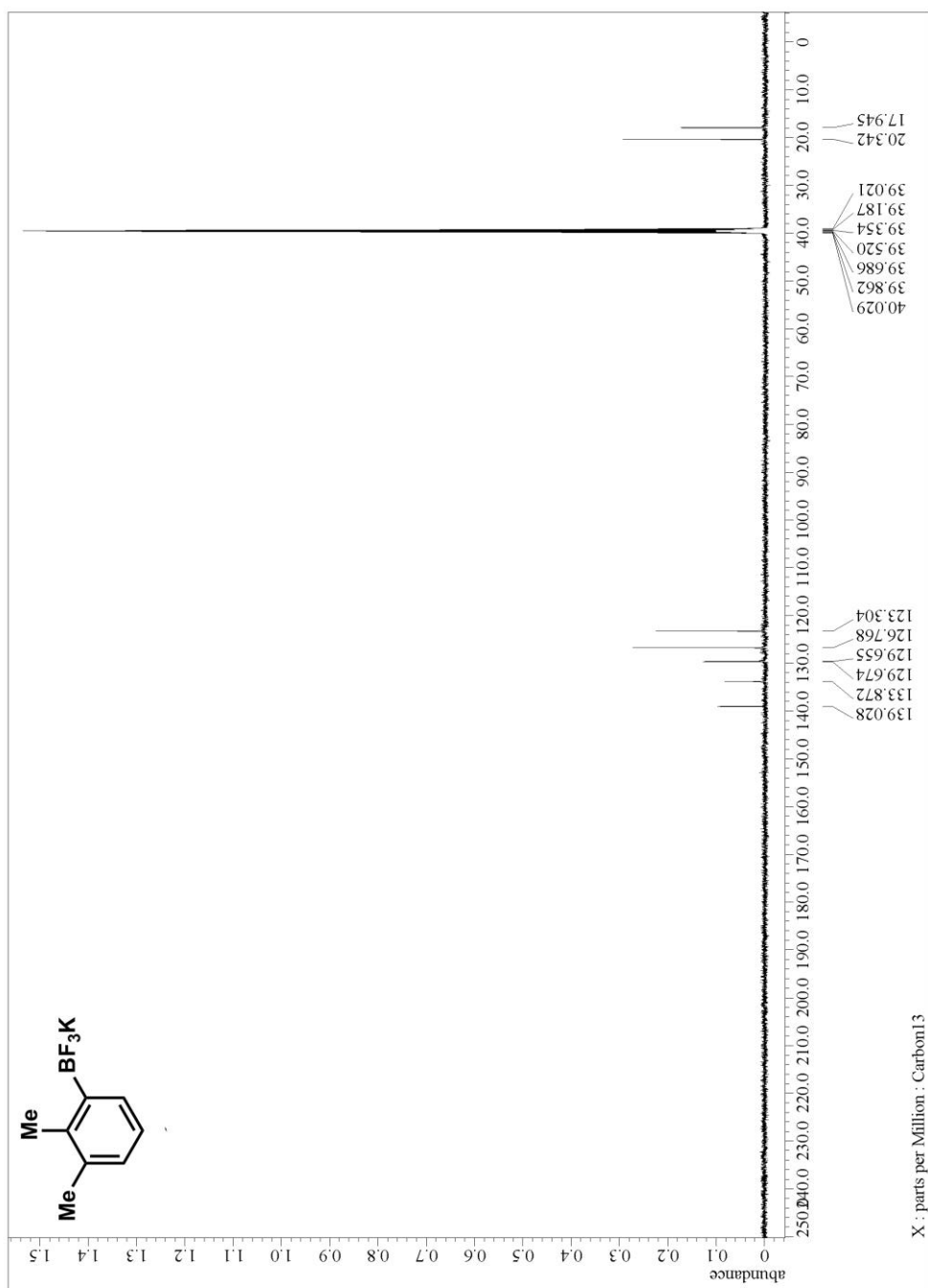


Figure A.2.45. ^{13}C NMR for precursor to compound 337

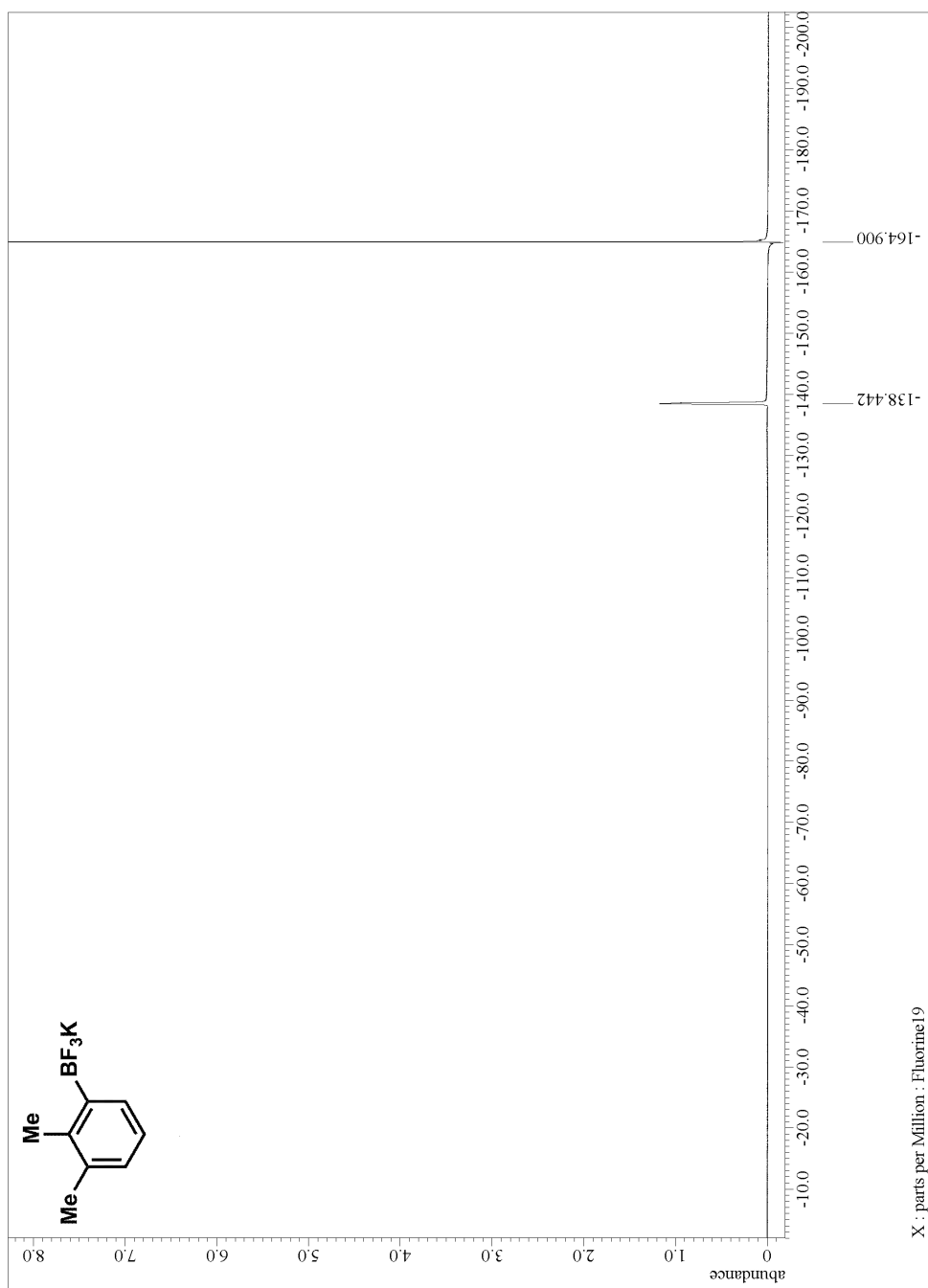


Figure A.2.46. ^{19}F NMR for precursor to compound 337

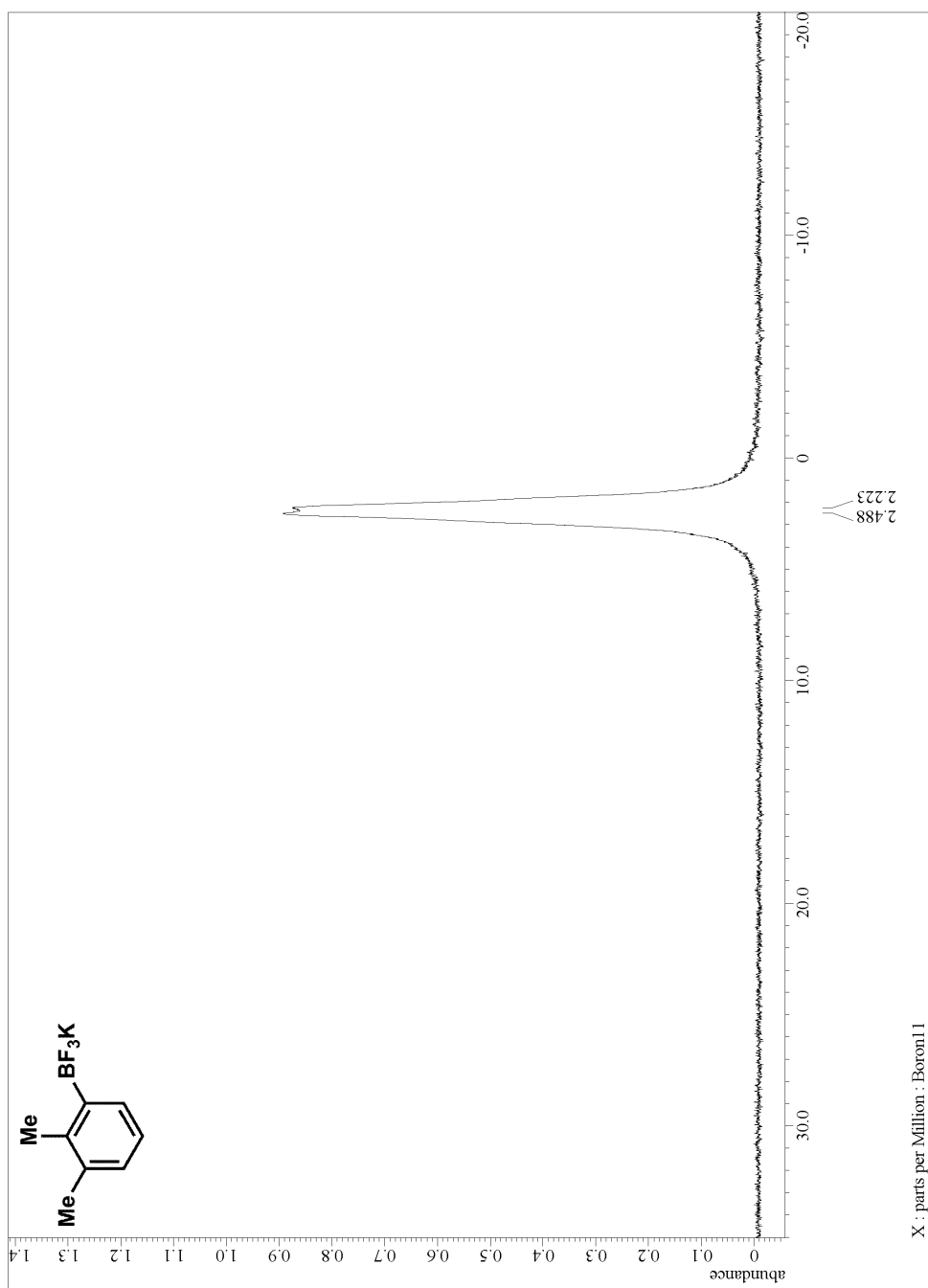


Figure A.2.47. ^{11}B NMR for precursor to compound 337

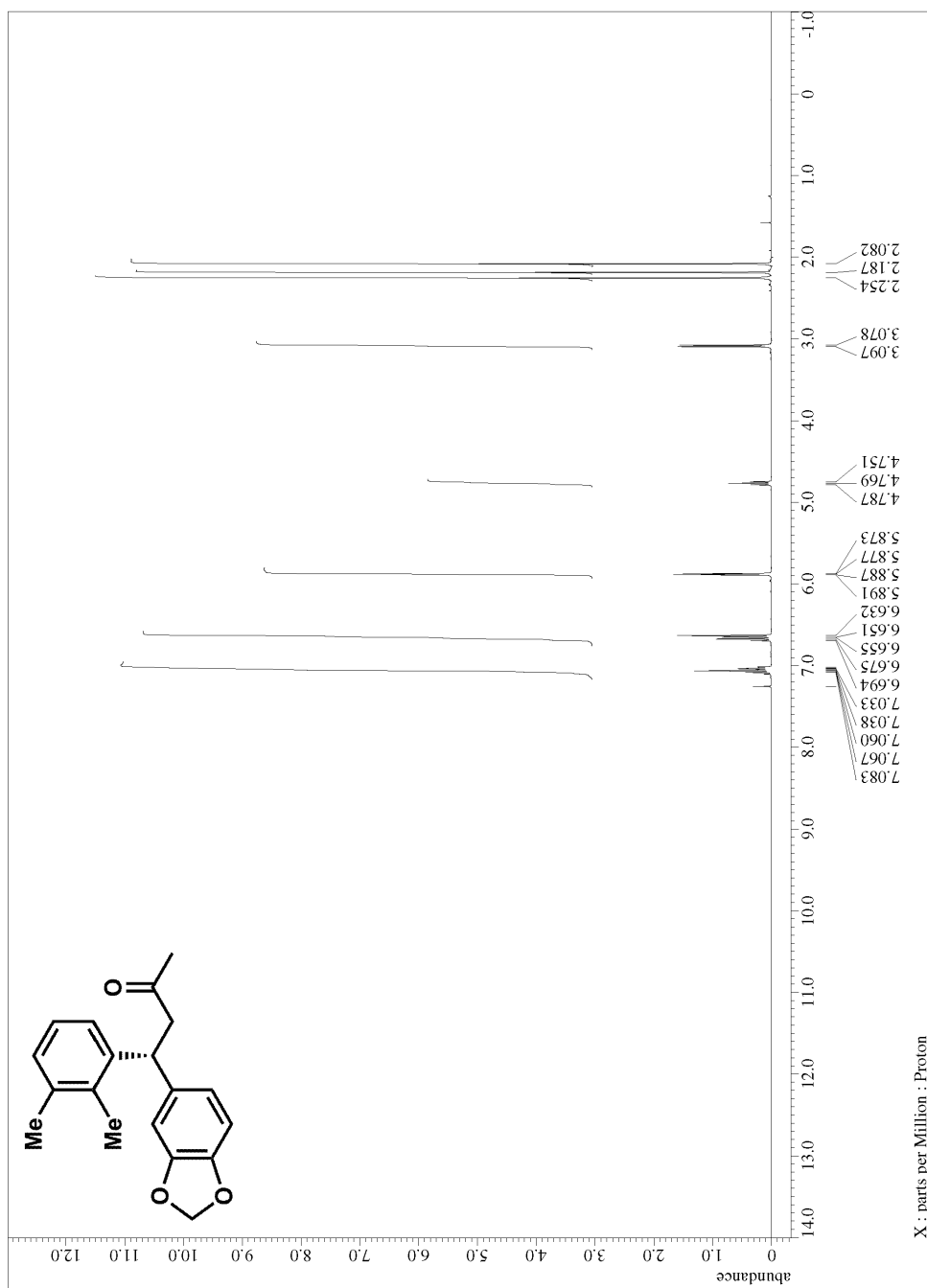


Figure A.2.48. ^1H NMR for compound 337

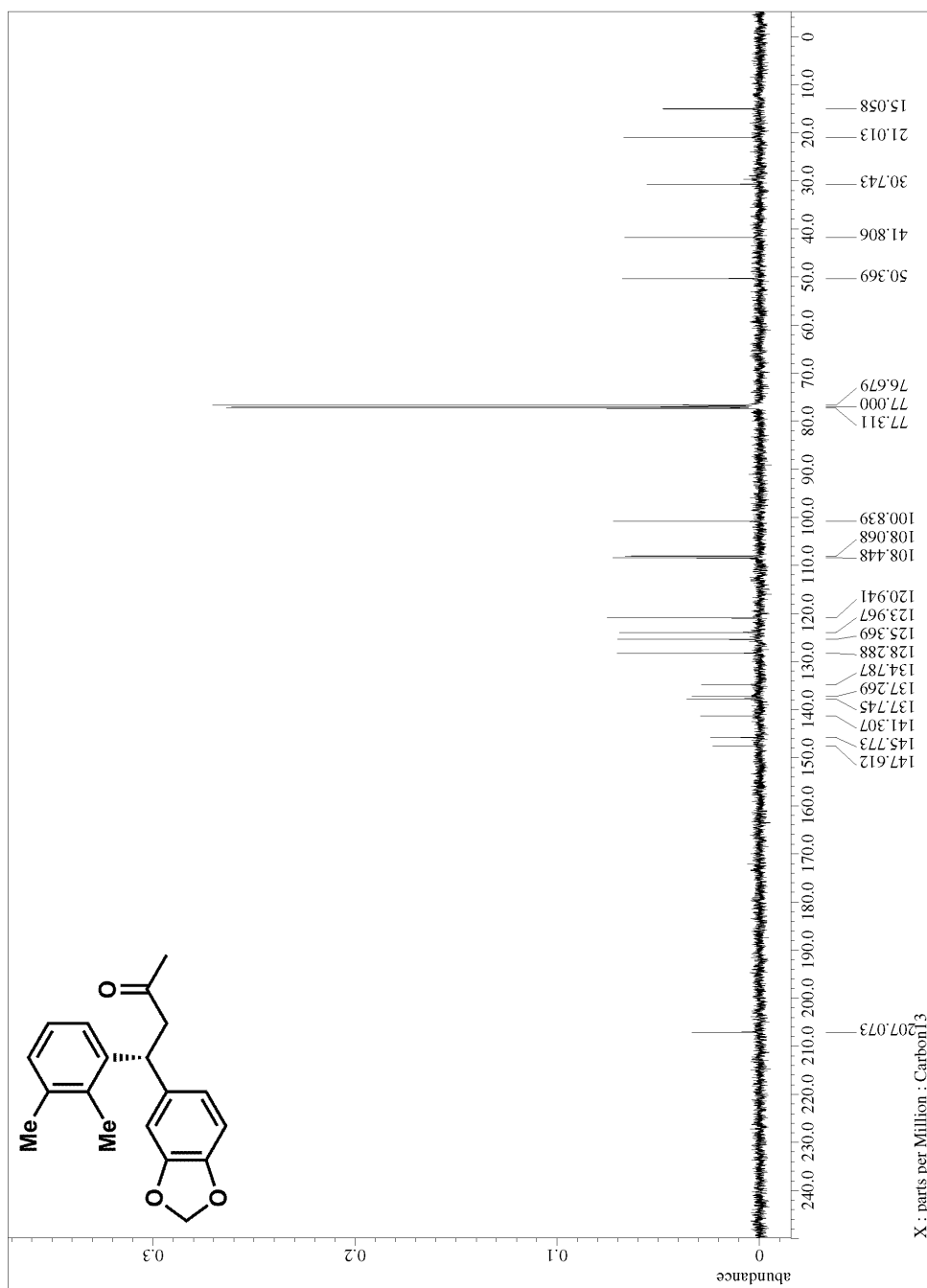
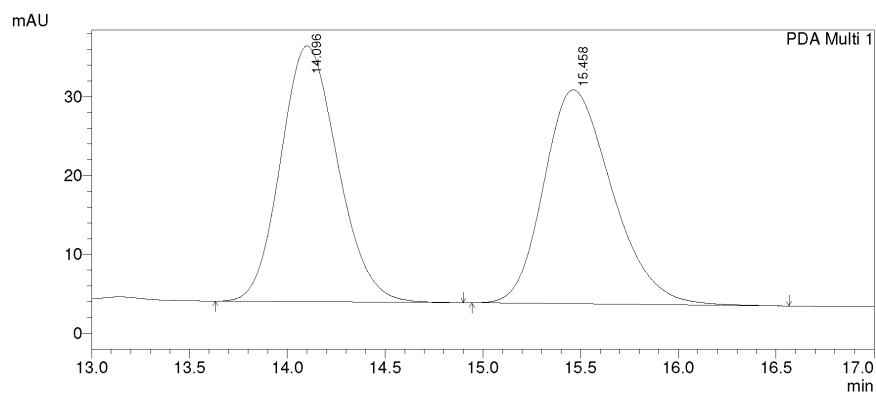
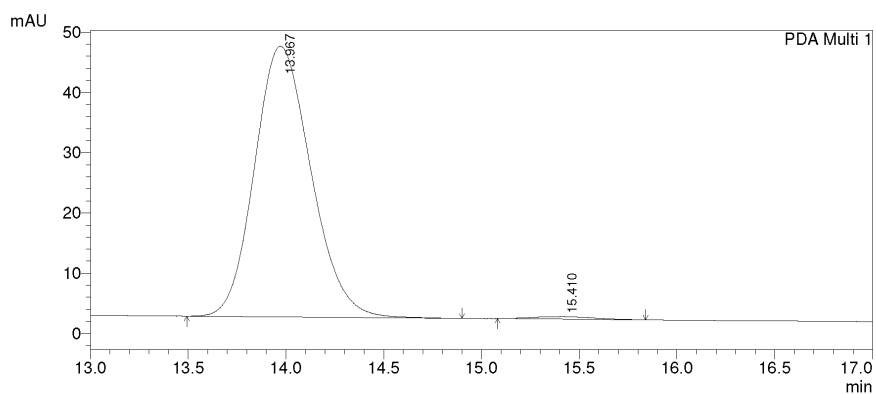


Figure A.2.49. ^{13}C NMR for compound 337



PeakTable

Peak#	Ret. Time	Area	Height	Area %	Height %
1	14.096	656721	32412	49.921	54.467
2	15.458	658802	27096	50.079	45.533
Total		1315523	59508	100.000	100.000



PeakTable

Peak#	Ret. Time	Area	Height	Area %	Height %
1	13.967	899299	44905	99.046	99.114
2	15.410	8664	401	0.954	0.886
Total		907962	45306	100.000	100.000

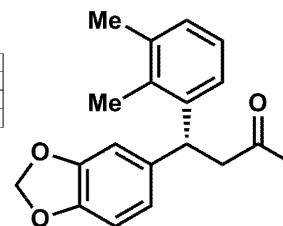


Figure A.2.50. HPLC trace for compound 337

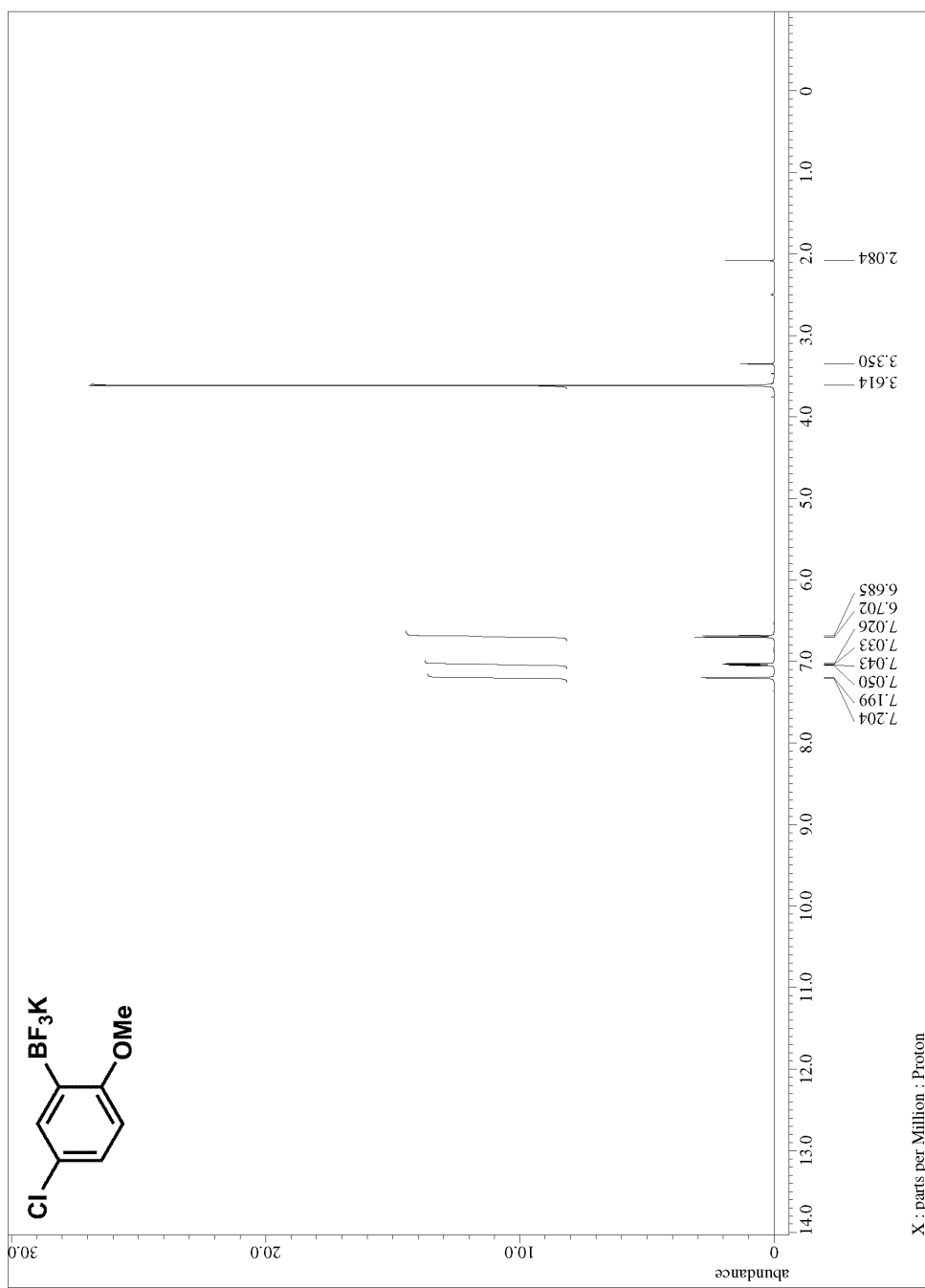


Figure A.2.51. ¹H NMR for precursor to compound 338

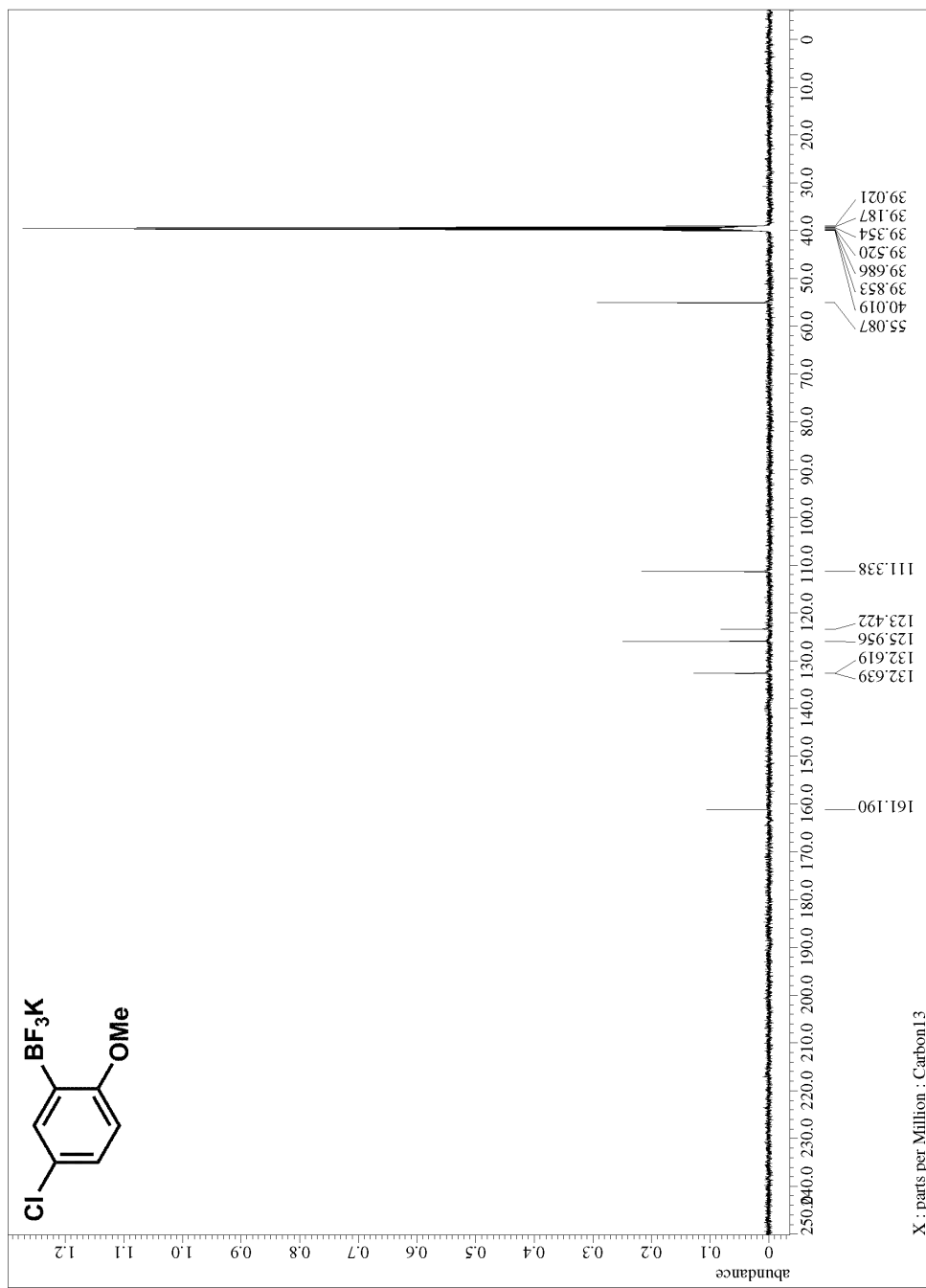


Figure A.2.52. ^{13}C NMR for precursor to compound **338**

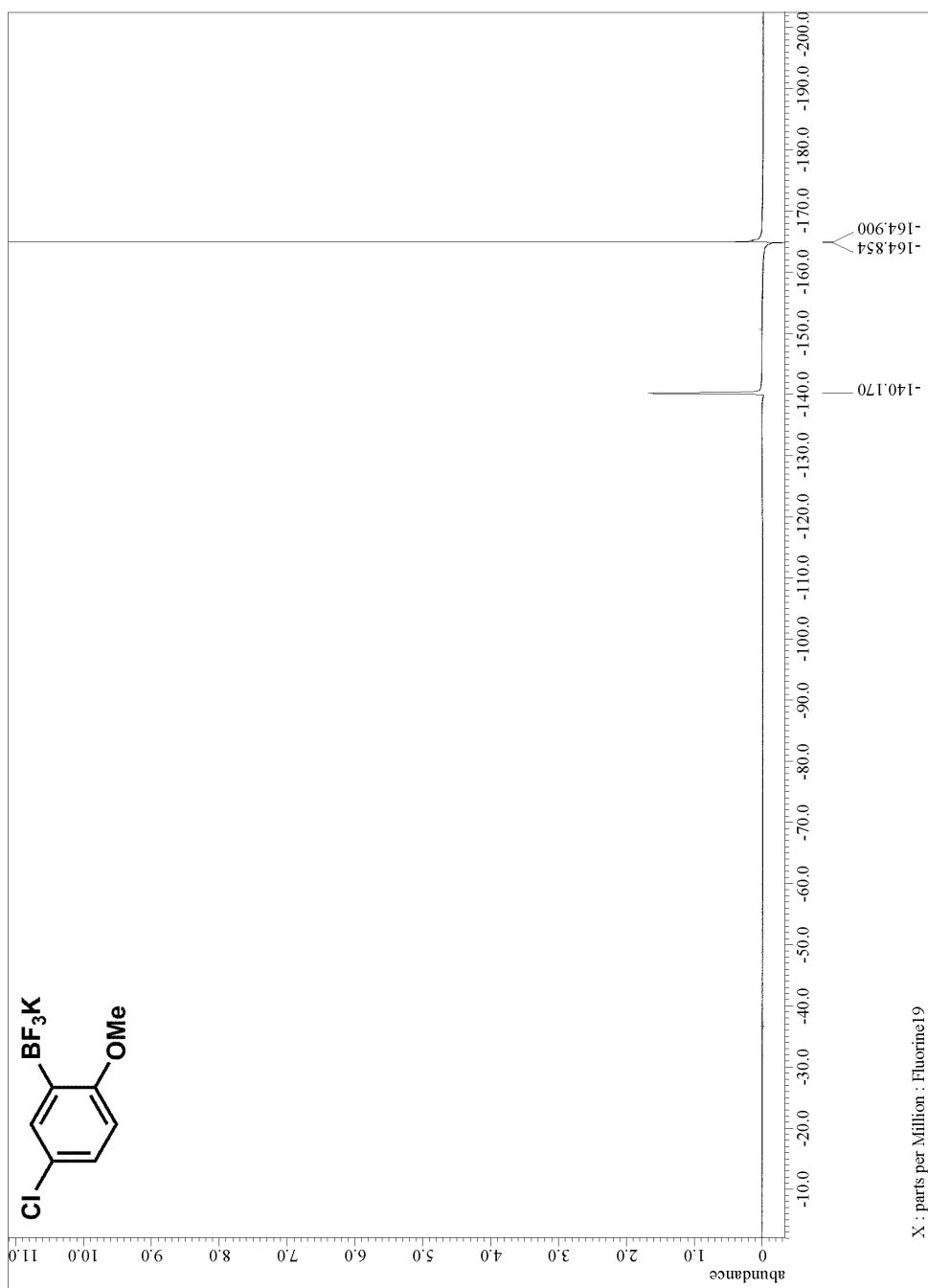


Figure A.2.53. ^{19}F NMR for precursor to compound **338**

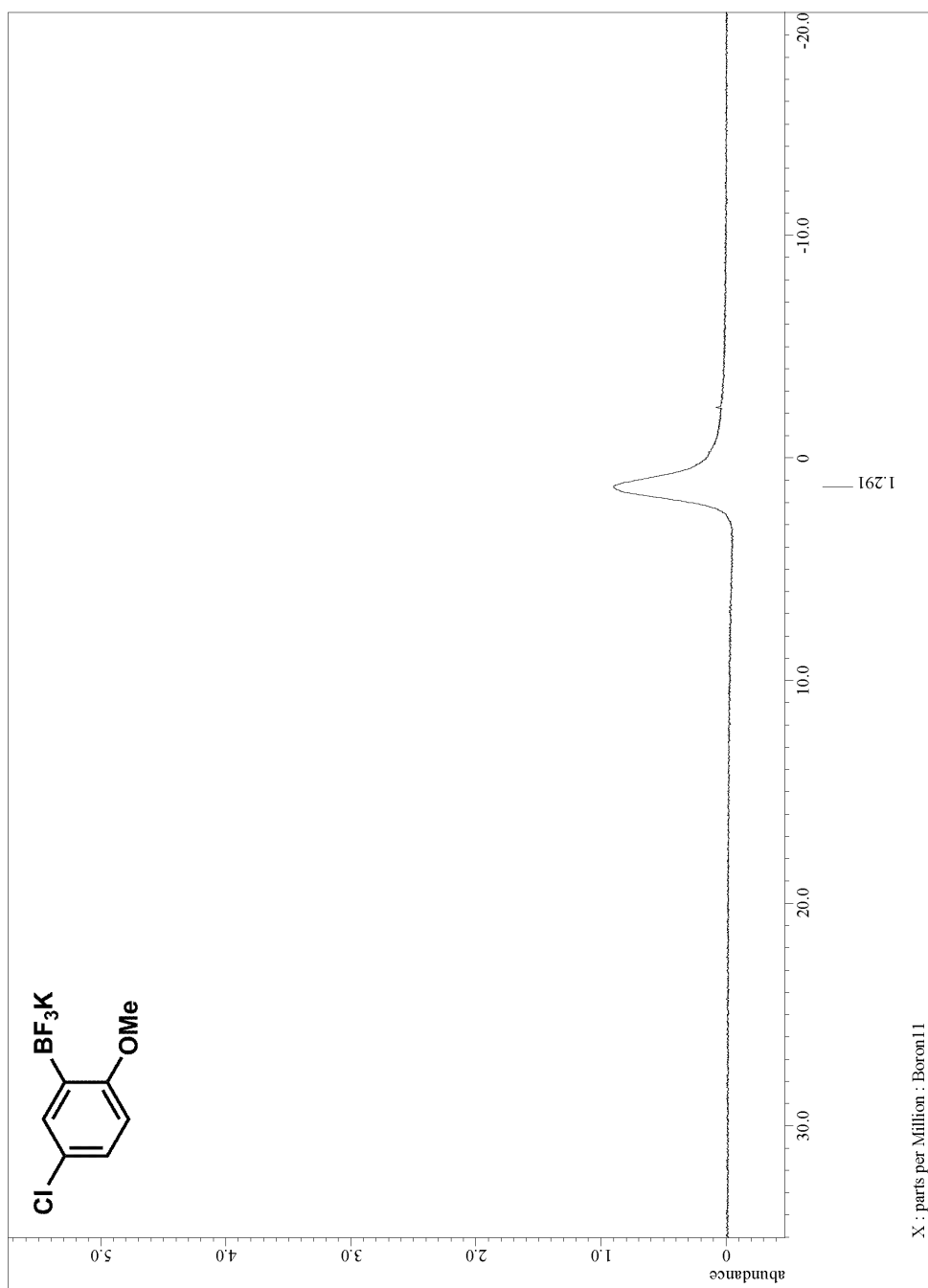


Figure A.2.54. ^{11}B NMR for precursor to compound 338

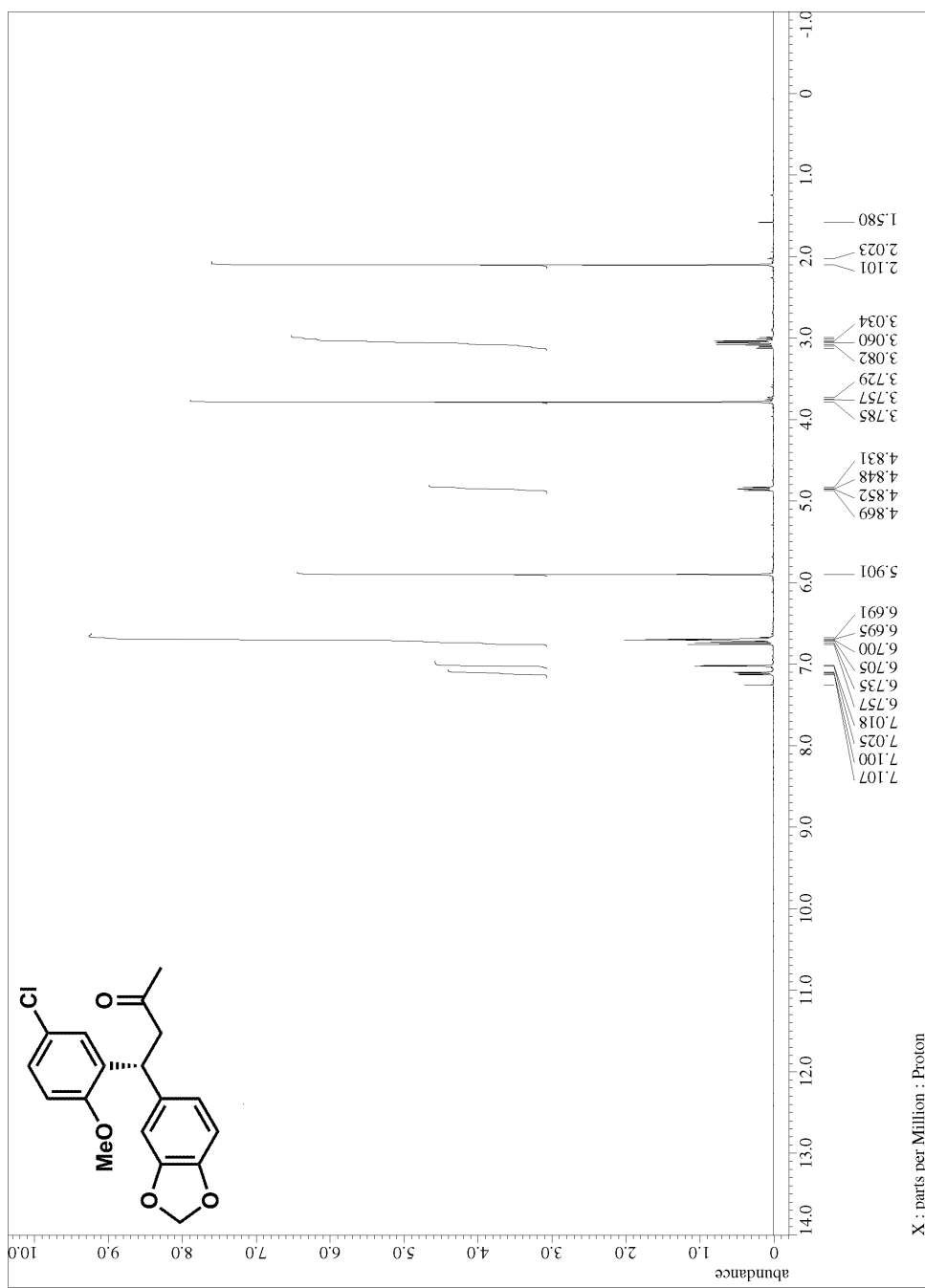


Figure A.2.55. ¹H NMR for compound 338

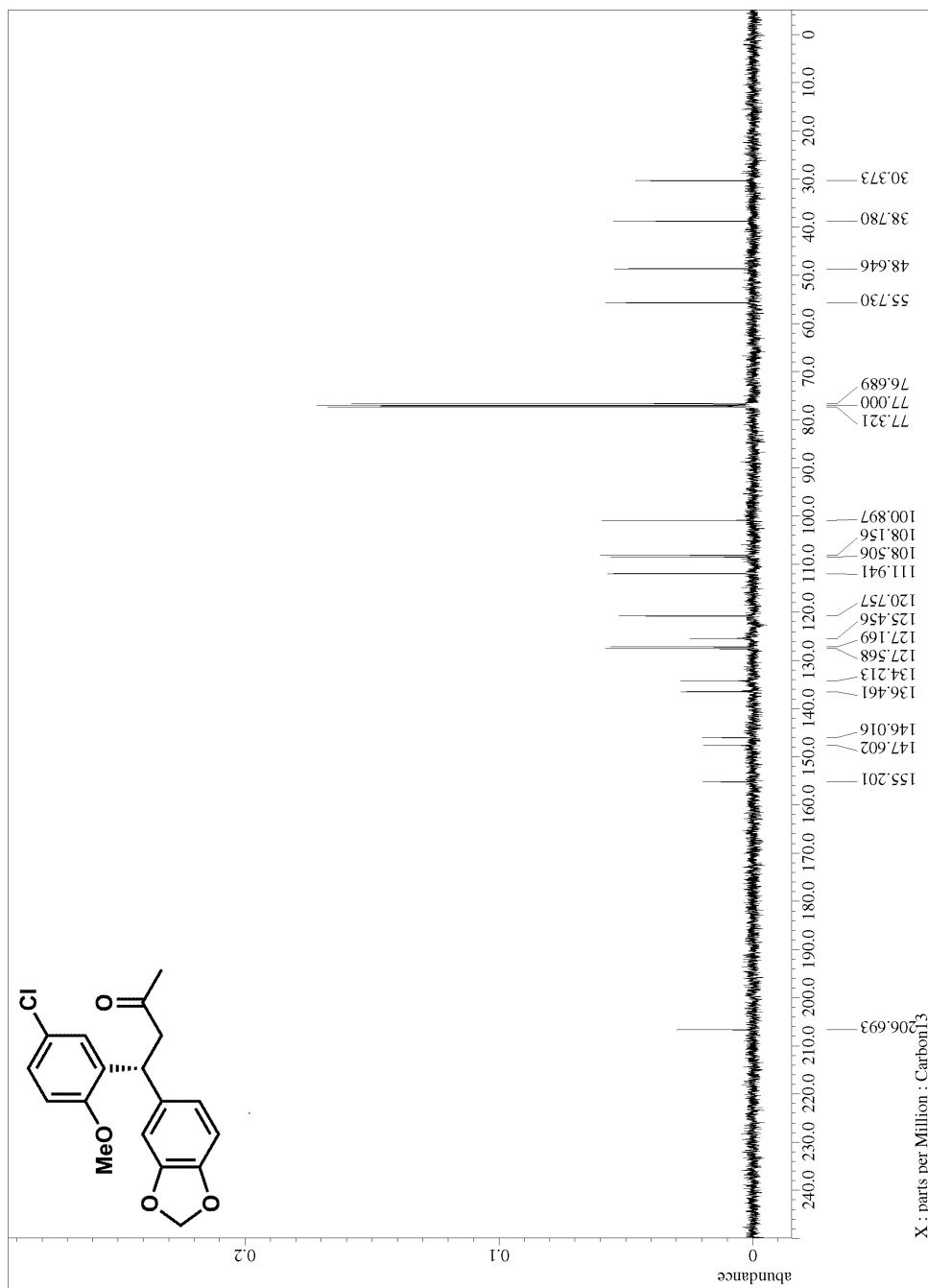
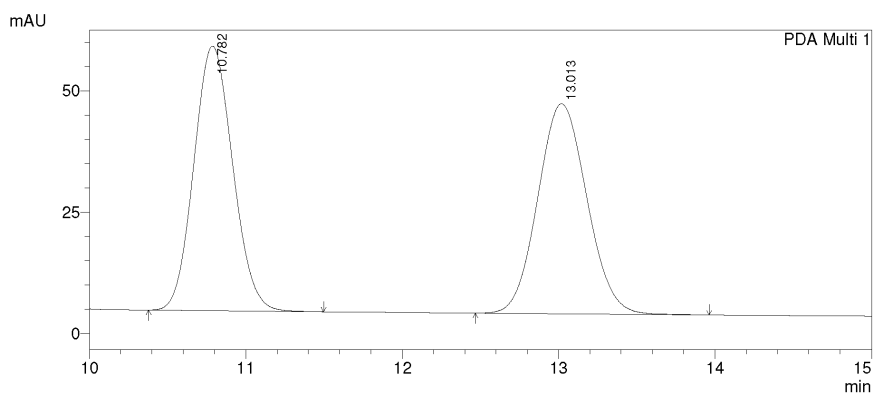
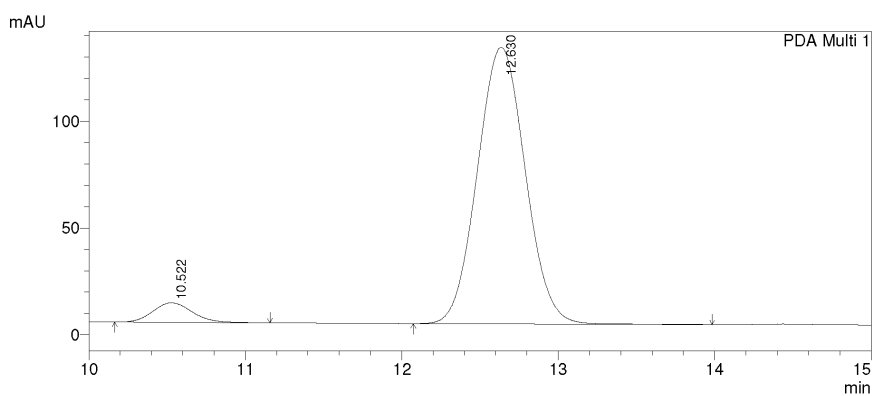


Figure A.2.56. ^{13}C NMR for compound **338**



PeakTable

Peak#	Ret. Time	Area	Height	Area %	Height %
1	10.782	939868	54485	49.996	55.764
2	13.013	940029	43222	50.004	44.236
Total		1879897	97707	100.000	100.000



PeakTable

Peak#	Ret. Time	Area	Height	Area %	Height %
1	10.522	160304	9136	5.511	6.596
2	12.630	2748518	129378	94.489	93.404
Total		2908822	138515	100.000	100.000

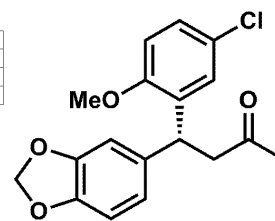


Figure A.2.57. HPLC trace for compound 338

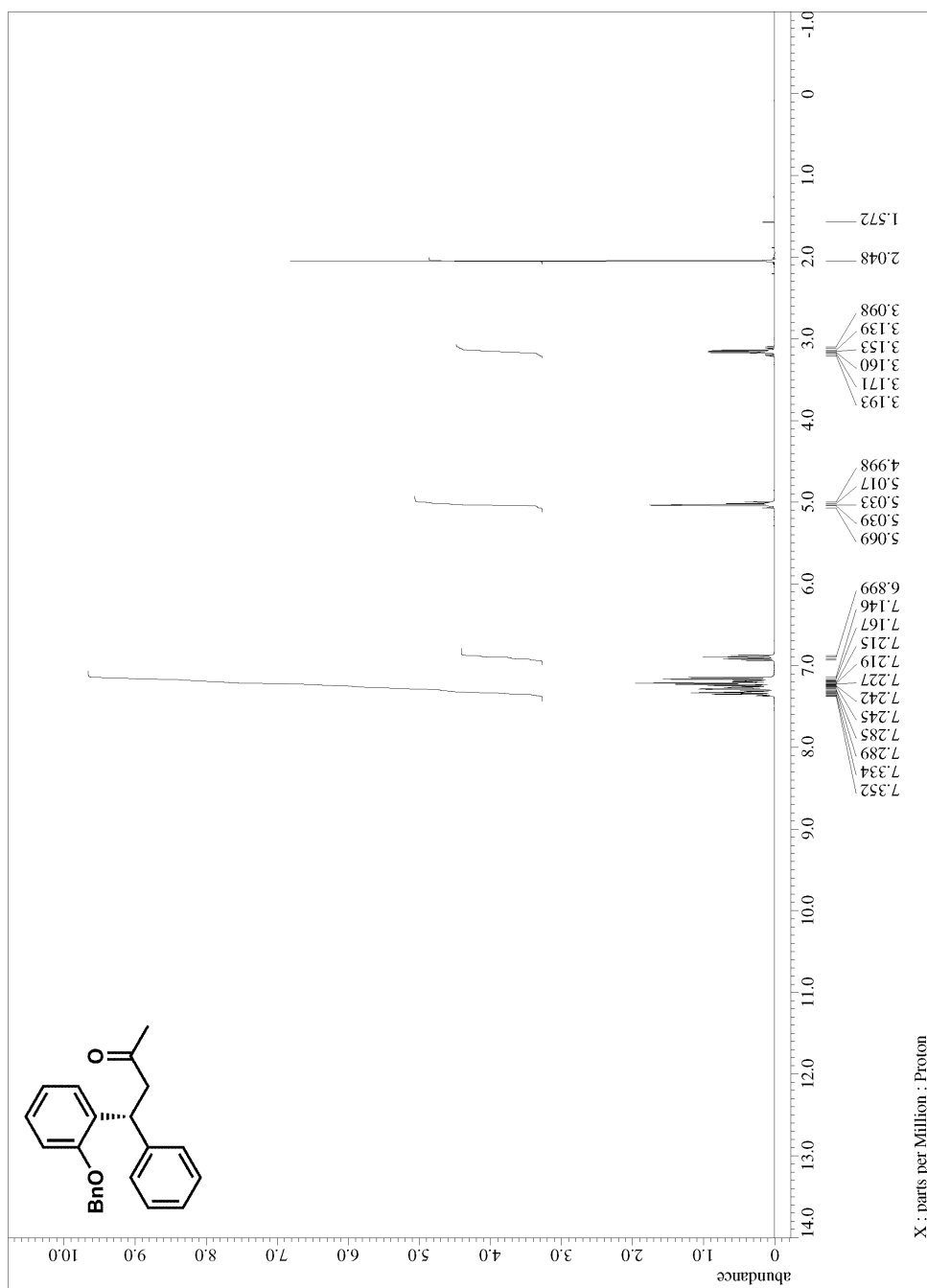


Figure A.2.58. ¹H NMR for compound **340**

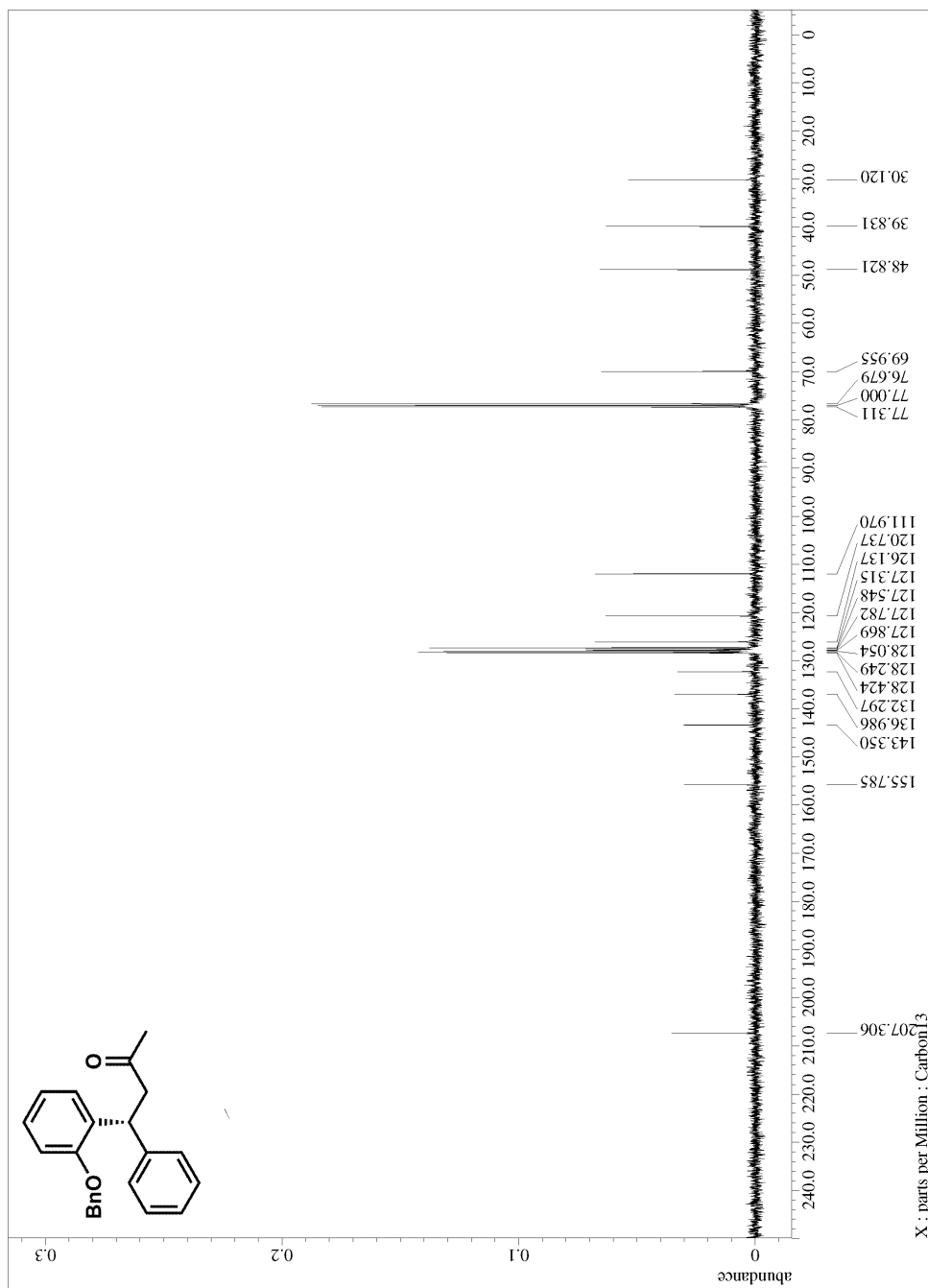
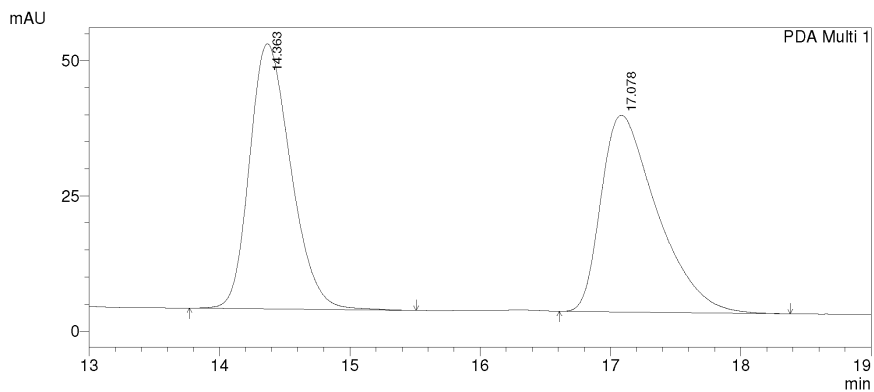


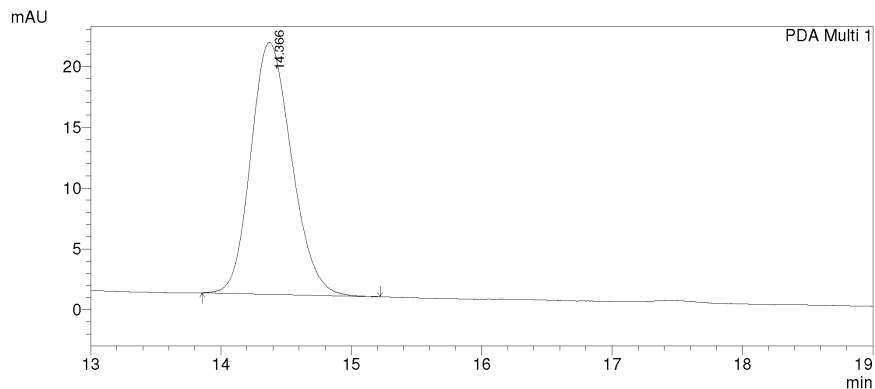
Figure A.2.59. ^{13}C NMR for compound **340**



PeakTable

PDA Ch1 254nm 4nm

Peak#	Ret. Time	Area	Height	Area %	Height %
1	14.363	1078666	49068	49.792	57.410
2	17.078	1087696	36401	50.208	42.590
Total		2166362	85469	100.000	100.000



PeakTable

PDA Ch1 254nm 4nm

Peak#	Ret. Time	Area	Height	Area %	Height %
1	14.366	450205	20687	100.000	100.000
Total		450205	20687	100.000	100.000

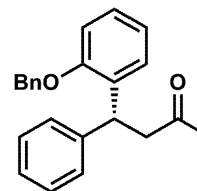


Figure A.2.60. HPLC trace for compound **340**

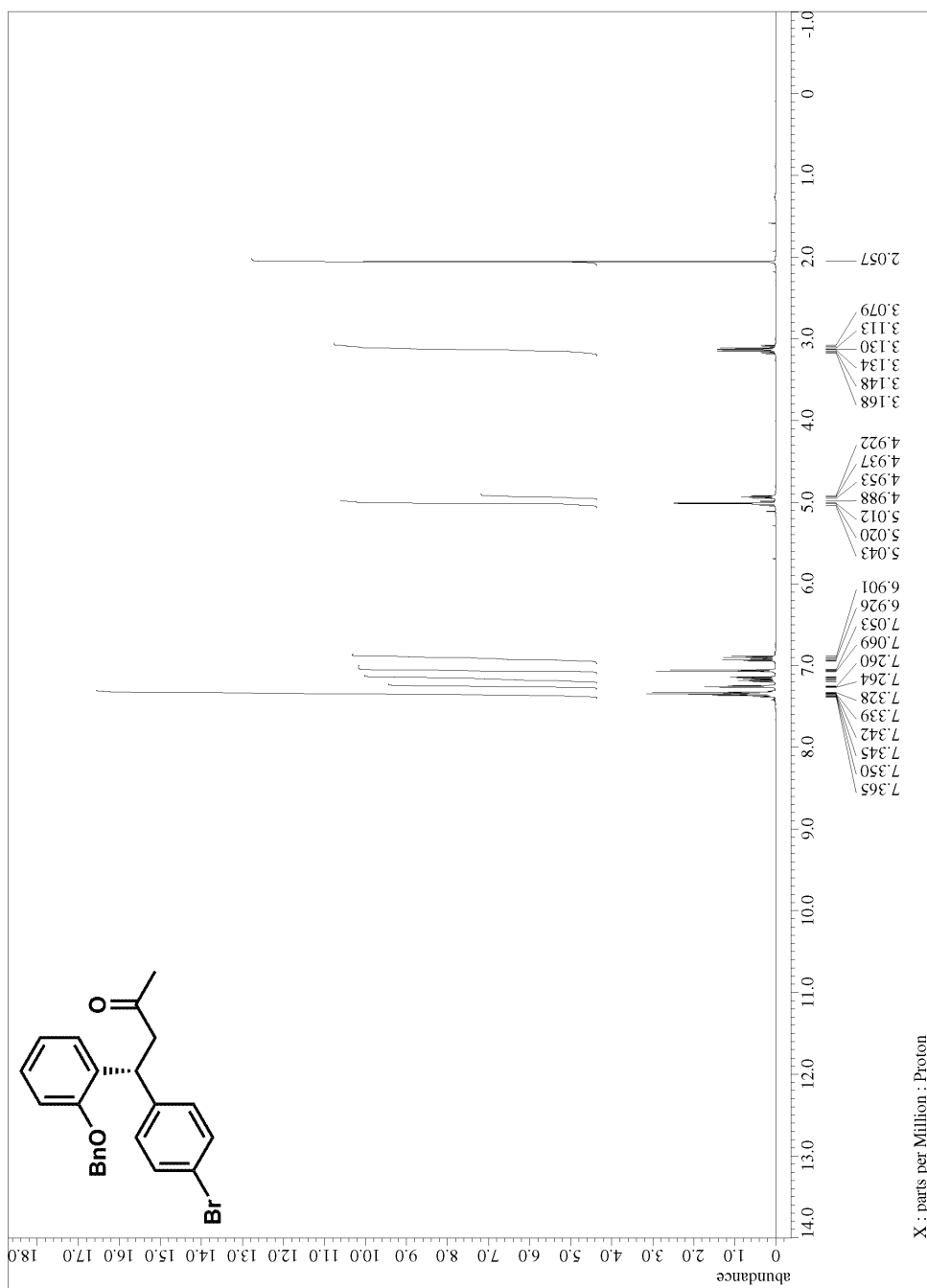


Figure A.2.61. ^1H NMR for compound 341

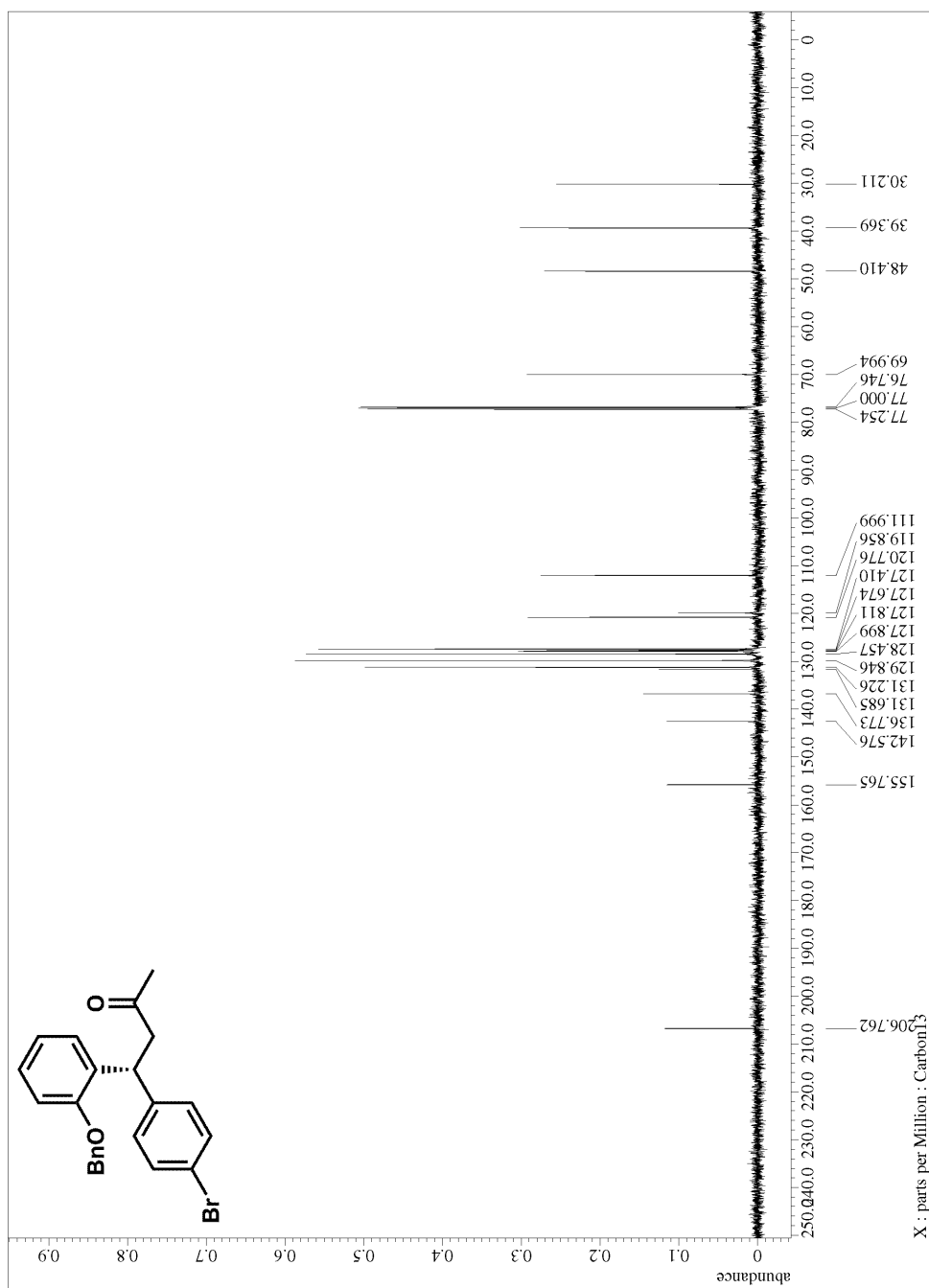
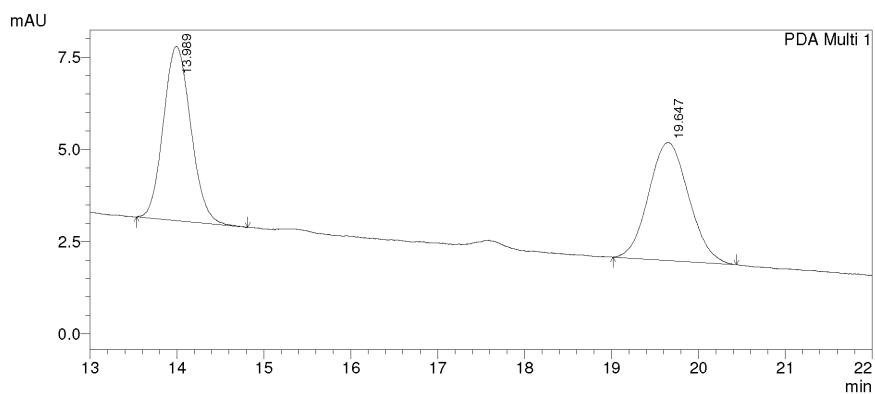
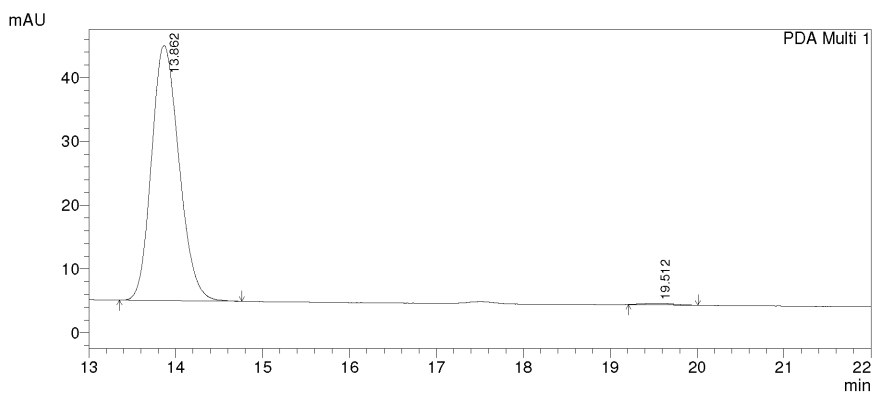


Figure A.2.62. ^{13}C NMR for compound 341



PeakTable

Peak#	Ret. Time	Area	Height	Area %	Height %
1	13.989	103696	4729	50.394	59.631
2	19.647	102076	3201	49.606	40.369
Total		205772	7930	100.000	100.000



PeakTable

Peak#	Ret. Time	Area	Height	Area %	Height %
1	13.862	879167	39985	99.295	99.414
2	19.512	6244	236	0.705	0.586
Total		885411	40220	100.000	100.000

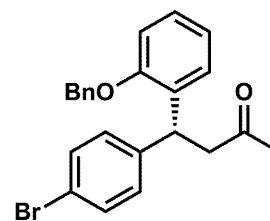


Figure A.2.63. HPLC trace for compound **341**

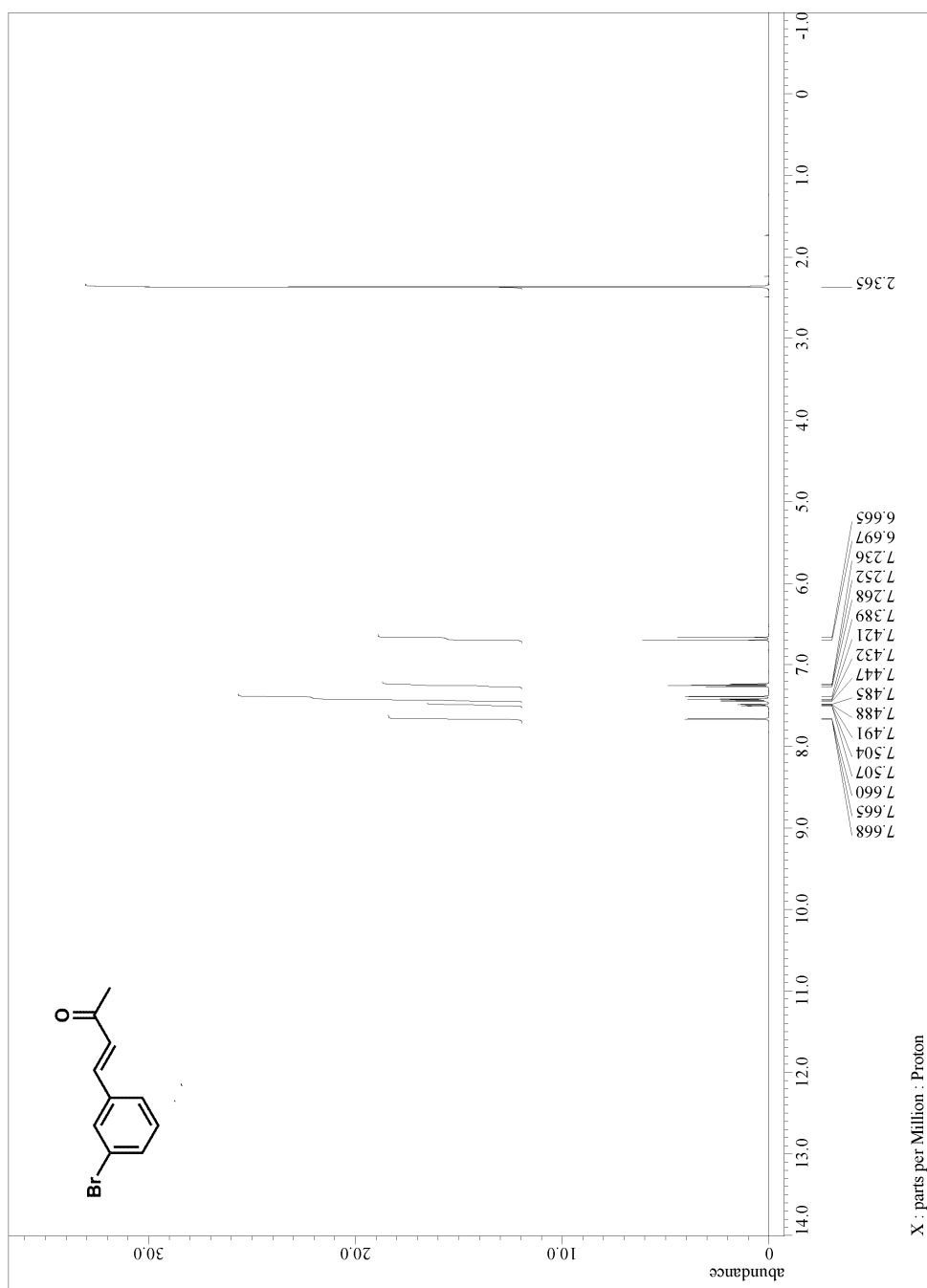


Figure A.2.64. ^1H NMR for precursor to compound **342**

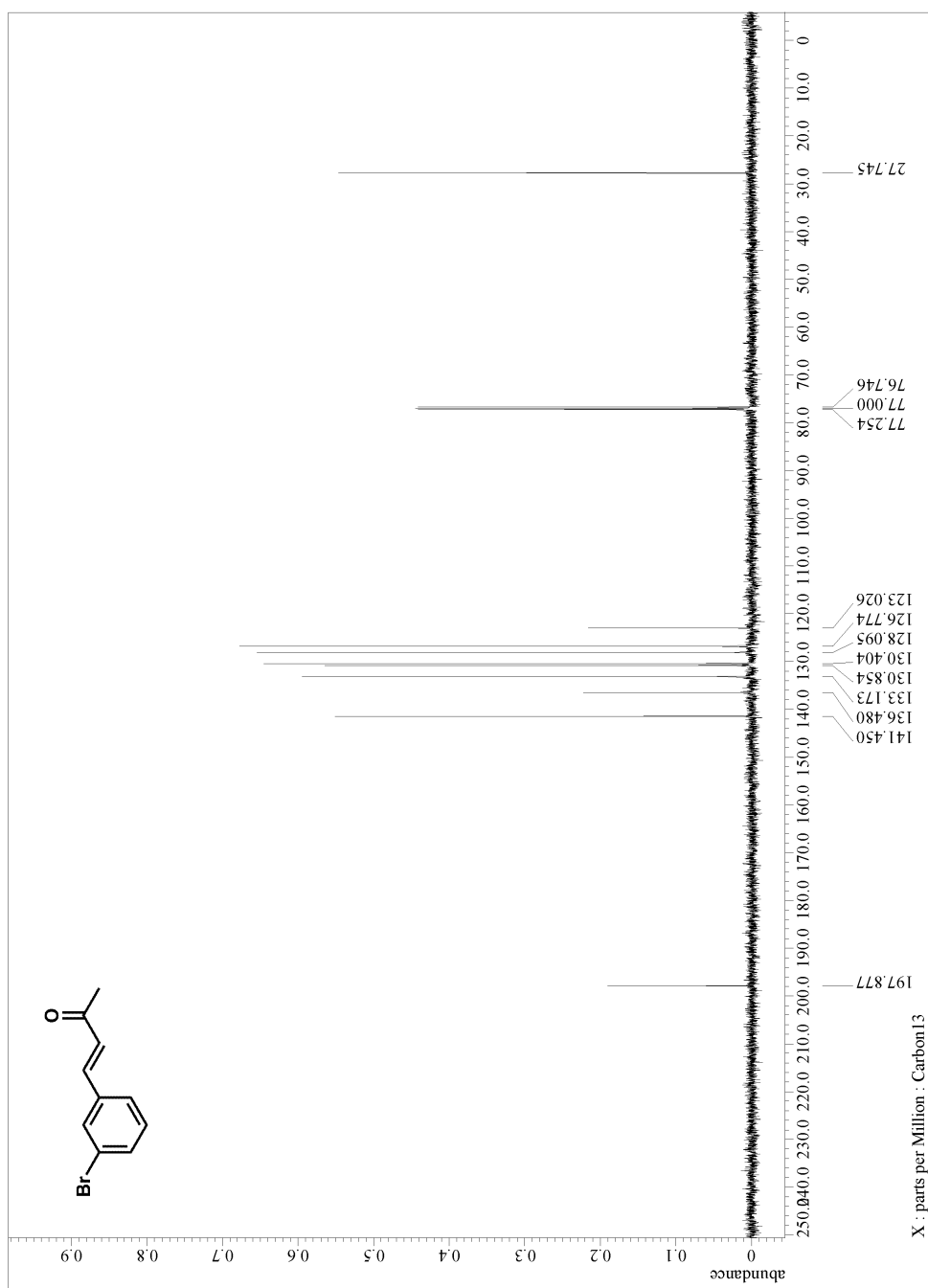


Figure A.2.65. ^{13}C NMR for precursor to compound 342

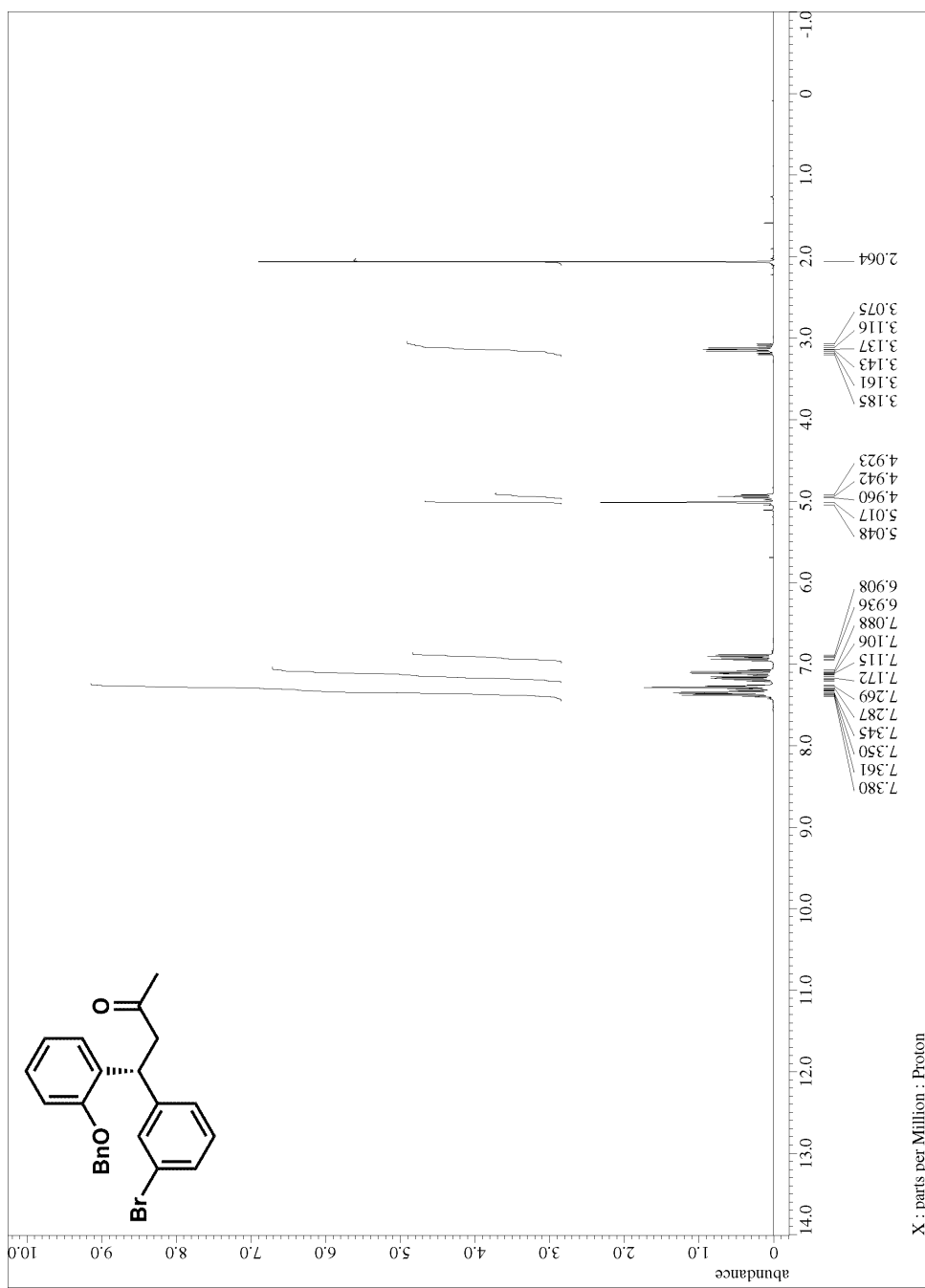


Figure A.2.66. ^1H NMR for compound **342**

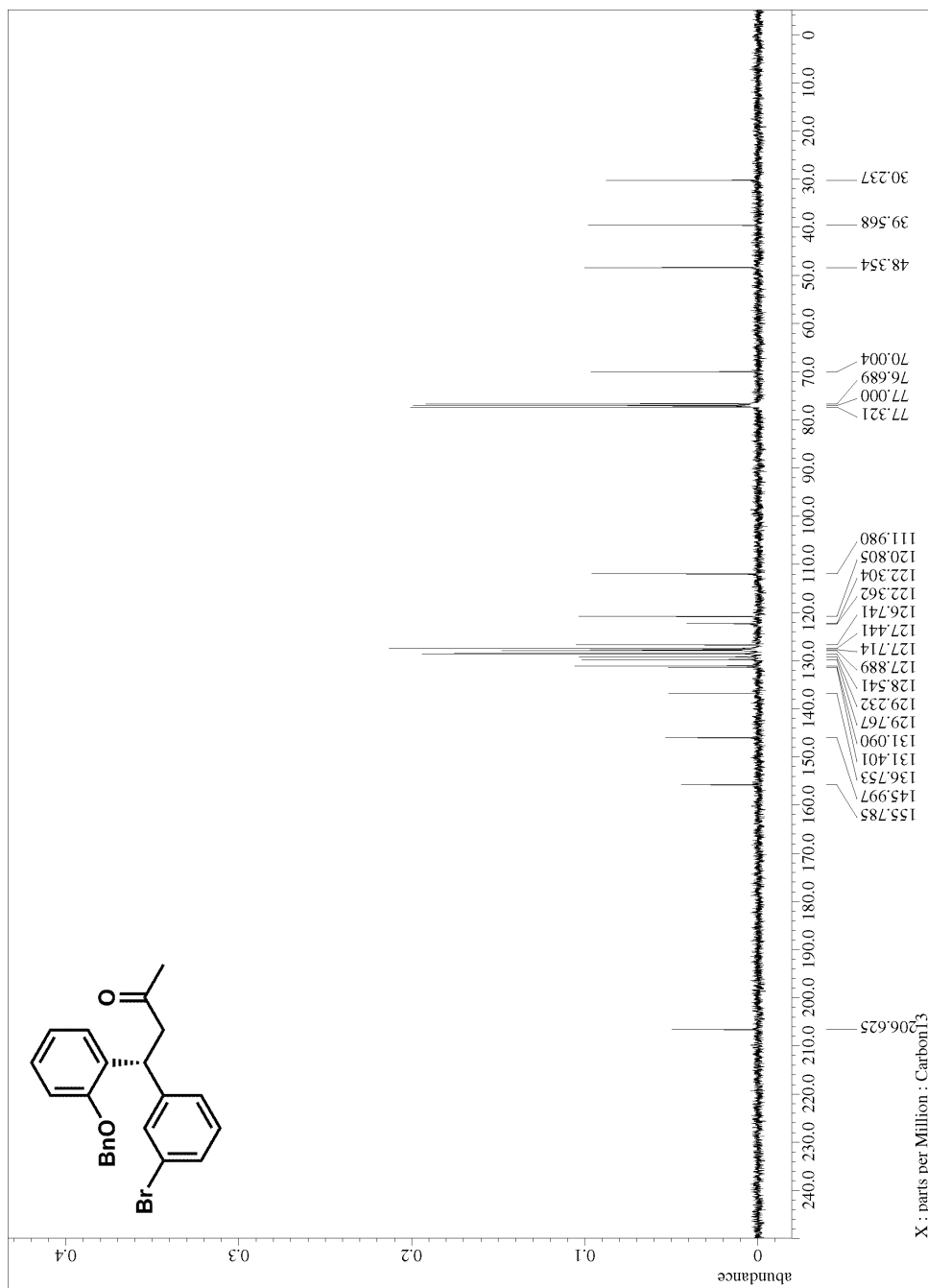
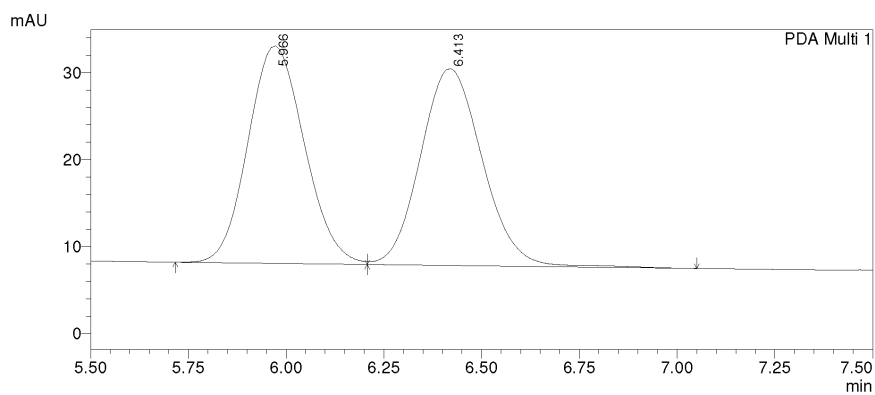
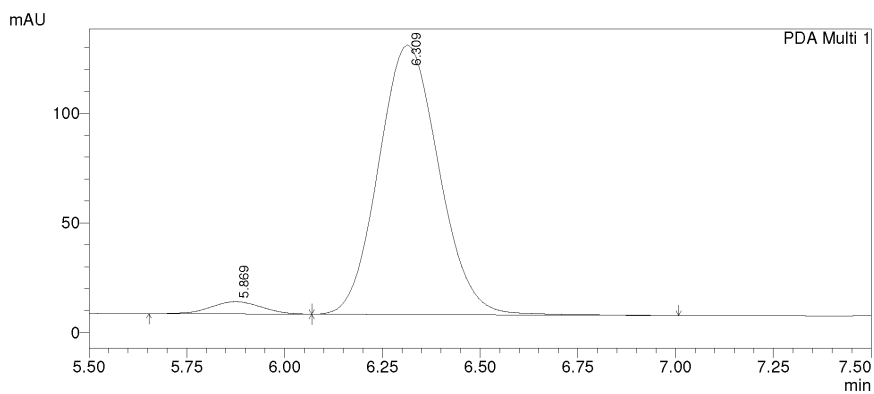


Figure A.2.67. ^{13}C NMR for compound 342



PeakTable

Peak#	Ret. Time	Area	Height	Area %	Height %
1	5.966	250291	25004	50.195	52.475
2	6.413	248346	22645	49.805	47.525
Total		498637	47649	100.000	100.000



PeakTable

Peak#	Ret. Time	Area	Height	Area %	Height %
1	5.869	50432	5622	3.692	4.371
2	6.309	1315654	122989	96.308	95.629
Total		1366086	128611	100.000	100.000

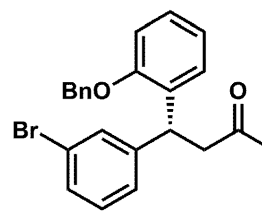


Figure A.2.68. HPLC trace for compound 342

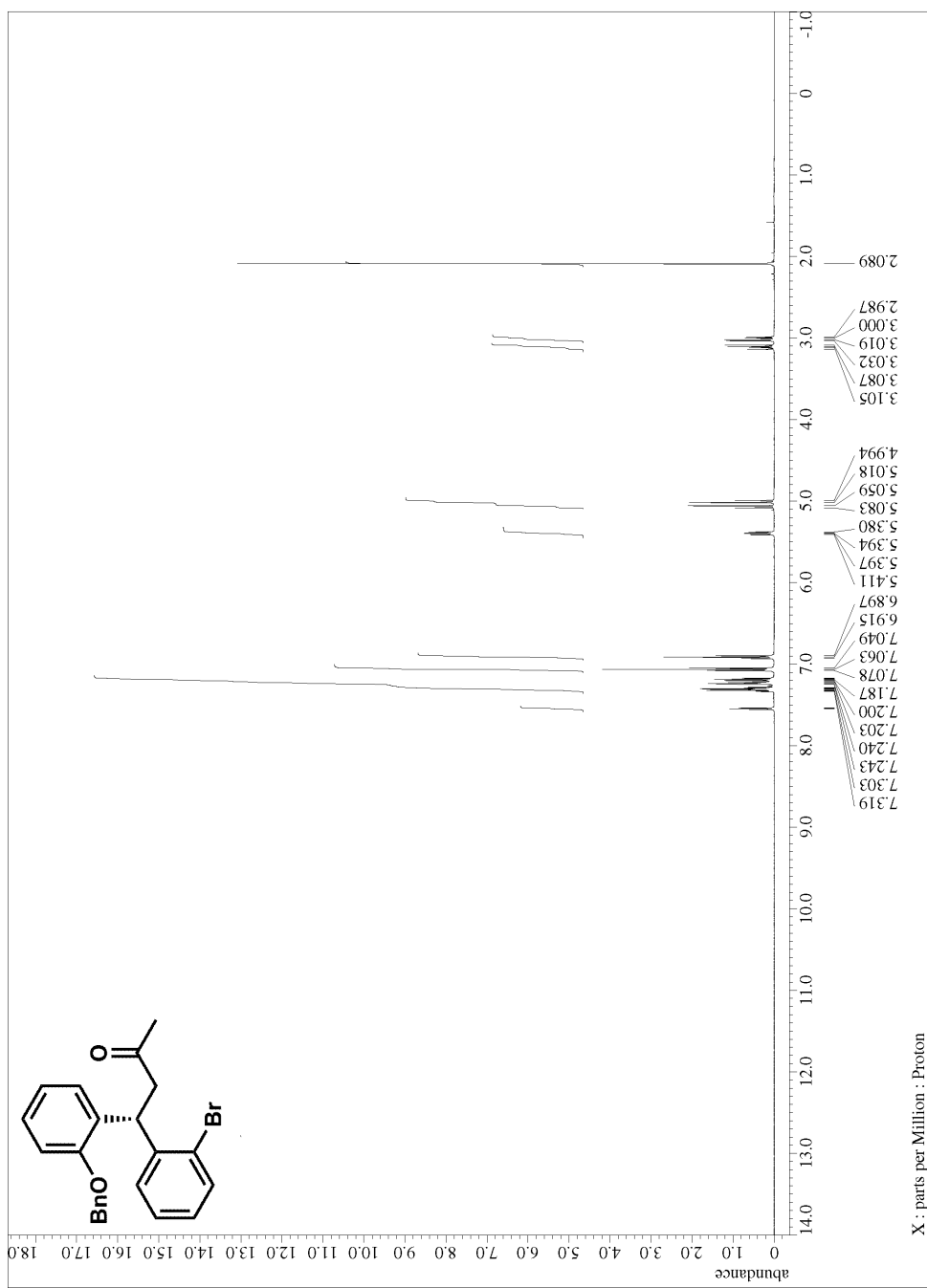


Figure A.2.69. ¹H NMR for compound 343

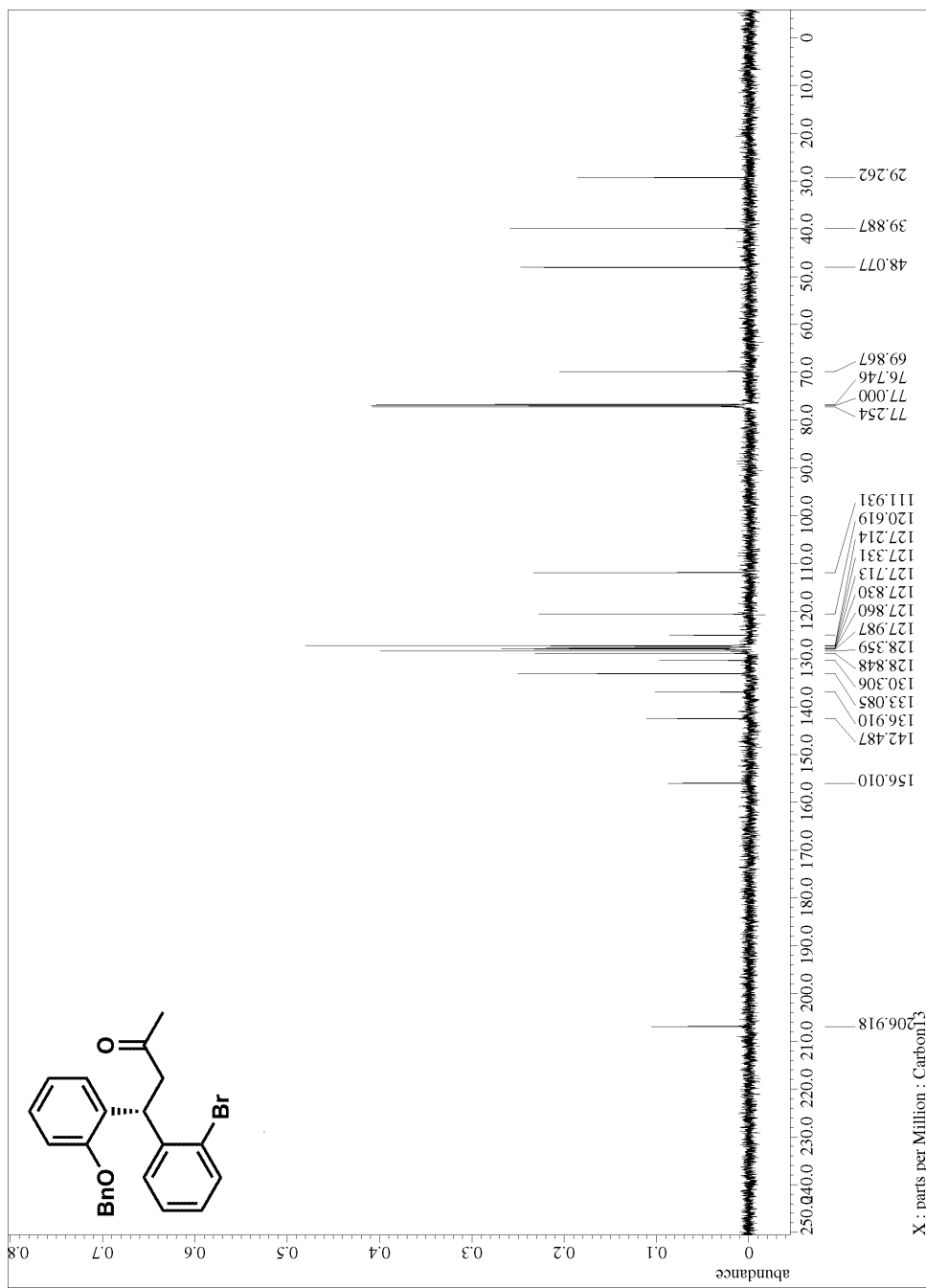
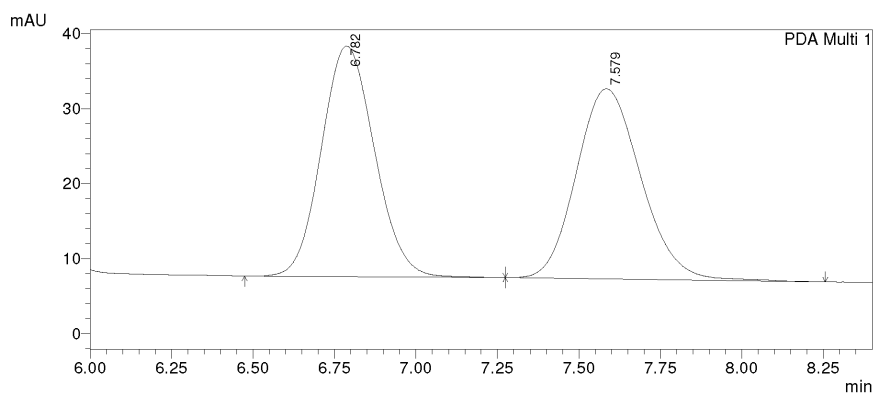


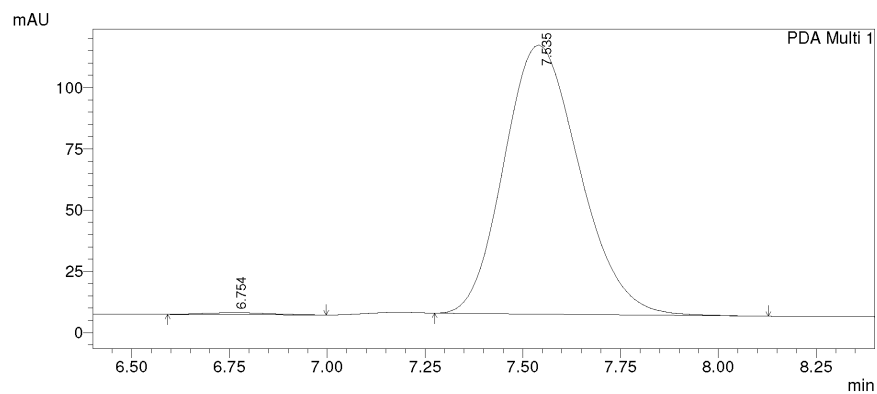
Figure A.2.70. ^{13}C NMR for compound **343**



PDA Ch1 254nm 4nm

PeakTable

Peak#	Ret. Time	Area	Height	Area %	Height %
1	6.782	348402	30742	50.012	54.785
2	7.579	348237	25372	49.988	45.215
Total		696639	56114	100.000	100.000



PDA Ch1 254nm 4nm

PeakTable

Peak#	Ret. Time	Area	Height	Area %	Height %
1	6.754	8840	747	0.597	0.676
2	7.535	1471103	109769	99.403	99.324
Total		1479943	110516	100.000	100.000



Figure A.2.71. HPLC trace for compound **343**

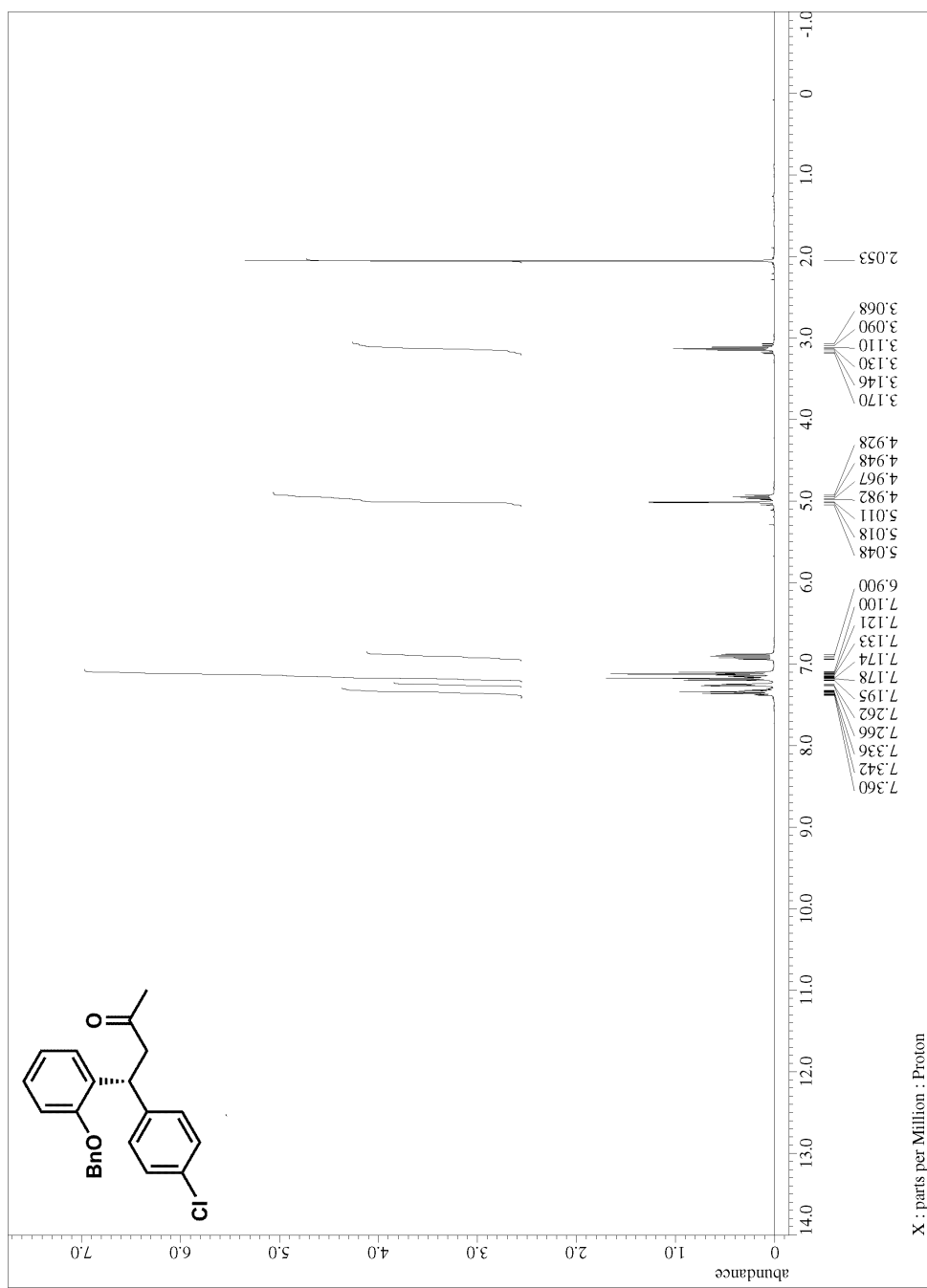


Figure A.2.72. ^1H NMR for compound **344**

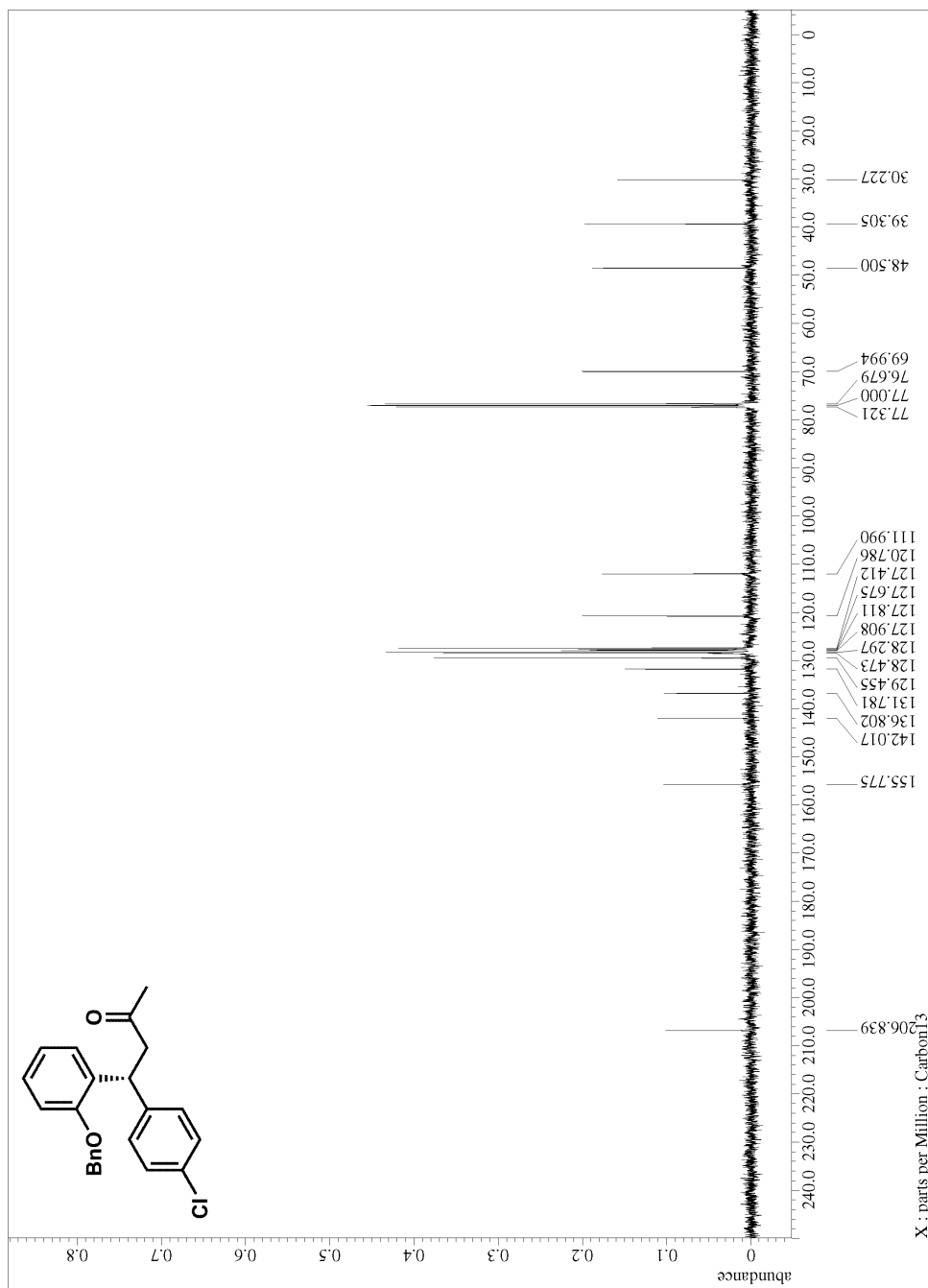
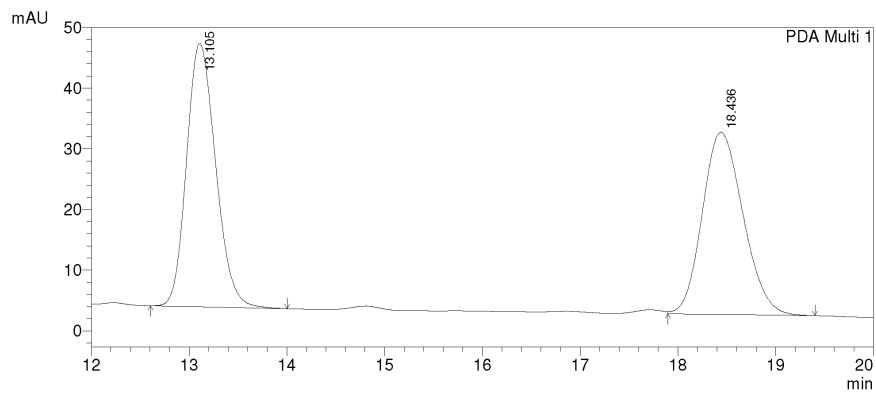
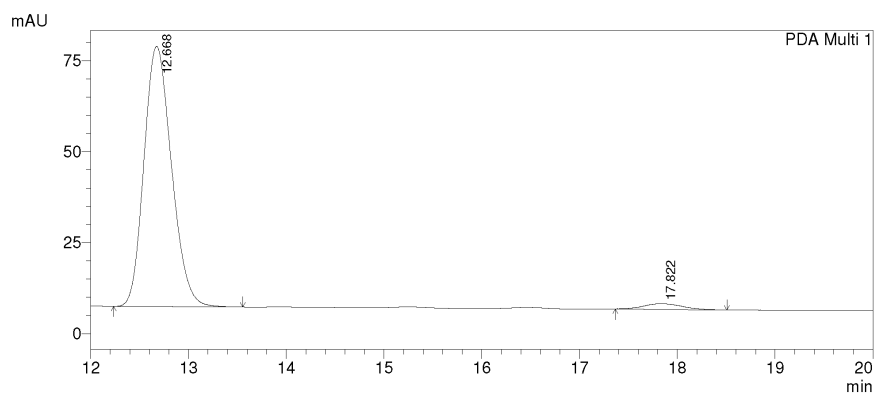


Figure A.2.73. ^{13}C NMR for compound 344



PeakTable

Peak#	Ret. Time	Area	Height	Area %	Height %
1	13.105	895866	43388	50.743	59.082
2	18.436	869620	30048	49.257	40.918
Total		1765486	73436	100.000	100.000



PeakTable

Peak#	Ret. Time	Area	Height	Area %	Height %
1	12.668	1397857	71544	97.058	97.866
2	17.822	42378	1560	2.942	2.134
Total		1440235	73104	100.000	100.000

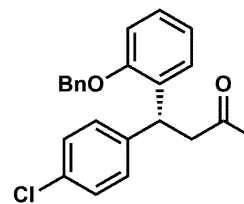


Figure A.2.74. HPLC trace for compound 344

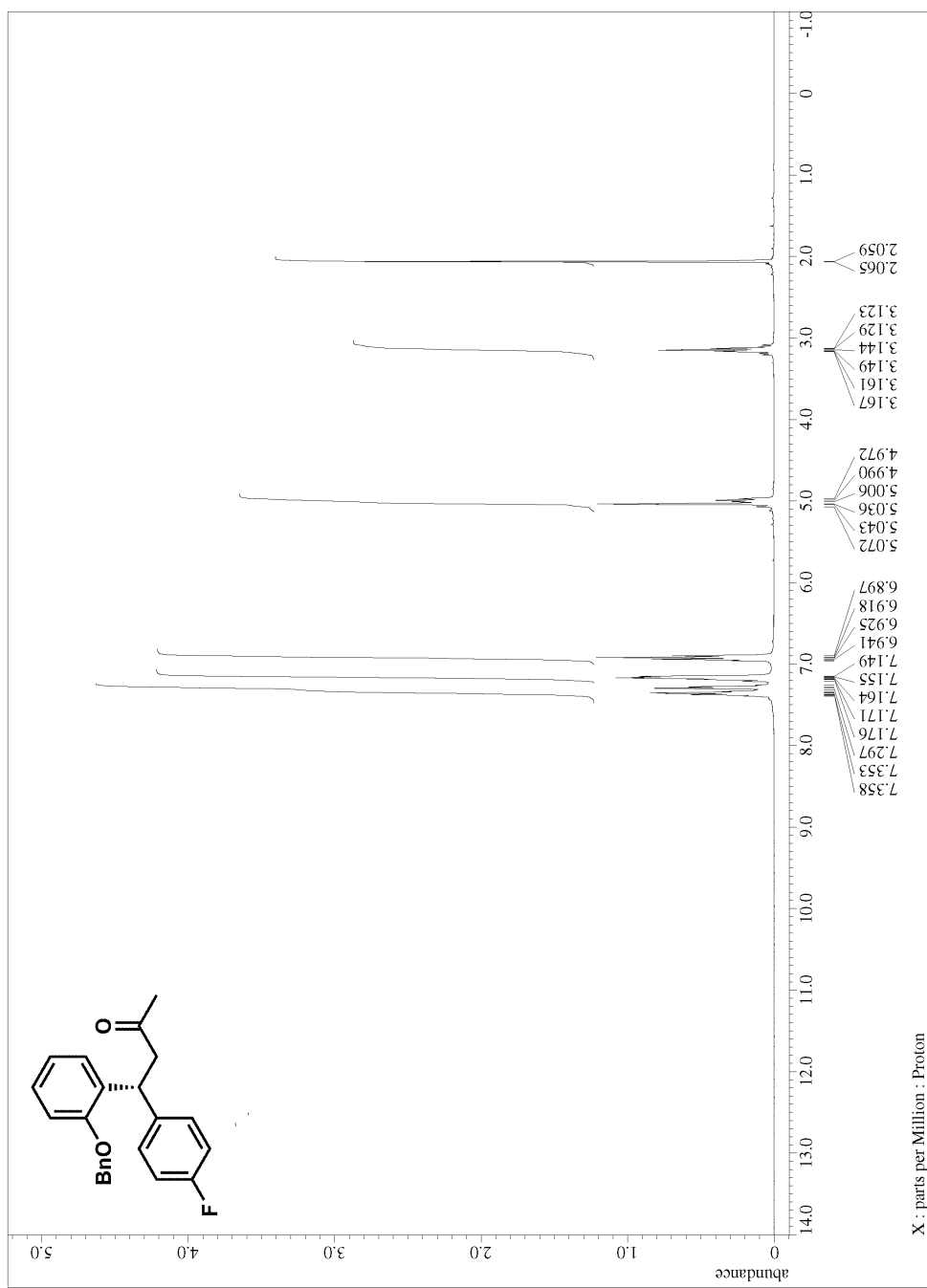


Figure A.2.75. ^1H NMR for compound 345

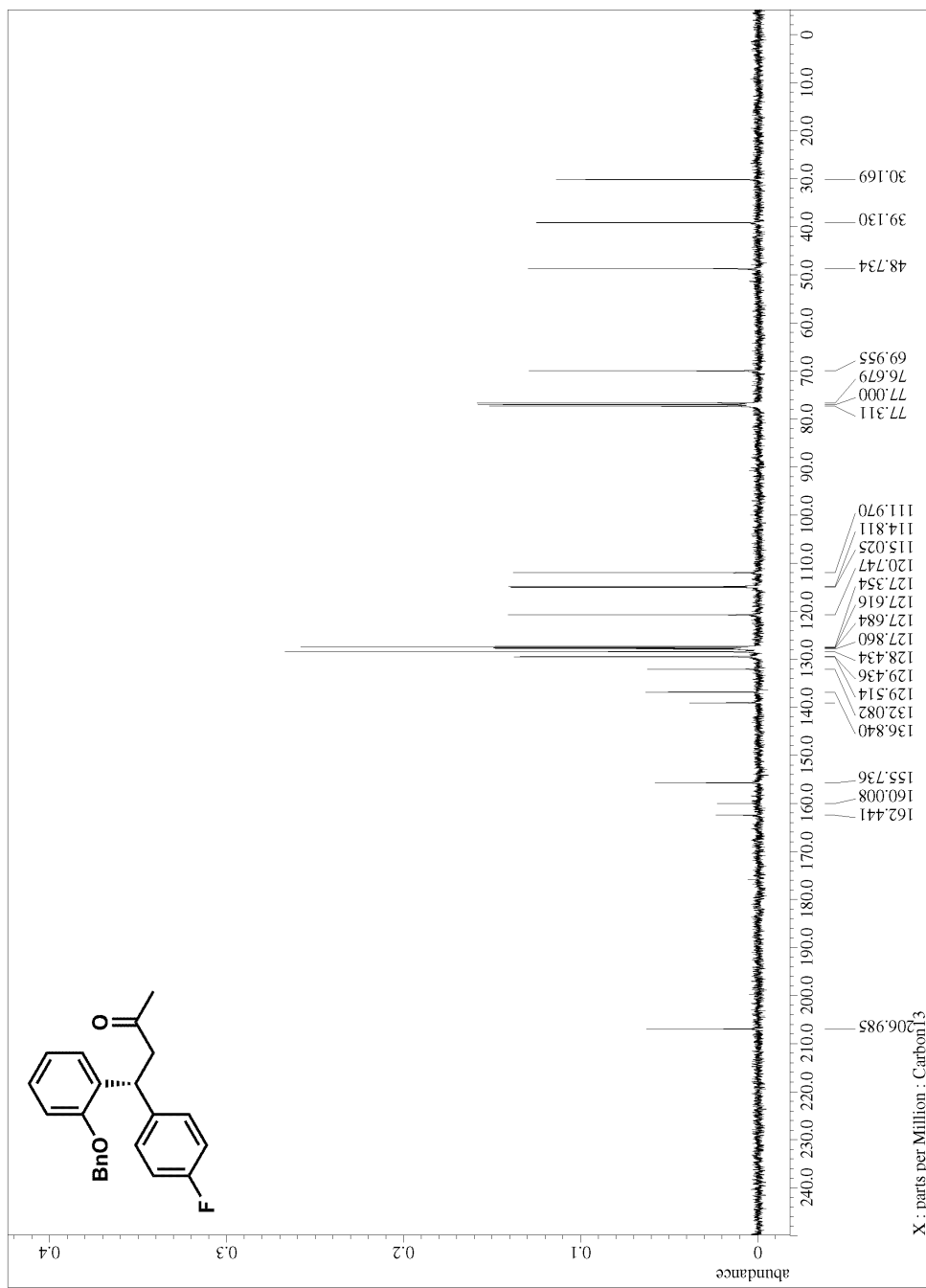


Figure A.2.76. ^{13}C NMR for compound **345**

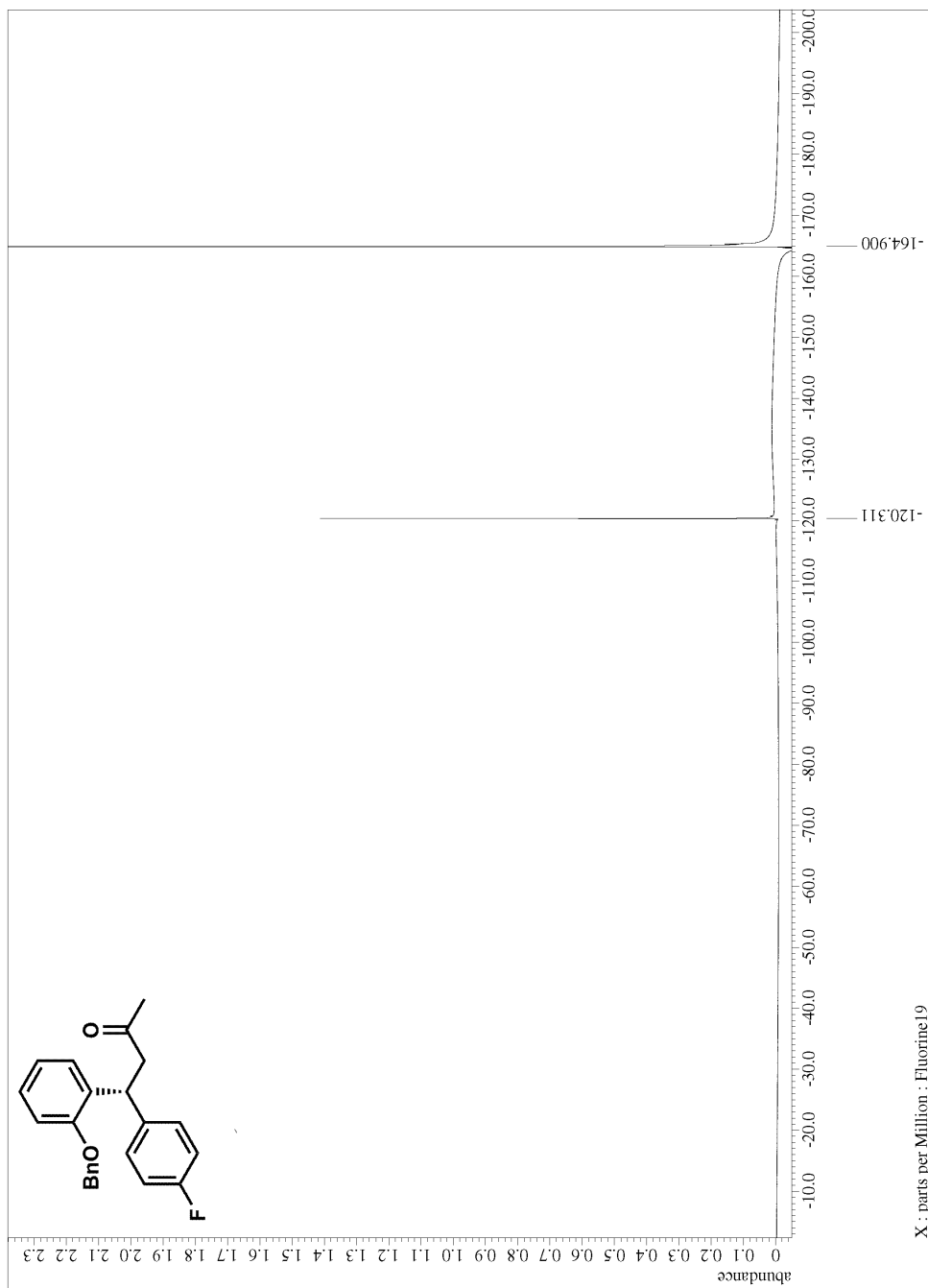
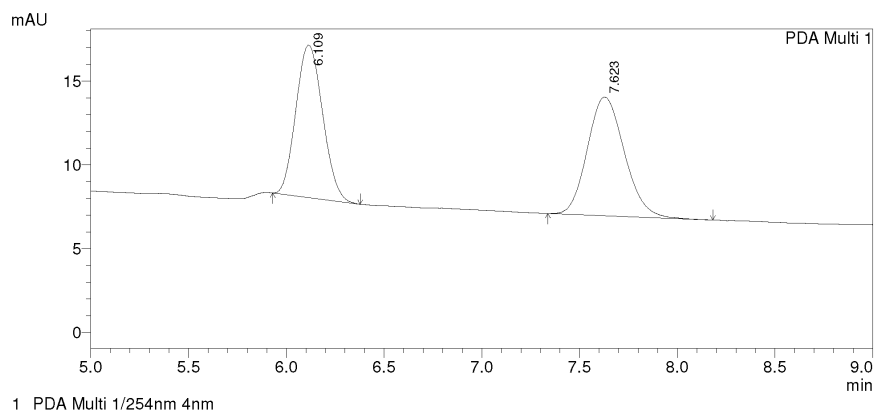


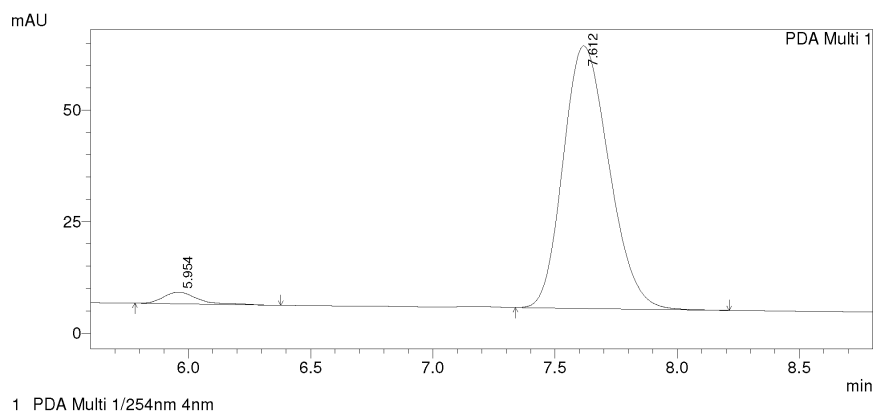
Figure A.2.77. ^{19}F NMR for compound 345



PDA Ch1 254nm 4nm

PeakTable

Peak#	Ret. Time	Area	Height	Area %	Height %
1	6.109	86482	9092	48.085	56.165
2	7.623	93372	7096	51.915	43.835
Total		179854	16188	100.000	100.000



PDA Ch1 254nm 4nm

PeakTable

Peak#	Ret. Time	Area	Height	Area %	Height %
1	5.954	25616	2614	3.228	4.250
2	7.612	768045	58895	96.772	95.750
Total		793661	61509	100.000	100.000

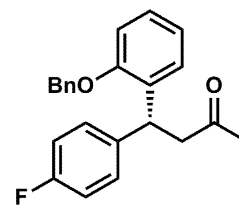


Figure A.2.78. HPLC trace for compound 345

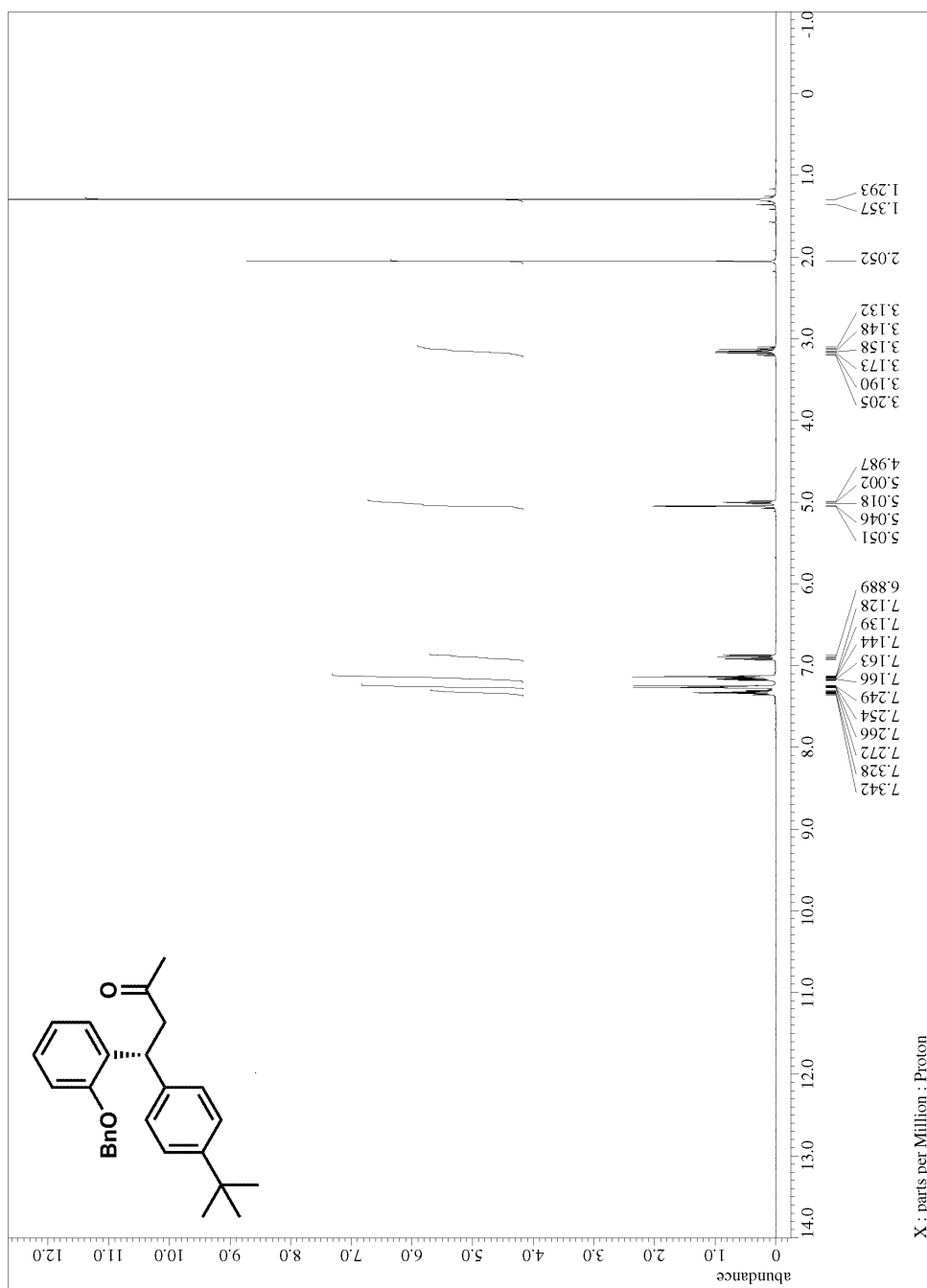


Figure A.2.79. ¹H NMR for compound **346**

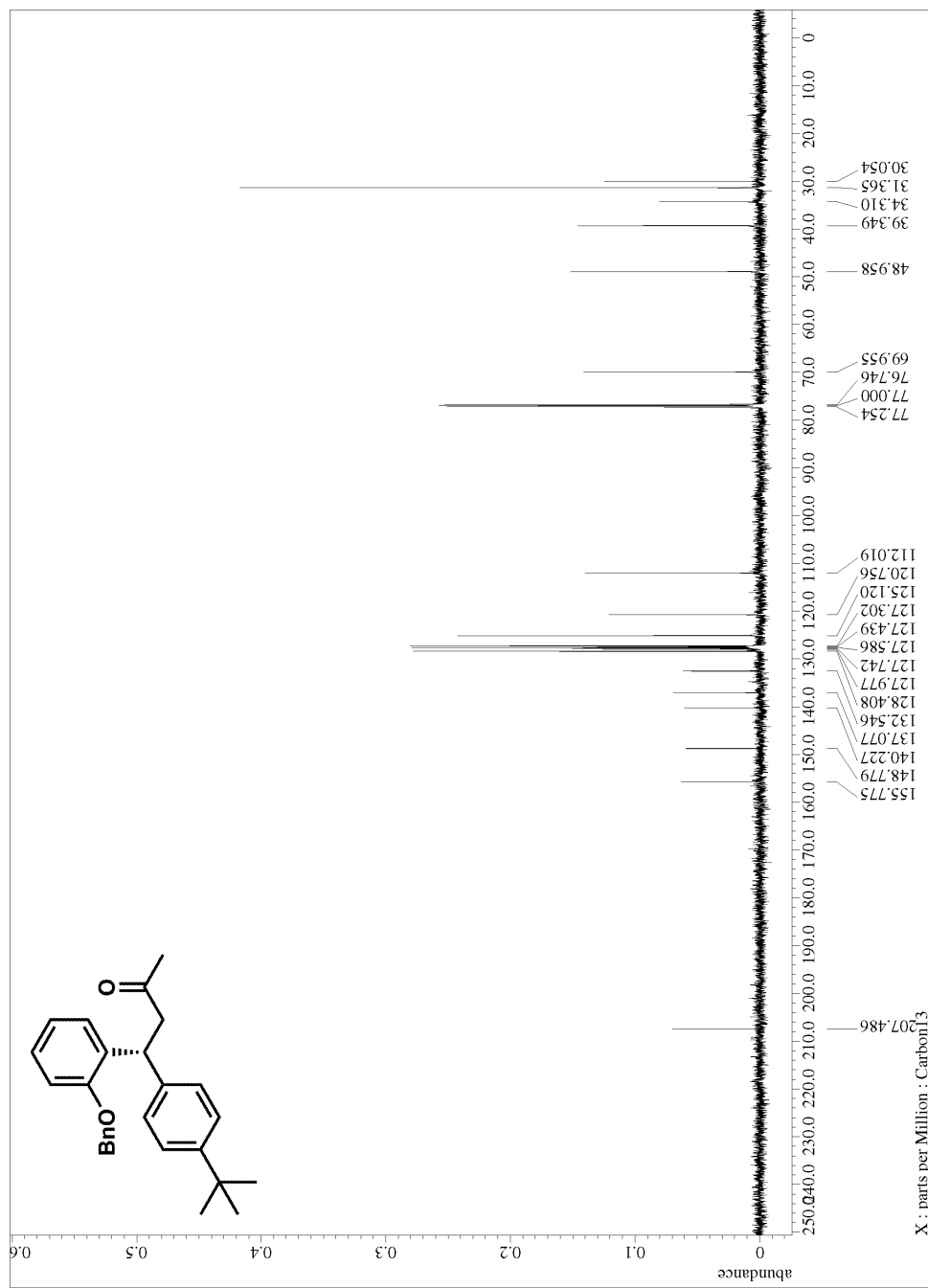
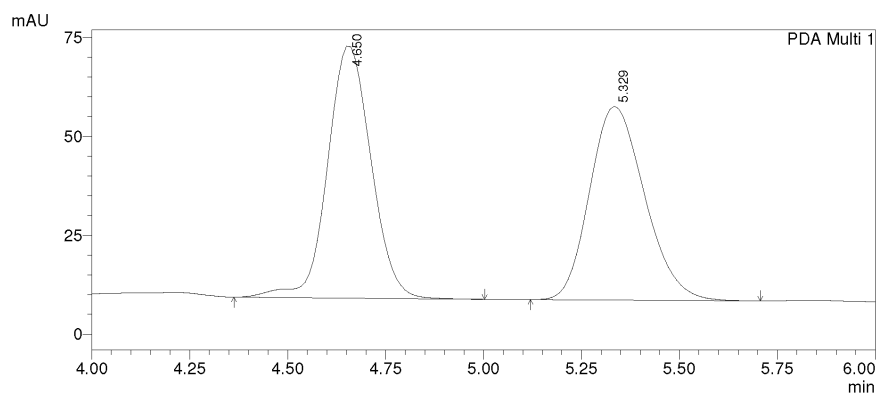


Figure A.2.80. ^{13}C NMR for compound **346**

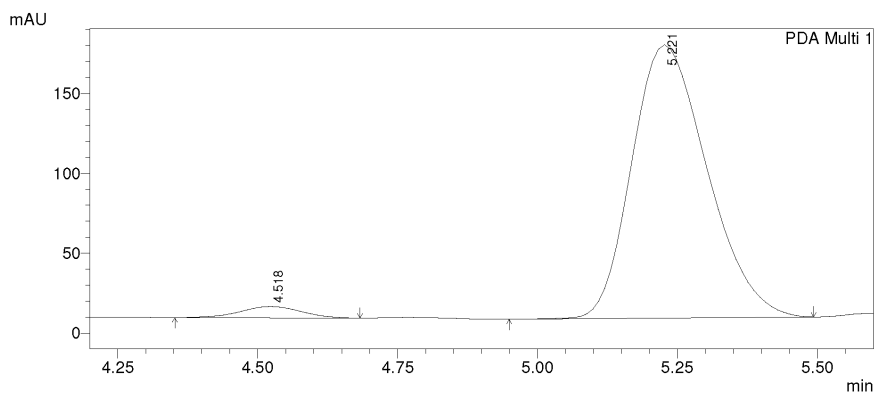


1 PDA Multi 1/254nm 4nm

PeakTable

PDA Ch1 254nm 4nm

Peak#	Ret. Time	Area	Height	Area %	Height %
1	4.650	492823	63706	50.820	56.525
2	5.329	476925	48998	49.180	43.475
Total		969749	112704	100.000	100.000



1 PDA Multi 1/254nm 4nm

PeakTable

PDA Ch1 254nm 4nm

Peak#	Ret. Time	Area	Height	Area %	Height %
1	4.518	54063	7132	3.266	4.002
2	5.221	1601042	171086	96.734	95.998
Total		1655105	178217	100.000	100.000

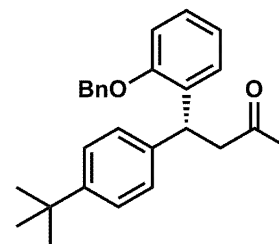


Figure A.2.81. HPLC trace for compound 346

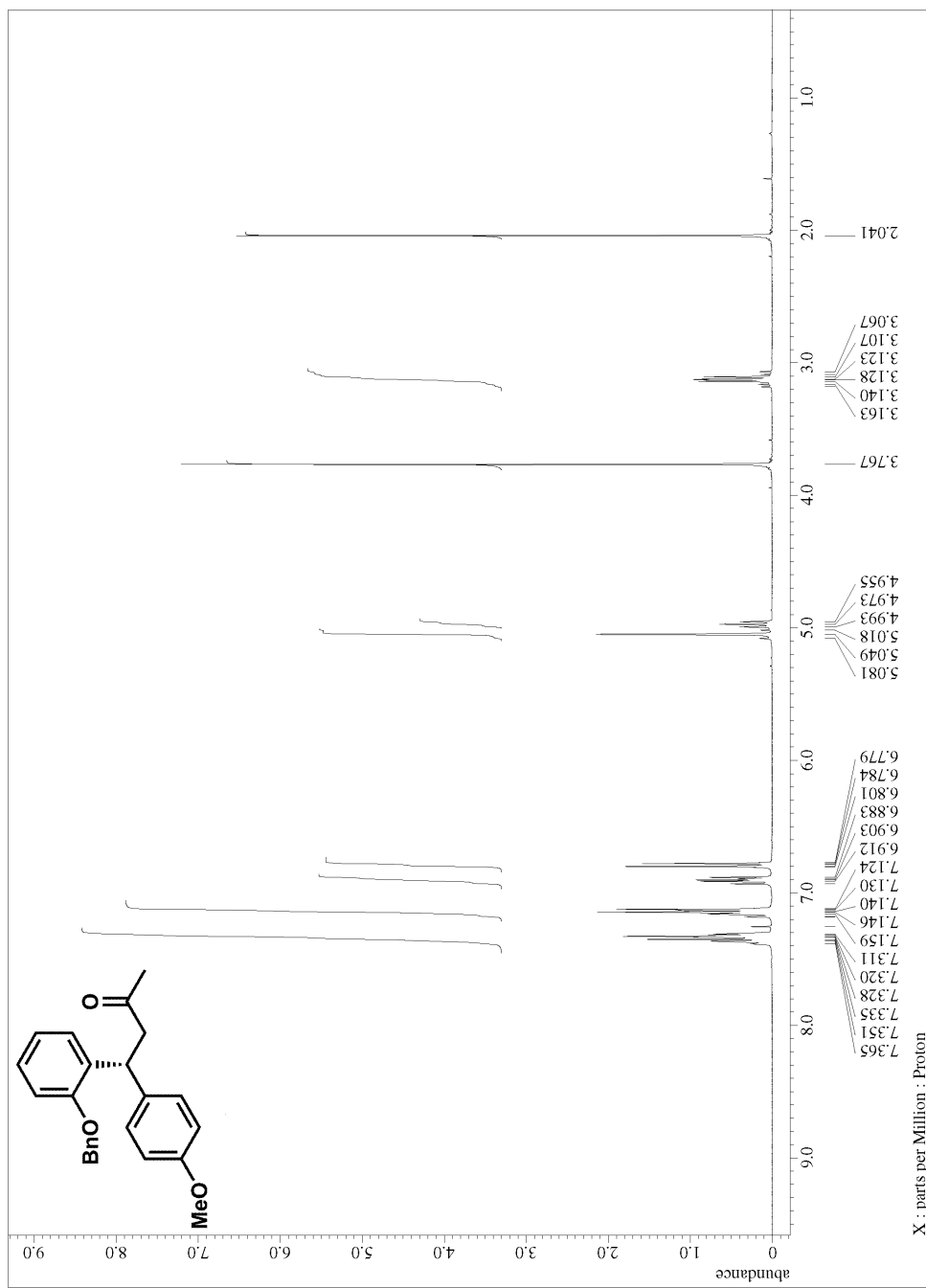


Figure A.2.82. ¹H NMR for compound **347**

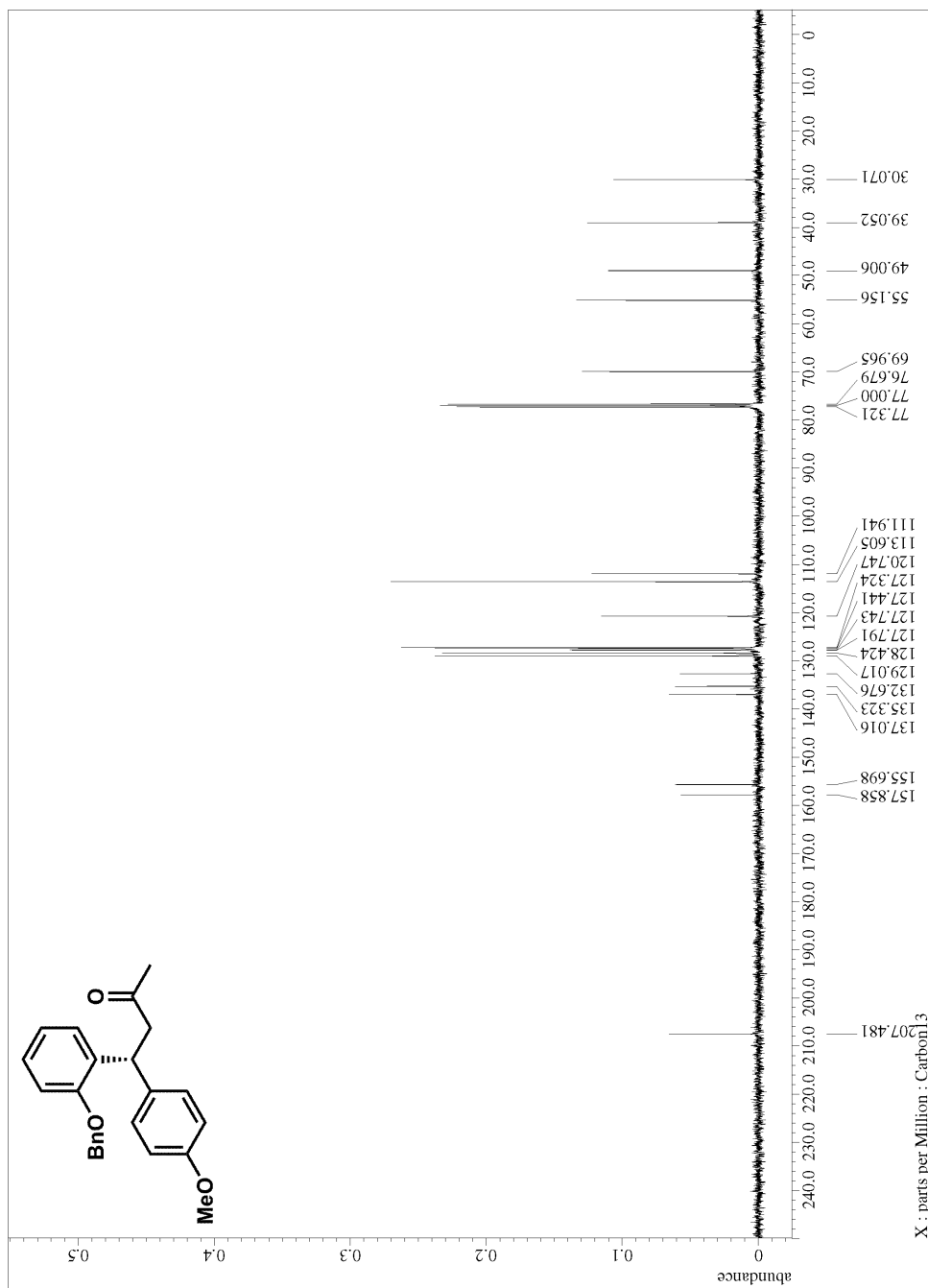
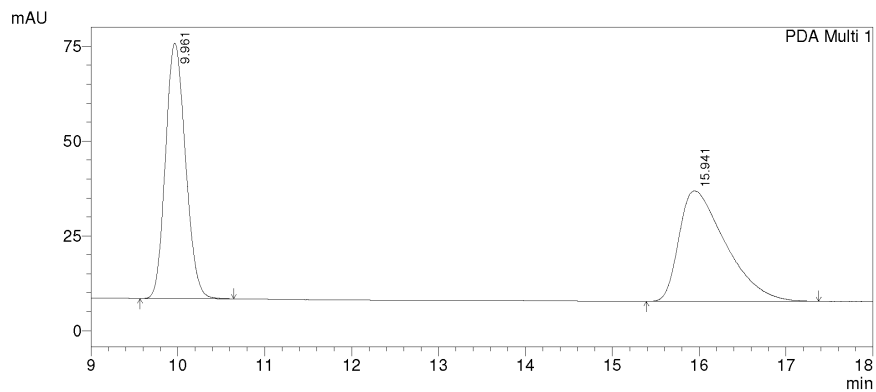
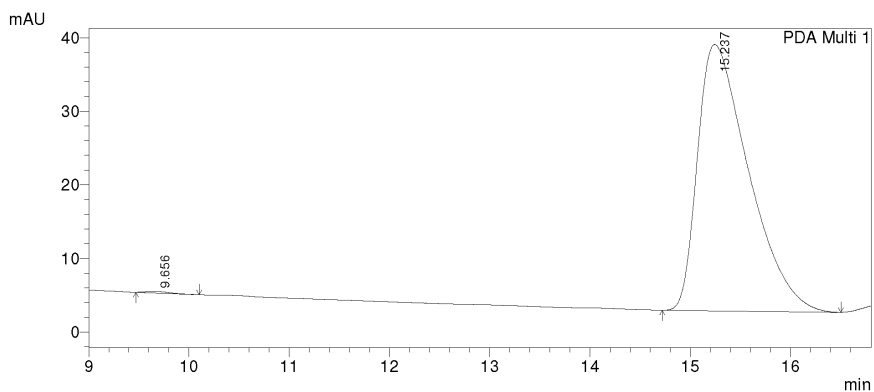


Figure A.2.83. ^{13}C NMR for compound 347



PeakTable

Peak#	Ret. Time	Area	Height	Area %	Height %
1	9.961	1075313	67266	49.739	69.757
2	15.941	1086600	29163	50.261	30.243
Total		2161913	96429	100.000	100.000



PeakTable

Peak#	Ret. Time	Area	Height	Area %	Height %
1	9.656	3538	223	0.276	0.613
2	15.237	1279798	36232	99.724	99.387
Total		1283336	36455	100.000	100.000



Figure A.2.84. HPLC trace for compound 347

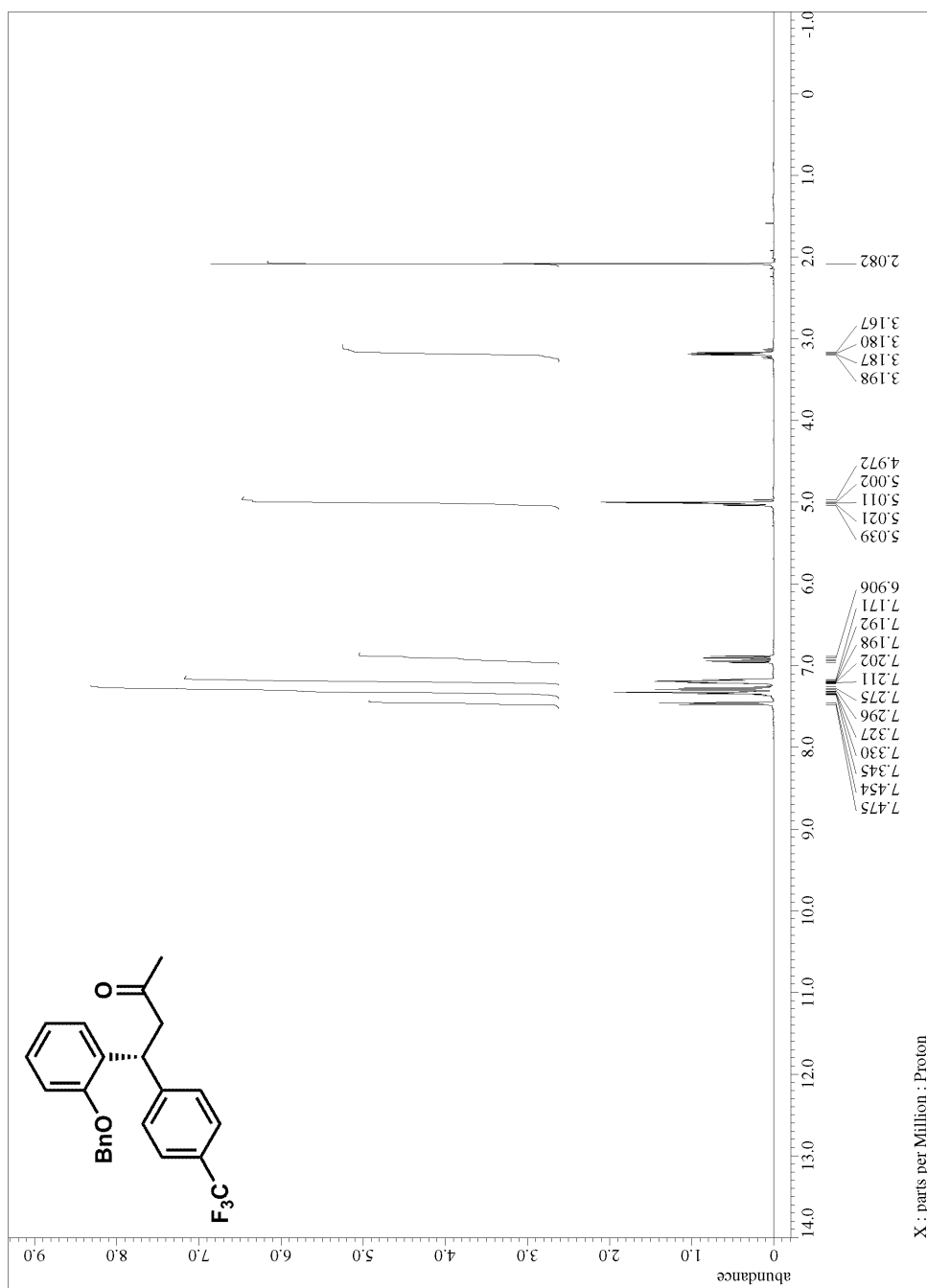


Figure A.2.85. ^1H NMR for compound 348

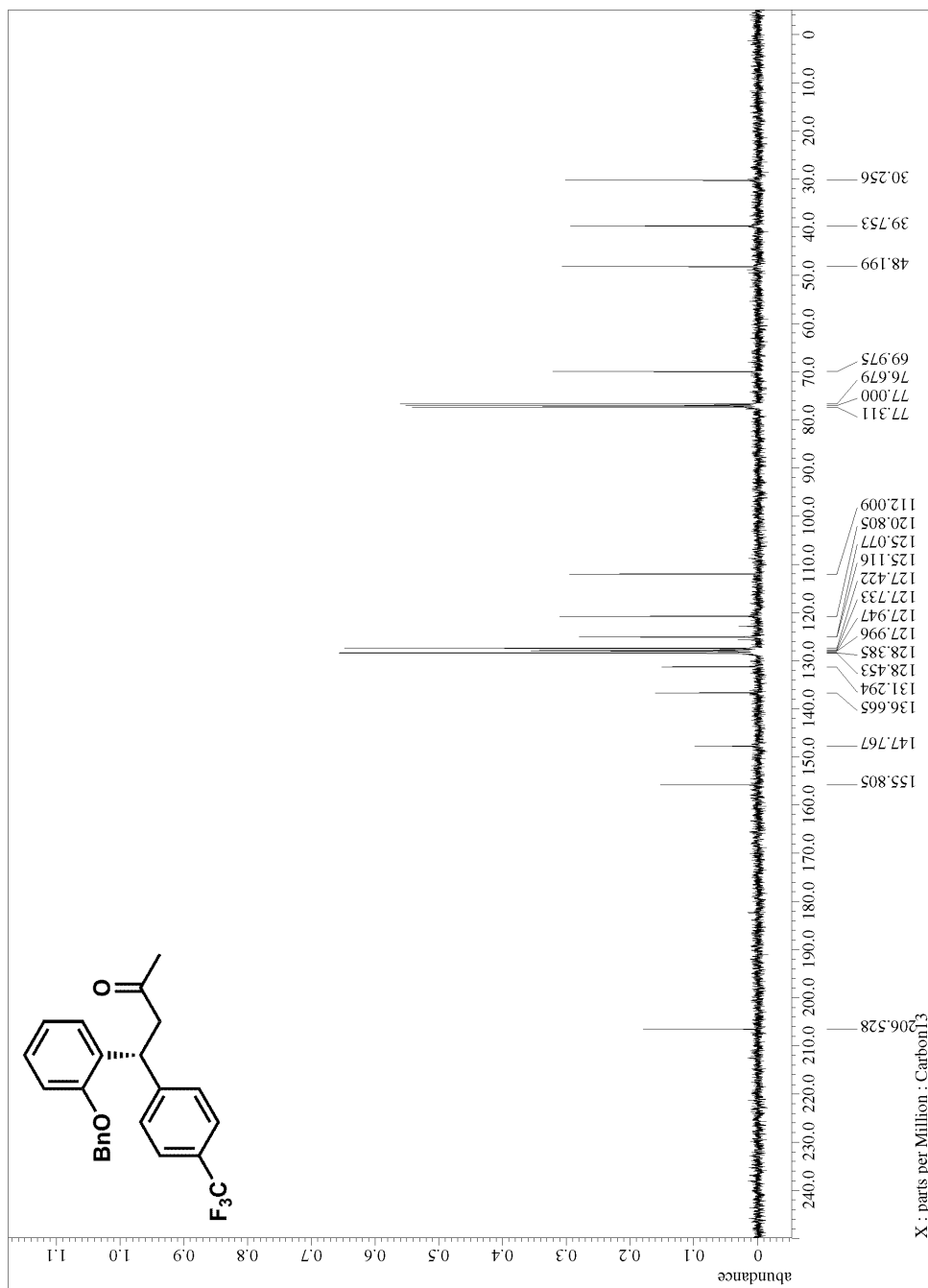


Figure A.2.86. ^{13}C NMR for compound 348

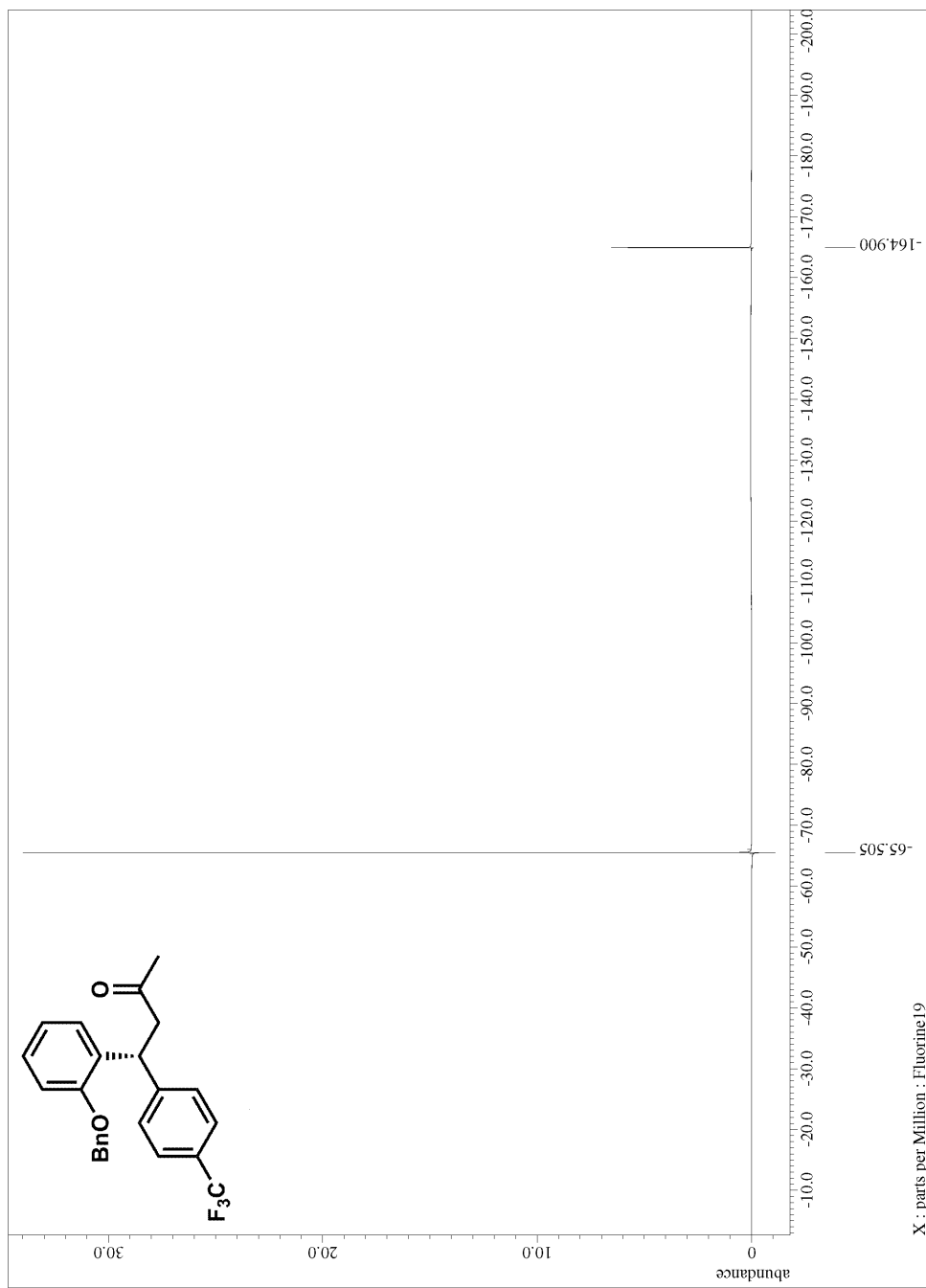
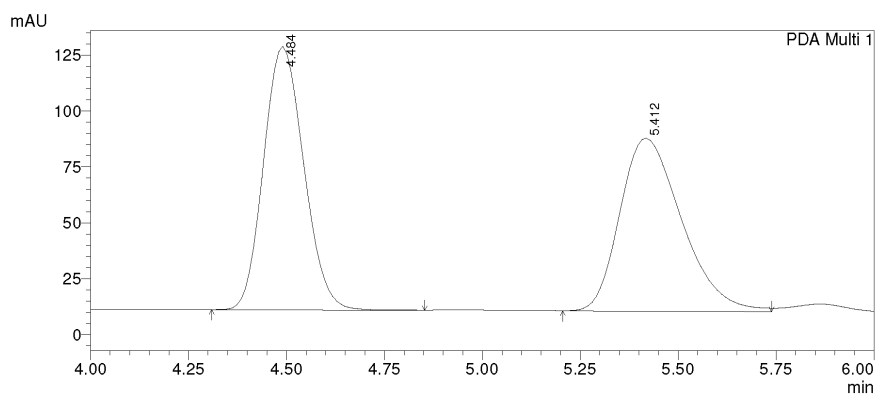


Figure A.2.87. ^{19}F NMR for compound **348**

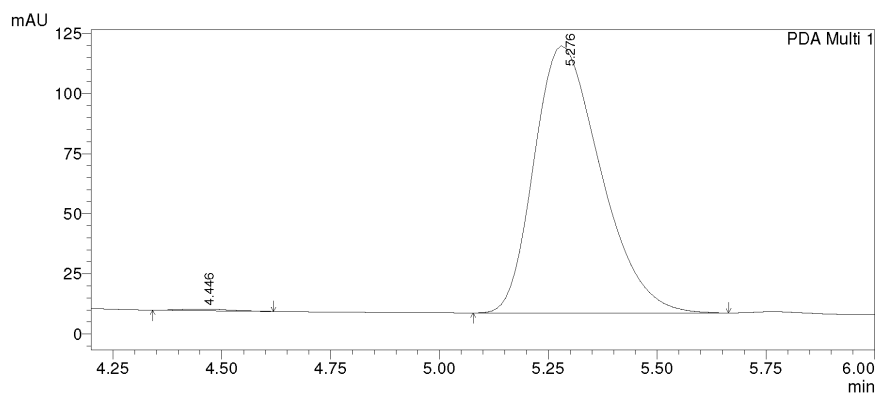


1 PDA Multi 1/254nm 4nm

PeakTable

PDA Ch1 254nm 4nm

Peak#	Ret. Time	Area	Height	Area %	Height %
1	4.484	840386	117776	49.804	60.357
2	5.412	847003	77358	50.196	39.643
Total		1687389	195133	100.000	100.000



1 PDA Multi 1/254nm 4nm

PeakTable

PDA Ch1 254nm 4nm

Peak#	Ret. Time	Area	Height	Area %	Height %
1	4.446	5119	669	0.433	0.599
2	5.276	1176648	110985	99.567	99.401
Total		1181767	111654	100.000	100.000

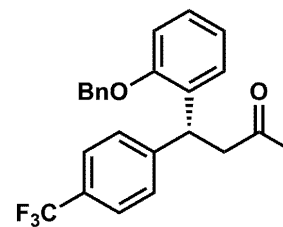


Figure A.2.88. HPLC trace for compound 348

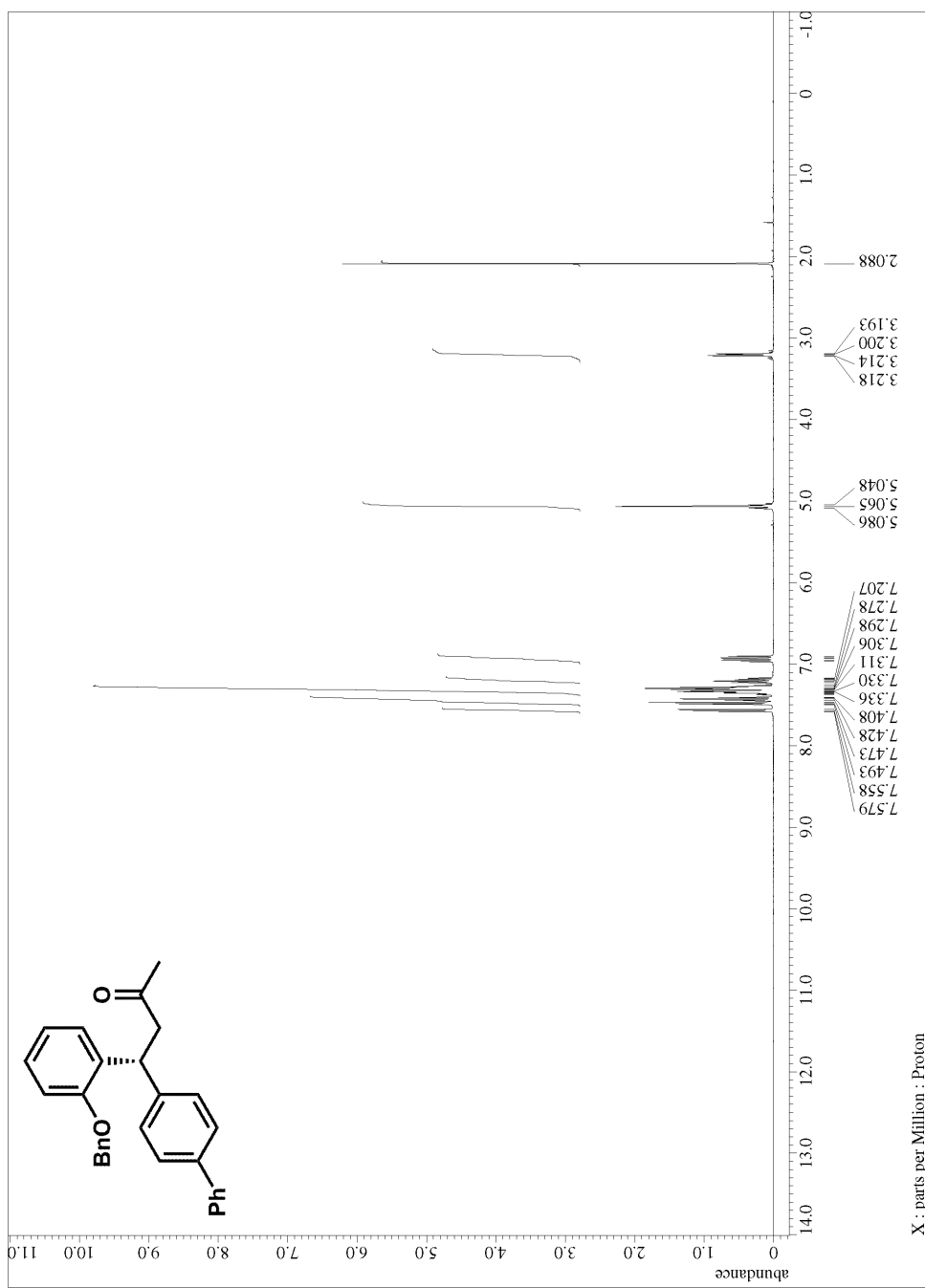


Figure A.2.89. ^1H NMR for compound 349

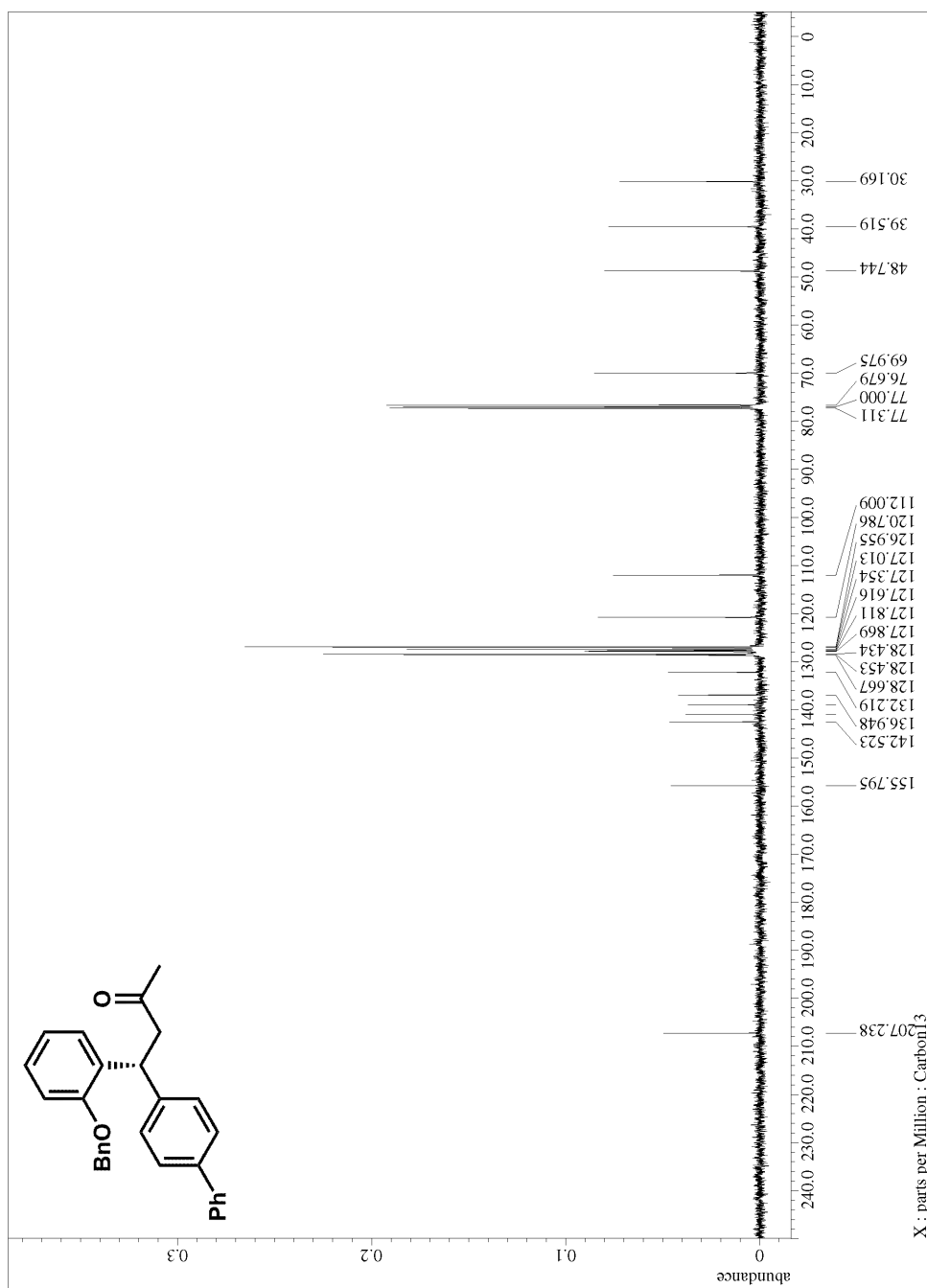
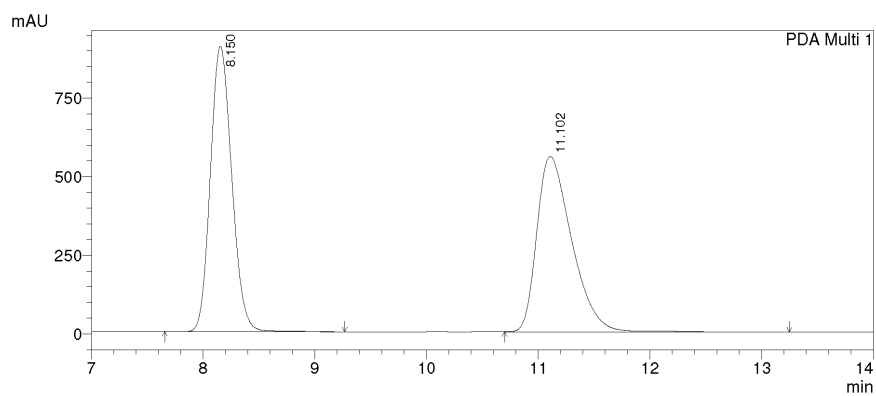


Figure A.2.90. ^{13}C NMR for compound **349**

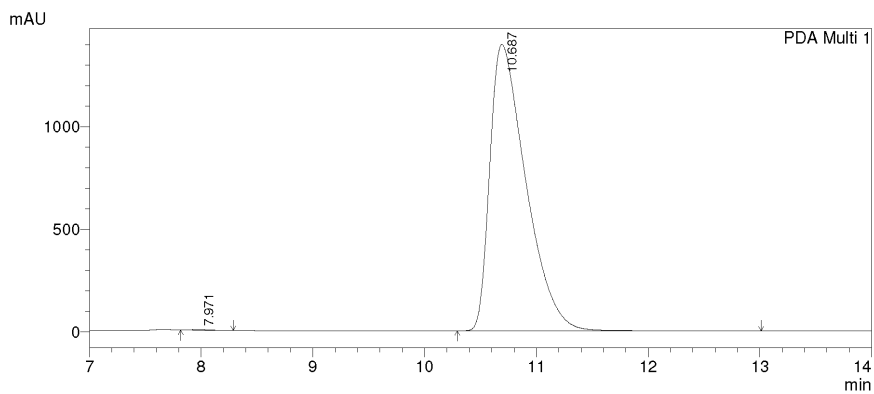


1 PDA Multi 1/254nm 4nm

PeakTable

PDA Ch1 254nm 4nm

Peak#	Ret. Time	Area	Height	Area %	Height %
1	8.150	12083222	906679	49.919	61.925
2	11.102	12122345	557468	50.081	38.075
Total		24205567	1464147	100.000	100.000



1 PDA Multi 1/254nm 4nm

PeakTable

PDA Ch1 254nm 4nm

Peak#	Ret. Time	Area	Height	Area %	Height %
1	7.971	39231	3355	0.126	0.240
2	10.687	31215480	1394776	99.874	99.760
Total		31254711	1398130	100.000	100.000

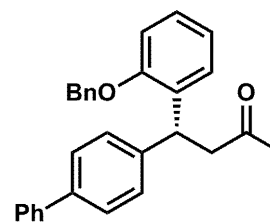


Figure A.2.91. HPLC trace for compound **349**

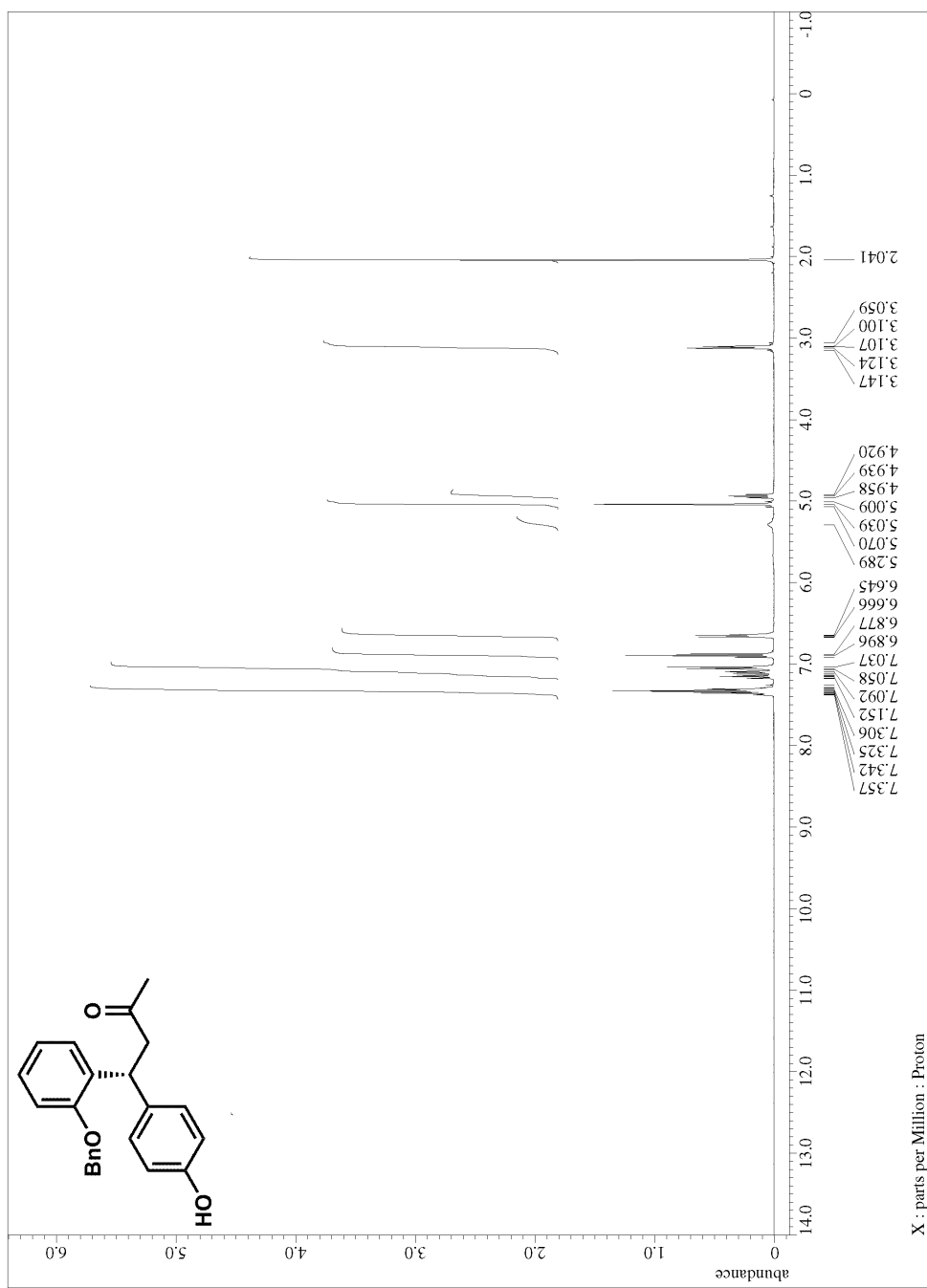


Figure A.2.92. ^1H NMR for compound **350**

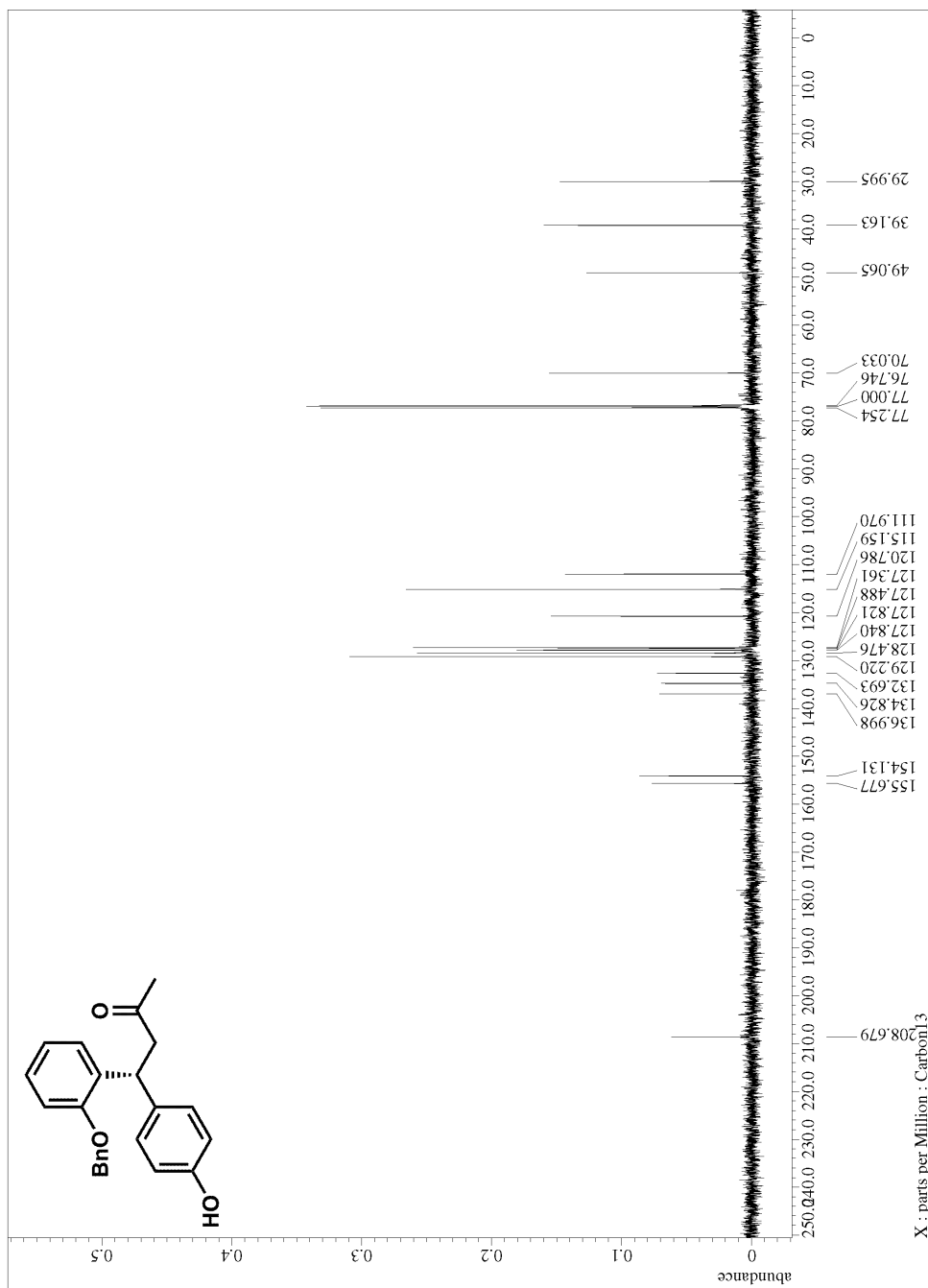
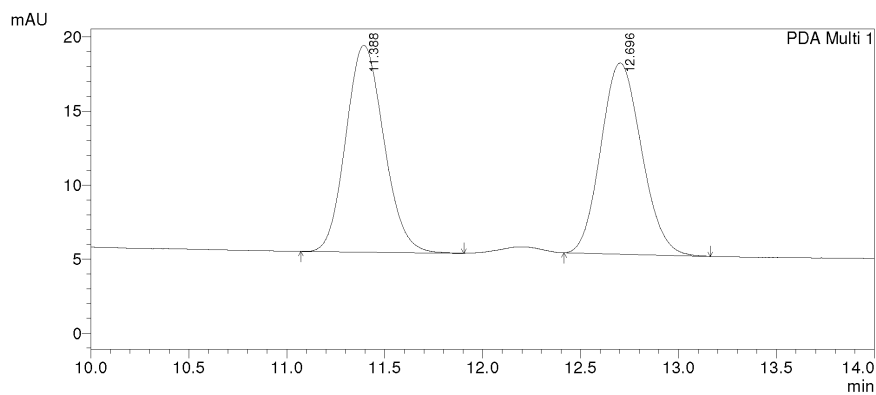
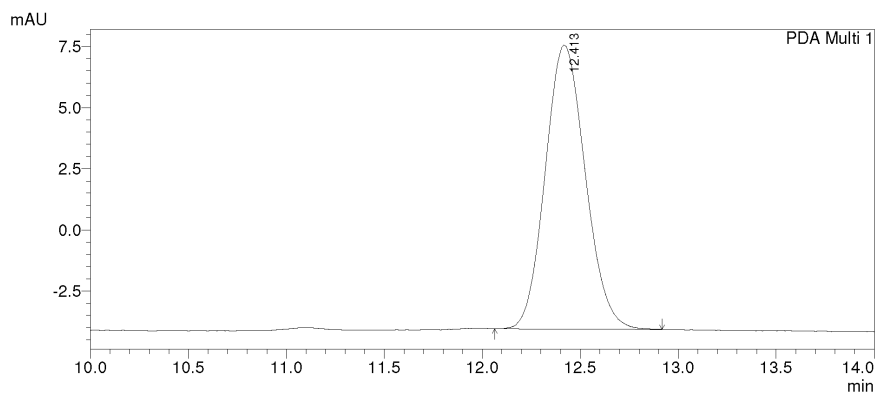


Figure A.2.93. ^{13}C NMR for compound 350



PeakTable

Peak#	Ret. Time	Area	Height	Area %	Height %
1	11.388	188734	13971	50.368	51.970
2	12.696	185978	12912	49.632	48.030
Total		374712	26883	100.000	100.000



PeakTable

Peak#	Ret. Time	Area	Height	Area %	Height %
1	12.413	165230	11605	100.000	100.000
Total		165230	11605	100.000	100.000

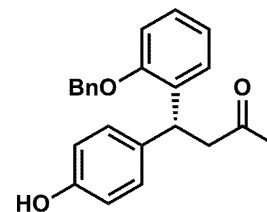


Figure A.2.94. HPLC trace for compound 350